SSCL-SR-1224

Design Report on the SSCL Prototype 80 K Synchrotron Radiation Liner System

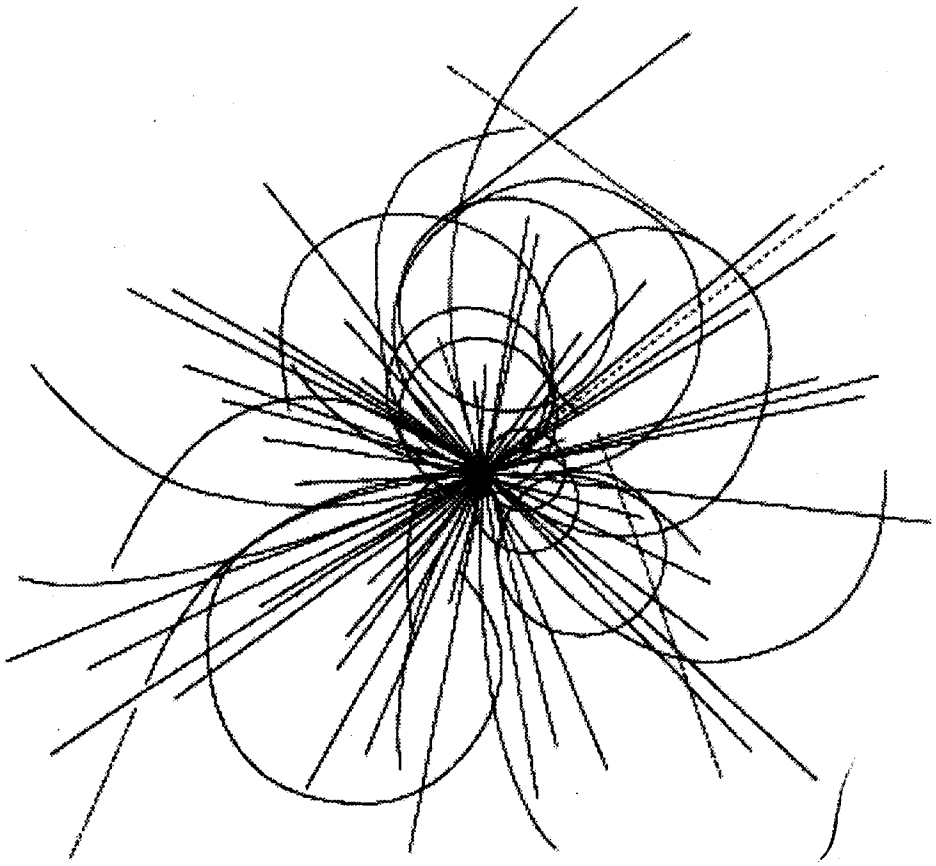

Superconducting Super Collider Laboratory

SSCL-SR-1224
September 1993
Distribution Category: 414

Prepared by Quen-Sheng Shu
SSCL Liner System Design Leader

Contributed by:
T. Barts
W. Chou
D. Clark
W. Clay
G. Goren
Y. Goren
E. Gray
W. Haddock
R. Kersevan
V. Kovachev
P. Kraushaar
S. Kurennoy
K. Leung
J. Maddocks
D. Martin
D. Meyer
R. Mihelic
G. Morales
K. Mountain
C. Murray
M. Neal
M. G. Rao
R. Richardson
E. D. Ruiz
N. Sday
N. Spayd
J. Simmons
W. Smith
G. Snitchler
G. Spalik
V. Thiagarajan
M. Tuli
W. Turner
L. Walling
K. Yu
A. Yücel
J. Zbasnik

SSCL-SR-1224

Design Report on the SSCL Prototype 80 K Synchrotron Radiation Liner System

Q. S. Shu, *et. al*

Superconducting Super Collider Laboratory*
2550 Beckleymeade Ave.
Dallas, TX 75237

September 1993

*Operated by the Universities Research Association, Inc., for the U.S. Department of Energy under Contract No. DE-AC35-89ER40486.

DESIGN REPORT ON THE SSCL PROTOTYPE 80 K SYNCHROTRON RADIATION LINER SYSTEM

Quan-Sheng Shu
SSCL Liner System Design Leader

Superconducting Super Collider Laboratory*
2550 Beckleymeade Avenue
Dallas, TX 75237

This report documents the effort to develop a viable design for an SSC prototype 80 K Synchrotron Radiation Liner System. This liner is designed to be tested in the Superconducting Super Collider Accelerator Systems String Test (ASST) facility. The liner is one method under consideration to minimize the presence of photodesorbed gases in the particle beam line vacuum environment. Secondly, the liner is aimed at improving the Collider cryogenic thermal efficiency which would allow a potential luminosity upgrade.

The SSC Collider is the first proton superconducting accelerator designed to operate at an energy of 20 TeV (each beam) and a beam current of 72 mA. The Collider will produce a synchrotron power of 0.14 W/m and a total of 18 kW into 4.2 K for the two rings. This radiated power may trigger a serious impact of photodesorbed gases on the operational availability of the Collider. The interaction between beam particle and photodesorbed gases may greatly reduce the beam lifetime and the scattered beam power may lead to quenching of the superconducting magnets. Collider availability may be unacceptable if this concern is not properly addressed. The liner is one method under consideration to minimize the presence of photodesorbed gases in the particle beam line vacuum. Secondly, the liner is aimed at improving the Collider's cryogenic thermal efficiency which would allow a potential luminosity upgrade. The ultimate goal is to require no more than one machine warm up per year for vacuum maintenance during operation of the SSC Collider.

A liner is a piece of scientific art and technical architecture that presents the challenge of developing a system inside the existing particle beam tubes that directly interfaces with the synchrotron light and compensates for the synchrotron by-products of photodesorbed gases and heat. The system addresses photodesorption, the particle beam, magnet fields, beam induced wakefields, the RF system, the cryogenic system, magnet quench conditions, especially quench induced Lorentz pressure, and many other interdisciplinary technical problems that must be considered and resolved in a timely manner. One of the challenges to the liner design is that there is no experience from which to draw directly. There is also a schedule challenge in that the liner design must catch up with many years of magnet design efforts.

The liner will be installed into all the dipole magnets, quadrupole magnets, and spool pieces in the entire arc region of the SSC Collider, if the liner is finally determined to be the best solution to the problem of synchrotron radiation and photodesorbed gases. As a liner Research and Development (R&D) program, it was decided by SSCL Project Management that a liner system prototype for a half cell be developed and tested at the Accelerator System String Test (ASST) facilities, since a half cell of the collider string (five dipoles, one quadrupole and one spool piece with a beam position monitor) is a basic unit of the SSC Collider.

---

*Operated by the Universities Research Association, Inc., for the U.S. Department of Energy Under Contract No. DE-AC35-89ER40486.

The liner's required operational temperature of 80 K was based on analyses of the photodesorption data available from the CDG and SCDG measurements at the time when the ASST liner design had been performed. In the case of an 80 K liner, there is a second purpose, namely, to replace the 4 K dynamic heat load of the synchrotron radiation with a static heat load, independent of the beam intensity, and to transfer the intercepted heat to the liquid nitrogen system. This has the advantage of upgrading the Collider luminosity over the lower temperature liners with a higher thermal dynamic coefficient.

The development of an 80 K Liner System for test and evaluation in the ASST was initiated through the auspices of Dr. Gerry Dugan of the SSCL Project Management Office resulting in the establishment of the Liner System Design Team in July of 1992. The team was created by enlisting key personnel from MSD, ASD, and PMO in the spirit of concurrent engineering represent the various critical elements of an 80 K system.

This development program was established with three major phases: (1) concept proposal and evaluation, (2) concept selection and design, and (3) fabrication and test of the selected design in the ASST facility.

The first phase was summarized in the "Report on the ASST II Liner Status" in November of 1992 (SSCL-N-805).

The second phase effort, design of an 80 K ASST liner, has been successfully accomplished. The trade studies, physics and engineering analyses, conceptual design developments, detailed engineering design, and the results from several experiments are briefly summarized herewith in the design report as well as in the associated technical papers..

The third phase has been suspended by the SSC pending the evaluation of other alternatives in light of recent measurements of photodesorption coefficients. This recent data indicate the viability of 4 K and 20 K systems, which were previously considered as not viable based on the old CDG and SCDG measurements.

This 80 K liner design development can not only be used for fabricating and testing of an 80 K liner, but can also serve as a solid foundation for developing the lower temperature liner (*i.e.* 20 K or 4 K liners). All of the logic, the trade studies, the analyses, and the design work will be very useful references when a lower temperature liner is pursued as a method to resolve the concern associated with the synchrotron radiation and the consequential photodesorbed gases. Costs associtated with this project can be obtained from Dr. Quan-Sheng Shu at the SSC Laboratory.

Tremendous progress has been made by the Liner team (Table 1) in completing the design of the 80 K Liner System for the ASST, due to their initiative and dedication to the project. Acknowledgement is equally due to G. Dugan, T. Bush, T. Kozman, R. Briggs, A. Chao, R. Coombes, M. McAshan, J. Tompkins, R. Meinke, W. Turner, and J. Franciscovich for supporting this unique interdivisional team approach towards accomplishing this task. Without their support, this progress would not have been possible. Finally, I would like to express my appreciation to M. Downes (student intern), R. Mihelic, and K. Yu for their contributions to the preparation of the design report.

TABLE 1. CONTRIBUTORS TO THE WORK SUMMARIZED IN THE LINER DESIGN REPORT.

No.	Description	Contributed by*
1	Liner Design Requirement	W. Turner
2	Leading Liner Design and Technical Management	Q. S. Shu
3	Liner Tubes for CDM, CQM	M. Tuli, W. Clay, G. Morales, Q. S. Shu, J. Zbasnik,
4	Liner Support	J. Maddocks, J. Zbasnik
5	Spool Piece Liner	D. Clark, J. Zbasnik, Q. S. Shu
6	BPM and Interface with Liner	D. Martin, D. Meyer, D. Clark
7	RF Joint, Cryogenic Box, and Interconnect Heat Exchangers of Liner	W. Clay, G. Morales, Q. S. Shu, J. Maddocks, K. Yu, J. Zbasnik
8	Cryogenic Cooling Loop and Refrigeration of Liner	J. Maddocks, Q. S. Shu, K. Yu,
9	Liner Cryosorber	R. Kersevan, W. Turner, M. Ganapati Rao (CEBAF)
10	Beam Tube Liner Vacuum Analyses	W. Turner
11	Thermal and Cryogenic Analyses of Liner System	Q. S. Shu, W. Clay, J. Maddocks, K. Yu
12	Quench Induced Lorentz Force, Stress, ASME Code Analyses of Liner System	K. Leung, G. Morales, Q. S. Shu, W. Haddock, G. Goren, K. Yu, J. Zbasnik
13	RF Impedance Analyses and Measurement	W. Chou, L. Walling, T. Barts, S. Kurennoy, V. Thiagarajan, E. D. Ruiz, Y. Goren, N. Spayd
14	Effect of Liner on Magnet Field Quality	G. Snitchler
15	Test of Liner Short Sample Quench Survivability	R. Richardson, J. Zbasnik
16	Test of Liner Support Heat Leak and the "Magic" Joint	J. Maddocks, J. Zbasnik
17	Test of Magnetoresistivity/Parasitic Heat/ Thermal Conductivity at Low Temperature and High Field	W. Chou, V. Kovachev, Q. S. Shu, J. Zbasnik, M. Tuli, G. Spalek, and E. Gray (LANL)
18	Liner ASST II Test	P. Kraushaar, Q. S. Shu, W. Turner
19	System Engineering and Schedule of Liner	R. Mihelic, J. Simmons, K. Mountain
20	System Design Package and Design Documents	Q. S. Shu, G. Morales, C. Murray, R. Mihelic, K. Yu

*Some names may be unintentionally omitted.

CONTENTS

CHAPTER 2 DESIGN ANALYSIS AND ENGINEERING DATA

CHAPTER 1

REQUIREMENTS AND DESIGN OVERVIEW

SECTION 1

Requirements for a Prototype 80 K Liner Vacuum System for the 4.2 K Cold Bore of the SSCL 20 TeV Proton Collider

W. C. Turner

SECTION 1

Requirements for a Prototype 80 K Liner Vacuum System for the 4.2 K Cold Bore of the SSCL 20 TeV Proton Collider

W. C. Turner

Superconducting Super Collider Laboratory*
2550 Beckleymeade Ave., MS 1002
Dallas, TX 75237

1.0 INTRODUCTION

This document describes the requirements for the 80 K liner design as they were written down at the beginning of the design effort in June 1992. For the most part these requirements are derived from the photodesorption data existing in June 1992,[1] the CDR[2] and SCDR,[3] the Collider 3B Specification[4] and various reports in the compilation by H. Edwards,[5] particularly A. Maschke's memo, "Initial Design Requirements and Goals," in Appendix 2. Other input will be noted in the discussion below.

2.0 REQUIREMENTS

Altogether there are 18 requirements listed in Table 1. We will briefly discuss the rationale for each of them.

The first requirement deals with the inside diameter of the liner. The number given for the liner ID in Table 1 is a minimum of 26 mm. The basis of this number is a discussion at the May 27, 1992, meeting of the Parameters Committee dealing with the minimum space needed for commissioning the Collider.[6] The number arrived at was 26 mm = 2*(4 mm 10σ beam size + 4 mm closed orbit errors + 3 mm mom. dispersion + 2 mm magnet misalignment). Arguments have been presented for a larger space. D. Johnson has argued for a 35 mm minimum physical aperture based on commissioning experience at the Tevatron and HERA.[7] Clearly, the larger the physical aperture the easier the commissioning; the price to be paid for a smaller aperture is a lengthier commissioning period. Quantifying this is somewhat elusive. Another consideration for minimum physical aperture is the impedance of the beam pipe and accessories, which increases sharply with decreasing diameter. W. Chou estimated that for the SCDR with an ID of 33 mm and no liner the transverse impedance safety margin is 4.[3] Scaling his results to 26 mm would reduce the impedance margin to 2, with no allowance yet for the impedance of pumping holes or slots in the liner. We will return to this in the discussion of the eighth requirement dealing with liner impedance.

The second requirement lists the maximum radial allotment for liner components as 7 mm. This number is the sum of liner wall thickness, cooling tube outer diameter, and radial gap between the cooling tube and magnet bore tube. In the actual design this number is 6.05 mm = 1.25 mm + 3.8 mm + 1.0 mm. The minimum magnet bore tube ID consistent with these numbers is the liner ID plus twice the radial allotment for the liner, or 38–40 mm. This runs into conflict with the 40 mm quad/spool aperture, since it would be desirable from impedance considerations to manufacture dipoles, quads, and spool pieces with a

* Operated by the Universities Research Association, Inc, for the U.S. Department of Energy under Contract No. DE-AC35-89ER40486.

common bore tube ID and, if needed, a common liner ID. An end-cooled liner would reduce the radial space requirement to about 3.5 mm and the minimum bore tube ID to 33 mm. Thermal design calculations indicate an end-cooled liner would work for the 5 m long quads but not for the 15 m dipoles,[8] so the minimum dipole bore tube ID with a 26 mm ID liner still stands at 38–40 mm. Exploiting end cooling in the quads and spools to reduce the bore tube ID requirement would not allow a liner solution with a uniform bore tube. These conflicts have been noted. Enlarging the quad/spool aperture has been under continuing evaluation prior to initiating this design effort. The possibility of preserving the option of installing a liner is one of several issues driving this evaluation.

TABLE 1. 80 K LINER REQUIREMENTS.*

1.	Liner ID	26 mm minimum
2.	Liner radial budget	7 mm maximum
3.	Liner temperature	80 K
4.	Inner wall conductivity and thickness	$\sigma^*t > 2x10^5\ \Omega^{-1}$
5.	Inner wall photodesorption coefficient for Ecrit = 284 eV	$\eta_{max} = 0.02$, $\alpha_{min} = 0.3$ for H_2 η(other gases)$<0.2^*\eta(H_2)$
6.	Liner pumping speed	~600 l/m/s for H_2
7.	Liner symmetry	4 fold *x-y*
8.	Liner impedance	$Z_L/n < 0.34\ \Omega$ $Z_T < 20\ M\Omega/m$
9.	Liner supports heat leak to 4K	< 0.5W/dipole
10.	Total liner heat leak to 4K	< 1W/dipole
11.	Cryosorber pumping speed	1200 to 3000 l/m/s for H_2
12.	Cryosorber pumping capacity	32 Torr l/m at 294K 60% H_2 10% CO_2 10% CO 10% H_2O 5% CH_4 5% He
13.	Cryosorber activation temperature	< 294 K
14.	Cryosorber regeneration temperature	< 80 K H_2 < 294 K all gases
15.	Cryosorber recovery fraction	> 98% per regeneration
16.	Quench survival	100 quenches in 25 yr
17.	Radiation dose tolerance	1400 Mrad in 25 yr
18.	Up to air accident recovery	> 90% recovery per accident

*All requirements apply to baseline collider operation at 20 TeV, 72 mA, and 140 mW/m of synchrotron radiation produced in the dipole bends.

The third requirement is the liner temperature, given as 80 K. At SSCL there are three options: 4.2 K, 20 K, and 80 K. When this study was initiated extrapolation of the existing photodesorption data indicated that 80 K was the only solution that could simultaneously satisfy beam stability impedance constraints and achieve the beam lifetime requirement of 300 h in a reasonable conditioning period. The 300 h beam lifetime requirement for the vacuum system is not listed in Table 1, but is taken as a top-level requirement from the CDR, SCDR, and the Collider 3B specification.

The fourth requirement specifies that the product of inner-wall conductivity and wall thickness of the high-conductivity inner layer of the liner tube exceed $2 \times 10^5\ \Omega^{-1}$. This is based on an analysis by W. Chou. It ensures that at baseline operating conditions the growth rate of the transverse multi-bunch resistive wall instability is of the order 120 turns at 2-TeV injection and is reasonable to stabilize by

feedback. Another wall resistivity issue is parasitic heating at GHz bunch frequencies. As long as the GHz resistivity is not too different from the low frequency (kHz) resistivity given by the $\sigma^*t = 2 \times 10^5 \Omega^{-1}$ requirement, parasitic heating is negligible compared to the synchrotron radiation heat load.

The fifth requirement is based on the photodesorption data of Bintinger *et al.*[1] and requires that photodesorption coefficients not exceed what was observed in that experiment. The sixth requirement gives the liner pumping speed (reciprocal sum of liner conductance and cryosorber pumping speed) for H_2 at 80 K as 600 l/m/s. With the data of Bintinger *et al.* as input, vacuum calculations with 460 l/m/s predict 17 days of conditioning at design current to achieve beam lifetime of 300 h. Running at reduced current would extend the conditioning time.

The inside of the liner was required to be up-down and left-right symmetric to avoid questions of x-y tune shift on the beam. This requirement mainly applies to the shape of the liner and the pattern of holes or slots and does not apply to the external supports, cryosorber, and cooling tubes, although the design chosen does have up-down, left-right symmetry.

The transverse and longitudinal liner impedances in Table 1 are required to be less than W. Chou's estimates of a 33 mm beam tube impedance without a liner.[8] The liner impedances listed in Table 1 are meant to exclude all the beam tube contributions without a liner and include only the contributions of holes (or slots) in the liner. If the ID is kept the same this would ensure impedance safety margins greater than two (safety margin = impedance threshold/2*calculated impedance). The SCDR impedance safety margins without a liner are 4 and 6 for transverse and longitudinal. The question of acceptable impedance safety margin for a liner is under review by M. Sypher's Impedance Committee. No requirement was written down for possible emittance degradation by high-frequency wakefields created by liner holes because it was not known how to do so and how to evaluate it. Since the design was initiated, Chou and Kurennoy have begun looking at this question, and it is possible that a new requirement on the spacing and/or shape of holes will emerge from this work.

The synchrotron radiation heat load at design intensity is 0.140 W/m, 2.1 W per 15 m dipole, 18 kW total for both Collider rings. The overall liner heat leak budget to 4.2 K is given as 1 W/dipole, and the heat leak through supports as 0.5 W per dipole. If these levels are achieved, the liner would reduce the 4.2 K refrigeration load by half the synchrotron heat load at design current, or by about 9 kW. These heat leak goals are the same as in Maschke's memo, "Initial Design Requirements and Goals," in Reference 4.

Requirements 11 through 15 deal with the cryosorber. Cryosorber pumping speed for H_2 should ideally be chosen to be large compared to the liner conductance so the liner conductance and not the cryosorber is the limiting factor. A range of values 2 to 5 times the liner conductance was chosen, since it isn't known exactly what can be achieved yet.

The cryosorber pumping capacity requirement was estimated by extrapolating the desorption coefficients of Bintinger *et al.*,[1] calculating the gas desorbed in one operational year (2×10^{23} photons/m) and requiring the cryosorber to hold this much gas. That way only of the order one beam tube warm up per year would be required for vacuum maintenance. Warm-ups of this frequency could most likely be done in a way that does not impact machine availability for HEP, which is the goal of this requirement and indeed of the entire liner.

The cryosorber activation and regeneration temperatures are chosen as room temperature, 294 K, so there is no interference with the 3B Specification for maximum dipole temperature 85±5F. The regeneration temperature for H_2 is specified as a lower temperature—80 K. The cryosorber recovery fraction (pumping speed and capacity) is specified as 98% so there would be less than a factor of two degradation over a 25-yr span, assuming one regeneration per year.

The sixteenth requirement specifies that the liner should survive 100 quenches (without thermal shorts, *etc.*) to be consistent with the number of quenches that could occur over a 25-yr period.

The seventeenth requirement of 1400 MRad radiation dose over 25 yrs is simply the 3B Specification radiation dose requirement for the beam tube.

The final requirement states that the liner system should have >90% recovery from an up to air accident to avoid a large retrofit expense when such an event occurs.

REFERENCES

1. D. Bintinger, P. Limon, H. Jostlein, and D. Trbjovic, "Status of the SSC Photodesorption Experiment," SSC-102, Dec. 1986, and D. Bintinger, P. Limon, and R. Rosenberg, *J. Vac. Sci. Technol.*, **A7**, 59. Jan./Feb. 1989.
2. SSC Central Design Group, "Conceptual Design of the Superconducting Super Collider," SSC-R-2020, Mar. 1986.
3. Site Specific Conceptual Design, SSC-SR-1056, July 1990.
4. Element Specification (Level 3B), Collider Arc Sections, Aug. 1992.
5. H. Edwards, "Study on Beam Tube Vacuum with Consideration of Synchrotron Light, Potential Liner Intercept and Collider Quad/Spool Coil Diameter," SSCL-N-771, August 1991.
6. Parameters Committee Minutes, May 27, 1992.
7. D. Johnson, "Collider/Tevatron Commissioning Aperture," memo dated Oct. 2, 1992.
8. Q.-S. Shu and K. Yu, "Thermal Analysis of the ASSTII Liner," SSCL-SR-1224/5, JULY 1993.

This Page Intentionally Left Blank

SECTION 2

Overview of the Design of the SSCL Prototype 80 K Synchrotron Radiation Liner

Q. S. Shu

SECTION 2

Overview of the Design of the SSCL Prototype 80 K Synchrotron Radiation Liner

Q.S. Shu

Superconducting Super Collider Laboratory*
2550 Beckleymeade Ave.
Dallas, TX 75237-3997 USA

Abstract

This paper presents an overview of the efforts that have led to the development of a viable design for an SSC Prototype 80 K synchrotron radiation liner system prototype. The liner is one method under consideration to minimize the presence of photodesorbed gases in the particle beam liner vacuum, thereby assuring acceptable operational availability of the SSC Collider. Otherwise, the interaction between beam particle and photodesorbed gases may greatly reduce the beam lifetime, and the scattered beam power may lead to quenching of the superconducting magnets. The 80 K liner is also aimed at improving the Collider's cryogenic thermal efficiency, which would allow a potential luminosity upgrade. The 80 K liner design development can be used not only for fabricating and testing of an 80 K liner, but can also serve as a solid foundation for developing lower temperature liners (at 4 K or 20 K). Trade studies and engineering analyses of an 80 K liner are briefly introduced. Also, the concept evaluation and engineering design are discussed. Finally, the eight concept verification and demonstration experiments are briefly summarized.

*Operated by the Universities Research Association, Inc., for the U. S. Department of Energy under Contract No. DE-AC35-89ER40486.

1.0 INTRODUCTION

The SSC Collider is the first proton superconducting accelerator designed to operate at an energy of 20 TeV (each beam) and a beam current of 72 mA. The Collider will produce a synchrotron power of 0.14 W/m and a total of 18 kW into 4.2 K for the two rings. This radiated power may trigger a serious impact of photodesorbed gases on the operational availability of the Collider. The interaction between beam particle and photodesorbed gases may greatly reduce the beam lifetime, and the scattered beam power may lead to quenching of the superconducting magnets. Collider availability may be unacceptable if this concern is not properly addressed.[1] The liner is one method under consideration to minimize the presence of photodesorbed gases in the particle beam line vacuum. Secondly, the liner is aimed at improving the Collider's cryogenic thermal efficiency which would allow a potential luminosity upgrade. The ultimate goal is to require no more than one machine warm-up per year for vacuum maintenance during operation of the SSC Collider.

A liner is a piece of scientific art and technical architecture that presents the challenge of developing a system inside the existing particle beam tubes that directly interfaces with the synchrotron light and compensates for the synchrotron by-products of photodesorbed gases and heat. The system addresses photodesorption, the particle beam, magnet fields, beam-induced wakefields, the RF system, the cryogenic system, magnet quench (especially quench induced Lorentz pressure) and many other interdisciplinary technical problems that must be considered and resolved in a timely manner. One of the challenges to the liner design is that there is no experience from which to draw directly. There is also a schedule challenge in that the liner design must catch up with many years of magnet design efforts.

The liner will be installed into all the dipole magnets, quadrupole magnets, and spool pieces in the entire arc region of the SSC Collider, as shown in Figure 1, if the liner is finally determined to be the best solution to the problem of synchrotron radiation and photodesorbed gases. As a liner R & D program, it was decided by SSCL Project Management that a liner system prototype for a half cell be developed and tested at the Accelerator System String Test (ASST) facilities, since a half cell of the collider string (five dipoles, one quadrupole, and one spool piece with a beam position monitor) is a basic unit of the SSC Collider.[2]

The liner's required operational temperature of 80 K was based on analyses of the photodesorption data available from the CDG and SCDG measurements at the time when the ASST liner design had been performed.[3] In the case of an 80 K liner, there is a second purpose, namely, to replace the 4 K dynamic heat load of the synchrotron radiation with a static heat load, independent of the beam intensity, and to transfer the intercepted heat to the liquid nitrogen system. This has the advantage of upgrading the Collider luminosity over the lower temperature liners with a higher thermal dynamic coefficient.

This development program was established with three major phases: (1) concept proposal and evaluation, (2) concept selection and design, and (3) fabrication and test of the selected design in the ASST facility. The first phase effort was summarized in the "Report on the ASST II Liner Status" in November 1992 (SSCL-N-805).[4] The second phase effort is documented in this report and associated papers. The third phase has been suspended by the SSCL pending the evaluation of other alternatives in light of recent measurements of photodesorption coefficients. This recent data indicate the viability of 4 K and 20 K systems, which were previously considered non-viable using the old CDG and SCDG measurements.

It should be noted that progress on the 80 K system also greatly facilitates evaluation of the 4 K and 20 K systems. It is recognized that the 80 K liner design development can be used not only for fabricating and testing an 80 K liner, but can also serve as a solid foundation for developing the lower temperature liners.

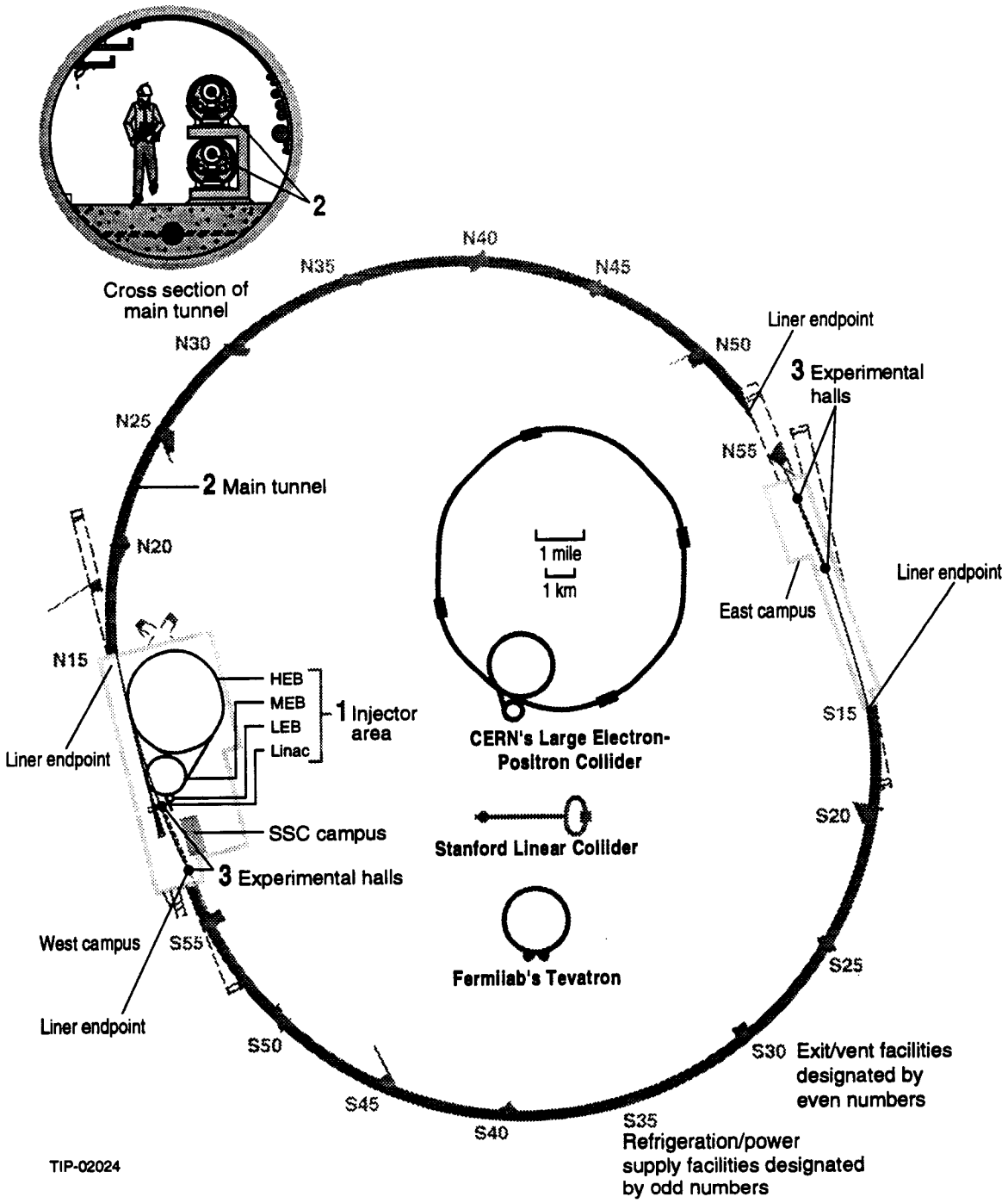

Figure 1. Location of Liner in Collider.

2.0 80 K ASST LINER CONFIGURATION

Figure 2 is a simplified schematic of the 80 K liner system prototype installed in a half cell of the ASST. The liner system consists of an 80 K perforated tube (the liner tube) located coaxially inside the 4.2 K magnet bore tube. An 80 K, high-pressure GHe loop of 0.25 g/s is used to maintain the dipole magnet liner temperature around 80 K; the GHe flow is then recooled by LN_2 in the LN_2 cooling pipe of the dipole magnet. A special end-conducting cooling structure is designed to cool the quadrupole magnet liner, since the ASST quadrupole beam tube ID (32.3 mm) will be installed with the BPM between the spool piece and quadrupole magnet.[5] The liner is much smaller than an ASST dipole ID (42.3 mm).[6] The end-cooling approach allows liners with a maximum uniform ID of 25.3 mm to pass through the magnets' beam tubes with different IDs. A thin layer of the cryosorber (0.5 mm) is pasted on the inner surface of the 4.2 K beam tube to pump the photodesorbed gases through the holes on the liner tube. The size and pattern of the holes on the liner tube are designed to meet both the requirement of pumping speed of photodesorbed gases and the requirement of the RF impedance.

The low thermal conductivity supports are designed to keep the liner tube in the magnet center line. The 80 K liner configuration also requires that the magnet interconnect allow a pathway for the 80 K cooling tubes into the beam vacuum environment and also provide access to the RF joint and the good thermal contact joint for assembly and maintenance. This interconnect is now called the cryogenic box. The thermal expansion and RF joints located in the cryogenic box between magnets are structured to assure the continuity of image current induced by the charged particle beams in the Collider beam tube.[7] These structures also take care of the different thermal contractions among magnets, liners, and spool pieces. However, the liner is discontinuous as routed through the beam position monitor (BPM). An interface design of the 80 K liner with the beam BPM has been conducted, and the interface will be installed with the BPM between the spool piece and the quadrupole magnet.[5] The liner cooling loop in the spool piece is specially arranged to pass the liner cooling pipe through the spool piece vacuum barrier that separates the magnet insulation vacuums between half cells of the magnet string.

In the design, the liner tube shall also meet the following requirements set forth in Table 1.

Figures 3(a) and (b) present an ASST quadrupole (CQM) magnet liner tube with a limiting aperture in the ASST system (25.3 mm ID). End cooling has been adopted for the ASST quadrupole liner, as shown in Figure 3(c). The liner tube is 1 mm thick copper, and the support will be either Vespel pegs or ceramic spheres. The conductive wall requirement is satisfied locally if $T < 110$ K. According to a calculation, a 1.5 mm diameter hole is efficient and requires 2800 holes/m. A radial space of 1.5 mm is required between the liner OD and cryosorber for acceptable backscatter of gas molecules. The quench-induced Lorentz force and resultant stress were found to be very low, so a stainless steel support layer outside the copper tube is not needed. Figure 4(a) is the cross section of a dipole magnet liner tube having the same aperture as the quadrupole liner of 25.3 mm ID. A copper thickness of 0.5 mm is required to meet the conductive wall requirement. To undertake the Lorentz force, which cannot be ignored in a dipole magnet, a 0.75 mm thick stainless steel shell is used to meet strength requirements. A 2 mm hole is adopted for pumping, and 1300 holes/m are required. Figure 4(b) is the ASST dipole liner tube. The cooling tube is sized to allow 0.25 g/s flow with an inlet pressure of 365 psi to provide flow to 48 half cells connected in series.[8] The ΔT across one dipole liner is ~ 2 K at 10^{33} baseline luminosity and ~ 6 K at 10^{34} upgraded. The GHe entering the flow tube is brazed on the liner tube to keep good heat exchange with the liner tube, and the returning GHe flow tube is mechanically attached to the liner tube to maintain a poor thermal contact. Figure 4(c) shows the dipole magnet liner assembly.

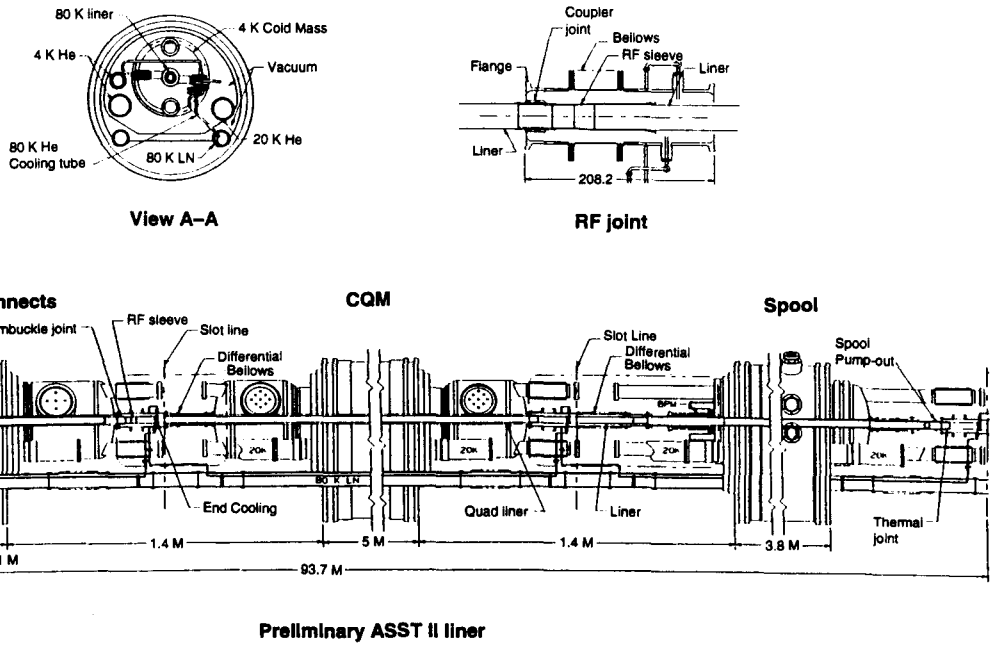

Figure 2. Schematic of an 80 K Synchrotron Radiation Liner System in an ASST Half Cell of the Magnet String.

TABLE 1. LINER TUBE REQUIREMENTS.

Inner wall conductivity and thickness	$\sigma*\delta > 2 * 10^5\ \Omega^{-1}$
Liner impedance	$ZL/n < 0.34\ \Omega$
	$Zt < 20\ M\Omega/m$
Inner wall photodesorption coefficient	$\eta = 0.02$
	$\alpha = 0.3$ for H_2
Liner pump speed	600 l/m/s for H_2
Total liner heat leak to 4 K	< 1 W for dipole
Cryosorber pump speed	1200–3000 l/m/s for H_2
Cryosorber pumping capacity	30 Torr l/m at 294 K
Cryosorber activation temperature	294 K
Cryosorber regeneration	< 80 K H_2, <194 K all gases
Recovery fraction regeneration	> 98%
Liner quench survivability and ASME code	100 quenches in 25 yr
Radiation dose tolerance	1400 MRad in 25 yr

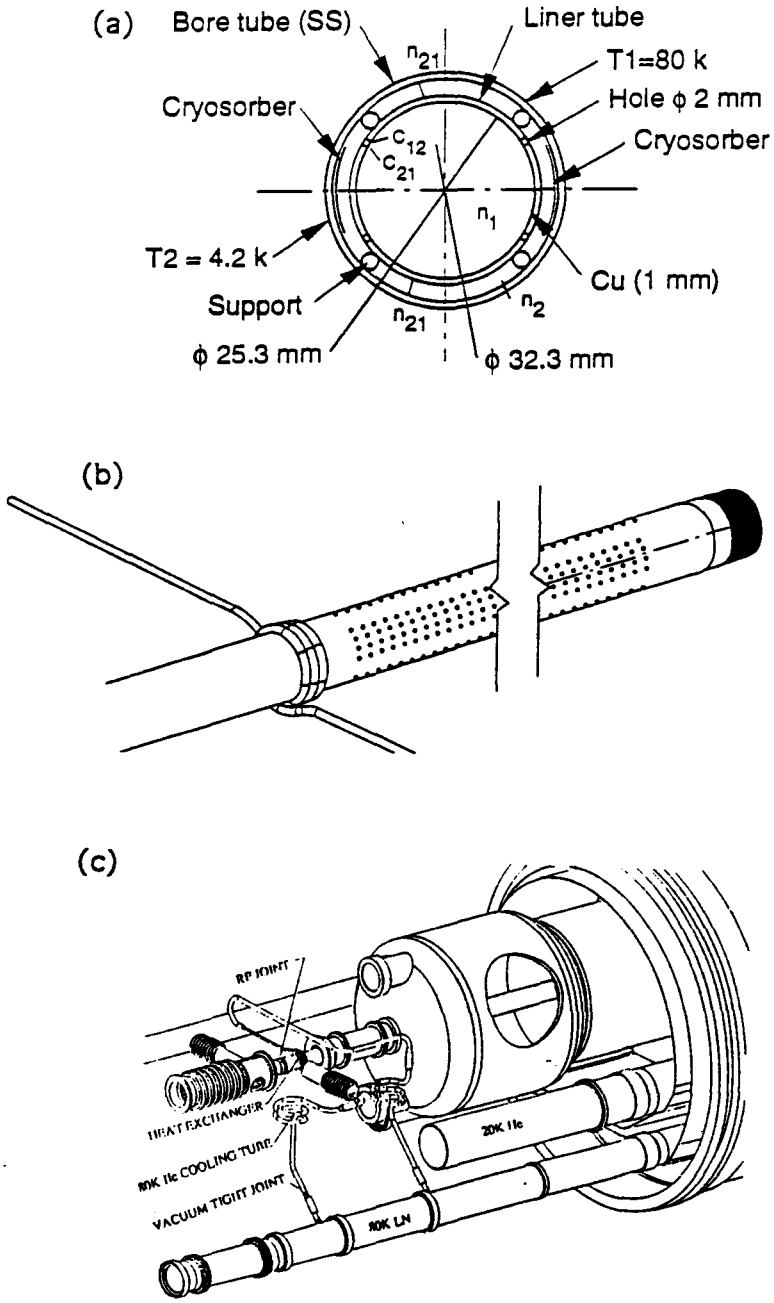

Figure 3. (a) A Cross Section of the 80 K ASST Quadrupole Liner Tube; (b) an 80 K ASST Quadrupole Magnet Liner Tube; (c) End Assembly of a Quadrupole Liner.

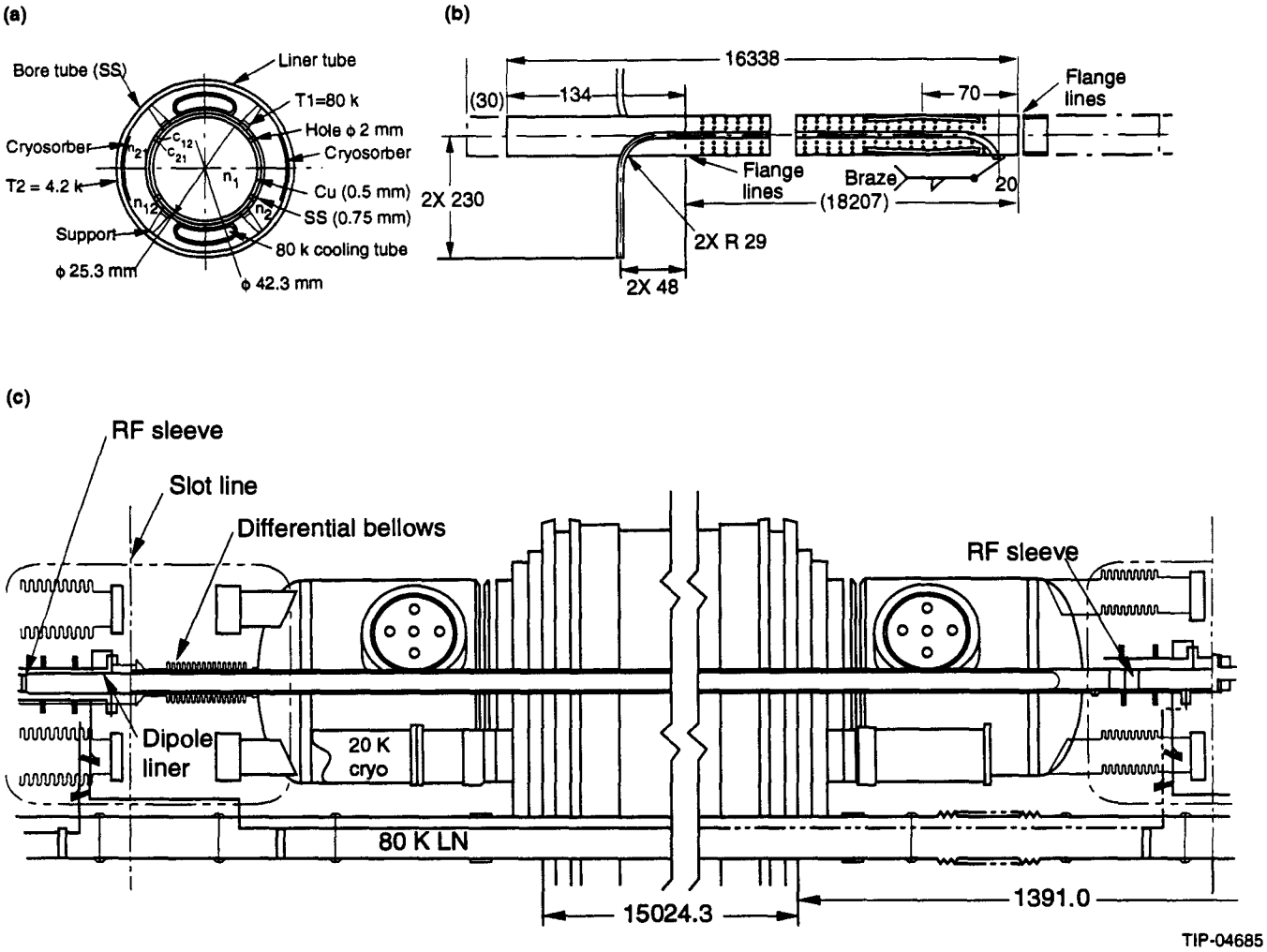

Figure 4. (a) A Cross Section of the 80 K ASST Dipole Liner Tube; (b) an 80 K ASST Dipole Magnet Liner Tube and its Support; (c) the Dipole Magnet Liner Assembly.

3.0 DESIGN ANALYSES AND CONCEPTS SELECTION

In order to minimize the cost and schedule impact and to remove or reduce the risks that a liner design can impact the Collider operation, trade studies, physics and engineering analyses, and concepts selection have been carried out.

4.0 80 K LINER VACUUM SUMMARY

Model equations have been developed to predict the vacuum performance of the SSCL Collider by using certain given assumptions and input data from photodesorption experiments by W. Turner.[9] Using data from the Central Design Group (CDG) experiments, the model predicted an initial beam tube warm-up interval of only one day for a 4.2 K beam tube without a liner. Furthermore, the increase in warm-up interval with increasing photon flux was predicted to be slow if the trend of decreasing photodesorption with photon flux was extrapolated from these experiments. If any part of the machine is let up to atmosphere for maintenance, the conditioning cycle will start over again. This is an unacceptable burden on operation and machine availability. An 80 K liner can be specified, which allows a beam instability safety

margin of two and, according to the vacuum model, eliminates the beam tube warm-up problem and meets the beam lifetime goal of 300 h after a reasonably short conditioning period, ~2×10^{22} photons/m, or two to three weeks at design intensity of 0.072 A and 20 TeV. Liners at lower temperatures, 20 K or 4.2 K, had either unacceptable impedance margins or excessively long conditioning periods, according to analyses of the CDG and SCFG data.[3]

In January 1993, the 80 K liner design effort had reached the point where the design was almost completed, and the component construction of this prototype was to begin. At the same time, new photodesorption data became available at 294 K and 4.2 K (from BINP).[10] The 294 K data has been taken for photon flux corresponding to one year of Collider operation with 2×10^{23} photons/m. The magnitude of photodesorption coefficients initially agree with the CDG experiments, but decrease more rapidly with increasing photon flux than does extrapolation of the CDG data. The beam tube warm-up interval without a liner would still be a large burden on machine availability. However, for the 80 K liner the vacuum model predicts only 1–3 $\times 10^{21}$ photons/m are needed to achieve a beam lifetime of 300 h. This opens up the possibilities of decreasing the number of holes in the liner (increasing the impedance margin) and decreasing the liner temperature to 20 K or 4.2 K. These conclusions do not depend on extrapolation of the data but do depend on the assumption that the desorption coefficients are independent of temperature so the 294 K data can be used. This was a conclusion reached in the CDG experiments that now seems to be at variance with new data at 4.2 K and 80 K. The new data indicate the desorption coefficients decrease significantly with temperature, making an even stronger case for reducing the liner impedance and considering the 20 K and 4.2 K liner possibilities.[10] The full implications of these possibilities will be the subject of future investigations.

4.1 Impedance of a Perforated Liner

The introduction of a perforated liner inside the magnet beam tube of the Collider leads to an increase of the RF coupling impedance. The increase comes from the holes as well as from the smaller diameter.

The impedance of the holes and slots has been studied by means of simulations (3D codes HFSS and MAFIA by W. Chou and L. Walling),[11] analytical modeling (Gluckstern and Kurennoy),[12] and wire measurements (L. Walling).[13] The results obtained from these approaches for different hole geometries are in general agreement. There is a premium to be gained by using slots. The wall thickness correction calculated by Gluckstern is corroborated by the measurements and simulations. In the coaxial region between the liner and the beam tube, the RF fields leaking through the holes are so weak in the frequency region of interest that both the impedance contribution and heating are negligibly small. Figure 5 shows the impedance of the holes for three different liner IDs and the comparison with the present Collider impedance budget. In the baseline design, the beam tube ID is 32.3 mm. If a smaller ID of the liner is used, the transverse impedance of other components (*e.g.*, the bellows, BPMs, *etc.*) will also be increased. The increase of the impedance implies the decrease of the safety margin (which is defined as the ratio of the instability threshold impedance to the Collider machine impedance). Table 2 shows impedance comparisons of the baseline beam tube design with liner tubes of different IDs and hole shapes.

W. Chou pointed out that the use of slots on the liner instead of holes reduces the impedance of the liner tube, but not enough to lower the total impedance significantly, since this is dominated by the liner ID. The possible approaches to increasing the safety margin include: (1) increasing the threshold impedance (*e.g.*, a larger longitudinal emittance, a higher RF voltage at injection of the Collider, *etc.*) or (2) reducing the machine impedance (*e.g.*, a larger liner diameter, an optimization in size and shape of the hole geometry, *etc.*) The high-frequency impedance (above cutoff) of the liner can be reduced by using short slots of random distribution. Figure 5 summarizes the liner impedance as functions of the liner ID and the hole diameters.

The impedance of the resistive wall is proportional to the liner ID^{-3}. A large wall impedance will result in coupled bunch instability. The growth time in the baseline design of a 32.3 mm beam tube ID is about

110 turns. When a liner ID of 25.3 mm is chosen, the growth time will be reduced to 44 turns. If the beam tube ID of the magnets is chosen to be around 40 mm, the liner ID and the consequent growth time will be in an acceptable region.

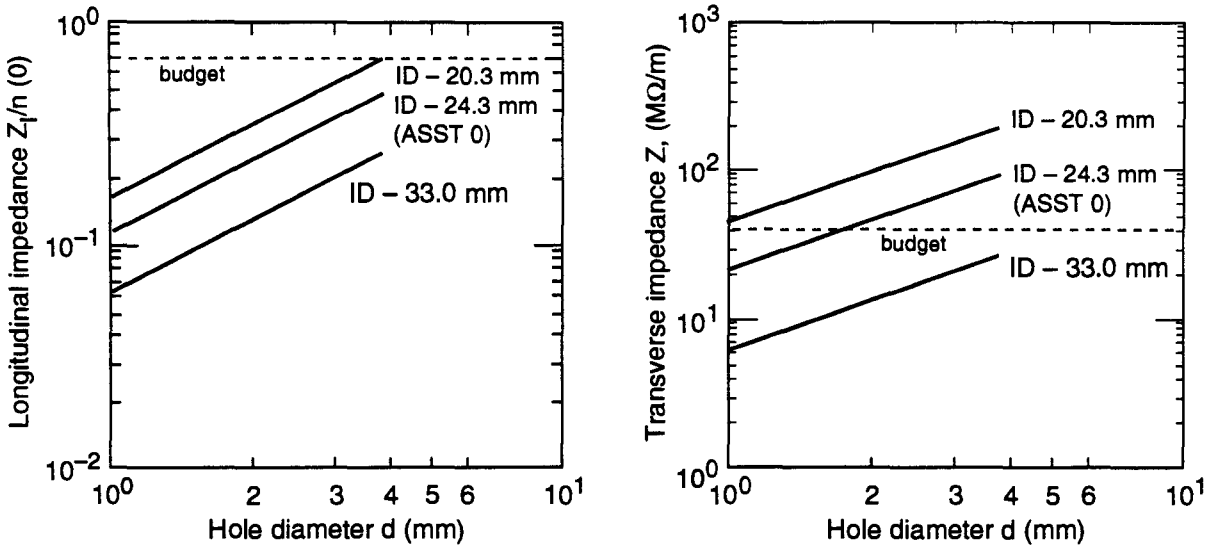

Figure 5. Comparison of Impedance of the Liners as Functions of the Liners' Diameters and Hole Sizes.

TABLE 2. COMPARISON OF IMPEDANCES AND SAFETY MARGIN.

CASE	ID (mm)	HOLE/SLOTS COVERAGE	Z (LINER) (MΩ/m)	Z (OTHER) (MΩ/m)	Z (TOTAL) (MΩ/m)	SAFETY MARGIN
Baseline	32.3			40	40	6.7
With liner	25.3	2 mm, 2%	22	112	133	2
With liner	25.3	2 mm, 4%	44	112	156	1.7
With liner	25.3	2 × 6, 2%	8	112	120	2.2
With liner	33	2 mm, 4%	15	40	55	4.9

4.2 Maximum Liner Inner Diameter (ID)

It is desirable to have a maximum uniform liner inner diameter (ID) due to the requirements of particle beam commissioning, and particle beam dynamic stability, as well as the requirement of the safety margin of the longitudinal and transverse impedance. However, the maximum liner ID is constrained by the following factors:

1. The available magnet beam tube inner diameter (ID) in which a liner tube is accommodated.
2. The minimum liner radial space required by the liner supports, liner cooling tubes, liner cryosorber/getter, and the thickness of the liner tube itself.

If a regular parallel tube cooling approach is used, the minimum radial space required by a liner is 12.1 mm: cooling tube 3.8 mm, liner wall 1.25 mm, vacuum gap between cooling tube and magnet beam tube 1 mm. If end-conducting cooling is utilized (Q-S. Shu, K. Yu),[14] the minimum radial space then is 7 mm: liner wall thickness 1 mm, vacuum gap between liner wall and cryosorber 1.5 mm, and cryosorber 1 mm.

However, the SSC superconducting magnet beam tube ID is either varied with different magnet categories or with a fabrication time of the same magnet category (*e.g.*, ASST CDM and GD CDM). Table 3 presents the different liner IDs in accordance with various magnets. It is clearly indicated that the liner ID is constrained by the smallest limitation if the uniform liner ID is required due to the beam dynamic requirement. **In the case of an 80 K ASST liner, the maximum liner ID should be 25.3 mm.**[4] Figure 6 shows the three options of liner ID in accordance with the three groups of different magnets.

TABLE 3. POSSIBLE MAXIMUM 80 K LINER ID IN VARIOUS CASES.

	DIPOLE MAGNET		QUAD. MAGNET		SPOOL PIECE	
OBJECT	BEAM TUBE ID (mm)	LINER ID (mm)	BEAM TUBE ID (mm)	LINER ID (mm)	BEAM TUBE ID (mm)	LINER ID (mm)
ASST	42.3	25.3	32.3	25.3	32.3	25.3
GD, and B & W	32.3	20.2	32.3	20.2	32.3	20.3
Desired future option	42.3	31	42.3	31	42.3	31

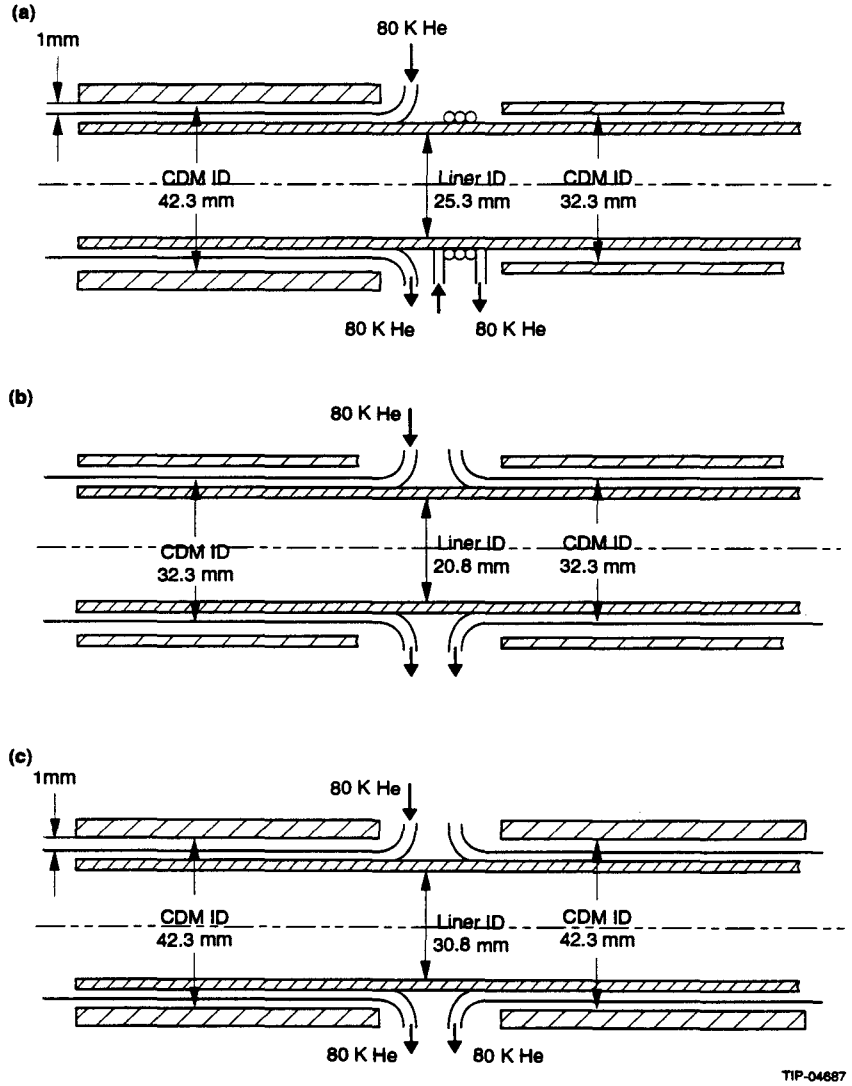

Figure 6. Three Options for the 80 K Liner IDs for Three Different Magnets' IDs. (a) Liner for ASST II test. (b) Liner for existent collider design. (c) Liner for desirable collider design.

4.3 End-Conducting Cooling For a Maximum Uniform Liner Diameter

As shown in Figure 7, a CQM liner is refrigerated through thermal conducting by 80 K GHe in a compact heat exchanger at the end of the liner tube outside the CQD cold mass. With this approach the required space between liner and beam tube can be reduced to 7 mm (3.5 mm for each side) from 11.5 mm. A thermal model was developed by Quan-Sheng Shu and Kun Yu to determine the optimum design parameters.[14] The different surface emissivities (0.05–0.3) and the copper thickness (0.5–2 mm) of the liners as well as the different beam tube emissivities were used in the analyses.

The maximum ΔT could be less than 5 K for the spool piece liner and less than 10 K for the CQM. A temperature difference between the pipe ends and the middle of 2 K with a copper layer of 2 mm and of 10 K with a copper layer of 0.5 mm was found for the spool. A ΔT of 6 K with a copper layer of 2 mm and of 26 K with a copper layer of 0.5 mm for the CQM were obtained. The correction of the effect of the magnetic field on copper thermal conductivity is considered in the calculation. Figure 8(a) presents several selected temperature distributions along a CQM liner and a SP liner. In order to utilize the end-cooling approach a good thermal contact joint must be located between both ends of the liner to assure an easy assembly.

During trade studies, both a 4 K BPM and an 80 K BPM option were considered. If a 4 K BPM is employed, the liner end-conductive cooling becomes more complicated. To reduce the heat leak through the copper liner tube from 80 K to the 4 K BPM, a piece of stainless steel tube of 10–30 mm is inserted between the BPM and the copper liner tube. The synchrotron radiation, the heat leak from liner to BPM, the heat leak from liner to 4 K beam tube, and the heat exchange between the liner and the 80 K GHe must meet the law of conservation of energy. Figure 8(b) shows a representative temperature distribution along the liner tube combination. The heat leak to 4 K from 80 K will be less than 150 mW. If an 80 K BPM is chosen, the interface between the liner and the BPM is simplified. The analysis on the 80 K BPM interface is presented in SSCL-SR-1224/15 (Chapter 3 Section 2) of this document.

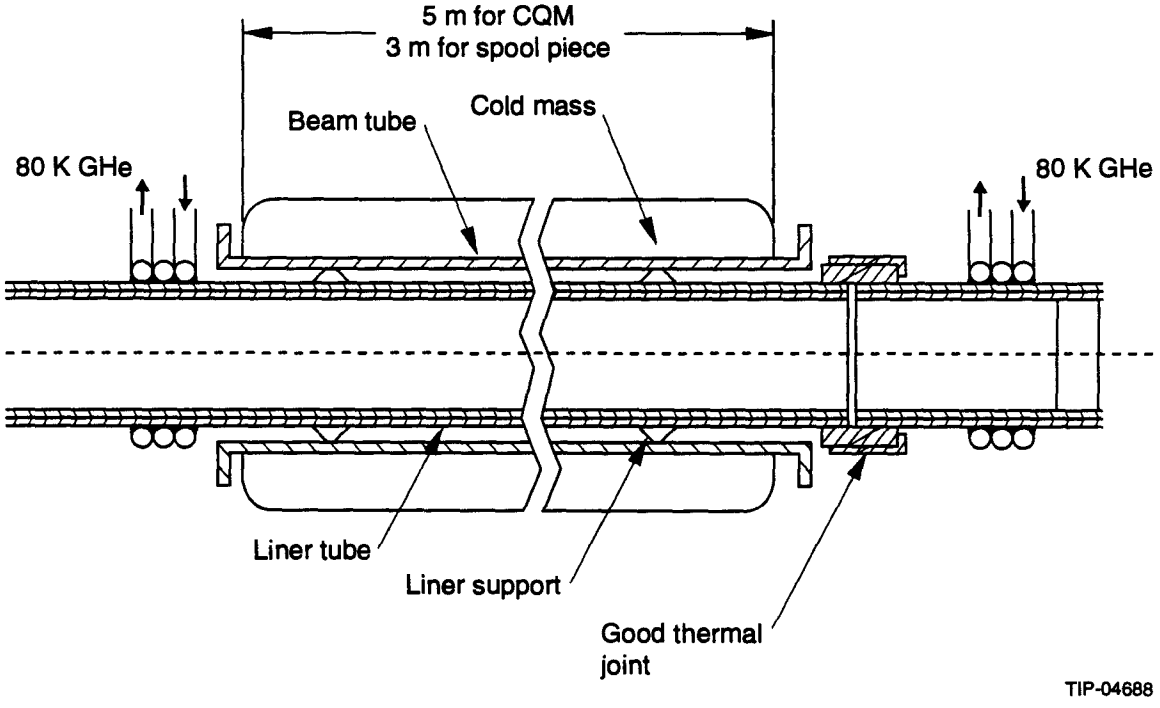

Figure 7. A Schematic of the End Conducting Cooling for a Quadrupole Magnet.

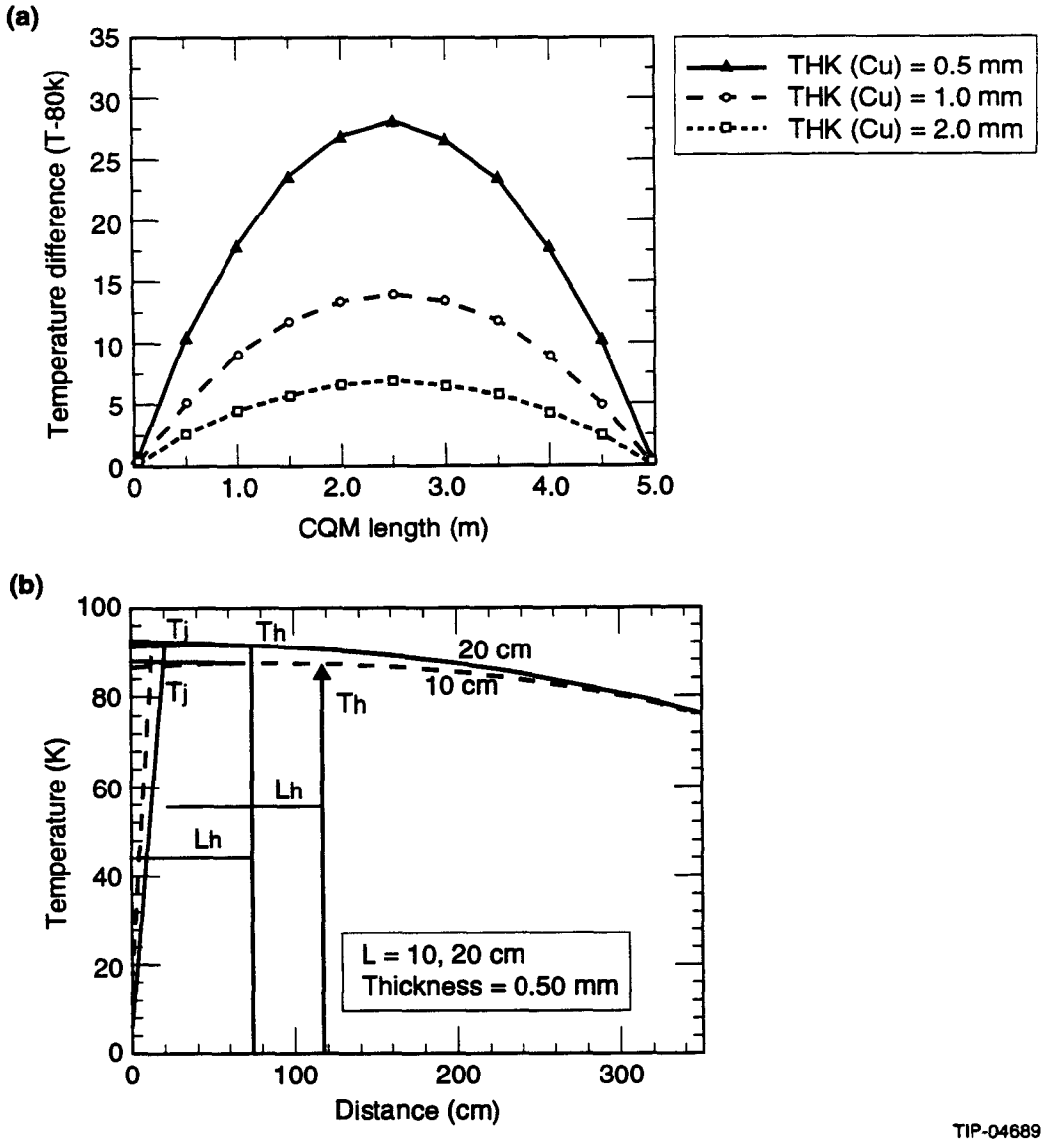

Figure 8. Temperature Profiles Along the Liner Tube with End-Conducting Cooling. (a) T along the CQM liner. (b) T along the spool piece liner with a 4 K BPM.

4.4 Retrofit Liner Structure Development

A trade study has been performed to develop a self-contained 80 K liner structure, a so-called Retrofit Structure.[15] Originally, the liner was designed to be inserted into the magnets after the magnet cryogenic test and prior to the installation in the tunnel. If an 80 K liner is chosen for the Collider upgrade, the retrofit structured liner will allow us to insert the liner into the magnets in the Collider tunnel in a relatively easy way.

A number of assembly procedures were considered for a liner in which the flow tube passes straight through each magnet and spool piece. None of them were acceptable. Consequently, a return flow pattern has been chosen. As shown in Figure 9, return flow refers to the fact that the liner cooling tube penetrates the magnet beam tube of a given component at the lead end, travels the length of that component, makes a 180° bend (still in the beam tube), and returns to the lead end where it exits the beam tube. The cooling-tube enter leg is thermally anchored to the liner by brazing, but the return leg is connected to the liner by

mechanical point contacts. Flow passes to each successive component through a cooling leg that is clipped to the outside of the 80 K shield line. Heat exchange between the 80 K line and the cooling leg is accomplished by wrapping the cooling leg around the shield line, creating a small heat exchanger (approximately 5 coils) in the interconnect. This design can minimize the cost and schedule impact on the magnet manufacturing process.

J. Maddocks calculated the half cell outlet pressure as a function of position in a string, as in Figure 10. There are 48 half cells in a string. Note that the required inlet pressure is much higher when interconnect effects are taken into account. The pressure drop calculations for a fixed mass flow rate of 0.25 g/s with and without interconnect effects are included.[16]

Estimates show that an inlet pressure as high as 1.9 MPa is required to pass the GHe of the liner cooling through 50 half cells. The maximum pressure available from a sector refrigeration station is 1.7 MPa. For this reason, the liner system will require an independent compressor. In addition, as a future upgrade it will require an independent transfer line, heat exchanger, and magnet string interface.

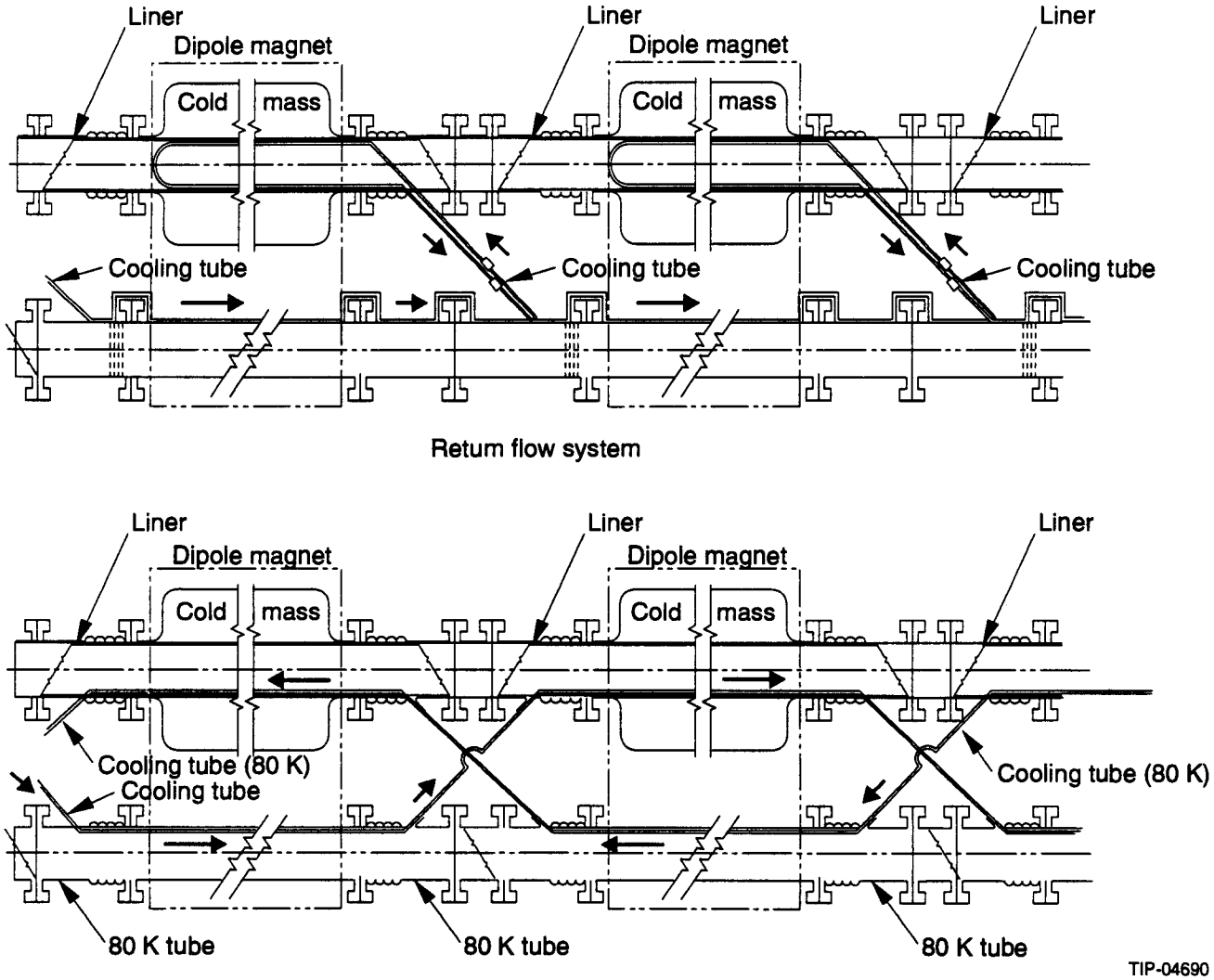

Figure 9. Comparison of the Flow Return Cooling Loop (a) and Flow Through Cooling Loop (b).

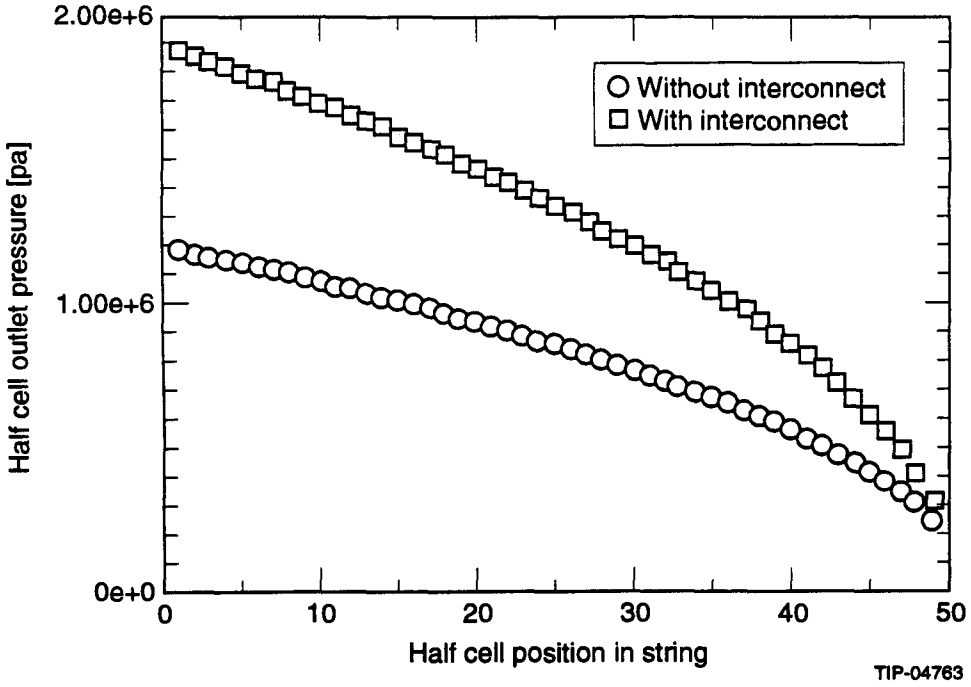

Figure 10. Half Cell Outlet Pressure as a Function of Position in an SSC String.

4.5 Liner Heat Load Budget and Impact on Existing System

In order to be of any positive cryogenic value, the liner must represent a smaller heat load to the 4 K refrigeration system than the synchrotron radiation does. The static heat load budget of the liner has thus been set at 1 W per dipole. Contributing heat loads arise from conduction through mechanical supports, blackbody radiation, end conduction through interconnect pieces, and conduction through the BPM. Details of the static 4 K heat budget are shown in Table 4 (J. Maddocks).[16]

TABLE 4. LINER HEAT LOAD BUDGET.

	DIPOLE (W)	QUADRUPOLE (W)	SPOOL (W)	HALF CELL (W)
Support	0.5	0.5	0.3	3.30
IR Radiation	0.2	0.06	0.04	1.1
Interconnects	0.05	0.05	0.05	0.35
BPM	–	–	0.26	0.26
Total	0.75	0.61	0.65	5.01

Radiation is difficult to reduce to the budgeted levels with the cryosorber, which is likely to have an emissivity near 1. However, electropolishing the liner and bore tube surfaces reduces the radiated heat load to 50% over the budgeted amount. Contact resistance is exploited to reduce the heat load in this case. The total liner heat load is currently projected to be 7.6 W per half cell. This is slightly over the budget of the liner design requirements, but well under the nominal synchrotron radiation load of 10.85 W per half cell.

For each cryogenic sector (total of 10 sectors for the entire Collider), comparison of the heat load budgets for 10 times baseline intensity have been conducted by J. Maddocks. The 4 K heat load remains constant, the 20 K system is nominally unaffected, and the 80 K system absorbs the additional synchrotron radiation load. The 80 K load is increased by 8.5 kW, or approximately 13%. Since the system has 4.4 kW of unallocated capacity, the net required increase in cooling capacity is 7%. However, piping in the nitrogen system is just large enough to handle the baseline. It therefore is likely that the addition of an 80 K liner would require additional nitrogen pumps and recoolers to keep the average temperature at 85 K.[16]

4.6 Magnetic Performance of the Liner

Magnetic finite-element models were performed to evaluate the harmonic risk from the beam tube liner (G. Snitchler).[17] The issue addressed is the change in the allowed harmonics based on a change in the susceptibility. Six F.E. cases were analyzed with changes in the susceptibility for the beam tube and liner. The impact in the allowed harmonics are b2 = –0.813, b4 = 0.261, b6 = –0.020, and b8 = –0.029 assuming a susceptibility of 0.005. The cooling tubes constitute most of the impact on the allowed harmonics. If the susceptibility is 0.005, the allowed harmonics are out of the systematic limit. Solutions to this problem may include adding permeable material to reduce the harmonics, selecting materials with a lower susceptibility, or changing the shape of the cooling tubes. No definitive solutions are available at the time of publication.

The F.E. model also addresses a 0.5 mm vertical offset in the liner from the central axis of the magnet. Two of the 180° model cases, a susceptibility of 0.000 and 0.005 for both liner tube and cooling tubes, could be used to compute the net skew quadrupole contribution. Unfortunately, the error in the calculation is on the same order of magnitude as the permeability affect. Therefore, the more accurate estimate is made from a simple feed down from the b2 term, which yields a skew quadrupole 0.04 units for an offset of 0.5 mm. If a 0.5 mm offset represents a systematic error in the liner, the systemic skew quadrupole term represents a significant adverse impact on the harmonics allocation. If the 0.5 mm represents a manufacturing rms error, this displacement represents a small impact on the rms harmonic allocation.

A simple eddy current model has also been performed for the copper liner. The eddy current dipole field is the only allowed term and is in the range of 0.2 G at 4A/s. All other harmonics would be the result of manufacturing errors in the copper-coated liner and should be small perturbations to the eddy current dipole field.

4.7 Lorentz Pressure, Stress, and ASME Code

The bimetallic and perforated liner tube is subjected to cooldown contraction and eddy current loads, now called Lorentz pressure, during magnet quench. Studies on the quench induced pressure, eddy current distribution, thermal dynamic loading, stress analyses, and ASME code issues have been performed (K. Leung, G. Goren, Q. S. Shu, K. Yu, *etc.*). The life of the liner tube is determined not only by the structural integrity of the steel tube, but also by preserving the high surface finish of the copper layer and keeping the copper within the yielding stress limit. The liner tube analysis is a three-dimensional stress problem with thermal and dynamic structural loads on non-linear material properties. Erroneous copper layer stress is found by using linear stress analysis. From the experimental data for quench performance of the SSC 50 mm CDM magnet, we have

$$B(t)\bullet[dB(t)/dt]_{max} = 147.26\ T2/sec$$

$$F_{max} = \sigma(B,T) \bullet \{B(t)\bullet[dB(t)/dt]\}|_{max} \bullet \iint r^2 \bullet dr \bullet d\phi = 1788\ N$$

$$P_{max} = 57\ Psi$$

According to K. Leung,[18] the calculations can be summarized as follows: The copper average yield is 44 MPa (6.4 ksi). The combined stress for the liner tube at the area away from the hole is 63.6 MPa (9.23 ksi), which is above the copper yield strength at 80 K. The stress at the area around the hole, however, will increase to 127 MPa (18.5 ksi), which is within the ultimate strength. The alternate solution is to increase the steel tube wall thickness to keep the copper stress within the yield strength limit. The steel

wall stress of the liner tube is 289 MPa (41.9 ksi). The stress at the hole area in the steel wall will increase to 578 MPa (83.8 ksi), which is smaller than the 1034 MPa (150 ksi) of the Nitronic-40 steel's yield stress at 80 K. Analysis on the CQM has also been performed. The Lorentz pressure is much smaller than that in the CQM. Figure 11 shows the Lorentz pressure distribution and the deformation distribution.

Non-axisymmetrical eddy current loading is a concern and analyses have been conducted. A tongue in the liner was found due to the non-axisymmetry, and a mechanical design to take care of the concerns was carried out.

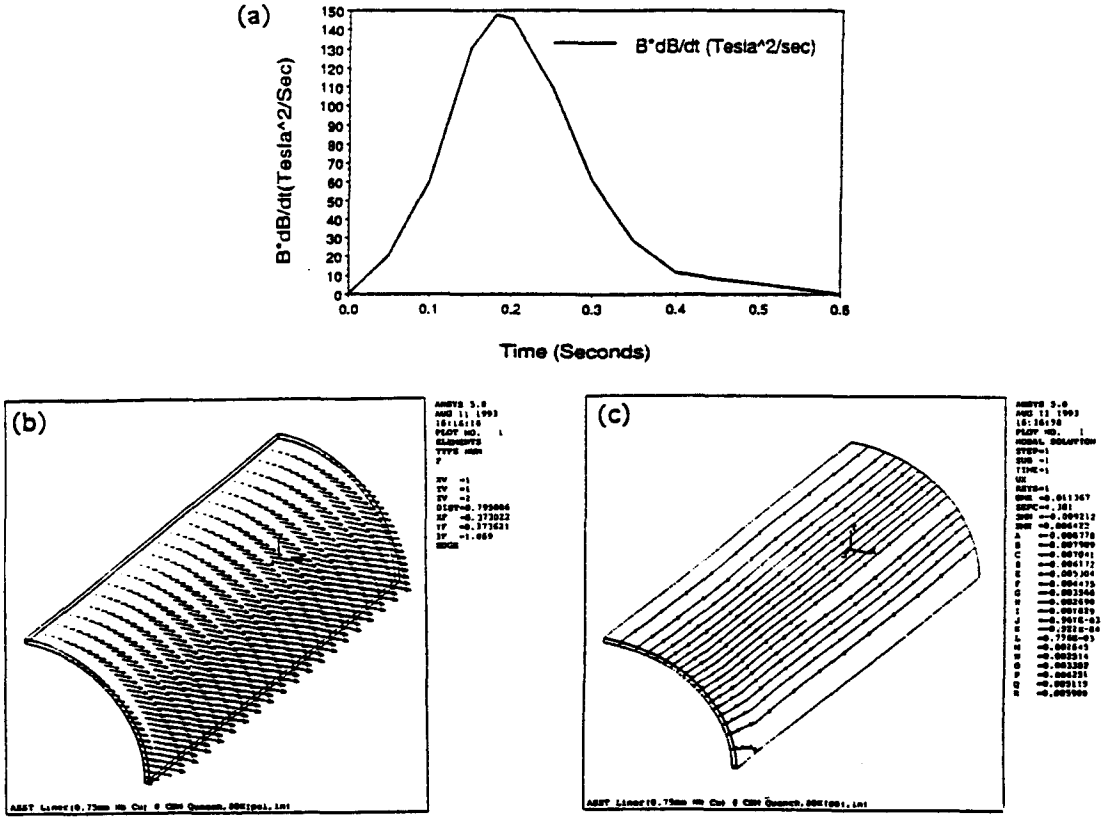

Figure 11. (a) Quench Behaviors of a 50 mm CDM Magnet: B · dB/dt vs. t; (b) Quench Induced Lorentz Pressure Distribution of a CDM Liner; (c) Deformation of a CDM Liner Under a Lorentz Pressure.

4.8 RF Resistivity, RR, and RRR at 80 K Under High B Field

The surface resistance of the liner tube is used to describe energy dissipating within the wall of the liner tube. The power dissipation occurs within a thin layer near the metal surface, because the electromagnetic fields are attenuated exponentially with distance from the surface:

$$d P_{loss}/dA = (R_s H_t^2)/2$$

$$R_s = 1/\sigma\delta = (\omega\mu/2\sigma)^{1/2} \qquad \text{mks unit,}$$

where, R_s is the surface resistance, δ is skin depth, H_t is the tangential magnetic field at the metal surface, σ is DC electrical conductivity, and μ is permeability.

However, when the electron mean free path becomes comparable to the skin depth, the R_S of normal metal becomes independent of temperature, the so-called "anomalous" skin effect. From room T to 4.2 K, copper R_S is reduced only by a factor of about 5, and this reduction is almost completed when cooling to LN_2 temperature. For copper, $R_S = 1.4 \times 10^{-2}\ \Omega$ at 2 K and 3 GHz. The parasitic heating of the liner by the proton beam-induced RF field is an important issue in the design of the Collider. The present heat load budget of the parasitic heating is based on some value of the surface resistance that has not yet been measured for the Collider beam tube under these conditions: low temperature (80 K or 4 K), high frequency, and high magnetic field. The surface resistance also affects the beam tube impedance and, therefore, the particle beam stability.

Copper dc resistance will increase when applying a magnetic field to the liner tube. The increase is also dependent on the temperature and the RRR of the tube materials. To use the real resistance values of the beam tube under the magnetic field becomes essential for calculating the Lorentz pressure and the resistive wall requirement. Q.S. Shu and K. Yu estimated that the magnetoresistance coefficient, $\Delta R/R_0$, may be in a region of 0.1–0.2 at 80 K. Using this estimation, the desired copper thicknesses and RRR for an 80 K liner design are listed in Table 5.

TABLE 5. THE REQUIRED RRR AND COPPER THICKNESS OF THE 80 K LINER WHEN $\sigma \times \delta > 2 \times 10^5\ \Omega^{-1}$.

RRR	$\Delta R/R_0$	$\sigma(0,80) \times 10^8$ $(M\Omega)^{-1}$	$\sigma(6.6,80) \times 10^8$ $(M\Omega)^{-1}$	$\sigma(6.6,80) \times \delta \times 10^5\ \Omega^{-1}$		
				d = 0.50 mm	d = 0.55 mm	d = 0.60 mm
20	0.1	3.45	3.14	1.57	1.73	1.88
50		4	3.64	1.82	2.01	2.18
57		4.6	4.18	2.09	2.3	2.51
100		5	4.55	2.28	2.5	2.73
20	0.2	3.45	2.88	1.44	1.58	1.73
50		4	3.33	1.67	1.83	2
57		4.6	3.83	1.92	2.11	2.3
100		5	4.17	2.08	2.29	2.5

However, magnetoresistance data appears not to be available at 80 K both for RF and dc. A corresponding experimental program to determine the RF and dc magnetoresistance has been performed (W. Chou, Q.S. Shu, V. Kovachev).[19, 20]

4.9 Interconnect Region and Cryogenic Box

The 80 K liner design requires that the magnet interconnect allow a pathway for the 80 K cooling tubes into the beam vacuum environment. The liner has an RF joint, but the beam tube does not. Also, the liner has a good thermal contact joint for assembly and maintenance. This interconnect for the liner is known as the cryogenic box (W. Clay, G. Morales).[21] Inside of this cryogenic box are housed the good thermal contact joint, and the RF joint (there is also a compact heat exchanger in the case of CQM liner). Figure 12 shows a quadrupole cryobox assembly.

A beam tube bellows assembly connects the beam tube flanges at the lead end and return end of adjacent magnets. This bellows assembly was modified to allow the cooling tubes access into the vacuum environment inside of this bellows assembly. The beam tube bellows assembly is at 4 K and the cooling tubes are at 80 K. To minimize the heat transfer from the cooling tubes to the beam tube bellows the cryogenic box requires some thermal standoffs to increase the thermal path.

Since the magnets are cooled from room temperature to a working temperature of 4 K, this produces a thermal contraction (51 mm) in the magnets. The cryogenic box is required to have a feature that will allow for this thermal contraction. The good thermal contact joint is used to connect sections of the quadrupole magnet. Rf flexible refers to a sleeve that is used to connect adjacent liner tubes.

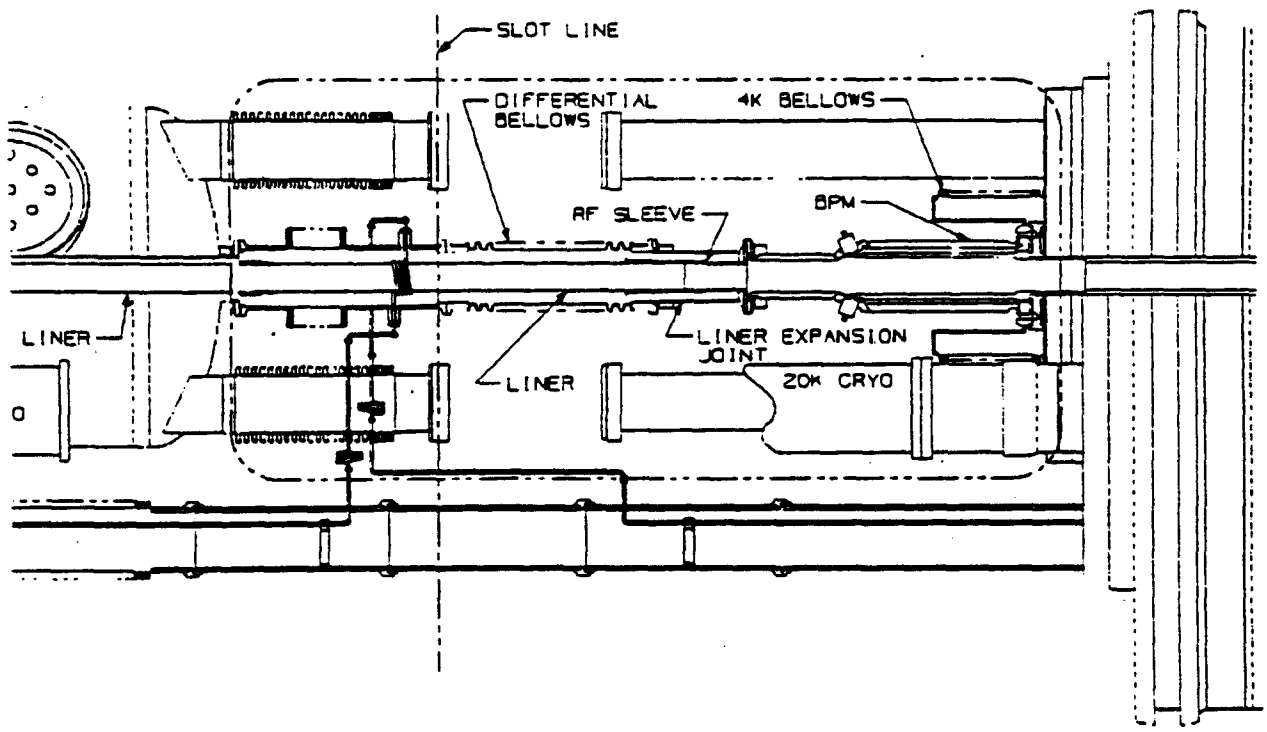

Figure 12. Interconnect Between a CQM Liner and Spool Piece.

4.10 Beam Position Monitor (BPM) and Spool Piece

The conceptual design of the BPM with the interface and the spool piece liner have been conducted by D. Martin, D. Clark, *etc.*[22,23] The problem faced was how to maintain the system performance of the BPM while incorporating changes in cryogenic design. The BPM system electrical centerline to sextupole magnetic axis must be known to be less than 0.1 mm. The BPM detector should have long-term mechanical stability and reliability. Additional heat leaks should be maintained below the 200 mW to 4 K budget. Rf continuity for image currents, good RF transitions, and impedance below 50 μΩ should be maintained.

Figure 13 shows two options for the proposed conceptual designs of the interface structure between the BPM and liner. Option A is a liner with an 80 K BPM. The advantage is that the liner copper tube connects directly to the BPM copper tube, so the RF impedance meets the requirement. But the heat leak through the re-enter tube is large. Option B is a liner with a 4 K BPM. The structure is simplistic, but there is a piece of stainless steel tube between the liner and BPM to reduce the heat leak. Therefore, the RF impedance hardly meets the requirement. Further study to define a final conceptual design structure is in progress.

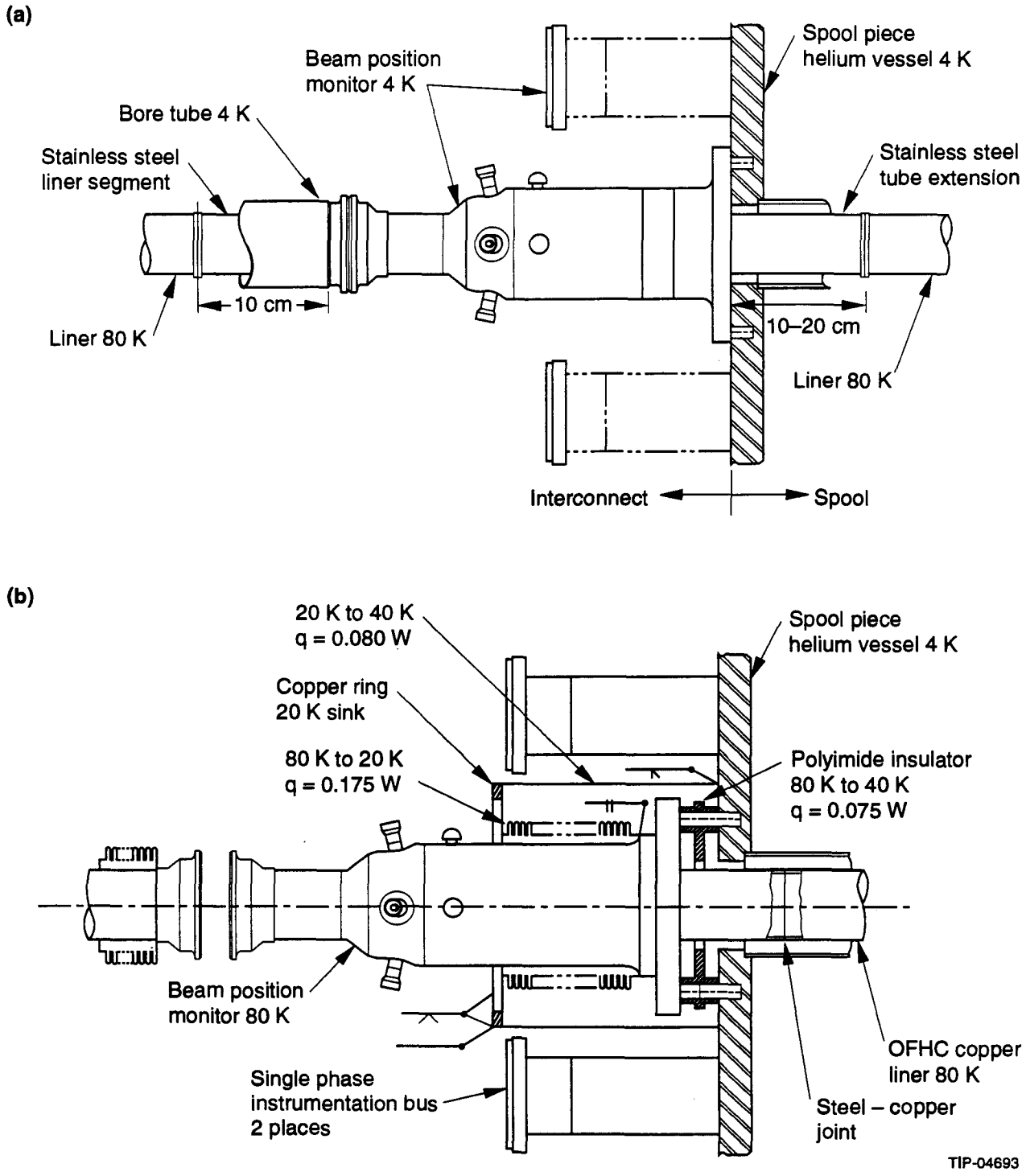

Figure 13. Two Options for the BPM with Interfaces to the Spool Piece and Liner. (a) 4 K BPM; (b) 80 K BPM.

4.11 Cryosorber

The cryosorber material needs to meet all the design requirements. R. Kersevan proposed three options for cryosorber materials to be further evaluated.[24] First, charcoals, carbonaceous particles in a granular form, are bonded/brazed into a matrix and possess a high specific surface. Next, zeolites, a class of synthetic materials used as molecular sieves for vacuum applications, provide very low pressure, a high pumping speed and capacity, and high radiation resistance. Also, they need to be baked out at 200–300°C to remove water. Finally, porous materials provide another alternative. In addition to the cryosorber material, the brazing or bonding material must be able to survive at least 100 quenches over a period of 25 yr. Furthermore, the material must have a radiation dose tolerance of 1400 MRad over 25 yr, good RF impedance behavior, and sufficiently low emissivity to reduce the heat leak to 4 K. In the meantime, charcoals are still the first candidates, and verification tests will be conducted.

5.0 ENGINEERING DESIGN AND DRAWING PACKAGE

The engineering design of the 80 K ASST Liner has been completed. The engineering design consists of four major assemblies and drawing trees. These assemblies are: dipole liner, quadrupole liner, spool liner lead end, and spool liner return end.

The dipole and quadrupole liner assembly consists of all the components required to have an assembly and complete installation through the lead end of the magnet. These assemblies are themselves made up of subassemblies and an interconnect kit. The subassemblies consist of the liner tube and all of the components that are physically attached to it before it is slid inside of the magnet beam tube. The interconnect kit consists of all of the components that are required to attach the cooling tubes and the RF flexible sleeve.

Another assembly consists of all of the components that make up the quadrupole/spool interconnect. The final assembly consists of all the components that make up the spool liner. The details of the engineering design are described in G. Morales's reports.[25]

6.0 THE VERIFICATION AND DEMONSTRATION EXPERIMENTS

Eight engineering experiments have been conducted or are planned to perform the design verification and concept demonstration. The following are brief summaries of their status:

1. The experiment of heat leak through liner supports has been conducted. The results have been produced and supported the design concept.

2. The test on the good thermal conducting joint has been carried out. The preliminary results are in agreement with the design analysis.

3. The equipment for the quench survivability test of a liner tube with supports is under construction. The test is planned to be performed at the SSCL Magnet Evaluation Laboratory.

4. The magnetoresistance of the combined liner tubes at 80 K has been tested at the SSCL Magnet Evaluation Laboratory.

5. The experiments on cryosorber will be developed and tested both through vendors by contract and at the SSCL.

6. The measurement of liner impedance with different perforated hole sizes and distribution patterns has been planned and started.

7. The RF surface resistivity of the liner tube at low temperature will be tested by Los Alamos National Laboratory (LANL) for the SSCL. In addition, the RF surface resistivity of the liner tube at low temperature under high magnetic field will be tested with LANL but at the SSCL Magnet Evaluation Laboratory.

8. The 80 K liner system test at the ASST is a cryogenic test of the entire 80 K liner system and will involve an entire Collider half cell. The liner vacuum performance, crysorber performance, RF impedance, liner thermal performance, cryo-cooling loop, heat leak through supports, quench survivability, and liner alignment will be validated.

7.0 DISCUSSION

Design of an 80 K ASST liner has been successfully accomplished. The trade studies, physics and engineering analyses, conceptual design developments, detailed engineering design, and the results from several experiments are briefly summarized herewith in the design report as well as in the associated technical papers.[4]

It is recognized that this 80 K liner design development can be used not only for fabricating and testing of an 80 K Liner, but can also serve as a solid foundation for developing the lower temperature liner (*i.e.,* 20 K or 4 K liners). All of the logic, the trade studies, the analyses, and the design work will be very useful references when a lower-temperature liner is pursued as a method to resolve the concern associated with the synchrotron radiation and the consequential photodesorbed gases.[26]

This Page Intentionally Left Blank

REFERENCES

1. H. Edwards, "Study on Beam Tube Vacuum with Consideration of Synchrotron Light, Potential Liner Intercept and Collider Quad/Spool Coil Diameter," SSCL-N-771, August 1991.
2. G. Dugan, SSCL internal memo on formation of the Liner R & D task force, (1992); W. Turner, SSCL internal memo on the ASST Liner Design Team, (1992).
3. W. Turner, SSC Vacuum Requirement, Proton Collider Vacuum Technical Meeting, SSCL, Dallas, TX, November 13, 1992;

   D. Bintinger, P. Limon *et al.*, "Status of the SSC Photodesorption Experiment," SSC-102, December 1986; "Site Specific Conceptual Design," SSCL-SR-1056, July 1990.
4. Q.S. Shu, "Report on the ASST II Liner Status," SSCL-N-805, November 1992;

   Q.S. Shu, "Design Report on SSC 80 K Synchrotron Radiation Liner," SSCL-SR-1224, July 1993.
5. D. Martin, Beam Position Monitor, Proton Collider Vacuum Technical Meeting, SSCL, Dallas, TX, November, 1992.
6. Q.S. Shu, Liner System Design Minutes, SSCL, (1992).
7. Q.S. Shu, Liner System Design Minutes, SSCL, (1992).
8. J. Maddocks, Proton Collider Vacuum Technical Meeting, SSCL, Dallas, TX, November 13, 1992.
9. W. Turner, Liner System Design Minutes, SSCL, (1992).
10. W. Turner, Liner System Design Minutes, SSCL, (1993).
11. W. Chou, Proton Collider Vacuum Technical Meeting, SSCL, Dallas, TX, November 13, 1992.
12. S. Kurennoy *et al.*, Liner Impedance Calculation and Beam Stability, Proton Collider Vacuum Technical Meeting, SSCL, Dallas, TX, November 13, 1992.
13. L. Walling *et al.*, Liner Impedance Measurements, Proton Collider Vacuum Technical Meeting, SSCL, Dallas, TX, November 13, 1992.
14. Q.S. Shu, "A Thermal Model for End Cooling Liner and Associated Novel Approaches," presented at *Particle Accelerator Conference*, Washington, D. C., May 1993.
15. Q.S. Shu, J. Maddocks *et al.*, Liner System Design Minutes, SSCL, (1993).
16. J. Maddocks, Thermal Budget Analysis and Impact to Collider Cryogenic System, Internal Technical Review of the 80 K ASST Liner Design, Dallas, TX, April 29–30, 1993.
17. G. Snitchler, Magnetic Performance of the ASST II Liner, Internal Technical Review of the 80K ASST Liner Design, Dallas, TX, April 29–30, 1993.
18. K. Leung *et al.*, "Design Report on SSC 80 K Synchrotron Radiation Liner," SSCL-SR-1224/8, July 1993.
19. Q.S. Shu, K. Yu, *et al.*, The Effects of Magnetoresistance on the Liner Design, Internal Technical Review of the 80 K ASST Liner Design, Dallas, TX, April 29–30, 1993.
20. V. Kovachev *et al.*, Magnetoresistance Test Data, Internal Technical Review of the 80K ASST Liner Design, Dallas, TX, April 29–30, 1993.
21. W. Clay and G. Morales, Interconnect Concept Design and Analysis, Internal Technical Review of the 80 K ASST Liner Design, Dallas, TX, April 29–30, 1993.
22. D. Martin, BPM System Concept Design and Analyses, Internal Technical Review of the 80 K ASST Liner Design, Dallas, TX, April 29–30, 1993.

23. D. Clark, Spool Piece Liner Concept Design and Analyses, Internal Technical Review of the 80 K ASST Liner Design, Dallas, TX, April 29–30, 1993.

24. R. Kersevan, Cryosorber Concept Design and Analyses, Internal Technical Review of the 80 K ASST Liner Design, Dallas, TX, April 29–30, 1993.

25. G. Morales and C. Murray, Liner Components and Assembly Detailed Design, Internal Technical Review of the 80 K ASST Liner Design, Dallas, TX, April 29–30, 1993.

26. Q.S. Shu *et al.*, Liner System Design Minutes, SSCL, June 14, 1993.

CHAPTER 2

DESIGN ANALYSIS AND ENGINEERING DATA

SECTION 1

Model of an 80 K Liner Vacuum System for the 4.2 K Cold Bore of the SSCL 20 TeV Proton Collider

W. C. Turner

SECTION 1

Model of a 80 K Liner Vacuum System for the 4.2 K Cold Bore of the SSCL 20 TeV Proton Collider

W. C. Turner

Superconducting Super Collider Laboratory*
2550 Beckleymeade Ave.
Dallas, TX 75237

1.0 INTRODUCTION

This report describes a model of a 80 K liner configuration for the beam tube vacuum system for the 87 Km SSCL Collider rings. The feature of the Collider which leads to the consideration of a liner is the combination of synchrotron light emitted by the ultra relativistic 20 TeV protons with superconducting magnets. The function of the type of liner described here is twofold; to pump gases photodesorbed by the synchrotron light emitted by ultra relativistic protons and to absorb the synchrotron radiation heat load at a temperature higher than the 4.2 K temperature of the superconducting magnet cryostats. The model described here is to be used for choosing parameters and estimating machine performance. Early considerations of a liner for the SSCL Collider rings are contained in the report by H. Edwards[1] and for the CERN Large Hadron Collider (LHC) in Chapter 7 of the design study for LHC.[2] The first clear statement of the potential problems that may be encountered by a smooth bore 4.2 K beam tube vacuum system without a liner was given by A. Maschke in Appendix 1 of Reference 1.

A schematic diagram of the liner configuration to be analyzed is given in Figure 1. The liner is a tube located coaxially inside the 4.2 K bore tube of the superconducting magnet cryostats. The liner shown in Figure 1 is maintained at 80 K by the flow of high pressure GHe in tubes brazed to the outside wall of the liner. Low thermal conductivity supports hold the liner in position. Holes in the liner allow photodesorbed gases to pass from the inside of the liner to the outside where it is cryosorbed on either the 4.2 K bore tube surface or the cryosorber that has been bonded to the bore tube surface. The inside surface of the liner is chosen to be Cu to avoid excessive parasitic heating by beam image currents and to have resistive wall instability growth time long enough for feedback stabilization. However the Cu by itself is not strong enough to withstand the Lorentz forces in a magnet quench so the liner tube has an outer layer of SS tubing. There are many technical details that need to be dealt with in the design of a practical liner system – heat leaks to the 4.2 K cryostat, differential thermal expansion and contraction, quench survivability, interface with beam position monitors, RF impedance and beam stability and so on. Here we will only deal with the vacuum performance. Some details of the design of a 80 K liner system may be found in the paper of Shu *et al.*[3]

From the vacuum viewpoint the purpose of the liner is to increase the pumping capacity for hydrogen and to reduce the accumulation of weakly bound photodesorbed gases on the surface of the beam tube that is directly exposed to synchrotron radiation. The operational gain is a reduction in the number of beam tube warm ups that are required in order to operate with acceptable beam current and luminosity. Hydrogen is a particular problem because of its relatively high isotherm pressure at 4.2 K, which precludes the

* Operated by the Universities Research Association, Inc, for the U.S. Department of Energy under Contract No. DE-AC35-89ER40486.

accumulation of even one monolayer due to the excessive heat deposited in the magnet cryostats by nuclear scattering on gas molecules. As Maschke has pointed out,[4] this is a local problem, the entire vacuum system availability is characterized by photodesorption from the least conditioned part of the system – *e.g.*, the components most recently vented to atmosphere or installed – and not by an average over the entire circumference of the Collider rings. Once the hydrogen pumping problem has been dealt with, as in the liner configuration with a cryosorbing material, then nuclear and Coulomb scattering of the high energy Collider proton beams are dominated by the photodesorption of heavier gases – primarily CO and CO_2.

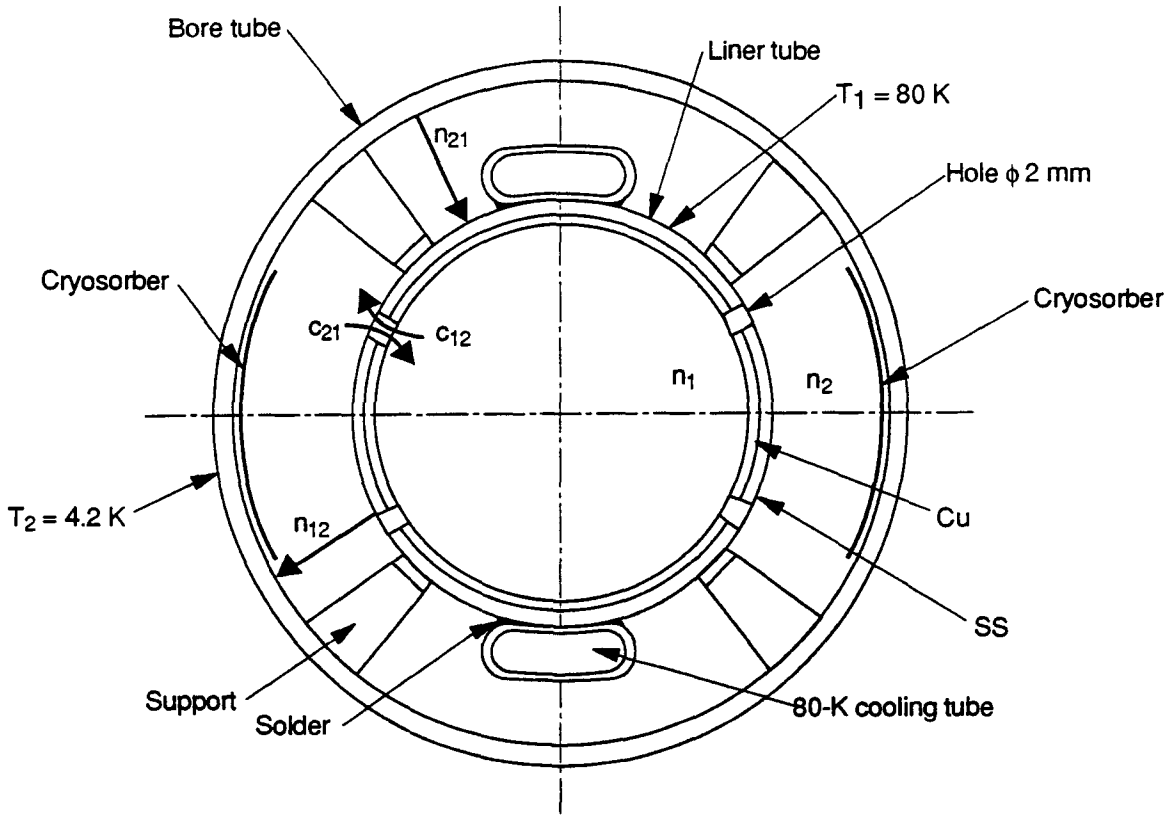

Figure 1. Liner Schematic.

At 20 TeV and design beam current 0.072 A in each ring the synchrotron radiation power is 0.140 W/m or 9 kW per ring. The photon flux is 10^{16} photons/m/s with critical energy 284 eV. This heat load amounts to about one third of the Collider 4.2 K refrigeration capacity (67.5 kW) and has been included in the baseline Collider configuration without a liner. From the heat load viewpoint the particular liner discussed in this paper is primarily of interest for upgraded operation – say at three times baseline beam current where it would be an alternative to increasing the 4.2 K refrigeration capacity.

The luminosity lifetime goal for the vacuum system is 150 hrs at 20 TeV and 0.072 A. Assuming the design luminosity 10^{33} $cm^{-2}s^{-1}$ is actually reached at 0.072 A this would ensure that the decrease in luminosity due to collisions at the interaction points (IP's) would dominate the vacuum effect.[5] From the viewpoint of 150 hrs luminosity lifetime the upper bound on density for each of the molecular species usually observed in photodesorption experiments is 3×10^8 H_2/cm^3, 6.5×10^7 CH_4/cm^3, 5×10^7 CO/cm^3 and 3.3×10^7 CO_2/cm^3.

The molecular densities given in the previous paragraph are global limits that apply to an average over the entire length of the Collider beam tube. Local upper bounds are determined by the limiting power density (~0.6 W/m)[6] that can be deposited in the dipole magnet cryostats by nuclear scattering without overloading the cryogenic system and/or causing a magnet quench. For the various gases the corresponding upper bounds on density are 4×10^{10} H_2/cm^3, 8.7×10^9 CH_4/cm^3, 7×10^9 CO/cm^3 and 4.4×10^9 CO_2/cm^3. H_2 presents a special case because its saturation isotherm density is 2.0×10^{12} H_2/cm^3 at 4.2 K.

The liner issues are somewhat different for the SSCL Collider than for the LHC proposed at CERN.[2] The LHC has 1.8 K magnet cryostats so removing the synchrotron radiation at a temperature higher than the superconducting magnets is the primary concern and a liner has been designed in from the beginning. At 1.8 K the vapor pressure of H_2 is low enough that it can be pumped by cryocondensation on the wall of the magnet bore tube and an additional cryosorber material is not required.

The goal of this report is to derive equations for the density of molecular species inside the liner tube in terms of the magnitude of photodesorption coefficients, the area of holes in the liner and the cryosorber pumping speed. The calculated densities are then used to estimate the nuclear scattering lifetime and the emittance growth time due to Coulomb scattering. The model equations are derived in paragraph 2, the trade off between liner hole pumping speed and impedance is described in paragraph 3, input data for the vacuum calculations are in paragraph 4 and numerical solutions to the vacuum equations are in paragraph 5. Additional experimental data has become available since this study was initiated and much work is in progress. The implications of this new information are contained in paragraph 6. A summary is provided in paragraph 7.

2.0 MODEL EQUATIONS

2.1 Two Region 80 K Liner Configuration

The equations for a two region model of the liner are given in this section. Conditions are assumed to be uniform in the axial direction. Conductances, volumes, surface areas and photon flux are understood to be per unit axial length of the beam tube. The treatment is first given for H_2, which is the most complicated case because of its higher isotherm density, and the simplifications for the heavier molecules are noted. The molecular density inside the liner is n_1 and outside is n_2. The density outside the liner is further divided into two components; molecules n_{12} that have collided with the liner and are moving toward the magnet bore tube and molecules n_{21} that have collided with the bore tube and are moving toward the liner. The molecules are assumed to move with velocity corresponding to the wall temperature of their last collision. The temperature of the liner is T_1 and the magnet bore tube T_2. We assume $T_1 >> T_2$ and that T_1 is high enough that we may neglect cryosorption on the liner surfaces. The conductance of the liner holes from inside to outside is C_{12} and outside to inside C_{21}. The conductances are given by:

$$C_{12} = p\langle v_1\rangle N_h\, A_h/4$$

$$C_{21} = p\langle v_2\rangle N_h\, A_h/2$$

where the molecular speeds are $\langle v_{1,2}\rangle = (8kT_{1,2}/\pi m)^{1/2}$, A_h is the area of a hole, p is the transmission probability through a hole and N_h the number of holes per unit length of beam tube. A factor 1/2 instead of the usual 1/4 appears in C_{21} because it applies the to the directed species n_{21}. The ideal pumping speed of the outside surface of the liner is S_1 and of the inside surface of the bore tube is S_2. These are given by:

$$S_1 = 2\pi a_1\langle v_2\rangle/2$$

$$S_2 = 2\pi a_2\langle v_1\rangle/2$$

where a_1 is the radius of the liner and a_2 the radius of the bore tube. Again the factor 1/2 instead of 1/4 appears because S_1 and S_2 apply to the directed species n_{21} and n_{12} respectively. The vacuum equations for n_1 and n_{12} may then be written as:

$$V_1 dn_1/dt = \eta * d\Gamma/dt - C_{12} * n_1 + C_{21} * n_{21} \quad (1)$$

$$V_2 dn_{12}/dt = C_{12} * n_1 + S_1 * n_{21} - C_{21} * n_{21} - S_2 * n_{12} \quad (2)$$

where V_1 is the volume inside the liner, V_2 the volume between the liner and bore tube, $d\Gamma/dt$ is the photon flux per unit length incident on the inside surface of the liner and η is the number of molecules desorbed per incident photon. In the Eqs. (1) and (2), $C_{12} * n_1$ and $C_{21} * n_{21}$ account for the leakage of molecules through the holes in the liner. In Eq. (2), $S_1 * n_{21}$ and $S_2 * n_{12}$ account for the conversion of n_{21} into n_{12} due to wall collisions. The vacuum equation for n_{21} is more involved since it must account for cryosorption on both the cryosorber and the 4.2 K SS bore tube surface that is not covered by cryosorber.

The number of molecules per unit length adsorbed on the cryosorber is N_c and on the SS bore tube surface N_w. The sticking coefficients on these surfaces are σ_c and σ_w, the ideal pumping speeds are S_{2w} and S_{2c} with $S_{2w} + S_{2c} = S_2$. The sojourn times are τ_w and τ_c. The vacuum equations for n_{21}, N_w and N_c are then given by:

$$V_2 \, dn_{21}/dt = -S_1 * n_{21} + (1-\sigma_w) S_{2w} * n_{12} + (1-\sigma_c) \, S_{2c} * n_{12} \quad (3)$$

$$+ N_w/\tau_w + N_c/\tau_c$$

$$dN_w/dt = \sigma_w S_{2w} * n_{12} - N_w/\tau_w \quad (4)$$

$$dN_c/dt = \sigma_c S_{2c} * n_{12} - N_c/\tau_c. \quad (5)$$

We have neglected cryosorption and condensation of molecules on the 80 K surfaces of the liner.

2.2 Approximate Solutions for the Two Region 80 K Liner Configuration

Solutions are now given for Eqs. (1) to (5). Since we are generally interested in time scales that are very long compared to the transit time of a molecule between wall collisions we simplify Eqs. (1) to (3) with the quasi-static density approximation $dn_1/dt = dn_{12}/dt = dn_{21}/dt = 0$. For the first solution we further assume the SS bore tube surface and the cryosorber are far from equilibrium, $N_w/\tau_w << \sigma_w S_{2w} n_{12}$ and $N_c/\tau_c << \sigma_c S_{2c} n_{12}$. In this approximation both the SS bore tube and cryosorber act as good pumps and the adsorbed flux far exceeds thermal evaporation. This approximation should be good for H_2 early in time at the beginning of photodesorption and always good for the heavier gases. We then have:

$$n_1 = (\eta * d\Gamma/dt)/C_{12} * [1 + (C_{21}/S_1) * (S_2/(S_c + S_w) - 1)] \quad (6)$$

$$\cong (\eta * d\Gamma/dt)/C_{12} * [1 + (pN_h A_h/2\pi a_1) * (1/\sigma_w - 1)]$$

$$n_{12} = (\eta * d\Gamma/dt)/(S_c + S_w) \quad (7)$$

$$n_{21} = [(S_2 - S_c - S_w)/S_1] * n_{12} \quad (8)$$

$$N_w = [S_w/(S_c + S_w)] * \int dt \eta * d\Gamma/dt \quad (9)$$

$$N_c = [S_c/(S_c + S_w)] * \int dt \eta * d\Gamma/dt. \quad (10)$$

For H_2 this solution begins to be invalid when the surface density $s \equiv (N_w + N_c)/2\pi a_1$ of H_2 approaches s_m and the density of H_2 thermally desorbing from the surface approaches n_{21}. The effective pumping of the surface dNc/dt then goes to zero and the SS bore tube surface reaches equilibrium. For the second solution we assume the SS surface is in equilibrium $N_w/\tau_w = \sigma_w S_{2w} n_{12}$ and obtain:

$$n_1 = \eta * d\Gamma/dt/C_{12} + (T_2/T_1)^{1/2} * ((S_2 - S_c)/S_1) * (\eta * d\Gamma/dt)/S_c \quad (11)$$

$$n_{12} = (\eta * d\Gamma/dt)/S_c \quad (12)$$

$$n_{21} = ((S_2 - S_c)/S_1) * (\eta * d\Gamma/dt)/S_c \quad (13)$$

$$N_w/\tau_w = \sigma_w S_{2w} * n_{12} \quad (14)$$

$$N_c = \int dt \eta * d\Gamma/dt. \quad (15)$$

This solution simplifies further with the reasonable assumption that the effective cryosorber pumping speed $S_c = \sigma_c S_{2c}$ is much less than the ideal pumping speed of the entire bore tube wall S_2. Then we have:

$$n_1 = (1/C_{12} + 1/S_c) * \eta * d\Gamma/dt \quad (16)$$

$$n21 = (T1/T2)1/2 * n12 \quad (17)$$

$$= (T1/T2)1/2 * (\eta * d\Gamma/dt)/Sc.$$

Since the SS surface is in equilibrium the surface density $x = s/s_m$ of H_2 is calculated from the BET equation for the normalized density $y = 2n_{21}/n_{sat}$, Reference 7. The BET eq. is described in paragraph 4.1. The transition between the regions of validity of the two solutions given by Eqs. (6) to (10) and (11) to (17) occurs when the surface densities of H_2 calculated in the two approximations cross over. When the cryosorber itself begins to saturate the assumption $N_c/\tau_c << \sigma_c S_{2c} n_{12}$ will no longer be valid and the hydrogen density will rise toward its saturation value, ~ 2×10^{12} H_2/cm^3 at 4.2 K. Operationally when this happens the cryosorber will need to be regenerated due to deterioration of the luminosity lifetime (τ_L = 150 hrs at 3×10^8 H_2/cm^3) or increasing heat load to the magnet cryostats (vacuum instability and quenching of the superconducting magnets set in at about 4×10^{10} H_2/cm^3). The capacity of the cryosorber is to be chosen so the time between beam tube warm ups is acceptably long – say once per operational year.

2.3 Single Region 4.2 K Beam Tube Configuration Without a Liner

In order to compare the beam tube vacuum with a liner to the case without a liner we write down the equations for a single region 4.2 K beam tube. There is then only one equation each for volume density n and surface density s:

$$V dn/dt = \eta d\Gamma/dt + \eta' d\Gamma/dt - \sigma_w S_w^* n + N_w/\tau_w \tag{18}$$

$$dN_w/dt = \sigma_w S_w^* n - N_w/\tau_w - \eta' d\Gamma/dt \, . \tag{19}$$

The ideal wall pumping speed is given by $Sw = \langle v \rangle Aw/4$ where $\langle v \rangle$ is the mean speed of desorbed molecules. Compared to the warm liner case an additional desorption term $\eta' d\Gamma/dt$ has been added to describe the desorption of cryosorbed molecules previously desorbed by the η process. In the case of a warm liner the cryosorbed molecules are hidden from the photons and this term does not appear. The cryosorbed molecules are relatively weakly bound to the surface and may be easily desorbed. For H_2 cryosorbed to a metal surface the sorption energy is in the range of 0.020 eV. At low surface coverage the desorption coefficient is expected to depend linearly on the surface concentration of cryosorbed molecules, $\eta' = \eta_0'(s/s_m)$. An alternative way of writing the thermal desorption term is $N_w/\tau_w = \sigma_w S_w^* n_e$ where n_e is the equilibrium vapor density given by the isotherm for surface density s. We are again interested in the quasi-static solution dn/dt = 0, which is given by:

$$n = (\eta d\Gamma/dt)/\sigma_w S_w + (\eta' d\Gamma/dt)/\sigma_w S_w + n_e, \tag{20}$$

$$s = (1/A_w) \int \eta d\Gamma. \tag{21}$$

There are three contributions to the density due to direct desorption, desorption of cryosorbed molecules and the isotherm. The first term would be expected to decrease with exposure to photon flux as the source of tightly bound molecules cleans up. The second term would increase with photon flux due to the accumulation of cryosorbed molecules. Furthermore the first term is linear in photon flux or proton beam current whereas the second term is quadratic in beam current and could become much more serious as the beam current in the Collider is increased. The additional desorption coefficient η' does not increase the inventory of desorbed molecules but amounts to a recycling of previously desorbed molecules. The isotherm density n_e is only important for H_2. The desorbed molecules steadily build up on the beam tube surface. In the case of H_2 this will necessitate a warm up and pump out of the beam tube at the very least when s approaches a monolayer s_m. In addition the desorption of cryosorbed molecules described by η' could well degrade the luminosity lifetime to the point where the beam tube would have to be warmed up well before reaching one monolayer.

In developing Eqs. (18) to (21) we have implicitly assumed that there is no place on the beam tube wall for the desorbed molecules to hide where they are not exposed to photons, either direct or scattered. When there is such a place the treatment is identical to the 4.2 K liner situation described in paragraph 2.5.

Comparing Eq. (16) with Eq. (20) we see that much less information is needed to specify a vacuum system with a 80 K liner than without. If the cryosorber pumping speed is to be chosen so $S_c >> C_{12}$, calculations are insensitive to the details of the cryosorber. With an 80 K liner present essentially only the desorption coefficient η is needed to calculate the density. Without a liner many more parameters are needed; η, η', s_w, $\langle v \rangle$ and n_e. With the 80 K liner the mean molecular speed may be assumed to be the wall temperature since the molecules are not absorbed on the liner wall and a molecule undergoes a large

number of wall collisions before passing through a hole to the outer region. With a 4.2 K beam tube and no liner the desorbed molecules may have a mean speed corresponding to a temperature higher than 4.2 K. It seems likely that the molecules desorbed by the η process, and relatively tightly bound, will have a mean speed much higher than 4.2 K whereas molecules desorbed by the η' process may have a speed comparable to 4.2 K. This complication has been ignored in Eq. (21).

The desorption of cryosorbed molecules in Eq. (18) has been written as though it is photon induced. It is also possible that energetic molecules of a few eV energy desorbed by the primary η process could desorb loosely bound molecules, say with a coefficient η'' molecules per incident molecule. In this case the desorption term would be written as $\eta''(\eta d\Gamma/dt)$ with $\eta'' = \eta_0''(s/s_m)$ at low surface coverage. The parametization is slightly different than with photon induced desorption but would also lead to a contribution to density increasing with Γ or time.

At 4.2 K it is possible to imagine a photon induced source of surface density in addition to the cryosorption of photodesorbed molecules. In that case Eqs. (18) and (19) are replaced by:

$$Vdn/dt = \eta_1 d\Gamma/dt + \eta' d\Gamma/dt - \sigma_w S_w^* n + N_w/\tau_w \tag{22}$$

$$dN_w/dt = \eta_2 d\Gamma/dt + \sigma_w S_w^* n - N_w/\tau_w - \eta' d\Gamma/dt\ . \tag{23}$$

A physical model of $\eta_2 d\Gamma/dt$ would be photon induced production of hydrogen followed by surface recombination to H_2 which remains cryosorbed to the surface. At temperatures high enough that cryosorption may be neglected these molecules would show up in the equation for Vdn/dt. The quasi static solution is:

$$n = (\eta_1 d\Gamma/dt)/\sigma_w S_w + (\eta' d\Gamma/dt)/\sigma_w S_w + n_e, \tag{24}$$

$$s = (1/A_w) \int (\eta_1 + \eta_2) d\Gamma. \tag{25}$$

2.4 20 K Liner Configuration

The primary purpose of this report is to develop a vacuum model for an 80 K liner. However we want to make some comparative statements for liners at other conveniently chosen temperatures where substantial refrigeration and cryogenic capacity is already being planned. For SSCL these temperatures are 20 K, the temperature of the intermediate thermal shield in the magnet cryostats, or 4.2 K, the temperature of the magnet cryostat cold mass. We will discuss the 20 K configuration in this section and 4.2 K in the following section.

The new feature of the 20 K liner compared to 80 K is that we must allow for cryosorption of CH_4, CO and CO_2 on the surfaces of the liner. H_2 may be treated the same way as at 80 K. For the molecules heavier than H_2 then we have to add an equation for the surface density on the inside of the liner and also allow for the possibility that these cryosorbed molecules may be photodesorbed. The isotherm density of these molecules may be neglected at 20 K. Since for the heavy molecules the pumping speed of the surfaces outside the liner is very high compared to the conductance of holes in the liner it is reasonable to neglect the streaming of molecules back into the liner from the outside region. This significantly simplifies the equations for the heavy molecules and since we are mainly interested in the density inside the liner we may drop the subscripts dealing with the different regions. We then have the following two equations describing the density n and surface density s for each species of heavy molecules inside the liner:

$$V dn/dt = \eta^* d\Gamma/dt + \eta'^* d\Gamma/dt - C^* n - \sigma_w^* S^* n \quad (26)$$

$$dN_w/dt = \sigma_w^* S^* n - \eta'^* d\Gamma/dt \quad (27)$$

where C is the hole conductance and S is the ideal pumping speed of the inside surface of the liner. We will again ignore the possible distinction in molecular velocities between molecules desorbed by the η and η' processes. Assuming a quasi-static approximation for the density $dn/dt \cong 0$ the solution to these equations is:

$$n = (\eta + \eta')d\Gamma/dt/(C + \sigma_w^* S) \quad (28)$$

$$s = (\sigma_w^* S/A_w)^* \int n dt - (1/A_w)^* \int \eta'^* d\Gamma$$

$$= (1/A_w)^* \int \eta^* d\Gamma - (C/A_w)^* \int n dt. \quad (29)$$

In the solution for s, conductance through the holes in the liner competes with the adsorption of molecules on the surface of the liner. A new feature of a cryosorbing wall with a liner compared to one without a liner, or indeed with any place for the molecules to be pumped other than the desorbing wall itself, is that the surface density s may also reach a quasi steady state $ds/dt \cong 0$, where the molecules sticking to the wall are balanced by those leaving due to recycling. This will only occur if the recycling coefficient η' is non zero. In the region where we may approximate η' by $\eta'_0(s/s_m)$ the solution then takes the form:

$$n = (\eta^* d\Gamma/dt)/C \quad (30)$$

$$\eta' = (\sigma_w S/C)^* \eta. \quad (31)$$

If a linear dependence of η' on s is assumed, $\eta' = \eta'_0(s/s_m)$ then the solution for surface density is:

$$s/s_m = (\sigma_w/\eta'_0)^* (S/C)^* \eta. \quad (32)$$

The characteristic time constant for s to reach a quasi steady state is $\tau_s = (A_w^* s_m)/(\eta'_0{}^* d\Gamma/dt)$. Eqs. (30) to (31) predict that as η decreases with increasing photon dose Γ, the density n and surface density s will both decrease with time and eventually all the desorbed gas winds up on the outside of the liner, or at least in a place where it cannot be photodesorbed.

2.5 4.2 K Liner Configuration

If the liner temperature is 4.2 K then we must allow for cryosorption of H_2 and the H_2 isotherm density inside the liner. The situation is similar to the 4.2 K beam tube without a liner discussed in paragraph 2.3 but with a conductance term added. The molecules heavier than H_2 are treated exactly the same as the 20 K liner, with appropriate change of conductances and pumping speed due to temperature. To simplify the equations we again neglect the streaming of molecules back into the liner from outside. Until the 4.2 K metallic surfaces approach a monolayer the error estimated from Eq. (6) is only a few percent. Once these surfaces approach a monolayer the fractional error from Eq. (16) is given by the ratio of hole conductance to cryosorber pumping speed, C_{12}/S_c. One would expect to choose S_c large enough that the hole conductance is the limiting factor for pumping but practical considerations may require C_{12}/S_c as large as a few tens of percent. The equations describing the density and surface density are:

$$V dn/dt = \eta d\Gamma/dt + \eta' d\Gamma/dt - C*n - \sigma_w S_w*n + N_w/\tau_w \tag{33}$$

$$dN_w/dt = \sigma_w S_w*n - N_w/\tau_w - \eta' d\Gamma/dt\ . \tag{34}$$

Again assuming a quasi-static approximation for the density $dn/dt \equiv 0$ the solution to these equations is:

$$n = (\eta + \eta')d\Gamma/dt/(C + \sigma_w*S) + n_e \tag{35}$$

$$s = (\sigma_w*S/A_w)*\int (n - n_e)dt - (1/A_w)*\int \eta'*d\Gamma$$

$$= (1/A_w)*\int \eta*d\Gamma - (C/A_w)*\int n dt. \tag{36}$$

For $t >> \tau_s = (A_w*s_m)/(\eta'_0*d\Gamma/dt)$ the surface density is also in a quasi steady state and the solution is:

$$n = (\eta*d\Gamma/dt)/C \tag{37}$$

$$\eta' = (\sigma_w S/C)*(\eta - C*n_e/d\Gamma/dt). \tag{38}$$

With $\eta' = \eta'_0(s/s_m)$ the solution for surface density is:

$$s/s_m = (\sigma_w/\eta'_0)*(S/C)*(\eta - C*n_e/d\Gamma/dt). \tag{39}$$

Comparing Eqs. (6), (11), (30) and (37) with 80 K, 20 K and 4.2 K liners we see that to good approximation, when the surface density has reached a quasi steady state, the density is always given by $n \approx (\eta*d\Gamma/dt)/C$ and remarkably does not depend on the recycling coefficient η', the isotherm density or the wall sticking coefficient. The solution for a 4.2 K beam tube without a liner given by Eq. (20) depends on all of these parameters as well as η. We are therefore in the situation where it is much easier to specify a satisfactory liner configuration than a beam tube without a liner since much less needs to be known. For the

80 K liner we can be reasonably sure that the mean molecular speed entering into C is just given by the velocity of molecules T = 80 K since there is no sticking and the molecules must make a large number of wall collisions before leaving through a hole. When the molecules stick at 20 K and 4.2 K the mean velocity of molecules exiting the holes may not correspond to the wall temperature. However it is reasonably certain that the wall temperature corresponds to a lower bound velocity and will give a conservative estimate of liner vacuum performance. For the 20 K and 4.2 K cases where there is sticking, it is true that $n = (\eta^* d\Gamma/dt)/C$ does not obtain until the surface has reached steady state and there is some uncertainty in the time for this to occur since the characteristic time constant depends on η'_0. However until the surface has reached a steady state it is effectively pumping so the true density will actually be lower than estimated by $n = (\eta^* d\Gamma/dt)/C$. Once again the liner performance will be underestimated, at least until the surface ceases to pump.

3.0 LINER HOLE GEOMETRY

For a given hole geometry the maximum allowable conductance is limited by beam impedance which must be less than the instability threshold by an agreed upon safety margin. For purposes here we will assume the holes are circular and calculate the impedance from the expression for a hole in a thin wall[8] with the Gluckstern correction for thickness applied.[9] This prescription is in reasonable agreement with experimental measurements[10] and numerical simulations[10,11] of hole impedance. If these assumptions are not the ones ultimately chosen it is a simple matter either to repeat these types of calculations or to match the chosen geometry to the numerical values of the pumping speed that are used here.

The conductance of N_h holes/m of diameter d and thickness t may be written as:

$$C = (\pi/16) f N_h d^2 \langle v \rangle. \tag{40}$$

where $\langle v \rangle$ is the mean molecular speed and $f = f(t/d)$ is the Clausing factor or transmission probability through a hole with finite thickness.[12] The transverse impedance of the holes is:

$$Z_{T,h} = (4/3\pi) g Z_0 R N_h d^3/D^4. \tag{41}$$

where $Z_0 = 377$ Ohms, D is the liner diameter, $2\pi R$ is the liner circumference (70.6 km) and $g = g(t/d)$ is the Gluckstern correction factor for hole thickness. For the transverse impedance of everything but the holes the results given by W. Chou[1] have been fit with:

$$Z_{T,t} = 22(33/D(\text{mm}))^{2.6} \ \text{MOhms/m}. \tag{42}$$

The total transverse impedance is then $Z_T = Z_{T,h} + Z_{T,t}$. For longitudinal impedance, $Z_{L,h}/n = (D^2/8R)^* Z_{T,h}$ and from W. Chou's Table 2, $Z_{L,t}/n = 0.34$ Ohms independent of liner diameter.

The instability threshold impedances given in the Collider SCDR are $Z_T = 170$ MOhms/m and $Z_L/n = 4.1$ Ohms.[12,13] In the SCDR the transverse "safety margin" (the instability threshold divided by twice the calculated impedance) is 4 and the longitudinal margin is 6. Here we need only be concerned with the transverse impedance since it has the smallest margin.

Assuming constant conductance C the dependence of $Z_{T,h}$ on hole diameter is $Z_{T,h} \sim (g/f)^*(d/t)$. The factors f and g and the "normalized impedance" $(g/f)^*(d/t)$ are plotted in Figures 2 and 3. Minimizing $Z_{T,h}$ with C constant leads one to choose the smallest practical hole size. This occurs in the range $d/t \sim 1$-2, below this the number of holes required and fractional surface area covered become very large. The hole thickness has been taken from our current liner designs t = 1.25 mm and the diameter of holes is taken as

d = 2 mm. The Gluckstern correction factor for t/d = 0.625 is essentially equal to its asymptotic thick hole limit g = 0.562. The impedance is reduced by a factor of almost two compared to an infinitesimally thin hole.

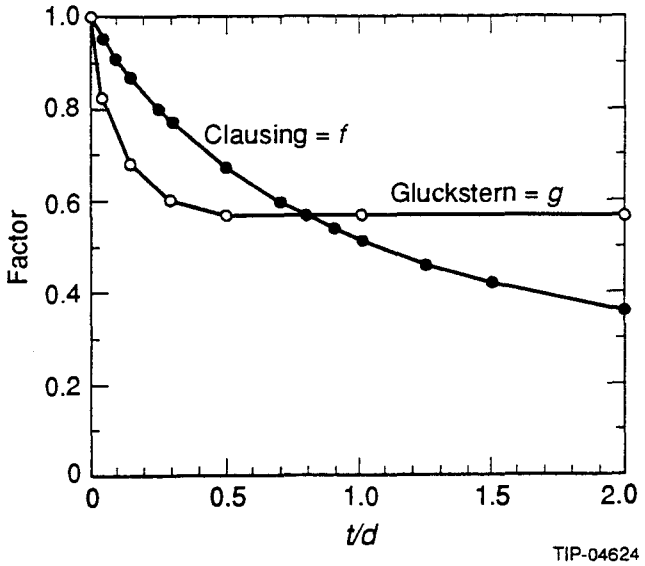

Figure 2. Clausing and Gluckstern Correction Factors Versus the Ratio of Hole Thickness Versus Diameter.

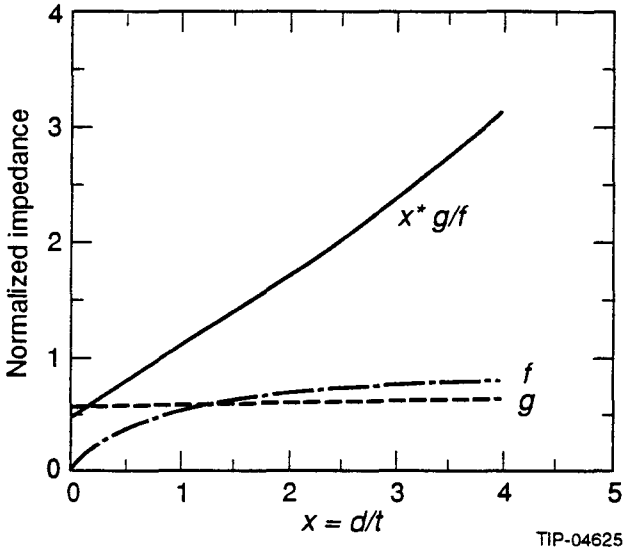

Figure 3. Hole Impedance Normalized for Constant Conductance Versus the Ratio of Hole Diameter to Thickness.

The impedance safety margin S is defined to equal the instability threshold impedance divided by twice the calculated impedance. For a given safety margin S = 1, 2, 3 and 4 the relationships between the number of holes per meter and liner diameter are plotted in Figure 4. The allowable safety margin is a strong function of the liner diameter. For a safety margin of 2.0 the minimum allowed liner diameter is 25.6 mm with no allowance left for holes, for a safety margin of 1.0 the minimum liner diameter is 19.6 mm. For most of the calculations reported here a minimum safety margin of 2.0 is regarded as acceptable and the

liner diameter has been chosen to be 30.2 mm. The corresponding maximum number of 2-mm holes per meter is then $N_h = 1546$. For a liner temperature T = 80 K the maximum conductance for H_2 is then C_{12} = 690 l/m/s. The transverse impedance for constant H_2 conductance C_{12} = 690 l/m/s is plotted in Figure 5 as a function of the diameter of liner holes for assumed liner diameters of 20.2, 25.2 and 30.2 mm. The instability threshold (S = 0.5) boundary is indicated by the horizontal dashed line.

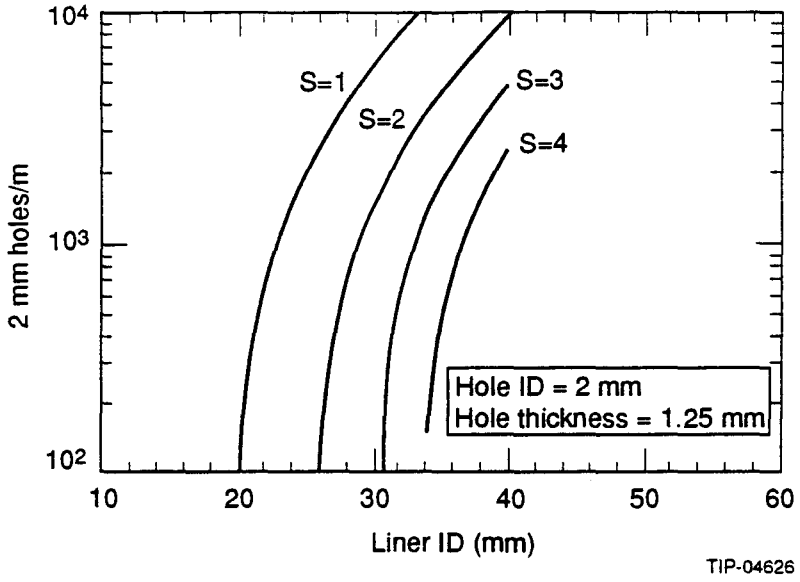

Figure 4. Number of Liner Holes Per Meter Versus Liner ID for Impedance Safety Margins S = 1 and 2, Hole Diameter = 2 mm, Hole Thickness = 1.25 mm.

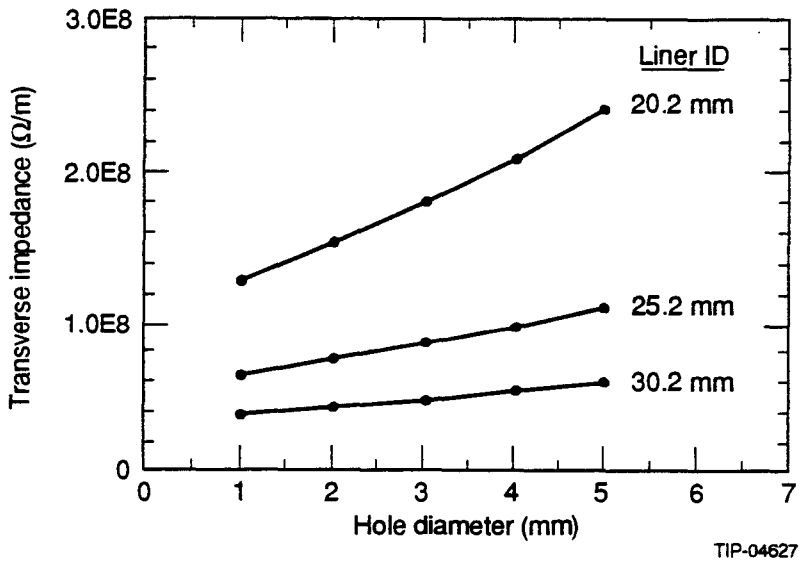

Figure 5. Transverse Impedance Versus Hole Diameter for H_2 Conductance C_{12} = 690 l/m/s.

The equations describing the liner vacuum have assumed that a negligible fraction of molecules exiting the liner holes hit the bore tube and scatter directly back through the holes. For this to be true the gap between the liner and bore tube must not be too small. Assuming a cos(θ) distribution for the backscattered molecules, upper and lower bounds for the backscatter fraction are:

$$f_U = 1 - r/(r^2 + (d/2)^2)^{1/2} \tag{43}$$

$$f_L = 1 - (r+t)/((r+t)^2 + (d/2)^2)^{1/2}.$$

where r is the radial gap width between the outside of the liner and the bore tube, d is the hole diameter and t is the liner thickness. These fractions are plotted in Figure 6 for d = 2 mm and t = 1.25 mm. For the present radial gap width r = 4.5 mm the backscatter fraction is less than a few percent and the gap could be reduced to 2 mm without large effect.

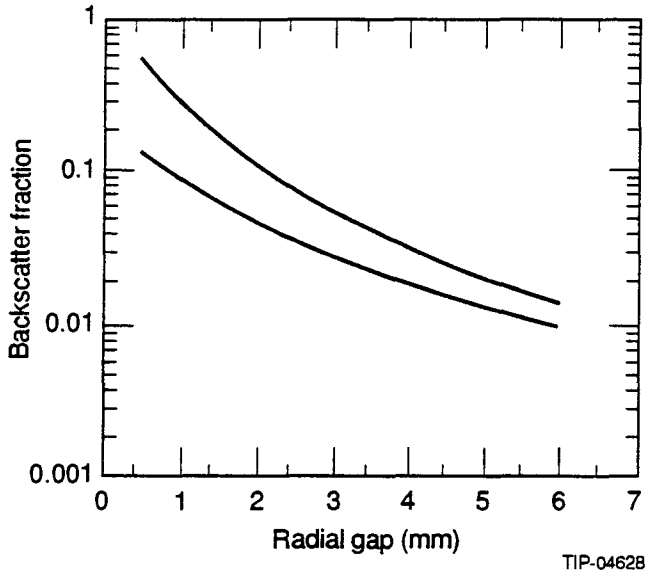

Figure 6. Backscatter Fraction Versus Radial Gap Between the Liner and Bore Tube.

4.0 INPUT DATA

4.1 Hydrogen Isotherm

Before discussing numerical solutions to the equations of the previous section it is useful to examine the H_2 isotherm on the 4.2 K SS bore tube wall that is not covered by cryosorber. This is shown in Figure 7 where we have plotted the BET equation and also normalized data from Benvenuti *et al.*[14] measured on SS at 4.17 K.

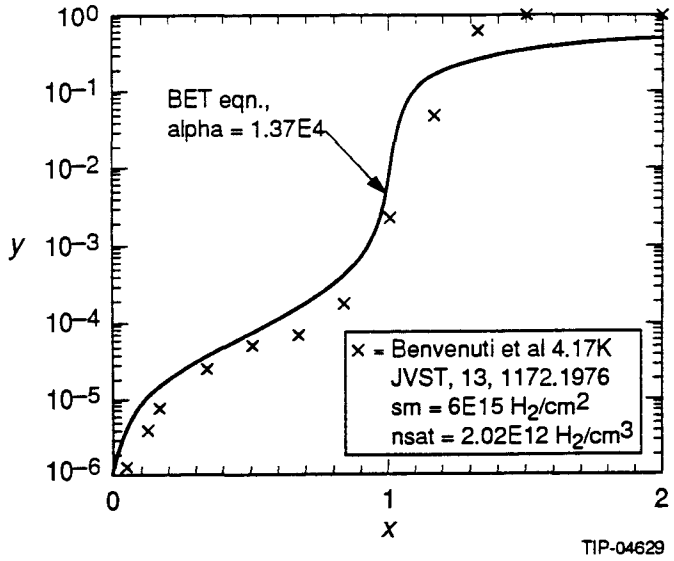

Figure 7. H_2 Isotherm on SS at 4.17 K.

The BET Eq. (44) has the saturation property y = 1 as x -> ∞. In Figure 7 the normalized variables are $x = s/s_m$, $y = n_e/n_{sat}$, s is the surface density of H_2, n_e is the equilibrium vapor density, s_m the density of one monolayer, n_{sat} the saturated vapor pressure ($n_{sat}(cm^{-3}) = 6.84\times10^{22}e^{-95.8/T}/T$) and $\alpha = e^{\Theta/T}$. The data of Benvenuti *et al.*, have been normalized with $s_m = 6\times10^{15}$ H_2/cm^2 and $n_{sat} = 1.73\times10^{12}$ H_2/cm^3. The BET Eq. (44) is plotted with $\Theta = 39.7$ K, $\alpha = e^{\Theta/T} = 1.37\times10^4$. The rapid rise in vapor pressure near one monolayer x~1 is of course the reason for pursuing a liner to avoid too frequent warm ups of the Collider beam tube to remove the photodesorbed H_2. Below x~1 the data of Benvenuti *et al.*, in Figure 7 are dominated by thermal desorption by 80 K and 300 K radiation from other parts of the vacuum system and the vapor pressure is higher than it would be in the absence of such radiation. However, this seems to be a reasonably accurate simulation of the situation here since the 4.2 K liner faces the 80 K bore tube.

$$x = \alpha y/[(1-y)(1 + (\alpha-1)y))] \ . \qquad (44)$$

If we make the approximation y<<1, which should be the case at very low photon dose, the BET Eq. (44) reduces to the simpler form:

$$y = x/[\alpha(1-x) + x] \ . \qquad (45)$$

Equation (45) accounts for the very rapid rise in vapor pressure as x~1 is approached, eventually invalidating the approximation y<<1. It is this rapid rise in vapor pressure near one monolayer which led to the two useful approximations for solving Eqs. (1) to (5) in paragraph 2.2. When the magnet bore tube surface reaches equilibrium $\sigma_w S_{2w} * n_{12} \equiv N_w/\tau_w$ it ceases to pump. The cryosorber is then chosen to clamp the H_2 vapor pressure well before it reaches the saturation value. Without the cryosorber the saturation vapor pressure would be reached and equilibration through the holes in the liner would lead to the same excessive pressure problem as occurs without the liner (the density decrease due to $(T_2/T_1)^{1/2}$ would not be enough to prevent overload of the cryogenic system and quenching of the magnets).

A useful estimate of the sojourn time for H_2 on SS can be obtained by using the equilibrium isotherm. When the surface is in equilibrium we have from Eq. (4):

$$\tau_w = N_w/\sigma_w S_{2w} n_{12}$$

$$\cong 2(a_1/a_2)*(1/\sigma_w<v_2>)*(s/n_{21}) \qquad (46)$$

$$\cong 4*(1/\sigma_w<v_2>)*(s_m/n_{sat})*(x/y).$$

where $x = s/s_m$ and $y = 2n_{21}/n_{sat}$. The sojourn time should be a function only of the surface temperature and the surface density of H_2 and not depend on whether or not the surface is actually in equilibrium – *i.e.*, not on the vapor density or incident molecular flux that is actually present. We therefore argue that Eq. (47), which has been derived from an equilibrium situation, can also be used when the surface is not in equilibrium providing n_{21} is properly calculated – *i.e.*, we use the equilibrium isotherm to calculate n_{21} for a given s rather than the n_{21} that is actually present. If $x<<1$, which should describe a clean surface, $x/y \cong \alpha$ and $\tau_w \cong 4*(1/\sigma_w<v_2>)*(s_m/n_{sat})*(\alpha) = 4.3$ hrs.

For the first approximation – that the surface be far from equilibrium – we should also have the time scale of interest since the start of photodesorption be short compared to the sojourn time. For the second approximation – that the surface be in equilibrium – the time should be long compared to the sojourn time.

4.2 Vapor Pressure of CH_4, CO and CO_2

Other gases besides H_2 are commonly observed in photodesorption experiments, the most important ones are CH_4, CO and CO_2. If the volume density of these molecules exceeds the isotherm saturation density then thick layers of these gases will build up by cryosorption. The saturation vapor density may be looked up in standard references. For example using the information in Barron[15] we obtain the following saturation densities at 80 K; 2.3×10^{18} CH_4/cm^3, 7.5×10^{19} CO/cm^3 and 2.2×10^{10} CO_2/cm^3. Generally these saturation densities exceed the expected gas densities inside the liner by a large margin so significant surface concentrations will not build up on the liner. At 4.2 K however the saturation vapor density of these molecules is vanishingly small so they will accumulate on the SS bore tube until it is warmed up.

4.3 Photodesorption Data from the Central Design Group Experiment of Bintinger *et al.*[16,17]

At the time the design study described in this report was initiated photodesorption data in a 4.2 K electroplated Cu tube was limited to the single experiment done by a SSC Central Design Group team. This experiment is described in two reports.[16,17] Numerical values for the parameters appearing in the model equations in paragraph 2 can be extracted from these reports. The results for the photodesorption coefficients η are given in Table 1 for each of the gases measured. Desorption coefficients for CH_4 were not reported. These coefficients were measured in a beam tube at 294 K, however the experimenters concluded that at least for H_2 η is about the same at 4.2 K and 294 K. The basis for this conclusion is three repetitions of a photodesorption experiment done at 4.2 K and 294 K with small samples cut out of the beam tube.[17] A limitation of the data from these experiments is that the maximum total integrated photon flux was 1×10^{21} photons/m which corresponds to only one day of SSC operation at design current. To obtain predictions beyond this flux it is necessary to extrapolate the data, which we have done assuming no change in the rate of decrease of η with accumulated photon flux. The motivation for this assumption is the 294 K data of Foerster *et al.*[18] on various materials which are reasonably well fit with single power law

decreases of η with photon flux up to 10^{23} photons/m. Furthermore this is most probably a conservative assumption since the rate of decrease with photon flux is lower than has usually been observed by other experimenters with different materials.[18,19] For the coefficients listed in Table 1 the inverse power law dependence of photon flux is approximately 0.3.

The data from the CDG experiment differ in some details from what will occur in the Collider. The critical energy for the CDG experiment was 478 eV and the angle of incidence was 9 mrad compared to 284 eV and 2 mrad for the Collider. The data of Gomez-Goni[20] *et al.*, on OFHC Cu show the desorption coefficients increasing linearly with energy up to 280 eV and then increasing about a factor of 2 up to 3 keV. The angular dependence of photodesorption coefficient hasn't been measured down to 2 mrad. However the data of Grobner *et al.*[21] indicate that at 3 keV critical energy the desorption coefficient is rather slowly increasing with decreasing angle of incidence at 11 mrad. As a result of these observations the data of the CDG experiment are used without correction for angle of incidence and critical energy. Additional details concerning the cutoff of low energy photons and different fractions of the wall circumference illuminated by the primary photon flux are also left uncorrected.

TABLE 1. PHOTODESORPTION COEFFICIENTS VERSUS PHOTON DOSE FROM REF. 16 FOR 294 K ELECTROPLATED CU MOLECULES/PHOTON.

Gases	Molecules/Photon				
	10^{19} photons/m	10^{20}	10^{21}	10^{22}*	10^{23}*
H_2	2.5×10^{-2}	8.5×10^{-3}	4.3×10^{-3}	2.1×10^{-3}	1.1×10^{-3}
CH_4	—	—	—	—	—
CO	9.0×10^{-3}	3.0×10^{-3}	1.4×10^{-3}	6.8×10^{-4}	3.3×10^{-4}
CO_2	2.6×10^{-3}	9.0×10^{-4}	4.2×10^{-4}	2.0×10^{-4}	9.3×10^{-5}

*all desorption coefficients above 10^{21} photons/m are extrapolated

The other parameters of interest are the sticking coefficient, mean molecular speed and recycling coefficient η'. These can be estimated from the data in Ref. 16, 17 taken at 4.2 K. The results for H_2 are f=1/13, $\langle v\rangle=1.8\times10^5$ cm/sec and $\eta' = 1.2$ at $\Gamma = 8.0\times10^{20}$ photons/m. Recycling is apparently quite large and efficient compared to primary desorption, having reached a value of approximately one molecule per photon at the conclusion of the experimental run when the direct term has fallen to less than one molecule per two hundred photons. If η' is parametized as $\eta' = \eta_0'(s/s_m)$ then $\eta_0' = 1.4$, where we have $\eta_{4\ K} = \eta_{294\ K}$ to calculate $s = 5.1\times10^{15}$ H_2/cm^2 at $\Gamma = 8\times10^{20}$ photons/m and $s_m = 6\times10^{15}$ H_2/cm^2.

One year of SSC operation is projected to be 2×10^7 sec, or 2×10^{23} photons/m at design intensity. The desorption coefficients listed in Table 1, admittedly extrapolated to a total flux one hundred times larger than the maximum measured flux, can be used to estimate the amount of gas desorbed in one operational year. The results are listed in Table 2 below together with intermediate values at photon fluxes at 10^{21}, 10^{22} and 10^{23} photons/m. The total amount of H_2 desorbed at 2×10^{23} photons/m is 2.5×10^{20} H_2/m, corresponding to 44 monolayers assuming a tube diameter of 30.2 mm and a monolayer density $s_m = 6\times10^{15}$ H_2/m. Clearly this would require an excessive number of beam tube warm ups per year of operation if a liner or distributed pump is not present. The total amount of all gases desorbed in one year is projected to be ~10 Torr l/m at 273 K. The cryosorber capacity of the distributed pump concept indicated in Figure 1 should be chosen in this range.

TABLE 2. QUANTITY OF DESORBED GAS VERSES PHOTON DOSE ESTIMATED FROM EXTRAPOLATION OF THE DATA OF REF 16.

Gases	Molecules/m (Torr l/m*)			
	10^{21} photons/m	10^{22}*	10^{23}*	2×10^{23}* (one oper yr)
H_2	6.1×10^{18}	3.0×10^{19}	1.6×10^{20}	2.5×10^{20} (7.1**)
CH_4	–	–	–	–
CO	2.1×10^{18}	1.0×10^{19}	4.8×10^{19}	7.7×10^{19} (2.2**)
CO_2	6.3×10^{17}	3.0×10^{18}	1.4×10^{19}	2.2×10^{19} (0.6**)

* Quantities of desorbed gas above 10^{21} photons/m are extrapolated

** Torr l/m at 273 K

4.4 Scattering Cross Section, Pumping Speed Ratios and Relative Weights of Gas Species in the Inverse Luminosity Lifetime

The luminosity lifetime of a Collider proton beam due to nuclear scattering is

$$1/\tau_L = 2^* \Sigma_j \, n_j \, \sigma_{jp} \, c \tag{47}$$

where the sum is over all molecular gas species j and σ_{jp} is the total scattering cross section of a 20 TeV proton with molecule j. From Eqs. (6) and (16), in a 80 K liner configuration the density n_j is proportional to the product of the desorption coefficient η_j and the square root of the mass m_j. It is of interest to calculate the weights of the heavier gases CH_4, CO and CO_2 relative to H_2 in $1/\tau_L$ due to the different desorption coefficients, cross sections and molecular weights. The total nuclear cross section for a 20 TeV proton hitting a stationary proton is taken as $\sigma_{pp} = 50$ mb. The cross section of a 20-TeV proton hitting an atom with atomic number A is assumed to be geometric so $\sigma = A^{2/3}\sigma_{pp}$, the molecular cross section is summed over the atoms. In Table 3 we list the weights relative to H_2 in the inverse luminosity lifetime due to desorption coefficient, scattering cross section and pumping speed. The product of all three weights is also given. Although the desorption coefficients of the heavier molecules are less than for H_2, the higher cross sections and molecular weights more than compensate. The result is that for the data of Bintinger *et al.*[16] the luminosity lifetime due to nuclear scattering on H_2 is reduced by a factor of ~12.3 when all gases are included.

TABLE 3. INVERSE LUMINOSITY LIFETIME WEIGHTS OF CH_4, CO AND CO_2 RELATIVE TO H_2.

Gases	w_η*	w_m	w_σ	w
H_2	1	1	1	1
CH_4	–	2.8	4.6	–
CO	0.33	3.7	5.8	7.1
CO_2	0.10	4.7	9.0	4.2
TOTAL				12.3

* from column 4 Table 1

5.0 NUMERICAL SOLUTIONS

5.1 4.2 K Beam Tube Without a Liner

In this section we present the prediction of H_2 build-up in a 4.2 K beam tube under Collider conditions and without a liner. The parameters of paragraph 4.3 deduced from Ref. 16 are used as input. A beam tube ID of 30.2 mm is assumed. H_2 density is plotted versus time in Figure 8a assuming a photon flux at design intensity 10^{16} photons/m/sec. The three components of the H_2 density are shown due to direct desorption, recycling and the isotherm. The isotherm density rises rapidly after 10^5 sec or about one day of operation as the surface density of H_2 approaches one monolayer and this would prevent further operation until the beam tube is warmed up and pumped out. This rapid rise was not observed in the photodesorption experiments. There are at least three possible explanations. One is that the experiments fell somewhat short of desorbing a monolayer and the isotherm pressure was still negligible. The condition $\eta_{4K} = \eta_{294\ K}$ is consistent with this explanation. The second possibility is that the desorption coefficient at 4.2 K is actually less than at 294 K. The third possibility is that some molecules are lost by axial diffusion so the build up of H_2 is reduced. Returning to Figure 8a, before a monolayer is reached the dominant density component is seen to be due to recycling except at very early times. Just before a monolayer has been reached the luminosity lifetime due to scattering on H_2 alone has fallen to ~11.25 hrs. Scattering by heavier gases hasn't been included. A luminosity lifetime this low would soon require a beam tube warm up and pump out even if the rapid rise in isotherm density didn't occur.

Since the results in Figure 8a predict an initial monolayer is reached in only one day's photon flux it is of interest to have an idea how long the second, third and following monolayers will take to form. For a simple power law dependence of desorption coefficient on photon flux $\eta = \eta_0/(\Gamma/\Gamma_0)^\alpha$ the time T_n to form the n-th monolayer is given by:

$$T_n = T_1[\ n^{1/(1-\alpha)} - (n-1)^{1/(1-\alpha)}]\ , \tag{48}$$

and for n>>1,

$$T_n \cong (T_1/(1-\alpha))*n^{\alpha/(1-\alpha)},$$

where

$$T_1{}^{1-\alpha} = (1-\alpha)A_w s_m/(\eta_0\Gamma_0{}^\alpha d\Gamma/dt^{1-\alpha}).$$

The monolayer time is plotted versus monolayer number in Figure 8b for the H_2 desorption coefficient extrapolated from the experiment of Bintinger *et al.*[4] ($\eta_0 = 0.017$, $\Gamma_0 = 10^{19}$ photons/m, $\alpha = 0.3$, $T_1 = 9.1\times10^4$ sec) and for baseline photon flux 10^{16} photons/m/s in the Collider. The monolayer formation time is predicted to be a rather slowly increasing function of monolayer number, behaving as the 0.43 power of the monolayer number n for n>>1 and reaching only about 5 days for n = 20. Beam tube warm up, pump out cycles with this frequency would place an unacceptable burden on Collider operation.

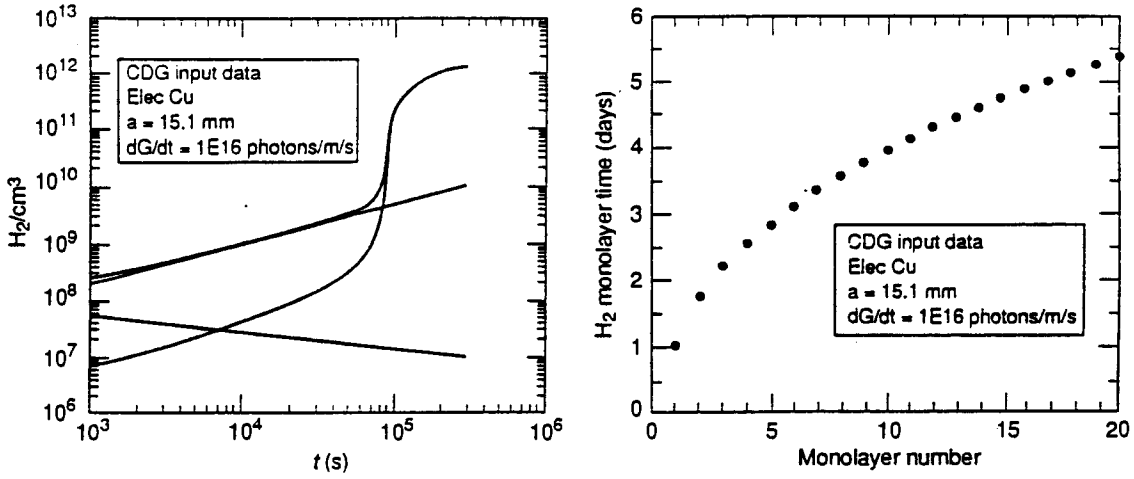

Figure 8. (a) Predicted H_2 Density vs. Time for $d\Gamma/dt = 10^{16}$ Photons/m/s and No Liner and (b) H_2 Monolayer Formation Time vs. Cumulative Number of Monolayers Desorbed.

5.2 80 K Liner Configuration

In order to obtain numerical results we need to assume specific values for liner hole conductance and cryosorber pumping speed in addition to the molecular desorption coefficients. For the desorption coefficients we take the values give in Table 1. Ideally the pumping speed of the cryosorber should be large compared to the conductance of the liner holes. The conductance of the holes are then the limiting factor determining molecular density inside the liner. We also need to choose the hole conductance large enough so the density of H_2 falls below that required to achieve the beam lifetime goal with reasonably short conditioning of the beam tube and consistent with beam instability impedance constraints. It will turn out that the nuclear scattering lifetime of the beam is dominated by the heavier gases CO and CO_2 however here we give the estimated requirement for H_2 alone. The goal for τ_L is 150 hrs which requires $n(H_2) < 3\times10^8/cm^3$. From Eq. (16) an estimate of C_{12} is:

$$C_{12} \equiv \eta^* d\Gamma/dt/n(H_2). \tag{49}$$

For the H_2 desorption coefficient we take a representative initial value for electrodeposited Cu $\eta = 0.02$, choose the Collider baseline value for photon flux $d\Gamma/dt = 10^{16}$ photons/m/s and obtain $C_{12} \equiv 667$ l/m/s for H_2 at 80 K as an estimate of the region of interest. This is very close to the upper bound allowed by impedance considerations. The numerical examples in Table 4 have been calculated for the cryosorber pumping speed equal to five and two times the hole conductance and for hole diameters 1, 2 and 3 mm. The molecular transmission probability p of the holes is tabulated assuming a hole thickness 1.25 mm. For all the cases given in Table 4 the reciprocal combination of C_{12} and S_c has been held constant at 460 l/m/s H_2 at 80 K.

TABLE 4. DENSITY OF 80 K LINER HOLES.

d (mm)	p	N_h(holes/m) C_{12}=552 l/m/s* Sc=2760 l/m/s*	N_h(holes/m) C_{12}=690 l/m/s* Sc=1380 l/m/s*
1	0.46	6668	8335
2	0.62	1237	1546
3	0.71	480	600

*for H_2 at 80 K

The final choice of hole size and shape and the pattern of the holes will depend on considerations of the RF impedance and cost. It isn't known yet what value of Sc can be achieved in a liner configuration with the cryosorber facing the 80 K surface. To get some idea of what is practical we calculate the fraction of the bore tube surface that must be covered with cryosorber in order to obtain the pumping speeds S_c = 1380 and 2760 l/m/s. The fractions are $0.045/\sigma$ and $0.09/\sigma$, respectively, where σ is the sticking coefficient. For a sticking coefficient near unity there is no problem. A sticking coefficient as low as 0.1 would give difficulty. Although the net pumping speed for all the cases listed in Table 4 is equivalent to an ideal pump with 2.1% of the liner area (assuming a liner ID = 30.2 mm), the actual fraction of the liner surface area perforated with holes is 5.5%, 4.1% and 3.6% for the C_{12} = 552 l/m/s cases in Table 2 and 6.9%, 5.1% and 4.5% for C_{12} = 690 l/m/s.

Calculations for the 80 K liner case are shown in Figures 9 to 12. For these calculations we have assumed the liner ID = 30.2 mm, the liner conductance is specified by N_h = 1546 2 mm diameter, 1.25 mm thick holes/m and the cryosorber H_2 pumping speed is Sc = 1380 l/m/s. H_2 densities inside and outside the liner are shown in Figures 9a and 9b, the surface density of H_2 building up on the 4.2 K bore tube is given in Figure 10. The H2 density shown in Figure 9b is actually a normalized density $2n_{21}$/nsat where nsat is the H2 saturation isotherm density at 4.2 K. In our two component model of the gas between the 80 K liner and 4.2 K bore tube this normalized density would approach unity in the absence of cryosorber and as the surface density of H_2 builds up to a monolayer on the bore tube. The actual density of H_2 in this region is $n_{21} + n_{12} = (1 + (T_2/T_1))^{1/2} * n_{21} = 1.23 * n_{21}$. The solutions are shown for the two approximations given by Eqs. (6) to (10) and (11) to (15) above, before and after the surface of the magnet bore tube reaches equilibrium. The transition from the first to the second approximation occurs when the two solutions for the surface density of H_2 on the bore tube are equal, or from Figure 10 at a photon flux ~8×10^{20} photons/m. Near the transition the surface density of H_2 on the bore tube is approaching a monolayer – actually reaching $s/s_m = 0.65$ in Figure 10 – and the isotherm density is rising rapidly until it reaches a value limited by the cryosorber pumping speed. When this happens the SS bore tube effectively ceases to pump H_2 and all the net pumping is by the cryosorber. This causes an upward jump in H_2 density inside and outside the liner at $\Gamma = 8\times10^{20}$ photons/m as evidenced in Figure 9a and 9b. In Figure 9b the density jump outside is to about 10^{-4} times the H_2 isotherm saturation density. Without the cryosorber the density $2n_{21}$ would have increased to the saturation density 2×10^{12} H_2/cm^3 outside the liner and $(T_2/T_1)^{1/2} * 2\times10^{12} = 4.6\times10^{11}$ H_2/cm^3 inside. When the cryosorber begins to saturate (not shown in Figures 9 to 12) the H_2 density will increase toward this level which of course would require warming up the beam tube and removing the H_2. The capacity of the cryosorber must be chosen so this occurs only infrequently, estimates of the minimum capacity required for one warm up per year are given in the right hand column of Table 2. What one gets with the liner is a photon shield for the cryosorbed molecules and an increase in the effective surface area of the bore tube. For the desorption coefficients given in Table 1 the desired increase in effective surface area is in the range of 50 to 100.

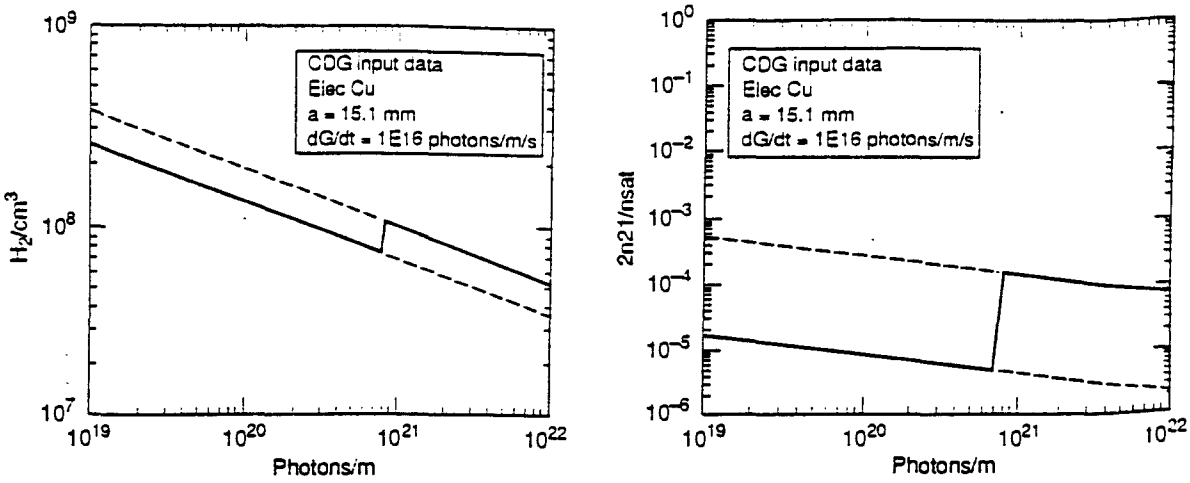

Figure 9. (a) H_2 Density Inside the 80 K Liner, (b) Normalized H_2 Density Between the 80 K Liner and 4.2 K Magnet Bore Tube.

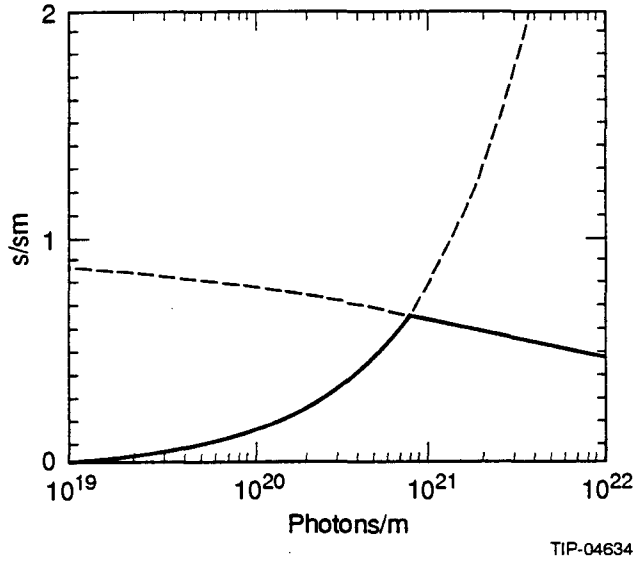

Figure 10. Normalized Surface Density of H_2 on the 4.2 K Magnet Bore Tube.

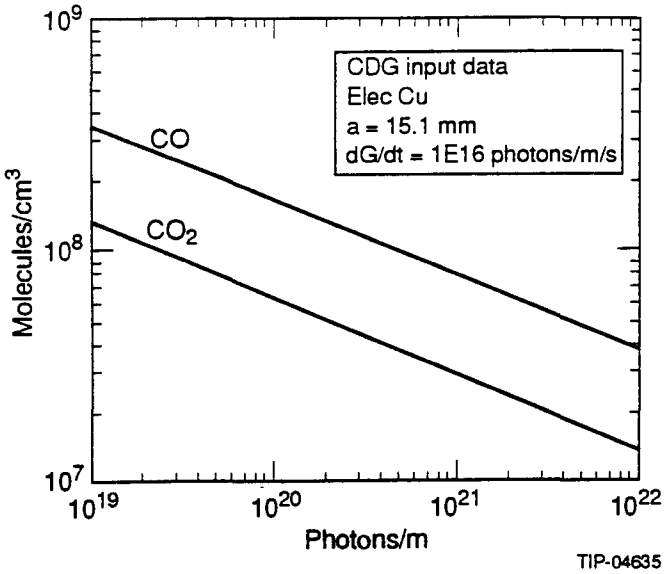

Figure 11. Density of CO and CO_2 inside the 80 K Liner.

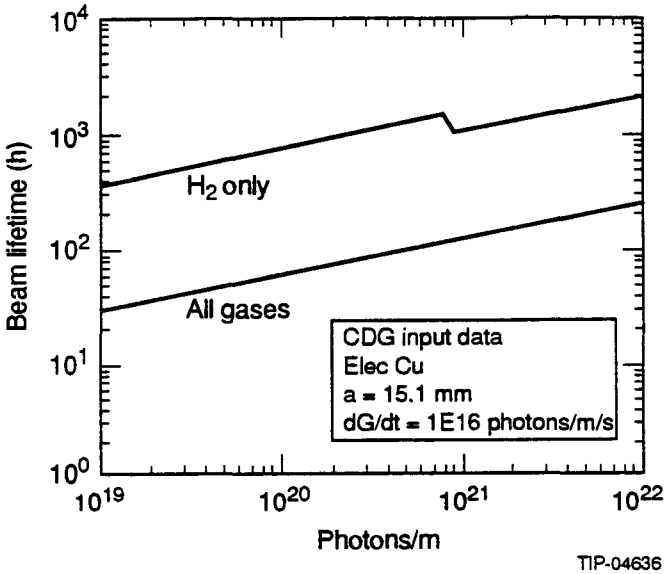

Figure 12. 20 TeV Proton Nuclear Scattering Lifetime with an 80 K Liner.

The density of H_2 inside the beam tube is less than $3\times10^8/cm^3$ even at 10^{19} photons/m and decreasing with increasing photon flux. The liner/cryosorber effectively solves the H_2 isotherm problem so we next look at the effect of heavier molecules. The isotherm densities of these molecules at 4.2 K are negligibly low so the 4.2 K magnet bore tube will always remain an effective pump for them. The densities of these molecules are given by Eqs. (6) to (10) with appropriate substitutions of the desorption coefficients from Table 1 and the mass dependence of conductances and pumping speeds. The densities of CO and CO_2 inside the liner are given in Figure 11. For the desorption coefficients that have been chosen the CO density

is actually comparable in magnitude to H_2. The beam lifetime estimates for nuclear scattering on H_2 only and on H_2, CO and CO_2 are given in Figure 12. At 10^{19} photons/m the beam lifetime is reduced from 380 hrs for H_2 only to 30 hrs with CO and CO_2 included. However the liner surface is cleaning up with increased exposure. By 1.5×10^{22} photons/m, or ~17 days of Collider operation at design intensity, the beam lifetime has reached the vacuum design goal of 300 hrs. If such a vacuum system were actually implemented it is likely that this vacuum conditioning would occur over a longer period of time during initial Collider operation at 20 TeV but at beam current less than the design goal. Since the synchrotron radiation intensity is proportional to beam current, the molecular densities and inverse scattering lifetime are also proportional to beam current.

6.0 WORK IN PROGRESS

When this study was started approximately one year ago, parallel efforts were initiated to increase the photodesorption data base relevant to the SSCL Collider. The thrust of these efforts is threefold; (1) to obtain photodesorption coefficients with total photon exposures equivalent to one year of Collider operation, (2) to revive photodesorption experiments at 4.2 K and (3) to expand the list of beam tube materials and preparation procedures under consideration. Most of the work in these areas still remains to be done; however, some new results are available and will be briefly described here.

Photodesorption coefficients for samples from the same batch of electrodeposited Cu tubing used in Refs. 16, 17 have recently been measured at 294 K up to 2×10^{22} photons/m at the Budker Institute of Nuclear Physics (BINP) VEPP-2M electron/positron collider and up to 2×10^{23} photons/m at the BNL NSLS UV ring.[22] In addition Mathewson *et al.* at CERN have been taking low intensity data on the EPA machine for the LHC.[20] Although most of CERN work is at the LHC critical energy 64 eV, some data is taken at the SSCL Collider critical energy 284 eV and this has been useful for comparing to the work at BINP and BNL. The desorption coefficients from the experiments at BINP and BNL are given in Table 5. The two data sets agree within a factor of two except for CO_2 which has somewhat larger photodesorption coefficient for the BNL data. For photon flux within the measurement range of the experiment in Ref. 16 (*i.e.*, less than 10^{21} photons/m) they are in reasonable agreement with that experiment as well. However for photon fluxes exceeding 10^{21} photons/m the photodesorption coefficients of the new data decrease more rapidly with increasing photon flux than extrapolation from Ref. 16 suggests. The amount of H_2 desorbed by one operating year of photon flux 2×10^{23} photons/m is 4.5×10^{19} H_2/m for the BNL data and 7.4×10^{19} H_2/m for the extrapolated BINP data.[22] This is significantly less than the 2.5×10^{20} H_2/m projected in Table 2 but still large enough that a liner would be an operational benefit. Anashin *et al.*[23] have used the isotherm method to measure the monolayer density of H_2 on the electroplated Cu used in these experiments, obtaining $s_m \equiv 3\times10^{15}$ H_2/cm^2. The number of equivalent monolayers desorbed in one year is then in the range 16 to 26 and a prohibitive number of beam tube warm ups.

The coefficients in Table 5 can be used as input to the liner calculations done in paragraph 5 and the operation time until the beam lifetime due to vacuum exceeds 300 hrs can be estimated. The result is that the clean up time for the 80 K liner is 1 to 3 days instead of 17 days. An obvious thing to do at this point is decrease the number of holes in the liner, thus increasing the impedance instability margin at the expense of some increase in clean up time. Another possibility is to keep the number of holes fixed and calculate the liner clean up times for lower liner temperatures –0 20 K and 4.2 K. These clean up times are given in Table 6 below for the extrapolated scaling obtained from Ref. 16 and for the recent BNL and BINP data. More detailed calculations of 20 K and 4.2 K vacuum performance will be given in a following report. The clean up time becomes progressively longer as the temperature is decreased because of the decreasing hole conductance in Eqs. (6), (11), (30) and (37). The molecular velocity has been assumed to equal that of a molecule in thermal equilibrium with the wall. We see from the Table 6 that with the new data even the 4.2 K liner has an acceptable clean up time, in the range of 15 days, and that this conclusion does not depend on extrapolation of data beyond its measurement range. This is in contrast to the earlier calculations

which gave a clean up time of 174 days for a 20 K liner and much longer for a 4.2 K liner. Because of these unfavorable clean up times and the desire to maintain an impedance margin of at least 2.0 we had originally selected 80 K for the liner temperature, The consequence of the new data is that more possibilities are opened up, each with their own advantages. The 20 K and 80 K options would have about equal engineering complexity since they both require GHe cooling tubes. The problem of heat leaks to the 4.2 K system due to thermal radiation and thermal conduction through supports is reduced for 20 K compared to 80 K. However the refrigeration capacity available in the Collider is much larger at 80 K (650 kw) than 20 K (150 kW) and the thermal efficiency is improved at 80 K. If sufficiently good thermal contact between the "4.2 K" liner and magnet bore tube can be made so that the GHe cooling tubes can be eliminated then the 4.2 K case is less complex than 80 K/20 K. Furthermore cryosorber could be applied to the outside of a 4.2 K liner rather than the inside of the bore tube and this would also be simpler. In this case it isn't necessary that the liner temperature be held right at the bore tube temperature, but the temperature should be low enough that the cryosorber performs adequately. The disadvantage of a 4.2 K liner compared to 80 K/20 K is that the beam operating current is tied to the 4.2 K refrigeration capacity (67.5 kW). A factor three increase in beam current would require 36 kW additional 4.2 K refrigeration due to the increase in synchrotron radiation.

TABLE 5. 294 K PHOTODESORPTION COEFFICIENTS FROM RECENT EXPERIMENTS.

(a) Photodesorption coefficients versus photon dose measured at BINP for 294 K electroplated Cu (Ref. 22)

Gases	Molecules/Photon				
	10^{19} photons/m	10^{20}	10^{21}	10^{22}	10^{23}*
H_2	3.4×10^{-2}	1.5×10^{-2}	3.7×10^{-3}	9.4×10^{-4}	2.4×10^{-4}
CH_4	6.8×10^{-4}	2.9×10^{-4}	7.3×10^{-5}	1.8×10^{-5}	4.5×10^{-6}
CO	5.7×10^{-3}	2.5×10^{-3}	6.2×10^{-4}	1.6×10^{-4}	3.9×10^{-5}
CO_2	1.2×10^{-3}	5.2×10^{-4}	1.3×10^{-4}	3.3×10^{-5}	8.2×10^{-6}

(b) Photodesorption coefficients versus photon dose measured at BNL for 294 K electroplated Cu (Ref. 22)

Gases	Molecules/Photon				
	10^{19} photons/m	10^{20}	10^{21}	10^{22}	10^{23}*
H_2	5.8×10^{-2}	1.55×10^{-2}	3.9×10^{-3}	6.6×10^{-4}	1.2×10^{-4}
CH_4	8.5×10^{-4}	2.9×10^{-4}	6.4×10^{-5}	8.0×10^{-6}	4.9×10^{-7}
CO	1.2×10^{-2}	4.5×10^{-3}	1.0×10^{-3}	1.4×10^{-4}	9.6×10^{-6}
CO_2	7.9×10^{-3}	3.5×10^{-3}	6.8×10^{-4}	8.5×10^{-5}	9.4×10^{-6}

*all desorption coefficients above 10^{22} photons/m are extrapolated

In addition to the new 294 K results the first 4.2 K photodesorption experiment at BINP has been completed with electrodeposited Cu.[23] These results and follow-on experiments will eventually have even more impact on the Collider beam tube vacuum design. It is too early to include an analysis based on these results in this report but some comments may be made. As observed in Ref. 16 the density in the 4.2 K tube, at least initially, increases with photon dose. At an integrated photon flux 8×10^{20} photons/m the magnitude of H_2 density rise observed in these two experiments appears to agree within a factor of about two. This confirms the importance of photodesorption of cryosorbed molecules. In contrast to Ref. 16 however the 4.2 K desorption coefficients seem to be much lower than at 294 K. More analysis and data at higher photon dose are needed to understand the full implications for the Collider. The results however are in the direction of decreasing the required pumping speed and therefore the number of holes and/or the temperature of the liner. For the electrodeposited Cu that has been tested it still seems that there would be a large operational benefit if a liner is installed.

TABLE 6. 80 K, 20 K AND 4.2 K LINER CLEAN UP TIME (1546 2-mm HOLES/m).

(a) CDG data[16,17]

Liner temp (K)	H_2 conductance (liters/m/s)	Photon flux to achieve t_b = 300 hrs (photons/m)	Operation time to achieve t_b = 300 hrs (days)
80	690	1.5×10^{22}	17
20	345	1.5×10^{23}	174
4.2	158	1.6×10^{24}	1852

(b) BNL024[22]

Liner temp (K)	H_2 conductance (liters/m/s)	Photon flux to achieve t_b = 300 hrs (photons/m)	Operation time to achieve t_b = 300 hrs (days)
80	690	2.8×10^{21}	3.2
20	345	6.5×10^{21}	7.5
4.2	158	1.3×10^{22}	15.1

(c) BINP009[22]

Liner temp (K)	H_2 conductance (liters/m/s)	Photon flux to achieve t_b = 300 hrs (photons/m)	Operation time to achieve t_b = 300 hrs (days)
80	690	1.05×10^{21}	1.2
20	345	3.5×10^{21}	4.1
4.2	158	1.3×10^{22}	15.1

Whether or not a beam tube material or preparation procedure can be found in a reasonable time frame that eliminates the vacuum need for a liner or distributed pump isn't yet known. A number of approaches are being investigated and much more information will be available in the coming year. The emphasis up to now has been on getting hardware in place so that evaluations can be made.

7.0 SUMMARY

Model equations have been developed for describing liner configurations of the SSCL Collider beam tube vacuum system that deal with the photodesorption of gases by synchrotron radiation in a superconducting magnet environment. The liner is an effective solution to the problems of desorption of cryosorbed gas and the H_2 isotherm which occur in a 4.2 K beam tube without a liner. Generally the prediction of vacuum performance depends on far fewer parameters with a liner than without. With conservative assumptions this makes it possible to specify a liner that will simultaneously meet design goals for accelerator availability and impedance constraints. Most of the calculations in the paper have dealt with an 80 K liner. Whereas a 4.2 K beam tube without a liner needs to be periodically warmed up to remove cryosorbed gases, a liner needs a certain amount of conditioning time before the beam lifetime goal can be reached. A particular example given in the report, with beam instability safety margin 2.0, indicated that an 80 K liner would need about two weeks of operating time at design intensity to reach the beam lifetime goal of 150 hrs. The 4.2 K beam tube without liner allowed only a few days of operation before it would need to be warmed up.

New photodesorption data have become available which indicate the photodesorption coefficients are significantly less than the values used when this work was begun. It is still an open question and under vigorous research whether a beam tube material or conditioning method can be found which will allow sufficient Collider availability without a liner or distributed pump. The new photodesorption data at 294 K allow consideration of 4.2 K and 20 K liners that meet impedance budget constraints and also have adequately short conditioning times. Furthermore recent 4.2 K and 77 K photodesorption experiments at BINP indicate that the desorption coefficients decrease with temperature so the impedance of a liner, if needed, can be reduced and still have short conditioning time. Ultimately the 4.2 K experiments should be able to resolve the question of whether a liner is needed for a given beam tube material and, if needed, to define the minimum liner conductance.

REFERENCES

1. H. Edwards, "Study on Beam Tube Vacuum with Consideration of Synchrotron Light, Potential Liner Intercept, and Collider Quad/Spool Coil Diameter," SSCL-N-771. August (1991).
2. LHC Study Group, "Design Study of the Large Hadron Collider (LHC)," CERN 91-03 (1991).
3. Q.-S. Shu *et al.*, "Prototype Liner System for the Interception of Synchrotron Radiation in a Half Cell for the SSCL Collider," to be submitted to the IEEE Particle Accelerator Conference, Washington, D.C., May 17-20, 1993.
4. H. Edwards, "Study on Beam Tube Vacuum with Consideration of Synchrotron Light, Potential Liner Intercept, and Collider Quad/Spool Coil Diameter,"SSCL-N-771. August (1991) and A. Maschke, "Hydrogen Desorption and the Search for the Higgs," SSCL-Preprint 86. March (1992).
5. SSC Central Design Group, "Conceptual Design of the Superconducting Super Collider," SSC-R-2020. March (1986).
6. R. Carcagno, W. Schieller, H.-J. Shih, X. Xu and A. Yucel, *Proceedings of Supercollider IV*, New Orleans (1992).
7. S. Brunauer, P. Emmett, and E. Teller, *J. Chem. Soc.* **60**:309 (1938).
8. S. Kurennoy, *Particle Accelerators* **39**:1 (1992).
9. R. Gluckstern, "Coupling Impedance of a Single Hole in a Thick Wall Beam Pipe," and Coupling Impedance of Many Holes in a Liner Within a Beam Pipe: *Phys. Rev. A* **46**:1106, **46**:1110 (1992).
10. E. Ruiz, L. Walling, Y. Goren, and N. Spayd, report in preparation.
11. W. Chou and T. Barts, report in preparation.
12. J. O'Hanlon, *A User's Guide to Vacuum Technology,* J. Wiley, New York (1989).
13. J. Sanford and D. Mathews, eds., "Site-Specific Conceptual Design of the Superconducting Super Collider," SSCL-SR-1056. July (1990).
14. C. Benvenuti, R. Calder, and G. Passardi, *J. Vac. Sci. Technol.* **13**:1172 (1976).
15. R. Barron, *Cryogenic Systems,* Oxford Univ. Press, 2nd edition (1985).
16. D. Bintinger, P. Limon, H. Jostlein, and D. Trbjovic, "Status of the SSC Photodesorption Experiment," SSC-102 (1986).
17. D. Bintinger, P. Limon, and R. Rosenberg, *J. Vac. Sci. Technol.* **A7**:59 (1989).
18. C. Foerster, H. Halama, and C. Lanni, *J. Vac. Sci. Technol.* **A8**:2856 (1990).
19. A. Mathewson, private communication.
20. J. Gomez-Goni, O. Grobner, and A. Mathewson, CERN, CH-1211 Geneve 23, Switzerland, Vac. Tech. Note 92-12 (1992).
21. O. Grobner, A. Mathewson, H. Stori, R. Strubin, and R. Souchet, *Vacuum* **33**:397 (1983).
22. I. Maslennikov *et al.*, "Photodesorption Experiments on SSC Collider Beam Tube Configurations," to be submitted to the IEEE Particle Accelerator Conference, Washington, D.C., May 17-20, 1993.
23. V. Anashin, V. Erstigneer, O. Malyshev, V. Osipov, I. Maslennikov, and W. Turner, "Summary of Recent Photodesorption Experiments at VEPP2M," SSCL-N-825 (June, 1993).

This Page Intentionally Left Blank

SECTION 2

Thermal Budget Analysis and Impact on a Cryogenic Sector of an 80 K Liner of the SSCL

J. Maddocks

SECTION 2

Thermal Budget Analysis and Impact on a Cryogenic Sector of an 80 K Liner of the SSCL

J. Maddocks

Superconducting Super Collider Laboratory*
2550 Beckleymeade Avenue
Dallas, TX 75237

1.0 INTRODUCTION

In general, a liner system is a distributed cryopump contained within the beam tube. It has associated with it a cryosorber and a synchrotron radiation intercept which shields the cryosorber. The primary purpose is to pump gases which are desorbed by the synchrotron radiation from the beam tube wall. Such a cryopump can be effected by attaching cryosorber to the cold (4 K) magnet bore tube. A concentric tube, or liner, centered within the magnet bore tube shields the cryosorber from the synchrotron radiation, and becomes the beam tube. By perforating a fraction of the liner surface with small (on the order of 1–3 mm) holes, the liner/cryosorber assembly becomes a distributed pump.

The liner temperature may be allowed to equilibrate at a temperature close to that of the 4 K bore tube. However, thermally coupling the liner to the 80 K shield supply is of interest because the synchrotron radiation heat can then be transferred to the liquid nitrogen system. This, at least partially, decouples the allowable beam current from the helium cryogenic system. Thermal coupling to the LN_2 system is accomplished by means of supercritical helium flowing through a trace tube attached to the outside of the liner which heat exchanges with the LN_2 supply line at every interconnect. A cross section of the magnet bore tube with an 80 K liner is shown in Figure 1.

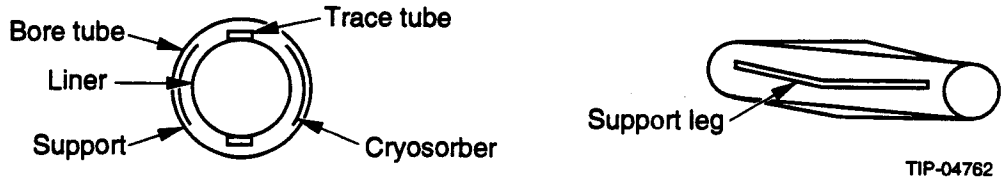

Figure 1. Cross Section of Magnet Bore Tube with Liner, and Schematic of Support Leg Attached To Liner.

* Operated by the Universities Reasearch Association, Inc., for the U.S. Department of Energy under Contract No. DE-AC35-89ER40486.

2.0 REQUIREMENTS

2.1 Temperature

The actual temperature of the 80 K supply line will fluctuate depending on local tunnel depth, location within the string, and unknown factors such as the number of LN_2 recoolers. A typical average temperature is likely to be 85 K. Since the liner will heat exchange with the LN_2 supply line in every component, it will experience similar fluctuations. Thus a temperature rise along the liner of 5 K is considered acceptable and taken to be a requirement.

2.2 Mass Flow Rate

The mass flow rate is determined from the $\Delta T \leq 5$ K requirement by

$$m \geq (Q \ / \ Cp \ \Delta T) \tag{1}$$

where Q is the heat due to synchrotron radiation and C_p is the specific heat of helium. Equation (1) uses the temperature rise of the bulk helium. Allowance has not been made for a temperature rise from the bulk helium to the liner wall, though this is expected to be small. A minimum mass flow rate of 0.09 g/s is indicated by Eq. (1) using the baseline dipole synchrotron heat $Q = 2.17$ W. The mass flow required for an upgrade to 3 times baseline current ($Q = 6.51$ W) is 0.25 g/s.

2.3 Inlet Pressure

The flow pattern within the magnet string is governed by the obvious need to be able to assemble the liner with relative ease. Any interconnect assembly procedure for a liner in which the flow tube passes straight through each component is exceedingly complex and labor intensive. Consequently, a return flow pattern has been chosen. Return flow refers to the fact that the liner trace tube penetrates the bore tube of a given component at the lead end, travels the length of that component, makes a 180 degree bend (still in the bore tube) and returns to the lead end where it exits the bore tube. The trace tube supply leg is thermally anchored to the liner by brazing, while contact between the return leg and the liner is kept to a minimum. Flow passes to each successive component through a cooling leg which is clipped to the outside of the 80 K supply line.

Heat exchange between the 80 K line and the cooling leg is accomplished by wrapping the cooling leg around the shield line, creating a small heat exchanger (approximately 5 coils) in the interconnect. The cooling leg diameter is large enough (1 cm) that it does not contribute significantly to the total pressure drop.

A kidney-bean shaped cross section has been chosen for the trace tube to maximize use of the limited radial space. The flow cross section and hydraulic diameter of the trace tube are determined by parametric study of their effects on required inlet pressure, stresses in the tubing wall, and radial space budget. The result is a trace tube with a hydraulic diameter of 4.2 mm and a cross sectional area of 26 mm^2. A flow path the length of a string has been chosen. This allows the flow to be controlled from a single point and minimizes the number of cryostat penetrations.

The pressure gradient for a compressible gas with heat transfer can be approximated at low velocities by,

$$dP/dx \ = \ (-2m^2 f/\rho A^2 d) + (4\rho q m \beta / A d C_p), \tag{2}$$

where m is the mass flow rate, f the friction factor, q the heat added or rejected, β the bulk compressibility, C_p the specific heat, A is the cross sectional area of the flow tube and d is the diameter. The second term in Eq. (2) is only important when q is large. The heat absorbed by the liner (even at upgrade intensity) is relatively small, and since heat is alternately absorbed and rejected in each component, the term will alternate in sign and cancel over the full length of a string.

Equation (2) is integrated over the effective length of trace tube (L) in a half cell, using the ideal gas law, to yield the outlet pressure (P_o) at the end of each half cell,

$$P_o = [(P_i^2) - (4m^2 fRTL/A^2 Md)]^{1/2} \quad (3)$$

where P_i is the inlet pressure, R is the universal gas constant, T is the temperature, and M is the atomic weight of helium. The length of pipe attached to the 80 K shield contributes a negligible amount to the pressure drop. The effective path length used in Eq. (3), then, is twice the length of a half cell (180 m).

It is instructive to calculate the outlet pressure for each half cell in a string and plot it versus its position in the string. The result is shown in Figure 2. The pressure drop is approximately linear near the inlet end of a string, but drops off very rapidly near the outlet end. If the inlet pressure is not high enough, interconnect effects, which have not yet been accounted for, can combine to reduce the mass flow rate below the desired level.

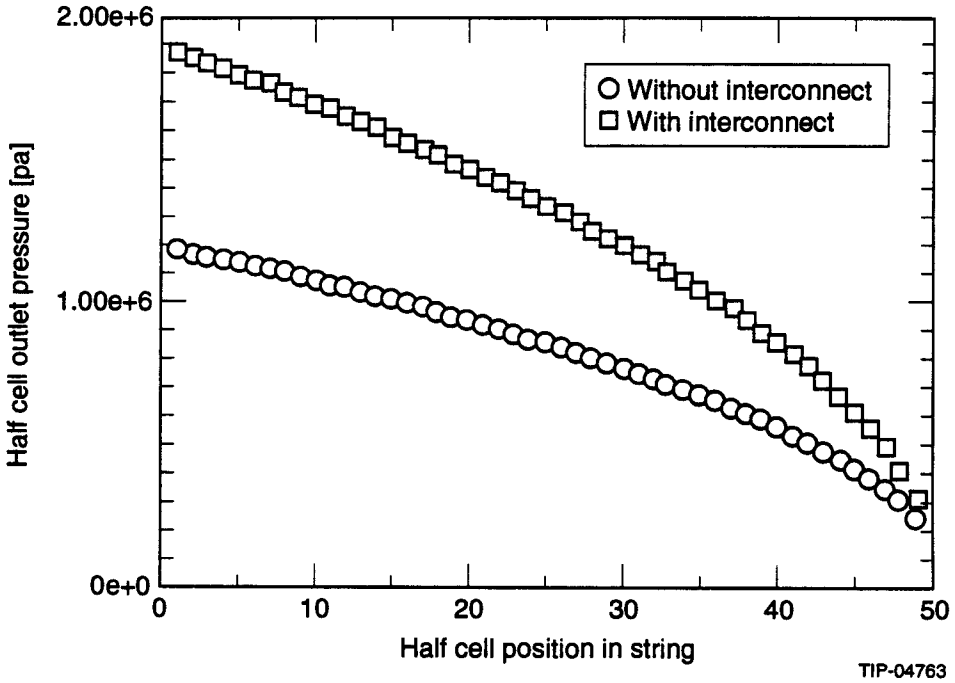

Figure 2. Half Cell Outlet Pressure as a Function of Position in String. There are 48 half cells in a string. Note that the required inlet pressure is much higher when interconnect effects are taken into account.

Interconnect effects are difficult to calculate. An estimate is arrived at as follows. Each interconnect is comprised of approximately 10 right angle bends, 2 expansion loops and at least one heat exchanger. The total length of piping is on the order of 3 to 4 meters. In the case of curved pipes and elbows the friction factor can be as much as an order of magnitude larger than it is in the same diameter straight tube. Thus, the additional pressure loss incurred in the interconnect region can be estimated by integrating Eq. (2) over an additional 30 to 40 meters of length for each interconnect in the half cell.

Admittedly, this is a worst case scenario. The interconnect piping may have a larger diameter than the 4.2 mm hydraulic diameter of the liner tubing, and friction factors may only be on the order of five times those in straight tubing. It is the uncertainty of these parameters, however, that dictates the conservative nature of the estimate.

Pressure drop calculations for a fixed mass flow rate of 0.25 g/s with and without interconnect effects are included in Figure 2. The results indicate that an inlet pressure of 1.2 MPa is sufficient if interconnect effects are ignored. Estimates including interconnect effects show that they can drive the necessary inlet pressure as high as 1.9 MPa, which is higher than what is available from a Sector Refrigeration Station. The consequences of this result are discussed in a later section entitled.

3.0 HEAT LOADS

In order to be of positive cryogenic value, the fixed heat load of the liner must be smaller than that portion of the dynamic heat load that it removes to the LN_2 system. The 4 K dynamic heat load, Table 1, arises from of a number of contributions. The primary source is the synchrotron radiation, which is generated in the dipole magnets. Other, much smaller, contributions result from splices in the power bus, microwave heating of the beam tube wall and collisions between beam protons and residual gas in the vacuum space.

The liner will intercept a significant fraction of the total dynamic heat load, including all the synchrotron radiation, the microwave heat, and approximately 17% of the beam/gas interaction heat. Table 2 gives a breakdown of the heat intercepted by the liner on a per component basis.

The fixed heat load budget of the liner has been set at 1 Watt per dipole, approximately one-half the nominal synchrotron radiation load. Details of the fixed 4 K heat budget are shown in Table 3. By far the largest heat load arises from the support system, so that half of the budget is allocated to it. Additional heat loads arise from thermal radiation, end conduction through interconnect pieces where the trace tube penetrates the 4 K bore tube, and conduction through the beam position monitor (BPM). Consideration is given to each in the following paragraphs.

TABLE 1. ORIGINS OF THE DYNAMIC HEAT LOAD.[1]

	DIPOLE	QUADRUPOLE	SPOOL	HALF CELL
Synchrotron Radiation	2.17	-	-	10.85
Splices	0.14	0.22	0.08	1.0
Microwave	0.2	0.17	0.17	1.34
Beam/gas	0.14	0.05	0.04	0.79
Total	2.65	0.44	0.29	13.98

TABLE 2. PORTION OF DYNAMIC HEAT LOAD INTERCEPTED BY LINER.[1]

	DIPOLE	QUADRUPOLE	SPOOL	HALF CELL
Synchrotron Radiation	2.17	-	-	10.85
Splices	-	-	-	-
Microwave	0.2	0.17	0.17	1.34
Beam/gas	0.024	0.009	0.007	0.136
Total	2.39	0.18	0.18	12.33

TABLE 3. FIXED LINER HEAT BUDGET.

	DIPOLE	QUADRUPOLE	SPOOL	HALF CELL
Supports	0.5	0.5	0.3	3.30
IR Radiation	0.2	0.06	0.04	1.1
Interconnects	0.05	0.05	0.05	0.35
BPM	-	-	0.26	0.26
Total	0.75	0.61	0.65	5.01

3.1 Mechanical Supports

The mechanical supports must be optimized to provide accurate centering of the liner within the bore tube while having minimal cross section for heat transport. Because the supports are located in the beam tube they must also be radiation resistant. This requirement precludes the use of insulating composites like G-10. Other material candidates, such as polyimides, have been shunned because relatively little is known of their low temperature radiation resistance, thermal conductivity, or mechanical properties. Thus a prototype support consists of four stainless steel legs, each with a rectangular cross section, approximately 6 mm × 1.2 mm thick. The legs are bent slightly in the middle, as shown in Figure 1, in order to position the liner concentric to the bore tube. To provide the necessary rigidity, support legs must be less than 17.2 cm long, have both ends welded to the liner, and be spaced at 2 m intervals.

The resistance to heat flow of each leg is the sum of the stainless steel resistance and the contact resistance between the support and bore tube. Neglecting contact resistance for the moment, the heat leak through a single leg is given by

$$Q = 2A/l \int k dT \tag{4}$$

where A is the cross sectional area of a support leg, l is half the leg length and k is the thermal conductivity of stainless steel. The integral is evaluated from 4 K to 80 K, and predicts a heat load of 0.06 W per leg. Assuming that all four legs are in contact with the bore tube, this results in a heat load of 0.12 W/m, which is less than the baseline synchrotron radiation load but more than the fixed heat load budget. Since the material and geometry of the support are more or less fixed by other considerations, the contact resistance is the only remaining design parameter with which to reduce the heat load. Contact resistance can be expressed as,

$$R_{\text{contact}} = f(\Delta T, k, F, G) \tag{5}$$

where ΔT is the temperature difference across the contact, k is the mean thermal conductivity of the materials in contact, F is the force with which the contacts are pressed together, and G is a geometric factor related to surface roughness. In general, R_{contact} is not well known. For this reason, tests were conducted to measure both the heat leak of a prototypic support and the average resistance of a stainless to stainless contact.

The total heat leak as a function of liner temperature for a number of cases tested is shown in Figure 3. Scatter in the data indicates the contact resistance is reproducible to approximately ±15%. In addition, oxide on the "as delivered" contact surfaces seems to have little effect on the heat leak, as expected for the rough contact surfaces tested.

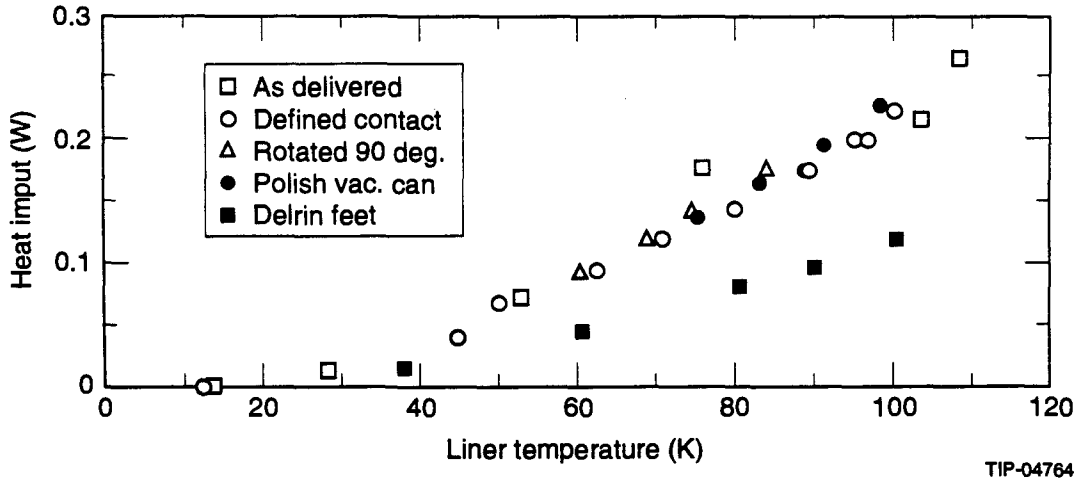

Figure 3. Measured Heat Load of a Mechanical Support Prototype, as a Function of Liner Temperature.

For a liner temperature of 80 K, the measured heat leak is 0.04 W per leg, a reduction of 30% from the estimate obtained by neglecting contact resistance.

To determine the heat load of the dipole support system it is necessary to know how many legs will be in contact with the bore tube and what the contact force will be. The contact force (F) in the collider will be determined by three factors: first, preloading by compression of the supports at the time of insertion in the bore tube, second, further loading or unloading of support legs due to differential contraction on cooldown, and third, compression of the lower legs and unloading of the upper legs due to the weight of the liner. Currently, it is believed that no preloading will be required.

The effects of differential contraction can be estimated by considering the following simple model of a dipole support (refer to Figures 4a and 4b).

Let:

l	=	length of one half dipole support leg
l'	=	length of liner between end of support leg and point of contact
r	=	thickness of radial gap
D	=	inner diameter of bore tube
d	=	outer diameter of liner
Δr	=	effective change in radial gap due to differential contraction

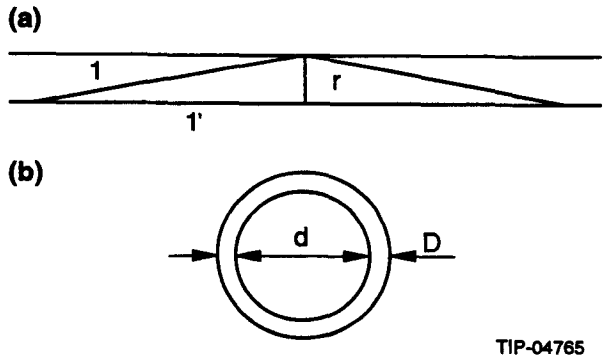

Figure 4. Model of Differential Contraction Between Liner Support and Bore Tube.

Assume:

(1) support leg has triangular shape (Figure 4a)
(2) average temperature along support leg is 70 K
(3) liner temperature is 80 K

Then:

$$\Delta r = [(l + \Delta l)^2 - (l'+\Delta l')^2]^{1/2} - r - (\Delta D - \Delta d)/2, \qquad (6)$$

where a positive value of Δr indicates compression on cooldown and a negative value indicates retraction. Results for dimensions that correspond to the test rig and the ASST dipole bore tube are given in Table 4. They show that additional compression upon cooldown does not occur, and that, nominally, only two support legs will be in contact with the bore tube during collider operation.

TABLE 4. CALCULATED RESULTS OF DIFFERENTIAL CONTRACTION FOR THE TEST RIG AND A 43 mm BORE TUBE WITH A 33 mm LINER.

	TEST RIG (mm)	ASST (mm)
l	65.00	86.00
r	5.00	5.00
l'	64.807	85.855
D	43.00	43.00
d	33.00	33.00
Δl	–0.187	–0.247
$\Delta l'$	–0.182	–0.241
ΔD (4 K)	–0.132	–0.132
Δd (80 K)	–0.093	–0.093
Δr	–0.048	–0.10

The contact force expected in the collider can be calculated, then, from the weight of the liner. The liner has a mass of approximately 1 Kg/m, so that supports spaced every two meters will experience a force of 20 N. This will be divided evenly between the two lower legs located at 45° to the vertical. The resultant contact force due to liner weight is 14 N per contact. This is the approximate contact force applied during the heat leak tests.

Finally, to calculate the dipole support heat load, the data in Figure 3 is used together with the assumption that only two legs of the support will be in contact with the bore tube. In practice, the liner temperature may be as high 90 K, so that the heat leak through a single leg is taken to be 42.5 mW. Then, given 8 supports per dipole, the heat load of the support system is 0.68 W per dipole. The result is listed in Table 5 where the heat load of the current design is tabulated for comparison with the budget (Table 3).

The support system of the quadrupoles and spools is different from that of the dipoles because of the end cooling scheme, which is necessitated by limited radial space in the smaller bore quads and spools. The supports in these components are stainless steel buttons 2 mm thick and 2 mm in diameter.

To calculate the heat leak through Quad/Spool supports the thermal resistance of the button itself is neglected and only the contact resistance is considered. The contact force will be approximately the same as in the dipoles so that the contact conductance measured in the heat leak tests is used.

In the test it was found that

$$h_c = \alpha T^n, \tag{7}$$

where $n = 1.5$ and $\alpha = 0.75$. Using these values and Eq. (7) in

$$Q_i = A_c \int h_c \, dT, \tag{8}$$

and assuming an average liner temperature of 90 K, a heat leak of 0.24 W per contact is predicted. Again it is assumed there will only be 2 contact points per support. The length of a quad is taken to be 5 m and that of a spool 3 m. Predicted heat leaks per quad and per spool are included in Table 5 together with those for the dipoles.

TABLE 5. FIXED LINER HEAT LOAD (CURRENT DESIGN).

	DIPOLE	QUADRUPOLE	SPOOL	HALF CELL
Supports	0.68	1.20	0.70	5.30
IR Radiation	0.30	0.10	0.06	1.66
Interconnects	0.05	0.05	0.05	0.35
BPM	-	-	0.26	0.26
Total	1.03	1.35	0.87	7.57

Finally, it is well known that stainless sliding on stainless can lead to galling. This behavior raises concerns regarding the result of sliding a support the length of a dipole on insertion of the liner into the bore tube. To solve this problem it is suggested that an electrically insulating material be put on the contact area of each support. Possible materials include: polyimides, specially manufactured composites and ceramics such as silica, alumina, and zirconia. Methods of attaching these materials need to be studied. Two possibilities that have been considered to date are (1) coating the contacts by sputtering or some similar technique (2) attaching machined buttons, perhaps by press fitting.

In order to test the effect of buttons on the heat leak, each contact point of a dipole support was fitted with a Delrin button. The data are included in Figure 3. Although Delrin is an unacceptable material for use in the bore tube, the data give an indication of the effect of attaching some sort of plastic buttons to the supports should an acceptable material be identified. In this case the heat leak is reduced by approximately a factor of two.

3.2 Radiation

The radiant heat exchange between two bodies is given by,

$$Q = \sigma E (T_H^4 - T_C^4), \tag{9}$$

where E is a function of the emissivities and geometry of the bodies in question. For concentric cylinders

$$E = \{(1/A_i e_i) + (1/A_o)(1/e_o - 1)\}^{-1}. \tag{10}$$

The subscripts refer to the inner and outer cylinders, e is the emissivity and A the surface area. In general the emissivity of a material is a function of temperature and surface preparation.

The heat transferred by radiation between a stainless steel surface at 77 K and one at 4.2 K has been measured by Obert *et al.*[2] The results for a variety of surface preparations are reported in terms of emissivities, and reproduced in Table 6.

TABLE 6. EMISSIVITY OF STAINLESS STEEL FROM OBERT. *et al.*[2]

SURFACE PREPARATION	EMISSIVITY BETWEEN 77 K AND 4.2 K
As Found	0.120 ± 5%
Mechanically Polished	0.074 ± 5%
Electro. Polished	0.065 ± 5%
Silver Plated	0.013 ± 5%

To determine the radiation heat load of an 80 K liner, it is necessary to include the effect of holes in the liner tube and cryosorber on the bore tube. To account for these effects, an average emissivity for the liner (e_L) and one for the bore tube (e_B) is defined. Each is taken to be the weighted average of the appropriate stainless steel emissivity (e_{ss}) and the hole (e_h) or cryosorber (e_c) emissivity. Further, the liner holes and cryosorber are both assumed to have an emissivity of 1. The resulting average emissivity of each tube is a linear function of the fraction of surface coverage (f_h) or (f_c).

$$e_L = f_h + (1 - f_h) e_{ss}, \tag{11}$$

$$e_B = f_c + (1 - f_c) e_{ss}. \tag{12}$$

To evaluate Eq. (9) it is necessary to know the bore tube and liner tube diameters, the surface preparation of the stainless steel, the number and size of holes in the liner and the surface area of cryosorber. The last two numbers are not well known. The fraction of holes may vary up to 0.05, while the fraction of cryosorber coverage may be as high as 0.15. Unfortunately, if (f_h) and (f_c) turn out to be near the maximum of their respective ranges, they will dominate the radiated heat leak. This is especially true in the case of the cryosorber. To get some idea, assume a 33 mm liner, a 42 mm bore tube, $f_h = 0.05$ and $f_c = 0.15$. This arrangement will radiate 0.6 W/dipole with as found stainless, and 0.4 W/dipole with electro-polished stainless. For the same geometry, reducing the hole coverage to 0.03 and the cryosorber coverage to 0.1 reduces the respective heat leaks to 0.5 W/dipole or 0.3 W/dipole. This last number is probably achievable, and is recorded in Table 5 as the current design. However, it is still twice the budgeted amount.

In order to meet the budget, hole and cryosorber coverages would have to be reduced to zero and electro-polished stainless used. Only the silver plated stainless has an emissivity low enough to meet the budget for any significant cryosorber coverage.

3.3 Interconnects

Calculation of the interconnect heat load is detailed elsewhere in this report. The result, included in Table 5, is equal to the budgeted heat leak of 0.05 W.

4.0 BPM

Two possibilities exist for the BPM. A 4 K model and an 80 K model. Details are included in another section of this report. It is unclear at this time exactly what the BPM heat load will be, the load reported in Table 5 just assumes it meets the budget.

5.0 IMPACT ON EXISTING SYSTEMS

A cryogenically cooled liner requires a constant supply of high pressure helium gas. While the mass flow rate is small (0.25 g/s for an 80 K liner), the path length is long and the tube diameter small. The flow scheme chosen represents a flow path more than 3 times the nominal length of a string, or approximately 13 km. For two-thirds of that length the hydraulic tube diameter is 4.2 mm. Thus, a high pressure at the inlet to the string is required.

The highest pressure available from a Sector Refrigeration Station (SRS) is 1.7 MPa at the discharge of the compressors. However, during normal collider operation this pressure can float as low as 1.3 MPa. Thus, the available pressure may not be adequate to supply the required mass flow rate of 0.25 g/s, and will not supply a constant mass flow rate unless a more complex control system is added to the liner.

In addition, use of the SRS compressors to supply a liner requires design modifications of the main cold box, the CCWP, the transfer lines, and the tunnel distribution box. The main cold box must have a spigot from which to obtain 1g/s flow. The CCWP must be modified to allow purging of the liner flow tube. Necessary transfer line modifications include the addition of holes in the stainless steel piping supports to accommodate the liner tube, and clips on the 80 K supply line for securing the liner tube. The distribution box must have additional internal piping, appropriate valving, and bayonet connections added at the outlet.

Since specification of the Sector Refrigeration Stations has progressed to the point that inclusion of the above features would require costly design changes, and since the compressor discharge pressure will not provide a constant mass flow rate without the addition of a complex control system, it is concluded that a cryogenically cooled liner must have an independent supply of helium.

Figure 5 illustrates one concept for the integration of a cryogenically cooled liner, into a Sector Refrigeration Station. A small compressor on the surface provides 1 g/s of helium gas at a discharge pressure of 1.7 MPa and a temperature of 300 K. A warm transfer line carries the gas to the tunnel where it is cooled to 80 K, and passes through a purifier. Purifying the gas before it enters the magnet string is important because the diameter of the flow tube is small. There are many bends in the interconnects where kinks in the line can occur and frozen impurities may collect. Finally, the gas flows from the purifier, through a valve box, to each of the four strings.

Entry to each string can conceivably be gained through the first interconnect, in order to eliminate the need for a redesign of the feed spools. At the end of each string, the last interconnect can be modified to provide for connection of a return line. The flow is then routed through the return line into the warm header and returned to compressor suction. The liner flow will increase the total flow in the warm header by 1 g/s and should not be a problem. The return line contains the necessary valves for adjusting the flow rate and dropping the line pressure to the header pressure.

During steady state operation of the collider an 80 K liner replaces the 4 K dynamic heat load of the synchrotron radiation with a fixed heat load independent of the beam intensity. The heat load budgets for operation at baseline intensity with and without a liner are compared in Table 6. The impact on the 4 K system is to lower the heat load by one half the nominal amount of the synchrotron radiation.

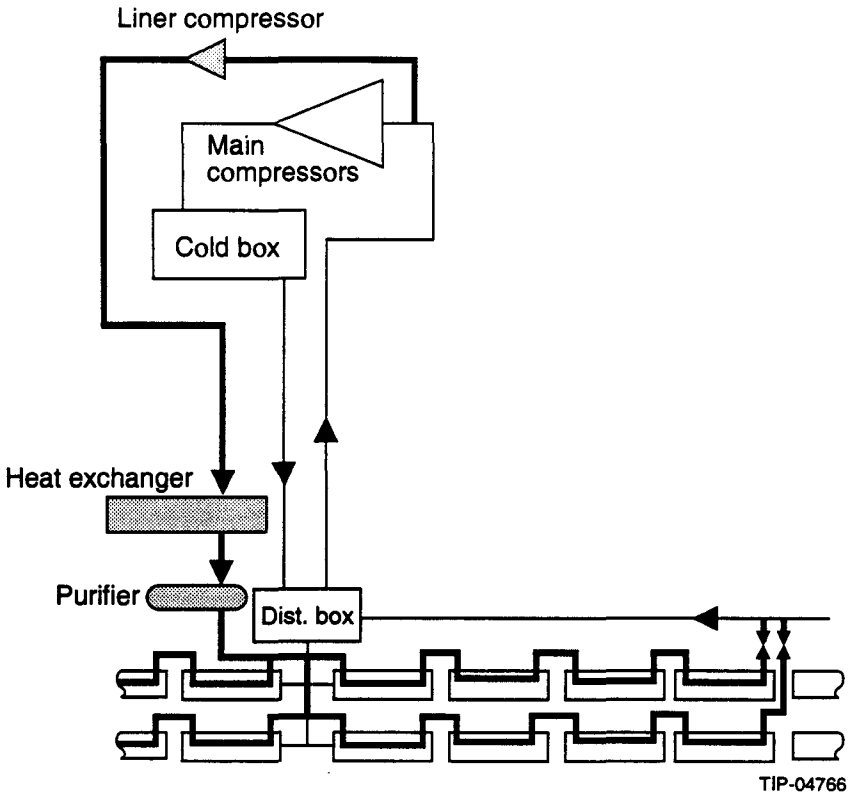

Figure 5. Schematic Representation of an 80 K Liner Integrated into a Sector Refrigeration Station.

Comparison of the heat load budgets for 10 times baseline intensity is also contained in Table 7. The 4 K heat load remains constant, the 20 K system is nominally unaffected, and the 80 K system, in the worst case, absorbs the entire synchrotron radiation load. Thus, the 80 K load is increased by 8.5 kW or approximately 13%. Since the LN_2 system has 4.4 kW of unallocated capacity, the net required increase in cooling capacity is only 7%. However, piping in the nitrogen system is just large enough to handle the baseline. It therefore is likely that the addition of an 80 K liner would require additional nitrogen pumps and recoolers to keep the average temperature at 85 K.

TABLE 7. 4 K HEAT LOADS —WITH AND WITHOUT A LINER.[1]

	BASELINE LUMINOSITY		10 × BASELINE LUMINOSITY	
	Without Liner	With Liner	Without Liner	With Liner
Static	1227	1227	1227	1227
Dynamic	2682	1478	7046	1478
Distribution	1491	1491	1491	1491
Total	5400	4196	9764	4196

A liner is expected to have minimal impact on operating procedures. Cooldown should be largely unaffected, since it will take place in parallel with cool down of the entire cold mass. It is not clear whether similar arguments apply to the warm up procedure. It is clear, however, that the liner tube will need to be purged before cooldown. Steady state operating procedures have not been considered in detail, but would be worked out for a system test, should one be initiated. Likewise what the response of the liner to upset conditions such as a quench or an up-to-air accident have not been studied, but would necessarily be included as part of a system test.

6.0 SYSTEM TEST

There are enough uncertainties and unknowns in the calculations, the operating procedures, and the response to upset conditions discussed above, that a system test in a string of magnets similar to the ASST is imperative prior to finalizing a design. In addition, the complexity of the design raises questions about installation procedure and reliability of operation. From a cryogenic point of view, the large number of bore tube penetrations increases the probability that unexpected thermal shorts from 80 K to 4 K will occur. Therefore, a cold test to measure the heat leaks associated with a half cell of liner is important.

Some preliminary work has been done on the integration of a liner into the ASST, using the ASST refrigerator. A schematic diagram is shown in Figure 6, where it is assumed that a full cell of magnets is in place and that the liner is to be inserted in the second half cell. The inlet pressure required to provide 0.25 g/s mass flow in a half cell of magnets is obviously much less than that required for flow through a string (48 half cells). The supply of helium can thus be taken from the discharge of the ASST refrigerator compressors.

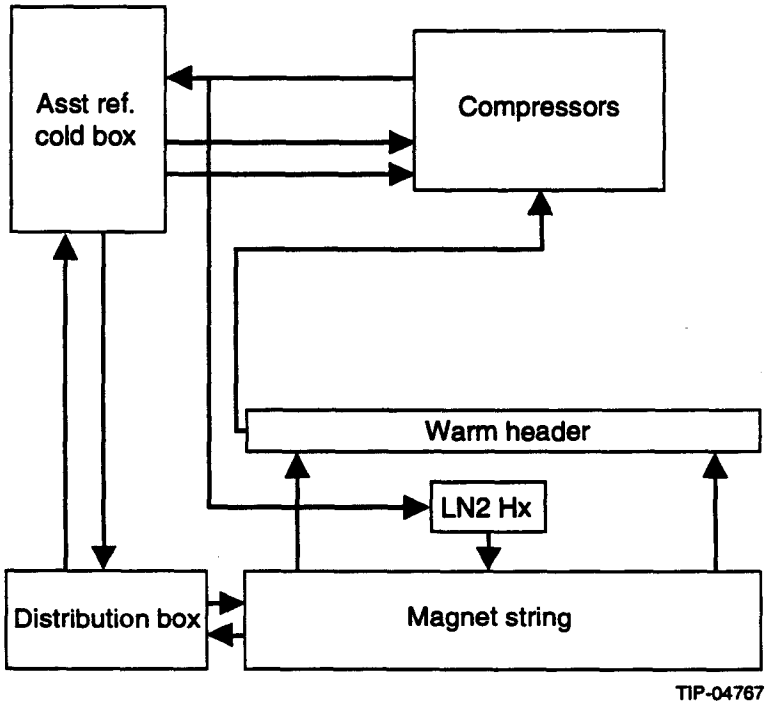

Figure 6. Schematic of Cryogenic Circuit for Testing an 80 K Liner in the ASST.

Figure 6 shows a warm supply line carrying high pressure helium gas from the compressors to the niche of the string building where it passes through an 80 K heat exchanger and a purifier before being transferred to the string. A shell and tube heat exchanger with a boil-off rate of 6 L/hr of LN_2 is sufficient to cool 0.25 g/s of room temperature helium to 80 K. An actively cooled U-tube from the heat exchanger

to the string keeps the helium temperature at 80 K. This could be accomplished by venting the shell side of the LN_2 heat exchanger through a trace tube that runs along the process line of the U-tube. Finally, the U-tube is connected to the magnet string through a 0.75" bayonet at the first interconnect of the second half cell.

Flow continues down the string, with the 80 K shield leg in each component being inserted directly into the LN_2 line in each cryostat. The helium flow exits the string at the last interconnect before the end spool and is tied, through a flow controller and J-T valve, to the warm header in the string building.

7.0 SUMMARY

The impact of heat load redistribution and the mechanical design of an 80 K liner on a sector refrigeration station have been considered. Pressure drop analysis of the liner cooling circuit, and consideration of the current design status of the sector refrigeration stations indicate that the supply leg of the circuit should be virtually independent of the refrigerator. In this way the impact of the liner will be minimal. Operating procedures have not been considered in detail, but the liner appears to have no adverse effect on cooldown warmup or steady state operation of the refrigerators.

A comparison of calculated heat loads from all sources, as shown in Table 5, with the fixed liner budget shown in Table 4, indicates that the total heat load is about a factor of 1.5 over budget. This stems primarily from an incomplete design for the support system and to a lesser extent from questions concerning surface treatments as they relate to thermal radiation loads.

With the present dipole support design, *i.e.*, no preloading of supports, it appears that only two legs will be in good contact with the bore tube. As a consequence, it is expected that the heat leak per dipole will be 0.68 W or 36% over budget. The heat leak through quadrupole and spool supports is determined primarily by the contact resistance, and is also over budget. In addition, it has been pointed out that this may not be the most conservative estimate. Given that there will be tolerances in the bore tube, liner, and support diameters, it may not be entirely correct to assume only two legs of a support are in contact with the bore tube. If some fractional number of legs is in contact, the heat load will go up proportionately. It is likely, however, that attaching an insulating coating or buttons to the contact points of each support will significantly reduced the heat load. This should be done for assembly purposes as well. As a consequence, the support design and development should be considered incomplete.

In the case of radiation, it is not clear that the savings generated by meeting the heat load budget will offset the cost of surface treatments required to reduce the stainless steel emissivity to an acceptable level. A cost optimization is necessary in this case.

REFERENCES

1. R. Than, S. Abramovich, and V. Ganni, "The SSC Cryogenic System Design and Operating Modes," SSC Cryo Note 92-12 (1992).
2. Obert *et. al.*, "Emissivity Measurements of Metallic Surfaces used in Cryogenic Applications," *Adv. Cryo Eng.*, **27**:293 (1982).

This Page Intentionally Left Blank

SECTION 3

Thermal Model and Associated Novel Approach for Synchrotron Radiation Liner with End Cooling

Q. S. Shu, K. Yu, W. Clay, J. Maddocks,
D. Martin, G. Morales, and J. Zbasnik

SECTION 3

Thermal Model and Associated Novel Approach for Synchrotron Radiation Liner with End Cooling

Quan-Sheng Shu, Kun Yu, Wayne Clay, Jim Maddocks, Don Martin,
and Gilberto Morales

Superconducting Super Collider Laboratory*
2550 Beckleymeade Avenue
Dallas, Texas 75237 USA

Abstract

An end-conductive cooling approach has been developed to reduce the radial space budget of a synchrotron radiation liner to permit the maximum possible liner tube inner diameter (ID). A thermal model has also been developed to analyze the thermal performance of such liners. This approach has been found to be acceptable for a liner in a 5 m long quadrupole magnet and 3 m long spool piece, but not for a longer 15 m dipole. The heat transfer and temperature distribution were calculated respectively along the axes of two different liner models: 20 K and 80 K liners with different thicknesses (0.5–2 mm) of liner tubes and different emissivities (0.05–0.3) of liner surfaces for a variety of magnets. The thermal model has also been applied to the case of an 80 K liner connected directly to a 4 K beam position monitor (BPM). In order to utilize the end cooling, a good thermal joint and a compact heat exchanger have been designed. Also, the case of an 80 K Liner with an 80 K BPM is briefly discussed.

* Operated by the Universities Research Association, Inc., for the U.S. Department of Energy under Contract No. DE-AC35-89ER40486.

1.0 INTRODUCTION

A uniform and maximum possible liner inner diameter (ID) is needed due to: (1) particle beam commissioning, (2) particle beam dynamic stability, and (3) safety margin of impedance. However, the maximum liner ID is constrained by: (1) the available magnet beam tube inner diameter (ID), and (2) the minimum liner radial space. Using regular cooling, the minimum liner radial space is 6 mm, and using end-conducting cooling, the radial space needs to be 3.5 mm. The 80 K synchrotron radiation liner prototype was designed to be tested at the SSCL Accelerator System String Test (ASST) facility. In the case of the 80 K ASST liner, the 25.3 mm design was chosen for the maximum liner ID.

Since the magnet quench-induced Lorentz pressure on a CQM liner is much smaller than that on a CDM liner, the pure copper tube was chosen for the CQM liner material. The RRR and thickness of the copper tube must be of sufficient value due to requirements for both the resistance wall (conductivity × Thickness > $2 \times 10\ \Omega^{-1}$) and for the conducting heat transfer. However, the RRR and thickness should not be too large in order to reduce the Lorentz pressure. This paper will focus on the thermal model used to predict the thermal performance of an end-cooling liner for different cases.

2.0 THERMAL MODEL AND RESULTS FOR END-CONDUCTIVE COOLING

An end-conductive cooling approach for the Spool Piece and CQM is shown in Figure 1. The 80 K GHe flows through a compact heat exchanger located at each end of the liner tube outside of the CQM cold mass. The rest of the liner tube is refrigerated by thermal conduction. A compact heat exchanger and a good thermal conducting joint are designed to utilize the end cooling approach and to assure an easy assembly.

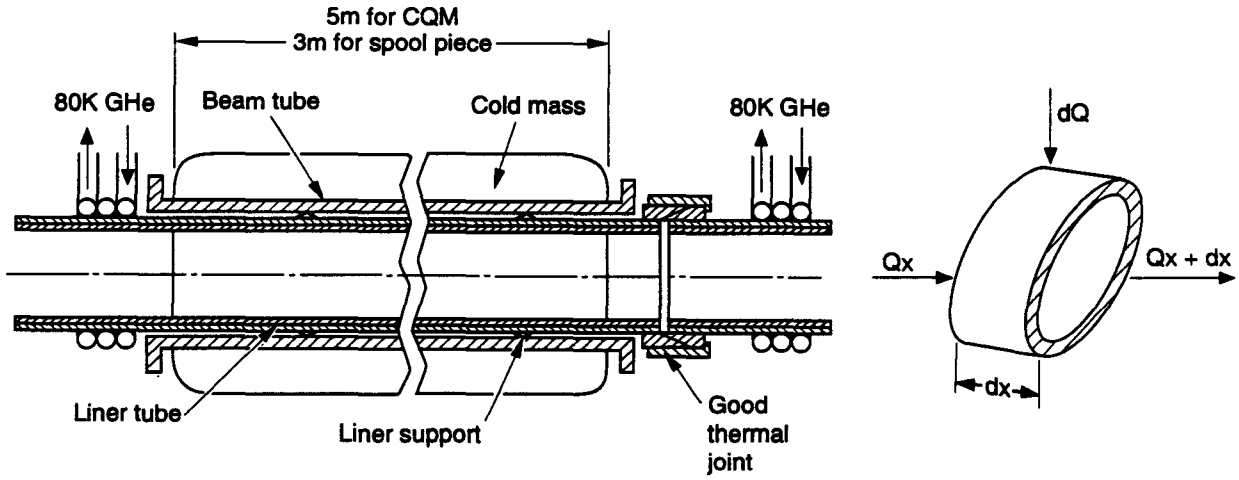

Figure 1. Schematic Drawing of a Liner with End-Conducting Cooling.

A thermal model to analyze the end-conductive cooling was developed by Q. S. Shu and K. Yu,[1,2] assuming: Q_1 = represents synchrotron radiation, 0.14 w/m; Q_L = (heat leak through supports)/2L; Q_r = (heat leak by radiations)/2L; L the half length of the CQM or the length of the Spool Piece; A the cross section area of the liner tube; $\lambda(T)$ the heat conductivity; $\lambda(80)_{Cu} \approx 5.50$ w/(cm·K); $\lambda(80)_{snl\ stl} \approx 0.08$ w/(cm·k); and ε_1 and ε_2 the emissivity,[3] as shown in Figure 1:

$$dQ = (Q_1 - Q_L - Q_r)dX, \tag{1}$$

if $q = (Q_1 - Q_L - Q_r)$,

$dQ = qdX$,

$$Q_X = -\lambda(T)\, A\, dT/dX, \tag{2}$$

and $Q_{X+dX} = -\lambda(T)\, A\, d[T + (dT/dX)dX]/dX$

$$= -\lambda(T)\, A\, [dT/dX + (d^2T/dX^2)dX]. \tag{3}$$

We know $Q_{X+dX} = dQ + Q_X$ (4)

$$-\lambda(T)\, A[dT/dX - (d^2T/dX^2)dX] = qdX - \lambda(T)\, A\, dT/dX$$

$$-\lambda(T)\, Ad^2T/dX^2 = q$$

$$d^2T/dX^2 = -q/[\lambda(T)A]. \tag{5}$$

We can get the equation,

$$T(X) = -\{\, q/[2\lambda(T)A]\,\}\, X^2 + C_1X + C_2, \tag{6}$$

with boundary conditions:

$$T(X)|_{X=L} = 80\ K; \qquad T(X)|_{X=-L} = 80\ K.$$

We obtain $80 = -\{\, q/[2\lambda(T)A]\,\}L^2 + C_1L + C_2,$ (7)

$$80 = -\{\, q/[2\lambda(T)A]\,\}L^2 - C_1L + C_2. \tag{8}$$

Equations (2) and (3) give: $C_1 \equiv 0$ (9)

$$\therefore\ 80 = -\{\, q/[2\lambda(T)A]\,\}L^2 + C_2$$

$$\therefore\ C_2 = \{\, q/[2\lambda(T)A]\,\}L^2 + 80. \tag{10}$$

Substitute Eqs. (4) and (5) into (1):

$$T(X) = -\{\, q/[2\lambda(T)A]\,\}X^2 + \{\, q/[2\lambda(T)A]\,\}L^2 + 80 \tag{11}$$

$$\Delta T(X) = T(X) - 80$$

$$= -\{\, q/[2\lambda(T)A]\,\}X^2 + \{\, q/[2\lambda(T)A]\,\}L^2$$

$$= -\{\, (Q_1 - Q_L - Q_r)/[2\lambda(T)A]\,\}X^2 + \{\, (Q_1 - Q_L - Q_r)/[2\lambda(T)A]\,\}L^2. \tag{12}$$

We assume that two planes' areas are the same and are parallel. Their emissivities are separately ε_1 and ε_2. The temperatures are separately T_1 and T_2. The mean of the heat transfer by radiation per unit time is Q_r.

We must take:

$$Q_r = \sigma A\, (T^4_1 - T^4_2)\, \varepsilon_1\varepsilon_2/(\varepsilon_1 + \varepsilon_2 - \varepsilon_1/\varepsilon_2)\, 2L. \tag{13}$$

The mean of the heat leak through the supports per unit time is Q_L, N is the number of supports, and J' is the length of a support.

We must take:

$$Q_L = (N/2L)\cdot(A/J')\cdot\int\lambda(T)dT. \tag{14}$$

Using the model: 1) The temperature distribution along the liners as functions of both the emissivities and the tube thicknesses were calculated. 2) The maximum ΔT could be less than 5 K for the Spool Piece liner and less than 10 K for the CQM. 3) The temperature difference between the Spool Piece pipe ends and the middle of the liner is 2 K when a copper layer of 2 mm is used and 10 K with a copper layer of 0.5 mm. 4) A CQM ΔT of 6 K is obtained with a copper layer of 2 mm, and 26 K with a copper of 0.5 mm. 5) The correction of the effect of the magnetic field on copper thermal conductivity is considered. Figures 2–5 show some of the calculated results.

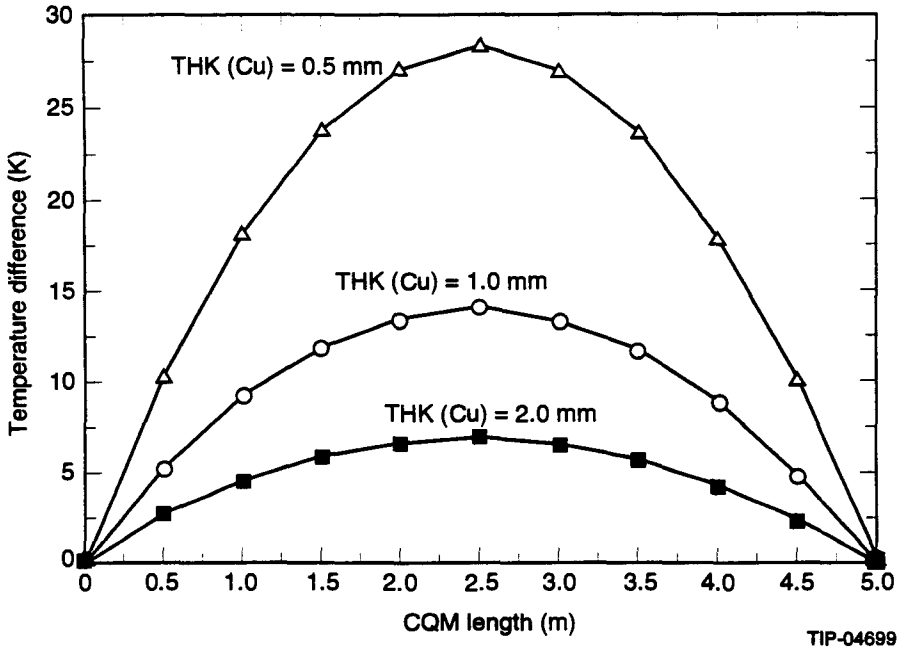

Figure 2. Temperature Distribution of 80 K Liners (CQM) as Function of Liner Tube Thicknesses.

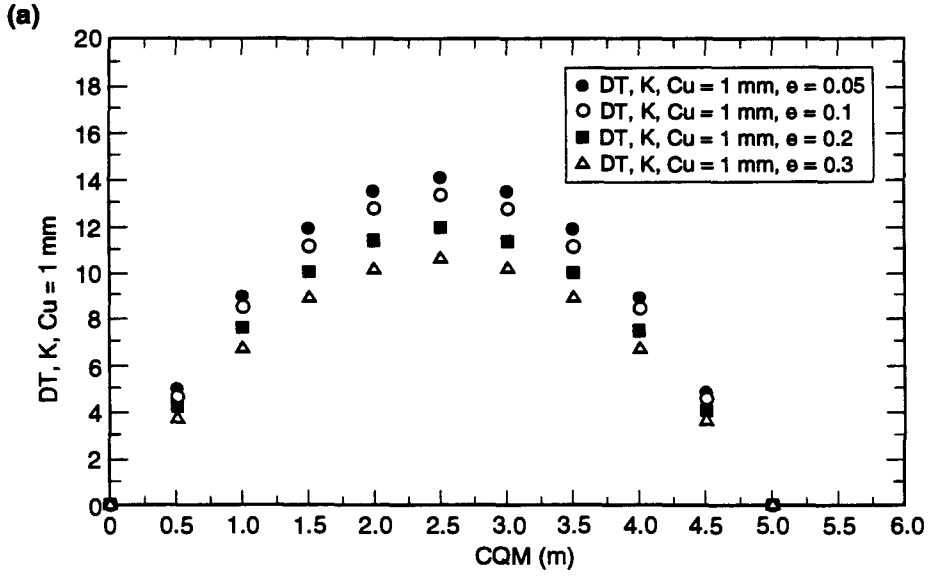

Figure 3(a). Temperature Distribution of 80 K Liner as Function of CQM Liner Surface Emissivity.

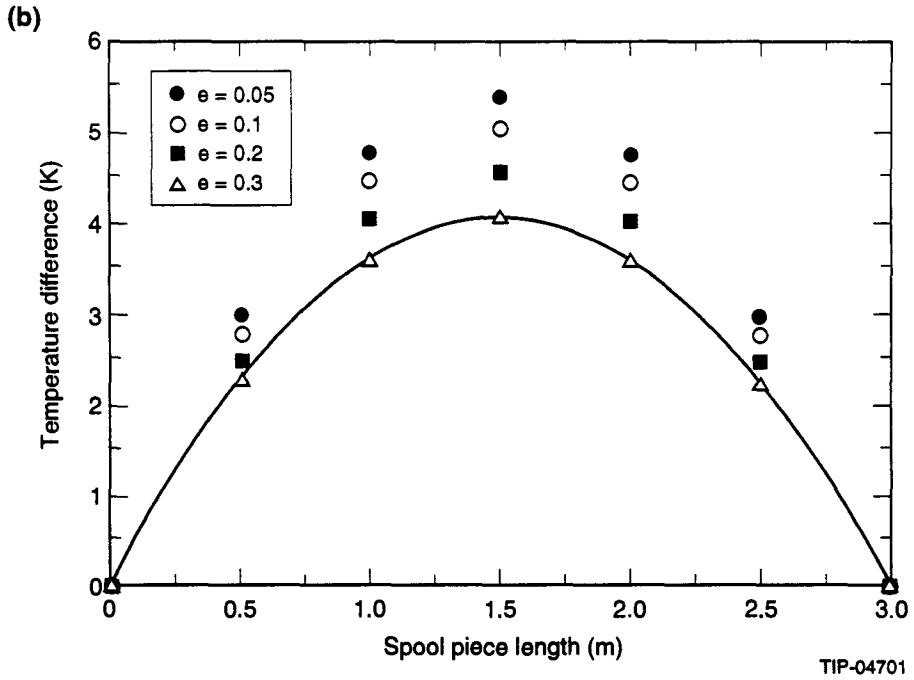

Figure 3(b). Temperature Distribution of 80 K Liner as Function of Spool Piece Liner Surface Emissivity.

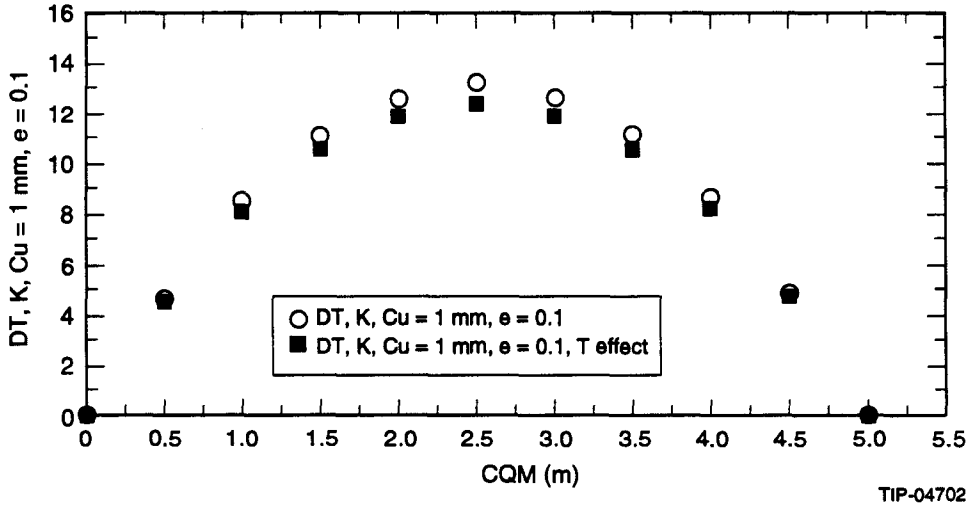

Figure 4. Effect of Surface Temperature Correction on the Temperature Distribution Along CQM by Conductively End Cooling.

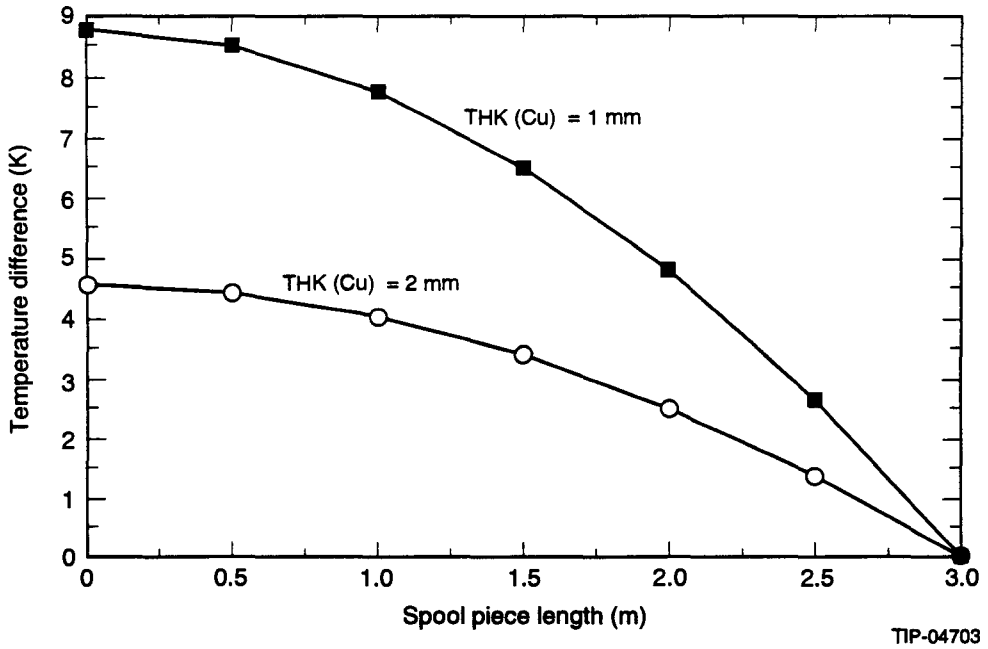

Figure 5. Temperature Distribution of 20 K Liners with One End Cooling Only.

3.0 THERMAL MODEL AND RESULTS FOR 80 K LINER WITH A 4 K BPM

If a 4 K BPM is used, the 80 K liner end-conductive cooling becomes more complicated, as shown in Figure 6. To reduce the heat leak through the copper liner tube from 80 K to the 4 K BPM, a 10– 20 cm long piece of stainless steel tube is inserted between the BPM and the copper liner tube. The synchrotron radiation, the heat leak from the liner to the BPM, the heat leak from the liner to the 4 K beam tube, and the heat exchange between the liner and the 80 K GHe must meet the law of conservation of energy.

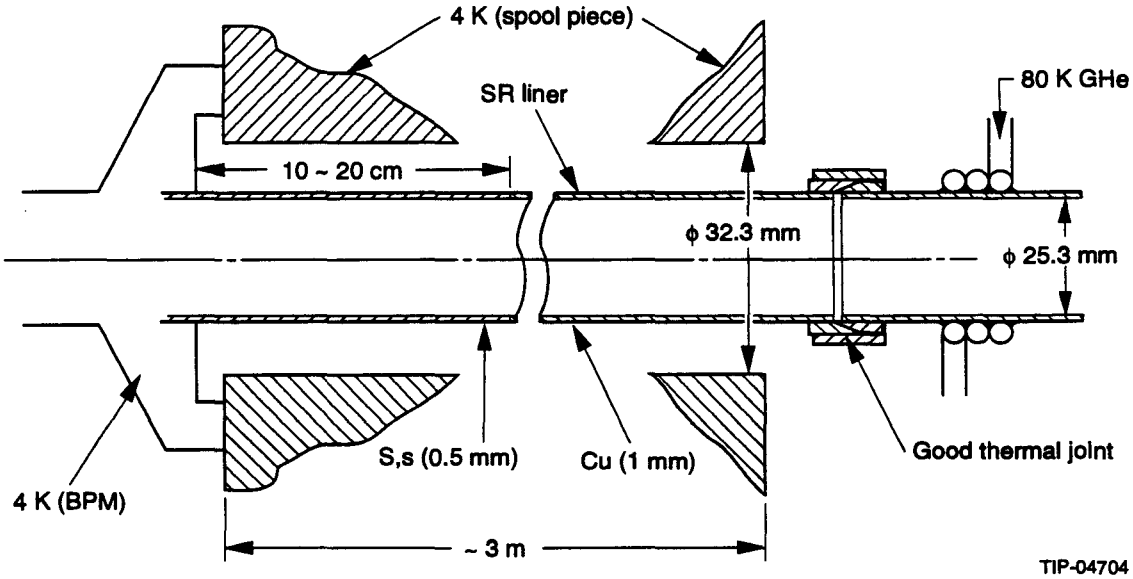

Figure 6. Schematic Drawing of an 80 K Liner with a 4 K BPM.

We know the parameters:

$L_o = 350$ cm	spool piece length
$\lambda_c = 5.0$ W/cm·k	we suggest copper thermal conductivity is constant between 100 K~80 K
$\lambda_s = 0.051$ W/cm·k	we suggest STN STL thermal conductivity is constant between 100 K~4 K also
Liner STN STL tube	ID = 2.53 cm OD = 2.63 cm
Liner copper tube	ID = 2.53 cm OD = 2.73 cm
$A_s = 0.405$ cm^2	cross section area (STN STL tube)
$A_c = 0.826$ cm^2	cross section area (copper tuber)
$q = q_1 - q_2 = 13.77 \times 10^{-4}$ w/cm	
$q_1 = 0.14$ W/m	synchrotron radiation
$q_2 = 0.0023$ W/m	liner supports heat leak
L = 10 cm; 20 cm	STN STL tube length between the BPM and a spool piece.

We obtained equations from a thermal model for end-conductive cooling:

$$dQ = (q_1 - q_2)dX = qdX \tag{15}$$

$$Q_x = -\lambda(T)\, A\, dT/dX \tag{16}$$

$$Q_{x+dx} = -\lambda(T)A\, d\{T + (dT/dX)dX\}/dX. \tag{17}$$

On account of $dQ + Q_x = Q_{x+dx}$ (18)

$$qdX - \lambda(T)AdT/dx = -\lambda(T)A\, d\{T + (dT/dX)dX\}/dX$$

$$= -\lambda(T)A\, dT/dX - \lambda(T)A(\, d^2T/dX^2)dX$$

$$\therefore \quad d^2T/dX^2 = -q/(\lambda(T)A). \tag{19}$$

First, we calculate a temperature distribution along the S.S. Liner tube:

When $0 \le X \le L$, we have

$$T_s(X) = -qX^2/(2\lambda_s A_s) + S_1X + S_2. \tag{20}$$

The temperature distribution along the copper tube shall satisfy Eq. (21).

When $L \le X \le L_0$, we have

$$T_c(X) = -qX^2/(2\lambda_c A_c) + C_1X + C_2. \tag{21}$$

Equations (20) and (21) must meet the following boundary conditions:

$$T_s(0) = 4 \tag{22}$$

$$T_c(L_o) = 80 \tag{23}$$

$$\lambda_c A_c \{\partial T_c(X)/\partial X\}|_{X=L} = \lambda_s A_s \{\partial T_s(X)/\partial X\}|_{X=L} \tag{24}$$

$$T_s(L) = T_c(L) \tag{25}$$

$$T_s(0) = S_2 = 4$$

$$\therefore \quad S_2 = 4. \tag{26}$$

Equation (26) was obtained from Eq. (22):

$$T_c(L_o) = -qL_o^2/(2\lambda_c A_c) + C_1 L_o + C_2 = 80$$

$$\therefore \; -qL_o^2/(2\lambda_c A_c) + C_1 L_o + C_2 = 80. \tag{27}$$

Equation (27) was obtained from Eq. (23):

$$\lambda_c A_c[-2qL/(2\lambda_c A_c) + C_1] = \lambda_s A_s [-2qL/(2\lambda_s A_s) + S_1]$$

$$\therefore \; \lambda_c A_c C_1 = \lambda_s A_s S_1. \tag{28}$$

Equation (28) was obtained from Eq. (24):

$$-qL^2/(2\lambda_s A_s) + S_1 L + S_2 = -qL^2/(2\lambda_c A_c) + C_1 L + C_2. \tag{29}$$

Equation (29) was obtained from Eq. (25):
The S_1, S_2, C_1, and C_2 can be determined from Eqs. (26)–(29):

$$S_2 = 4. \tag{30}$$

$$S_1 = [\lambda_c A_c/(\lambda_s A_s)]\,[80 + qL_o^2/(2\lambda_c A_c) - qL^2/(2\lambda_c A_c) + qL^2/(2\lambda_s A_s) - 4]$$

$$/[\lambda_c A_c L/(\lambda_s A_s) - L + L_o]. \tag{31}$$

$$C_1 = [80 + qL_o^2/(2\lambda_c A_c) - qL_2/(2\lambda_c A_c) + qL^2/(2\lambda_s A_s) - 4]$$

$$/\,[\lambda_c A_c L/(\lambda_s A_s) - L + L_o]. \tag{32}$$

$$C_2 = 80 + qL_o^2/(2\lambda_c A_c) - L_o\{[80 + qL_o^2/(2\lambda_c A_c) - qL^2/(2\lambda_c A_c)$$

$$+ qL^2/(2\lambda_s A_s) - 4] / [\lambda_c A_c L/(\lambda_s A_s) - L + L_o] \}. \quad (33)$$

To put S_1, S_2, C_1, C_2 in Eqs. (20) and (21):

$$T_s(X) = -qX^2/(2\lambda_s A_s) + [\lambda_c A_c/(\lambda_s A_s)] [80 + qL_o^2/(2\lambda_c A_c) - qL^2/(2\lambda_c A_c) + qL^2/(2\lambda_s A_s) - 4]/[\lambda_c A_c L/(\lambda_s A_s) - L + L_o]X + 4. \quad (34)$$

$$T_c(X) = -qX^2/(2\lambda_c A_c) + [80 + qL_o^2/(2\lambda_c A_c) - qL_2/(2\lambda_c A_c) + qL^2/(2\lambda_s A_s) - 4] / [\lambda_c A_c L/(\lambda_s A_s) - L + L_o]X + 80 + qL_o^2/(2\lambda_c A_c) - L_o\{[80 + qL_o^2/(2\lambda_c A_c) - qL^2/(2\lambda_c A_c) + qL^2/(2\lambda_s A_s) - 4] / [\lambda_c A_c L/(\lambda_s A_s) - L + L_o] \}. \quad (35)$$

Using Eqs. (34) and (35) the temperature distribution can be calculated and is shown in Figure 7 and Table 1.

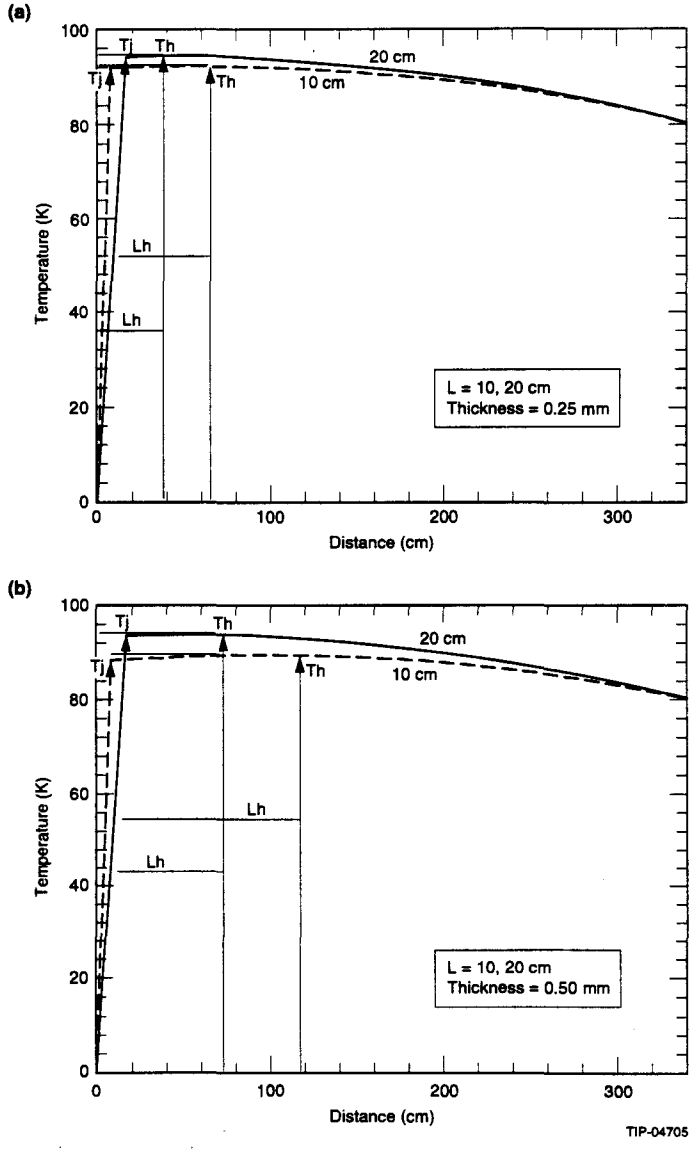

Figure 7. Temperature Distribution Along an 80 K Liner with a 4 K BPM (a), (b).

TABLE 1. CALCULATION DATA OF AN 80 K LINER WITH A 4 K BPM. (Q_{E4K} IS THE HEAT LEAK THROUGH THE 4 K END OF THE LINER.)

STAINLESS STEEL TUBE LENGTH	PARAMETERS	STAINLESS STEEL TUBE THICKNESS = 0.50 mm	STAINLESS STEEL TUBE THICKNESS = 0.25 mm
L = 10 cm	T_i, K	86.75	92.25
	L_h, cm	114.52	62.71
	T_h, K	88.41	92.52
	Q_{e4K}, w	0.158	0.086
L = 20 cm	T_i, K	91.57	94.54
	L_h, cm	67.99	39.6
	T_h, K	92.06	94.6
	Q_{e4K}, w	0.094	0.055

4.0 THE THERMAL RESULTS FOR AN 80 K LINER WITH AN 80 K BPM

In order to simplify the interface structure of a BPM with an 80 K Liner, an 80 K BPM has been developed, as shown in Figure 8. However, to reduce the heat leak from an 80 K BPM to the 4 K part of the spool piece becomes a big concern. A polyimide insulator was used to thermally separate the 80 K BPM from the 4 K spool piece. To keep the required ultrahigh vacuum, a shield was utilized to separate the beam vacuum and the thermal insulation vacuum. A bellow was placed in the shield, and a 20 K thermal bridge has been designed to intercept the heat from 80 K to 4 K.

The results of the thermal calculations for the structure are summarized as follows:

The heat leak is 0.175 W from the 80 K BPM to the 20 K copper ring sink through the stainless steel bellows, 0.080 W from the 20 K copper ring sink to a 4 K spool piece helium vessel end wall through a stainless steel tube, and 0.075 W from the 80 K BPM to a 4 K spool piece helium vessel end wall through a polyimide insulator.

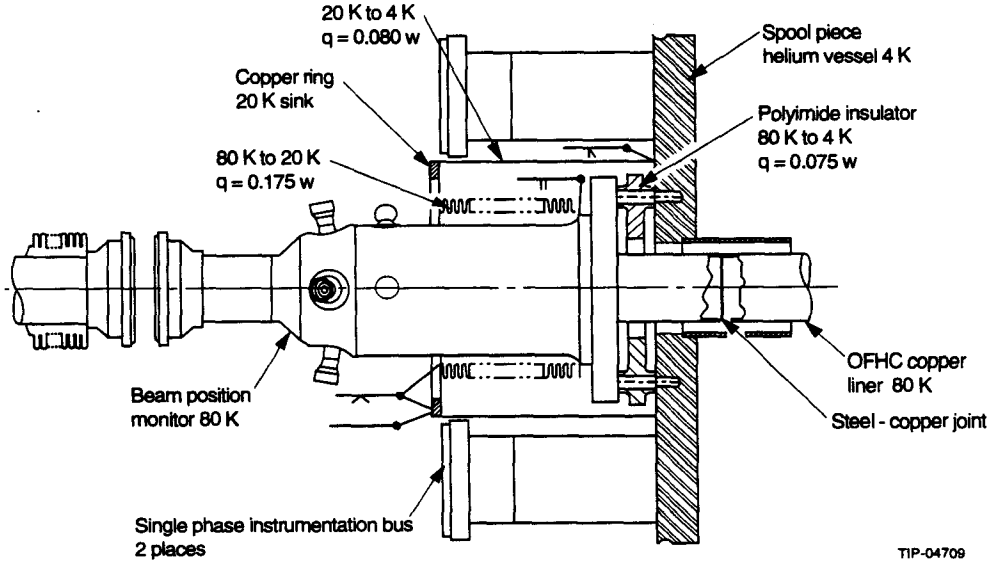

Figure 8. Schematic Drawing of an 80 K Liner with an 80 K BPM.

5.0 GOOD THERMAL CONDUCTING JOINT

A good thermal conducting joint concept, as shown in Figure 9, was proposed by Q. S. Shu and K. Yu. The joint makes liner assembly easier. Assume synchrotron radiation of a quadrupole to be 1 W. The heat transferred at each liner end is 0.5 W. If the pressure on the Cu-Cu machined contact is 7 MPa, the thermal conductance of the contact (in the temperature range 5–25 K) is h(T) = 0.13T (W/cm^2 K). The Cu-Cu contact area is S:

$$S = \pi(R_1 + R_2) L = 4.0134 \text{ cm}^2, \tag{36}$$

as $Q = S \cdot h(T)\, dT,$ (37)

$\Delta T(25 \text{ K}) = Q/(S \cdot h(T)) = 0.012 \text{ K},$

$h(80 \text{ K}) \cdot \Delta T_{80 \text{ K}} = h(25 \text{ K}) \cdot \Delta T_{25 \text{ K}} \cdot$

We know h(80 K) > h(25 K) for the same contact and same pressure:

$\Delta T_{80 \text{ K}} < \Delta T_{25 \text{ K}}$

$\therefore \quad \Delta T_{80 \text{ K}} < 0.012 \text{ K}.$

So at its largest,

$\Delta T_{80 \text{ K}} \leq 1 \text{ K}.$

The temperature across the joint is $\Delta T(\text{at } 80 \text{ K}) \leq 1 \text{ K}$.

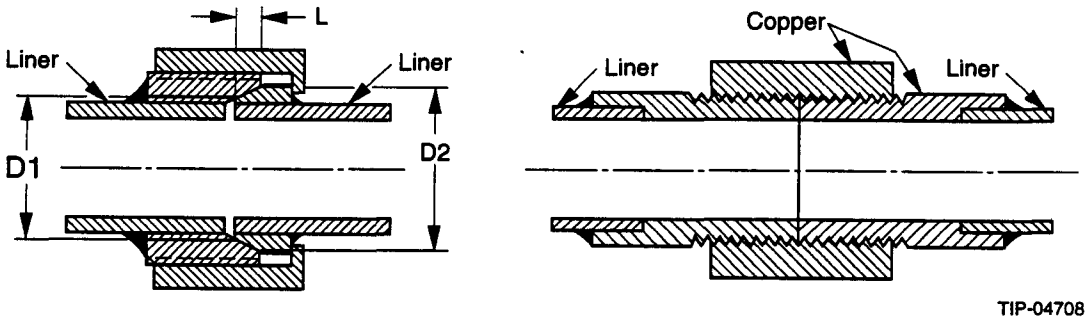

Figure 9. Schematic Drawing of a Good Thermal Conducting Joint.

6.0 COMPACT HEAT EXCHANGER

To make end cooling work, a compact heat exchanger with a length of less than 5 cm was developed. The total heat to be transferred by the heat exchanger is Q = 2 W. The design parameters used were: Copper cooling tube ID = 0.25 cm; mass flow rate of the 80 K GHe, dM/dt = 0.25 g/sec; the temperature increase of GHe is ΔT, as shown in Figure 10.

η	Viscosity
h	Heat transfer coefficient for turbulent flow
P_r	Prandtl's number
R_e	Reynolds number
D_e	Effective diameter
G	Mass flow rate per unit area
M	Mass
C_p	Heat capacity

λ Thermal conductivity of GHe

ΔT_L Different temperature between enter tube GHe and Liner

ΔT Different temperature between exit tube GHe and Liner.

Since $Q = C_p(dM/dt)\Delta T_L$, (38)

$C_p = 5.2$ [J/(g·K)] for GHe under 80 K,

$\Delta T_L = [\ Q/C_p(dM/dt)\ ] = 1.54$ K, (39)

we have $G = 4M / \pi D^2 = 5.09$

$h = 40 \times 10^{-6}$ (P)

$\lambda = 14\ 0 \times 10^{-6}$ (cal/s·k·cm)

$R_e = GD/\ h = 31812.5$

$\therefore$ $R_e > 2300$ (turbulent)

$P_r = \eta C_p / \lambda = 0.357$

$h = 0.023\ C_p\ G^{0.8}\eta^{0.2} /(P_r^{0.6}\ D_e^{0.2}) = 0.0345$

$c = \pi\ D = 0.785$ cm

$L = [(dM/dt)C_p / (hc)]\ \ln[\Delta T_L/\Delta T]$. (40)

If three turns are used,

$L = 28.75$ cm

$\Delta T = 0.13$ K

$\Delta T < 1$ K.

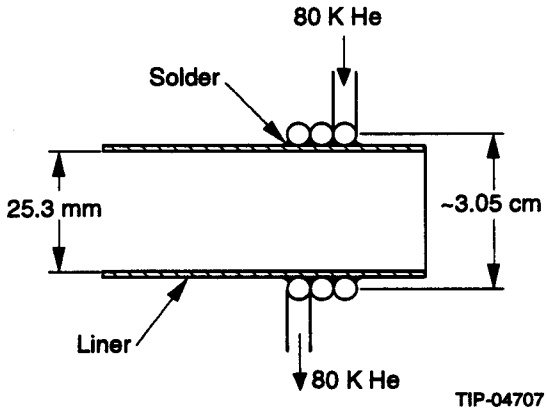

Figure 10. Schematic Drawing of a Compact Heat Exchanger.

ACKNOWLEDGEMENTS

The authors sincerely thank A. Yucel, D. Clark, and W. Turner of the SSCL for their contributions to this work.

REFERENCES

1. Q. S. Shu, "Status Report on the ASST Liner System Design," SSCL-N-805, November 1993.
2. "80K ASST Liner Design Report," (in preparation).
3. G. K. White, *Experimental Techniques in Low-Temperature Physics,* 1979.

This Page Intentionally Left Blank

SECTION 4

Wakefield and Impedance Studies of a Liner Using MAFIA

W. Chou and T. Barts

SECTION 4

Wakefield and Impedance Studies of a Liner Using MAFIA

W. Chou and T. Barts

Superconducting Super Collider Laboratory*
2550 Beckleymeade Avenue
Dallas, Texas 75237

Abstract

The liner is a perforated beam tube that is coaxial with an outer bore tube. The 3D code MAFIA (version 3.1) is used to study the wakefields, impedances, and resonances of this structure. The short-range wakes and low-frequency (below the cutoff) impedances are in agreement with the theoretical model. The long-range wakes and high-frequency resonances are associated with the distribution of the holes (or slots). The dependence of the impedance on the size, shape, and pattern of the holes (or slots) is studied. The impact of the liner impedance on the Superconducting Super Collider impedance budget is discussed.

* Operated by the Universities Research Association, Inc., for the U.S. Department of Energy under Contract No. DE-AC35-89ER40486.

1.0 INTRODUCTION

One novel feature of the Collider at the Superconducting Super Collider (SSC) is that synchrotron radiation from the 20 TeV proton beam becomes an important issue. This radiation creates a significant heat load to the cryogenic system, and it causes a large amount of gas load from the photon-induced desorption process. The latter may result in a poor vacuum in the beam tube and an eventual short luminosity lifetime. One possible solution to the problem is to install a perforated liner inside the bore tube.[1] The principal function of the liner is to decouple the synchrotron radiation from the bore tube. The photo-desorbed gas from the inner surface of the liner would be pumped out by the bore tube (which is at 4 K) and absorbed by the cryosorber that is located in the coaxial region between the liner and the bore tube.

The introduction of the liner brings up a list of issues that need to be studied. Among them is the additional RF impedance. There have been some theoretical studies on the hole impedance in the low-frequency region.[2] This paper reports the simulation studies using the 3D code MAFIA (version 3.1).[3] It is found that, at the frequencies below the cutoff, MAFIA results are in agreement with the theoretical model. At high frequencies, impedance resonance peaks and long-term wakes are observed in the simulations. The size, shape, and distribution of the holes (or slots) on the liner surface have significant impact on the liner impedance.

The MAFIA code runs on an IBM RS 6000/560 workstation. Statistics of the code performance are also included.

2.0 LOW-FREQUENCY REGION

2.1 Analytical Model

For some structures, such as a pipe attached to a small pillbox or a pipe with small holes on its surface (*e.g.*, the perforated liner), the longitudinal and transverse impedances can be approximated by a pure inductance L at low frequencies (below the cutoff):

$$Z_{\parallel}(\omega) = i\omega L \tag{1}$$

$$Z_{\perp}(\omega) = i\frac{2c}{b^2}L, \tag{2}$$

in which b is the radius of the pipe, c the velocity of light. The corresponding wakefields $W_{\parallel}$ and $W_{\perp}$ are, respectively, the derivative of the δ and δ' :[4]

$$W_{\parallel}(\tau) = \frac{1}{2\pi}\int_{-\infty}^{\infty} d\omega\, e^{-i\omega\tau}\, Z_{\parallel}(\omega) = -L\,d'(\tau) \tag{3}$$

$$W_{\perp}(\tau) = \frac{-i}{2\pi}\int_{-\infty}^{\infty} d\omega\, e^{-i\omega\tau}\, Z_{\perp}(\omega) = \frac{2c}{b^2}L\,\delta(\tau). \tag{4}$$

Letting $\tau = z/c$, one obtains

$$W_{\parallel}(z) = -c^2 L\, \delta(z) \tag{5}$$

$$W_{\perp}(z) = \frac{2c^2}{b^2} L\, \delta(z)\,. \tag{6}$$

For a Gaussian bunch with rms length σ, the line charge density is

$$\lambda(z) = \frac{1}{\sqrt{2\pi}\,\sigma}\, e^{-\frac{z^2}{2\sigma^2}}\,. \tag{7}$$

The longitudinal and transverse wake potentials generated by this Gaussian bunch are, respectively,

$$W_{\parallel}(z) = \int_{-\infty}^{\infty} dz'\, \lambda(z-z')\, W_{\parallel}(z') = \frac{c^2 L}{\sqrt{2\pi}\,\sigma^3}\, z\, e^{-\frac{z^2}{2\sigma^2}} \tag{8}$$

$$W_{\perp}(z) = \int_{-\infty}^{\infty} dz'\, \lambda(z-z')\, W_{\perp}(z') = \frac{2c^2 L}{\sqrt{2\pi}\,\sigma b^2}\, e^{-\frac{z^2}{2\sigma^2}}\,. \tag{9}$$

They are shown in Figures 1(a) and 1(b).

The magnitudes and locations of the peaks of the wake potentials are as follows:

$$W_{\parallel}^{max(min)} = \pm \frac{c^2 L}{\sqrt{2\pi}\,\sigma^2}\, e^{-1/2}\,, \text{ at } z = \pm\sigma \tag{10}$$

$$W_{\perp}^{max} = \frac{2c^2 L}{\sqrt{2\pi}\,\sigma b^2}\,, \text{ at } z = 0\,. \tag{11}$$

Therefore, if the inductance L is known, then Eqs. (8)–(11) give the wake potentials for specified beam pipe radius b and rms bunch length σ.

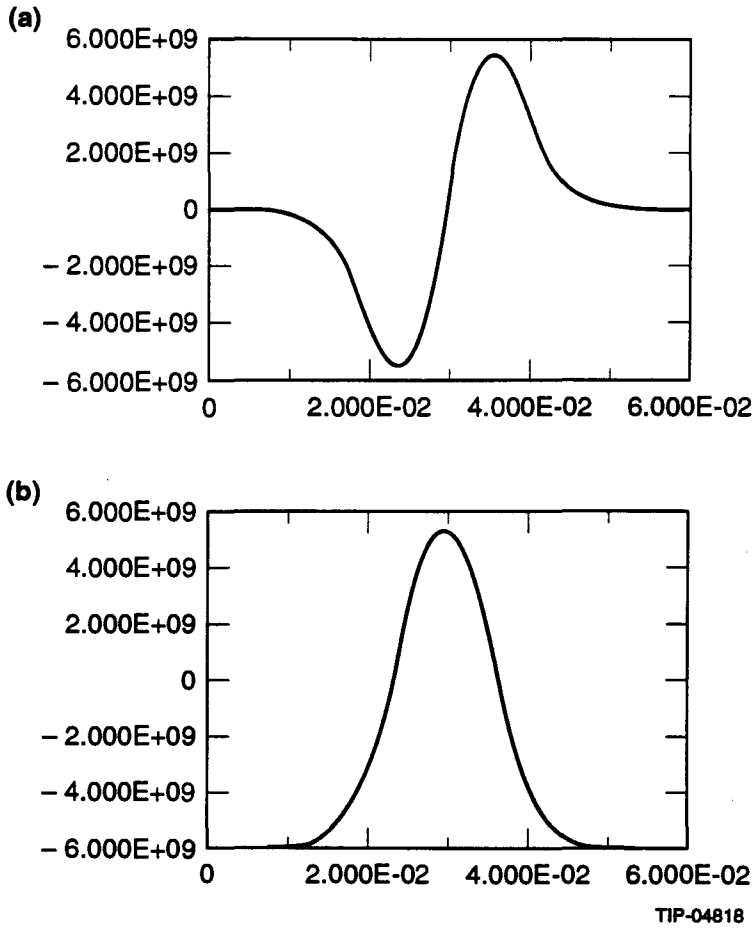

Figure 1. The Wake Potentials of a Purely Inductive Impedance for a Gaussian Bunch: (a) Longitudinal, (b) Transverse.

2.2 MAFIA Results

The inductance of a small hole with diameter d has been worked out:[2]

$$L = \frac{Z_0}{48\pi^2 c}\,\frac{d^3}{b^2}, \tag{12}$$

where $Z_0 = 377\ \Omega$. Therefore, the peaks of the wake potentials of the liner are given by (all dimensions in meters):

$$W_{\parallel}^{max} = \frac{Z_0 c}{48\pi^{5/2}\sqrt{2e}}\,\frac{d^3}{\sigma^2 b^2} = 5.77\times 10^{-2}\times\frac{d^3}{\sigma^2 b^2}\ \text{V/nC (per hole)} \tag{13}$$

$$W_{\perp}^{max} = \frac{Z_0 c}{24\pi^{5/2}\sqrt{2}}\,\frac{d^3}{\sigma b^4} = 1.90\times 10^{-4}\times\frac{d^3}{\sigma b^4}\ \text{V/nC/mm (per hole)}\,. \tag{14}$$

Equations (13) and (14) can be directly compared with the MAFIA results as shown in Figures 2(a) and 2(b).

When the hole size is small and bunch length is large, the theory and simulations agree with each other. This implies that the low-frequency approximation is valid. However, when the hole becomes larger ($d \geq$ 4 mm) or the bunch becomes shorter ($\sigma = 0.25$ and 0.6 cm), the simulation results appear to be larger than what the theory would predict. This probably indicates the breakdown of the low-frequency assumption.

The hole shape in the simulations is a square rather than a circle. It would thus give an inductance larger than that of a circular one as predicted by Eq. (12). On the other hand, Eq. (12) is derived from a zero-thickness liner. The finite thickness (1 mm) used in the simulations would lead to a smaller inductance.[5] It is interesting to see from Figures 2(a) and 2(b) that these two effects seem to cancel each other, resulting in a good agreement between Eqs. (13), (14) and the MAFIA results.

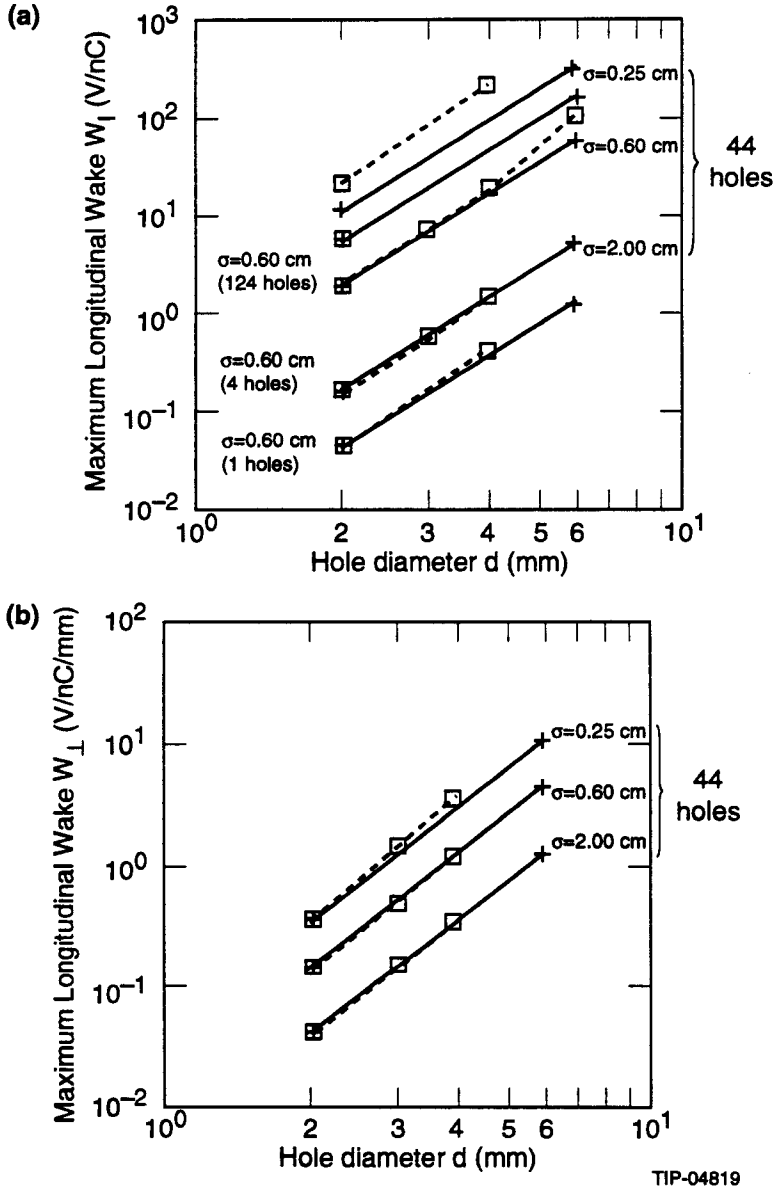

Figure 2. The Peak Values of the Wake Potentials of a Liner. The solid lines are computed using Eqs. (13)–(14). The squares and dashed lines are the MAFIA results. (a) $W_{\parallel}^{max}$, (b) $W_{\perp}^{max}$.

3.0 HIGH-FREQUENCY REGION

One interesting observation in the simulations is the long-term wakes for large holes or short bunches. These long-term wakes are potentially dangerous because they may cause coupling among successive bunches, which could be a source of multiple bunch instability and/or emittance growth. In order to understand these wakes, a fast Fourier transform (FFT) is carried out to convert the wakes to the impedance in the frequency domain.

3.1 Benchmark Test

Because of the lack of an appropriate analytic model of the perforated liner in the high-frequency region, the MAFIA results are at first compared with the known impedance spectra of a small pillbox. For this simple structure, the impedances obtained from several different methods (field matching,[6] TBCI,[7] and transmission line[7]) agree with each other and, therefore, can be used for a benchmark test.

Figures 3(a) and 3(b) show the longitudinal impedance of a small pillbox obtained from the FFT of the wakes computed by MAFIA.

Below the cutoff (which is about 5.75 GHz for a beam pipe radius of 2 cm used in the simulation), the impedance is purely inductive:

$$Z_{\parallel}(\omega) = i\omega \frac{\mu_0}{2\pi} \frac{4g\varepsilon}{b}, \tag{15}$$

where $2g$ and 2ε are the width and depth of the pillbox, respectively, and $\mu_0 = 4\pi \times 10^{-7}$ H/m. The difference between Eq. (15) and the MAFIA results in Figure 3(b) is only about 3%. Above the cutoff, the impedance spectra also agree reasonably well with those in Refs. 6 and 7.

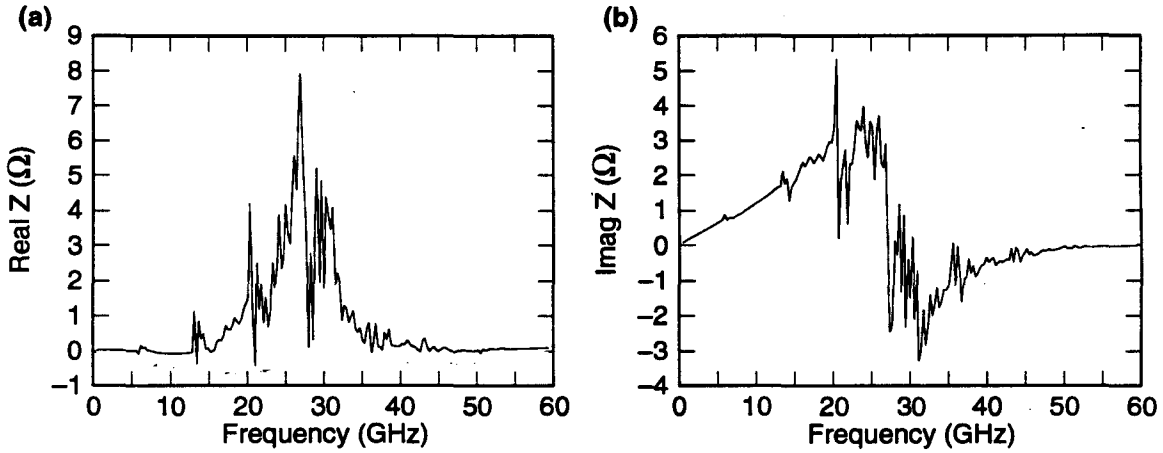

Figure 3. The Longitudinal Impedance of a Small Pillbox Obtained from MAFIA and FFT: (a) the Real Part, (b) the Imaginary Part.

3.2 Periodic Distributions of Holes on a Liner

The simulations use 20 holes along the azimuthal direction of the liner, which is called a column, and 21 columns along the axial direction. The total number of holes is 420. Each hole is a 2 mm × 2 mm square. The columns are uniformly distributed with 1 cm spacing between each other. Figure 4(a) shows the structure, and 4(b) the longitudinal wake. The long-term wake indicates the existence of resonance impedance, which is clearly seen in Figures 4(c) and 4(d). The liner radius is 1.65 cm, which gives the longitudinal cutoff at approximately 7 GHz. Below the cutoff, the impedance is purely inductive. The analytical value is obtained from Eqs. (1) and (12):

$$Z_{\parallel}(\omega) = i\omega \frac{Z_0}{48\pi^2 c} \frac{d^3}{b^2}. \tag{16}$$

The difference between the value given in Figure 4(d) and that given by Eq. (16) is again only a few percent, as in the case of the pillbox. The resonance peaks at high frequency are associated with the periodicity of the holes. The first peak occurs near 15 GHz, which corresponds to a half wavelength of 1 cm, the periodic spacing between two columns. The transverse impedance is shown in Figures 5(a) and 5(b).

The transverse cutoff is approximately 11 GHz. Below it, the impedance is also purely inductive. The analytical value from Eqs. (2) and (12) is

$$Z_{\perp}(\omega) = i \frac{Z_0}{24\pi^2} \frac{d^3}{b^4}. \tag{17}$$

This value agrees within a few percent with that given in Figure 5(b) at zero frequency. But the falloff of Im $Z_{\perp}$ from dc to the cutoff is not predicted by the theoretical model. Similar to the longitudinal case, the long-term wakes and the resonance impedance at high frequencies are observed.

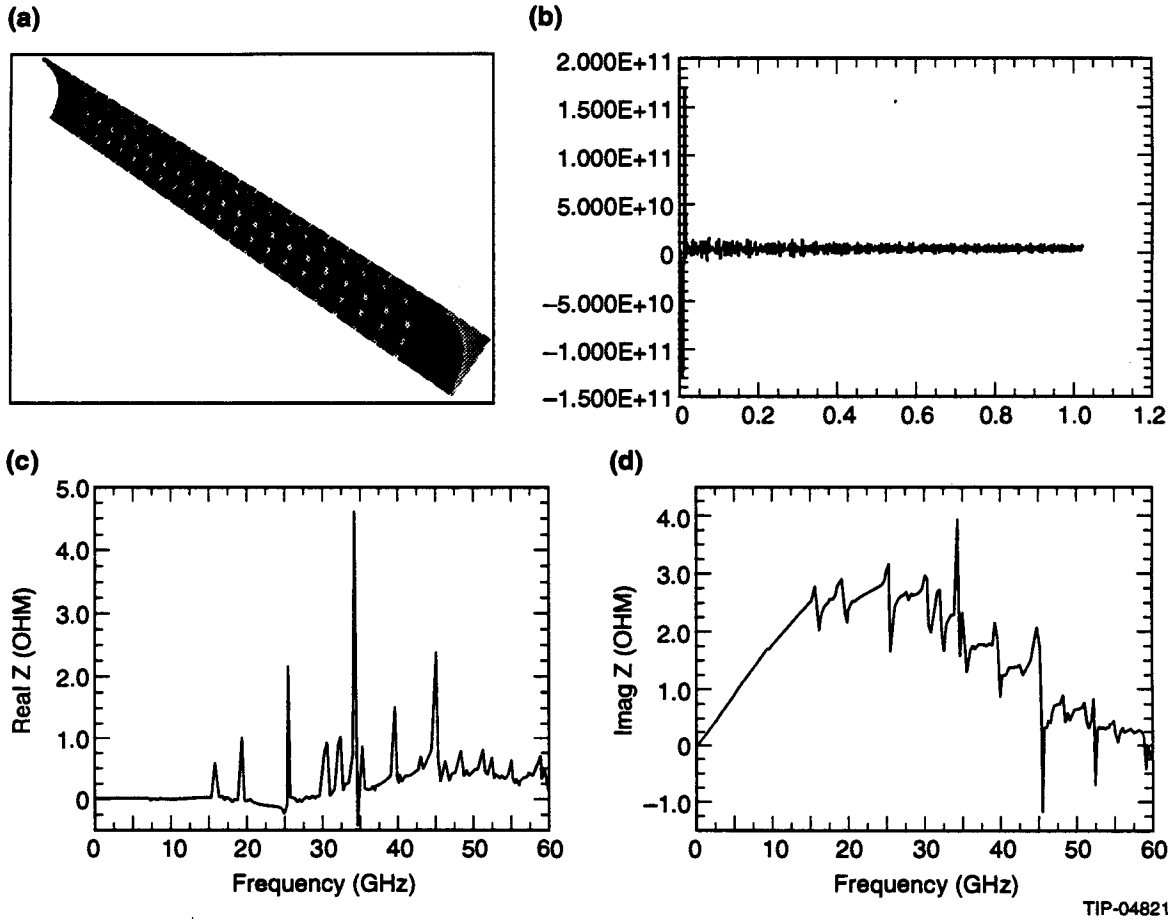

Figure 4. (a) The Liner with 420 Holes of the Size 2 mm × 2 mm, Randomly Distributed. (b) The longitudinal wake of this structure. (c) The real longitudinal impedance. (d) The imaginary longitudinal impedance.

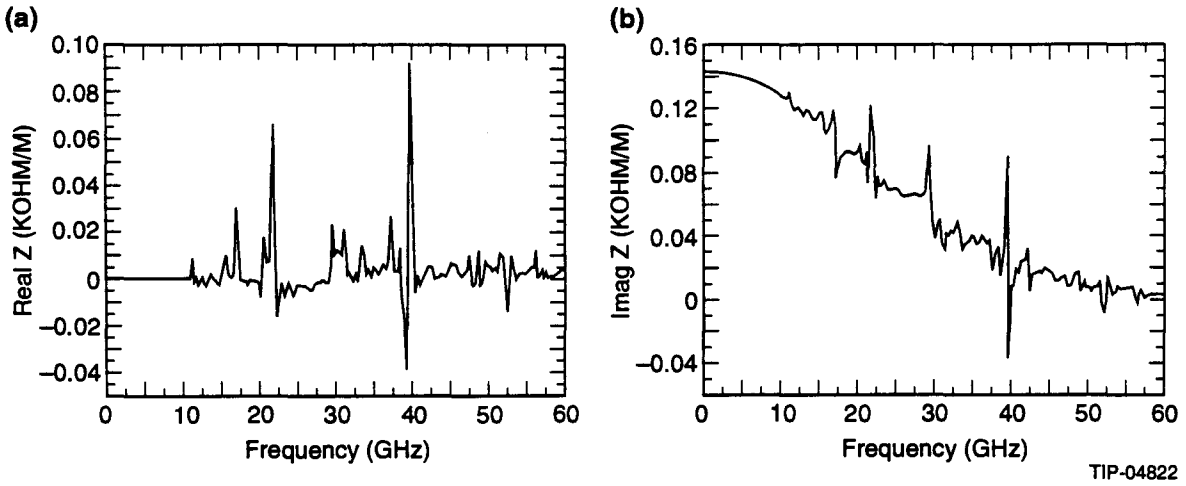

Figure 5. The Transverse Impedance of the Structure in Figure 4(a): (a) the Real Part, (b) the Imaginary Part.

3.3 Random Distribution of Holes on a Liner

One effective way to reduce the long-term wakes and resonance impedance is to destroy the periodicity of the hole distribution. For this purpose, the spacing between two neighboring holes in the axial direction is randomized. Figures 6(a)–6(d) show the structure and the resulting longitudinal wakes and impedance. Compared with Figures 4(a)–4(d), the short-term wakes and low-frequency impedance remain about the same (as they should, due to the additivity), whereas the long-term wakes and resonance impedance at high frequencies are greatly decreased. However, by using the same technique, the reduction in the transverse direction is less dramatic. This needs to be understood.

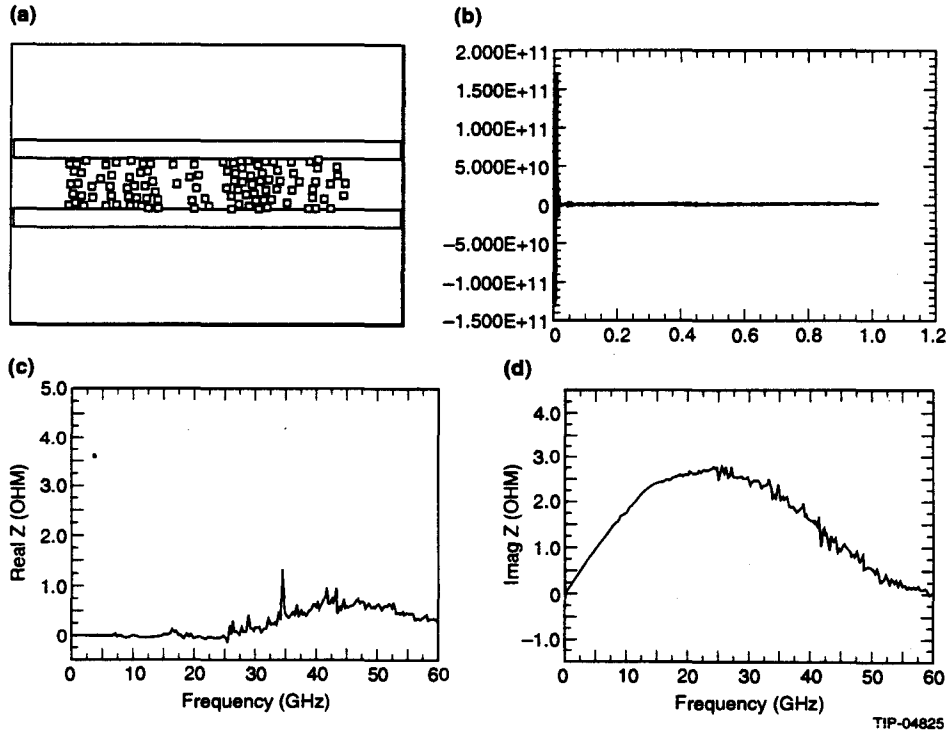

Figure 6. (a) The Liner with 420 Holes of the Size 2 mm × 2 mm Randomly Distributed. (b) The longitudinal wake of this structure. (c) The real longitudinal impedance. (d) The imaginary longitudinal impedance.

3.4 Slots on a Liner

When the holes are replaced by the slots that have the same area and have the major axis parallel to the pipe axis, the low-frequency impedances are reduced, whereas the long-term wakes (*i.e.*, the high-frequency resonances) are enhanced because it becomes easier to resonate. This is shown in Figures 7(a) and 7(b). Therefore, the tradeoff should be studied carefully. The short slots with rounded edges seem to be a good compromise.

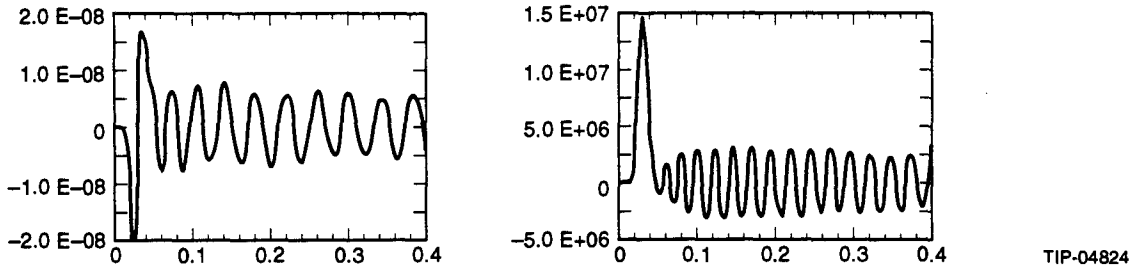

Figure 7. The Wake Potentials of a Liner with Four Long Slots of the Size 2 mm × 22 mm: (a) Longitudinal, (b) Transverse.

4.0 DISCUSSION

Based on the good agreement of the theory with the simulations as well as with some measurements,[8] it is believed that the low-frequency part of the impedance of a perforated liner can be estimated accurately. These impedances are plotted in Figures 8(a) and 8(b) for three possible liner IDs. In these calculations, the area coverage of the holes is kept the same for different hole sizes, namely, 1000 holes/m for d = 2 mm. This is about 3%, 4%, and 5% coverage for ID = 33 mm, 24.3 mm, and 20.3 mm, respectively.

As a comparison, the impedance budget of the Collider is also plotted. It is seen that when the liner ID is 24.3 mm—as designed for the Accelerator System String Test (ASST II)—and the hole diameter 2 mm, the longitudinal impedance of the liner would be about 34% of the present budget, and the transverse impedance about 110%. This represents a significant increment of the budget. Because of a relatively large safety margin reserved in the present impedance budget (which is 6 times greater than the instability threshold impedance), this increment should not jeopardize the beam dynamics at the baseline design current of 72 mA. Rather, its main impact would be to limit the potential of beam current upgrade.

The size, shape, and distribution of the holes or slots on the liner surface have significant impact on the impedance. The rounded, short slots with random pattern may present the best choice to minimize the impedance while meeting the vacuum pumping requirements.

The code MAFIA (version 3.1) runs on an IBM 560 workstation with 128 MB RAM. It is a virtual memory machine. The maximum number of mesh points in the simulations can reach approximately 1.8 million. When this number is exceeded, the CPU usage would be greatly degraded. A typical job calculating approximately 10^6 mesh points and 10^3 wake points takes approximately 4 h CPU time. The same job would take approximately 7 h CPU time on the NERSC Cray.

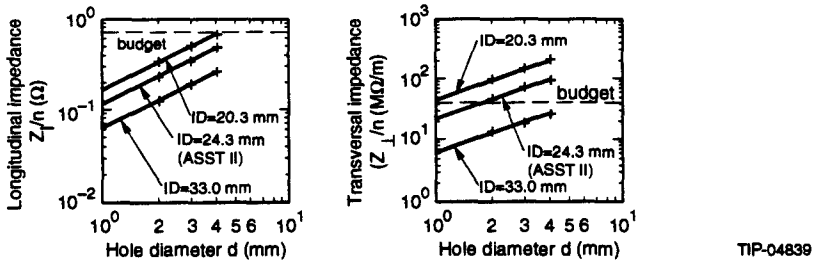

Figure 8. The Total Impedance of the Liner in the SSC Collider for Three Possible Liner IDs: (a) Longitudinal, (b) Transverse. The dashed lines are the impedance budget.

This Page Intentionally Left Blank

REFERENCES

1. H. T. Edwards, SSC Laboratory Report SSCL-N-771 (1991).
2. S. Kurennoy, CERN Report SL/91-29; R. L. Gluckstern, CERN Report SL/92-05.
3. MAFIA is a commercial code for general purpose electromagnetic simulations.
4. W. Chou and T. Barts, SSCL internal technical note PMTN-0057C (1992).
5. R. L. Gluckstern and J. A. Diamond, *IEEE MTT*, v. **39**, p. 274 (1991).
6. H. Henke, CERN Report LEP-RF/85-41 (1985).
7. W. Chou, *Proc. 4th Advanced ICFA Beam Dynamics Workshop*, KEK Report 90-21, p. 161 (1991).
8. L. Walling, private communication.

This Page Intentionally Left Blank

SECTION 5

Impedance of a Perforated Liner and Its Impact on the SSCL Collider

W. Chou and T. Barts

SECTION 5

Impedance of a Perforated Liner and Its Impact on the SSCL Collider

W. Chou and T. Barts

Superconducting Super Collider Laboratory*
2550 Beckleymeade Avenue
Dallas, Texas 75237

Abstract

Various approaches (analytical, numerical, and experimental) have been tried to investigate the impedance and wakefields of a liner. At low frequencies, the results obtained from different approaches are in agreement. At high frequencies, the simulations show that the resonance peaks and the associated long term wakes are related to the periodicity of the hole distribution. The dependence of the impedance on the size, shape and pattern of the holes and slots has been studied. The rounded short slots of random distribution are recommended for minimizing the impedance. The RF coupling between the area inside the liner and the annulus is negligibly small in the frequency range of interest. The impact of the liner on the safety margin and resistive wall instability has been studied.

* Operated by the Universities Research Association, Inc., for the U.S. Department of Energy under Contract No. DE-AC35-89ER40486.

1.0 INTRODUCTION

The synchrotron radiation in the SSC Collider will cause a large amount of gas load from the photon-induced desorption process and may result in a poor vacuum in the beam tube. A possible solution to the problem is to install a perforated liner inside the bore tube.[1] The introduction of the liner brings up a number of issues that need to be studied. Among them, one is the increase of the RF impedance. The increments come from the holes (or slots) as well as from the smaller ID of the liner.

The impedance of the holes and slots has been studied by means of 3D simulations (MAFIA[2] and HFSS[3]), analytical modeling,[4] wire measurements[3] and electron beam measurement.* The impedance increments of the bellows, beam position monitors and other components due to a smaller liner ID have also been computed. The increase of the impedance implies the decrease of the safety margin, which is defined as the ratio of the instability threshold impedance to the machine impedance. This is now under study to determine the minimum allowable ID of the liner.

2.0 LOW FREQUENCY REGION

2.1 Analytical Model

For some structures, such as a pipe attached to a small pillbox or a pipe with small holes on its surface (*i.e.*, the perforated liner), the longitudinal and transverse impedances can be approximated by a pure inductance L at low frequencies (below the cutoff):

$$Z_{\parallel}(\omega) = i\omega L, \qquad Z_{\perp}(\omega) = i\frac{2cL}{b^2} \tag{1}$$

in which b is the radius of the pipe, c the velocity of light. When a Gaussian bunch traverses the pure inductance, it will generate the longitudinal and transverse wake potentials:[2]

$$W_{\parallel}(z) = \frac{c^2 L}{\sqrt{2\pi}\,\sigma^3} z\, e^{-\frac{z^2}{2\sigma^2}}, \qquad W_{\perp}(z) = \frac{2c^2 L}{\sqrt{2\pi}\,\sigma b^2} e^{-\frac{z^2}{2\sigma^2}}, \tag{2}$$

in which σ is the rms bunch length. The magnitudes and locations of the peaks of the wake potentials are:

$$W_{\parallel}^{max(min)} = \pm\frac{c^2 L}{\sqrt{2\pi}\,\sigma^2} e^{-1/2}, \qquad \text{at } z = \pm\sigma \tag{3}$$

$$W_{\perp}^{max} = \frac{2c^2 L}{\sqrt{2\pi}\,\sigma b^2}, \qquad \text{at } z = 0 \tag{4}$$

---

* J. Simpson 1993: personal communication. Measurements of the liner impedance with large size holes have been made by J. Simpson's group using the short electron pulses of AATF at ANL. The results show that a better resolution is required in order to perform quantitative analysis.

2.2 MAFIA Results

The inductance of a small hole with diameter d at low frequency has been worked out:[4]

$$L = \frac{Z_0}{48\pi^2 c}\frac{d^3}{b^2}, \tag{5}$$

in which $Z_0 = 377\ \Omega$. Therefore, the peak of the wakes of each hole are given by (all dimensions in meters):

$$W_{\parallel}^{max} = \frac{Z_0 c}{48\pi^{5/2}\sqrt{2e}}\frac{d^3}{\sigma^2 b^2} = 0.0577 \times \frac{d^3}{\sigma^2 b^2}\left(\frac{\mathrm{V}}{\mathrm{nC}}\right), \tag{6}$$

$$W_{\perp}^{max} = \frac{Z_0 c}{24\pi^{5/2}\sqrt{2}}\frac{d^3}{\sigma b^4} = 0.00019 \times \frac{d^3}{\sigma b^4}\left(\frac{\mathrm{V}}{\mathrm{nC}\cdot\mathrm{mm}}\right). \tag{7}$$

Equations (6) and (7) can be compared with the MAFIA results as shown in Figures 1(a) and (b). When the hole size is small and bunch length large, the theory and simulations agree with each other. However, when the hole becomes larger ($d \geq 4$ mm) or the bunch becomes shorter (σ= 0.25 and 0.6 cm), the simulation results appear to be larger than what the theory would predict. This probably indicates the breakdown of the low frequency assumption.

The hole shape in the simulations is a square rather than a circle. It would thus give an inductance larger than that of a circular one as predicted by Eq. (5). On the other hand, Eq. (5) is derived from a zero-thickness liner. The finite thickness (1 mm) used in the simulations would lead to a smaller inductance.[5] It is interesting to see from Figure 1 that these two effects seem to cancel each other and result in a good agreement between Eqs. (6) and (7), and the MAFIA results.

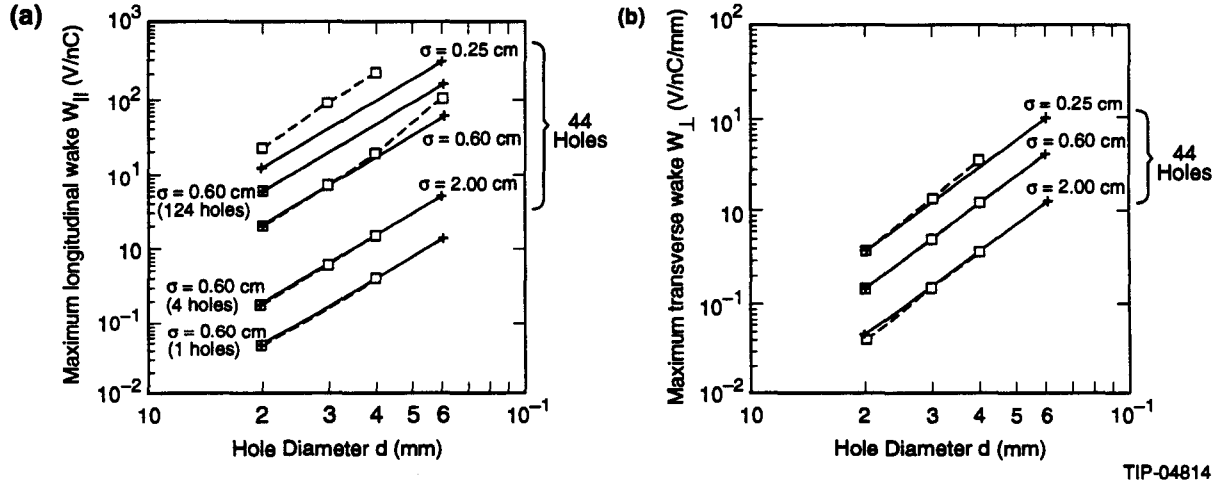

Figure 1. The Solid Lines are Computed Using Eqs. (6) and (7). The squares and dashed lines are the MAFIA results. (a) $W_{\parallel}^{max}$, (b) $W_{\perp}^{max}$.

3.0 HIGH FREQUENCY REGION

3.1 Fields in the Annulus

The annulus region allows the existence and propagation of a TEM wave, which has zero cutoff and travels with the speed of the light. In order to understand whether this should be a concern, the frequency domain simulation with periodic boundary conditions was carried out. Many modes have been identified and compared with the theoretical values of the frequencies. The errors are in general less than 1%. Two of them are shown in Figures 2(a) and (b). Up to 30 GHz, no coupling is seen between the inner and outer regions. Therefore, the impact of the co-axial structure to the impedance is considered to be insignificant.

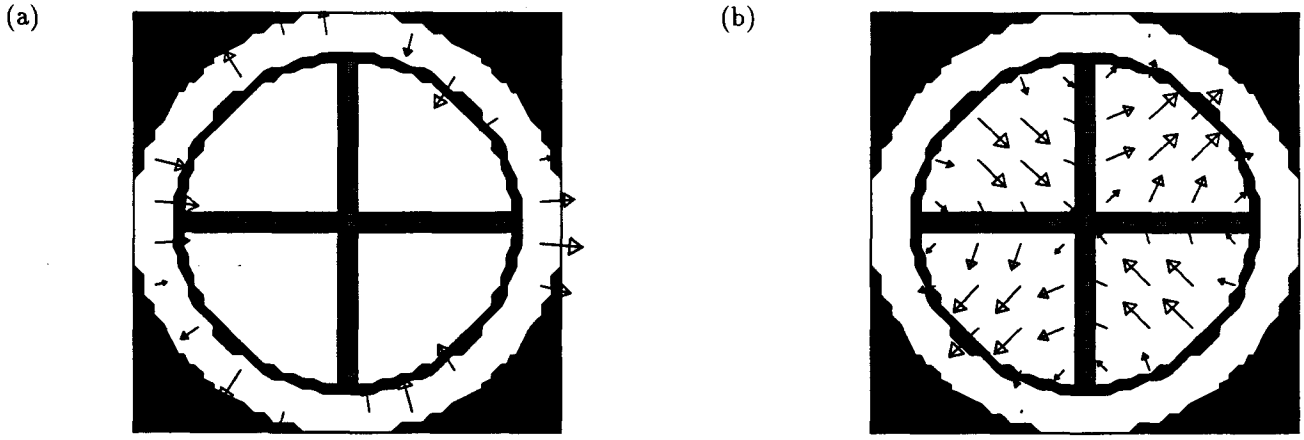

Figure 2. Electric Field Vectors for: (a) the TE31 Mode (10.4 GHz) and (b) the TE21 Mode(11.5 GHz).

3.2 Periodic Distributions of Holes on a Liner

When the holes are periodically arranged along the axis with 1-cm spacing, resonance peaks above the cutoff (~ 7 GHz) are observed in the longitudinal impedance spectrum as shown in Figures 3(a) and (b).

Below the cutoff, the spectrum agree with the analytical value (5) within a few percent. Similar results have also been obtained for the transverse impedance.

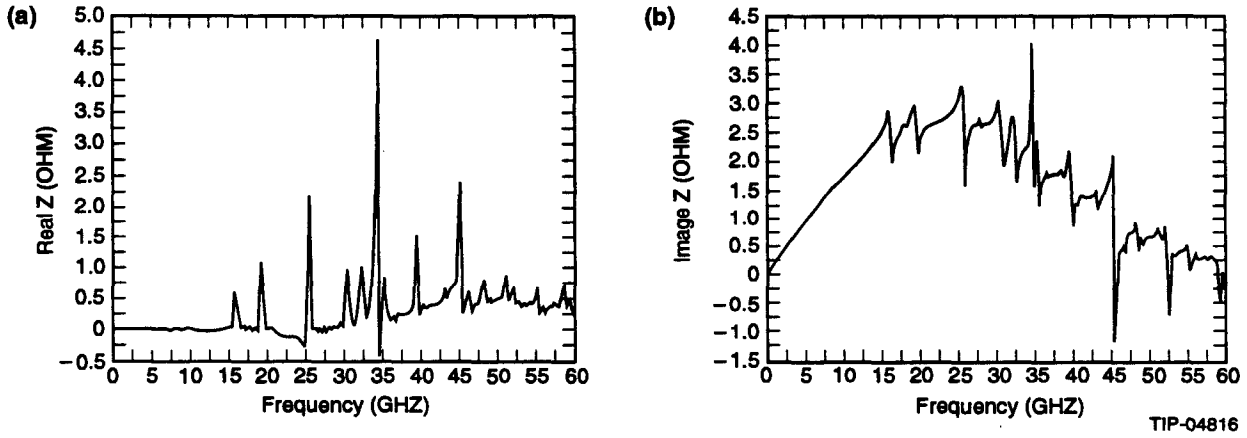

Figure 3. The Longitudinal Impedance for a Liner with 420 Square Holes (2mm), Periodically Distributed.

3.3 Random Distribution of Holes on a Liner

One effective way to reduce the resonance impedance is to destroy the periodicity of the hole distribution. This is demonstrated in Figures 4(a) and (b), when the spacing between two neighboring holes in the axial direction is randomized. Compared with Figures 3(a) and (b), the low frequency impedance remains about the same (as it should be due to the additivity), whereas the resonance peaks at high frequencies are greatly suppressed. However, by using the same technique, the reduction in the transverse direction is less dramatic. This needs further study.

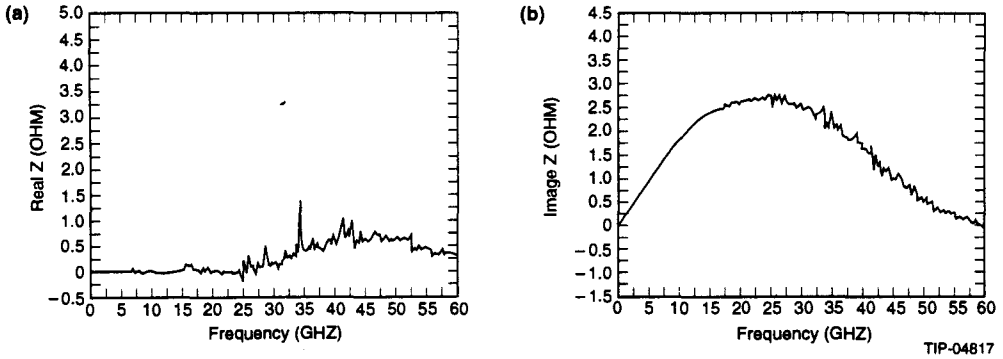

Figure 4. The Longitudinal Impedance for a Liner with 420 Square Holes (2mm), Randomly Distributed.

3.4 Slots vs. Holes

When the holes are replaced by the slots that have the same area and have the major axis parallel to the pipe axis, the low frequency impedance is reduced, whereas the long term wakes and high frequency resonances are enhanced because it becomes easier to resonate.[2] Therefore, the trade off should be studied carefully. The short slots with rounded edges seem to be a good compromise.

4.0 SAFETY MARGIN

The baseline beam tube ID is 33 mm. The impedance threshold before any coherent transverse instability could occur is 270 MΩ/m. Assuming the liner ID be 25.3 mm (as designed for the string test), hole diameter 2 mm, and 4% area coverage of the holes on the liner surface, then the safety margin will be reduced by a factor of 3, as listed in Table 1.

TABLE 1. SAFETY MARGIN.

CASE	$Z_{\perp}^{(liner)}$ MΩ/m	$Z_{\perp}^{(others)}$ MΩ/m	$Z_{\perp}^{(total)}$ MΩ/m	SAFETY MARGIN
Baseline	–	40	40	6.7
With liner	37	80	117	2.3

There are several possible measures that will increase the safety margin: (a) To increase the threshold impedance by increasing the longitudinal emittance and RF voltage at injection of the Collider; (b) To reduce the machine impedance by maximizing the liner ID and optimizing the size and shape of the holes or slots.

5.0 RESISTIVE WALL INSTABILITY

The growth time of the resistive wall instability is proportional to ID^{-3}. The baseline specification is 110 turns. When a liner of 25.3 mm ID is installed, the growth time will be reduced to 50 turns. It will be further reduced if the stainless steel pieces are introduced near the BPM for thermal insulation purposes. As a consequence, the requirement of the feedback system becomes more demanding.

This Page Intentionally Left Blank

REFERENCES

1. H. T. Edwards, SSCL-N-771 (1991).
2. W. Chou and T. Barts, "Wakefield and Impedance Studies of a Liner Using MAFIA," *Proc. Computational Accelerator Physics Conference (CAP93)*, San Francisco, February 22–26, 1993; also see SSCL-Preprint-204 (1993).
3. L. Walling, private communication.
4. S. Kurennoy, CERN Report SL/91-29; R. L. Gluckstern, CERN Report SL/92-05.
5. R. L. Gluckstern and J. A. Diamond, IEEE MTT, v. **39**, p. 274 (1991).

This Page Intentionally Left Blank

SECTION 6

Beam Coupling Impedance Measurements and Simulations of a Beam Tube Liner with Pumping Holes or Slots

E. Ruiz, L. Walling, Y. Goren, and N. Spayd

SECTION 6

Beam-Coupling Impedance Measurements and Simulations Of a Beam Tube Liner With Pumping Holes or Slots

E. Ruiz, L. Walling, Y. Goren, and N. Spayd

Superconducting Super Collider Laboratory*
2550 Beckleymeade Avenue
Dallas, TX 75237

1.0 INTRODUCTION

To avoid reduction of beam lifetime due to photodesorption and to shield the SSC collider ring bore tube from synchrotron radiation, it is proposed to include a holed liner within the bore tube that intercepts the synchrotron radiation while allowing required vacuum to be achieved. Discontinuities in the liner, such as pumping holes or slots, interrupt the beam image currents, resulting in beam coupling impedance. In addition, electromagnetic coupling through the holes in the liner allow power to circulate between the liner and bore tube in synchronism with the beam. This TEM wave would couple back into the beam pipe, thereby possibly presenting an unacceptably high impedance. The coupling impedance of pumping holes and slots is estimated analytically, and numerical and measurement results are presented.

2.0 ANALYTICAL ESTIMATION

Analytical determination of the coupling impedance of small apertures in metallic walls has been studied extensively, but only recently has their collective coupling impedance in a beam tube liner been described analytically. The pumping holes or slots in the liner excite electric and magnetic dipoles that scatter energy back into the beam pipe and couple some energy through the aperture into the coaxial region formed between the liner and bore tube. Gluckstern[1] calculates the impedance due to holes in a liner, including the effect of wall thickness and the outer coaxial region:

$$z_{\parallel} = \frac{jZ_o kP}{8\pi^2 b^2}\left[\psi_{in} - \chi_{in} - \frac{(\psi_{out} - \chi_{out})^2}{\psi_{in} - \chi_{in} - j8\pi b^2 \left(\frac{a}{k}\right) Lln\left(\frac{a}{b}\right)}\right]$$

and

$$z_{\perp} = \frac{Z_{\parallel}}{n}\left(\frac{2R}{b^2}\right),$$

* Operated by the Universities Research Association, Inc., for the U.S. Department of Energy under Contract No. DE-AC35-89ER40486.

where

$$\frac{a}{k} ln\left(\frac{a}{b}\right) = \frac{1}{4}\left(\frac{\delta_a}{a} + \frac{\delta_b}{b}\right)$$

and $\Psi_{out}, \chi_{out}, \Psi_{in}$, and χ_{in} are the magnetic susceptibility and electric polarizability for the inside and outside of the liner, Z_o is 377 Ω, $k = 2\pi f/c$, P is the number of holes, b is the liner radius, a is the bore tube radius, δ_a and δ_b are the skin depth for the bore tube and outer surface of the liner, respectively, L is the average axial hole spacing, and R is the ring radius. For small pumping holes, the contribution to the coupling impedance due to power circulating outside the liner is shown by Gluckstern to be negligible.

3.0 SIMULATION AND MEASUREMENT

First, the triaxial geometry for low-frequency longitudinal impedance was simulated. The beam pipe had a radius of 16.5 mm and thickness of 1 mm. We found that the outer coax contributed insignificantly to the coupling impedance, so to speed up the simulations the outer coax was eliminated. Since holes this size represent a very small impedance, it was necessary to detect minute phase shifts due to the holes. The simulations were converged until the uncertainty in the phase was much smaller than the phase shift (θ-θ_0), where θ_0, the electrical length of the reference liner, was calculated using c specified to about 5 decimal places. However, there was an error that could not be extracted by further adaptive passes when merely subtracting the length of the reference liner. This phase shift is due to small errors in the mapping of the 3-D tetrahedrons to the 2-D port surfaces. Another order of magnitude in phase accuracy was obtained by modeling the holes and the beam tube as separate elements, meshing and running the problem with both specified as vacuum, then, without changing the mesh, re-specifying the holes as metal and re-running over the frequency range. This was used as the "reference pipe" to normalize the data, and removed the port mapping errors as well as the baseline transmission.

3.1 Longitudinal Impedance

Measurements were made of a liner 2 m in length with 1010 pumping holes or 160 rounded slot using the wire technique[2] as shown in Figure 1. Initially, these were made with a center conductor of diameter 12.7 mm. However, simulation of the measurement using HFSS revealed that a 3.2-mm-diameter center conductor yielded more accurate results. For this reason, the longitudinal impedance data shown in Figure 1 was made with the 3.2 mm center conductor. In addition, measurements confirmed that the presence of the outer triaxial region did not significantly affect the observed impedance data, so later measurements were made without a bore tube.

Many variations of liner holes were simulated. These included variation in the number of holes axially from 2 to 20, variation of the number of holes longitudinally from 2 to 20, and varying the depth of the holes. These simulations confirmed that for low frequencies, the longitudinal impedance of the holes add, and the impedance is reduced by the wall thickness, as theory predicts. Simulations were also performed with small and large center conductors and compared to measurement results for the same parameters. We found very good agreement between the HFSS simulation of the wire technique and wire measurements. Extensive simulations were also performed for comparison with MAFIA simulations done by Chou and Barts.[3]

To reduce the low-frequency beam impedance, short slots are being considered. Simulations were run to study the influence of the shape of the slot, and measurements were performed using the wire technique on 3.2 × 31-mm rounded slots. The results of longitudinal impedance measurements and simulation at 5.0 GHz for holes and slots are shown in Table 1. A large savings in low-frequency impedance is achieved by using slots; the high-frequency behavior should be acceptable for short slots.

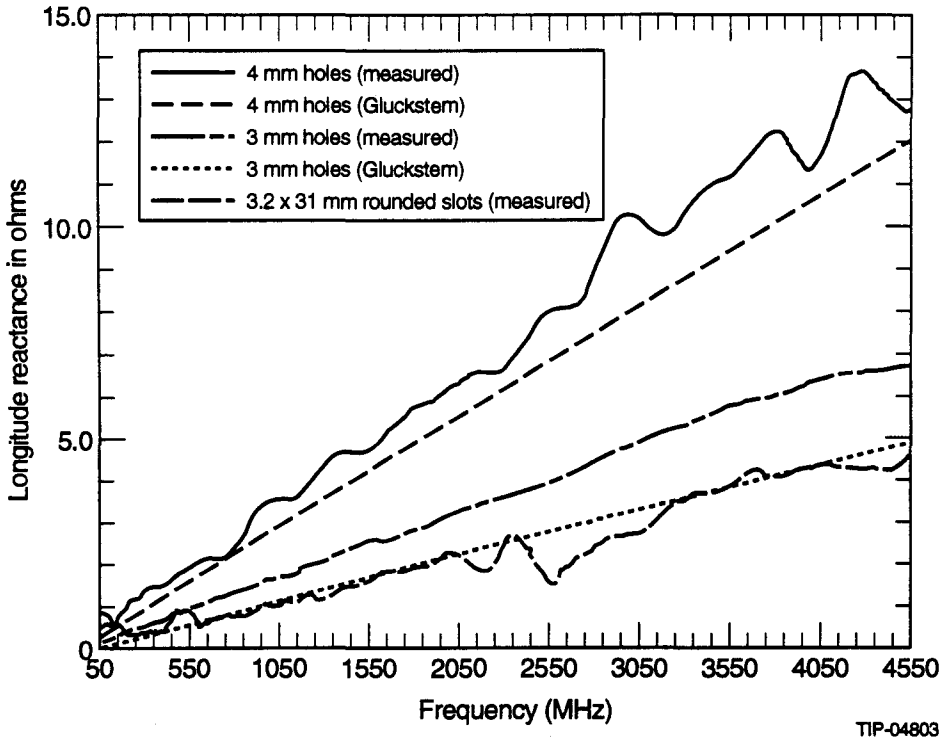

Figure 1. Measured Longitudinal Reactance of 1010 3-mm and 4-mm Diameter Holes and 160 Rounded Slots.

Table 1. LONGITUDINAL IMPEDANCE OF VARIOUS HOLE AND SLOT GEOMETRIES AT 5.0 GHz (b = 16 mm, thickness = 1 mm).

Slot Shape	Longitudinal Impedance per Slot (Ω)	Z/n Scaled To Number Required for Vacuum (Ω)
Rectangular (2 × 6 mm)*	0.0038	7.8×10^{-2}
Rounded (2 × 6 mm)*	0.0027	5.8×10^{-2}
Rounded (3.2 × 31 mm)	0.0172	4.0×10^{-2}
Elliptical (2 × 6 mm)*	0.0017	4.3×10^{-2}
Square Hole (2 × 2 mm)	0.0021	14×10^{-2}
Hole (dia = 3.0 mm)	0.0075	27×10^{-2}
Hole (dia = 2.0 mm)	0.0012	11×10^{-2}
Hole (dia = 1.5 mm)	0.00050	9.0×10^{-2}
Hole (dia = 1.0 mm)	0.00015	7.5×10^{-2}

*These values have been refined since their original publication.

3.2 Transverse Impedance

The transverse impedance was measured using two parallel center conductors driven 180° out of phase relative to each other (odd mode). The spacing between the 3.2-mm-diameter conductors is 16 mm. Holes and slots are distributed in rings with 10 holes or slots azimuthally per ring.

Measurements were made of a liner 2 m in length with 1010 pumping holes or 160 rounded slots using the wire technique.[2] Initially, these were made with a center conductor of diameter 12.7 mm. However, simulation of the measurement using HFSS revealed that a 3.2-mm-diameter center conductor yielded more accurate results. For this reason, the longitudinal impedance data shown in Figure 1 was made with the 3.2 mm center conductor. In addition, measurements confirmed that the presence of the outer triaxial region did not significantly affect the observed impedance data, so later measurements were made without a bore tube.

Transverse impedance for various hole and slot geometries was also simulated and compared to calculations by Kurennoy[4] for a zero-thickness liner. Kurennoy predicts a factor of 2 reduction in transverse impedance when there are 3 or more holes in one radial cross section. We find results half of Kurennoy's predictions, which is consistent when the reduction due to wall thickness is taken into account. Simulation results are shown in Table 2, while measurement results are shown in Figure 2.

TABLE 2. TRANSVERSE IMPEDANCE OF VARIOUS HOLE AND SLOT GEOMETRIES (b = 16 mm, thickness = 1 mm).

Slot Shape	Transverse Impedance per Slot (Ω/m)	Z/meter Scaled To Number Required for Vacuum (Ω/m^2)
Rectangular (2 × 6 mm)*	0.22	75
Rounded (2 × 6 mm)*	0.15	54
Rounded (3.2 × 31 mm)	0.88	34
Elliptical (2 × 6 mm)*	0.10	42
Square Hole (2 × 2 mm)	0.17	185
Hole (dia = 3.0 mm)	0.31	186
Hole (dia = 2.0 mm)	0.087	135
Hole (dia = 1.5 mm)	0.037	111
Hole (dia = 1.0 mm)	0.011	92

*These values have been refined since their original publication.

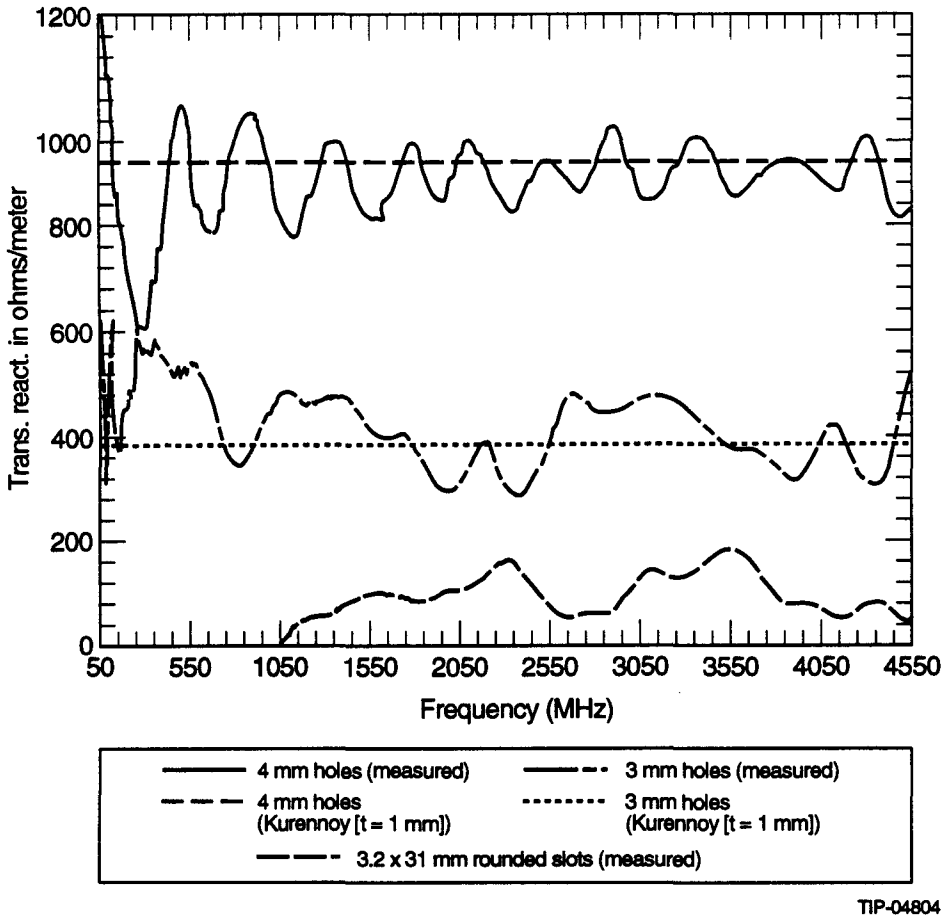

Figure 2. Measured Transverse Reactance of 1010 3-mm and 4-mm Diameter Holes and 160 Rounded Slots.

4.0 LINER LEAKAGE

Measurements of leakage were made using a triaxial impedance measurement technique,[5] as shown in Figures 3–5. The test liner is 2 m long, with 1010 holes in the center 1 m, and 0.5 m of solid pipe on both ends. The outer bore tube has a radius of 23 mm, while the liner has an inner radius of 16 mm and is 1 mm thick. The center conductor diameter was 12.7 mm for the leakage measurements. To measure leakage, the center conductor is placed on axis within the liner and the transmission through the pumping holes, S_{41}, is measured. A transmission measurement is also made through the coaxial regions formed between the liner and bore tube (S_{43}), and between the center conductor and liner (S_{21}), to correct the effects of hardware mismatches and multiple reflections in the triax on the S-parameters. S_{41} is time-gated, and divided by the square root of gated S_{43} and S_{21}. Liners with holes of diameter 1 mm, 2 mm, and 3 mm were measured. Results of leakage measurements and simulation are shown in Figure 3.

To estimate the contribution to the coupling impedance of the TEM wave traveling in the region outside the liner and 'feeding back' on to the beam, a two-step calculation was performed. A triaxial model, representing 20 holes axially and 22 longitudinally, was driven at the inner coax on one side. The other side has enough blank pipe forming the outer coax such that the maximum radial electric field, E_0, due to forward-leaked power could be determined. Thus, the ratio E_0/I was determined where I is the current on the center conductor within the liner. Then, the center conductor is removed from the model, the outer coax is driven, and the ratio of E_z, the maximum longitudinal electric field on axis, to the radial

electric field in the outer coax is determined. This ratio is then multiplied by the scaling ratio to yield the coupling impedance, which is the length of the liner segment with holes in it, and is the attenuation length in the outer coax. Numerical simulations were performed for holes of 2 mm, 3 mm, and 4 mm diameter. This inquiry confirmed that this contribution was much smaller than the inductive impedance for reasonably sized holes at low frequencies.

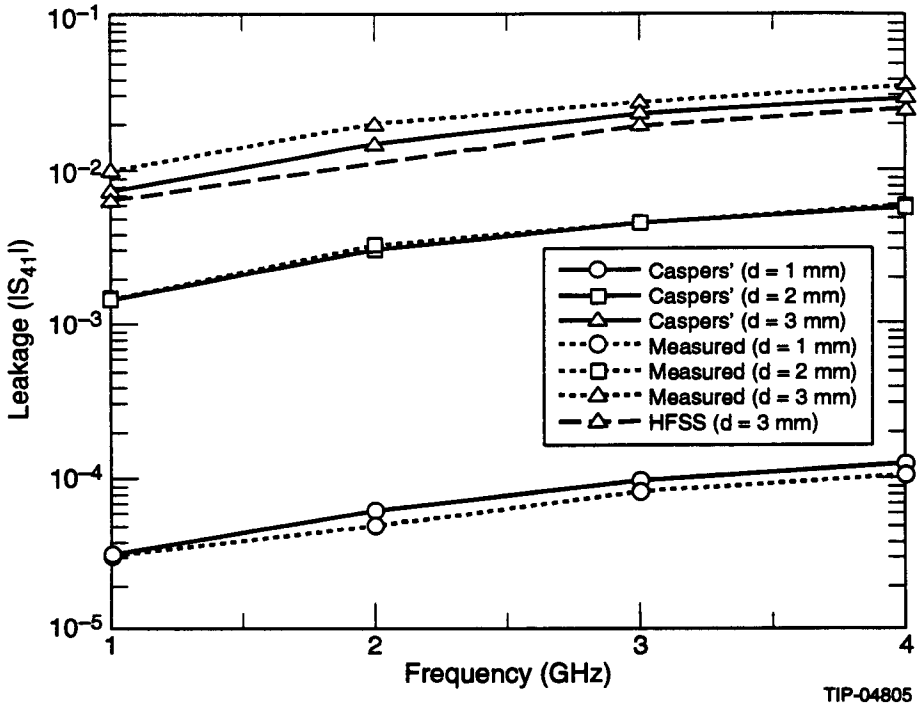

Figure 3. Leakage through a 1-mm-Thick Liner With 1010 Holes of Various Diameters.

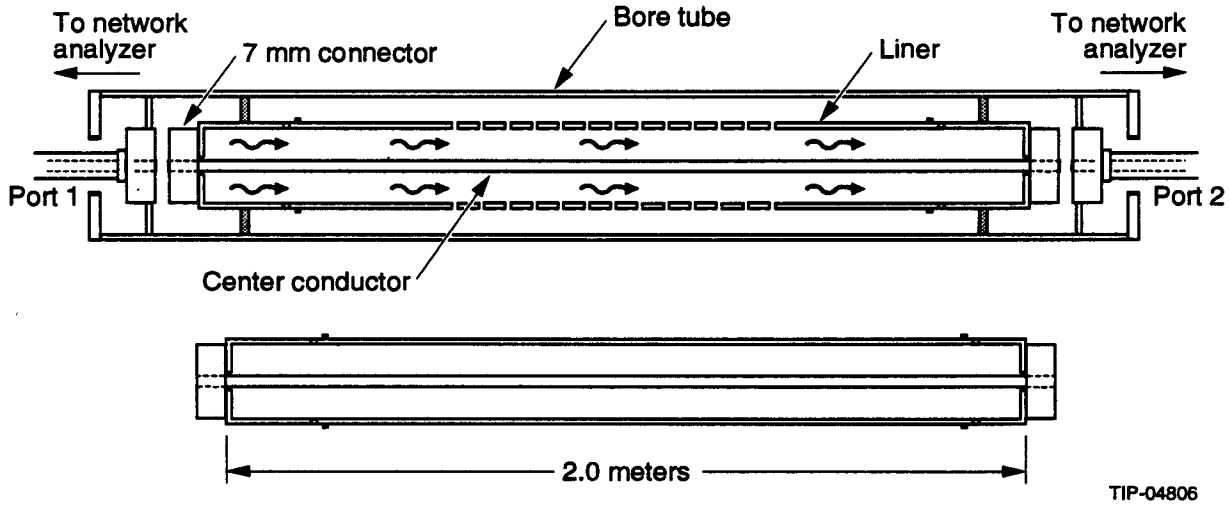

Figure 4. Schematic Diagram of Coupling Impedance Measurement.

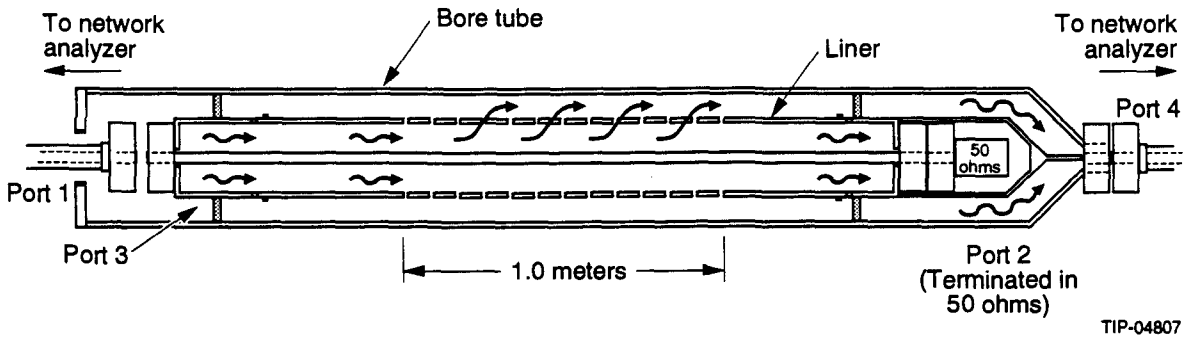

Figure 5. Schematic Diagram of Leakage Measurement.

5.0 DISCUSSION OF RESULTS

The simulations and the measurements both yielded low-frequency longitudinal impedances that are in good agreement with Gluckstern's thickness corrected estimate for the longitudinal impedance of round holes. Transverse impedance for round holes fit Kurennoy's theory well. Slots reduce the impedance but must be kept short to avoid the potentially large coupling impedance caused if the slots themselves become resonant.

We have investigated the high-frequency coupling impedance using TM_{01} excitation.[6] Because of disagreement between HFSS and MAFIA simulations done by Chou and Barts, we plan to measure the high-frequency impedance.[7]

This Page Intentionally Left Blank

REFERENCES

1. R. L. Gluckstern, "Coupling impedance of many holes in a liner within a beam pipe," CERN SL/92-05 (AP) (1992).
2. "Transmission-Line Impedance Measurements for an Advanced Hadron Facility," L. S. Walling, D.E. McMurry, D.V. Neuffer, and H.A. Thiessen, *Nucl. Instr. and Meth.* **A281** (1989) 433.
3. W. Chou and T. Barts, "Wakefield and Impedance Studies of a Liner Structure Using MAFIA," *Proc. of the 1993 Computational Accelerator Physics Conference*, Pleasanton, CA.
4. S. Kurennoy, "Beam Coupling Impedance of Holes In Vacuum-Chamber Walls," IHEP, Protvino. No. 92-84, 1992.
5. F. Caspers, "Triaxial line technique," in *Proc. of the Coupling Impedance Measurement Workshop*, Argonne National Laboratory-Advanced Photon Source, August 12–13, 1991.
6. E. Ruiz, L. Walling, and Y. Goren, "Liner Impedance Calculations Using HFSS," *Proc. of the 1993 Computational Accelerator Physics Conference*, Pleasanton, CA.
7. G. Lambertson, A.F. Jacob, R.A. Rimmer, and F. Voelker, "Techniques for Beam Impedance Measurements Above Cutoff," LBL-28190.

This Page Intentionally Left Blank

SECTION 7

Magnetic Field Considerations for the 80 K Beam Tube Liner

G. Snitchler

SECTION 7

Magnetic Field Considerations for the 80 K Beam Tube Liner

G. Snitchler

Superconducting Super Collider Laboratory*
2550 Beckleymeade Avenue
Dallas, TX 75237

1.0 INTRODUCTION

As part of the 80 K beam tube liner program it is important to determine the impact of the liner on the field performance. This paper discloses an initial estimate of the permeability effects associated with the liner. These estimates are performed with the finite element software called PE2D.[1] A brief discussion of eddy current effects is also presented.

2.0 PERMEABILITY MODEL

A relatively simple finite element model was generated to represent a beam tube with cooling channels. The dipole field was represented by enforcing boundary conditions on the vertical axis of $v\ (x = 0) = 0$ and $v\ (x = 4\ \text{cm}) = 260\ 000$ G/cm where v is the value of the potential. This generated a field of 65 000 G. The horizontal boundary conditions were defaulted to a field normal condition. An 180 degree model was required since the primary objective is the skew quadrupole effect of the unallowed harmonics.

Quadratic elements were used which are by definition six node triangles and approximately 9600 elements were incorporated into the model. This is probably an excessive number of elements but, skew quadrupole calculations are frequently difficult models to converge. The model has the beam tube and cooling passages vertically offset by 0.5 mm. The basic model configuration is displayed in Figure 1. In Figure 2, the elements are displayed near the cooling passages.

Several cases of the model were run to demonstrate the effect of individual components. The first case contained a permeability of 1.005 for the liner tube and for the cooling passages. The second case had all elements set to a permeability of 1.000 to represent a baseline for comparison with the first case. Case 3 had the permeability of the liner tube set to 1.005 and the cooling channels were set to 1.000 and case 4 the permeability of the liner tube set to 1.000 and the cooling channels were set to 1.005.

The four cases of the basic model were processed as linear models. The results of the three models are listed in Table 1. The sextupole information is reproducible and has the expected effect that the cooling tubes generate significant allowed harmonics but, the linear tube does not generate a significant effect to the allowed terms.

* Operated by the Universities Research Association, Inc., for the U.S. Department of Energy under Contract No. DE-AC35-89ER40486.

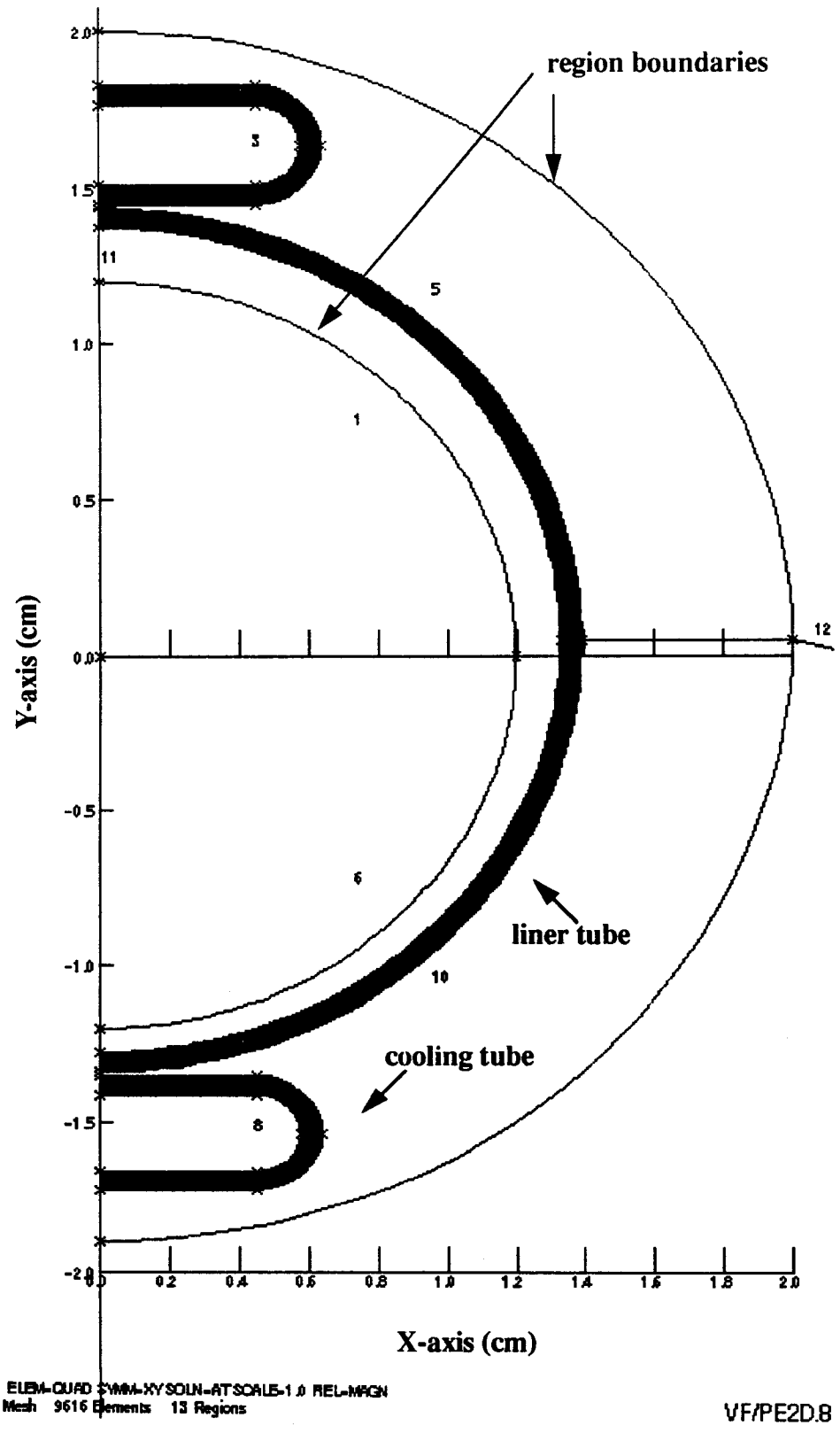

Figure 1. The Finite Element Model of the 80 K Liner and Cooling Channels.

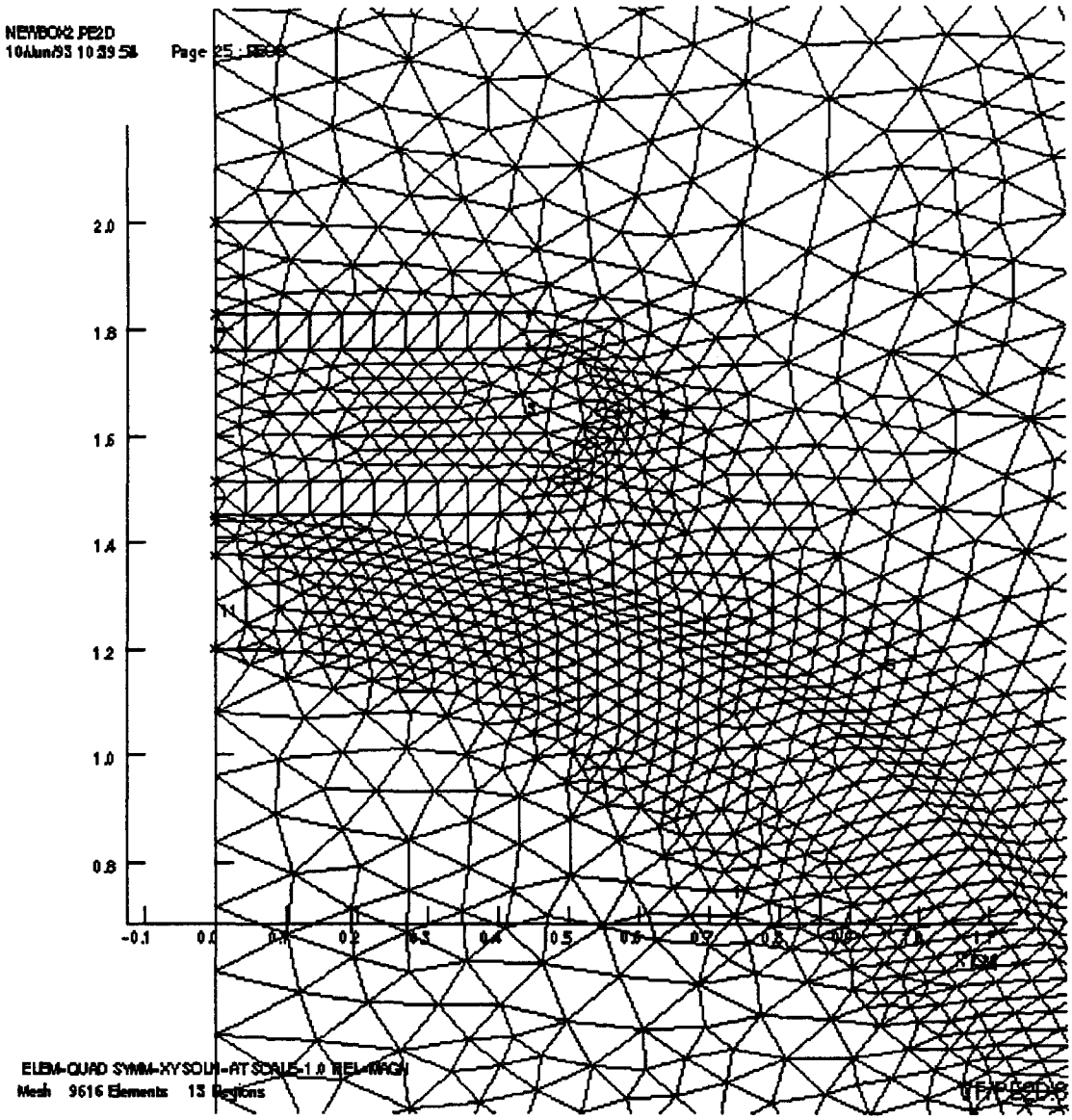

FIGURE 2. MESH NEAR TO THE UPPER COOLING CHANNEL.

A significant concern is that a vertical displacement would generate a skew quadrupole term. The skew quadrupole should be a feed down from the normal sextupole. If an offset of 0.5 mm is assumed, the skew quadrupole would be approximately 0.037 units.

Another technique which has been employed in non-linear models to address the field harmonic impact of the bus bar.[2] This technique involves running a case with and without the magnetization feature. In the case of the bus bar, the feature is the current density which alters the saturation profile of the yoke material. In this case, the change in the model is the permeability of the liner or cooling tubes. If this is a valid technique, one would expect a result similar to the feed down from the sextupole term. If a delta of the $a1$ term is taken from case 1 and case 2, one gets – 0.12 units which appears to be a high estimate.

A disturbing result is seen when summing cases 2 through 4. If the effects are truly linear, then the sum of each of the effects should total case 1. Yet, the sum is 0.04 units of $a1$ and case 1 has –0.07 units. The geometric element structure is identical between all cases. The only major difference is the change in element error function in cases 1 and 4 relative to cases 2 and 3. A possible conclusion is that the only way to have a valid model is to find and significantly reduce the error in cases 1 and 4. Most of the error in the calculation is generated in the cooling tubes. The mesh near the cooling tube is displayed in Figure 2. Consequently, the only valid information about $a1$ would be the feed down estimate from the normal sextupole. The skew harmonics calculation is the difference of two large numbers from upper plus lower coil integrations. The numerical integrations are very sensitive to the mesh and integration direction. In general, it is not clear that this is a valid technique in subtracting the results of two linear models when there appears to be a significant change in the error functions.

TABLE 1. RESULTS FROM PE2D MODELS.

CASE	μ LINER TUBE	μ COOLING TUBE	$a1$	$b2$	$b4$	$b6$
1	1.005	1.005	–0.07	–0.747	0.234	–0.025
2	1.000	1.000	0.05	–0.001	0.001	0.000
3	1.005	1.000	0.01	–0.011	0.000	0.000
4	1.000	1.005	–0.02	–0.737	0.234	–0.025

A second higher resolution model was developed to confirm the allowed harmonics results from the first F.E. model. The model is a symmetric 180 degree model with more meshing near the cooling tubes. There is no compelling reason why the model needed to be an 180 degree model except to test the convergence of an a1 calculation. The two permeability cases, 5 and 6, were run to demonstrate that the harmonics scale linearly with the susceptibility. The results are shown in Table 2 and are linear as expected.

TABLE 2. RESULTS FROM SYMMETRIC PE2D MODEL.

CASE	μ LINER TUBE	μ COOLING TUBE	$b2$	$b4$	$b6$	$b8$
5	1.0050	1.0050	–0.813	–0.261	–0.020	–0.029
6	1.0025	1.0025	–0.408	–0.131	–0.010	–0.015

Cases 5 and 6 is a more accurate estimate than the asymmetric model from Table 1. This is primarily because the allowed harmonics were only integrated in quadrant 1 and the 0.05 mm vertical offset moves the cooling tubes away from the integration radius. In any case, a material selection which reduces the permeability of the cooling tubes also reduces the harmonic error. Nitronic-40 has a permeability of approximately 1.0025 and would be approximately represented as case 6. Even in this case the effects and too large for the $b4$ and $b6$ terms.

Finally, attempts were made to introduce permeable material to offset the effects of the liner. At the time of publication, no reasonable solutions were found for reducing $b4$ and $b8$. The concentration of permeable material at nearly one angle, the cooling tube curved section, is the primary reason why it is difficult to reduce the $b4$ contribution. Optimization of the cooling passage shape may be the best alternative to reducing the allowed harmonic contribution. More studies would be required to resolve this issue.

3.0 EDDY CURRENT CONTRIBUTION

Another concern for a copper coating in the liner or in a standard beam tube without a liner, is the eddy current effects on the field harmonics. One can estimate the impact by computing the current density,

$$J = \dot{B}\sigma r\cos\theta, \tag{1}$$

where the change in the central field is $\dot{B}$ = 0.004 T/s, the conductivity of copper is $\sigma = 5 \times 10^9$ at 0.6T and rrr = 100, Reference 3. Wilson[4] expresses this as $J = J_1 \cos\theta$ and derives the eddy current dipole as

$$B_e = -\mu_o J_1 \frac{\Delta r}{2}.$$

The B_e would be approximately 0.15 G for the parameters listed above. This is a 4.2-K case with a 100 micron copper coating. If the $\sigma\Delta r$ is held constant, the impact would be the same on an 80 K copper liner. Any harmonics generated in a dipole magnet liner tube would be an asymmetry perturbation on this 0.15-G dipole field and would be very small.

4.0 CONCLUSIONS

This initial estimate of the permeability effects on the multipoles reveals a large impact on the allowed field harmonics. This would require design tune for the CDM magnet to meet the required performance specifications or a redesign of the beam tube liner cooling tubes to minimize the contribution to the allowed terms. If an 80 K liner is implemented, a redesign of the liner or a harmonic tune of the CDM would be required with field harmonics as a key concern. If the liner is implemented in the CQM and corrector magnets there may also be a significant impact to systematic but traditionally called unallowed harmonics since the liner has dipole symmetry.

One can use the allowed terms in the CDM magnet to estimate dislocations and rotations. The skew quadrupole term appears to be small if the dislocations are random. The $a1$ systematic specification is very small and even 0.037 units of systematic error nearly takes up the whole allowance.

The asymmetric finite element model does not appear to be stable and the technique of subtracting two models results to remove error inherent in the "geometric" element configuration may not be a sound approach. It is still possible that improving the error function in cases 1 and 4 could improve the reliability of the results.

Other concerns expressed at the liner PDRR were related to permeability effects associated with the brazing material. Since no information is available at this time related to the material and its permeability, it is impossible to estimate the effects. It must be emphasized that top-bottom asymmetries must be avoided. For example, if the brazing material has a significant permeability, it must be symmetrically applied to the top and bottom junctions between the cooling tubes and the liner tube.

This Page Intentionally Left Blank

REFERENCES

1. PE2D is a product of Vector Field, Inc., 1700 N. Farnsworth Ave., Aurora, IL 60505.
2. This technique has been used at Brookhaven National Laboratory (Gupta and Morgan), at the SSCL (Snitchler and Orrell), and at General Dynamics (D. Bliss). The GD publication was in the form of the Preliminary Design Review document.
3. Information was obtained from MAGDATA which is a database developed by the SSCL Magnet Division Test Department.
4. M. Wilson, *Superconducting Magnets,* Oxford Science Publications, (1983).

This Page Intentionally Left Blank

SECTION 8

Quench Induced Stress Analysis and Simulation for an 80 K CDM Liner

K. K. Leung

SECTION 8

Quench Induced Stress Analysis and Simulation for an 80 K CDM Liner

K. K. Leung

Superconducting Super Collider Laboratory*
2550 Beckleymeade Avenue
Dallas, TX 75237

Abstract

This report presents an finite element structural analysis,[1] instead of code,[2] for an 80 K liner [3] in a collider dipole magnet. The new issue for the Collider compared to earlier accelerators is the combination of synchrotron radiation with the 4.2 K bore tube of the superconducting magnets.[4] One of the design options is to use a liner within a bore tube to remove the radiated power and the accompanying photodesorbed gases that impair the beam tube vacuum. The SSC 80 K liner design conditions are vacuum luminosity lifetime = 150 hours and liner electrical conductivity $\sigma^*t>2E5\ \Omega-1$.[4] The bimetallic liner tube is subjected to cooldown and eddy current loads.[5,6] The liner tube is a two-shell laminate[3] with Nitronic-40 steel for strength and a copper inner layer for low impedance to the image currents induced by the circulating protons. The high electrical conductivity of the copper layer is essential for minimizing the power losses. Perforated holes are used to remove the photodesorbed gases for vacuum maintenance. The tube is cooled by 80 K lines. The code[2] is not applied to the structural design of the liner. The life of the liner involves structural integrity and keeping the copper laminate within yield stress limits to avoid change in conductivity for minimizing the power losses. The copper layer stress governs the structural design. The use of two dimensional linear elastic analysis and code[2] has been found to be inadequate for liner design. The liner is a three dimensional non-linear stress problem especially the axial thermal stress produced by the steel and the copper. Ignoring the copper stress in designing a liner or beam tube may produce an inadequate liner with high heat loss. This analysis will address the effect of thermal stress, non-axisymmetrical eddy current loads, and dynamic and non-linear material effect.

* Operated by the Universities Research Association, Inc., for the U.S. Department of Energy under Contract No. DE-AC35-89ER40486.

1.0 INTRODUCTION

The proposed SSC liner is a beam tube with two concentric tubes. A perforated liner tube inside a bore tube is designed to remove the photodesorbed gases and synchrotron radiation heat, and to withstand the eddy current and cooldown load without stressing the copper beyond yield. The steel bore tube is subjected to external buckling pressure caused by vaporized liquid helium from the quenching dipole.[7] The liner is designed to have the same reliability level as the ASME code.[2] The liner design can be predicted by nuclear quality analysis methods[8] in modeling for various loading conditions including eddy current load, bimetallic effect, and dynamic amplification. This effective stress analysis shall use SSC 50 mm dipole test data to establish the eddy current loadings of the liner. By designing the copper stress within the yield strength limit, the liner can be operated over hundreds of quench cycles in the 25 years of operation without additional power loss.

2.0 LINER TUBE DESIGN

Mechanical Design of the 80 K Liner System[3]

A minimum steel tube wall thickness is required to provide a maximum Collider Dipole Magnet (CDM) aperture and adequate annular cooling, but adequate strength is needed to keep the copper layer within yield strength. Nitronic-40 Stainless is employed for its non-magnetic property, for its matching of statistical thermal coefficience to the copper, and to provide structural strength to withstand the eddy current and thermal loads at cryogenic temperatures. copper is employed for maximum electrical conductivity to satisfy the requirement[4] of $\sigma \cdot t > 2E5\ \Omega{-}1$. The copper layer thickness is calculated as 0.5 mm for Cu's RRR = 7 @ 80 K with $\sigma = 4E8(\Omega m)^{-1}$. The life of the liner tube is lengthened by keeping the copper layer within the yield stress limit and to maintain the high surface finish of the copper layer by avoiding residual stress from post yield stress condition. Figure 1 shows the proposed liner system.

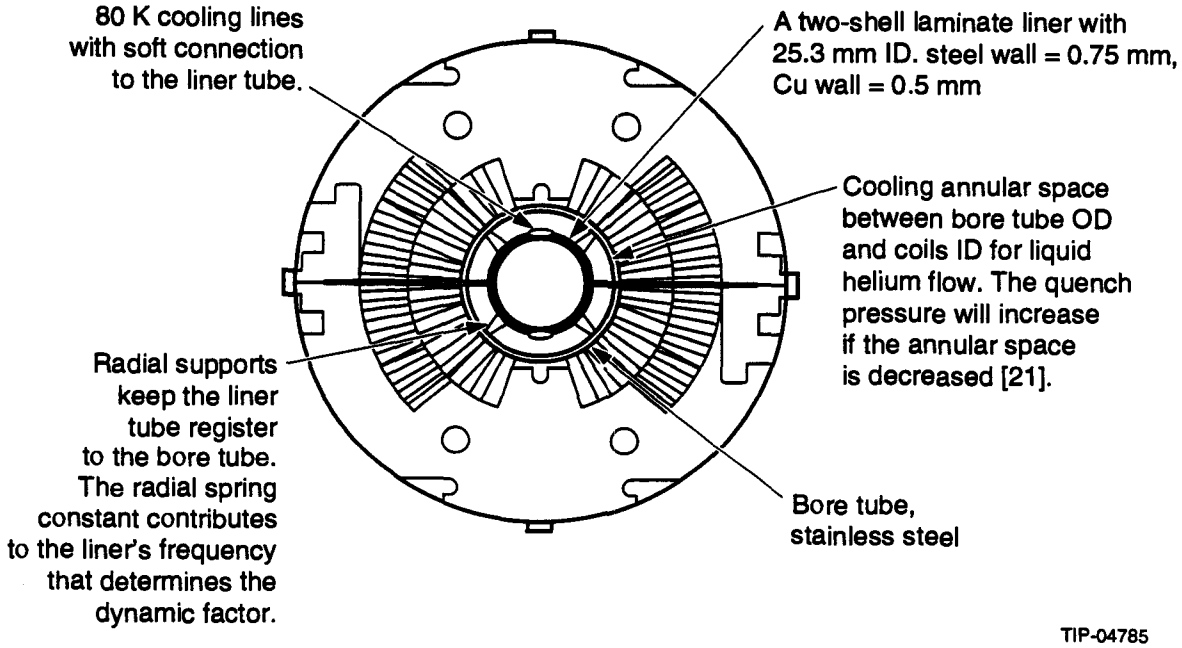

Figure 1. 80 K Synchrotron Radiation Liner System.

3.0 LOADING CONDITIONS, NON-LINEAR STRESS-STRAIN PROPERTIES AND BUCKLING EFFECT

The proposed SSC liner system replaces a beam tube that acts as a vacuum chamber for proton beams with two concentric tubes, a bore tube with a liner tube inside. The bore tube analysis is not included but the loading conditions are described as follows.

3.1 Bore Tube

The steel bore tube is subjected to external buckling pressure caused by vaporized liquid helium from the quenching dipole. The bore tube subjected to external pressure will be designed with the ASME code[2] providing that a bellow is employed to release the thermal load from the thermal strain from large statistical variation in coefficience of thermal expansion between the cold mass shell and bore tube and from a 150 K temperature rise in the quenching CDM.[24] In case a bellow is not used, inelastic buckling from tangent-modulus[22,26] $Et = d\sigma/de$, and an unstable deflected equilibrium controlling the critical stress must be carefully evaluated to prevent the low cycle fatigue failure of the bore tube and welded joints in long term service. Eddy current torque or lateral eddy current pressure[5,6,9,24,27] needs to be included for the bore design to account for additional local and global bending moments induced by the liner radial supports. The importance of designing the beam tube with eddy current torque[9] is also applied to the liner system design because the liner tube's radial supports must be designed with adequate strength to withstand the torque or the lateral force.[10]

The MSD specification[30] for vaporized liquid helium pressure is 2 MPa (290 psi). SSC test data[7] indicates that at 0.21 seconds after quench, the He Pressure is 0.86 MPa (125 psi) (DCA315.QB003 Feed End). SSC Helium venting computer simulation during dipole quenches[21] shows that a 37 mm OD's beam tube on 50 mm dipole has (2.33 MPa) and is 1.5 times lower than the 40 mm dipole (3.5 MPa) even though the 50 mm CDM contains 2.7 times more helium within and around the windings. The vaporized liquid helium pressure needs to be adjusted according to the bore tube OD and may double the specification's 2 MPa value for the bore tube design. The dynamic response factor[8,12,16,19,25] (1.2 to 1.75) needs to be considered in the liner system structural analysis. Some structural analysts[9,11,14] may not have included the dynamic factor in their analysis. The SSC data[7] indicates the pulse frequency $w = 1.19$ that is much lower than the pulse frequency $w = 0.05$ that produces a strain rate effect on the material. The hoop frequency of the tube is used to determine the response factor for He pressure and the eddy current loads. It is recommended that test data on a specified bore tube and the appropriate dynamic factor are used in the optimum design of the bore tube. A dynamic amplification factor of 1.25 should be applied for liner system preliminary design without detailed analysis of the liner system compliance. Bore tube analysis is not included in the present analysis.

3.2 Liner Tube

The liner tube is not part of the pressure vessel component but needs to be designed with the same confidence level in reliability as the ASME code.[2] The service life of the liner tube can be predicted by finite element analysis with a procedure proposed in this note to include the following loads and factors that increase the stress level on the tube.

3.3 Axisymmetrical and Non-axisymmetrical Eddy Current Loading[5,6,9,27]

The non-axisymmetrical eddy current load is simply the result of the eddy current seeking the minimum conductivity paths that formed from the mechanical tolerances of the tube as well as the residual stress or cold work imbalance in the current paths. Some structural analysts[28,29] discount these loads and their structural analyses[11,14] offer different results. It appears necessary to perform tests using two identical size copper tubes and to make one tube by jointing two half circular sections of the two tubes made from annealed and full hard copper. Test the tube in the SSC CDM to substantiate the net

Lorentz force.[15] A lateral pressure of 10 psi uniformly distributed along the axial direction of the beam tube is recommended to be used in liner design. A 3D magnet code analysis from EMAS27 indicates the net Lorentz existed.

3.4 Cooldown Load on the Bimetallic Two-shell Laminated Tube

Some beam tube structural analysts[9,11,14] may not include the bimetallic effect in their analysis because the copper is not considered to be a critical element in their beam tube design. A 2D linear elastic analysis by a finite element method or closed form solution can adequately predict the steel laminate layer stress. However, the state of the copper layer stress must be addressed to ensure that the liner would not generate additional power loss after many quenches. The present analysis indicates that the bimetallic cooldown load contributes a significant portion of the copper stress in a static state thermal stress analysis. It will certainly contribute more stress if thermal transient stress analysis[10,18] is performed. Stress factors are used to represent the stress concentration[31] and the hole's pattern on the liner strength effect. The hole shape and pattern are under intense study by the SSC to determine the impedance impact that is limited to < 170 mΩ/m for a single bunch fast head tail instability threshold.[4] The present analysis is based on an effective hoop section area of 7/9 = 0.777 with 2 mm diameter circular holes located away from the maximum stressed area at plus and minus 20 degrees from the equatorial axis. The latest consideration of hole shape is a long slot with a random pattern for low impedance. If the random hole pattern is selected for the liner design, the carry-over factor is no longer applied. A complex 3D model needs to be used for FEM analysis. The calculated copper stress on the exiting hole design is on the yield stress threshold. Post yield analysis of the liner should be performed to determine the service life of the liner. An increase in the steel thickness may be needed to lower the copper stress in the new configuration of hole shape and pattern to keep the copper stress within the safe stress limit. A non-linear stress-strain property needs to be used for the liner analysis due to the fact that the copper strength is about 3% of the stainless steel strength. The elastic modulus is changed not only with temperature but also with the copper stress level. Micro cracks may be developed on the copper layer from low cycle fatigue under multi-quench. This stress analysis is to design the copper layer to the safe stress level to avoid cycle fatigue problems for the hundreds of quench cycles[3] required in the 25 years of operation of the CDM. The copper yield stress limit is about 6 ksi.

4.0 LINER TUBE CONFIGURATION[3]

Figure 2 shows the proposed SSC dipole magnet liner system design. The liner tube (25.3 mm I.D.) is a bimetallic lamination with a 0.5 mm copper layer bonded by a stainless steel (Nitronic-40) tube with wall thickness of 0.75 mm.

Radial standoffs are used to support the liner tube from the bore tube. Torsional restraints are placed in some locations to avoid disturbing the dipole magnetic field. Bellows are used in the liner tube end to reduce the axial load induced by statistical variation in coefficient of thermal expansion of the cold mass shell and the bore tube materials and the temperature rise of the tube from the heated coils during quench. Two 80 K cooling tubes are attached to the liner tube for removing synchrotron radiation heat rated as 0.14 watts per meter. The holes are designed to maximize the luminosity lifetime of the liner system.The shape and the pattern of the holes have significant effects on the stress and impedance (<170 mΩ/m) of the liner tube. The present design uses circular holes arranged in a bend pattern with the cut-out hoop area in a ratio of 2/9 along the axial direction. Final hole shape and pattern are under intensive study in the liner program.

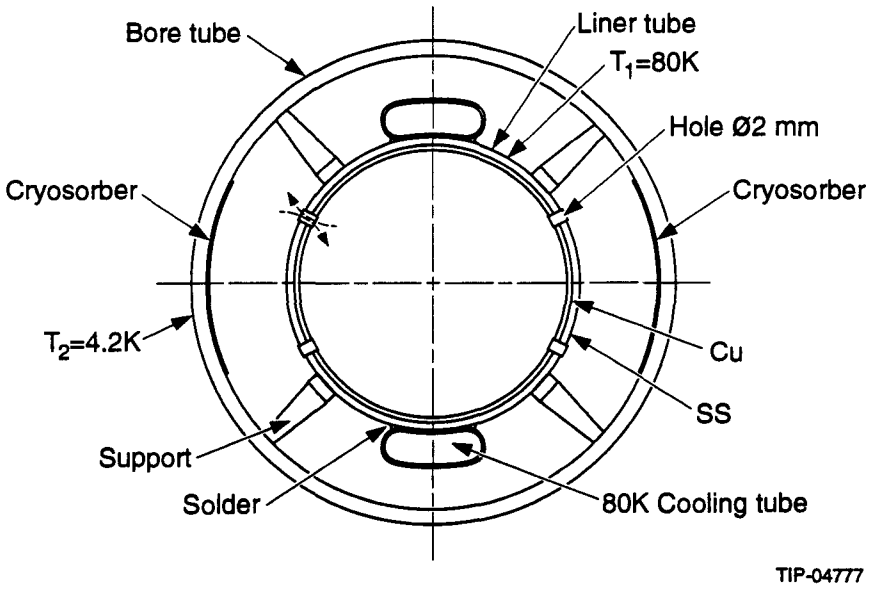

Figure 2. SSC Dipole Liner System.

5.0 EDDY CURRENT LOAD EVALUATION

The equation of equatorial eddy current pressure 4 (Lorentz pressure), also see Figures 3 through 9, is given as:

PLmax = B * (dB / dT) * b* t * σ = (1.45E – 4) * B(tesla) * dB/dT (tesla/sec) * b (m) * t (m)* σ (Ω–1 * m–1) [PSI].....(a)

Where B = dipole field strength.[6.01 T @ t = 0.18 sec]
dB/dt = the rate of change in during quench. [24.52 T^2/sec][13]
b = the mean radius of the copper layer. [1.29E–2 m][13]
t = the layer thickness of the copper. [5E–4 m]
σ = the copper electrical conductivity which depends on temperature, magnetic flux density and cold-worked condition. {4E8 Ω–1 * m–1}[4]

PLmax = 56 psi * 1.25 = 70 psi {0.482 MPa}

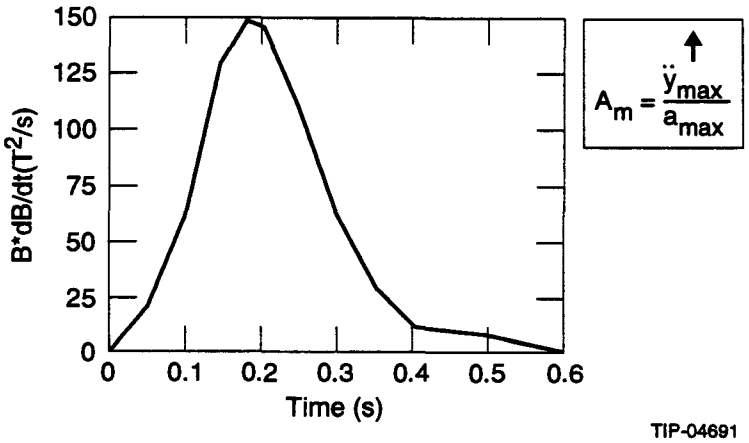

Figure 3. Dipole Field Strength.[13]

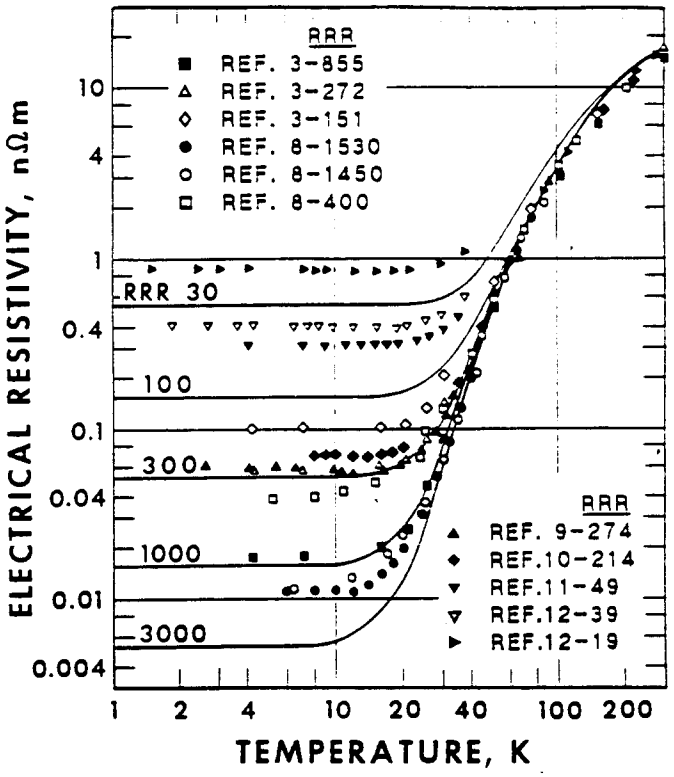

Figure 4. Copper Resistivity at Zero Magnet Field and Zero Cold Work.[23]

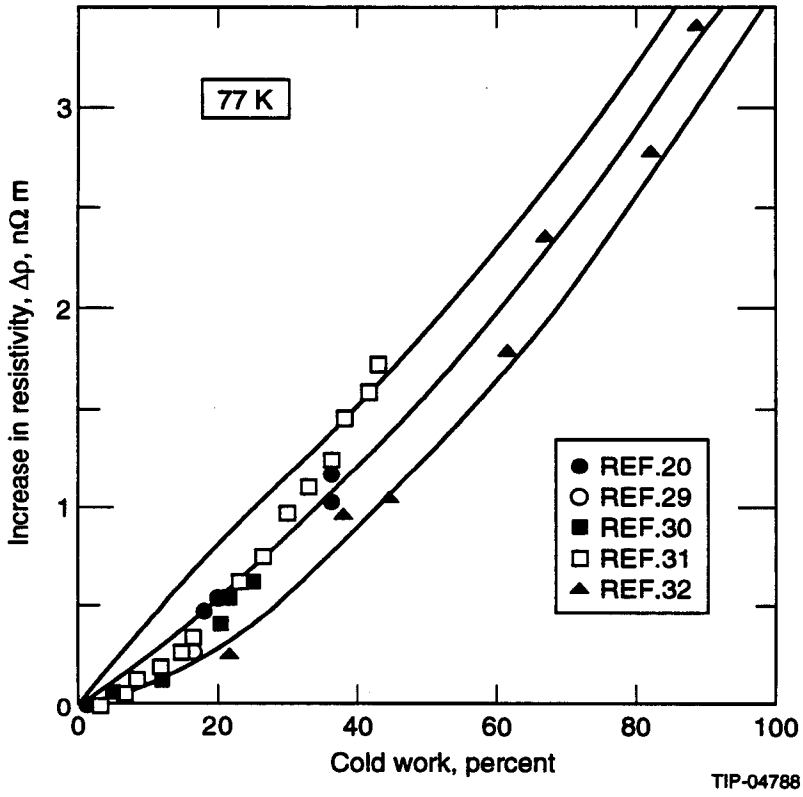

Figure 5. Copper Resistivity at Zero Magnet Field with Cold Work.[23]

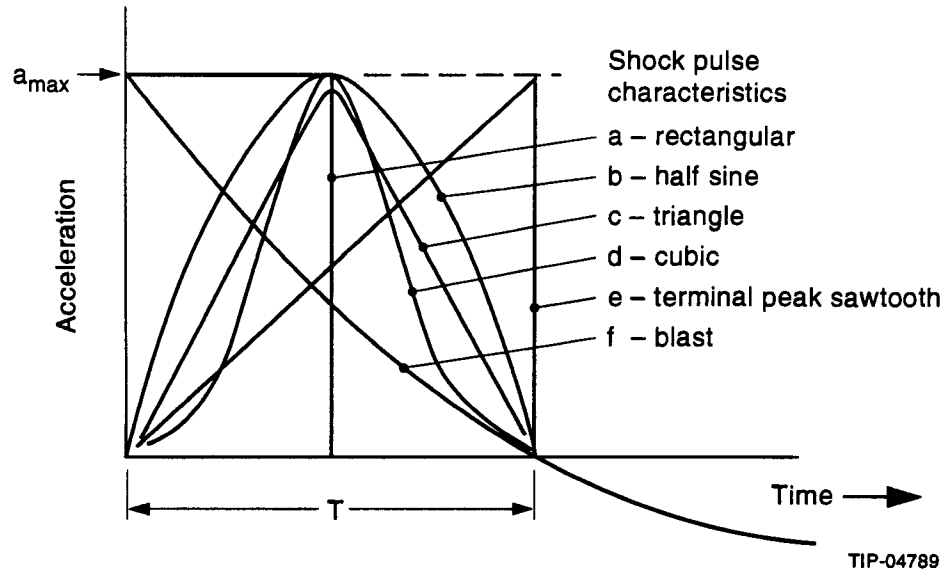

Figure 6. Dynamic Factor on Various Pulse Shapes.

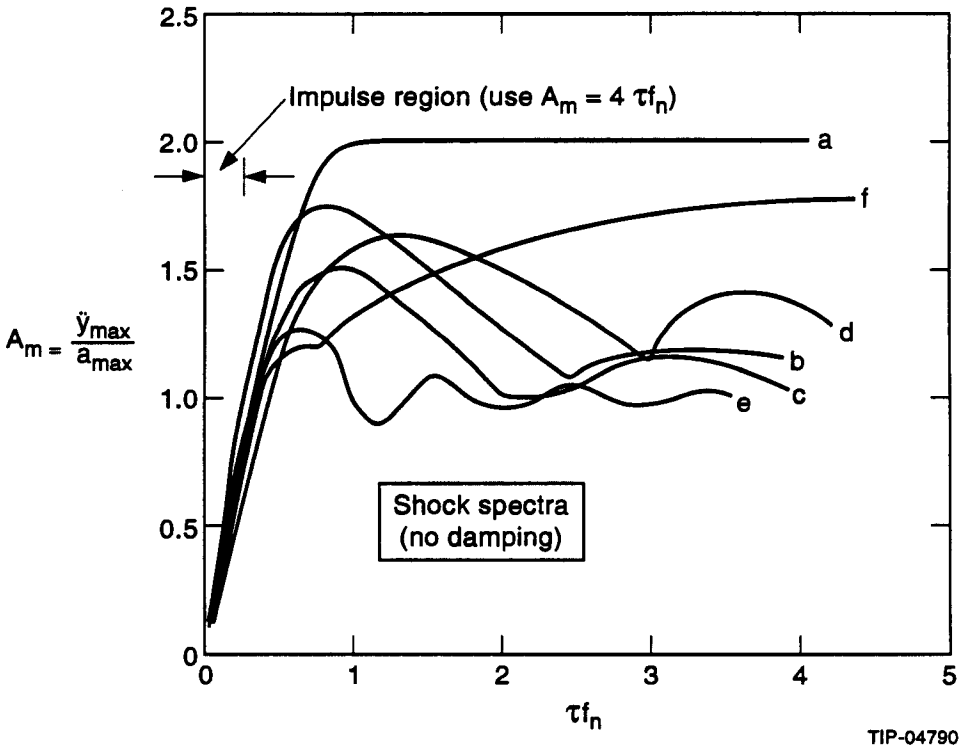

Figure 7. Dynamic Factor on Cubic Pulse.

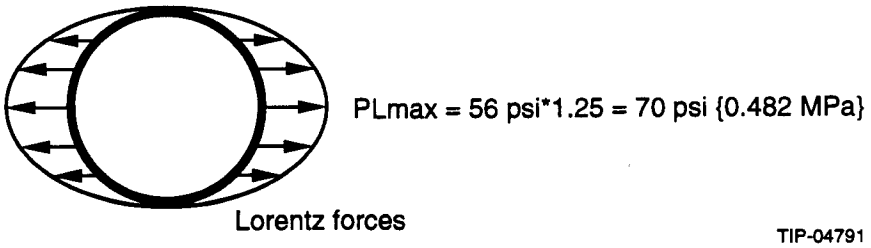

Figure 8. Eddy Current Pressure Distribution at Copper Liner.[14]

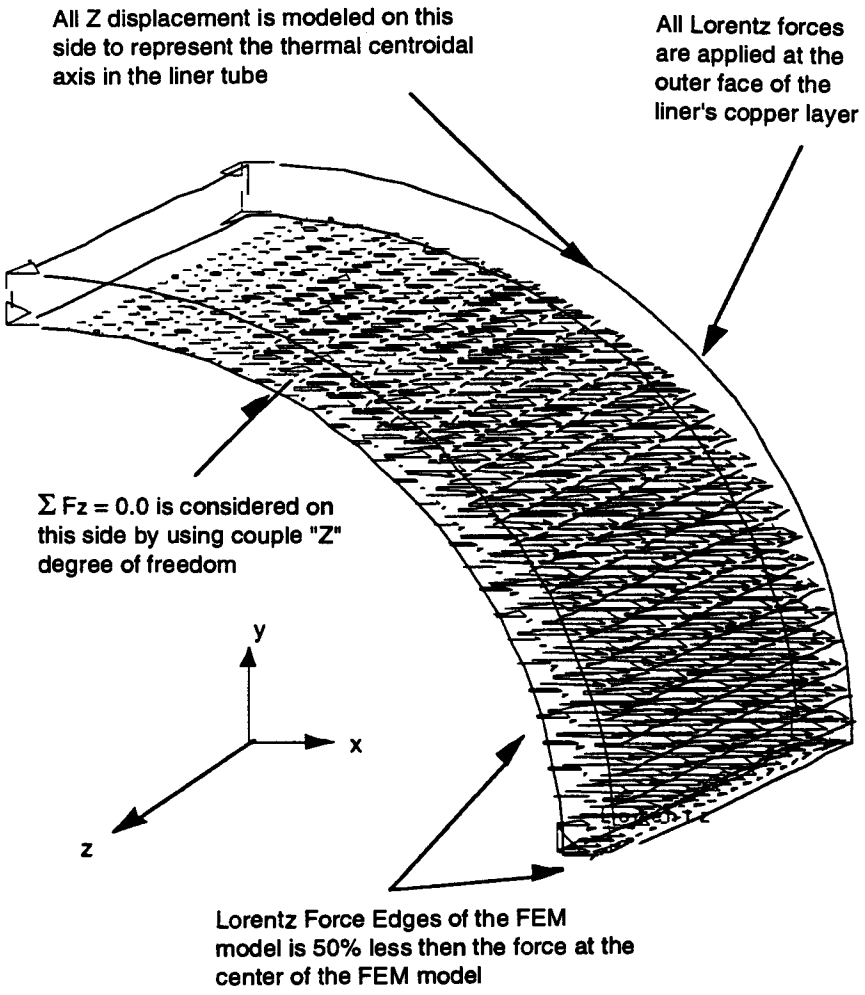

Figure 9. SSC Dipole Liner Tube FEM Model.

Eddy current torque, and lateral bending[6] forces are developed on the liner from geometrical tolerances in the tube by forming and plating processes. Torque and lateral bending stresses need to be determined for designing the bellow and torque restraints on the supports and all welded joints in the liner system.

6.0 FINITE ELEMENT MODEL

A three dimensional finite element model is employed to study the liner. The axial bimetallic effect combined with eddy current load may collapse the tube, develop bimetallic bond separation, or produce stress beyond the copper yield limit that diminishes the thermal and electrical performance of the liner tube and produces unacceptable power loss. A 2D model has proved to be inadequate for this kind of analysis.[7]

Effective stress analysis of the liner tube by the finite element method requires loadings with factors obtained from test data; (a) carryover factor for hoop strength of the liner as reduced by the perforated holes, the factor is 1.286 (9 mm/7 mm); (b) dynamic load factor based on the eddy current pulse shape is estimated as 1.25; and (c) stress concentration factor for circular hole is 2.0. This factor is applied on the FEM result for hole effect.

7.0 RESULT OF ANALYSIS (Stress, material properties plots are shown in Appendix)

Yield strength is dependent on copper grain size and purity and temperature. Figures 12 through 16 in the Appendix show the calculated stress, deflection of the liner, and material properties data. From Table 2.2 of Reference 7, the average yield is 44 MPa (6.4 ksi). The combined stress for the liner tube at the area away from the hole is 63.6 MPa (9.23 ksi) which is above the copper yield strength at 80 K.[7] The stress at area around the hole however, will increase to 127 MPa (18.5 ksi) which is within the ultimate strength. How much of the high stress around hole in the liner tube would affect the electrical performance of the liner system requires additional investigation. The alternate solution is to increase the steel tube wall thickness to keep the copper stress within yield strength limit. The steel wall stress of the liner tube is 289 MPa (41.9 ksi). The stress at the hole area in the steel wall will increase to 578 MPa (83.8 ksi) which is smaller than the 1034 MPa (150 ksi) of the Nitronic-40 steel's yield stress at 80 K.

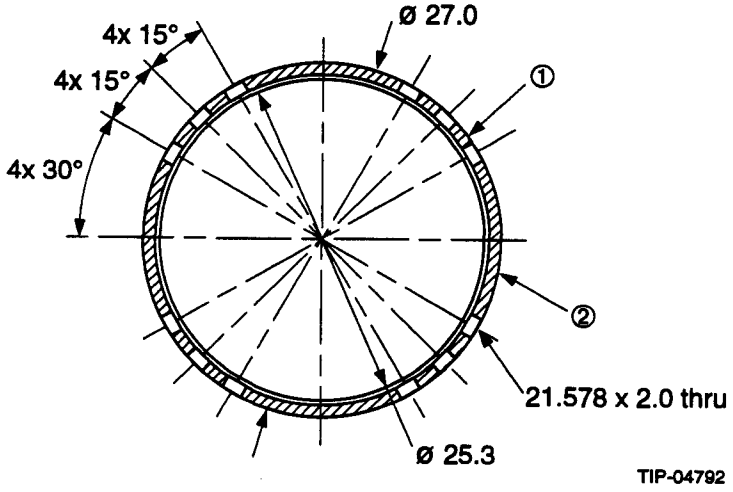

Figure 10. Steel and Copper Layer and Hole Location on the Liner.[3]

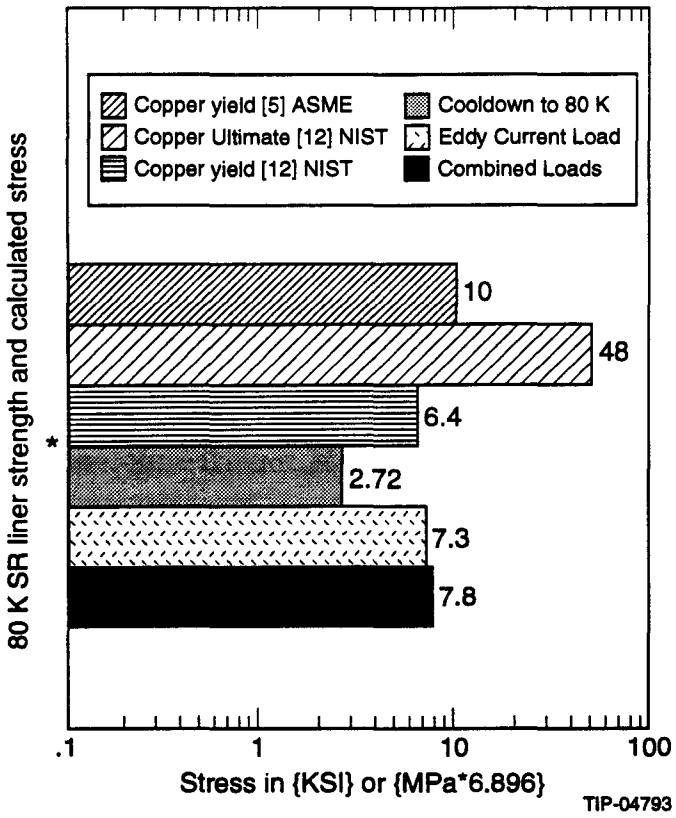

Figure 11. Copper Layer Stress In Annealed Copper.

8.0 CONCLUSIONS AND DISCUSSIONS

(1) High local stress on the copper layer reduces the service life the liner because the copper's resistivity may increase and micro-cracks may be developed in the copper surface leading to high heat load and power loss. Steel wall thickness may need to be increased to keep the copper within the yield stress limit.

(2) The analytical result is based on the shape and pattern of the perforated holes in the existing design[3] that shall produce the lowest stress. Changing the existing circular hole shape to the shape of an ellipse or a square, and rearranging the hole in a random array will increase the copper layer stress.

(3) A bellow and torque stoppers are parts of the design on the liner. The high slenderness ratio of the liner tubes ($l/\gamma > 200$) practically deducts the liner to zero axial load capacity. The non-axisymmetrical eddy current Loads[5] will destroy the bellow and the liner supports if torque stoppers are not used.[3,11]

(4) This analysis is based on annealed copper properties. Cold work or residual stress will raise the resistivity in post yield. Figure 5 indicates that the resistivity would double with a 10% to 20% increase in cold-work. We need to establish the amount of cold-work created by the yield copper under quench condition. The residual resistivity ratio (RRR) is a measure of the extent of physical defects such as lattice imperfections due to cold-working.[12] Additional analysis shows that stress at the hole area is 414 MPa (60 ksi) for a hard copper layer which has a yield stress of 207 MPa [30 ksi]. Hard copper is not recommended to be used. Pure copper wire has an RRR of 50, but very high-purity copper, well annealed, could have an RRR of 2000.[12] The liner fabrication technique by electrode-posited method is preferable. It is possible to use high purity copper or gold for the liner with 0.25 mm wall for the conductive layer or to increase the steel layer to 1.0 mm from the existing 0.75 mm. If the design guideline[1] for the copper conductivity as σ = 4E8(Ωm)–1 (80 K in 6.1 T. dipole field) is modified to = 8E8(Ωm)–1 with an identical liner as specified[4] [the liner stress will be reduced to a comfortable level.

(5) This report employs methods from various references[2,16,17,18,19,20,21,22,26,31,32] to establish a procedure to a design a liner with the steel layer structural safety equal to 3.0 as specified in code.[2] The copper stress is critical and a factor of safety based on the copper resistivity test with a value compatible to other system factor of safety such as 2.4 for the liner heat budget or 2.6 for the liner impedance is recommended.

This Page Intentionally Left Blank

REFERENCES

1. J. Swanson, "ANSYS Finite Element Code Revision 5.0," Swanson Analysis Systems, Inc. December 23, 1992.
2. American Society of Mechanical Engineers, "ASME Code Section VIII, Division 1," 1992.
3. Q. S. Shu, "Report on the ASST II Liner Status," SSCL Report, SSCL-N-805, Nov. 1992.
4. W. C. Turner, "Collider Beam Tube Vacuum," Presentation at the Beam Tube Size and Coating Meeting at SSCL, March 31, 1993.
5. A. Chao, "More on Copper Coating Considerations," SSCL Report, SSC-N-434, 1988.
6. K. K. Leung, "Non-Axisymmetrical Eddy Current Loads on Beam Tube in A Quenching Dipole Magnet," SSCL, Magnet Division Report, MD-TA-243. 1993.
7. Q. S. Shu, "Status of Tests on RF Surface & Magneto-Resistance," Presentation at the Beam Tube Size and Coating Meeting at SSCL, March 31, 1993.
8. K. K. Leung, "Seismic Stress of Piping and Heat Exchanger Supporting Structures," Section K-7/6, *Transactions of the 3rd International Conference on Structural Mechanics in Reactor Technology*, London, 1975.
9. K. Ng, J. Peterson, "Allowable Stress in The SSC Beam Tube During A Quench," SSCL Report, SSC-168, March, 1988.
10. K. K. Leung, "Nonlinear Stress Analysis of Superconducting Dipole Magnet Shell," MD-TA-167, September 1990.
11. S. Smith, R. Jaykumar, "Mechanical Analysis of Beam Tube Assemblies for SSC Dipoles During a Quench," IEEE Particle Accelerator Conference, San Francisco, May, 1991.
12. K. K. Leung, "Structural Analyses of SSC Collider 4.2 K Beam Tube," Presentation at the Beam Tube Size and Coating Meeting at SSCL, March 31, 1993.
13. Q.S Shu, K. Yu, SSC, Private Communication on "Analysis of Effect of H & T on Lorentz Force," April 21, 1993.
14. G. Snitrchler, Chris Ogle, "Structural Analysis of Collider Dipole Magnet Beam Tube," General Dynamics Space System Divisions Document Number M3A-100054, Preliminary Design Review Data Package-Presentations, Volume 1, March 23, 1992.
15. C. Haddock, "Lorentz Pressure on a Copper lined Beam Tube During a Quench for a 50 mm SSC Dipole," SSCL, Magnet Division Report, MD-TA-165. 1992.
16. K. K. Leung, "A Frequency Response Study of Collider Dipole Magnet Cold Mass For the SSC," *Supercollider 3*, Edited by J. Nonte, Plenum Press, NY & London, 1991.
17. K. K. Leung, "Engineering Design Study of CDM Cold Mass End Shell," *Supercollider 3,* Edited by J. Nonte, Plenum Press, NY & London, 1991.
18. K. K. Leung, "Transient Cooldown Stress in SSC Dipole Magnet Shell," *Supercollider 4*, Edited by J. Nonte, Plenum Press, New York & London, 1992.
19. K. K. Leung, Q.S. Shu *et al.*, "Effective Stress Of A 4.2 K Beam Tube in a Quenching Collider 50 mm Dipole Magnet For The SSC," pre-print of 1993 IEEE Particle Accelerator Conference, Washington, DC, May, 1993.
20. K. K. Leung, A. Paterson, "Advanced Light Source Accelerator Seismic Design Procedures," Lawrence Berkeley National Laboratory Mechanical Engineering Report, LSME-135, May, 1989.

21. R. Carcagno, W. Schiesser, "Helium Venting Computer Simulation During An SSC Dipole Quench," *Advances In Cryogenic Engineering*, Vol. **37**, Part A, Edited by R. Fast, Plenum Press, NY, 1992.
22. B. Johnston, *Design Criteria for Metal Compression Members*, John Wiley, Inc. NY 1966.
23. N. J. Simon *et al.*, "Properties of Copper and Copper Alloys at Cryogenic Temperatures," National Institute of Standards and Technical, NIST Monograph 177, February 1992.
24. J. Shuy, SSC, private communication.
25. "Environment Test methods and Engineering Guidelines," MIL-STD-810D, Department of Defense, USA.
26. F. Bleich, *Buckling Strength of Structures*, McGraw-Hill, 1952.
27. Y. Goren, SSC, private communication.
28. G. Snitchler, SSC, private communication.
29. C. Haddock, SSC, private communication.
30. SSCL Specification, Doc. No: M80-000001 Rev: A, Magnet System Specification, SSCL, Jan. 1992.
31. G. N. Savin, "Stress Concentration Around Holes," Kontsentratsiya Napryazhenii Okolo Otverstii, Moscow/Leingrad. 1951.
32. S. P. Timoshenko, *Theory of Elastic Stability*, pp 1–45, McGraw-Hill.

APPENDIX

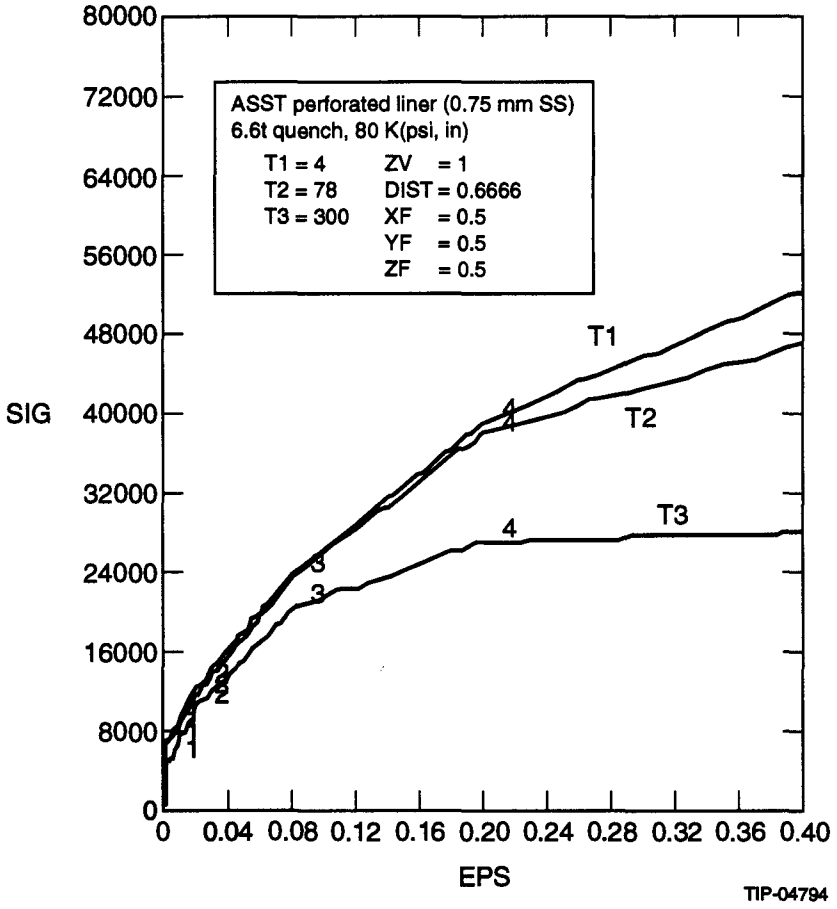

Figure 12. Non-linear Copper Stress-Strain at Annealed Condition.

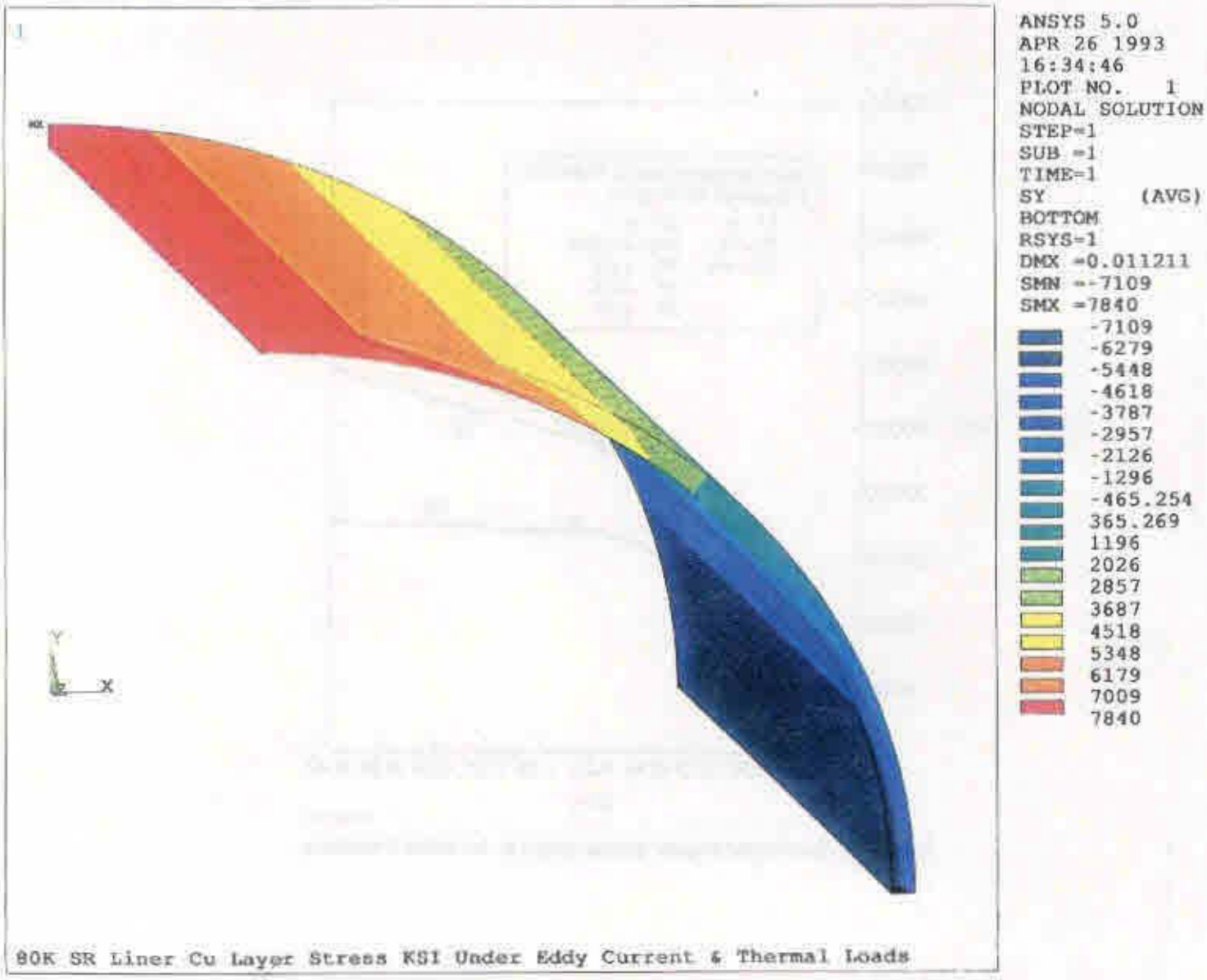

Figure 13. Combined Stress on Copper Layer in PSI.

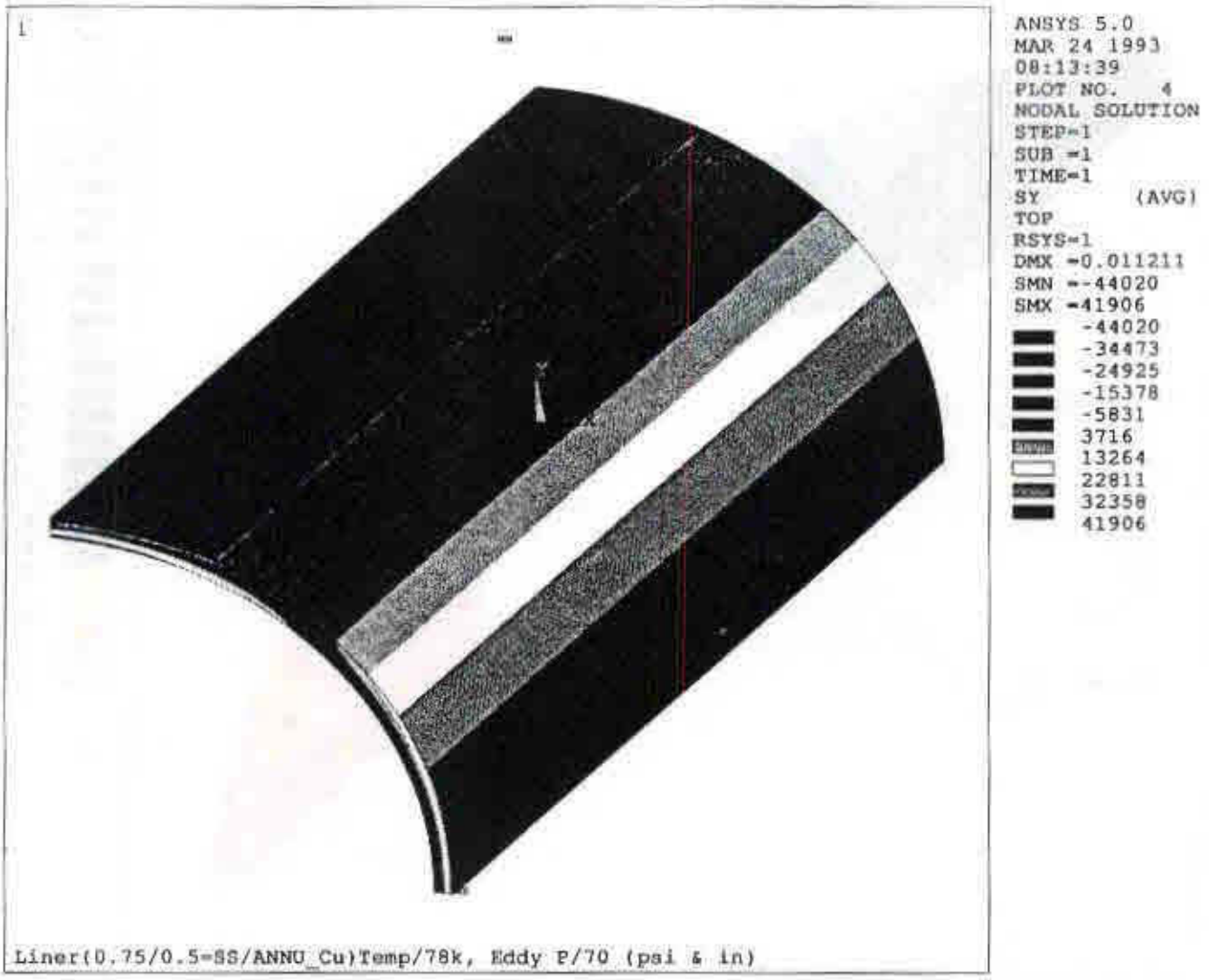

Figure 14. Combined Stress on Steel Layer in PSI.

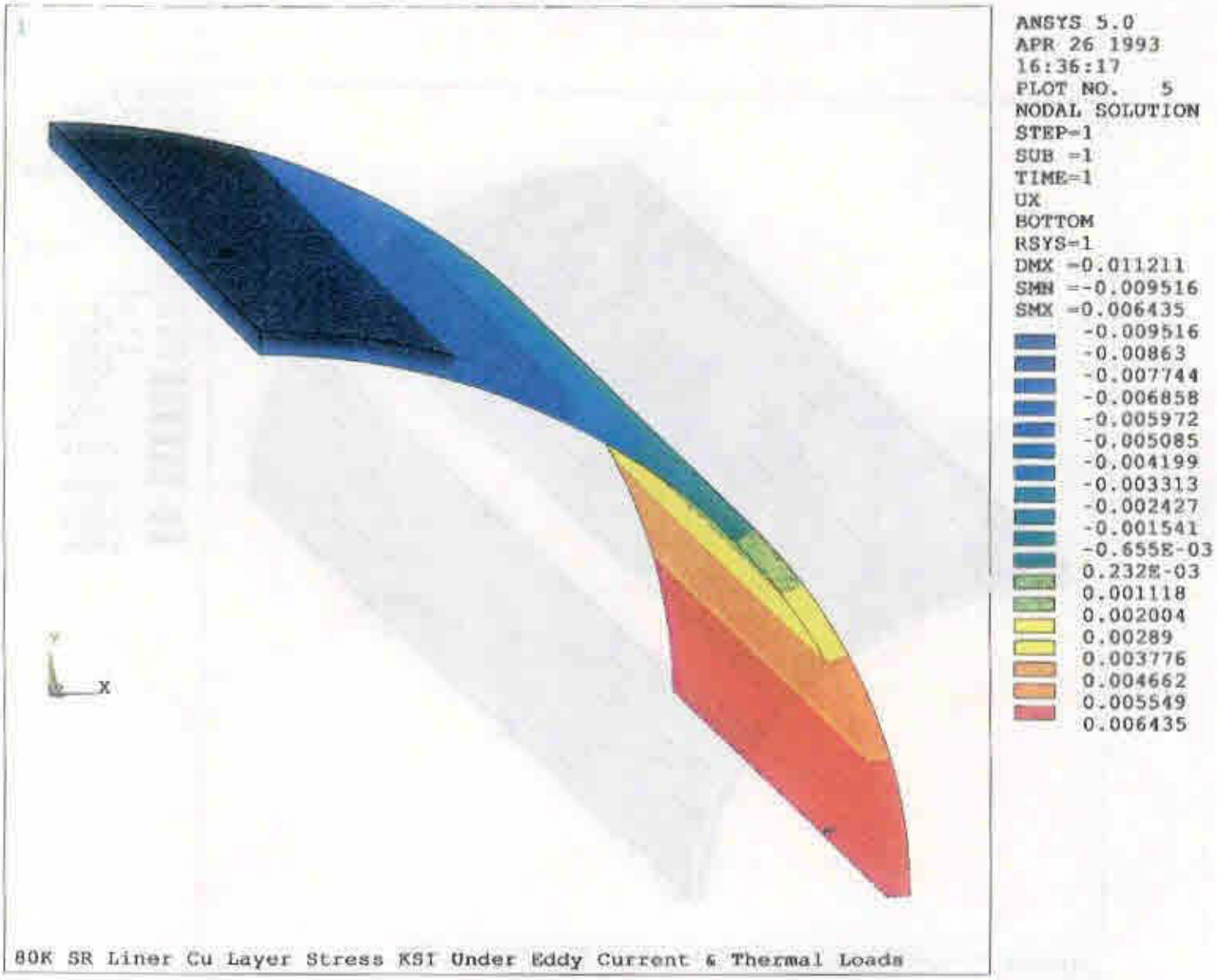

Figure 15. Radial Deformation of Liner in Inches.

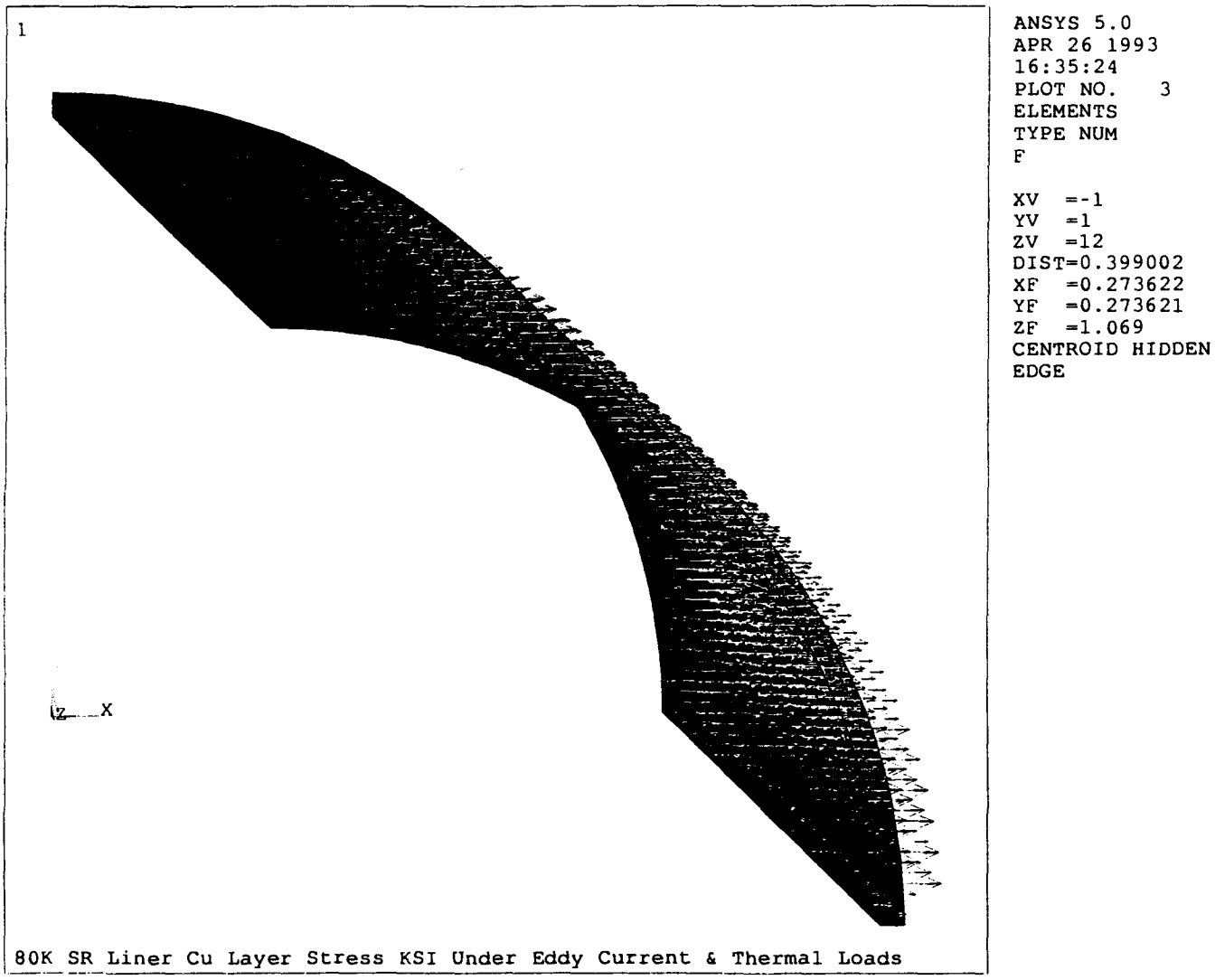

Figure 16. Eddy Current Forces on Liner.

This Page Intentionally Left Blank

SECTION 9

Quench Induced Stress Analysis and Simulation for an 80 K CQM Liner

K. K. Leung

SECTION 9

Quench Induced Stress Analysis and Simulation for an 80 K CQM Liner

K. K. Leung

Superconducting Super Collider Laboratory*
2550 Beckleymeade Avenue
Dallas, TX 75237

Abstract

This report presents a finite element structural analysis[1,2] for an 80 K all copper liner [3] in a Collider Quadrupole Magnet (CQM). The 1.0 mm copper wall thickness of the CQM liner tube with 24.3 mm ID is a design option to remove the radiated power and the accompanying photodesorbed gas that impair the beam tube vacuum. The SSC liner design conditions are vacuum luminosity lifetime = 150 hours and liner electrical conductivity $\sigma^*t > 2E5\,\Omega-1$.[4] The all copper CQM liner tube is free from cooldown thermal load but needs to withstand the eddy current loads.[5,6] The CQM liner tube is a monocoque copper structure for strength and for low resistivity to the image currents induced by the circulating protons. High electrical conductivity of the copper liner is essential for minimizing the sychrotron power losses. The copper stress must be held under the yield limit with adequate safety margin to prevent the substantial increase of copper resistivity from residual stress under post yield conditions. Reduction of copper conductivity is the main design objective to control the sychrotron heat within the heat load budget and to prevent degradation of the collider machine operation margin from "Beam Tube" heating induced quench. The copper liner stress needs to be considered as the predominant concern in the liner design. Ignoring the copper stress yield limit in designing a liner appears to produce an inadequate machine with a low operating margin. This design perception is also applied to the structural design of the "Beam Tube," "Beam Pipe" or "Beam Conduit" in general. It makes sense to coin the term "Beam Conduit" to adumbrate that this precarious accelerator component, beam conduit, is not an ordinary pipe used in the boiler shop. Perforated holes are located at the low stress positions of the liner to remove the photodesorbed gases for vacuum maintenance. The ASME B31.3 code is not applied to the structural design of the liner.[2] Two dimensional nonlinear analysis has been found to be adequate for the CQM liner design because the all copper monocoque structure is autarchic from the axial thermal stress from cooldown condition. This analysis will address the CQM liner stress induced by eddy current loads, holes, dynamic pressure and non-linear material effect.

* Operated by the Universities Research Association, Inc., for the U.S. Department of Energy under Contract No. DE-AC35-89ER40486.

1.0 INTRODUCTION

The proposed SSC CQM liner is a beam-conduit with two concentric tubes. A perforated all copper liner tube inside a bore tube is designed to remove the photodesorbed gases and synchrotron radiation heat, and to withstand the eddy current load without stressing the copper beyond its yield stress limit. The steel bore tube is subjected to external buckling pressure caused by vaporized liquid helium from the quenching CQM.[7] The liner is designed to have the same reliability level as the ASME code,[2] and a safety margin of 4.0 is recommended. The liner design can be predicted by nuclear quality analysis methods[8] in modeling for various loading conditions, including eddy current load, hole cut out effect and dynamic amplification. This effective stress analysis shall use SSC 50 mm CQM test data to establish the eddy current loadings of the liner. By designing the copper stress within the yield strength limit, the liner can be operated over hundreds of quench cycles in the 25 years of operation without additional power loss.

2.0 LINER TUBE DESIGN

Mechanical Design of the CQM 80 K Liner System[3]

Minimum copper wall thickness is required to provide the maximum CQM aperture and adequate synchrotron power heat cooling, but adequate strength is needed to keep the copper within yield strength. Copper is employed for maximum electrical conductivity to satisfy the requirement[4] of $\sigma \bullet t > 2E5\ \Omega{-}1$. The copper thickness is calculated as 1 mm. Figure 1 shows the data for the 80 K liner system.

3.0 LOADING CONDITIONS, NON-LINEAR STRESS-STRAIN PROPERTIES AND BUCKLING EFFECT

The proposed SSC liner system replaces a beam tube that acts as a vacuum chamber with two concentric tubes, a bore tube with a liner tube inside. The bore tube analysis is not included, but the loading conditions are described as follows.

3.1 Bore Tube

The steel bore tube is subjected to external buckling pressure caused by vaporized liquid Helium from the quenching CQM. The bore tube subjected to external pressure will be designed with the ASME code[2] providing that a bellow is employed to release the thermal load from thermal strain of statistical variation in coefficient of thermal expansion in cold mass shell and the bore tube and the 100 K temperature rise in the quenching CQM.[24] In case a bellow is not used, inelastic buckling from tangent-modulus[22,26] $Et = d\sigma/de$, and an unstable deflected equilibrium controlling the critical stress must be carefully evaluated to prevent the low cycle fatigue failure of the bore tube and the welded joints in long term service. Eddy current torque or lateral eddies current pressure[5,6,9,24,27] needs to be included for the bore design to account for additional local and global bending moment induced by the liner radial supports. The importance of designing the beam conduit with eddy current torque[9] is also applied to the liner system design because the liner tube's radial supports must be designed with adequate strength to within the torque or the lateral force.

The MSD specification[30] for vaporized liquid helium pressure is 2 MPa (290 psi). SSC test data[7] indicates that the pressure's peak is at 0.21 seconds after quench, the quench He. pressure is 0.86 MPa (125 psi) (DCA315.QB003 Feed End) and 1.41 MPa (205 psi) (DCA313 at ASST). SSC helium venting computer simulation during dipole quenches[21] shows that a 37 mm OD's beam tube on 50 mm dipole has 2.33 MPa (338 psi) and is 1.5 times lower than the 40 mm dipole 3.5 MPa (507.5) even through the 50 mm CDM contains 2.7 times more helium within and around the windings. The maximum buckling pressures which is located at the center portion of the magnet needs to be considered and most of the test pressures are recorded at the end of the magnet and therefore registered a factor of 2 in the pressure

difference. Futhermore, the vaporized liquid helium pressure needs to be adjusted according to the bore tube OD because the less the annular space between the coil and the bore tube the higher the buckling pressure that will be induced. The dynamic response factor[8,12,16,19,25] (1.2 to 1.75) needs also to be considered in the liner system structural analysis. The hoop frequency of the tube is used to determine the response factor for the He. pressure and the eddy current loads. It is recommended that test data on a specified bore tube and appropriate dynamic factor be used in the final design of the bore tube. A dynamic amplification factor of 1.25 should be applied for liner system in the preliminary design without detail analysis of the liner system compliance. Bore tube analysis is not included in the present analysis.

3.2 Liner Tube

The liner tube is not part of the pressure vessel component but needs to be designed with the same confidence level in reliability as the ASME code.[2] The service life of the liner tube can be predicted by finite element analysis[10,13,14,17,18,20,28,32] with a procedure proposed in this note to include the following loads and factors that increase the stress level on the tube. Axisymmetrical and Non-axisymmetrical eddy current loading[5,6,9,27] are to be considered the final design and some test data are needed because the unaxisymmetrical distribution of the liner copper resistivity induces from tube making process that cannot be determined analytically. The non-axisymmetrical eddy current load[6,9] is simply the result of the eddy current seeking the minimum conductivity paths that formed from the mechanical tolerances of the tube as well as the residual stress or cold work that are not uniformly distributed in the current's paths. A 3D model using magnet code analysis from EMAS27 also indicates the net Lorentz[15] existed based upon the ASME tolerances on wall thickness and diameter.[27]

Two dimensional non-linear elastic analysis by the finite element method is sufficient to predict the monocoque CQM liner stress. The state of the copper layer stress is used to ensure that the liner would not generate additional power loss after many quenches. Stress factors are used to represent the stress concentration[31] and the hole's pattern on the liner strength effect. The hole shape and pattern are under intense study by the SSC to determine the impedance impact.[4] The present analysis is based on an effective hoop section area of 4.5/6 = 0.75 that produces a carryover factor of 1.33. The 2 mm diameter circular holes are positioned away from the maximum stressed area. The copper's elastic modulus is changed not only with temperature but also with the copper stress level. This stress analysis is to design the copper layer to the stress level to ensure the liner is good for the hundreds of quench cycles[3] required in the 25 years of operation of the CQM. The copper yield stress limit is about 6 ksi.

The eddy current forces (Figure 2) acting on the CQM are calculated by PE2D Code.[29] The forces are larger than the forces as evaluated by the code EMAS.[27] Conservative eddy loads are used for this analysis.

Eddy current torque, and lateral bending[6] forces are developed on the liner from geometrical tolerances in the tube by forming and plating processes. Torque and lateral bending stresses are needed for designing the bellow and torque restraints on the supports and all welded joints in the liner system.

4.0 FINITE ELEMENT MODEL

A two dimensional finite element model, Figure 3, is employed to study the liner.

Effective stress analysis of the liner tube by the finite element method requires loadings with factors obtained from test data: (a) carryover factor for hoop strength of the liner as reduced by the perforated holes, the factor is 1.286 (9 mm/7 mm); (b) dynamic load factor (Figures 6 and 7) based on the eddy current pulse shape is estimated as 1.25; and (c) stress concentration factor for circular hole is 2.0. This factor is applied to the FEM result for hole effect.

5.0 RESULT OF ANALYSIS (Stress, material properties plots are shown in Appendix, Figures 14–16)

Yield strength is dependent on copper grain size and purity and temperature. From Table 2.2 of Reference 7, the average yield is 44 MPa (6.4 ksi). The combined stress for the liner tube at the area away from the hole is 25.5 MPa (3.7 ksi) which is below the copper yield strength at 80 K.[7] The stress at area around the hole however, will increase to 51 MPa (7.4 ksi) which is within the ultimate strength. How much the high stress around the hole in the liner tube would affect the electrical performance of the liner system requires additional investigation.

6.0 CONCLUSIONS AND DISCUSSIONS

(1) High local stress on the copper layer reduces the service life of the liner because of the reduction of copper conductivity. Micro-cracks may be developed in the copper surface leading to high heat load and power loss. The maximum CQM stress is 25.5 MPa (3.7 ksi) in over 60% of the liner area. Refer to Figures 8 through 13 for stress data. Also see Appendix, Figures 15 and 16. The low stress regions are located at 25/75 degrees (plus or minus 10 deg.) from the equatorial axis. Considering 44 MPa (6.4 ksi) as the copper yield stress. A safety margin of 1.73 is provided in the present design. A factor of 4.0 is applied in the analysis as the ASME safe factor to cover hole stress concentration effect as well as the residual stress that may exist according to ASME consideration.

(2) The analytical result is based on the shape and pattern of the perforated holes anywhere in the existing design.[3] The 1.73 safe margin in the present design will increase if the holes are designed for the low stress locations.

(3) A bellow and torque stoppers are part of the design on the liner. The high slenderness ratio of the liner tubes (l/g >200) practically deducts the liner to zero axial load capacity. The non-axisymmetrical eddy current Loads[5] will destroy the bellow and the liner supports if torque stoppers are not used.[3,11]

(4) This analysis is based on annealed copper properties. Cold work or residual stress will raise the resistivity in post yield stress condition. Figure 5 indicates that the resistivity would double with a 10% to 20% increase in cold-work. We need to establish the amount of cold-work created by the yield copper under quench conditions. The residual resistivity ratio (RRR) is a measure of the extent of physical defects such as lattice imperfections due to cold-working.[12]

(5) The copper stress is critical and a factor of safety based on the copper yield stress to 2.4 that is compatible with other system safety factors, such as 2.4 for the liner heat budget or 2.4 for the liner impedance, is recommended.

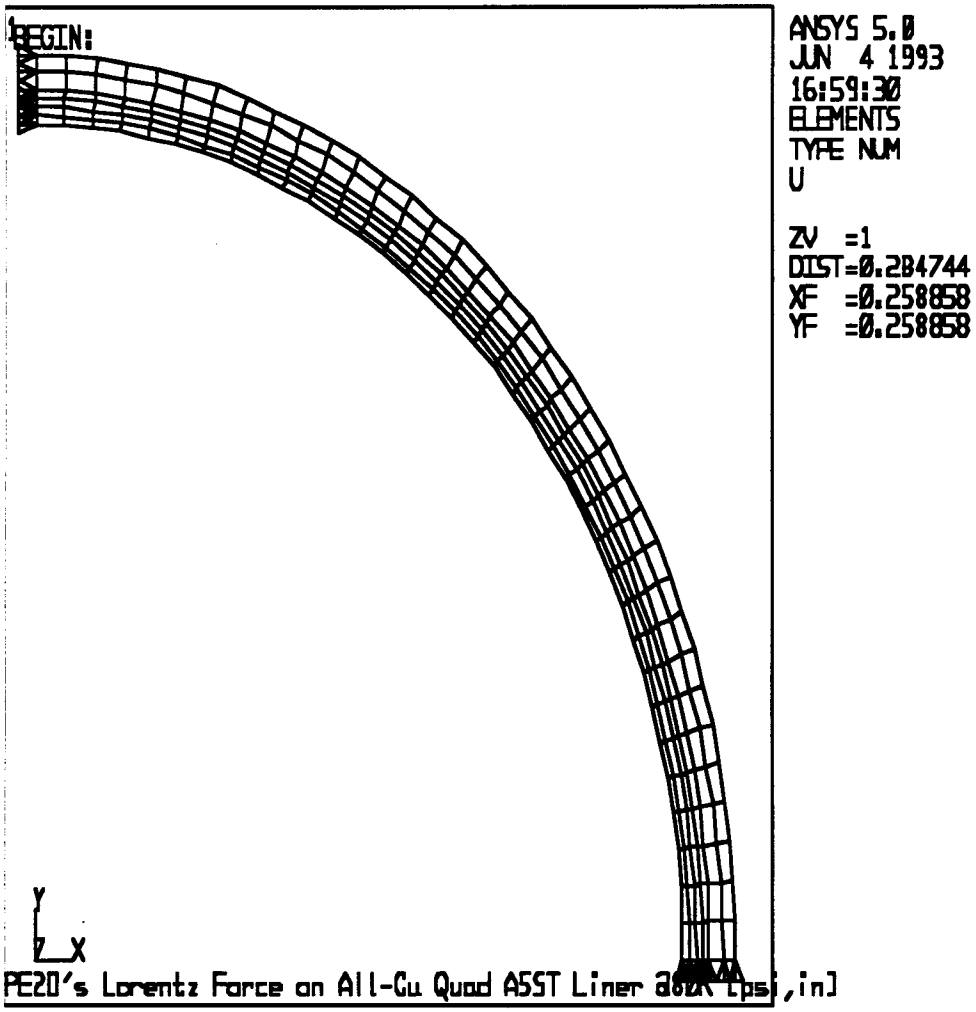

Figure 1. 80 K CQM Synchrotron Radiation Liner System (Lorentz Force).

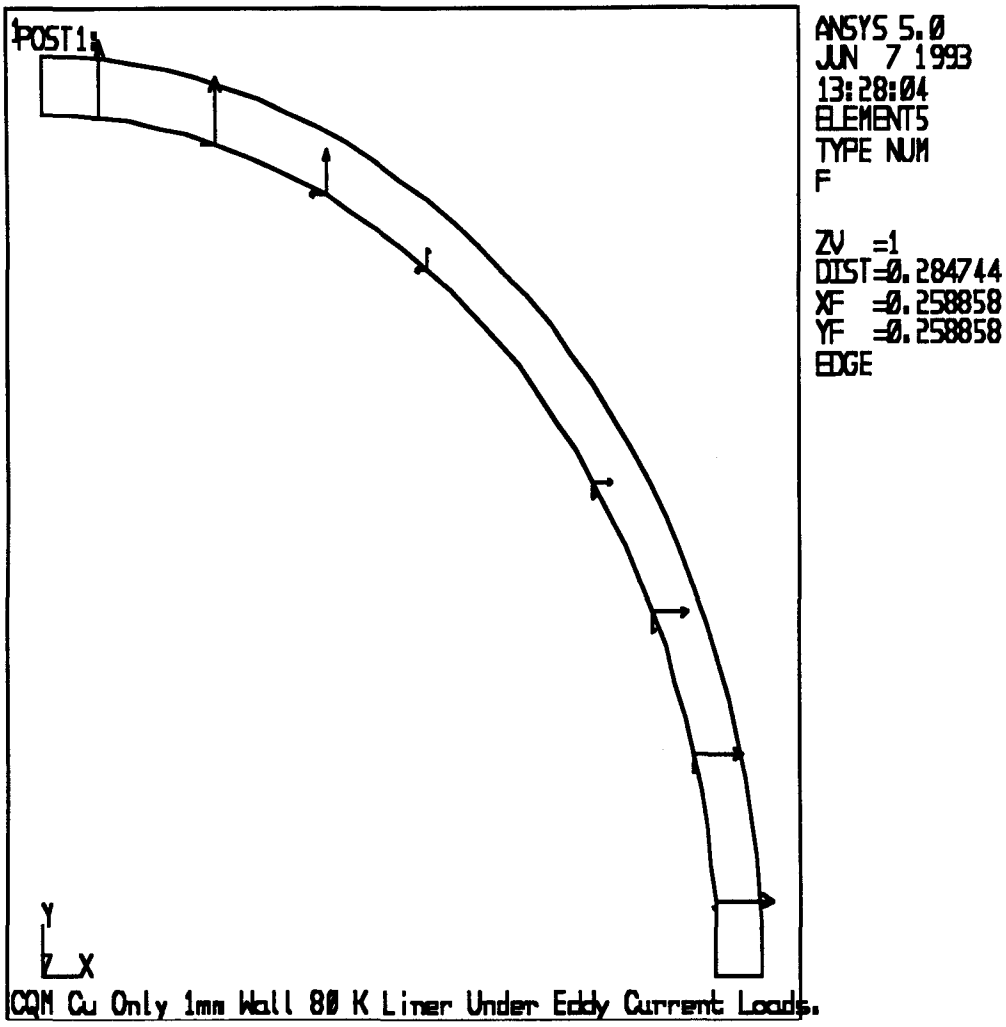

Figure 2. SSC CQM Liner System (Eddy Current Loads).

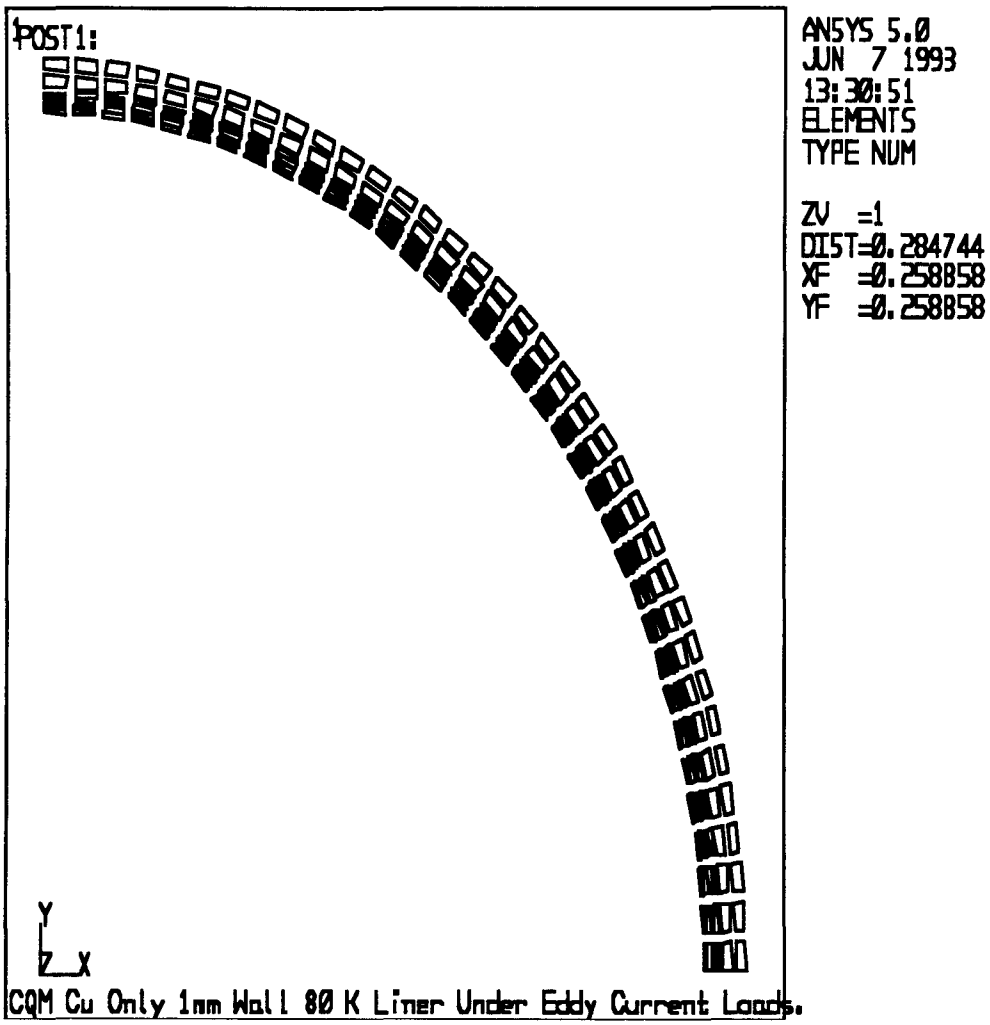

Figure 3. SSC CQM Liner Tube FEM Model.

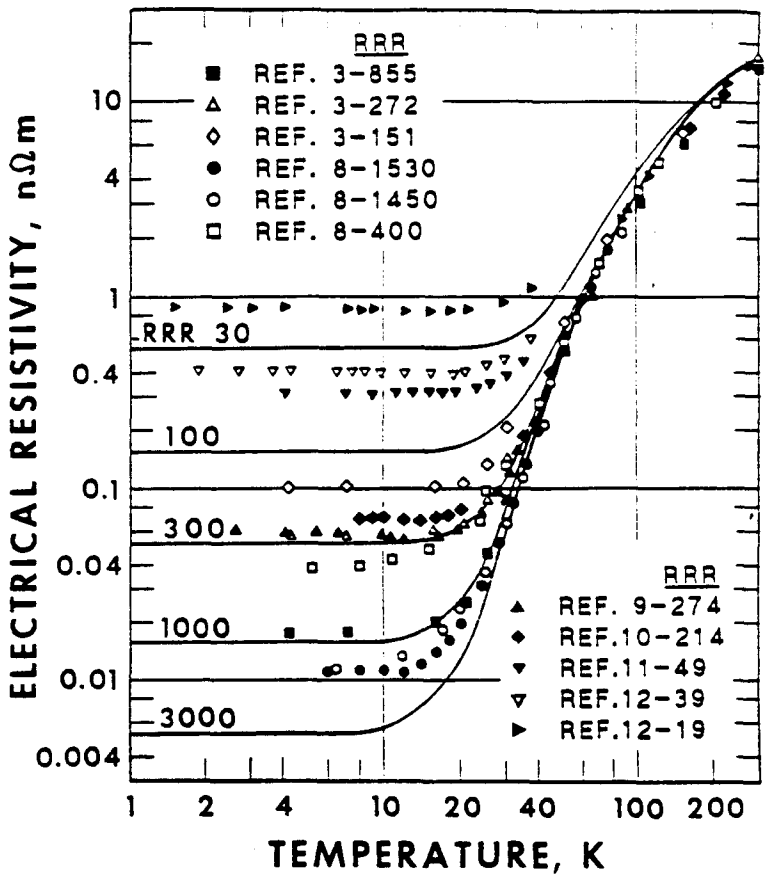

Figure 4. Copper Resistivity at Zero Magnet Field and Zero Cold Work.[23]

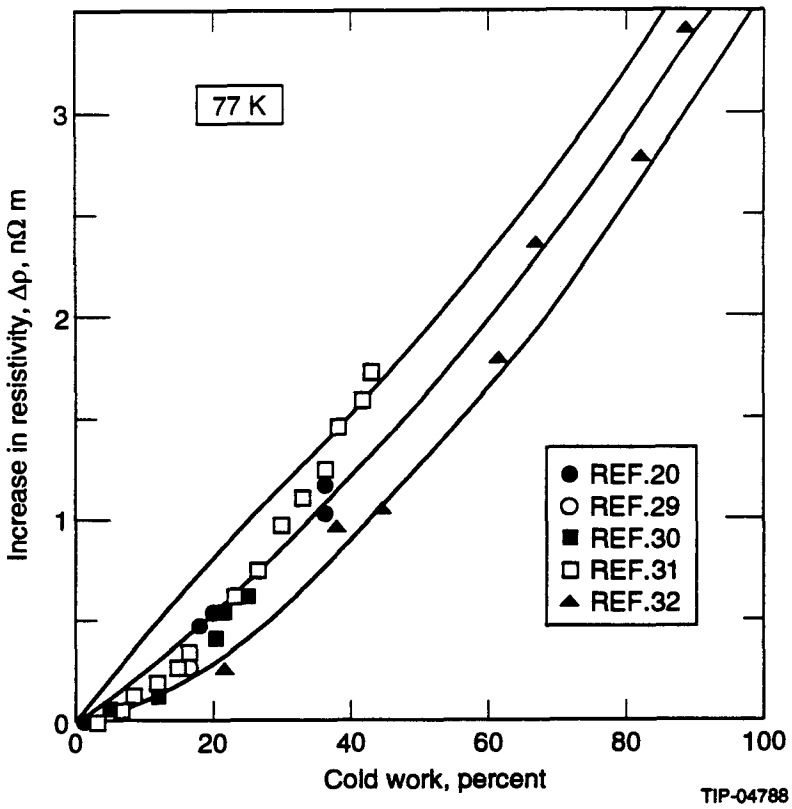

Figure 5. Copper Resistivity at Zero Magnet Field with Cold Work.[23]

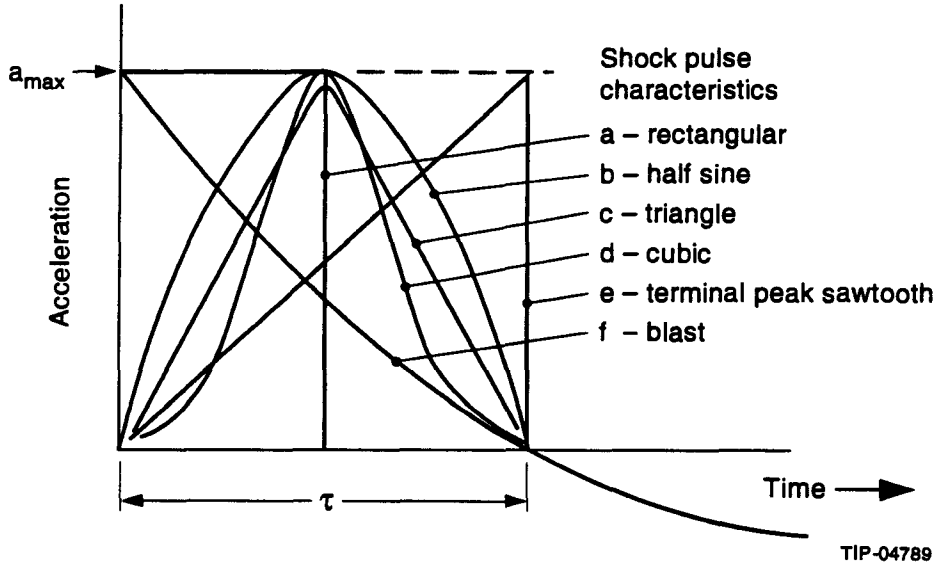

Figure 6. Dynamic Factor on Various Pulse Shapes.

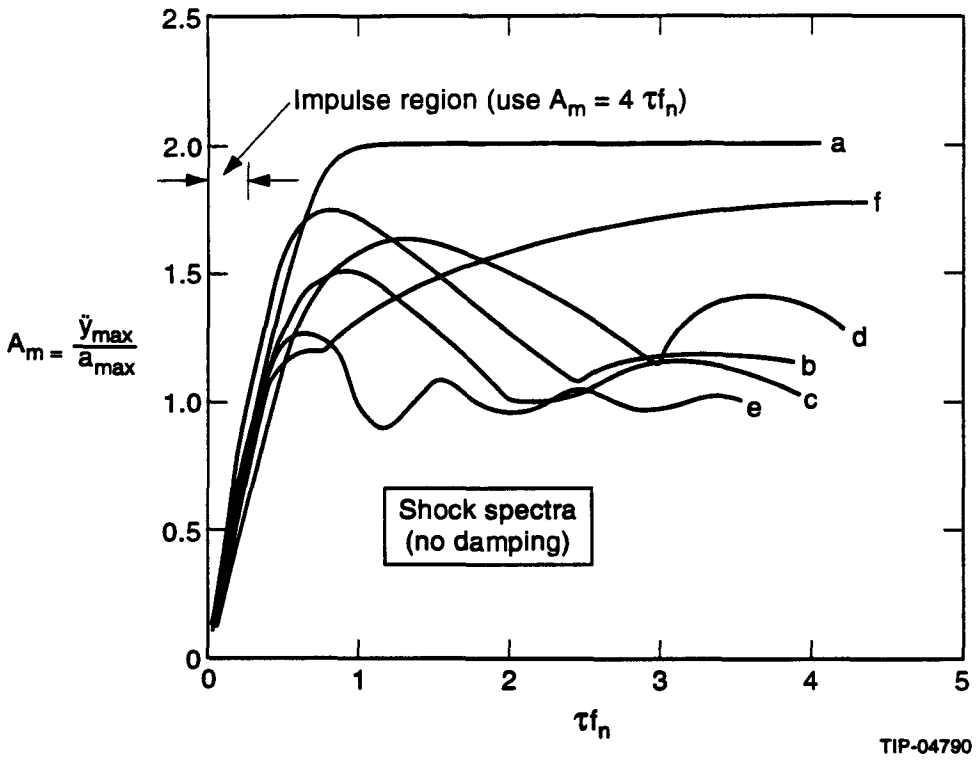

Figure 7. Dynamic Factor on Cubic Pulse.

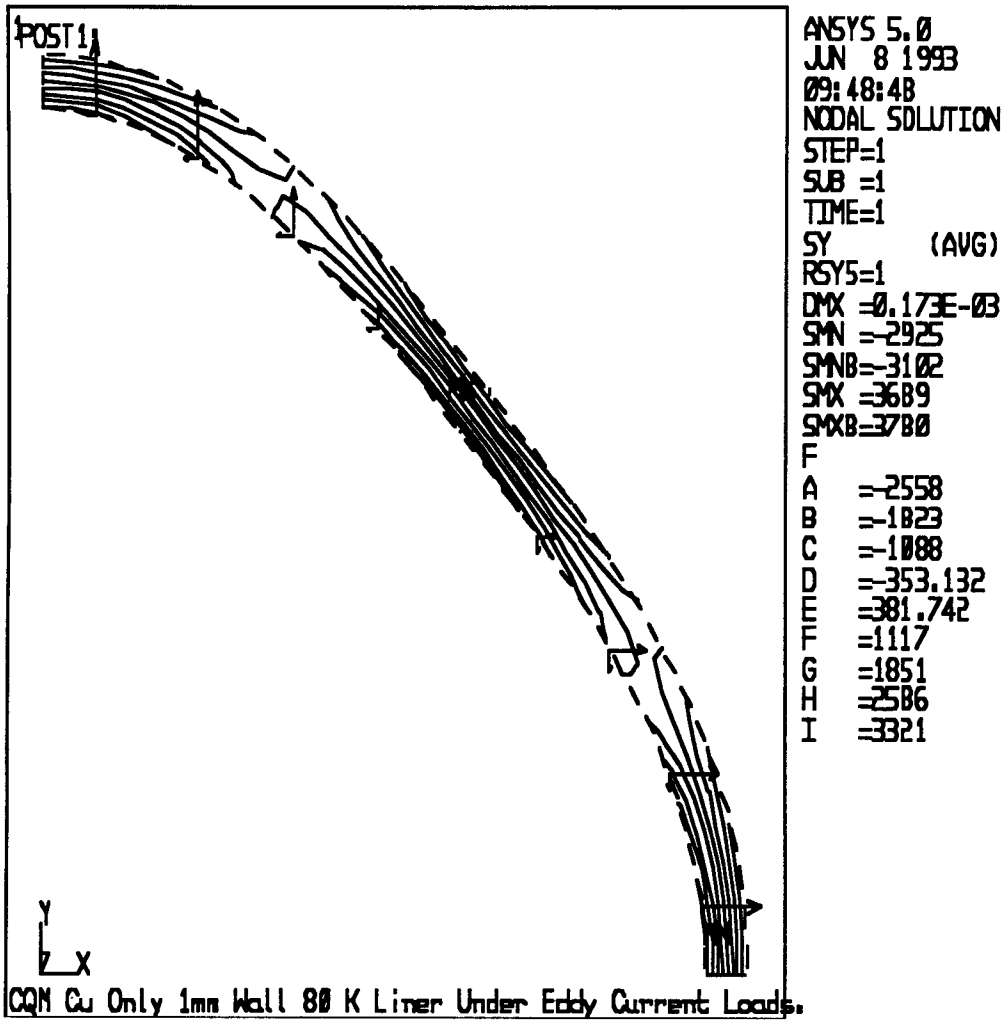

Figure 8. Copper Stress from Eddy Current, Stress in Circumferential Direction (KSI).

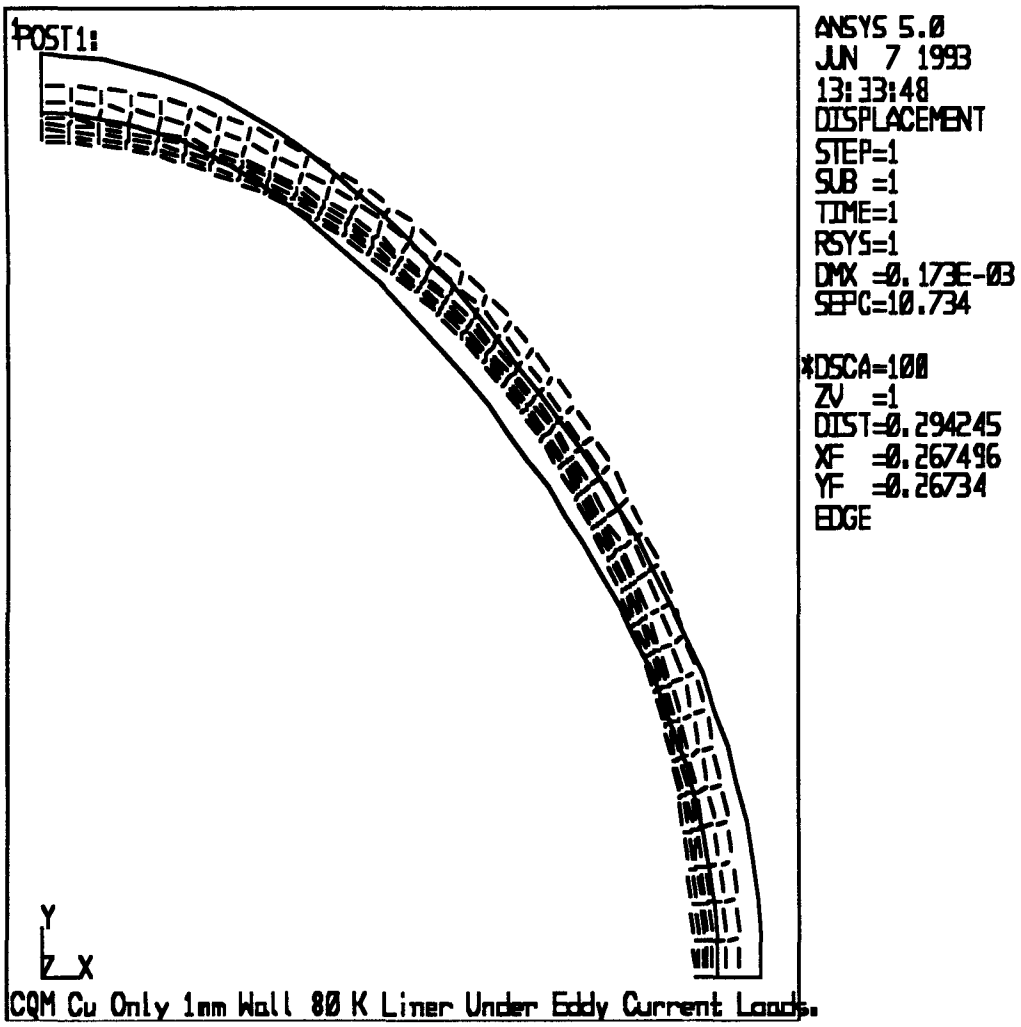

Figure 9. Deformed Shape of the CQM Liner.

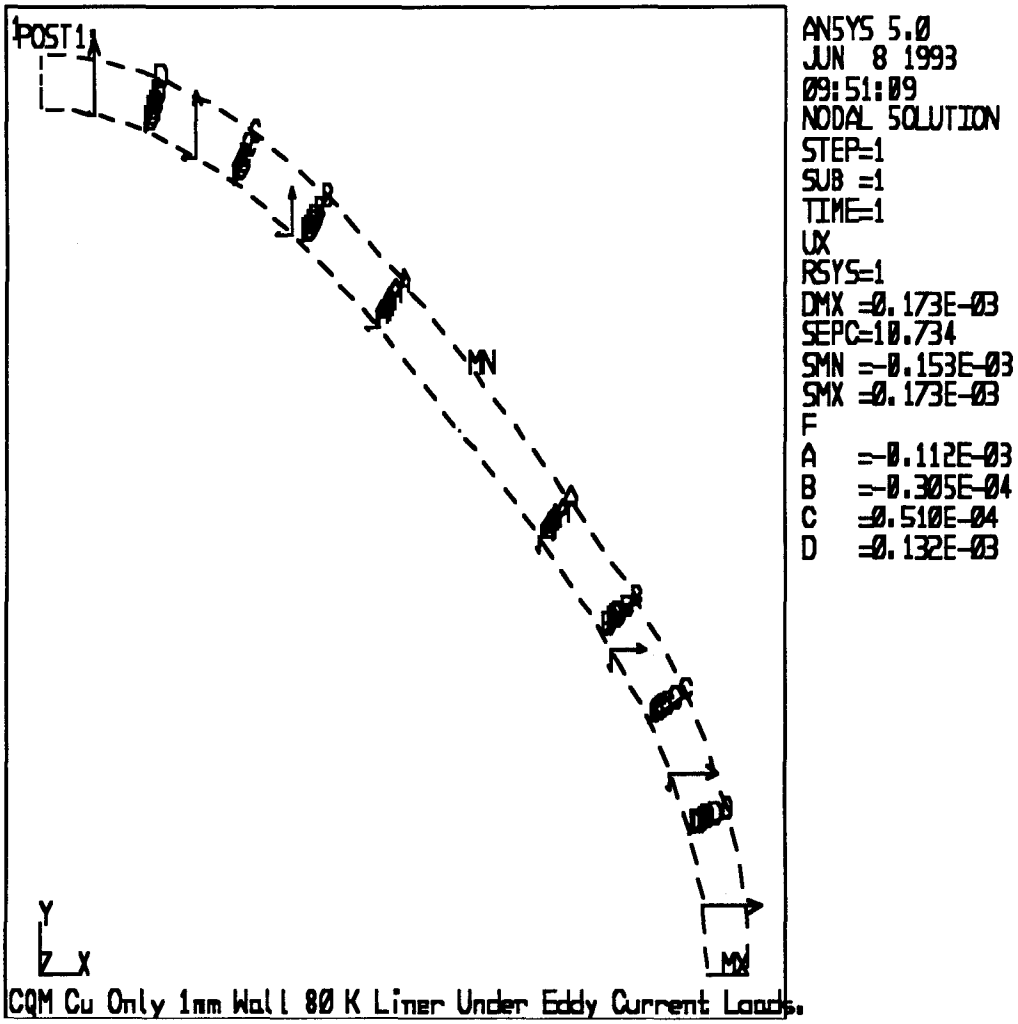

Figure 10. Radial Deflection of the Copper Liner (1.0 mm Wall Thickness) Deflection Unit {in.}.

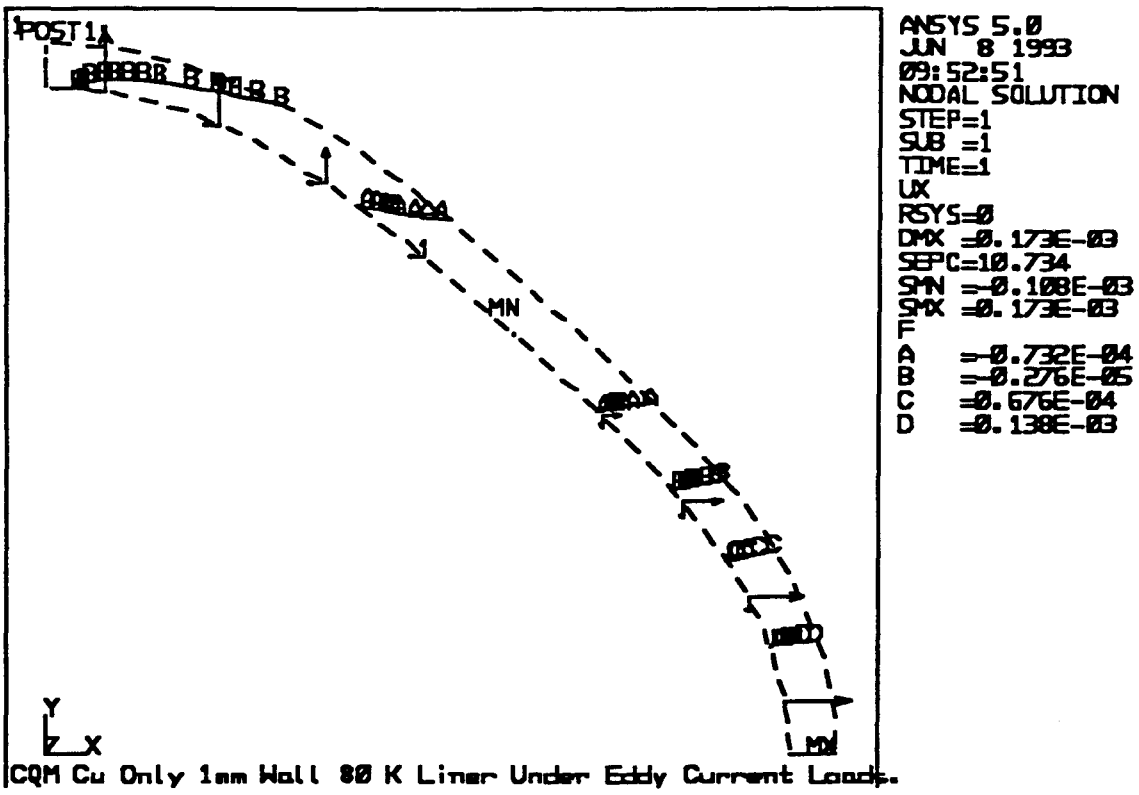

Figure 11. Horizontal Deflection of the CQM Liner (in.)

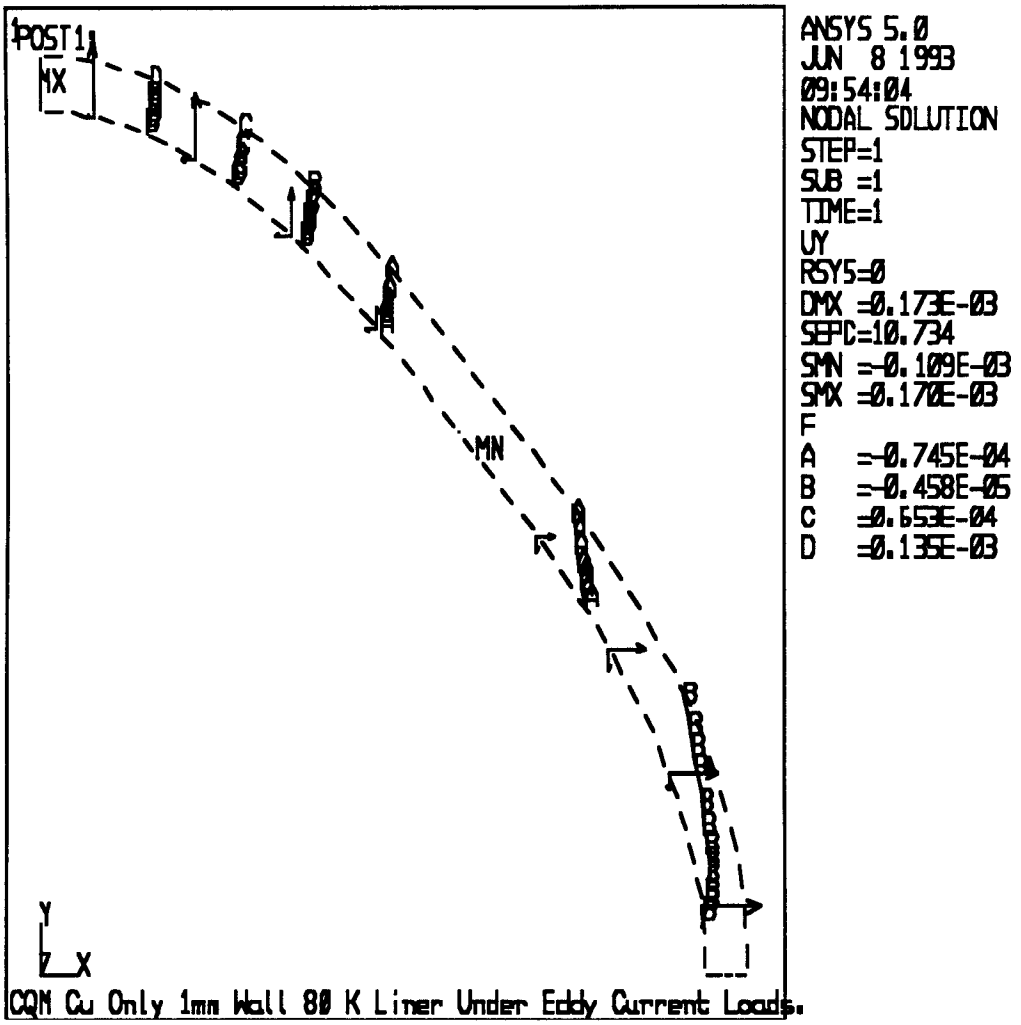

Figure 12. Vertical Deflection of the CQM Liner (In.)

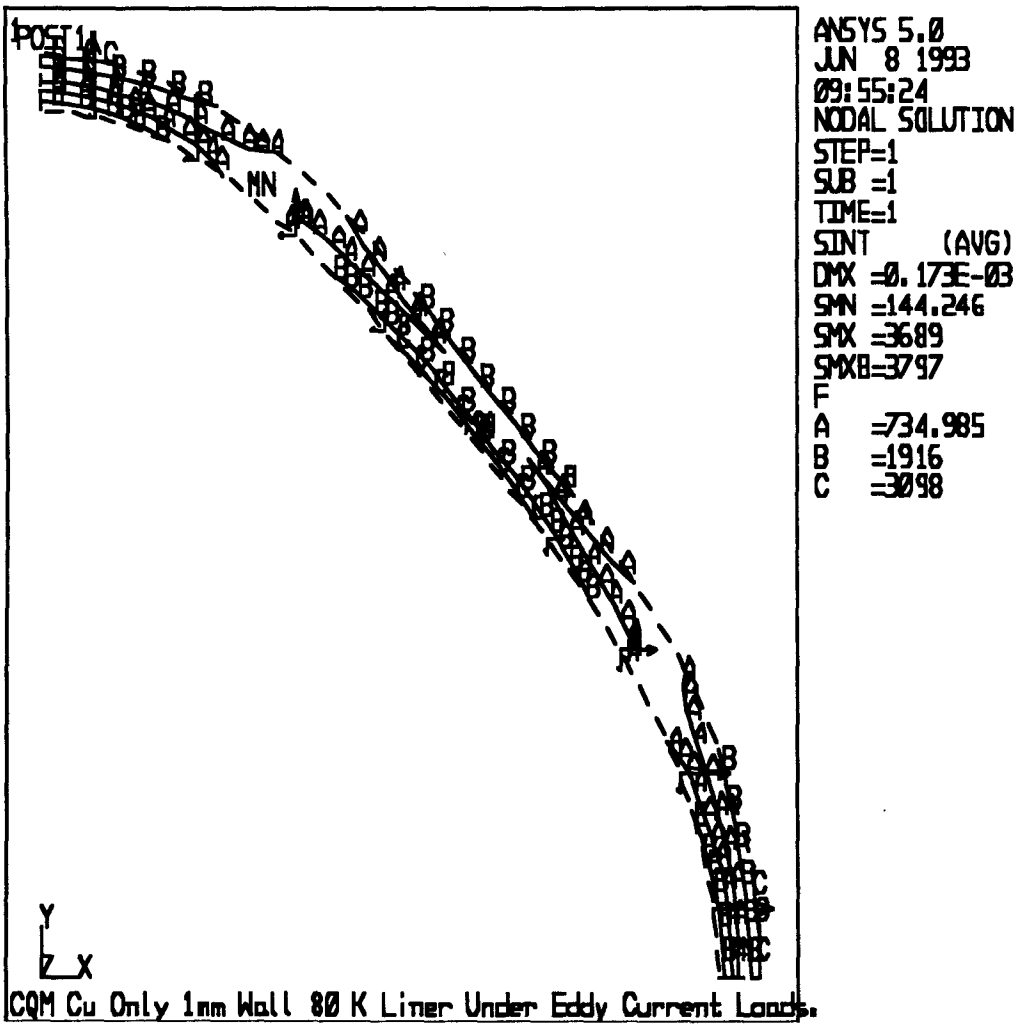

Figure 13. Maximum Combined Stress of the CQM Liner (KSI).

REFERENCES

1. J. Swanson, "ANSYS Finite Element Code Revision 5.0," Swanson Analysis Systems, Inc., December 23, 1992.
2.. American Society of Mechanical Engineers, "ASME Code Section VIII, Division 1," 1992.
3. Q. S. Shu, "Report on the ASST II Liner Status," SSCL Report, SSCL-N-805, Nov. 1992.
4. W. C. Turner, "Collider Beam Tube Vacuum," Presentation at the Beam Tube Size and Coating Meeting at SSCL, March 31, 1993.
5. A. Chao, "More on Copper Coating Considerations," SSCL Report, SSC-N-434, 1988.
6. K. K. Leung, "Non-Axisymmetrical Eddy Current Loads on Beam Tube in A Quenching Dipole Magnet," SSCL, Magnet Division Report, MD-TA-243, 1993.
7. Q. S. Shu, "Status of Tests on RF Surface & Magneto-Resistance," Presentation at the Beam Tube Size and Coating Meeting at SSCL, March 31, 1993.
8. K. K. Leung, "Seismic Stress of Piping and Heat Exchanger Supporting Structures," Section K-7/6, *Transactions of the 3rd International Conference on Structural Mechanics in Reactor Technology*," London, 1975.
9. K. Ng, J. Peterson, "Allowable Stress in The SSC Beam Tube During A Quench,," SSCL Report, SSC-168, March, 1988.
10. K. K. Leung, "Nonlinear Stress Analysis of Superconducting Dipole Magnet Shell," MD-TA-167, September 1990.
11. S. Smith, R. Jaykumar, "Mechanical Analysis of Beam Tube Assemblies for SSC Dipoles During a Quench," IEEE Particle Accelerator Conference, San Francisco, May, 1991.
12. K. K. Leung, "Structural Analyses of SSC Collider 4.2 K Beam Tube," Presentation at the Beam Tube Size and Coating Meeting at SSCL, March 31, 1993.
13. Q.S Shu, K. Yu, SSC, Private Communication on "Analysis of Effect of H&T on Lorentz Force," April 21, 1993.
14. G. Snitchler, Chris Ogle, "Structural Analysis of Collider Dipole Magnet Beam Tube," General Dynamics Space Systems Division Document Number M3A-100054, Preliminary Design Review Data Package-Presentations, Vol. 1, March 23, 1992
15. C. Haddock, "Lorentz Pressure on a Copper lined Beam Tube During a Quench for a 50 mm SSC Dipole," SSCL, Magnet Division Report, MD-TA-165, 1992.
16. K. K. Leung, "A Frequency Response Study of Collider Dipole Magnet Cold Mass for the SSC," *Supercollider 3*, Edited by J. Nonte, Plenum Press, NY & London, 1991.
17. K. K. Leung, "Engineering Design Study of CDM Cold Mass End Shell," *Supercollider 3*, Edited by J. Nonte, Plenum Press, NY & London, 1991.
18. K. K. Leung, "Transient Cooldown Stress in SSC Dipole Magnet Shell," *Supercollider 4*, Edited by J. Nonte, Plenum Press, New York & London, 1992.
19. K. K. Leung, Q.S. Shu *et al.*, "Effective Stress Of A 4.2 K Beam Tube in a Quenching Collider 50 mm Dipole Magnet for the SSC," pre-print of 1993 IEEE Particle Accelerator Conference, Washington, DC, May, 1993.
20. K. K. Leung, A. Paterson, "Advanced Light Source Accelerator Seismic Design Prodecures," Lawrence Berkeley National Laboratory Mechanical Engineering Report, LSME-135, May, 1989.

21. R. Carcagno, W. Schiesser, "Helium Venting Computer Simulation During An SSC Dipole Quench," *Advances In Cryogenic Engineering,* Vol.**37**, Part A, Edited by R. Fast, Plenum Press, NY, 1992.

22. B. Johnston, *Design Criteria for Metal Compression Members*, John Wiley, Inc. NY 1966.

23. N. J. Simon *et al.*, "Properties of Copper and Copper Alloys at Cryogenic Temperatures," National Institute of Standards and Technical, NIST Monogrph 177, February 1992.

24. J. Shuy, SSC, private commuication.

25. "*Enviroment Test Methods and Engineering Guidelines*," MIL-STD-810D, Department of Defense, USA.

26. F. Bleich, *Buckling Strength of Structures*, McGraw-Hill, 1952.

27. Y. Goren, SSC, private communication.

28. G. Snitchler, SSC, private communication.

29. C. Haddock, SSC, private communication.

30. SSCL Specification, Doc. No: M80-000001 Rev: A, Magnet System Specification, SSCL, Jan. 1992.

31. G. N. Savin, "Stress Concentration Around Holes," Kontsentratsiya Napryazhenii Okolo Otverstii, Moscow/Leingrad, 1951.

32. S. P. Timoshenko, *Theory of Elastic Stability*, pp1–45, McGraw-Hill.

APPENDIX

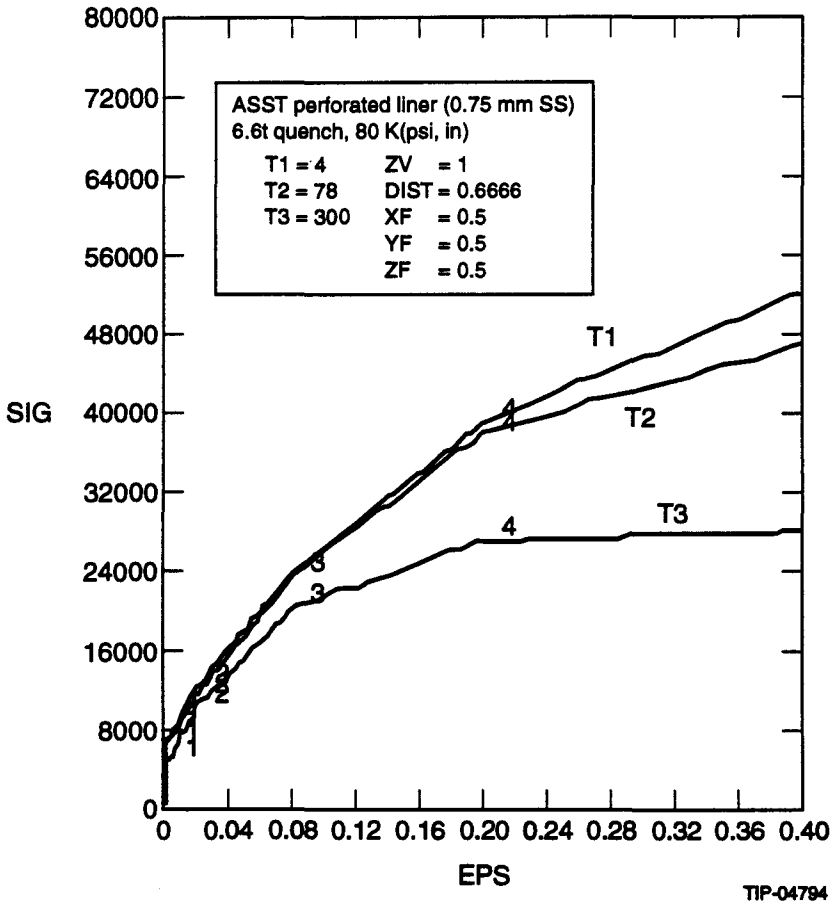

Figure 14. Non-linear Copper Stress-Strain at Annealed Condition.

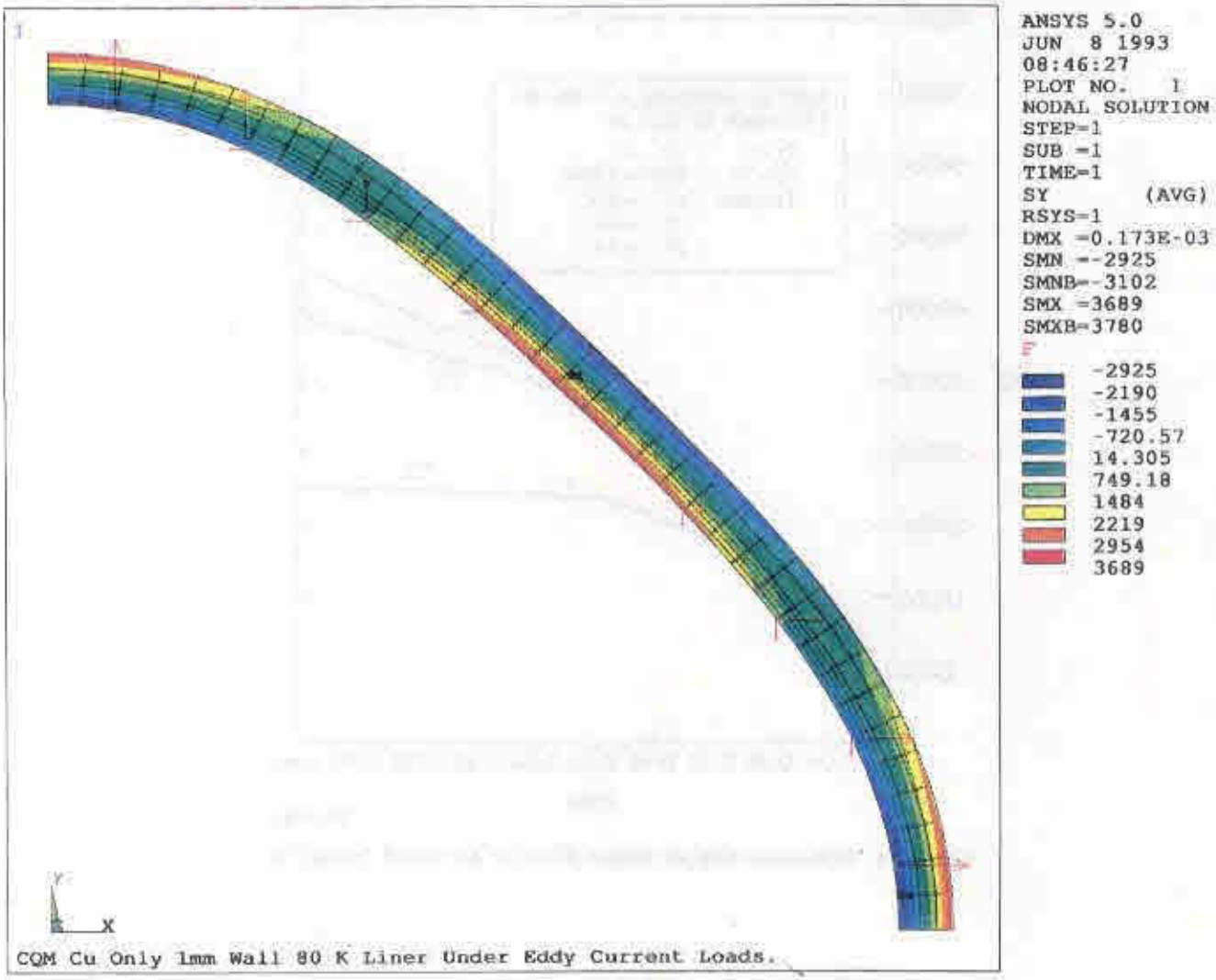

Figure 15. The Stress on the CQM Liner Copper Layer. The yield stress is 6000 PSI which is greater than the maximum of 3689 PSI as shown here. The copper layer will not be subjected to cold work, and the copper resistivity will not increase.

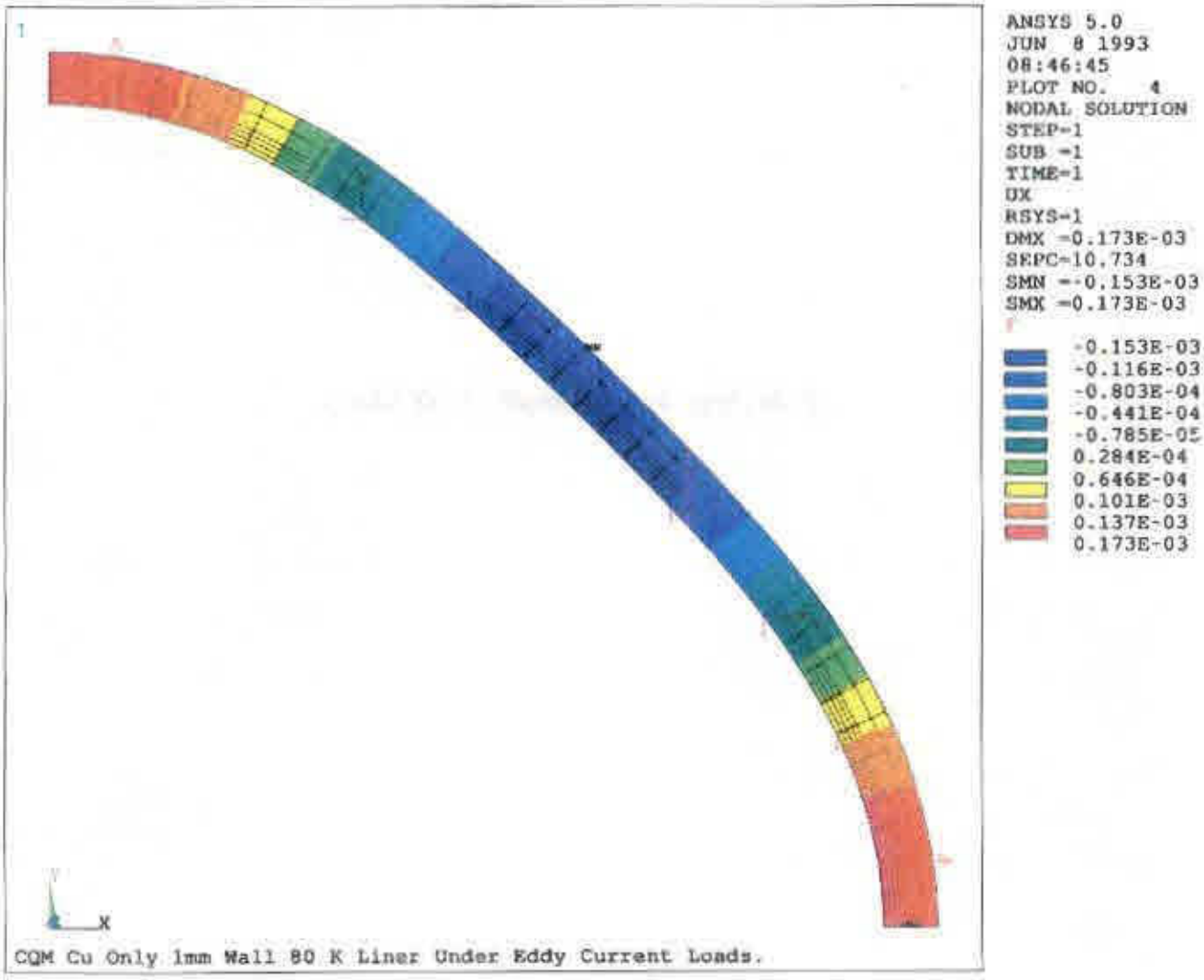

Figure 16. The Radial Deflection of the CQM Liner Copper Layer. The vertical and horizontal positions of the liner are deflected outward. The 45° portion is deflected inward.

This Page Intentionally Left Blank

SECTION 10

Effect of Magnetoresistance on Liner Design

Q. S. Shu and K. Yu

SECTION 10

Effect of the Magnetoresistance on Liner Design

Q. S. Shu and K. Yu

Superconducting Super Collider Laboratory*
2550 Beckleymeade Ave.
Dallas, TX 75237-3997

Abstract

For beam particle dynamic stability, the inner wall of the liner tube (or beam tube) must meet the resistive wall requirement: conductance (σ) · thickness (δ) $\geq 2 \times 10^5\ \Omega^{-1}$. Due to magnetoresistance, the σ in collider operation will be smaller than that value without B fields. The magnitude of the change is dependent on: (1) the RRR of the material, (2) the operational temperature, and (3) the applied magnetic fields. This paper will briefly introduce the concept of magnetoresistance, and the effects of magnetoresistance on the choice of the RRR of the copper coating layer in both the case of a 4 K liner and of an 80 K liner. Calculations of the temperature increase of a liner tube during a magnet quench are presented. The Lorentz pressure is estimated for liners at different operational temperatures and with different copper thicknesses.

*Operated by the Universities Research Association, Inc., for the U. S. Department of Energy under Contract No. DE-AC35-89ER40486.

1.0 INTRODUCTION

The image current in the inner wall of a liner tube (or beam tube) is induced by the charged particle bunches that move along the center line of the liner (or beam) tube with a speed close to that of light. From the point of view of beam dynamic stability, the product of the conductance and thickness of the liner tube must meet the following requirements:

conductance (σ) · thickness (δ) $\geq 2 \times 10^5\ \Omega^{-1}$. ID = 25~30 mm

conductance (σ) · thickness (δ) $\geq 1 \times 10^5\ \Omega^{-1}$. ID $\approx$ 40 mm

In the SSC Collider, the liner tube is under a strong magnetic field of 6.6 T. An extra resistance in a metal, a so called magnetoresistance, must be considered in the presence of a magnetic field. This magnetoresistance may be changed by a change in the direction of the magnetic field and/or its magnitude, depending on the Fermi surface topology. If there is a distribution of electron velocities, then it is clear that only those electrons of a certain "average" velocity will be undeflected. The remaining carriers, having velocities either larger or smaller than the "average" will be deflected and will traverse longer paths, thus increasing the resistance of the conductor. We have

$$\Delta\rho/\rho = aB^2 / (1 + \mu^2 B^2), \tag{1}$$

where $a = 0.38\ \mu^2 \times 10^{-16}$,

μ - Hall mobility, cm^2/V - s,

B - Oe.

For the reasons discussed and the fact that $\Delta\rho/\rho_0$ varies as B^2 in weak fields, magnetoresistance is a second-order effect. It tends to saturate in strong magnetic fields, unless there is a disturbance of the Hall field. Magnetoresistance is even in B, and it is related to the symmetric components of the resistivity tensor.

Also, we know the magnetoresistance will increase both with a reduction in temperature and with an increase in the material's RRR. The magnetoresistance can be varied by a factor of 0.5–10 at 4 K, and by a factor of 0.1–0.2 at 80 K. A good amount of experimental data is available at 4 K, but little is available at 80 K. For reference, we calculated from experimental data and assumptions the relative magnetoresistance, $\Delta R/R_0$, as functions of the copper RRR of the liner tube at 4 K, 30 K, and 80 K under magnetic fields of 5 T and 6 T, as summarized in Figure 1. The detail considerations of the effects of the magnetoresistance on the liner design are discussed in the following sections.

(calculated by Q. S. Shu and K. Yu, 4/93)

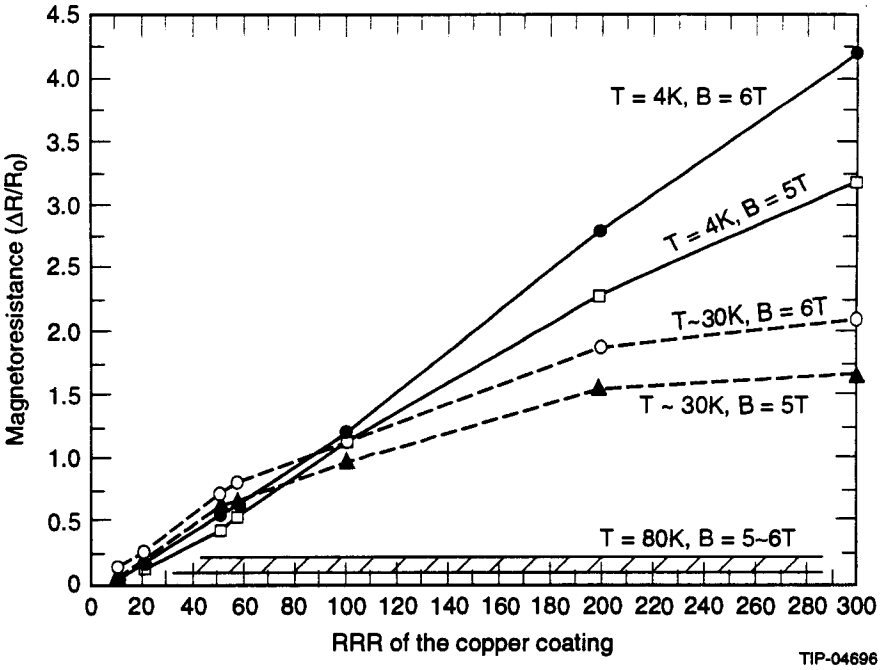

Figure 1. Copper Magnetoresistance vs. H, T, and RRR.

2.0 EFFECT OF MAGNETORESISTANCE ON CHOICE OF RRR AND COPPER THICKNESS OF THE LINER TUBE

As mentioned, if the liner (or beam) tube ID = 25~30 mm,

$$\sigma(B,T) \cdot \delta \geq 2 \times 10^5\ \Omega^{-1}. \tag{2}$$

It is essential to use the real copper resistance values for the liner tube under magnetic fields to meet the resistive wall requirement.

Definition,

$$RRR = \rho(0,273)\cdot\sigma(0,4) \tag{3}$$

$$RR = \rho(0,273)/\rho(0,T) \tag{4}$$

$$\Delta R/R_0 = [\rho(B,T) - \rho(0,T)]/\rho(0,T) \tag{5}$$

$$\rho(0,273) = 1.545 \times 10^{-8}\ (\Omega.m)$$

$$\sigma(B,T) = \sigma(0,T)/[\Delta R/R_0 + 1]. \tag{6}$$

2.1 In the Case of a 4 K Liner (or Beam Tube)

Temperature, $T = 4$ K

Magnetic field, $B = 6.6$ T

Proposed copper coating layer thickness, $\delta = 0.1$ mm.

1) If the effect of magnetoresistance is not taken into account in determining the minimum required RRR:

$$\sigma(0,4) \geq 2.0 \times 10^9\ (\Omega.\mathrm{m})^{-1}$$

$$\mathrm{RRR} = 2.0 \times 10^9\ (\Omega.\mathrm{m})^{-1} \cdot \rho(0,273)$$
$$= 31.$$

2) If the effect of magnetoresistance is taken into account in determining the minimum required RRR:

$$\sigma(6.6,4) \geq 2.0 \times 10^9\ (\Omega.\mathrm{m})^{-1}$$

$$\sigma(B,T) \cdot [\Delta R/R_0 + 1] = \sigma(0,T)$$

$$\sigma(6.6,4) \cdot [0.6 + 1] = \mathrm{RRR}/[\rho(0,273)]$$

$$\mathrm{RRR} = 2.0 \times 10^9\ (\Omega.\mathrm{m})^{-1} \cdot \rho(0,273) \times 1.6$$
$$= 50.$$

To satisfy the resistive wall requirement, the RRR must be ≥ 50, but not = 31.

3) Now, we would like to recommend the choices of copper RRR and coating thickness under the different resistive wall requirements in Figure 2.

(calculated by Q. S. Shu and K. Yu, 4/93)

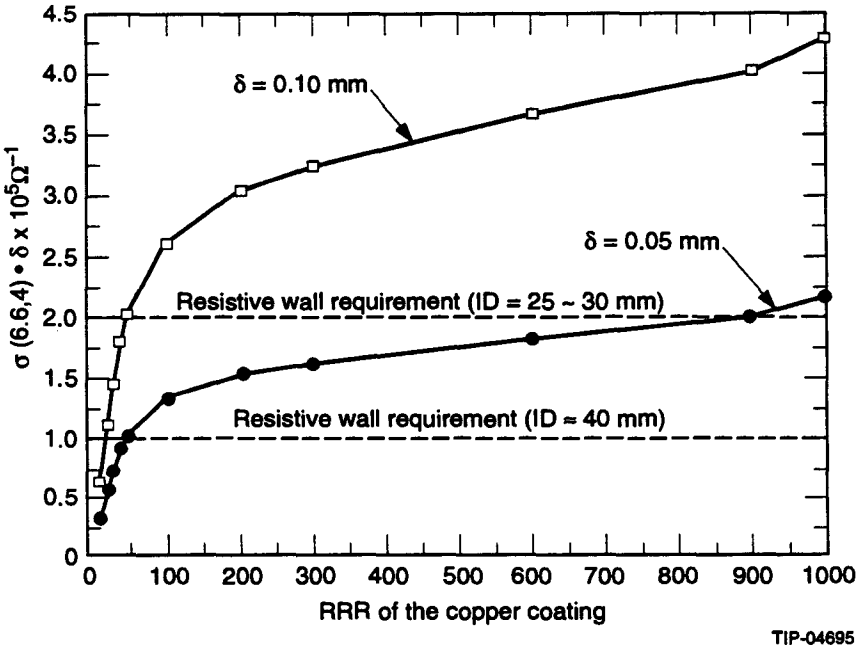

Figure 2. RRR vs. s(B = 6.6T, T = 4K) · d(m) x 10^5 W^{-1}.

For example:

If $\sigma(B = 6.6\ T, T = 4\ K) \cdot \delta(m) \geq 2 \times 10^{-5}\ \Omega^{-1}$, $\delta = 0.1$ mm, RRR ≥ 50

$\delta = 0.05$ mm, RRR ≥ 900.

If $\sigma(B = 6.6\ T, T = 4\ K) \cdot \delta(m) \geq 1 \times 10^{-5}\ \Omega^{-1}$, $\delta = 0.1$ mm, RRR ≥ 20

$\delta = 0.05$ mm, RRR ≥ 50.

2.2 In the Case of an 80 K Liner

Temperature T = 80 K

Magnetic field B = 6.6 T

Possible copper coating thickness $\delta = 0.5$ mm, 0.55 mm, 0.60 mm

From graphs in Appendices B and C, when RRR = 20,

$\sigma(0,80) \approx 3.45 \times 10^8\ (\Omega.m)^{-1}$

If $\Delta R/R_0 \approx 0.1$, $\sigma(6.6,80) \approx 3.14 \times 10^8\ (\Omega.m)^{-1}$

If $\Delta R/R_0 \approx 0.2$, $\sigma(6.6,80) \approx 2.88 \times 10^8\ (\Omega.m)^{-1}$.

The $(\sigma \cdot \delta)$ can be calculated with different RRR and $\Delta R/R_0$, as shown in Table 1.

TABLE 1. THE VALUE OF s(B = 6.6T, T = 80 K) · d(m).

RRR	$\Delta R/R_0$	$s(0,80) \times 10^8$ $(M.\Omega)^{-1}$	$s(6.6,80) \times 10^8$ $(M.\Omega)^{-1}$	$s(6.6,80) \cdot d \times 10^5 \Omega^{-1}$		
				d = 0.50 mm	d = 0.55 mm	d = 0.60 mm
20	0.1	3.45	3.14	1.57	1.73	1.88
50		4	3.64	1.82	2.01	2.18
57		4.6	4.18	2.09	2.3	2.51
100		5	4.55	2.28	2.5	2.73
20	0.2	3.45	2.88	1.44	1.58	1.73
50		4	3.33	1.67	1.83	2
57		4.6	3.83	1.92	2.11	2.3
100		5	4.17	2.08	2.29	2.5

1) If magnetoresistance is $\Delta R/R_0 \approx 0.10$ at T = 80 K, B = 6.6 T, to meet the resistive wall requirement, the thickness vs. the required minimum RRR is listed as follows:

$\delta = 0.50$ mm RRR ≥ 54

$\delta = 0.55$ mm RRR ≥ 50

$\delta = 0.60$ mm RRR ≥ 32.

2) If magnetoresistance is $\Delta R/R_0 \approx 0.20$ at T = 80 K, B = 6.6 T, to meet the resistive wall requirement, the thickness vs. the required minimum RRR is listed as follows :

$\delta = 0.50$ mm RRR ≥ 77

$\delta = 0.55$ mm RRR ≥ 54

$\delta = 0.60$ mm RRR ≥ 50.

3.0 TEMPERATURE INCREASE OF THE COPPER COATING OF A LINER DURING MAGNET QUENCH

The quench performance of an ID = 50 mm dipole magnet, DCA320, was calculated from experimental data. When discharge time is t = 0.18 s, the B(t)·[dB(t)/dt] has reached its maximum and the Lorentz force is F_{max}. At t = 0.18 s, we have:

$$B(t) = 6.01 \text{ T}$$

$$dB(t)/dt = 24.52 \text{ T/s}$$

$$B(t)\cdot[dB(t)/dt]\,|_{max.} = 147.26 \text{ T}^2/\text{s},$$

as shown in Figure 3 (a), (b), (c).

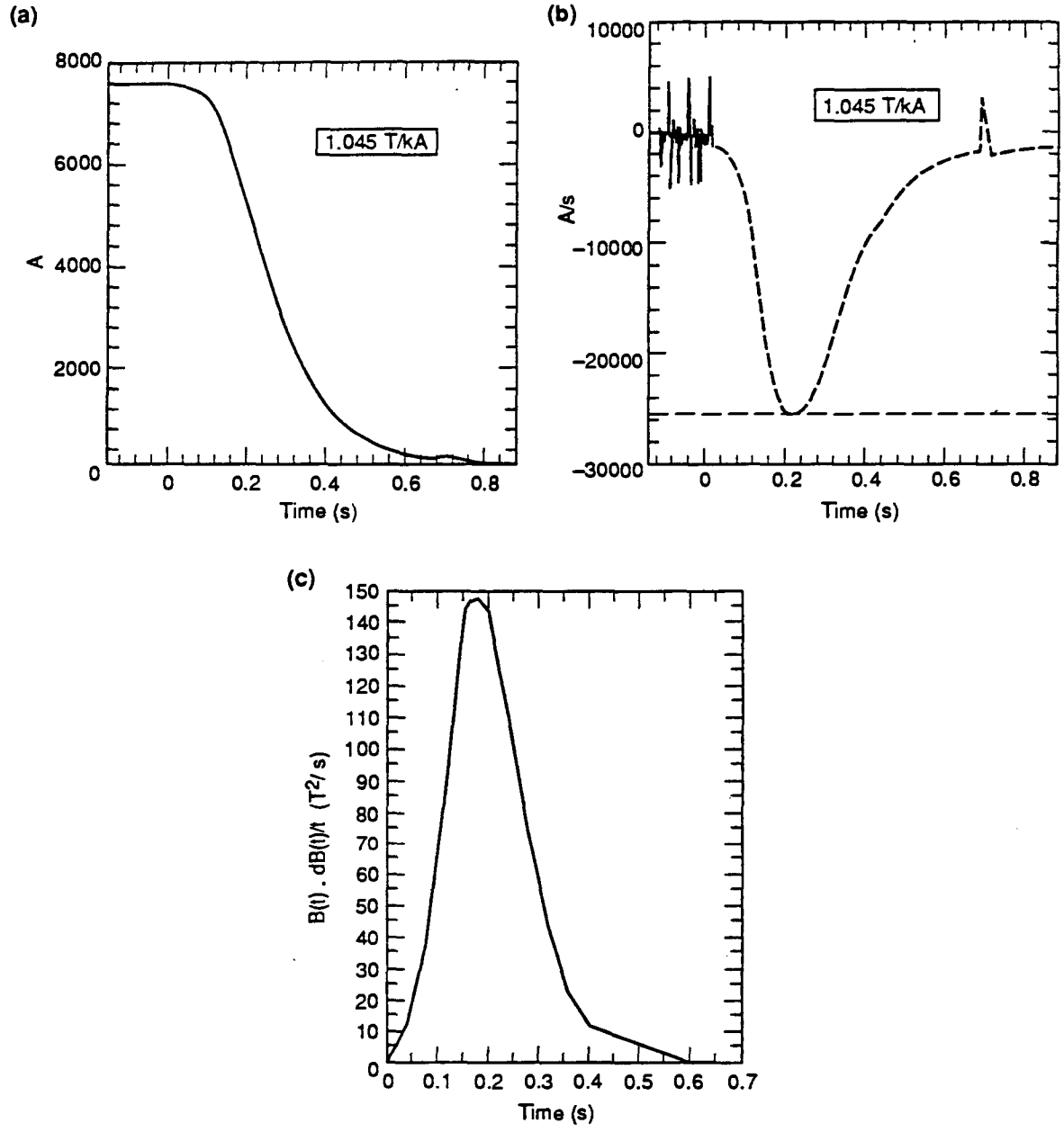

Figure 3. The Above Experimental Quench Data Were Taken from the SSC CDM DCA320. (a) Current decay after quench. (b) Current decay rate as function of time. (c) B(t) · [dB(t)/dt] as function of time.

3.1 In the Case of a 4 K Liner

The heat change between the copper coating and the stainless steel tube is ignored.

Heat capacity of copper at 40 K	$C_p = 60$ (J/kg.K)
Copper density	$\zeta = 9.02 \times 10^3$ (kg/m^3)
Eddy current density	$J(t) = \sigma(B,T) \cdot \{[dB(t)]/dt\} \cdot r'$ (7)
Proposed copper coating thickness	$\delta = 0.1$ mm
	ID = 25.3 mm ($r_1 = 1.265 \times 10^{-2}$ m)
	OD = 25.5 mm ($r_2 = 1.275 \times 10^{-2}$ m)
Mean radius of copper coating layer	$r' = (r_1 + r_2)/2 = 1.27 \times 10^{-2}$ m
Copper mass	M
	RRR = 57
Electrical conductivity	$\sigma(6,40) \approx 14.7 \times 10^8$ $(\Omega.m)^{-1}$
At the midplane	$\sin\varphi = 90^o$

On account of

$$C_pMdT = I^2Rdt \quad (8)$$
$$= [(J \cdot S)^2 \cdot \rho \cdot L/S]dt$$
$$= (J^2SL/\sigma)dt$$
$$= (J^2V/\sigma)dt$$
$$C_pdT = (J^2/\sigma) \cdot (V/M)dt \quad (9)$$
$$= (J^2/\sigma) \cdot (1/\zeta)dt$$
$$\therefore \quad dT/dt = J^2/(\sigma \cdot \zeta C_p) \quad (10)$$
$$= 263 \text{ K/s.}$$

When the Lorentz force reaches maximum, discharge time is dt = 0.18 s.

$$\therefore \quad dT \approx 47 \text{ K}$$

Therefore, the temperature of the liner tube is T ≈ 4 K + 47 K =51 K during the quench (at dt = 0.18 s).

Note: The approximation method of successive substitution is utilized in choosing the "heat capacity of copper at 40 K" and the "electrical conductivity σ(6, 40)" for the above calculation of temperature increase.

3.2 In the Case of an 80 K Liner

The heat change between the copper coating and the stainless steel tube is ignored.

Heat capacity of copper at 80 K	$C_p = 200$ (J/kg.K)
Copper density	$\zeta = 9.02 \times 10^3$ (kg/m^3)
Eddy current density	$J(t) = \sigma(B,T) \cdot \{[dB(t)]/dt\} \cdot r'$
Proposed copper coating thickness	$\delta = 0.5$ mm
	ID = 25.3 mm ($r_1 = 1.265 \times 10^{-2}$ m)
	OD = 26.3 mm ($r_2 = 1.315 \times 10^{-2}$ m)

Mean radius of copper coating layer	$r' = (r_1 + r_2)/2 = 1.29 \times 10^{-2}$ m
Copper mass	M
	RRR = 57
Electrical conductivity (if $\Delta R/R_0 \approx 0.10$)	
	$\sigma(6,80) \approx 4.2 \times 10^8\ (\Omega.m)^{-1}$
At the midplane	$\sin\varphi = 90^o$

use $C_p dT = J^2/(\sigma \cdot \zeta)dt$

$dT/dt = J^2/(\sigma \cdot \zeta C_p)$

$= 27$ K/s.

When the Lorentz force reaches maximum, discharge time is dt = 0.18 s.

$$\therefore \qquad dT \approx 5 \text{ K}.$$

Therefore, the temperature of the liner tube is T ≈ 80 K + 5 K =85 K during the quench (at dt = 0.18 s).

4.0 EFFECT OF T AND δ ON LORENTZ PRESSURE

1) Lorentz pressure P_{max}:

The differential Lorentz force

$$dF = \mathbf{I} \times \mathbf{B}(t) = I \cdot B(t) \sin\Omega \tag{11}$$

due to $$F = \iint 1/[1 + \pi(r/l)\cdot(\varphi/90)]\sigma(B,T)\cdot B(t)\cdot[dB(t)]/dt \cdot r^2 \cdot dr \cdot \sin\varphi \cdot d\varphi \tag{12}$$

$$F_{max} = \sigma(B,T)\cdot\{B(t)\cdot[dB(t)/dt]\}|_{max} \cdot \iint 1/[1 + \pi\,(r/l)\cdot(\varphi/90)]\cdot r^2 \cdot dr \cdot \sin\varphi \cdot d\varphi \tag{13}$$

$$P_{max} = F_{max}/(2 \times r' \times \varnothing) \tag{14}$$

If $\delta << r$, $r << 1$ and $\varphi = 90^0$

$$\therefore \qquad F_{max} = \sigma(B,T)\cdot\{B(t)\cdot[dB(t)/dt]\}|_{max} \cdot \iint r^2 \cdot dr \cdot d\varnothing \tag{15}$$

we have $$P_{max} = \sigma(B,T)\cdot\{B\cdot[dB/dT]\}|_{max} \cdot r' \cdot \delta \tag{16}$$

The detailed deduction is presented in the Appendix A.

4.1 In the Case of a 4 K Liner

If we choose:

RRR = 57

ID = 25.3 mm ($r_1 = 1.265 \times 10^{-2}$ m)

Copper coating thickness $\delta = 0.10$ mm, 0.5 mm

Electrical conductivity $\sigma(6,4) \approx 18 \times 10^8\ (\Omega.m)^{-1}$

$\sigma(6,51) \approx 10.8 \times 10^8\ (\Omega.m)^{-1}$

$P_{max} \approx 49$ Psi, when $\delta = 0.10$ mm, $r' = 1.27 \times 10^{-2}$ m.

If the temperature increase of the copper coating layer is taken into account during magnet quench,

$P_{max} \approx 30$ Psi.

$P_{max} \approx 248$ Psi, when $\delta = 0.50$ mm, $r' = 1.29 \times 10^{-2}$ m.

If the temperature increase of the copper coating layer is taken into account during magnet quench,

$P_{max} \approx 149$ Psi.

4.2 In the Case of an 80 K Liner

If we choose:

RRR = 57

ID = 25.3 mm ($r_1 = 1.265 \times 10^{-2}$ m)

Copper coating thickness $\delta = 0.50$ mm, 0.55 mm, 0.60 mm

Suggested magnetoresistance $\Delta R/R_0 \approx 0.10$

Electrical conductivity $\sigma(6,80) \approx 4.2 \times 10^8\ (\Omega.m)^{-1}$

$\sigma(6,85) \approx 3.3 \times 10^8\ (\Omega.m)^{-1}$

$P_{max} \approx 57$ Psi, when $\delta = 0.50$ mm, $r' = 1.29 \times 10^{-2}$ m.

If the temperature increase of the copper coating layer is taken into account during magnet quench,

Pmax ≈ 46 Psi.

$P_{max} \approx 64$ Psi, when $\delta = 0.55$ mm, $r' = 1.2925 \times 10^{-2}$ m.

If the temperature increase of the copper coating layer is taken into account during magnet quench,

$P_{max} \approx 50$ Psi.

$P_{max} \approx 70$ Psi, when $\delta = 0.60$ mm, $r' = 1.295 \times 10^{-2}$ m.

If the temperature increase of the copper coating layer is taken into account during magnet quench,

$P_{max} \approx 55$ Psi.

REFERENCES

1. Q. S. Shu, "Report on the ASSTII Liner Status," SSCL-N-805, Nov. 1992.

This Page Intentionally Left Blank

APPENDIX A

A Lorentz pressure, P_{max}, is estimated on the liner tube during a magnet quench for the SSC dipole. The Lorentz force formula was deduced as below.

$$dF = \mathbf{I} \times \mathbf{B}(t) = I \cdot B(t) \sin\Omega \tag{A.1}$$

because, $\Omega = \pi/2$

$$I = j(t) \cdot ds = j(t) r \cdot dr \cdot d\phi. \tag{A.2}$$

To put Eq. (A.2) into Eq. (A.1), the force per unit length is given by:

$$dF = j(t) \cdot B(t) \cdot r \cdot dr \cdot d\phi, \tag{A.3}$$

and due to

$$j(t) = \sigma(B,T)E(t)$$

$$I(t) = \varepsilon(t)/R$$

$$R = \rho L/S = L/[\sigma(B,T) \cdot S]$$

$$I(t) = \varepsilon(t)/\{ L/[\sigma(B,T) \cdot S] \}$$

$$I(t)/S = \varepsilon(t)\sigma(B,T)/L$$

$$\therefore \quad j(t) = [\sigma(B,T) \cdot \varepsilon(t)]/L \tag{A.4}$$

therefore,

$$L = 2l + 2\pi\, r \cdot 2\varphi/180 \text{ (m)}$$

$$= 2[l + \pi\, r\varphi/90]. \tag{A.5}$$

To put Eq. (A.5) into Eq. (A.4),

$$j(t) = 1/[l + \pi\, r\varphi/90] \cdot [\sigma(B,T) \cdot \varepsilon(t)]/2, \tag{A.6}$$

and due to $\varepsilon(t) = -d\phi / dt = -S' [dB(t)/dt]$

$$S' = l \cdot 2r \cdot \sin\varphi$$

$$\therefore \quad \varepsilon(t) = l\{[dB(t)]/dt\} \cdot 2r \cdot \sin\varphi. \tag{A.7}$$

To put Eq. (A.7) into Eq. (A.6), the current density is given by:

$$j(t) = 1/[1 + \pi\, (r/l) \cdot \varphi/90] \cdot \sigma(B,T) \cdot \{[dB(t)]/dt\} \cdot r \cdot \sin\varphi. \tag{A.8}$$

To put Eq. (A.8) into Eq. (A.3),

$$dF = 1/[1 + \pi\, (r/l) \cdot \varphi/90] \cdot \sigma(B,T) \cdot B(t) \cdot [dB(t)]/dt \cdot r^2 \cdot dr \cdot d\phi \cdot \sin\varphi$$

$$F = \iint 1/[1 + \pi\, (r/l) \cdot \varphi/90] \cdot \sigma(B,T) \cdot B(t) \cdot [dB(t)]/dt \cdot r^2 \cdot dr \cdot d\phi \cdot \sin\varphi.$$

If the Lorentz force reaches maximum F_{max}, $B(t) \cdot [dB(t)/dt]$ must reach maximum, $\varphi = 90^o$ also. For this reason,

$$F_{max} = \sigma(B,T) \cdot \{B(t) \cdot [dB(t)/dt]\}|_{max} \cdot \iint 1/[1 + \pi\, r/l] \cdot r^2 \cdot dr \cdot d\phi \tag{A.9}$$

$$P_{max} = F_{max} /(2 \times r' \times \phi).$$

If $\delta << r$, and $r << l$

we have

$$P_{max} = \sigma(B,T) \cdot \{B \cdot [dB/dT]\}|_{max} \cdot r' \cdot \delta. \tag{A.10}$$

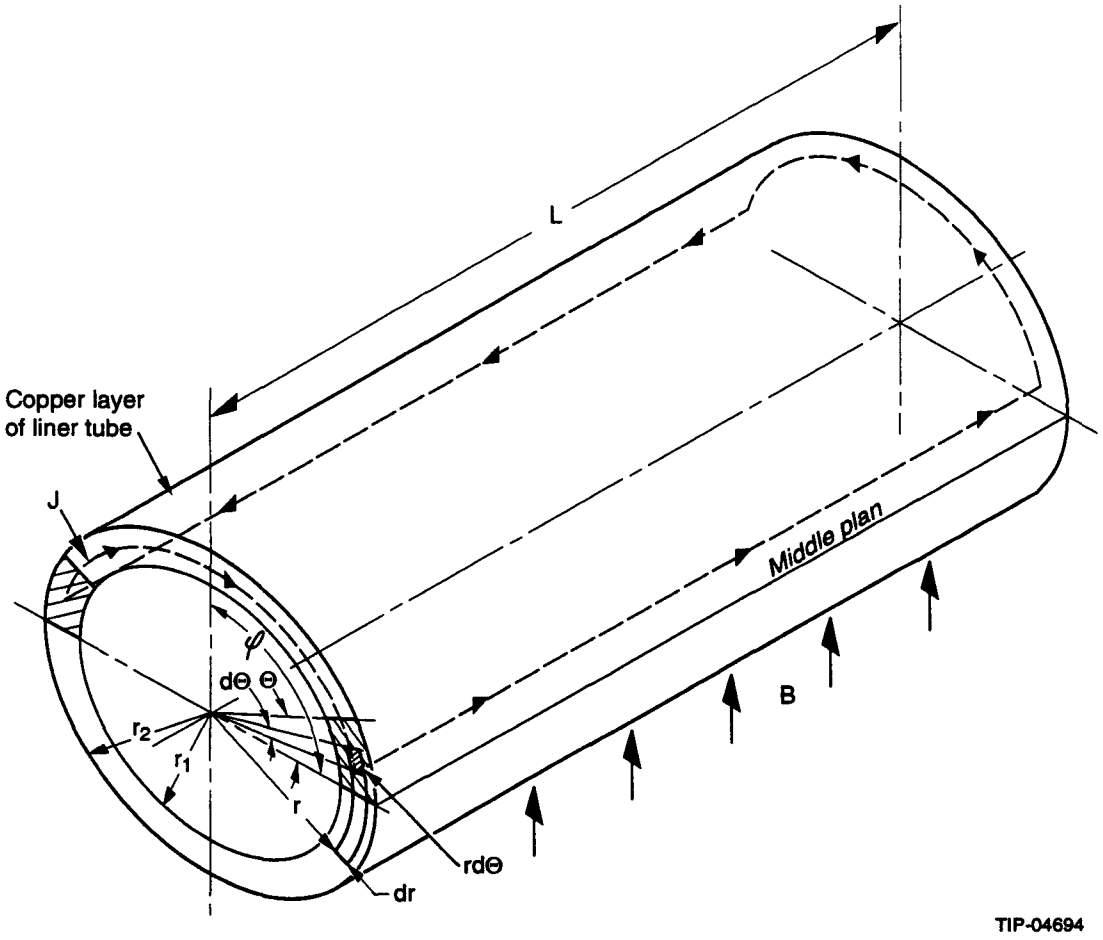

Figure A-1. A Schematic of a Liner Copper Coating for Lorentz Pressure Calculation.

APPENDIX B

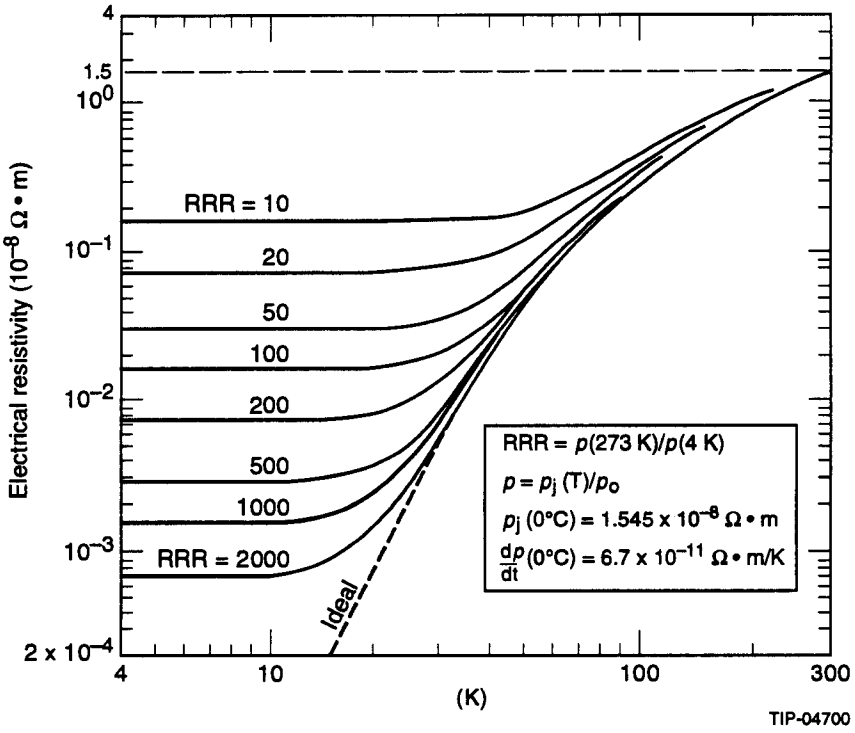

Figure B-1. Graph of Copper Electrical Resistivity vs. Temperature at B = 0 (Taken from NIST).

APPENDIX C

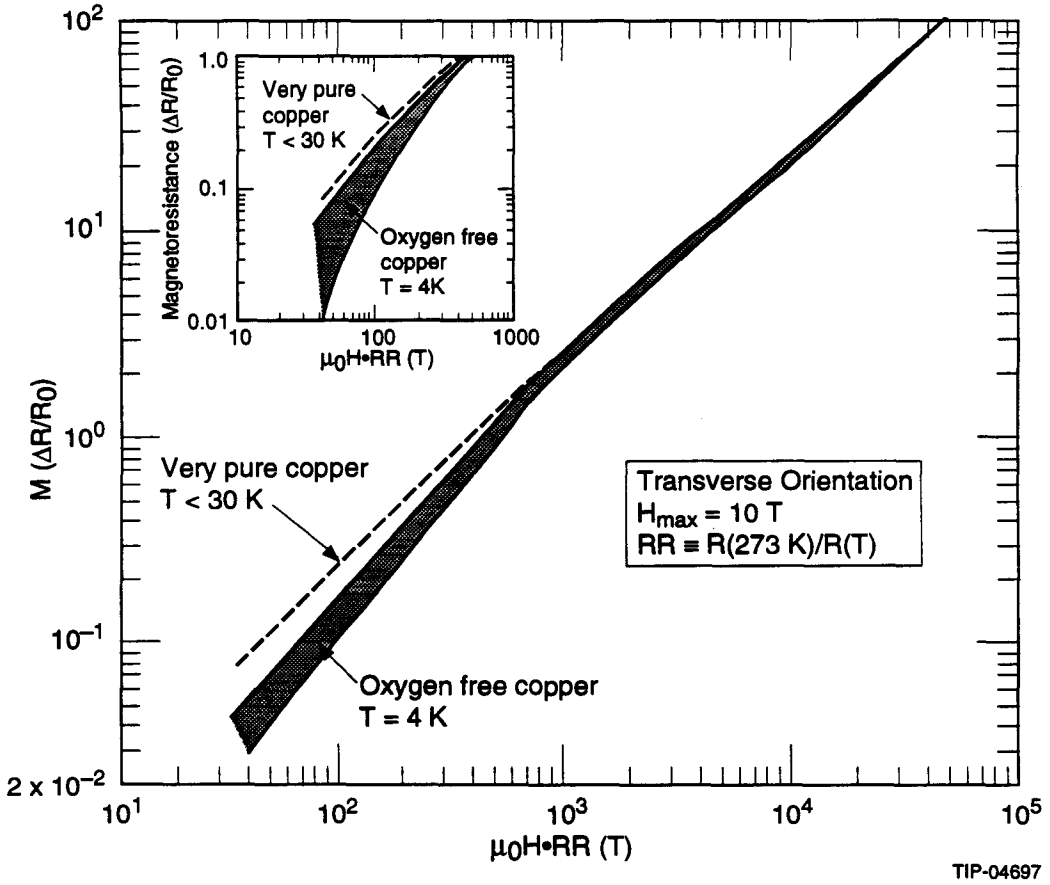

Figure C-1. Graph of Fractional Change in Copper Electrical Resistance Under Transverse Magnetic Field (Taken from NIST).

SECTION 11

Quench Induced Eddy Current Analyses

Y. Goren

HEADLINES

1) **Basic theory of eddy currents**
2) **Liner inside a dipole magnet**
   a) Eddy currents distribution
   b) Lorentz forces
   c) Heat dissipation
   d) Error analysis
3) **Liner inside a quadropole magnet**
   a) Eddy currents distribution
   b) Lorentz forces
   c) Heat dissipation
4) **Summary**

BASIC THEORY of EDDY CURRENTS

Neglect displacement currents in Maxwell's eqs.

1) The magnetic field is given by a diffusion eq.

$$\nabla^2 \mathbf{B} = \mu_0 \sigma \, \partial \mathbf{B}/\partial t$$

togather with appropriate boundary conditions.

2) The eddy currents are

$$\mathbf{J}_{eddy} = 1/\mu_0 \, \nabla \mathbf{x} \mathbf{B}$$

3) The Lorentz force

$$\partial^3 \mathbf{F}/\partial x^3 = \mathbf{J} \mathbf{x} \mathbf{B} = 1/\mu_0 \, (\nabla \mathbf{x} \mathbf{B}) \mathbf{x} \mathbf{B}$$

BASIC THEORY of EDDY CURRENTS (cont.)

Approximate solution to the liner case assumes

$$\Delta / \delta_s << 1$$

where Δ liner thickness δ_s skindepth.

Dipole Magnet

1) Eddy current distribution

$$\mathbf{J} = \sigma/2 \, \partial \mathbf{B}_{ext}/\partial t \; r \cos(\theta)$$

2) Lorentz force

$$\partial^3 \mathbf{F}/\partial l = \sigma/2 \; \mathbf{B}_{ext} \, \partial \mathbf{B}_{ext}/\partial t \; r^2 \cos(\theta) \, dr \, d\theta$$

BASIC THEORY of EDDY CURRENTS (cont.)

Quadrupole magnets

1) Eddy current distribution

$$\mathbf{J} = \sigma/2 \; T \; dI/dt \; r^2 \sin(2\theta)$$

where I is the quadrupole drive current
and T the quadrupole transfer function

2) Lorentz force (1st quadrant)

$$\partial^3 F_x/\partial l = \sigma/2 \; T^2 \; I \; dI/dt \; r^4 \sin(2\theta) \sin(\theta) \, dr \, d\theta$$

$$\partial^3 F_y/\partial l = \sigma/2 \; T^2 \; I \; dI/dt \; r^4 \sin(2\theta) \cos(\theta) \, dr \, d\theta$$

EDDY CURRENTS in the

COLLIDER DIPOLE

MAGNET (CDM)

LINER

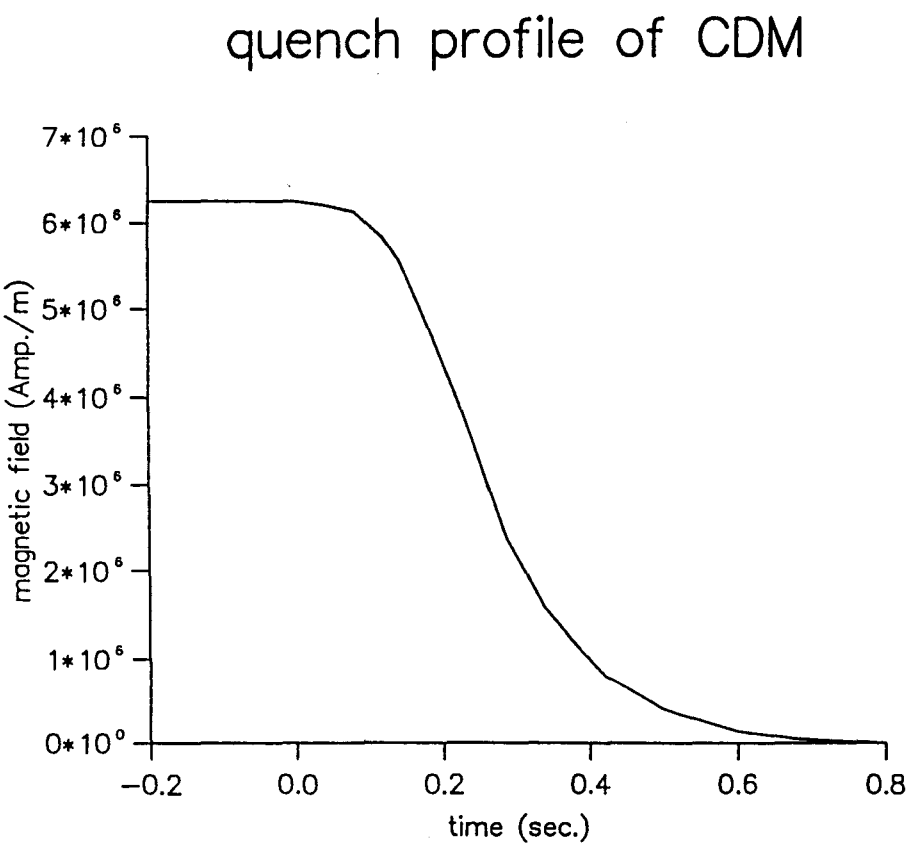

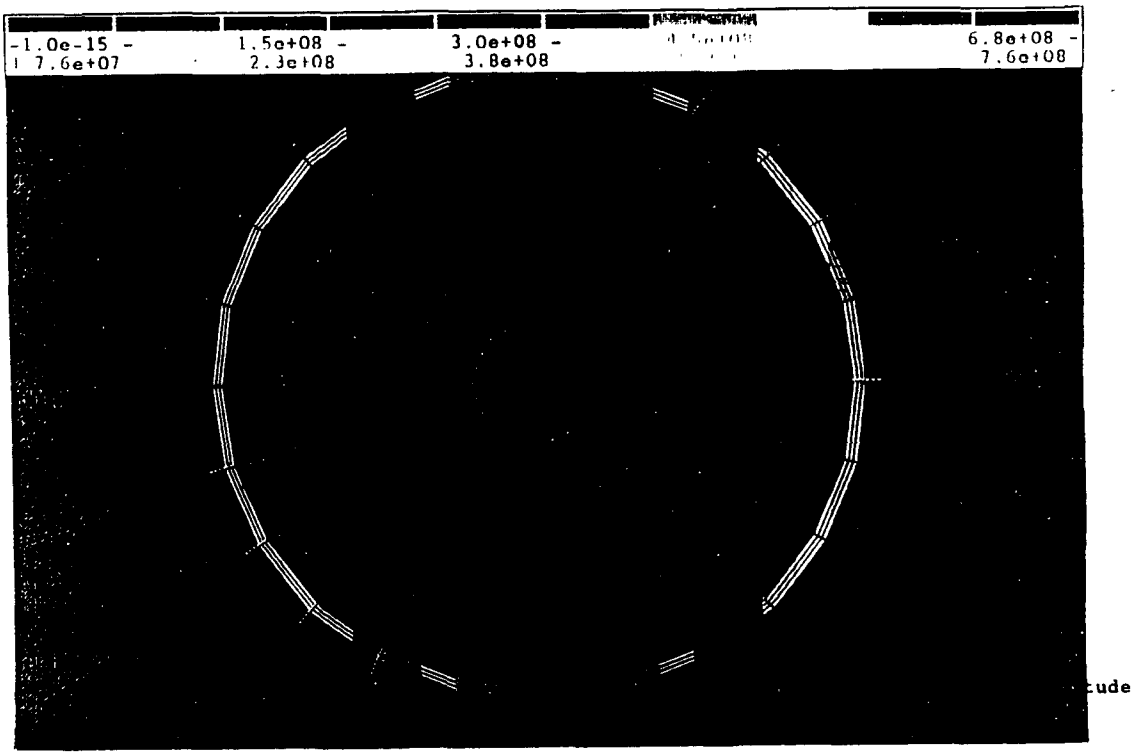
-1.0e-15
7.6e+07
1.5e+08
2.3e+08
3.0e+08
3.8e+08
6.8e+08
7.6e+08

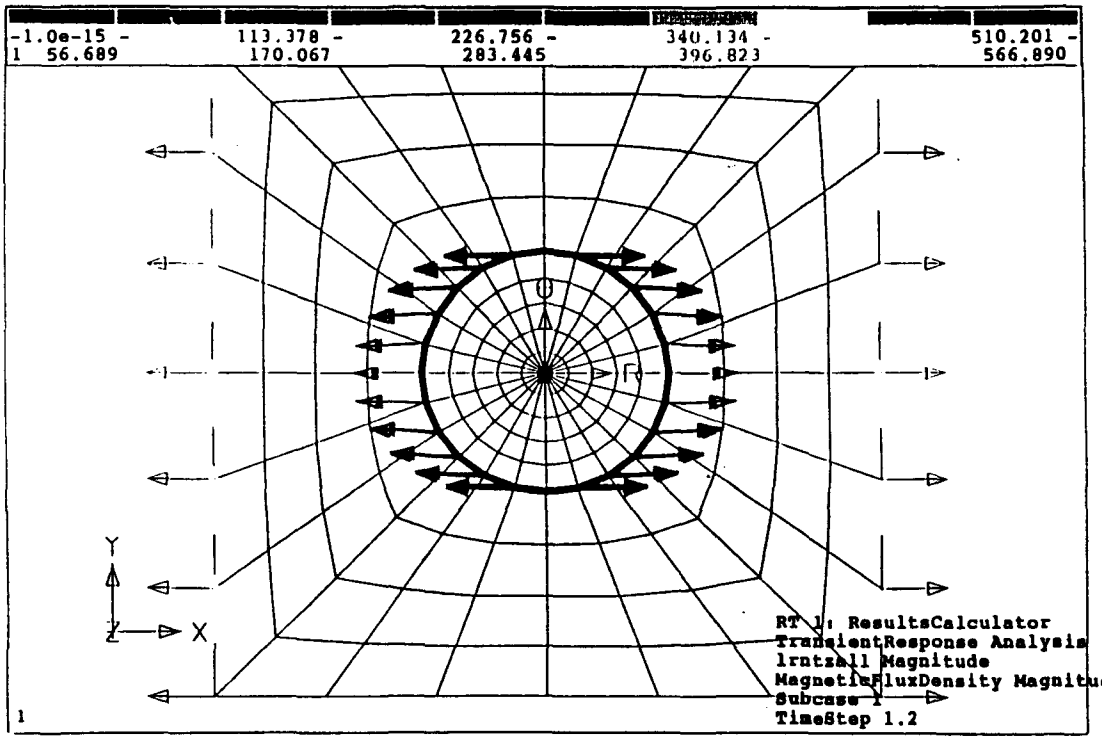
-1.0e-15
1 56.689
113.378
170.067
226.756
283.445
340.134
396.823
510.201
566.890
Y
Z
X
RT 1: ResultsCalculator
TransientResponse Analysis
Irntsall Magnitude
MagneticFluxDensity Magnitude
Subcase 1
TimeStep 1.2
1

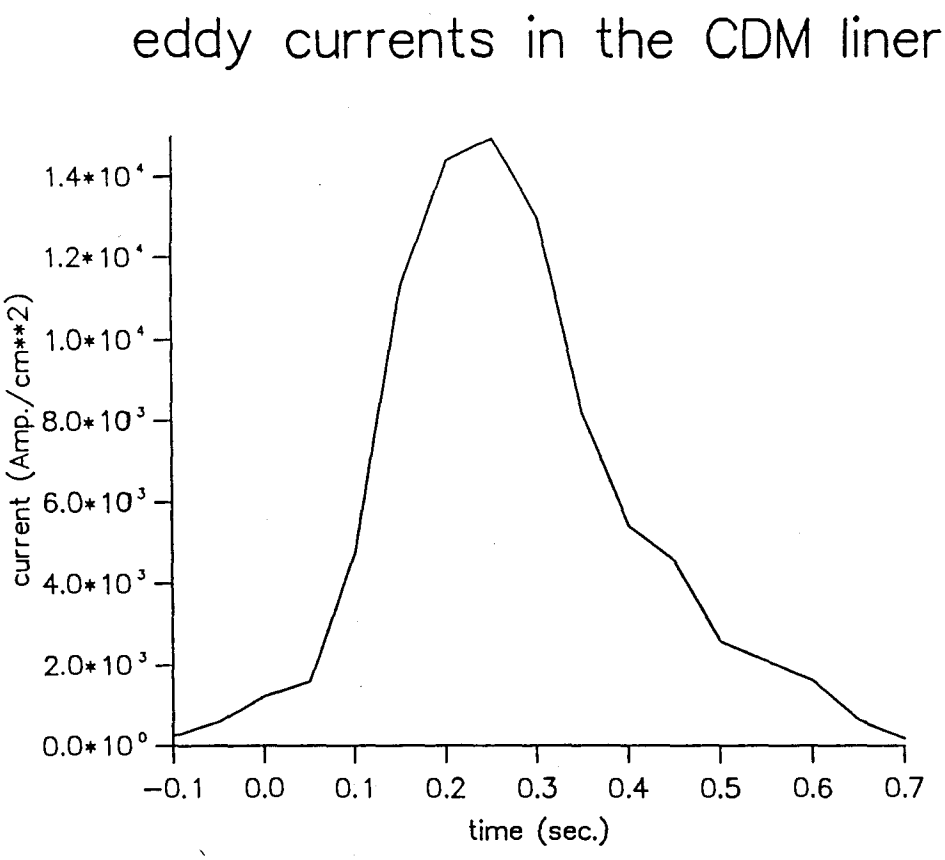
eddy currents in the CDM liner
current (Amp./cm**2)
1.4*10⁴
1.2*10⁴
1.0*10⁴
8.0*10³
6.0*10³
4.0*10³
2.0*10³
0.0*10⁰
−0.1
0.0
0.1
0.2
0.3
0.4
0.5
0.6
0.7
time (sec.)

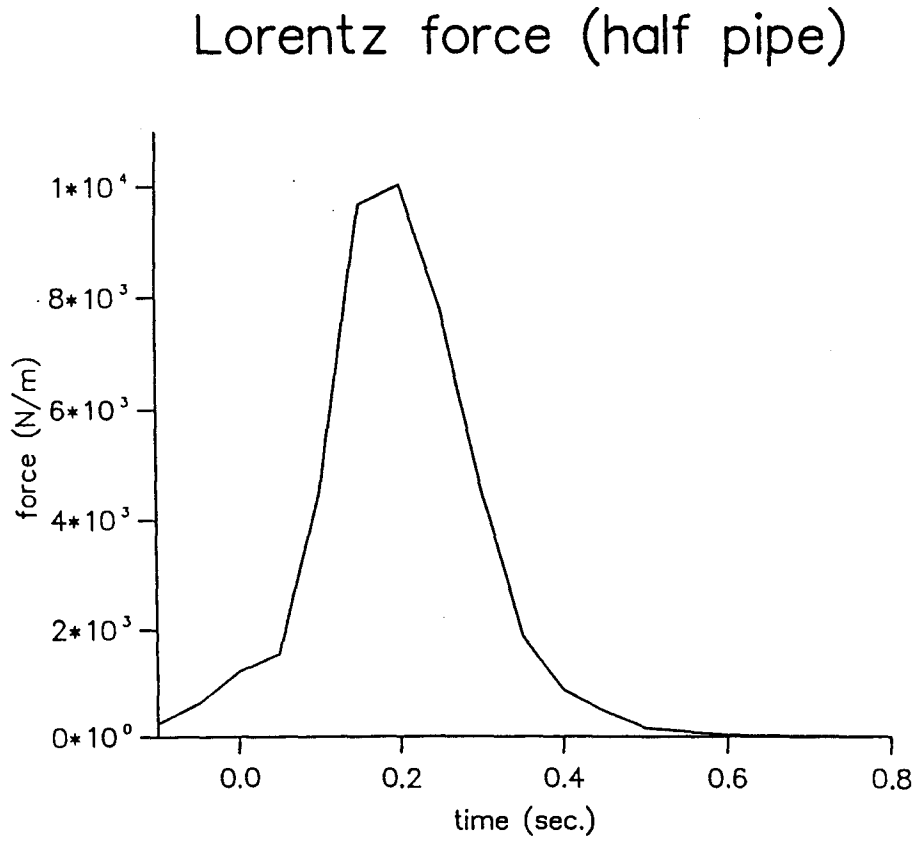
Lorentz force (half pipe)
force (N/m)
1*10⁴
8*10³
6*10³
4*10³
2*10³
0*10⁰
0.0
0.2
0.4
0.6
0.8
time (sec.)

power dissipation in the CDM liner

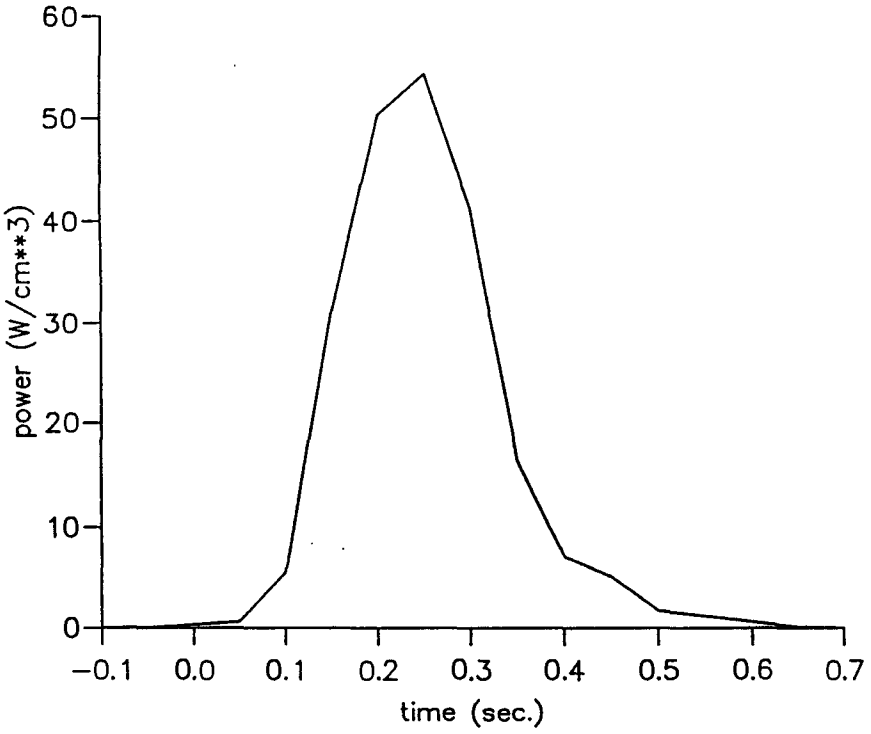

net force max. asymmetry

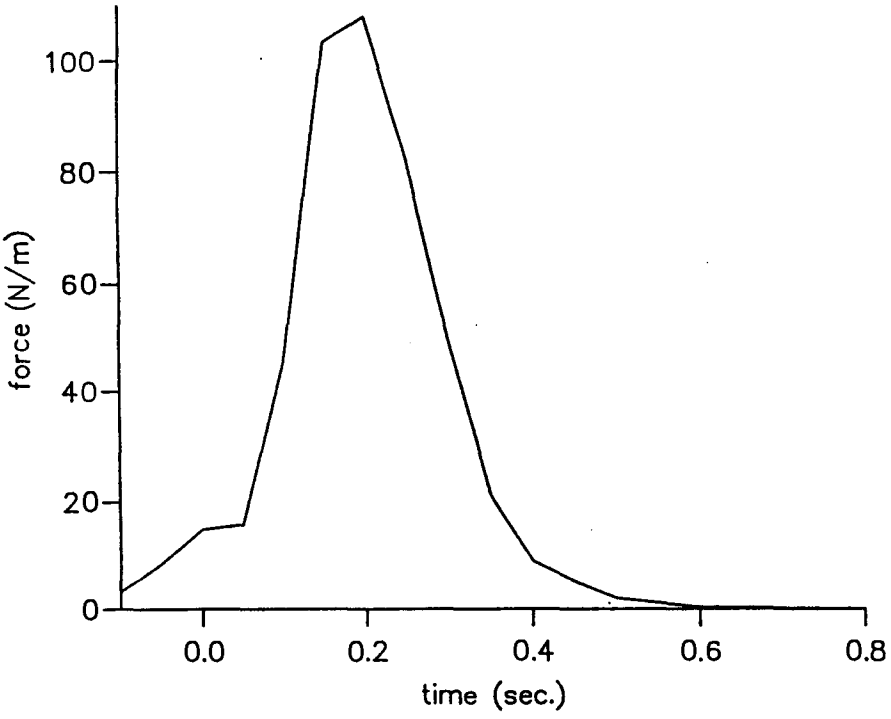

EDDY CURRENTS in the COLLIDER QUADRUPOLE MAGNET (CQM) LINER

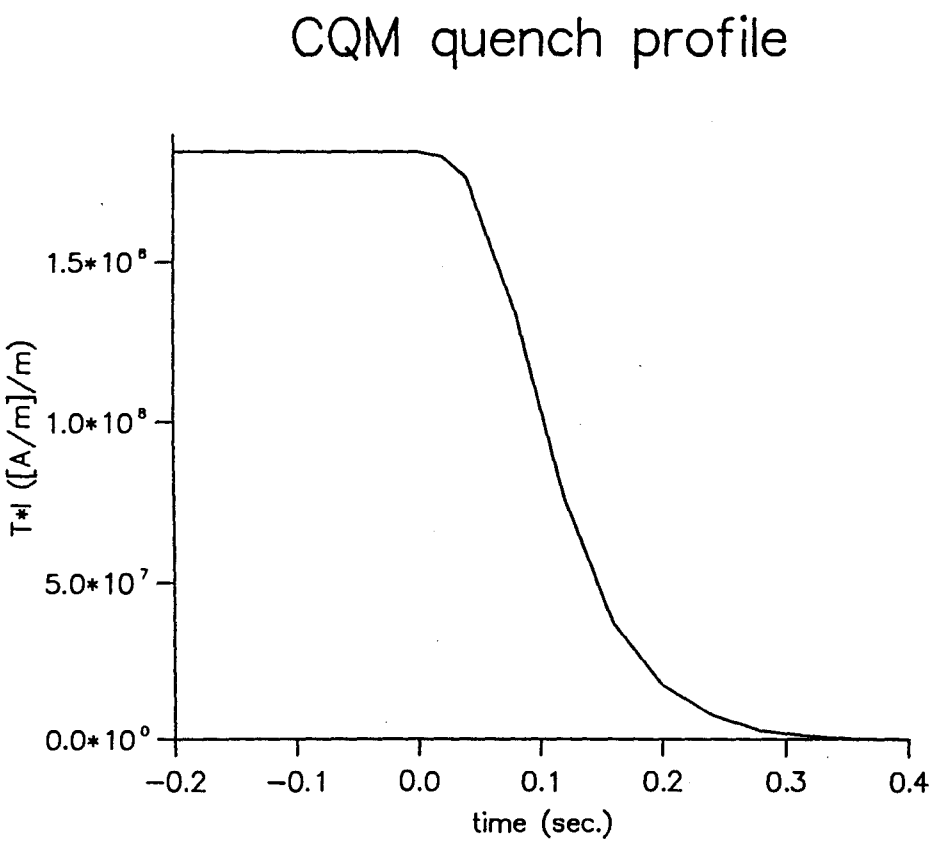

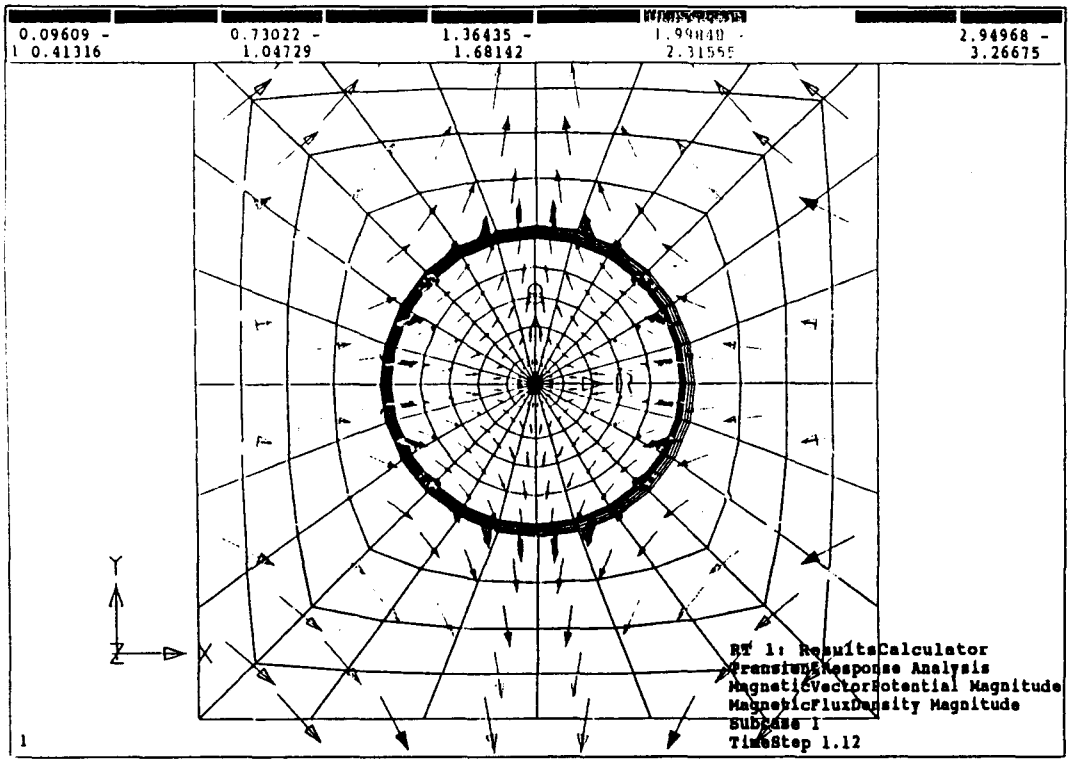
0.09609 -
0.41316
0.73022 -
1.04729
1.36435 -
1.68142
2.94968 -
3.26675
RT 1: ResultsCalculator
TransientResponse Analysis
MagneticVectorPotential Magnitude
MagneticFluxDensity Magnitude
Subcase 1
TimeStep 1.12
1

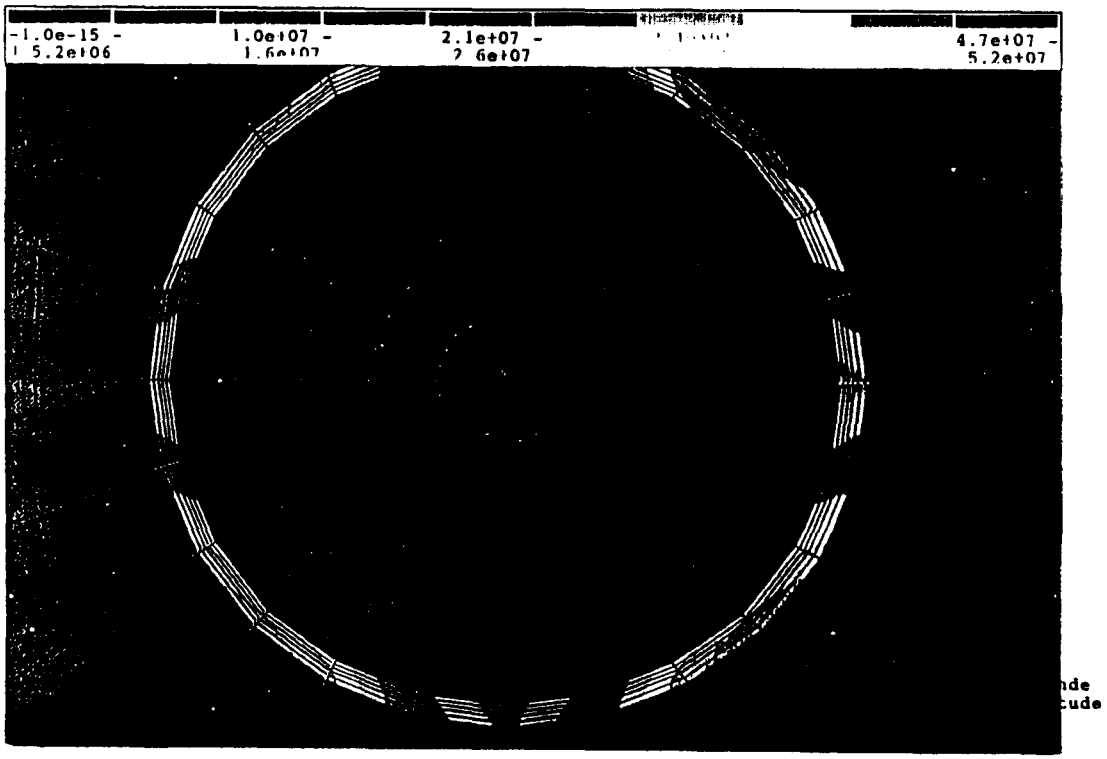
-1.0e-15 -
5.2e+06
1.0e+07 -
2.1e+07 -
4.7e+07 -
5.2e+07

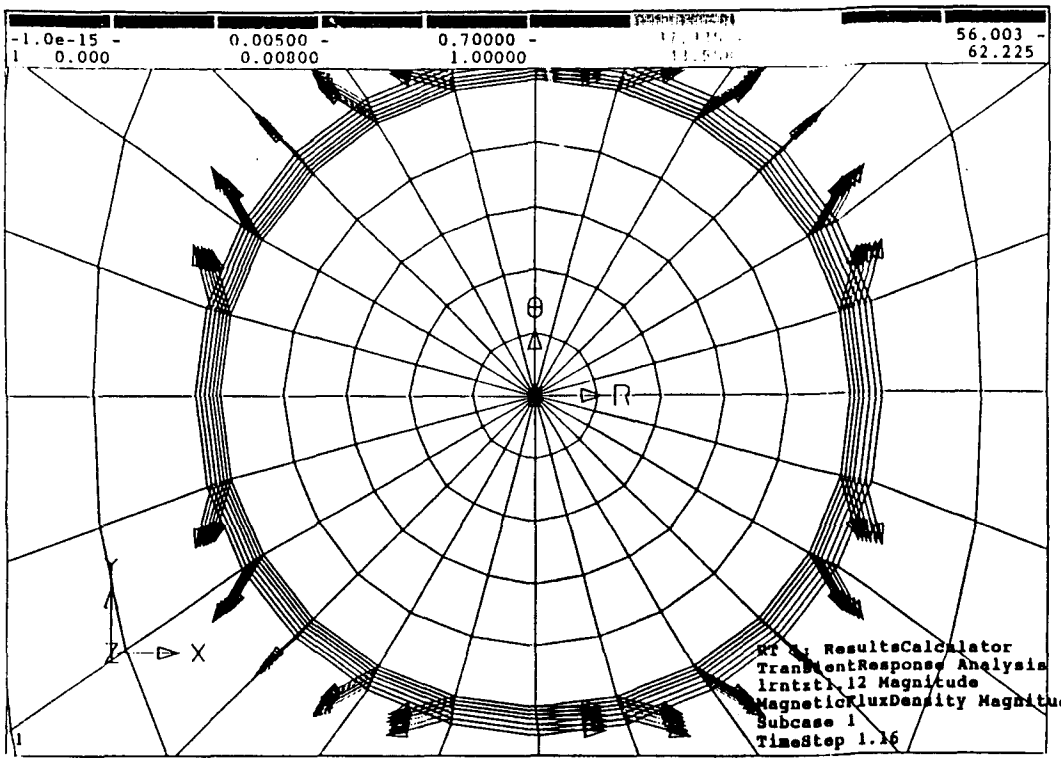

eddy currents in the CQM liner

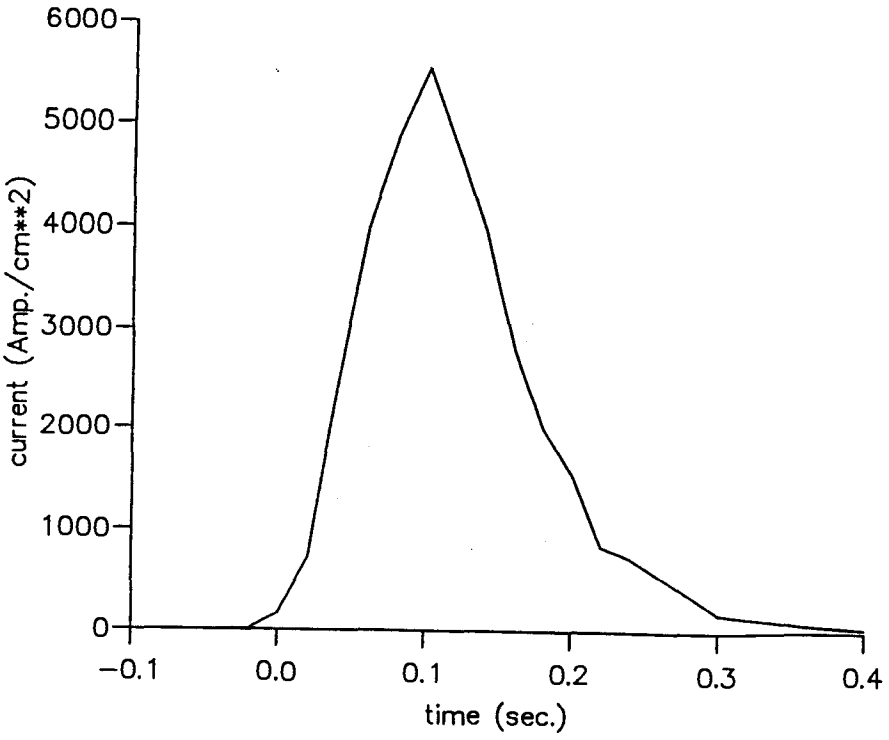

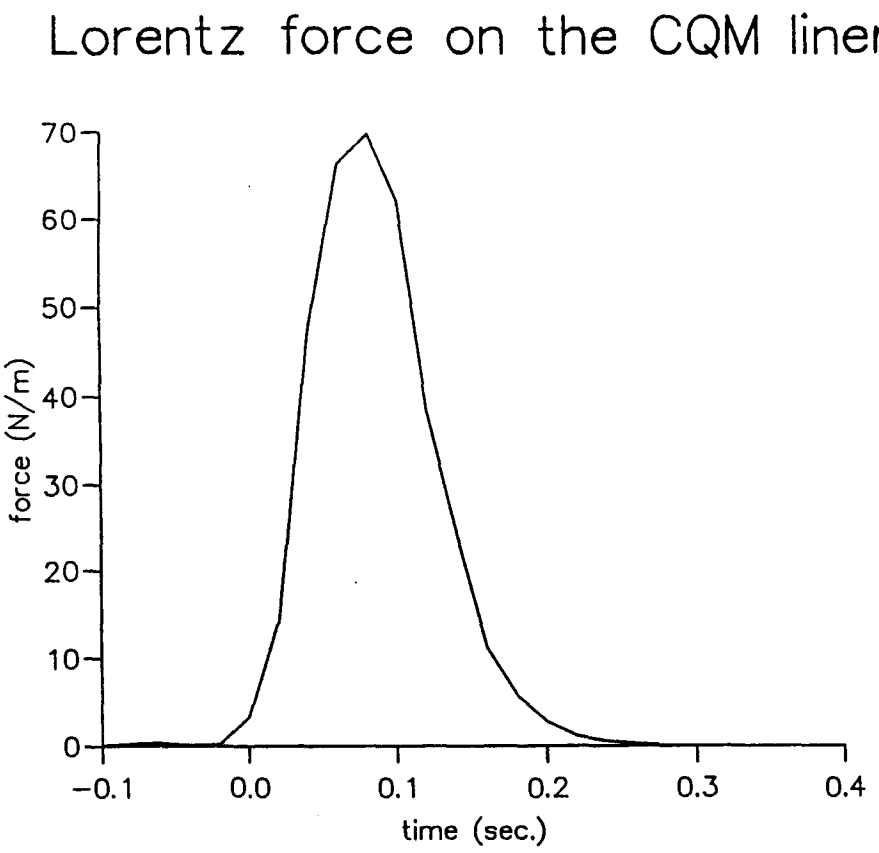
Lorentz force on the CQM liner
force (N/m)
70
60
50
40
30
20
10
0
−0.1
0.0
0.1
0.2
0.3
0.4
time (sec.)

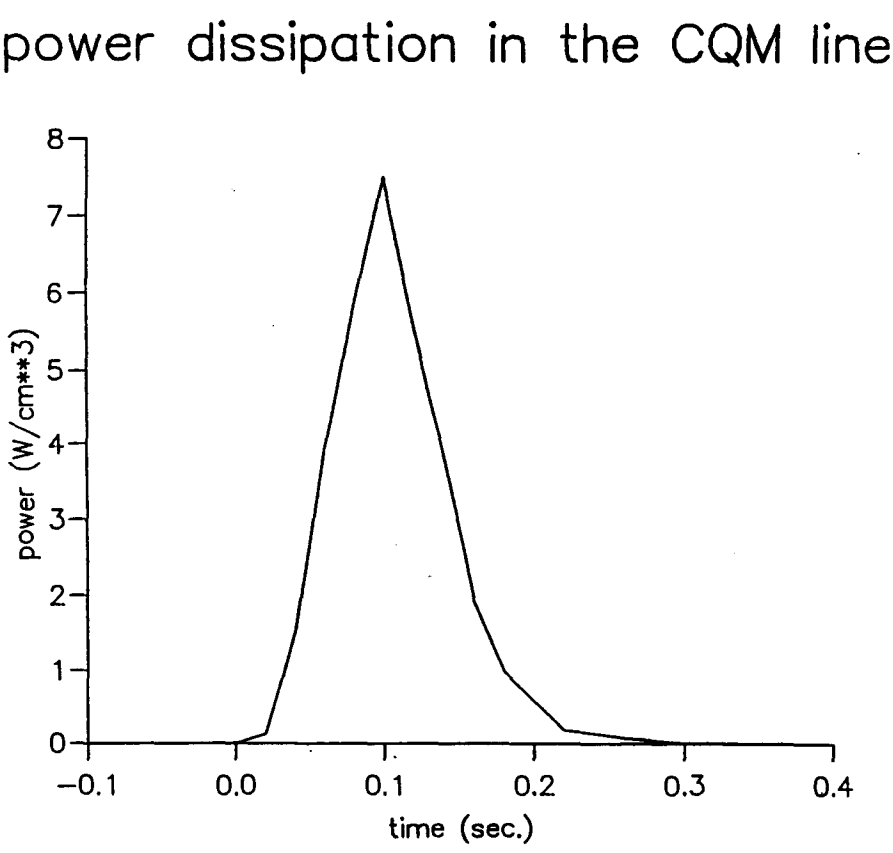
power dissipation in the CQM liner
power (W/cm**3)
8
7
6
5
4
3
2
1
0
−0.1
0.0
0.1
0.2
0.3
0.4
time (sec.)

SUMMARY

CDM LINER

* High rate of Ohmic heating during quench
* Moderate pressure on stainless steel
* No sever effects from mechanical errors

CQM LINER

* No severe mechanical or thermal effects during quench

This Page Intentionally Left Blank

CHAPTER 3

ENGINEERING DESIGN

SECTION 1

80 K Liner Tube Concept Design and Analysis

M. Tuli, J. Zbasnik, W. Chou, K. Leung,
J. Maddocks, G. Morales, Q. S. Shu and W. Turner

SECTION 1

80 K Liner Tube Concept Design and Analysis

M. Tuli, J. Zbasnik,* W. Chou, K. Leung, J. Maddocks, G. Morales,
Q.S. Shu, and W. Turner

Superconducting Super Collider Laboratory†
2550 Beckleymeade Ave.
Dallas, TX 75237-3997

*Lawrence Livermore Laboratory
P.O. Box 808
Livermore, CA 94550

1.0 INTRODUCTION

Developing an 80 K synchrotron radiation liner concept design presents technical challenges. The design must meet the requirements of photodesorption, particle beam stability, magnetic field quality, cooling for the liner tubes, RF impedance, quench induced Lorentz pressure and many other interdisciplinary technical, as well as fabrication, problems.

The SSC beam tube for Collider Dipole Magnets (CDMs) is designed as a two shell laminate. Nitronic-40 steel has been selected as the outer layer for its structural strength in a cryogenic environment, its non-magnetic properties, and its matching in statistical coefficient of thermal expansion to the copper layer. The steel layer is designed to withstand the thermal and eddy current loads and the buckling external pressure. Copper has been selected as the inner layer because of its low electrical resistivity.

The liner design for collider dipole magnets differs from that for collider quadrupole magnets with respect to the beam tube wall thickness, copper deposition, and support and cooling mechanisms.

This paper covers the design requirements and the design concept for both the CDM and CQM along with supporting analysis. Further work in the areas of components fabrication, prototype building, and testing needs detailed consideration.

2.0 COLLIDER DIPOLE MAGNET

The main features of the CDM design are:

A. Liner tube with holes and cooling loop

B. Supports

C. Materials and processes

†Operated by the Universities Research Association, Inc., for the U.S. Department of Energy under Contract No. DE-AC35-89ER40486.

2.1 Liner Tube with Holes and Cooling Loop

The liner tube must be maintained at 80 K in the presence of heat input due to synchrotron radiation heat input of 0.42 W/m. The cooling tube, as shown in Figure 1, is intended to carry the heat away. To ensure proper operation we have shown the tube with good thermal contact (brazing) at the top only—at the bottom it is insulated and is held in place with thin clips which are spot brazed every meter.

The cooling tube will require the following geometry, as shown in Figure 2, to meet ASME B31.3 piping codes.

The cooling tube is required to supply 48 half cells with 0.25 gm/sec of helium gas. The smaller the angle, the higher the pressure has to be to deliver the required flow rate.

The results, as presented in Table 1, show that the stress in a tube with an angle of 14 degrees and a wall thickness of 0.64 mm will meet the ASME pressure codes. ASME B31.3 piping code requires that the stress not exceed a value of 155.13 Mpa. In this tube the maximum Von Mises stress is only 143 which is below that required by ASME.

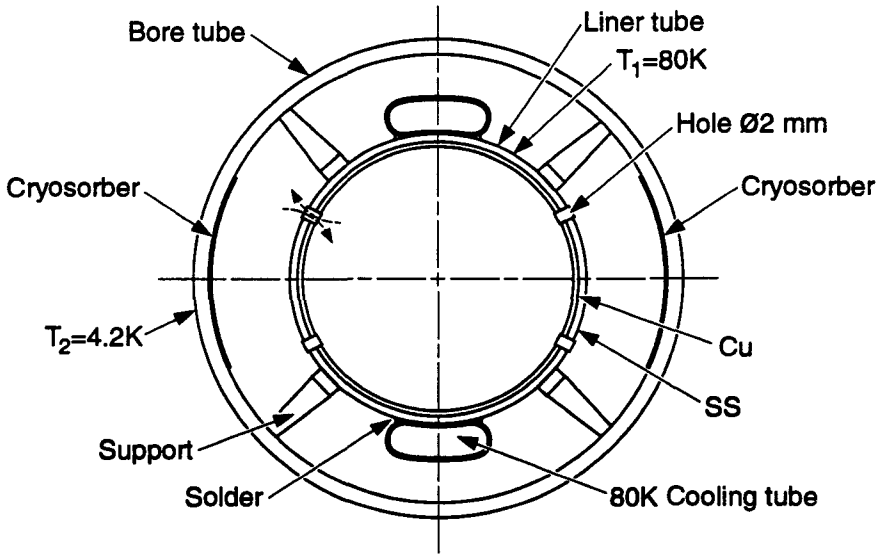

Figure 1. Cross Section View of the CDM Liner.

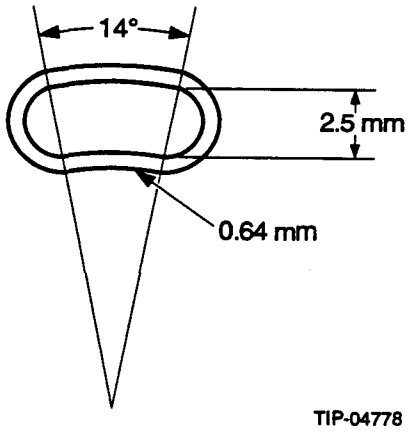

Figure 2. Cooling Tube Geometry.

TABLE 1. STRESS VALUES FOR COOLING TUBE WITH DIFFERENT GEOMETRIES.

ANGLE (DEGREES)	WALL THICKNESS (mm)	PRESSURE (MPa)	MAX VAN MISES STRESS (MPa)
15	0.635	2.517	157
15	0.64	2.517	155
14	0.635	2.586	147
14	0.64	2.586	143

Finally, the liner tube must be perforated to allow the liberated gas to be pumped by the cryosorber, which is attached to the 4 K bore tube. As shown in Figure 3, the cooling tube length is 32 800 mm. A series of 2 mm diameter holes are spaced 9 mm on center. There are 12 holes, arranged in four quadrants.Thus there are 12 holes per strip, 110 strips per meter, and 1286 holes per meter. In a full length tube we have a total of 21 576 holes.

However, beam impedance and stability considerations may demand that the hole shape and distribution be changed for the collider operation.

Virtually nothing has been done in the hole drilling area, except to make informal contact with laser drillers.

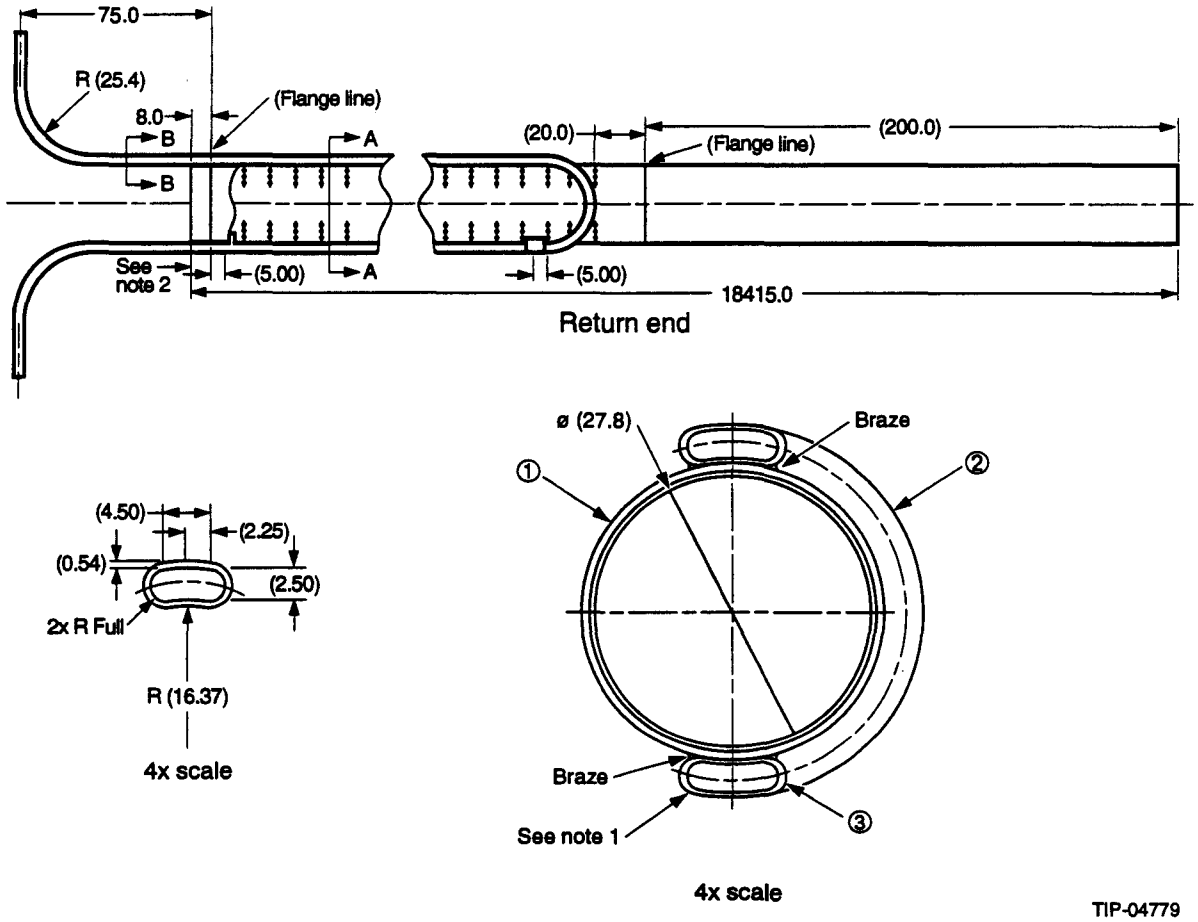

Figure 3. CDM Cooling Tube.

2.2 Supports

The 80 K liner tube is supported in the 4 K bore tube by stainless steel elements as shown in Figure 1. The mechanical analysis has determined the required spacing of the support to be under 2 m. The design constraint is to limit the distance from center to center of the beam tube to within 0.5 mm radially.

As shown in Figure 4, two constraints were analyzed, one with the "bird cage" fixed at both ends, and the another with it fixed at one end only. The mechanical analysis is presented in Tables 2 to 4. Both constraints are workable. The next step should be to build both models and test them to finalize the design. From the data presented below, model A has the maximum stiffness with an acceptable safety margin.

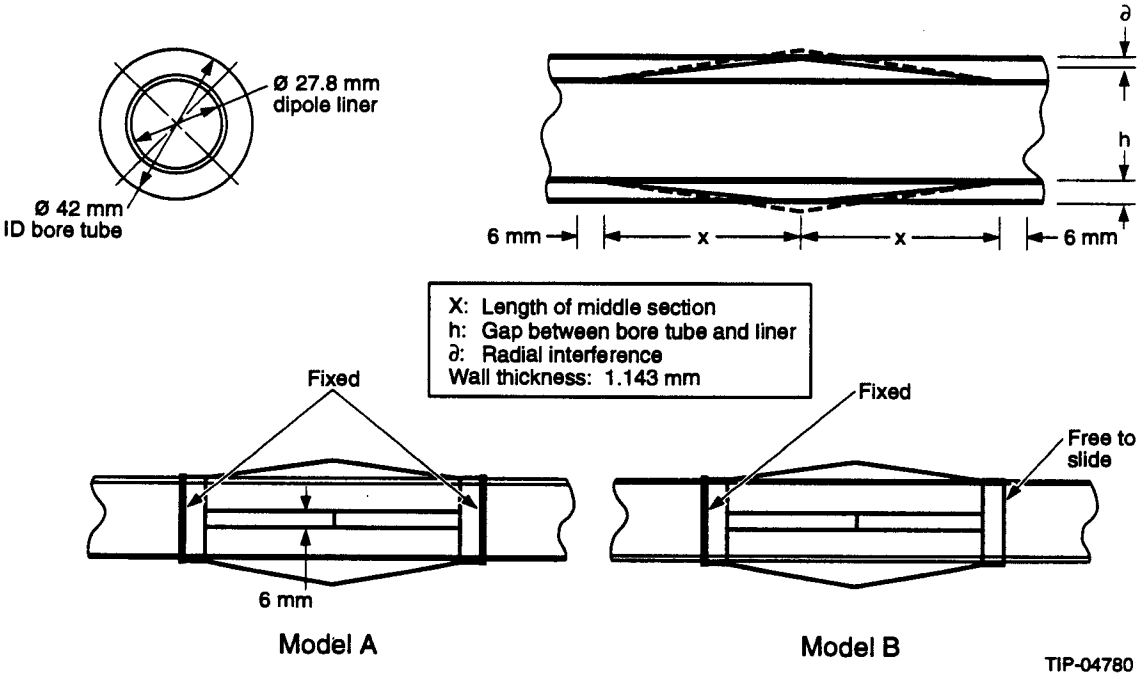

Figure 4. The Support System.

TABLE 2. STRESS VALUES FOR THE LINER SUPPORTS.

	MODEL DISPLACEMENT (mm)	MAXIMUM VON MISES STRESS (MPa)	FACTOR OF SAFETY (YIELD STRENGTH/ VON MISES)
A	0.25	136	2.94
A	0.50	284	1.38
B	0.25	72	5.57
B	0.50	143	2.79

Yield Strength = 400 MPa

TABLE 3. STIFFNESS COEFFICIENTS FOR THE LINER SUPPORTS.

MODEL	K (kN/m)
A	464
B	20.9

TABLE 4. DEFLECTION OF SUPPORTS WITH VARIOUS SPRING CONSTANTS.

SPRING CONSTANT (kN/m)	DEFLECTION OF SUPPORT (mm)	TOTAL MAX DEFLECTION OF LINER (mm)	SAG IN PIPE (mm)
10	1.00	1.70	0.70
20	0.50	1.20	0.70
27.3	0.35	1.10	0.75
30	0.32	1.00	0.68
40	0.24	0.97	0.70
50	0.20	0.89	0.69
60	0.16	0.85	0.69
70	0.14	0.83	0.69
Infinite	0.00	0.69	0.69

2.3 Materials and Processes

2.3.1 Liner Thickness

The inner wall conductivity and thickness are given by:

$$d * t > 2 \times 10E5\ \Omega e{-}1$$

For OFHC @ 80 K electric resistivity = $2 \times e{-}9\ \Omega$ m = 1/d

$$t = 2 \times 10e5(1/\Omega) * 2e{-}9\ (\Omega\ m) = 0.0004\ m = 0.4\ m$$

If we use 0.5 mm

$$d * t = 2.5e5\ \Omega e{-}1$$

So a thickness of 0.5 mm meets the multibunch resistivity wall instability of

$$d * t > 2 \times 10E5\ \Omega e{-}1$$

A 0.75 mm layer of stainless steel is added to the tube to give it more strength.

When the outer layer of stainless steel is 0.75 mm, the combined stress @ Cu layer will be under 30 KSI for approx. 1/4 hard copper

A low cycle fatigue analysis using data from the National Bureau of Standards indicates that this yielding would be acceptable for a maximum of 150 quench cycles, 30 thermal cycles to room temperature, and 10 000 magnetic cycles. (Kent Leung)

Thus the wall thickness for the dipole liner is 1.25 mm (0.5 Cu + 0.75 SS).

2.3.2 Fabrication Techniques

Several approaches are being pursued in parallel on a development scale to determine which, if any, are feasible for producing long tubes.

(1) Brazing Method

This method is being pursued by Handy & Harman. Handy & Harman will attempt to produce 5 short (0.6–1 m) copper/stainless liner tubes, without the pumping holes or attached cooling tubes.

This procedure involves reducing a stainless tube around a copper tube, with a suitable brazing alloy at the interface. The unit will then be furnace brazed to achieve a good bond between copper and stainless.

(2) Electrodeposited Method

In this method, the copper is applied to the inside of the stainless tube via electrodeposition. This method is being pursued by two vendors–Silvex Surface Technology and Babcock and Wilcox. Each vendor will provide three to four 6 meter long liner tubes without holes and cooling tube attached.

Each vendor will electroplate a 100 mm thick copper layer onto the I.D. of the tubes. Two of the four copper plated tubes will also receive a 1–10 mm gold layer over the previously plated and heat treated copper layer.

(3) Explosive Bonding Techniques

This method involves cladding the stainless onto a copper tube by an explosive bonding technique. This is being pursued by Northwest Technical Industries.

(4) Coextrusion Process

This process is being pursued at Supercon to develop a Cu/SS composite liner tube. This effort includes both the liner tube configuration (500 mm copper) as well as the baseline beam tube design (100 mm copper).

As an alternate to the composite tube, we are also pursuing development of a liner tube which is fabricated entirely from a copper that is strengthened by incorporating Nb dendrites in the microstructure.

The objective is to determine if there is a composition which has the proper combination of electrical conductivity and mechanical strength after the brazing operation that needs to be done to attach the cooling tubes to the liner. This has the attractive feature of eliminating thermal induced stresses, which will improve the reliability.

(5) Sputtering Process

This process is being pursued at Surface Solution, Inc. Sputtering is a PVD (physical vapor deposition) process. It includes the plasma cleaning of the I.D. of the tube prior to deposition of the desired copper coating utilizing SSI'S proprietary LMS (Linear Magnetron Sputtering) process.

(6) Chemical Vapor Deposition (CVP)

This process is being pursued by Virginia Polytechnical Institute. VPI will supply short tubes for testing.

2.4 Testing

The following tests (Table 5) will be conducted on the composite beam tube samples.

TABLE 5. BEAM TUBE SAMPLE TESTS.

TEST	TEMP.	CONDUCTED AT
Photodesorption/ Out Gassing	293 K/ 4.2 K	BNL and Novosibirisk
Surface Resistance (at dc or low frequencies)	293 K/77 K/4.2 K	Los Alamos Nat. Lab. and SSCL
Radiation	293 K/4.2 K	General Atomic
Bend test	ASTM B571	SSCL
Heat quench test	ASTM B571	SSCL
Grain Size	ASTM E112-88	SSCL

3.0 COLLIDER QUADRUPOLE MAGNET

The main features of CQM design (Figure 5) are:

A. End cooling

B. Hole configuration

C. Support

D. Materials

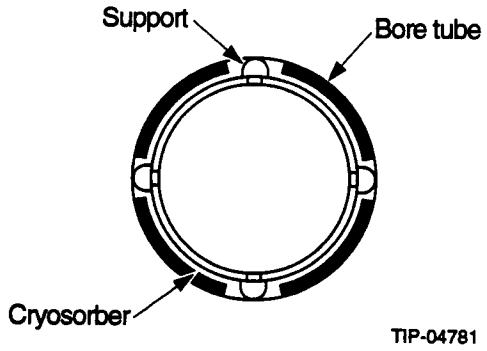

Figure 5. Cross Section View of the CQM Liner.

3.1 End Cooling and Hole Configuration

For a 1.5 mm hole in the quadrupole liner, a total of 3000 holes/m are required to yield sufficient conductance. As shown in Figure 6, a total of 16 holes are placed on each strip. Since the design requires 3000 holes/m and there are 16 holes/strip this means that there are 187 strips/m or 0.187 strips/mm. Taking the inverse says that for every 6 mm there must be a strip of holes.

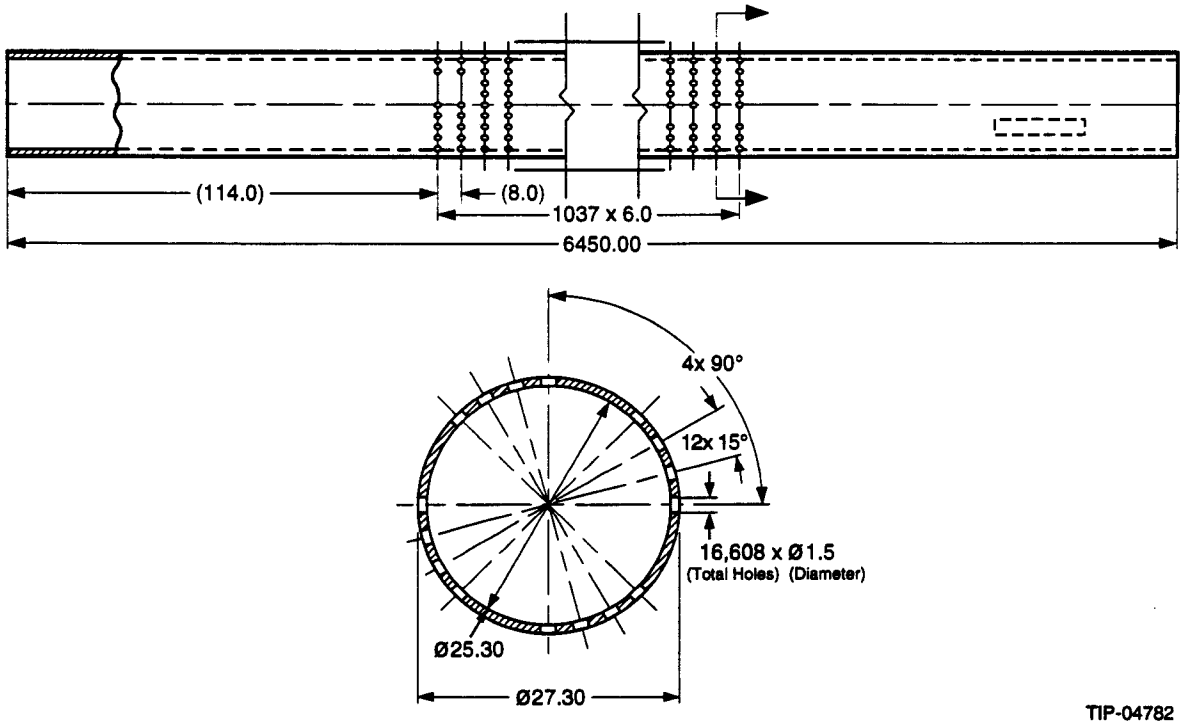

Figure 6. Cooling Configuration of CQM.

3.2 Support

In order to increase the thermal resistance between the liner support and the 4 K bore tube, plasma spraying of Zirconia or Alumina is under consideration. The initial design for a support is given in Figure 7.

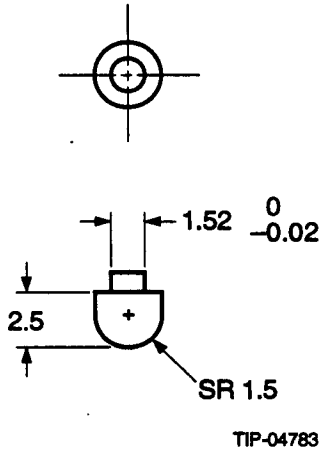

Figure 7. Support, CQM.

3.3 Materials

The quench force on a quadrupole is about one quarter of that in a dipole liner. The maximum stress calculated for the quadrupole liner is 8 Ksi. The yield stress of copper (OFHC) is 10 Ksi. A 0.5 mm thick Cu layer is needed for the quadrupole liner, since the stress for the copper layer is 8 Ksi and the yield stress of copper is 10 Ksi.

The conductivity × thickness requirement is satisfied locally if T < 100 K (Figure 8).

Since the CQM design uses end conductive cooling and, as shown, the maximum delta T = 14 K for 1.0 mm thick Cu.

Thus the liner is 1.0 mm thick copper (OFHC)

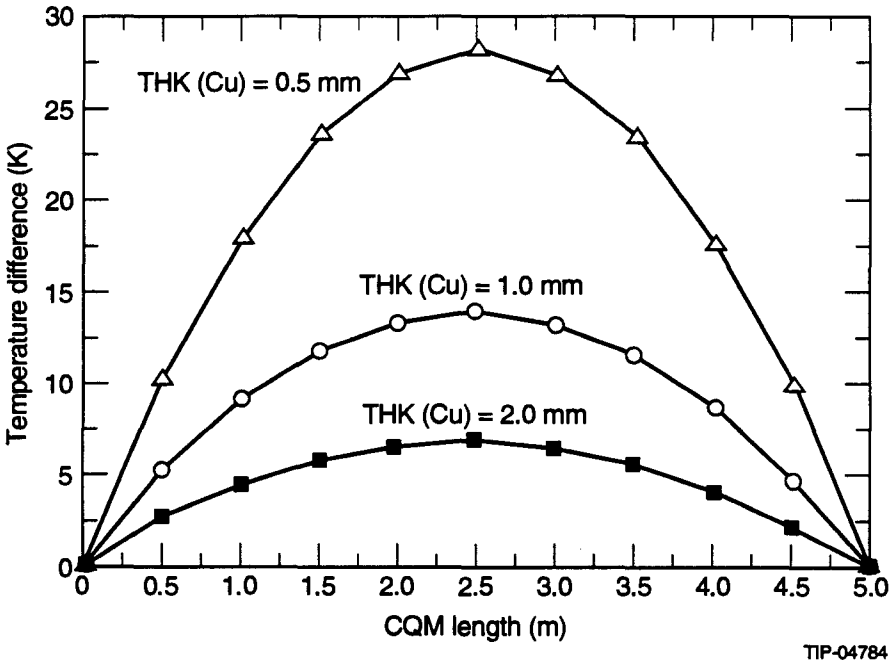

Figure 8. Temperature Distribution Along the Liner.

3.4 Future work

Further work in the areas of brazing methods, support materials, and selection of a liner bimetallic tube fabrication technique needs to be performed.

This Page Intentionally Left Blank

SECTION 2

80 K Liner Interconnect Design

G. Morales, D. Clark, W. Clay, J. Maddocks,
Q. S. Shu, M. Tuli, W. Turner, K. Yu, and J. Zbasnik

SECTION 2

80 K Liner Interconnect Design

G. Morales, D. Clark, W. Clay, J. Maddocks, Q. S. Shu,
M. Tuli, W. Turner, K. Yu, and J. Zbasnik

Superconducting Super Collider Laboratory*
2550 Beckleymeade Ave.
Dallas, Texas 75237-3997

1.0 INTRODUCTION

The operating energy of 20 TeV and beam current of 0.072 A of the Superconducting Super Collider (SSC) will produce considerable photodesorbed gases in the beam vacuum.[1] These gases may greatly reduce the beam lifetime, and the scattered beam power may lead to quenching of the superconducting magnets. One method being considered to minimize these gases is to install an 80 K liner inside of the magnets[2] (see Figure 1).

A prototype liner has been developed for installation and testing in a half cell at the Accelerator System String Test (ASST). This 80 K liner design consists of a perforated tube located coaxially inside of the magnet bore tube and sustained at 80 K with cooling tubes carrying pressurized GHe.

Installing such a liner requires redesigning the magnet interconnect and providing a means of connecting the tubes that make up the liner. The beam tube bellow has to be modified to allow the cooling tubes entry into the beam vacuum environment, while minimizing the heat transfer into the 4 K system. A RF joint is required to connect adjacent liner tubes while providing for thermal contraction; a magic joint is required to connect it to the liner. A good thermal contact joint is required to allow for easy assembly of the quadrupole/spool liner into the magnets.

This report covers the components required to assemble the liner in the magnets.

2.0 CRYOGENIC BOX

2.1 Requirements

The 80 K liner requires that the magnet interconnect allow a pathway for the 80 K cooling tubes into the beam vacuum environment, and also provide access to the RF joint and the good thermal contact joint for assembly and maintenance. This interconnect assembly for the liner is known as the cryogenic box (see Figures 2, 3, 4, and 5).

Cooling for the liner tubes is achieved with pressurized GHe cooling tubes that conduct the heat away from the liner. The dipole liner is cooled with a tube that is brazed to the top of the liner for approximately 16 meters and then returns strapped to the bottom of the liner (see Figures 1a and 6a). Compact heat exchangers at the extremes of the quadrupole liner are used to cool it to 80 K (see Figure 1b, 3b, 5, and 6c).

---

* Operated by the Universities Research Association, Inc., for the U.S. Department of Energy under Contract No. DE-AC35-89ER40486.

To minimize the heat transfer between the 4 K bellow and the 80 K cooling tubes, thermal standoffs are attached to the cryogenic box (see Figure 8).

The good thermal contact joint, the RF joint, and the magic joint are housed inside of this cryogenic box. The good thermal contact joint is used to connect sections of the quadrupole/spool liner (see Figure 9). RF flexible sleeve refers to the component used to connect adjacent liner tubes (see Figure 10); the magic joint connects it to the liner (see Figure 11).

The cryogenic box is required to have a feature that will absorb the themal contraction of the magnets.

2.2 Description of Components

The cryogenic box is made up of a flange lead end, a split cylinder, two thermal standoffs, and a beam tube bellow.

The first component is the flange lead end which connects to a flange on the magnet to make a vacuum seal (see Figure 12). It must have an inner diameter (ID) larger than 40 mm to be able to slide over the RF joint or the good thermal contact joint; however, this ID must not exceed 55 mm since the ID of the Helicoflex vacuum seal that goes between the flanges is 59 mm. The other face of the flange has a groove to provide for self aligning of the cryogenic box.

Connected to the flange lead end is the split cylinder which provides the means for assembly over the cooling tubes. This split cylinder is made up of two half cylinders which assemble over the cooling tubes and connect all of the components (see Figure 13). Its ID has to be large enough to allow room for the liner and cooling tubes.

To minimize the heat transfer into the 4 K system, thermal standoffs are attached to the split cylinders. The thermal standoff, which consists of a 22.2 mm OD $\times$ 0.97 mm wall tube with a bellow attached to it, provides an entrance into the beam vacuum environment (see Figures 8 and 14). This assembly provides a long thermal pathway needed to minimizes the heat transfer from the 80 K cooling tube into the 4 K split cylinder.

Attached to the other end of the split cylinder is the beam tube bellow (see Figure 15). This bellow has a flange on one end to mate with the split cylinder, and on the other side it has a flange to mate with the flange on the magnet. Moreover, it expands 51 mm when the magnets contract and compresses 51 mm to allow access to the good thermal contact joint and the RF joint. Its OD is similar to the one on the bellow shown in Figure 7a, and its ID has to be larger than the OD of the previously mentioned joints. The spring rate for the bellow was kept as low a possible to make it easy to compress the bellow during assembly.

The thermal standoff bellow requires an OD of 33 mm, an ID of 22 mm, and a ratio of the cross sectional area to length of 0.078 mm. The diameters are set by the OD of the cooling tube and the space in the interconnect. The ratio is required to maintain a long thermal path.

2.3 Calculations

A heat transfer analysis was performed on the thermal standoffs to determine the dimensions of their components. The analysis assumes that one end is at 80 K, the other end is at 4 K, and the point where the two connect is at 25 K (see Figure 8). To determine the dimensions the following equation was used:

$$Q = \frac{A}{L} \int_{T_1}^{T_2} K dt \qquad (1)$$

where Q is the rate of heat conduction in watts, A is the cross sectional area in cm^2, and K is the thermal conductivity in $\frac{W}{cm}$.

For the section going from 25 K to 4 K the calculations and results are as follows:

$$Q = 0.025 \text{ W}$$
$$\int_{T_4}^{T_{25}} \bar{K} dt = 0.277 \frac{W}{cm}. \quad (2)$$

Assuming an OD of 2.223 cm and a wall thickness of 0.0889 cm, the length becomes 6.6 cm.

For the section going from 80 K to 25 K the calculations and results are as follows:

$$Q = 0.025 \text{ W}$$
$$\int_{T_{25}}^{T_{80}} \bar{K} dt = 3.213 \frac{W}{cm}. \quad (3)$$

Using these values results in a ratio of A/L of 0.00778 cm.

2.4 Assembly

All of the components are assembled and welded together in a controlled environment (see Figures 4 and 5). The thermal standoffs will be welded to the split cylinder and then assembled over the liner. Finally, the end flange and the beam tube bellow are assembled around the split cylinder and the whole assembly is welded together.

2.5 Materials

All components are made of 316 L or 304 L stainless steel because of its non magnetic and corrosion resistant properties.

2.6 Operation/Maintenance

Once the cryogenic box is assembled around the liner, the Helicoflex seals are placed on each end of the cryogenic box, and the whole assembly is inserted into the magnet bore tube.

To complete the assembly, a Helicoflex clamp is placed and tightened around the mating flanges. This clamp can be removed, and the beam tube bellow can be compressed 51 mm to allow access to the magic joint or the good thermal contact joint.

3.0 RF JOINT

3.1 Requirements

The RF joint is used to connect the liner tubes of adjacent magnets while providing for thermal contraction and minimizing RF impedance (see Figure 9).[3] Since the liner tubes only extend from end to end of a dipole or quadrupole magnet, a connection is required to connect adjacent liner tubes.

One requirement of this joint is to maintain geometric and electric continuity between adjacent liner tubes, which is necessary to minimize transverse and longitudinal impedance.[3]

Another requirement for the joint is to have a feature that will absorb the 51 mm of thermal contraction in the magnets. While doing this it must also absorb ± 2.6 mm of axial misalignment.[3]

This RF joint will be located inside of the cryogenic box; therefore, its physical dimensions are dominated by those of the cryogenic box.

3.2 Description of Components

The RF joint is accomplished with an RF flexible sleeve, which has a cylindrical shape and flexible fingers, (see Figure 10). The solid part mechanically connects to the return end of the liner, and the flexible fingers clamp around the adjacent liner. The fingers allow the liner to slide inside of them during thermal contraction; these fingers are flexible enough to allow for radial misalignment.

The RF flexible sleeve is a scaled down version of that used in the collider RF joint. Its ID was reduced to match that of the liner and its length was also reduced to fit inside of the cryogenic box.

3.3 Materials

Beryllium copper is used to manufacture the sleeve because of its good electrical conductivity and high strength.

3.4 Assembly

In a controlled environment the components of the magic joint that go on the RF flexible sleeve and liner are braced on (see Figure 6).

Before the liner is inserted inside the magnet, the beam tube bellow is compressed 51 mm so the RF flexible sleeve can be inserted around the lead end of the liner and then clamped to the liner with a spring (see Figure 9).

Once the liner is installed inside of the magnet, the beam tube bellow is contracted again, and the rest of the components of the magic joint are used to connect the sleeve to the liner.

4.0 MAGIC JOINT

4.1 Requirements

The magic joint is the mechanical connection between the RF flexible sleeve and the liner tubes required to allow for ease of connecting and disconnecting the RF flexible sleeve from the liner. Its length and maximum diameter are set by the ID of the bellow and the maximum amount that the bellow can be compressed.

Another requirement for the joint is that it provides a smooth interface between the liner tube and the RF flexible sleeve to minimize impedance. Any discontinuities in the inner surface of the liner will increase the transverse and longitudinal impedance.

4.2 Description of Components

A turnbuckle design is used on this joint. This design consists of threaded sleeves that are brazed to the liner and RF joint and in turn are connected with a turnbuckle nut (see Figure 11).

The first component is a right hand threaded section that is brazed to the return end of the dipole liner (see Figures 16 and 6a). This section is brazed to the liner before it is inserted into the bore tube of the magnet. To allow this the OD of this threaded section must be smaller than the ID of the bore tube minus one millimeter for the cryosorbing material. The ID of the brazed section must also be greater than 27.8 mm, which is the OD of the dipole liner.

Threads with a nominal diameter of 30 mm and loose tolerance are needed for this section. The 30 mm diameter allows this section to slide inside of the bore tube and also to leave enough material, providing a shoulder that can be brazed to the liner tube. The loose tolerance on the threads is needed to allow a path for pumping a vacuum between the threads.

The next component is a similar sleeve except with left handed threads (see Figures 17 and 6).

Connecting the two threaded sections is a turnbuckle nut (see Figure 18). One side of this nut has right hand threads and the other side has left hand threads. Loose tolerance is also needed for the threads.

To make sure the joint does not unscrew itself during thermal cycling, a jam nut is added to the magic joint (see Figure 19).

On both nuts, holes are drilled all the way through to provide a path for pumping a vacuum between the threads. The holes are also used by a spanner wrench to tighten the joint.

4.3 Materials

All of the components of the magic joint are made of C10100 copper. This material is required to maintain good electric conductivity between the components. All of the components are made of the same material so they contract the same amount, ensuring that the contact between components is maintained.

4.4 Assembly

The beam tube bellow is contracted 51 mm to allow access to the magic joint. Then the turnbuckle nut is placed next to the threaded section on the liner. Once the RF flexible sleeve is slid next to the turnbuckle nut, this nut is turned until the two threaded sections make appropriate contact. Finally, the jam nut is unscrewed until it makes good contact with the turnbuckle nut, locking the joint.

5.0 GOOD THERMAL CONTACT JOINT

5.1 Requirements

The quadrupole liners are cooled with compact heat exchangers at both ends of the liner tube (see Figure 1). In order to easily assemble the liner into the quadrupole magnet, a joint is required between the two heat exchangers.[2] The spool liner also requires this joint since it has a heat exchanger on one end and the Beam Position Monitor at the other (see Figure 1). The joint must minimize RF impedance and provide good thermal and electrical contact. Also, since this joint is located inside of the beam tube bellow, its size is limited by this bellow.

5.2 Description of Design

A turnbuckle design is used on this joint. This design consists of threaded sleeves that are brazed to the ends of the liner tubes which are connected with a turnbuckle nut (see Figure 20).

The first component is a threaded section that is brazed to the return end of the quadrupole or spool liner (see Figures 21 and 6c). Its OD must be smaller than the ID of the bore tube minus a one millimeter layer of cryosorbing material.

Threads with a nominal diameter of 30 mm and loose tolerance are needed for this section. The 30 mm diameter allows this section to slide inside of the bore tube and also to leave enough material to provide a shoulder that can be brazed to the liner tube. The loose tolerances on the threads are chosen to allow a path for pumping a vacuum between the threads.

To the end of the other component of the quadrupole or spool liner, a left handed threaded section is brazed. This threaded section has the same properties as the right-handed sections except that it has left-hand threads (see Figure 20).

Thermal contact between all of the components is provided through the threads. The threaded section provides a thermal contact of 16 cm which is larger than the 4.013 cm required.[2]

Connecting these two threaded sections is a Turnbuckle Nut. One side of this nut has right hand threads and the other side has left hand threads. Loose tolerance is also needed for these threads.

To make sure the joint does not unscrew itself as the magnets are cooled and warmed up, a jam nut is added to the joint.

On both nuts, holes are drilled all the way through to provide a path for pumping a vacuum between the threads. These holes are also used by a spanner wrench to tighten the joint.

5.3 Material

All of the components of the good thermal contact joint are made of C10100 copper. This material is required to maintain good electric and thermal conductivity between the components. All of the components are made of the same material so they contract the same amount, ensuring that the contact between components is maintained.

5.4 Operation and Assembly

The beam tube bellow is contracted 51 mm to allow access to the magic joint. Next, the jam nut is screwed on the liner. Then the turnbuckle nut is placed next to the threaded section on the liner. Once the other sleeve is slid next to the turnbuckle nut, this nut is turned until the two threaded section make appropriate contact. Finally, the jam nut is unscrewed until it makes good contact with the turnbuckle nut, locking the joint.

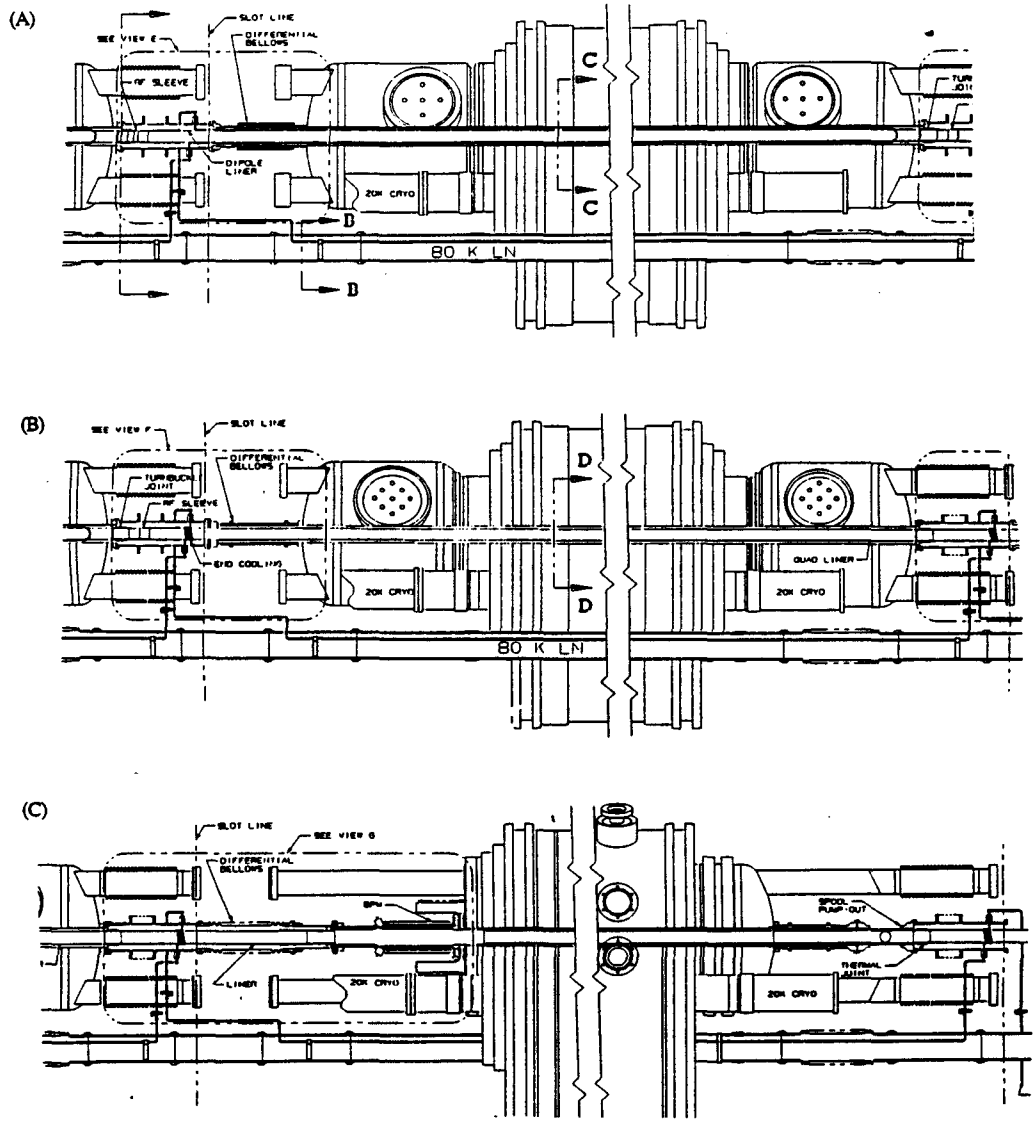

Figure 1. (A) Dipole Liner. (B) Quadrupole Liner. (C) Spool Liner.

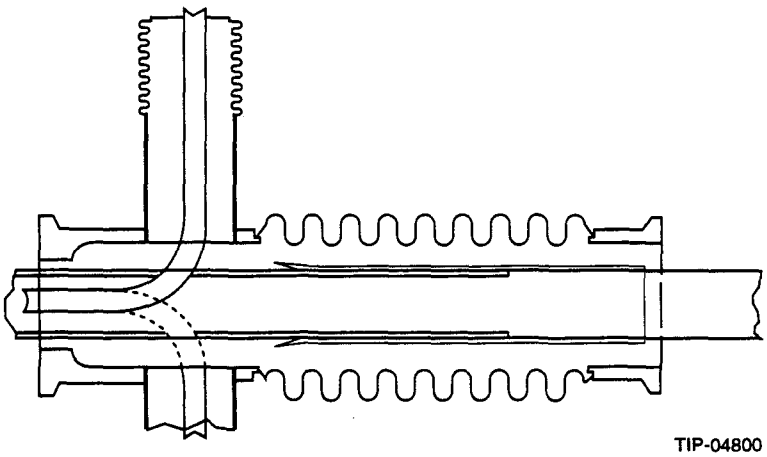

TIP-04800

Figure 2. Cryogenic Box Assembled Over the Dipole Liner.

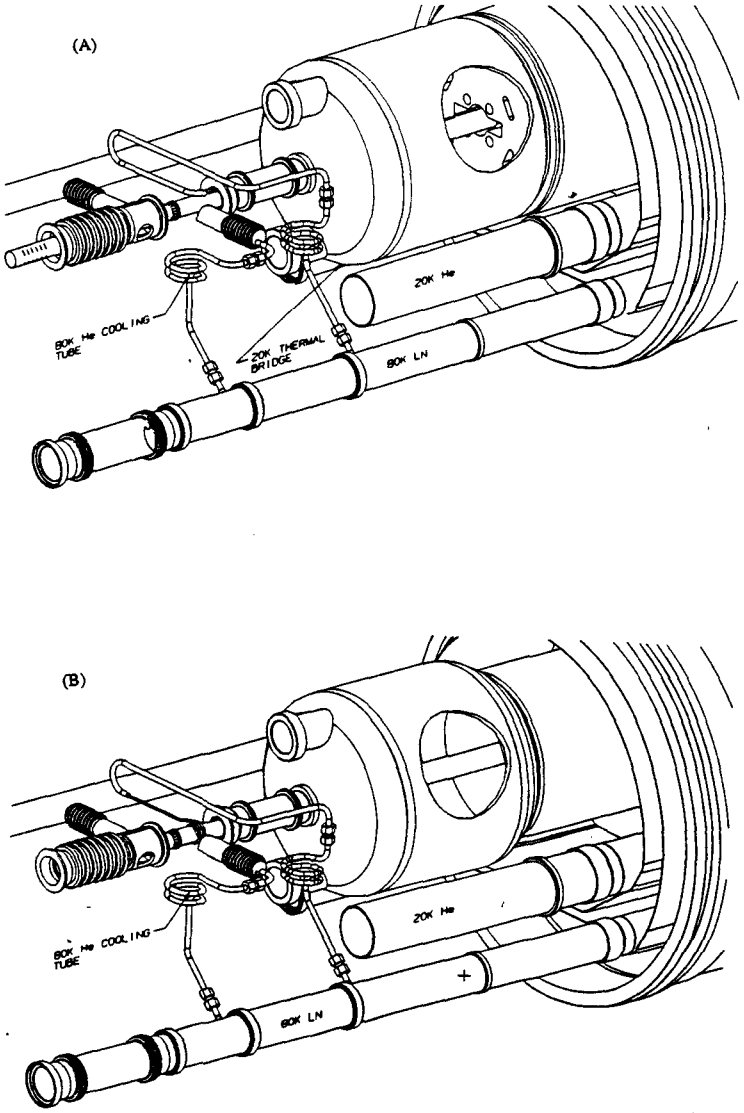

Figure 3. (A) Assembly of Dipole Liner. (B) Assembly of Quadrupole Liner.

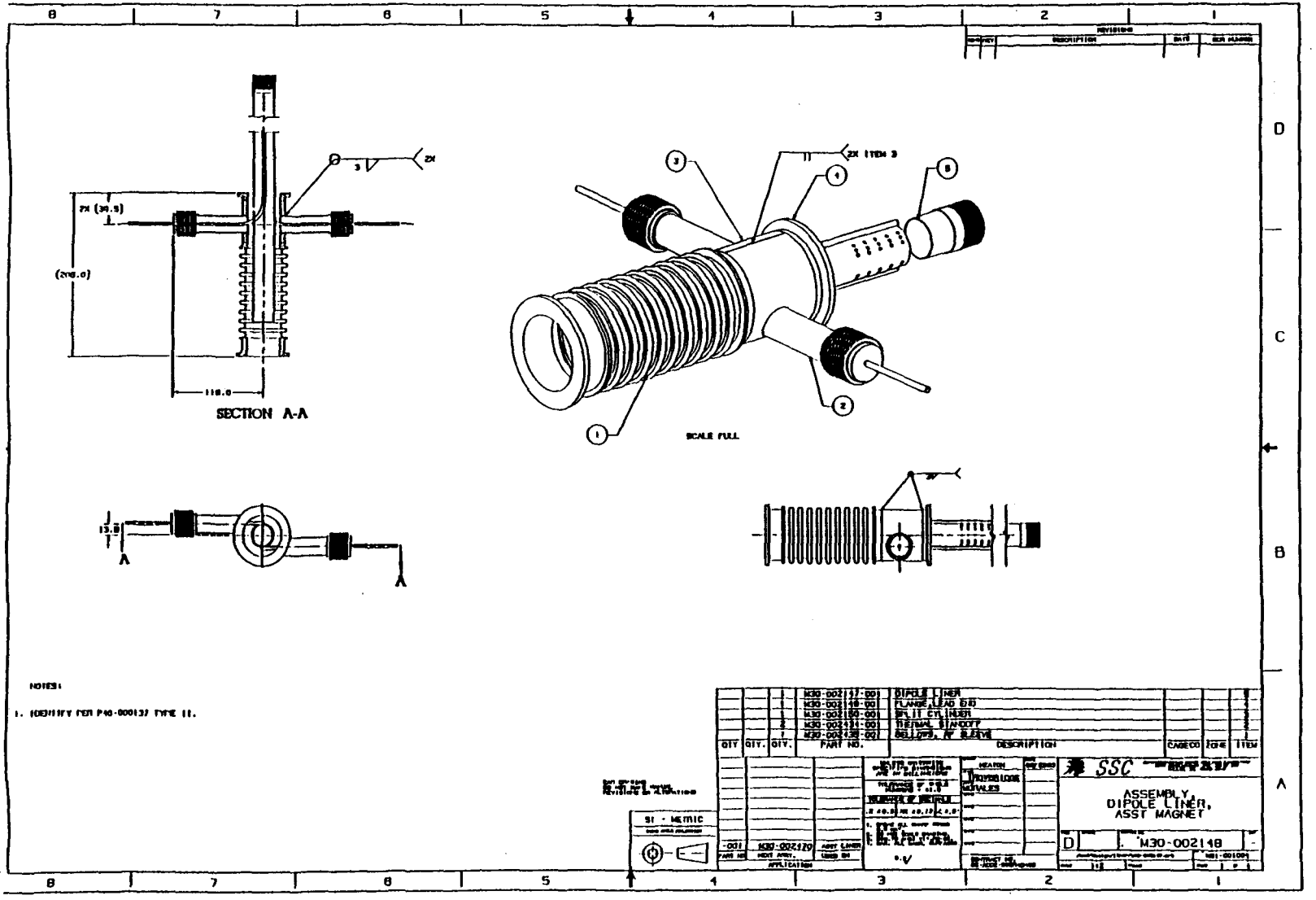

Figure 4. Dipole Liner Cryogenic Box Assembled on Dipole Liner.

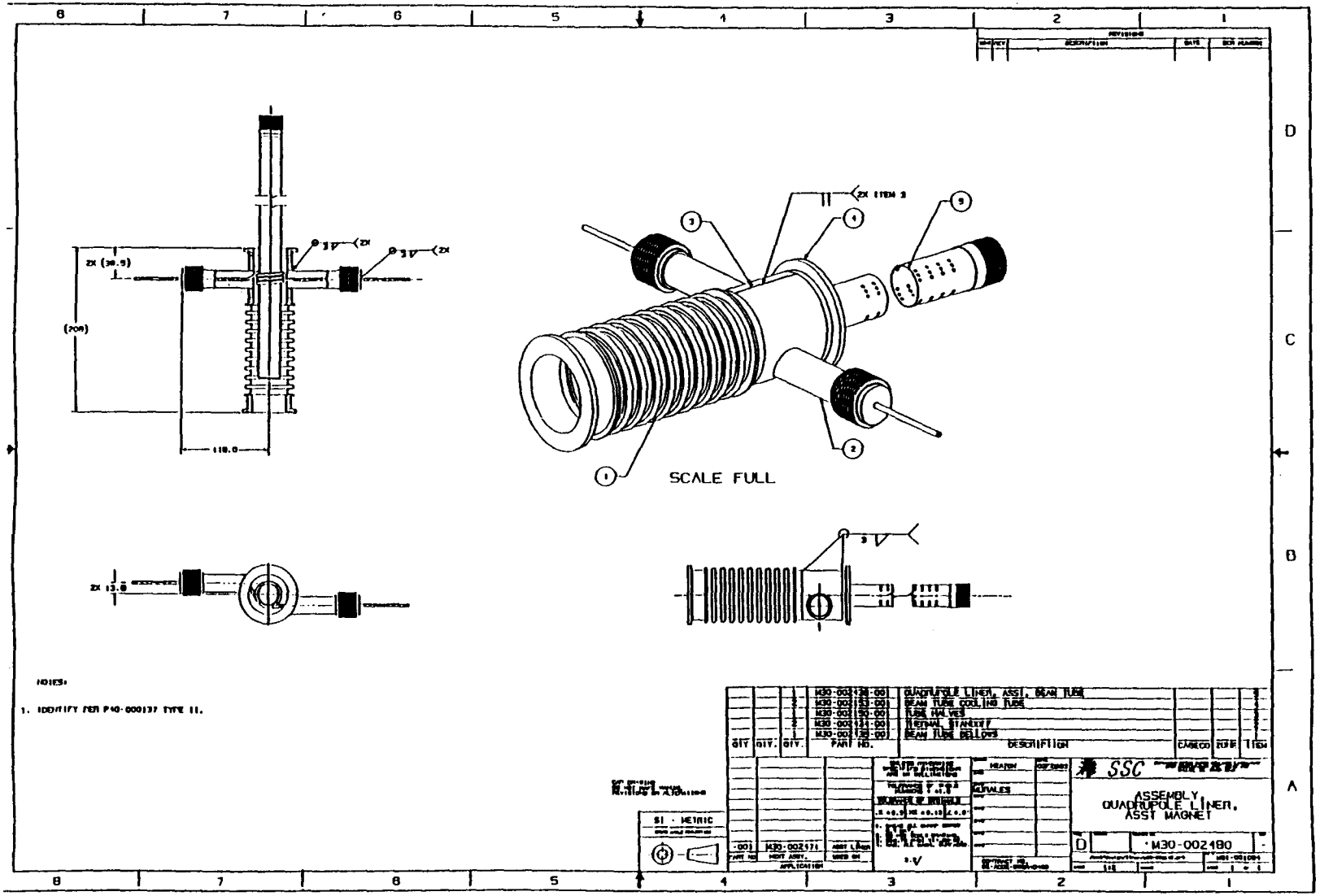

Figure 5. Quadrupole Liner Cryogenic Box Assembled on Quadrupole Liner.

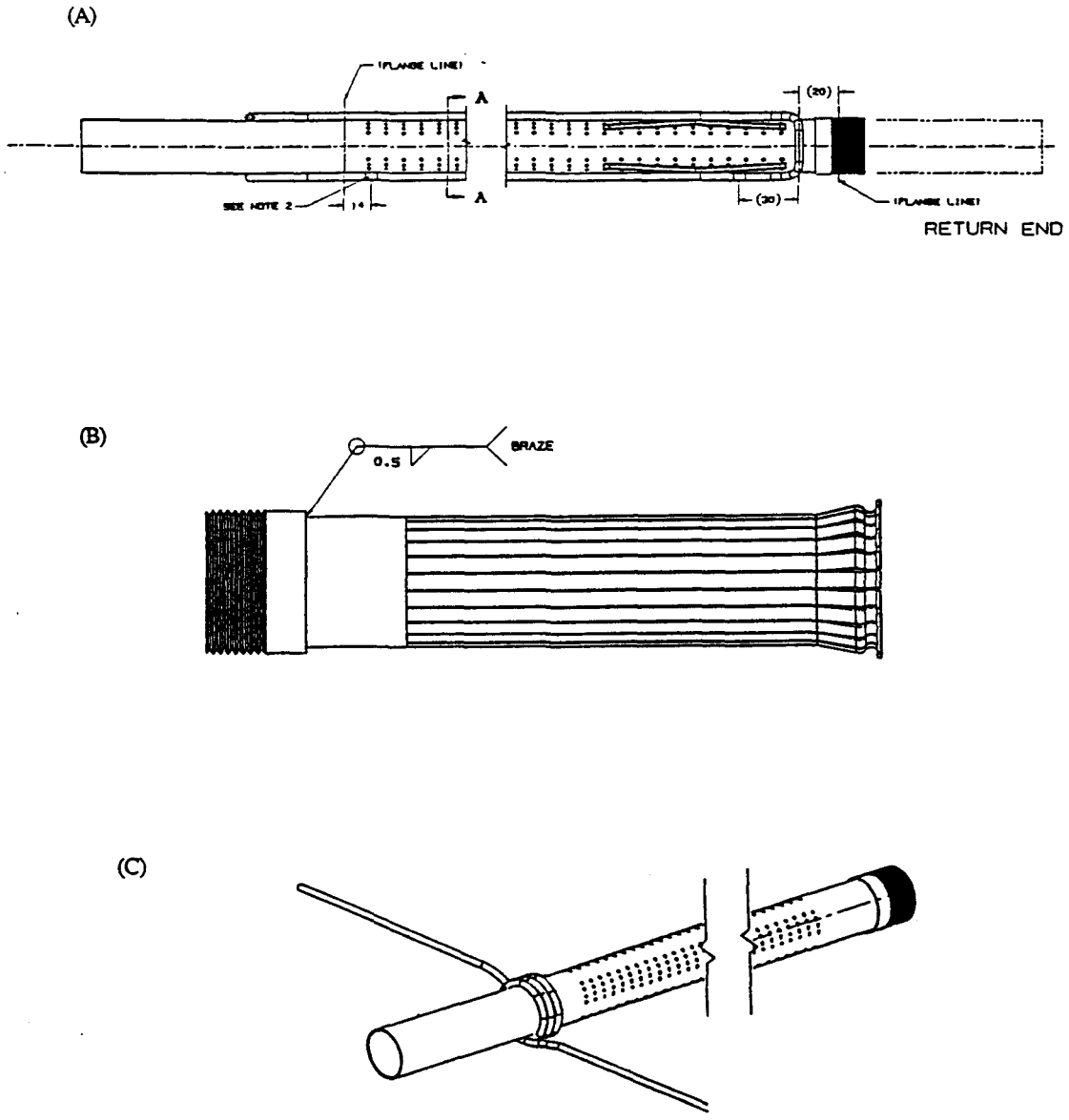

Figure 6. (A) Brazed Sleeve on Dipole Liner. (B) Brazed Sleeve on RF Flexible Sleeve. (C) Brazed Sleeve on Quadrupole Liner.

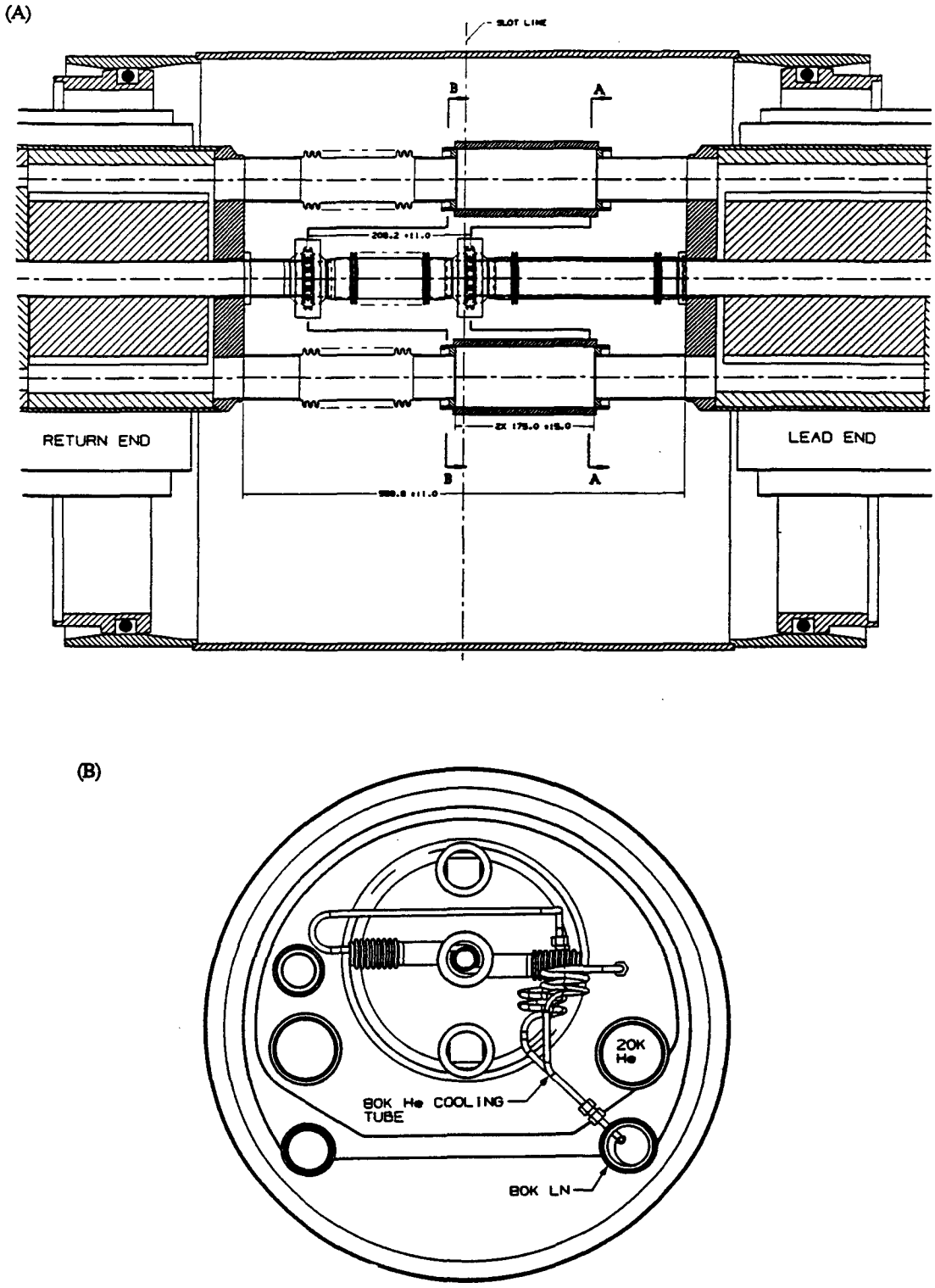

Figure 7. Cryogenic Box Envelope. (A) Space Between Magnets. (B) Space Within 20 K Shield.

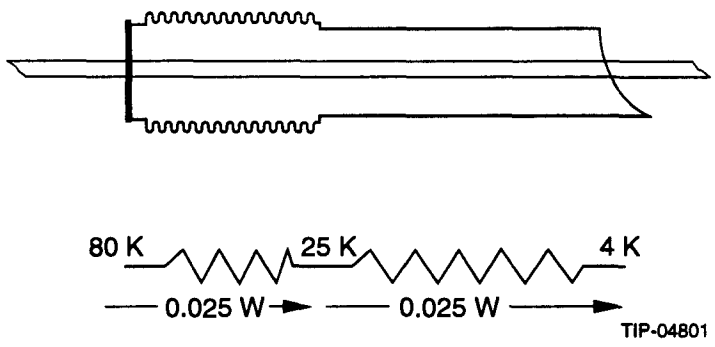

Figure 8. Thermal Analysis of Thermal Standoff.

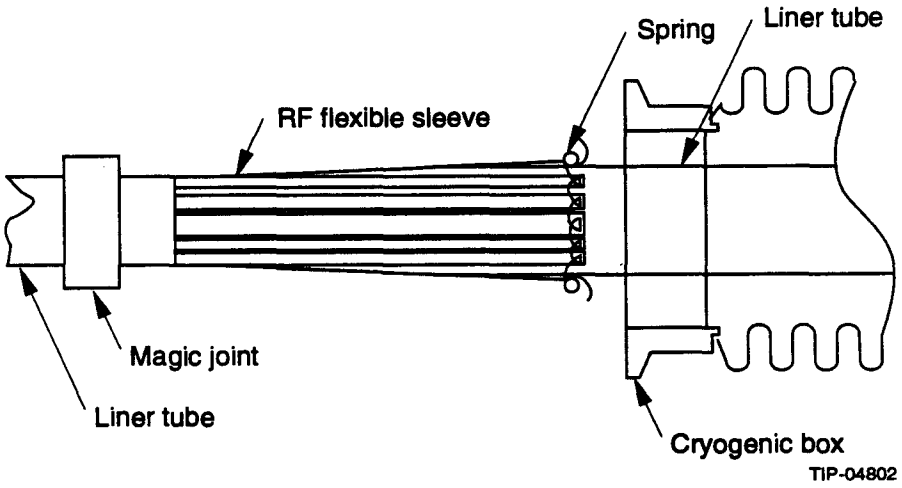

Figure 9. RF Joint Installation.

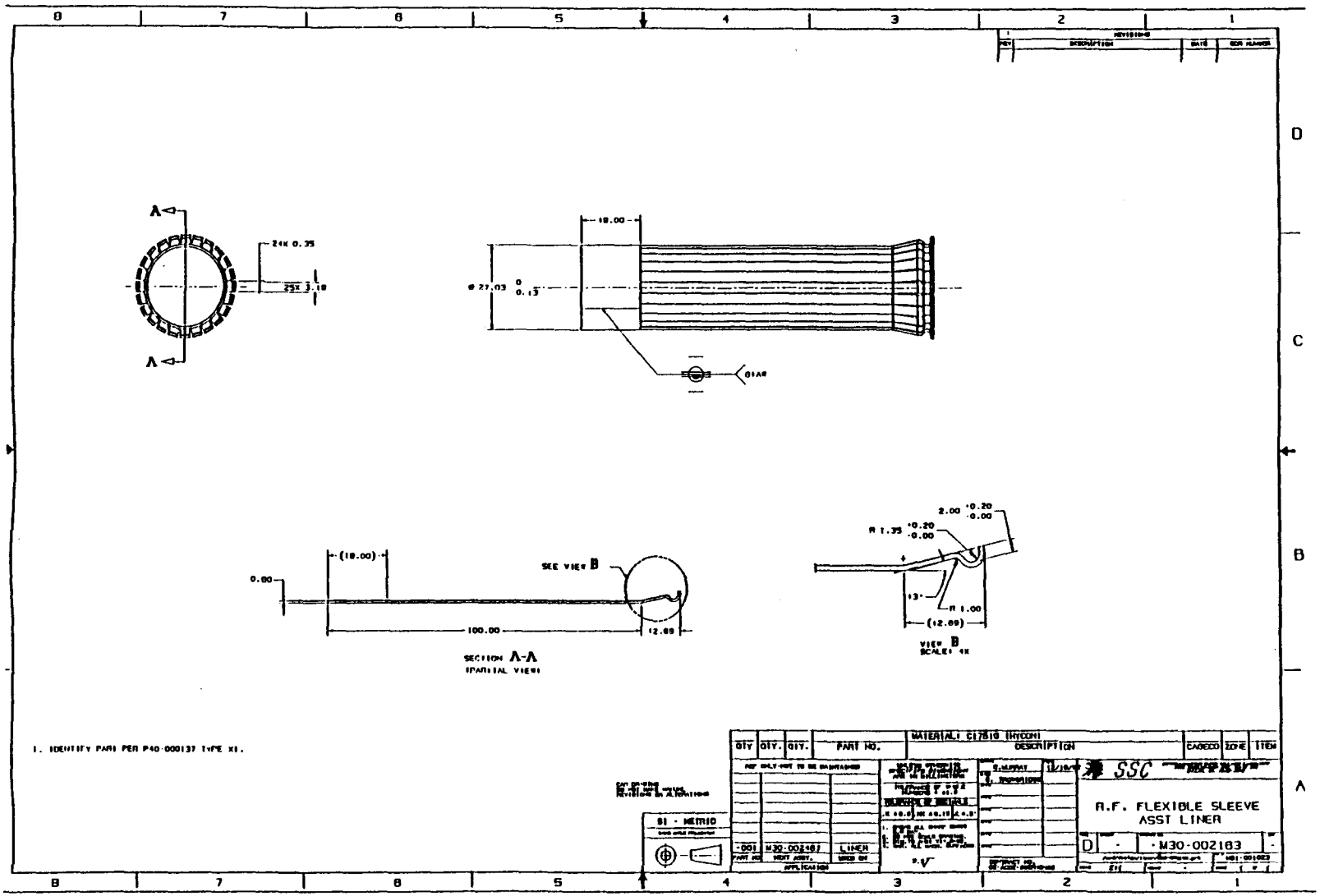

Figure 10. RF Flexible Sleeve.

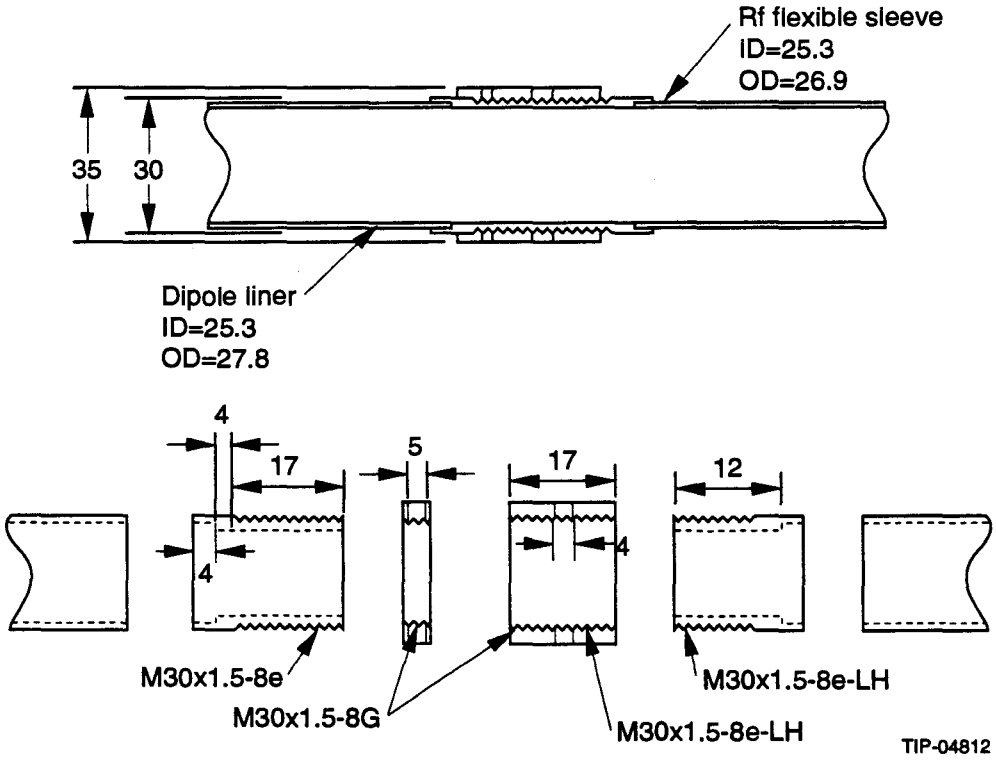

Figure 11. Magic Joint Components.

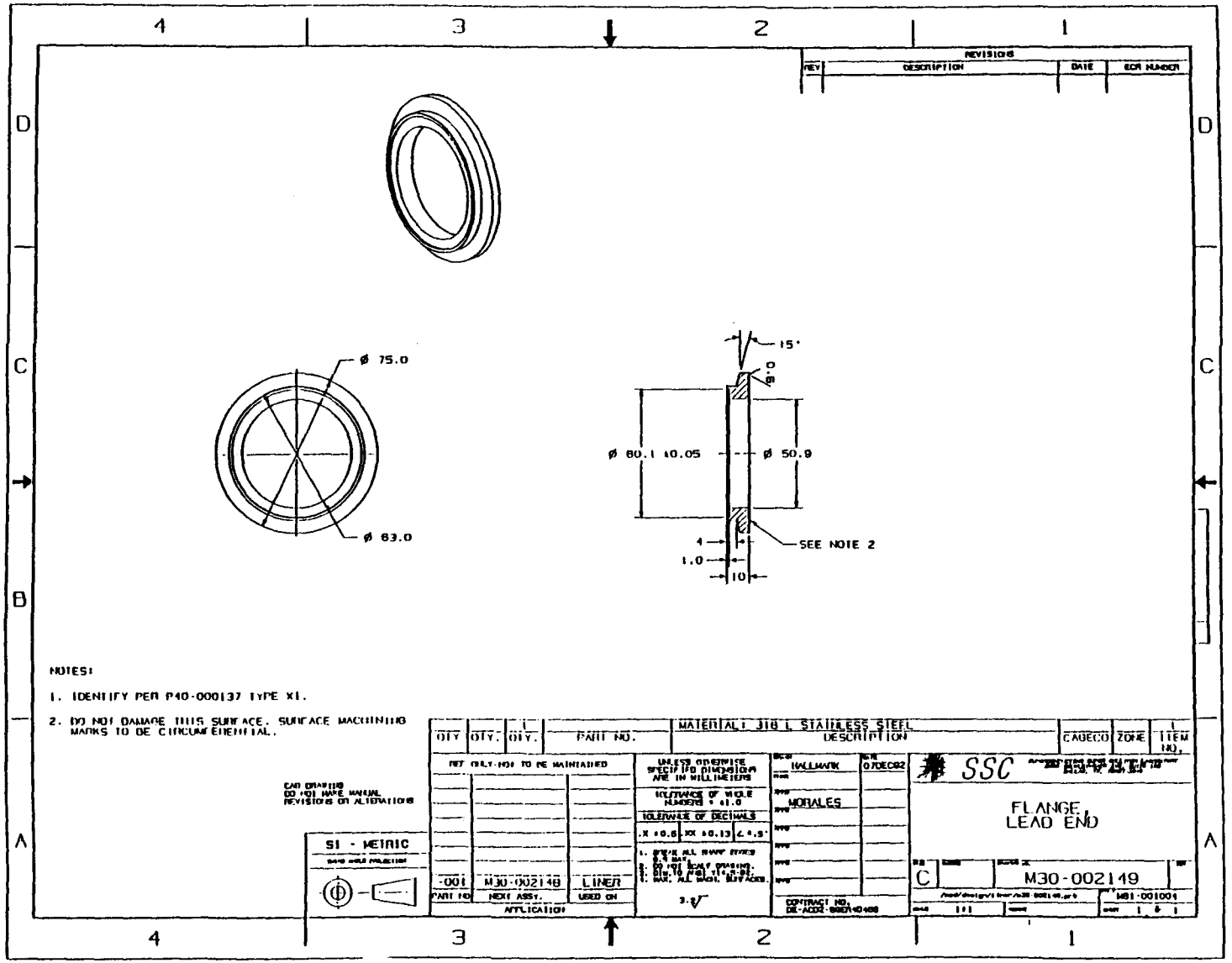

Figure 12. Flange Lead End.

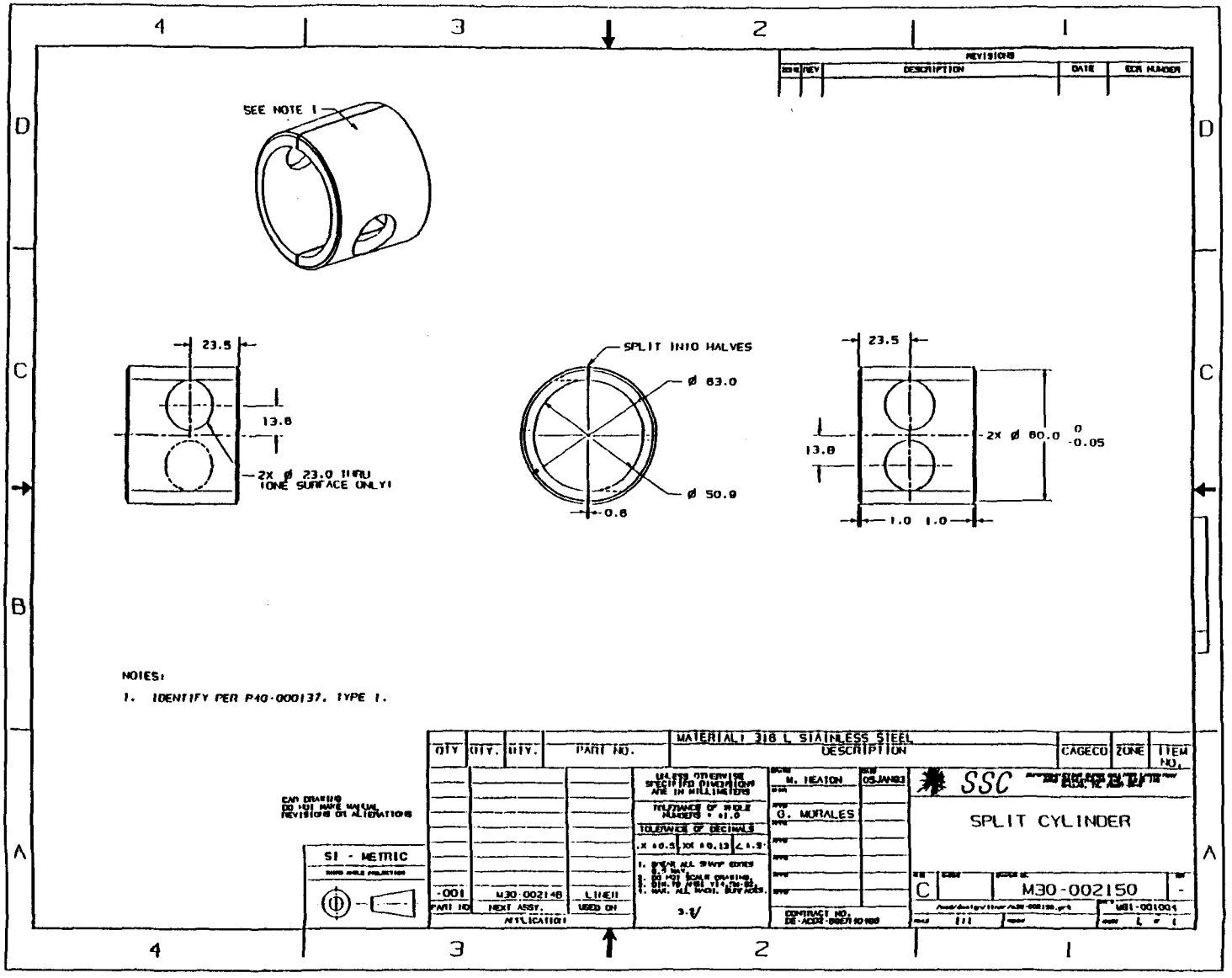

Figure 13. Split Cylinder.

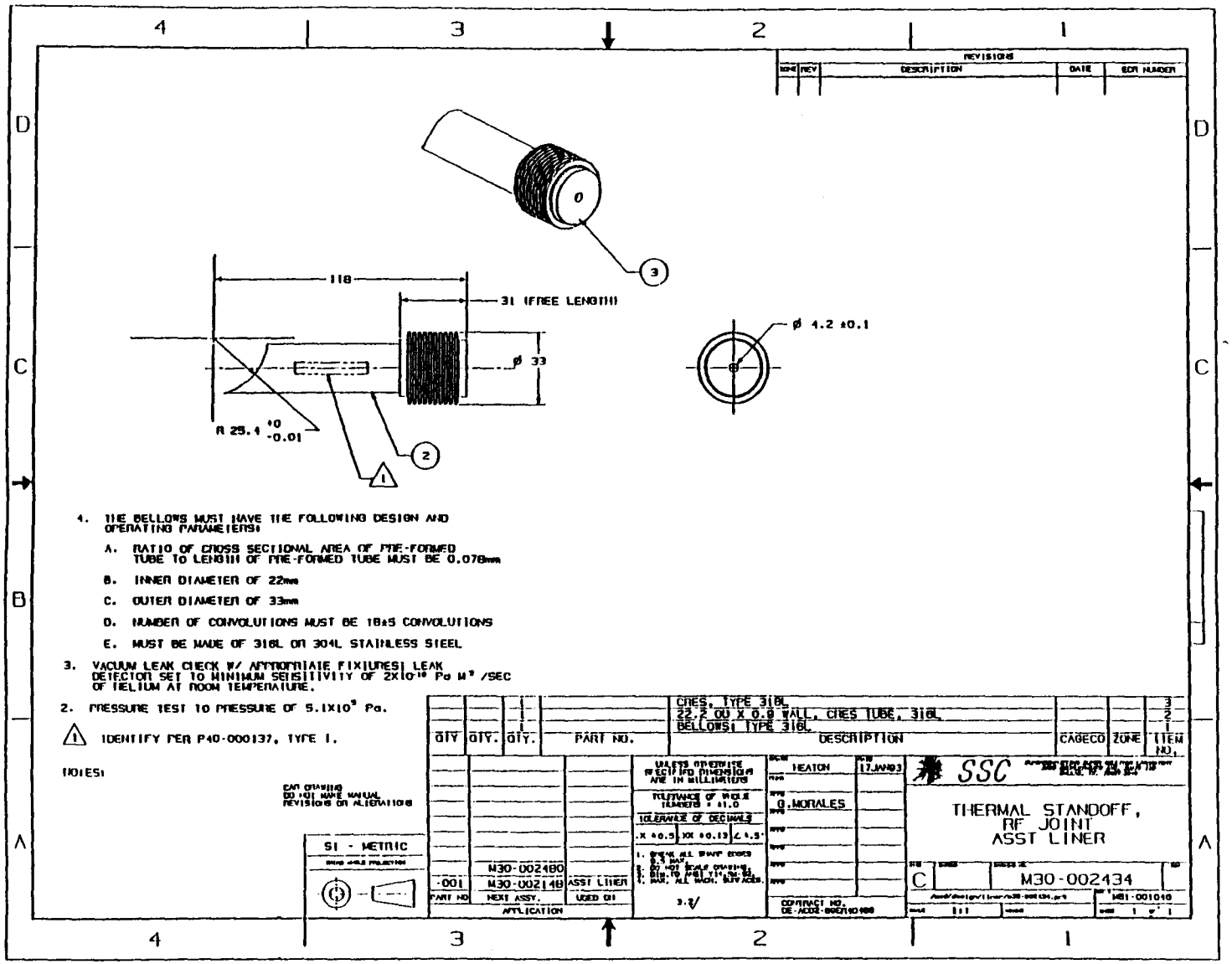

Figure 14. Thermal Standoff.

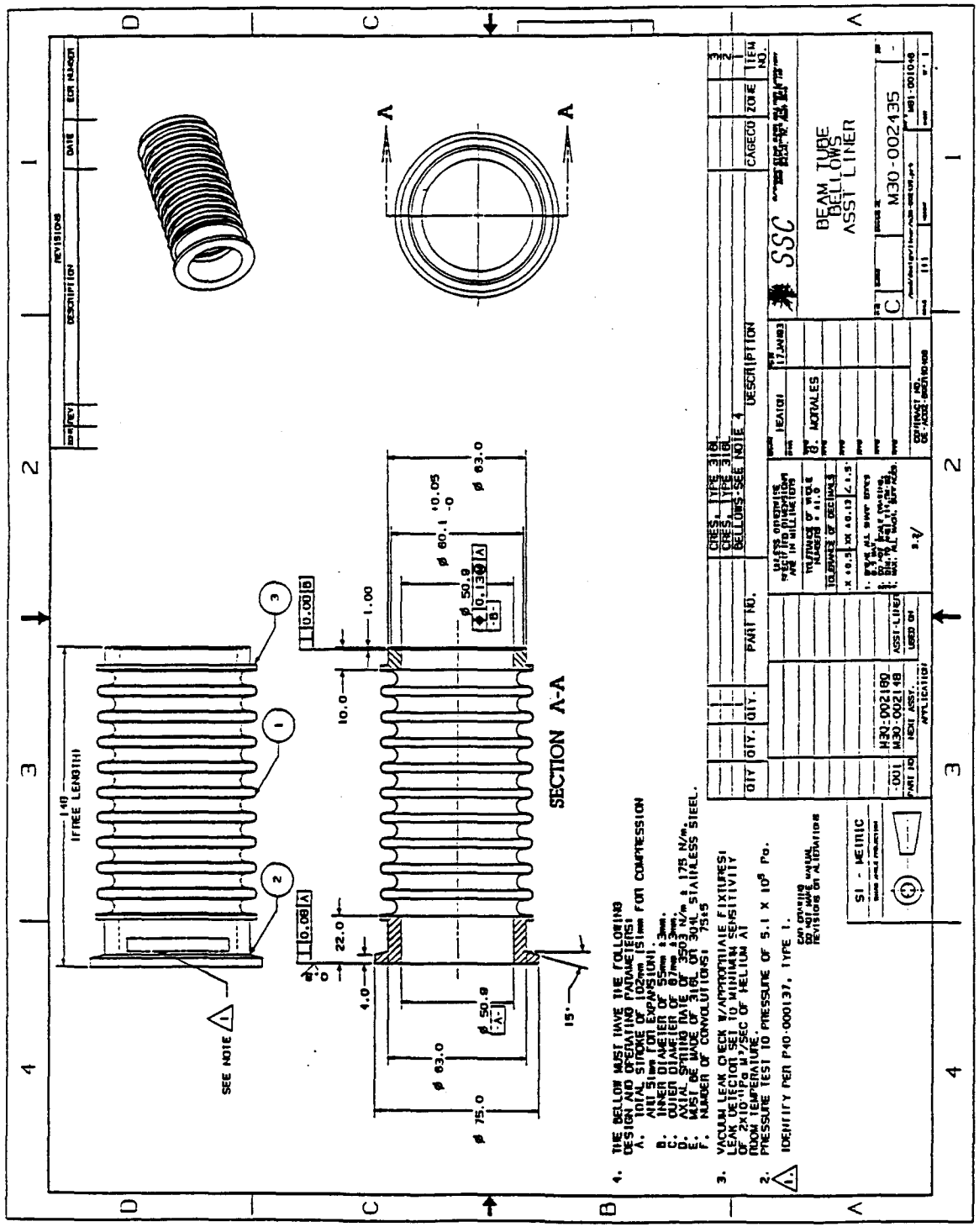

Figure 15. Beam Tube Bellow.

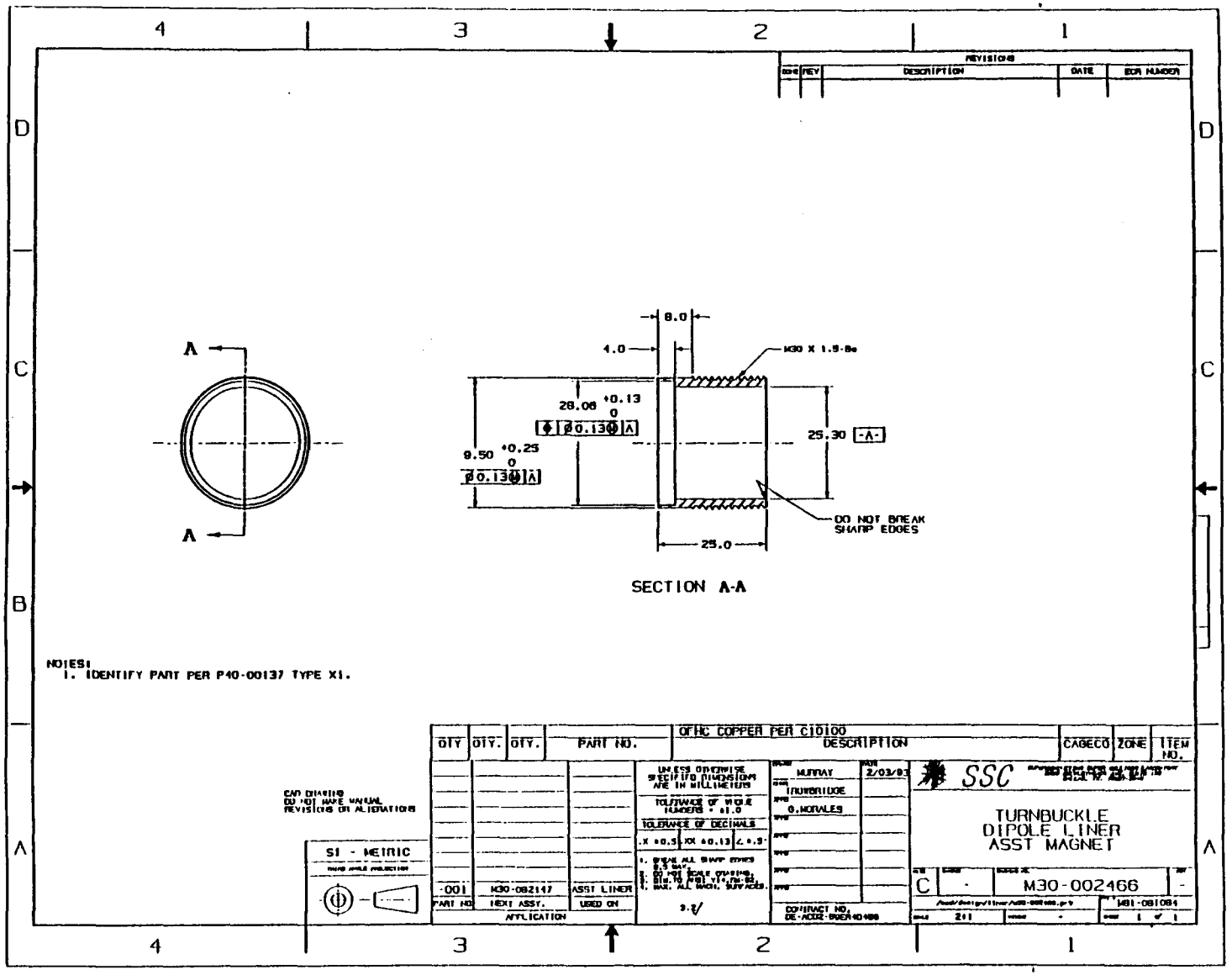

Figure 16. Sleeve of Majiic Joint which Brazes to Dipole Liner.

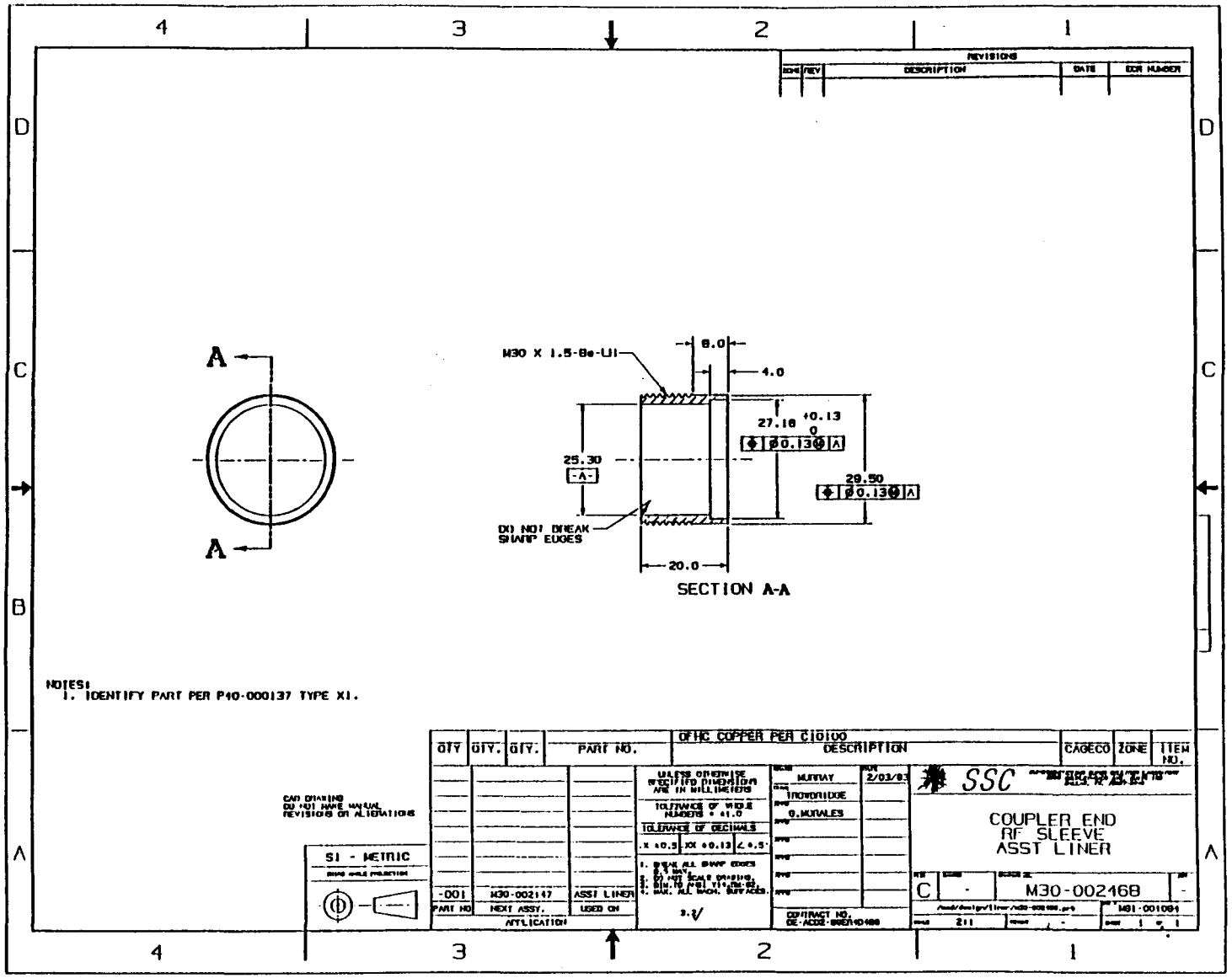

Figure 17. Sleeve of Majlic Joint which Brazes to RF Flexible Sleeve.

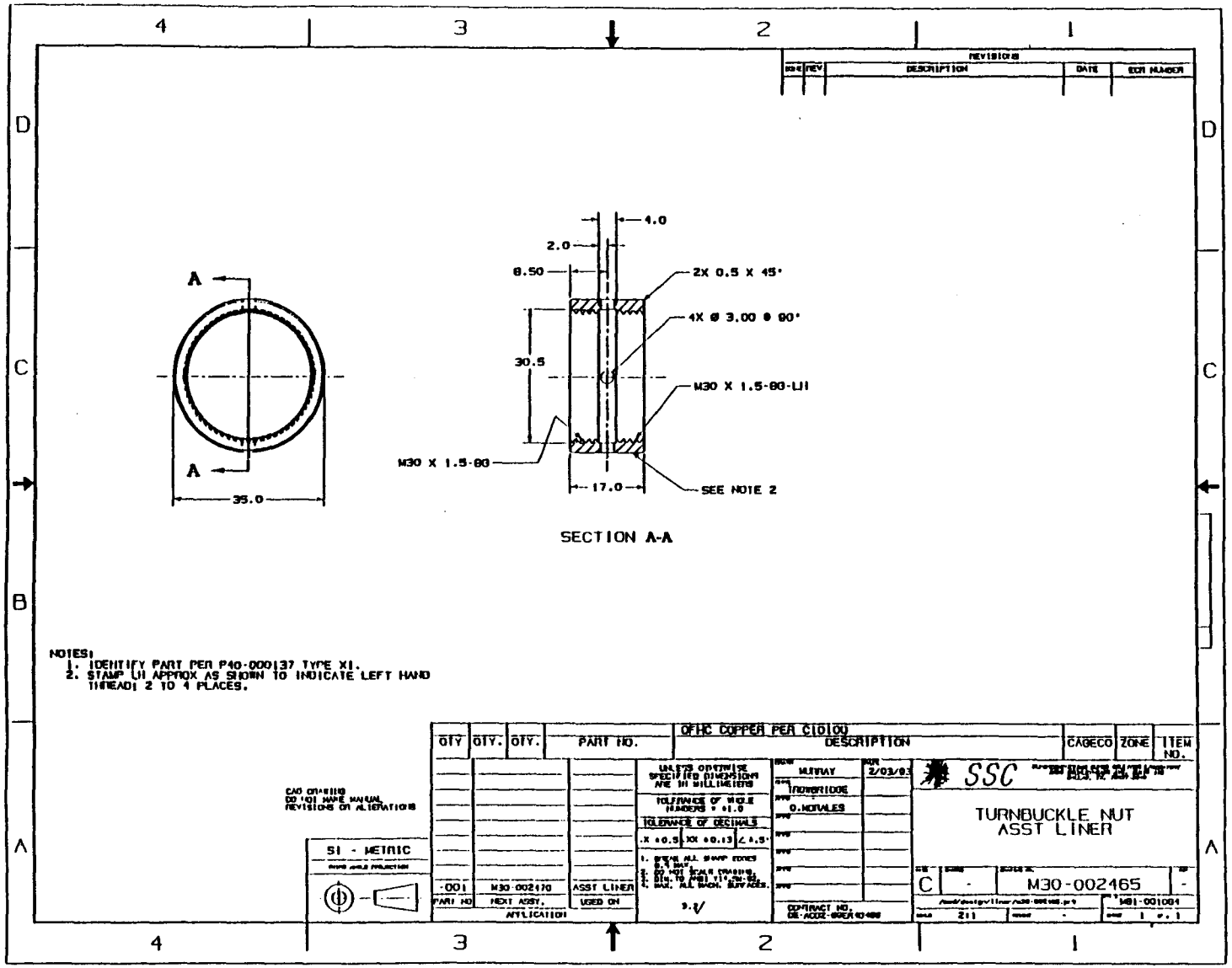

Figure 18. Turnbuckle Nut.

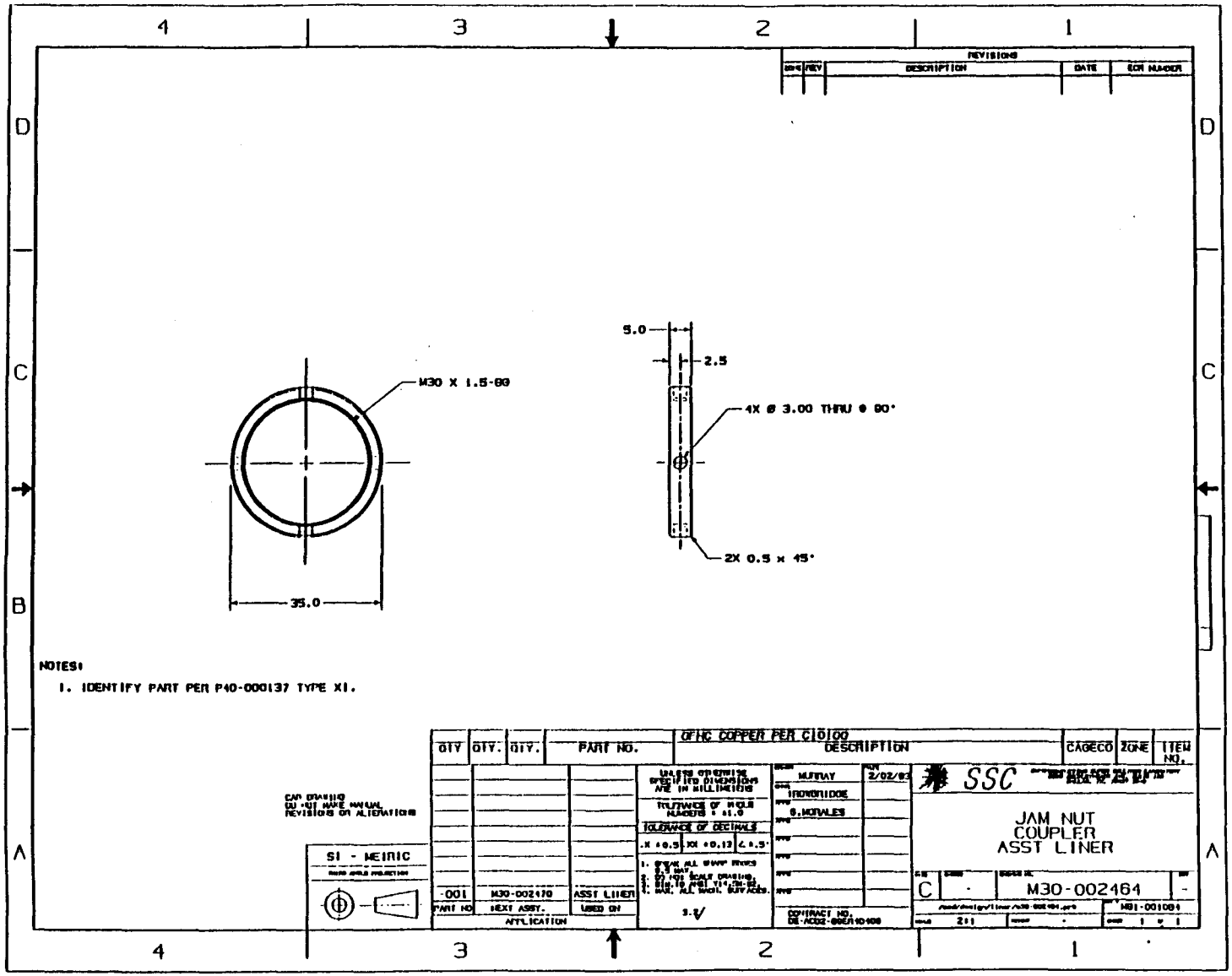

Figure 19. Jam Nut.

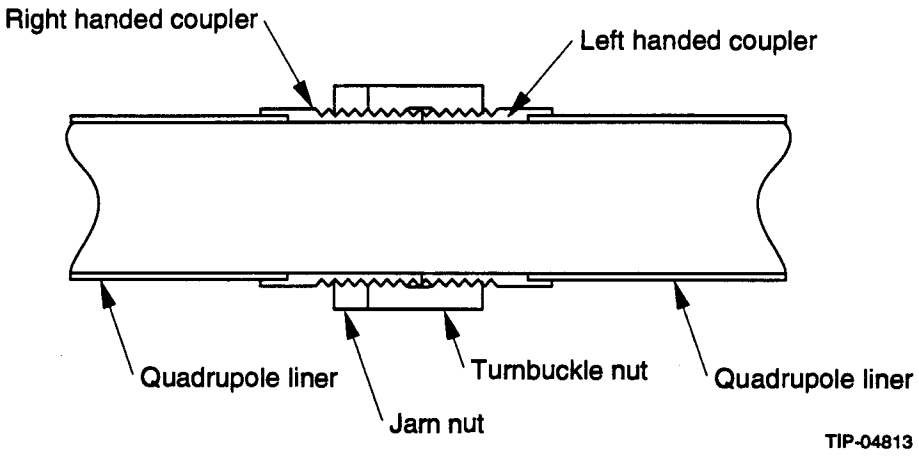

Figure 20. Good Thermal Contact Joint.

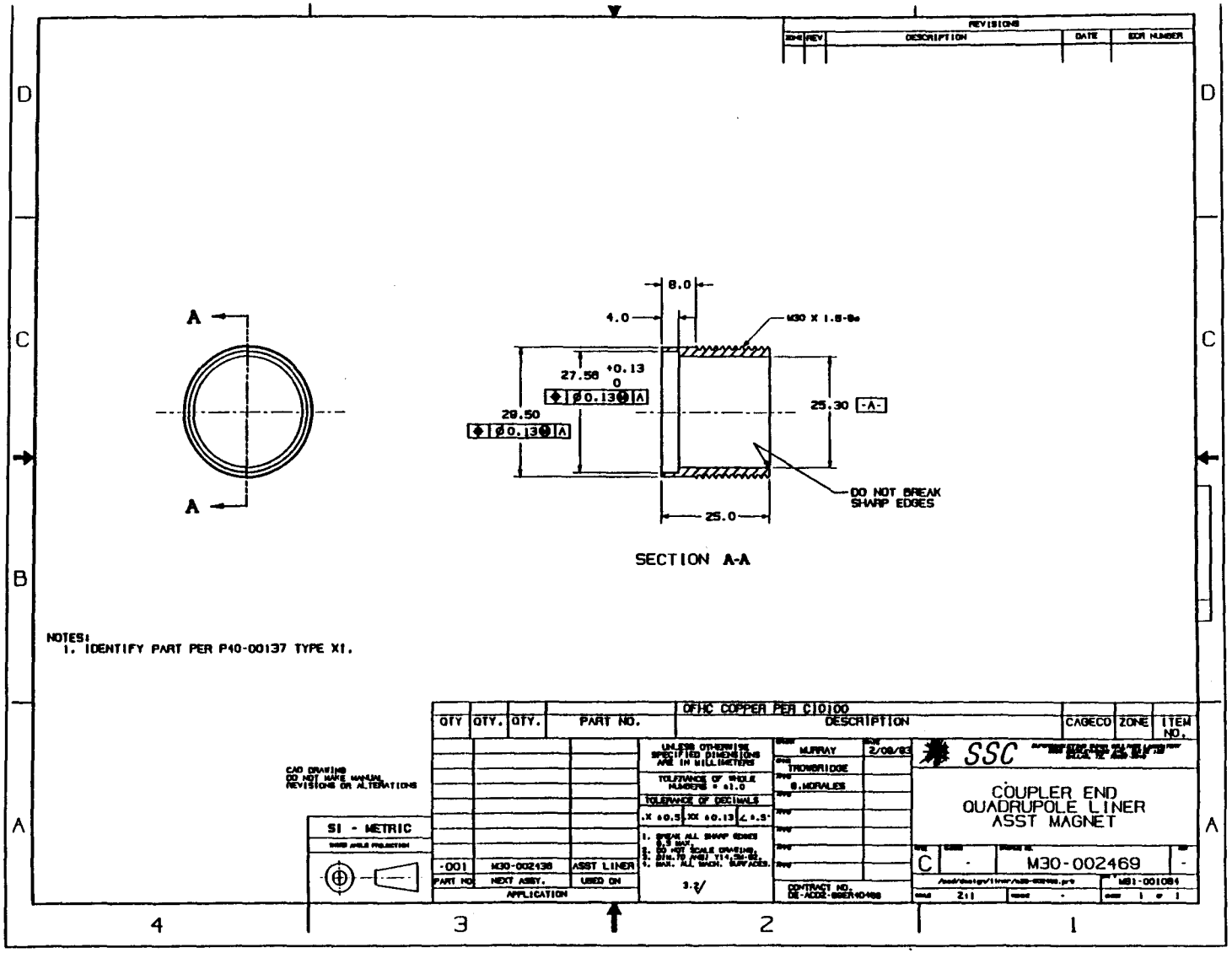

Figure 21. Sleeve of Good Thermal Contact Joint Which Brazes to Quadrupole Liner.

REFERENCES

1. Quan-Sheng Shu, "Design of an 80 K Liner Prototype in SSCL ASST for Synchrotron Light Interception," SSCL-N-818/1 (May, 1993).
2. Quan-Sheng Shu, "Report on the ASST II Liner Status," SSCL-N-805 (November 1992).
3. Jon Simmons, "Superconducting Magnet Radio Frequency (RF) Joint Specification," M80-000072 (November 1992).

This Page Intentionally Left Blank

SECTION 3

Spool Piece Liner Design Within the SPXA (SPRA)

D. M. Clark

SECTION 3

Spool Piece Liner Design Within the SPXA (SPRA)

Donald M. Clark

Superconducting Super Collider Laboratory*
2550 Beckleymead Ave.
Dallas, TX 75237

Abstract

The Collider spool pieces identified refer to the SPXA and the SPRA. Either of these spool pieces is positioned adjacent to a quadrupole magnet within the half cell. The 80 K helium liner is designed to be routed through the Collider arc magnets; however, because of the design of the beam position monitor, the 80 K liner will be discontinuous through the spool piece. Liner design within the spool piece involves end cooling by coil wrapping the spool piece liner with a 6.35 mm diameter stainless steel tube. The circulating 80 K helium is configured as a heat exchanger at the lead end and return end of the spool piece liner.

* Operated by the Universities Research Association, Inc., for the U. S. Department of Energy under Contract No. DE-AC35-89ER40486.

1.0 INTRODUCTION

80 K liner installation into the Superconducting Super Collider Arc Sections involve insertion of the liner into Collider Dipole Magnets (CDM), Collider Quadrupole Magnets (CQM), and Spool Pieces. The assortment of Spool Pieces is identified as SPXA, SPRA, SPRE, SPRF, and SPRI. The Spool Pieces are the standard model, standard model with recooler, (see Figure 1) special configuration with recooler and cryogenic end configured with power leads, special configuration with recooler and cryogenic feed configured with power leads, and special configuration with recooler and cryogenic isolation, respectively.

The initial studies by the Liner System Design Task Force Committee were made on an 80 K liner design and how best to implement that design into the Accelerator Systems String Test (ASST). A SPRA is employed within the ASST.

The scope of the 80 K liner in this discussion involve the 80 K liner design and the 80 K liner engineering required to ensure an 80 K liner installation within the Collider magnets and SPXA (SPRA) during initial Collider Arc installation.

The unit measure of the Collider Arc is designated as the half cell which is 90 meters in length. The Collider Arc half cell contains five CDM, one CQM, and a Spool Piece. The SPXA and SPRA are the majority of Spool Pieces within the Collider Arc and ordinarily each alternates within the half cell. A full cell at 180 meters contains one SPXA and one SPRA. The SPXA (SPRA) is located adjacent to and follows the CQM in respect to position within the half cell. The three remaining specialized Spool Pieces are positioned to interface with cryogenics and power at distinct locations within the Collider Arc. Liner development for these specialized Spool Pieces must be investigated and is addressed briefly in this discussion.

2.0 DISCUSSION

2.1 80 K Liner Within Spool Piece Bore Tube

The Spool Piece liner is positioned and supported within the beam tube of the SPXA (SPRA) which becomes the bore tube after insertion of the liner. The liner supports are of a material and design that allows for the minimum of heat conduction between the liner and bore tube. The heat conduction design budget for each support must be less than 0.050 W/m.

The single phase super critical helium at 4.2 K flows between the annulus of the Spool Piece Cold Mass Pipe and the outside diameter of the bore tube. The liner is circular, metallic, nonmagnetic, and perforated. Liner installation for magnets and Spool Pieces requires the insertion of the liner tube within the 32.2 mm ID stainless steel beam tube with the 0.05 mm copper coating. Liner design operating temperature is 80 K.

The Spool Piece liner follows the liner design of the CQM, being a 25.3 mm ID copper tube perforated with approximately 1500 2 mm diameter holes per meter in a pattern configuration that optimizes conductance.

2.2 BPM and Liner Interface

Each SPXA (SPRA) contains a Beam Position Monitor (BPM) which is located at the lead end of the Spool Piece. The BPM must operate at 80 K for an effective 80 K liner design. The current BPM design is anchored at a 4 K interface and this 4 K operating temperature of the BPM is not acceptable for the 80 K liner design. The BPM must be engineered to be isolated from this 4 K interface.

The internal design of the BPM employs electrodes that measure the transverse position of the proton beam in the beam tube. The design of these BPM electrodes do not allow for the insertion of a liner while continuing to function as an electrical circuit. Insertion of a liner through the BPM

would make the BPM completely inoperable. Therefore, the liner that is employed within the Spool Piece is of two pieces. There is a short length that interfaces with the lead end of the BPM to the CQM. And there is the liner that is much the length of the Spool Piece that interfaces with the return end of the BPM to the CDM. This longer length of liner is attached to the return end of the BPM. Therefore, liner installation must follow as a completed subassembly of BPM and liner prior to installation within the Spool Piece bore tube.

2.3 Liner 80 K Cooling Tube

The design of the 80 K liner into the SPXA (SPRA) involves end cooling of the liner. Cooling of the liner from the ends has been shown by heat transfer calculations to prove successful for Spool Piece liner design. Heat exchangers are mounted to the lead end liner and the return end liner with an 80 K cooling tube which provides the means to allow the Spool Piece liner to operate at 80 K with circulating helium.

The 6.35 mm diameter liner cooling tube is attached by wrapping around the liner in a single row configuration with a minimum of four complete circular wraps and brazed to secure the configuration. Liner cooling tube circulates 80 K helium at 1.82 MPa. The liner cooling tube is accessible at the Interconnect Regions (IR) of the CQM-BPM for the lead end arrangement and the Spool Piece-CDM for the return end arrangement. This arrangement of the liner cooling tube that provides 80 K cooling of the liner is known as the cryogenic box. And the cryogenic box contain the RF joint, bellows, and other joint components necessary for 80 K heat conduction along the liner, a beam current transport surface, and liner anchor points necessary for liner stability during magnet quenches.

The routing of the 80 K helium cooling tube through the magnets and Spool Pieces is achieved by attaching this tube to the 80 K LN_2 tube. The design of this tube with attachment points to the 80 K LN_2 tube and end connections must be identified for the manufacturers of the magnets and Spool Pieces. The SPXA (SPRA) will require this line to penetrate the vacuum barrier which is an integral component of the Spool Piece. Attachment of the liner cooling tube to the 80 K LN_2 tube will require the 80 K helium tube to be wrapped around the 80 K LN_2 tube at each IR to ensure the optimum design temperature of the circulating helium. This heat exchanger design which involves wrapping and securing of the 80 K helium tube to the 80 K LN_2 tube must be properly engineered to ensure optimal design temperature for the circulating helium.

2.4 Bore Tube Cryo-Absorber/Getter Material

The cryo-absorber/getter material necessary to serve as a cryo-pump for the liner is mounted on the inside surface of the bore tube. This material is in contact with the 4.2-K bore tube wall in order to perform as an effective cryo-pump with a minimum pumping speed of 3000 l/sec/meter for hydrogen.

This material and the process necessary for installation within the bore tube must be made available to magnet and Spool Piece manufacturers such that liner installation minimizes damage to this material.

3.0 SPECIALIZED COLLIDER SPOOL PIECES, SPRE, SPRF, SPRI

The design of the 80 K liner within the specialized Spool Pieces (SPRE, SPRF, and SPRI) (see Figures 2 and 3) would follow that of the SPXA (SPRA) at each IR. The design would involve end cooling each liner. The routing of the 80 K helium tube on the 80 K LN_2 tube would not be possible as each of the cryogenic tubes in these specialized Spool Pieces are terminated at bayonet interfaces such that these Spool Pieces and the cryogenic lines may be physically isolated.

These specialized Spool Pieces will be in two halves and isolated by a warm beam tube gate valve and many bayonets. The design of the 80 K helium tube must enter and exit these specialized Spool Pieces within each half and effectively provide 80 K end cooling for the liner at each IR.

The 80 K liner design difficulty for these specialized Spool Pieces will be identifying how best to introduce the 80 K helium tube to the 80 K LN_2 tube. The 80 K liner design for the specialized Spool Pieces within the Collider Arc requires engineering study.

4.0 CONCLUSIONS

The 80 K liner for the Superconducting Super Collider Arc Sections Spool Pieces has been engineered and a design has been discussed to present to the magnet and SPXA (SPRA) manufacturers. The design involves end cooling of the SPXA (SPRA) at each Interconnect Region with 80 K helium routed through an 6.35 mm-diameter stainless steel tube that is wrapped around the liner and all other engineering details are contained within the heat exchanger identified as a cryogenic box.

The Collider Arc design of the 80 K liner requires the insertion of the 80 K liner into the 32.2 mm ID beam tube that becomes a bore tube after the insertion of the 80 K liner. The end cooling designs for the CQM and the SPXA (SPRA) are essentially identical.

The BPM 4 K to 80 K interface within the SPXA (SPRA) requires additional engineering development in order to achieve temperature optimization of the 80 K liner within the Spool Pieces.

The routing of the 80 K helium cooling tube is identified as a 6.35 mm ID stainless steel tube that is routed and attached to the 80 K LN_2 tube located within the magnets and the SPXA (SPRA).

The bore tube cryo-absorber/getter material and the process necessary for installation within the bore tube must be made available to magnet and Spool Piece manufacturers such that liner installation minimizes damage to this material.

The 80 K liner design for the Collider Arc specialized Spool Pieces (SPRE, SPRF, and SPRI) will follow the design of the SPXA (SPRA) with circulating 80 K helium to provide end cooling of the liner. The routing of the 80 K helium tube within these specialized Spool Pieces must be engineered.

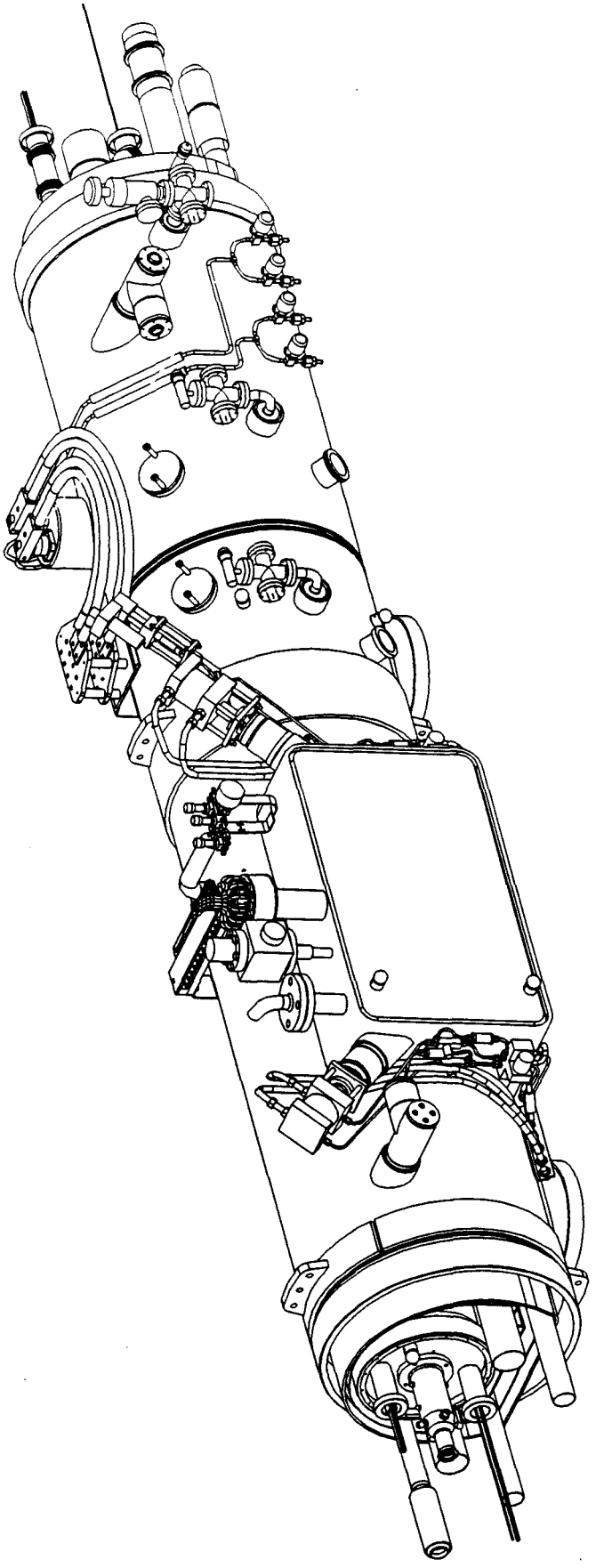

Figure 1. Standard Spool Piece with Recooler (SPRA).

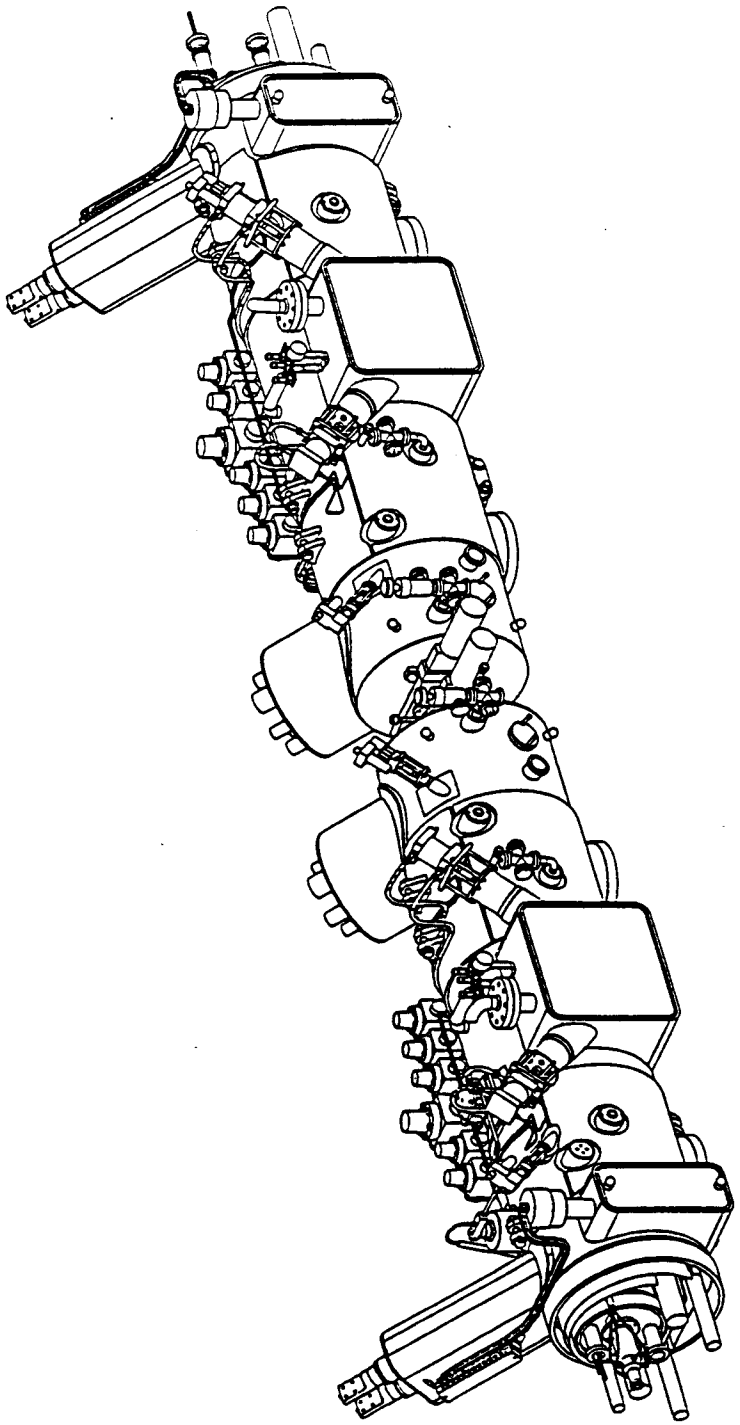

Figure 2. Spool Piece with Recooler and Cryogenic End (SPRE), Spool Piece with Recooler and Cryogenic Feed (SPRF).

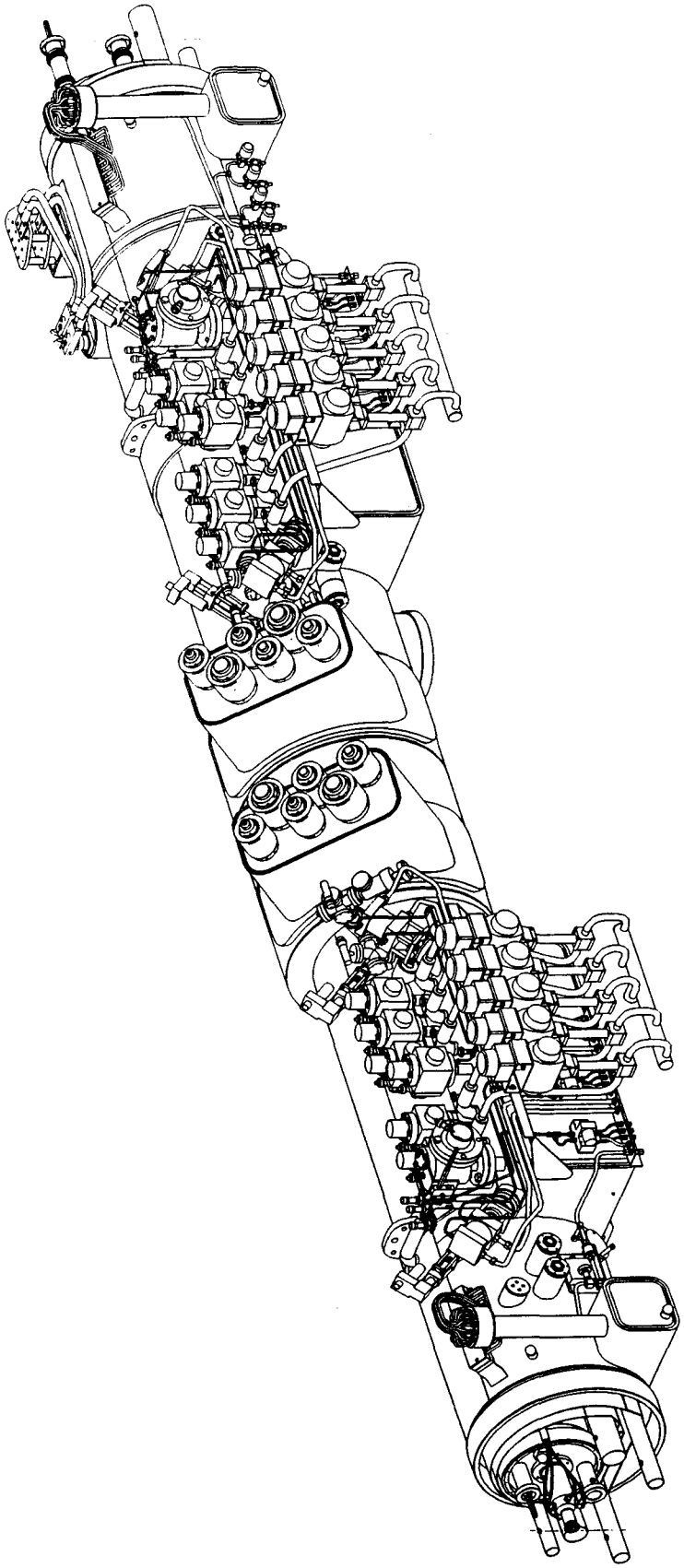

Figure 3. Spool Piece with Recooler and Cryogenic Isolation (SPRI).

This Page Intentionally Left Blank

SECTION 4

Spool Piece Liner Retrofit into the Collider

D. M. Clark

SECTION 4

Spool Piece Liner Retrofit into the Collider

Donald M. Clark

Superconducting Super Collider Laboratory*
2550 Beckleymeade Avenue
Dallas, TX 75237

1.0 INTRODUCTION

In the event that the Collider has been built to the 1989 baseline design and the 80 K helium liner is approved as a retrofit, one might ask what additional components this liner retrofit would add to the collider design? The following discussion addresses those components that are effected by a liner retrofit and identifies components that are required for an 80 K liner retrofit.

2.0 DISCUSSION

The baseline design of the beam tube for the Collider is 34.54 mm OD × 32.3 mm ID, with a 0.05-mm copper coating located on the inside surface wall. Because of the length of the Collider Dipole Magnet (CDM) the liner must have a cooling tube attached to the length of the liner. The annular space between the liner and the bore tube is limited by beam physics and the diameter of the cooling tube. The Collider Quadrupole Magnet (CQM) and the standard Spool Piece (SPXA) liners are cooled by attaching heat exchangers to the lead and return ends of the liner. The CDM has more annular space available as compared to the CQM, thus the liner design for CDM allows for cooling tube attached to the full length of the liner.

The first design issue to be addressed is defining the size of the liner with cooling tubes and heat exchangers that is available to fit within the beam (bore) tube. The beam tube becomes the bore tube with the installation of a liner. The bore tube size in the magnets and Spool Pieces will determine the physical size available for a liner and the cooling tubes associated with the liner.

The second design issue is that of the process of applying the cryo-absorber/getter material to the inside surface of the bore tube. The bore tube temperature at 4.2 K ensures effective cryopumping by the cryo-absorber/getter material. The 80 K liner installation must not damage the liner supports or the getter material.

A third design issue would be the modification to the interconnect region. This modification involves the bore tube/liner interface with the cooling lines and associated heat exchangers. The RF joint, bellows, and other joint components must be designed to carry the beam currents and withstand magnet quench forces.

The fourth design issue is that of the Beam Position Monitor (BPM) and addressing how the Spool Piece liner interfaces with the lead end and the return end of the BPM. The BPM is located on the lead end of the Spool Piece and provides a beam position diagnostic tool. The current BPM

* Operated by the Universities Research Association, Inc., for the U. S. Department of Energy under Contract No. DE-AC35-89ER40486.

design does not allow for a liner to be inserted through the Spool Piece as is the case for magnet bore tubes. In fact, the current BPM will allow the Spool Piece liner to be two liners in series coupled by the BPM. Also the current BPM design operates within a 4 K temperature region. The 80 K liner retrofit would require the BPM to operate at 80 K.

A fifth design issue in retrofitting the Collider would be that of routing the 80 K helium line through the collider ring via the 80 K LN_2 line within the magnets and Spool Pieces. The routing through the magnets and the SPXA (SPRA) will be internal through the 80 K LN_2 tube. However, the SPRE, SPRF, and SPFI would require another approach to routing the 80 K helium line because these specialized Spool Pieces have bayonets to decouple the Arc sections cryogenic lines.

3.0 CONCLUSIONS

The Interconnect Regions (IR) will require additional components at the interfaces of the beam (bore) tube. Also, the 80 K LN_2 line must be modified at the IR to accommodate the 80 K helium cooling tube. The 80 K helium cooling tube maintains the design operating temperature for the liner by either being routed through the 80 K LN_2 line or wrapping in sufficient loops the 80 K helium cooling tube around the 80 K LN_2 tube located in the IR just below the bore tube/liner interface. The 80 K liner cooling tubes are either a design by which the cooling tube is attached to the length of the liner as in the example of the CDM liner and the design by which the cooling tube is wrapped around the lead end and return end of the liner as in the example of the CQM and the SPXA (SPRA) to provide the heat exchanger to maintain the design temperature of the circulating helium.

The liner employed in the SPRE, SPRF, and SPRI may be retrofitted as that of the liner and the BPM of the SPXA (SPRA). The liner and associated heat exchangers will be a design of end cooling only and the heat exchangers within the IR will be positioned at both the lead end and return end of these specialized Spool Pieces. The routing of the 80 K helium line through these specialized Spool Pieces has to be resolved.

Areas which will require upgrading are identified as follows:

1. Beam tube bellows at the IR becomes obsolete and is replaced as the liner heat exchanger replaces this bellows.
2. BPM design within the Spool Pieces must be isolated from the 4 K region and operated at a temperature of 80 K.
3. BPM at the return end must be joined to the 80 K liner.
4. Beam tube becomes a bore tube and must be fitted with cryo-absorber/getter material.
5. 80 K helium liner heat exchanger must be installed on CDM, CQM, and SPXA (SPRA) liners.
6. 80 K helium liner heat exchanger must be installed on SPRE, SPRF, and SPRI liners.
7. 80 K helium cooling tube routed through or around the 80 K LN_2 tube.
8. 80 K helium cooling tube must be routed through the SPRE, SPRF, and SPRI.

The list of typical 80 K liner components is identified as follows:

Dipole Liner, CDM
- Dipole Liner Tube
- Support, Dipole Liner
- Coupler End Dipole Liner
- Flange, Lead End
- Split Cylinder
- Rigid Dipole Liner Support
- Thermal Standoff
- Bellows, RF Flexible Sleeve
- Fitting, Re-cooling tube
- Support, Re-cooling tube
- RF Flexible Sleeve
- Turn-Buckle Sleeve, RF Flexible Sleeve
- Jam Nut
- Turn-Buckle Nut

Quadrupole Liner, CQM
- Quadrupole Liner Tube
- Support, Quadrupole/Spool Liner
- Coupler End, Quadrupole Liner
- Flange, Lead End
- Split Cylinder
- Rigid Quadrupole Liner Support
- Thermal Standoff
- Bellows, RF Flexible Sleeve
- Fitting, Re-cooling Tube
- Fitting, Compact Heat Exchanger
- Re-cooling Tube, Quadrupole
- Support, Recoolant Tube
- Jam Nut
- Turn-Buckle Nut

Spool Liner Lead End, SPXA (SPRA)
- Spool Liner Lead End Tube
- Left Hand Turn-Buckle Sleeve, Spool
- Split Cylinder
- Rigid Spool Liner Support
- Thermal Standoff
- Bellows, RF Flexible Sleeve
- Spool Interconnect Bellows
- Flange Lead End
- Fitting, Recooling Tube
- Fitting, Compact Heat Exchanger
- Support, Re-cooling Tube
- Re-cooling Tube, Spool

Spool Liner, Return End SPXA (SPRA)
- BPM Liner
- Spool Liner Tube
- Support, Quadrupole/Spool
- Right Hand Turn-Buckle Sleeve, Spool
- Flange, Lead End
- Split Cylinder
- Thermal Standoff
- Bellows, RF Flexible Sleeve
- Spool Liner Return End Tube
- Rigid Spool Liner Support
- Left Hand Turn-Buckle Sleeve, Spool
- Fitting, Re-cooling Tube
- Fitting, Compact Heat Exchanger
- Jam Nut
- Turn-Buckle Nut

80 K Helium Supply Line
- 80 K LN_2 Spool with 80 K Helium Heat Exchanger/Port
- Fitting, Re-cooling Tube

Cryo-Absorber/Getter Material

BPM 4 K/80 K Isolation

SECTION 5

BPM System Concept Design and Analysis

D. Martin

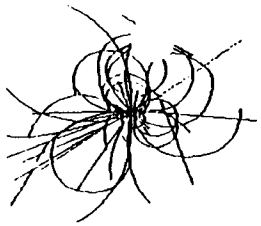

SSC Laboratory 80K SR Liner Program

ASD BEAM INSTRUMENTATION DEPARTMENT

Collider Beam Position Monitor

Design Team: ***D. Martin***
D. Meyer

April 29 & 30, 1993

Discussion of BPM Detector hardware

as modified for a Synchrotron Radiation Liner

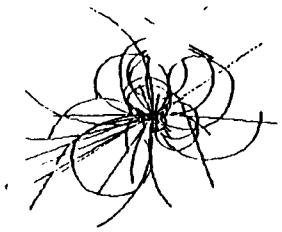

SSC Laboratory 80K SR Liner Program

BASELINE BPM DETECTOR REQUIREMENTS

Collider Requirements	***Proposed***
• X, Y and I_b at niches; other X or Y	• 2/4 electrode 50Ω Stripline
• Pos. knowledge sext. 100 μm. rms	• Spool Piece assy. measurement
• Long term reliability and stability	• Testing/Robustness/Materials
• 13 MGray radiation field	• 316LN SS/ Alumina/ PEEK cable
• Heat Load 200 mW max. @ 4K	• <100 mW conducted thru cables
• Image current continuity	• Smooth, vac. tight beam tube
• Impedance budget $(Z/n)_L < +j\ 50\mu\Omega$	• $+j\ 82\ \mu\Omega$
• BPM not an aperture restriction	• Electrodes recessed

D. Martin

29 & 30 April 1993

DIRECTIONAL COUPLER POSITION DETECTOR

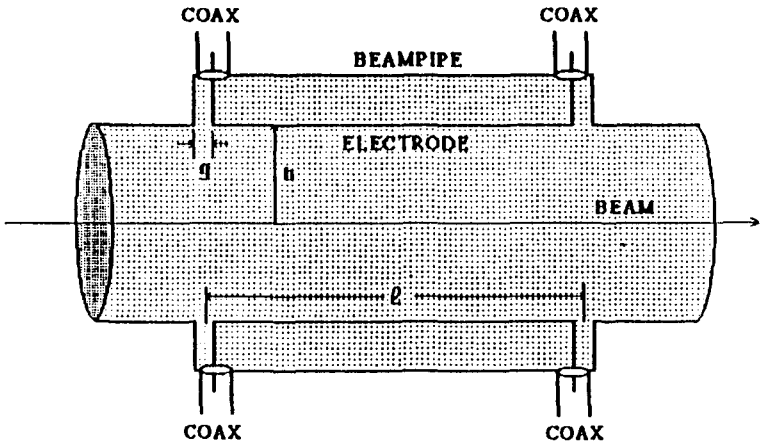

Each BPM electrode is a section of an impedance-matched transmission line, with the center conductor exposed to the electromagnetic fields of the passing beam. Induced signals exit through the upstream port without reflection.

In the SSC Collider, no signal is present at the downstream port. The downstream port is therefore electrically short-circuited to the beam tube.

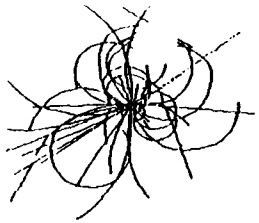

SSC Laboratory 8uK SR Liner Program

BPM THEORY OF OPERATION/ TIME DOMAIN

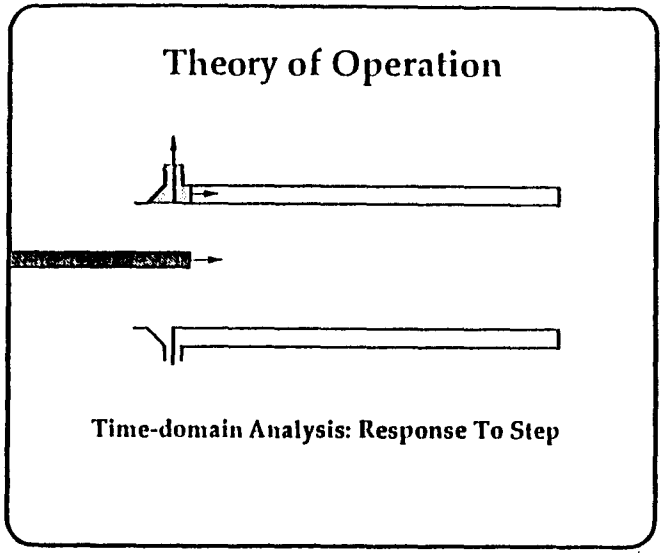

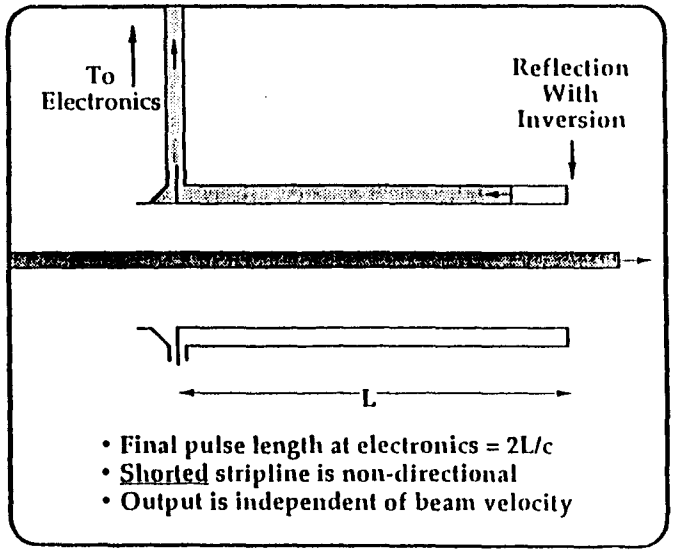

BPM TIIEORY OF OPERATION/ FREQUENCY DOMAIN

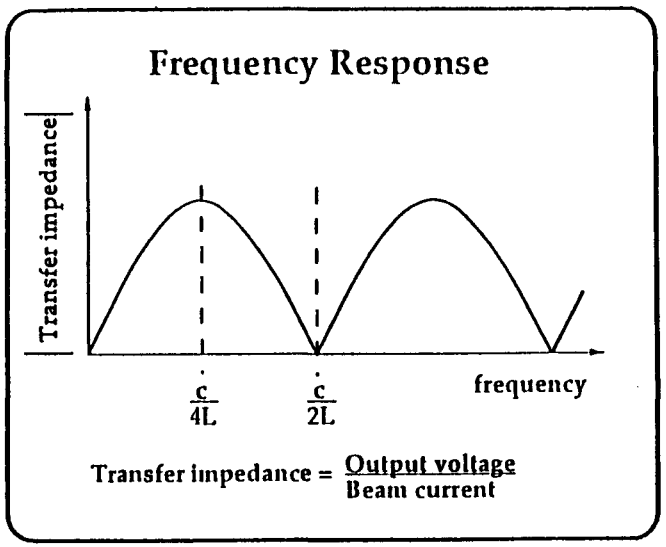

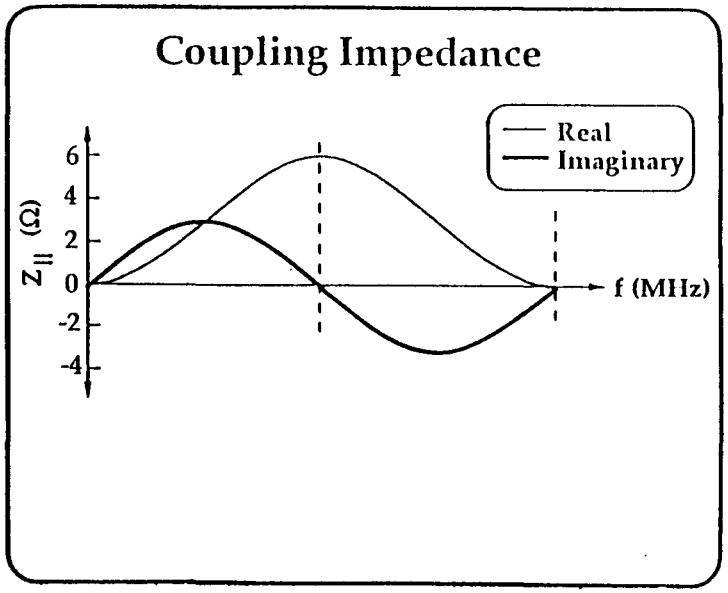

SSC Laboratory 80K SR Liner Program

BASELINE COLLIDER BPM

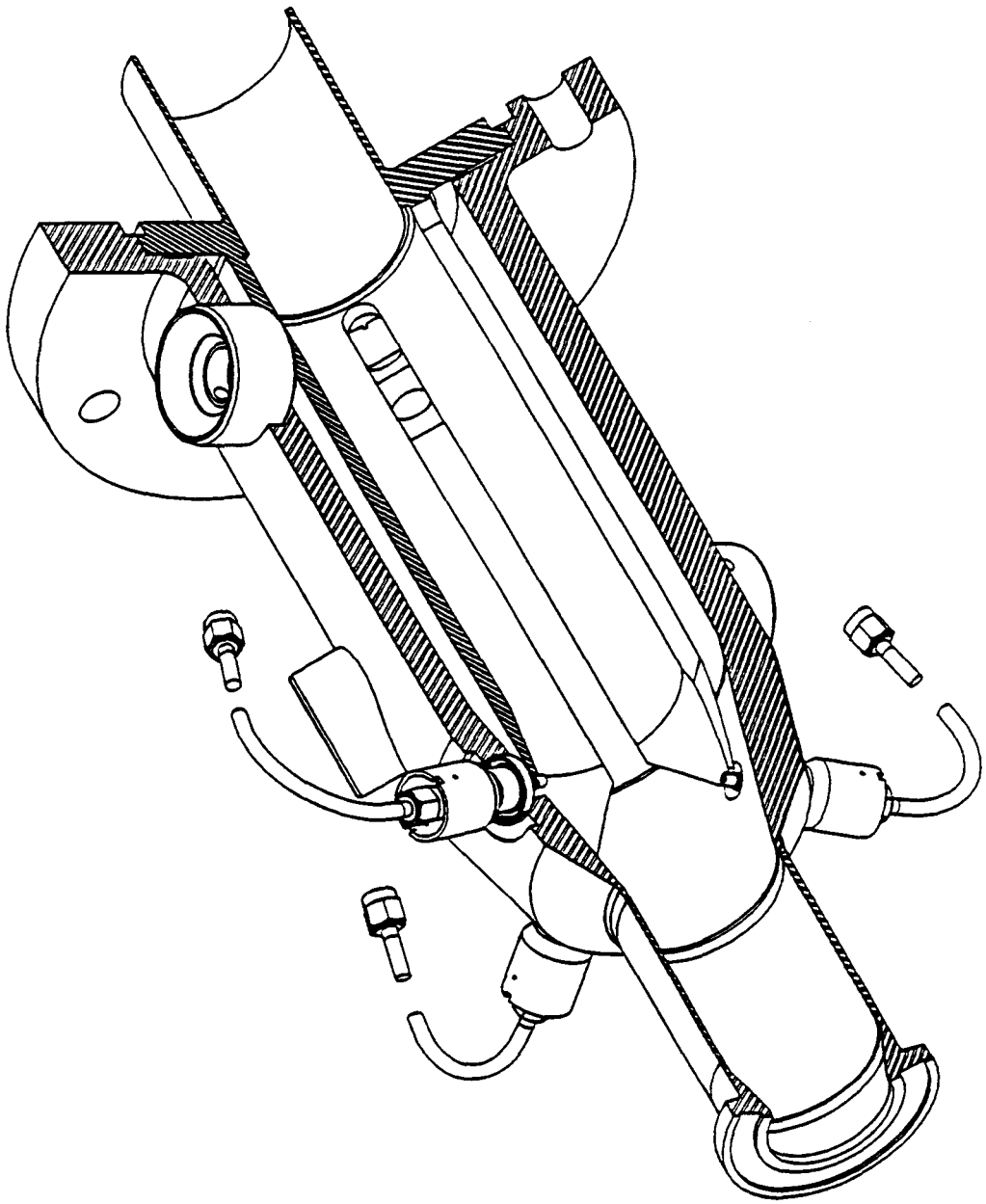

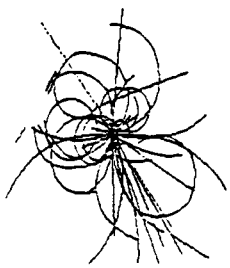

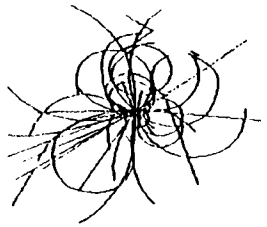

BPM/ LINER HARDWARE PROPOSAL

Design Approach

- The BPM design has been optimized to meet the baseline performance requirements. The existing design shall be the starting point to meet Liner requirement.
- Why? The existence of a suitable alternate concept cannot be disproved. However, the baseline functional requirements provide a very limited "design space".

The Baseline BPM Design

- Stripline beam monitor, l_e = 150 mm, Z_o = 50 Ω, r = 22 mm, ϕ = 70°, end short-circuited. Package dimensions z = 215 mm, ϕ = 85 mm.
- The 60 MHz signal level at monitor is 700 mV*pp* to 1.4 mV*pp* (dependent upon beam current) into 50 Ω, for a centered beam.

SSC Laboratory 80K SR Liner Program

COLLIDER BPM/ SPOOL PIECE CONFIGURATION

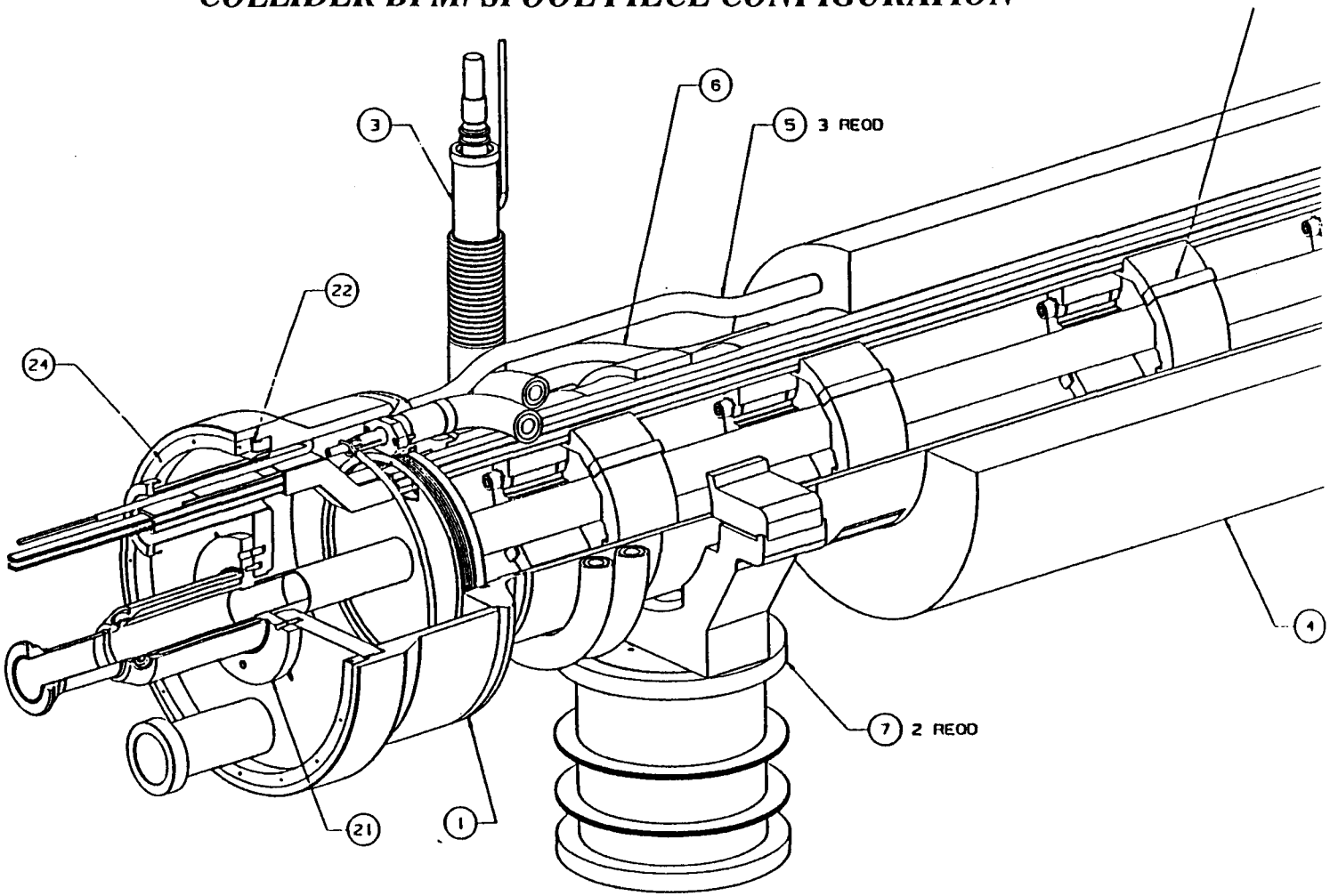

4K BPM CONCEPT

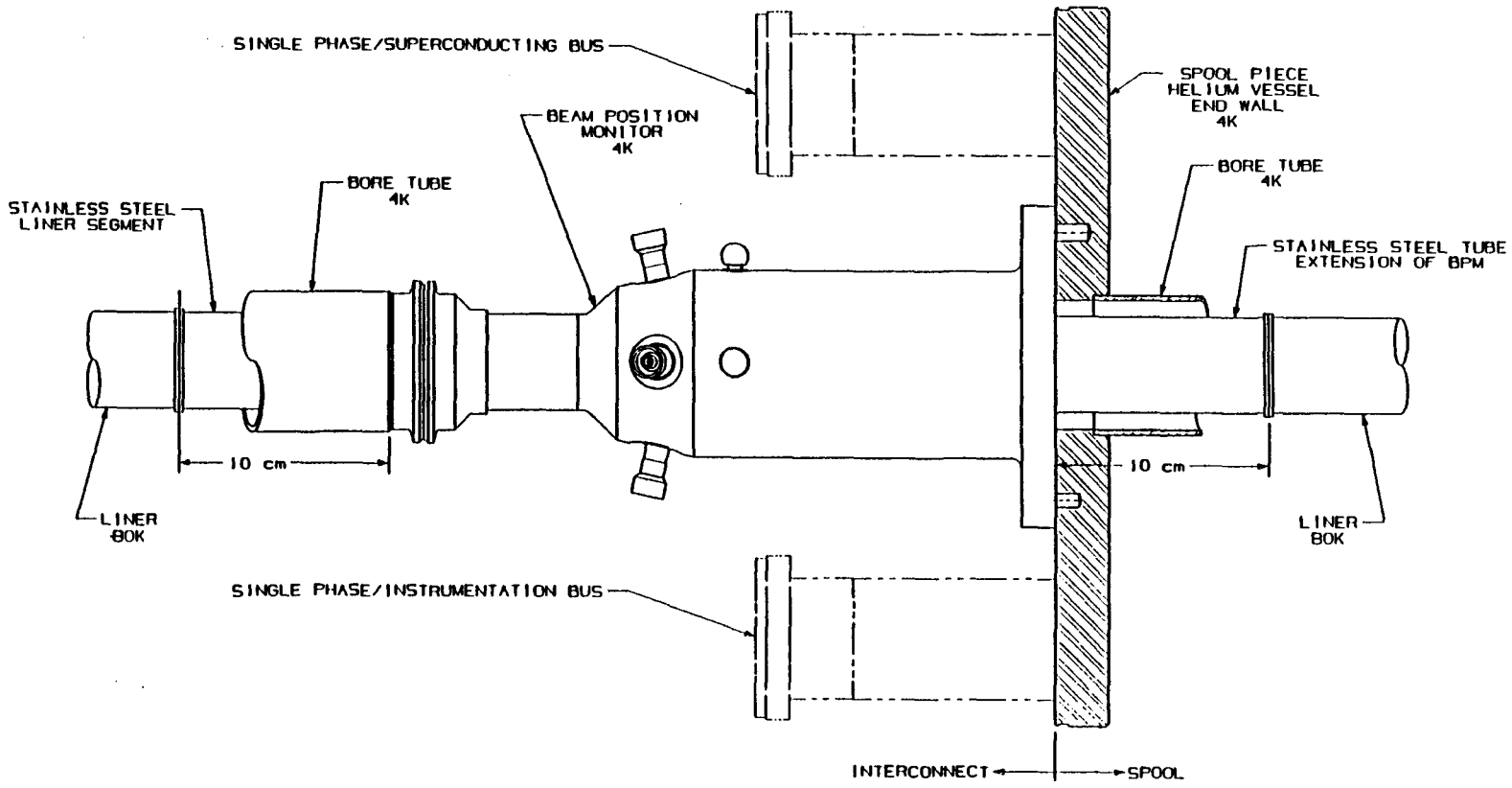

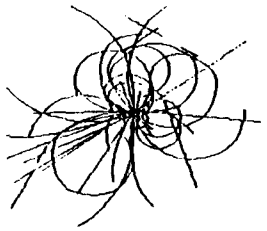

SSC Laboratory 80K SR Liner Program

4K CONCEPT/ HEAT LEAK

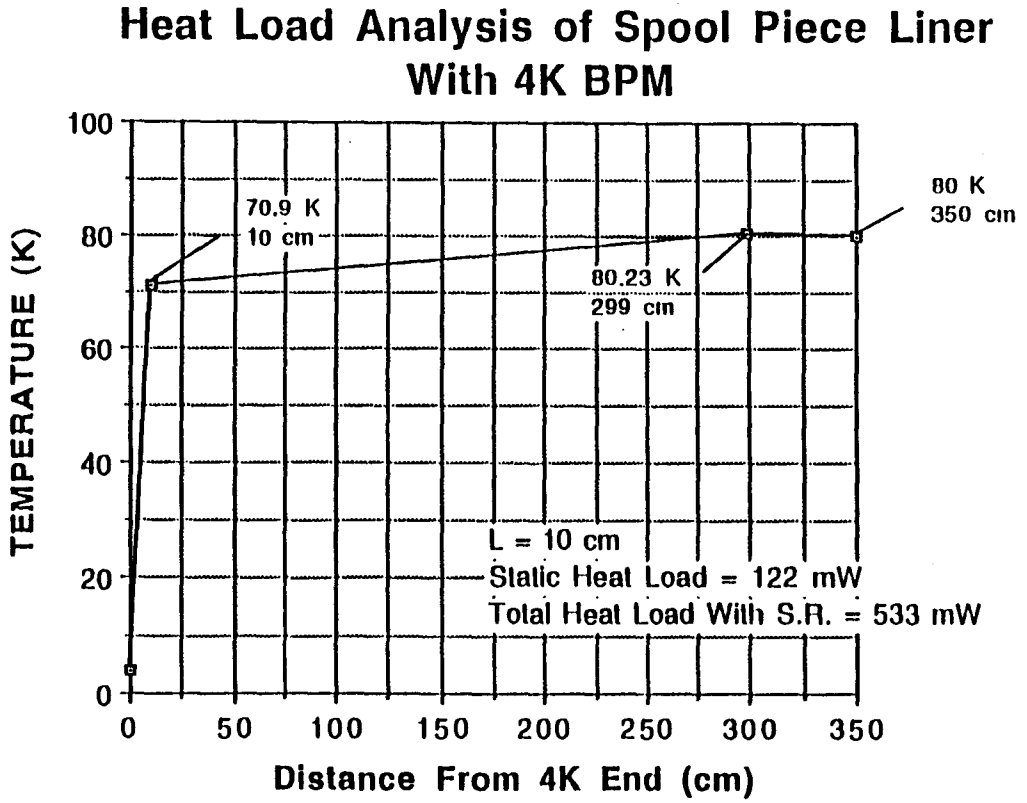

Analysis kindly supplied by Quan-Sheng Shu and Kun Yu.

4K CONCEPT/ HEAT LEAK

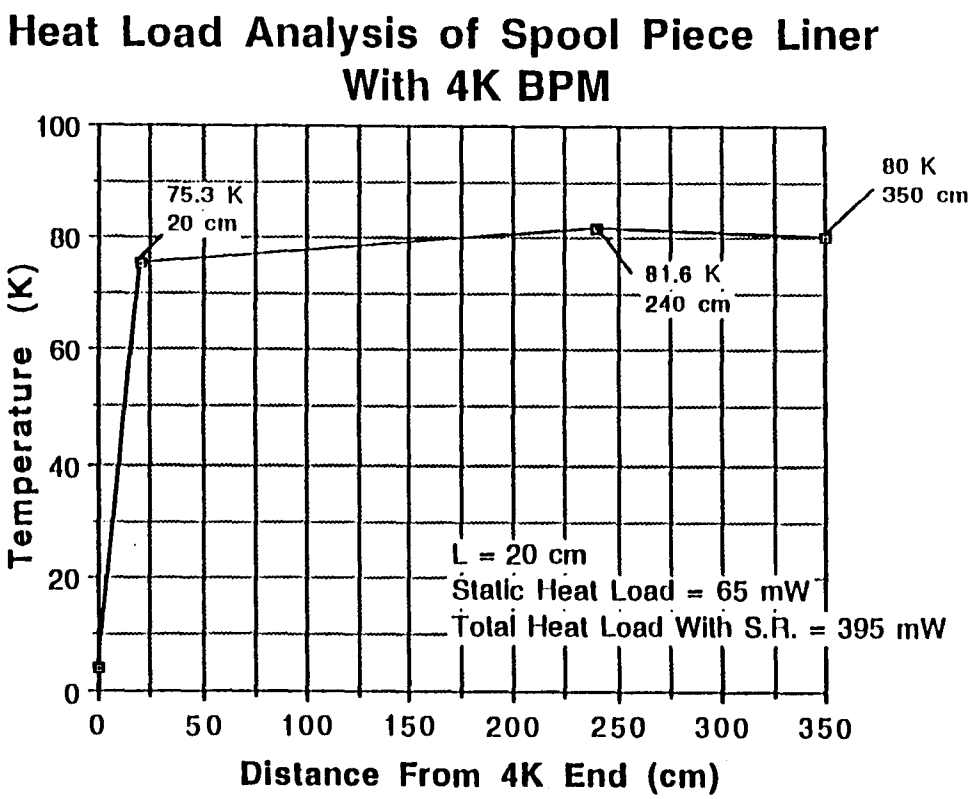

Analysis kindly supplied by Quan-Sheng Shu and Kun Yu.

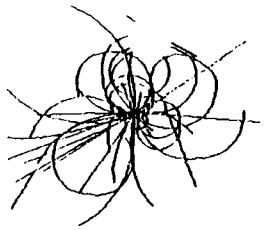

SSC Laboratory 80K SR Liner Program

4K CONCEPT/ RESISTIVE WALL IMPEDANCE

The 4K BPM concept requires thermal isolation between each end of the BPM and the 80K liner. This may be achieved using 2000 each 10 cm. sections of 316LN SS beam tube. The wall impedance presented by a beam tube in the low conductivity regime is given by:

$$R + i\omega X = \sqrt{\frac{2}{i}}\frac{R_s}{2\pi r_i}\left[\frac{J_o(Tr_i)H_o^{(1)'}(Tr_o) - J'_o(Tr_o)H_o^{(1)}(Tr_i)}{J'_o(Tr_i)H_o^{(1)'}(Tr_o) - J'_o(Tr_o)H_o^{(1)'}(Tr_i)}\right]$$

where r_o = liner outer radius = 14.15 mm

r_I = liner inner radius = 12.65 mm

$T^2 = -i\omega\mu\sigma$ $\qquad R_s = \sqrt{\frac{\omega\mu_o\mu_r}{2\sigma}}$

$\rho_{SS} = 1/\sigma_{SS}$ = 714 nΩm over the range 4-80K

$\rho_{Cu} = 1/\sigma_{Cu}$ = 2.5 nΩm at 80K

Neglect magnetoresistance and anomalous skin effect.

The expression for $R + i\omega X$ is evaluated for various Liner configurations.

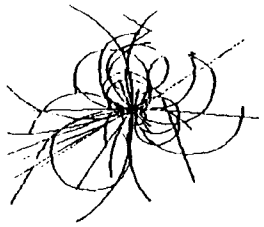

SSC Laboratory 80K SR Liner Program

4K CONCEPT/ RESISTIVE WALL IMPEDANCE

The addition of ~200 meters of Stainless Steel liner tube raises the arc resistive wall impedance (relative to Cu/Cu plated Liner) according to the scenarios shown:

Low Frequency Regime Δ (***wall thickness***) << δ (***skin depth***)	**Resistance**
1. Liner 0.5 mm Cu plating. Stainless Steel tube 1.5 mm wall.	**+22%**
2. Liner 1.5 mm Cu wall. Stainless Steel tube 1.5 mm wall.	**+65%**
3. Liner 0.5 mm Cu plating. Stainless Steel tube 0.5 mm wall. (Scenario No. 3 is appropriate to the heat leak calculation).	**+65%**

High Frequency Regime $\Delta >> \delta$	
1. Liner Cu or Cu plating. Stainless Steel tube.	**+3%**

SSC Laboratory 80K SR Liner Program

80K BPM CONCEPT

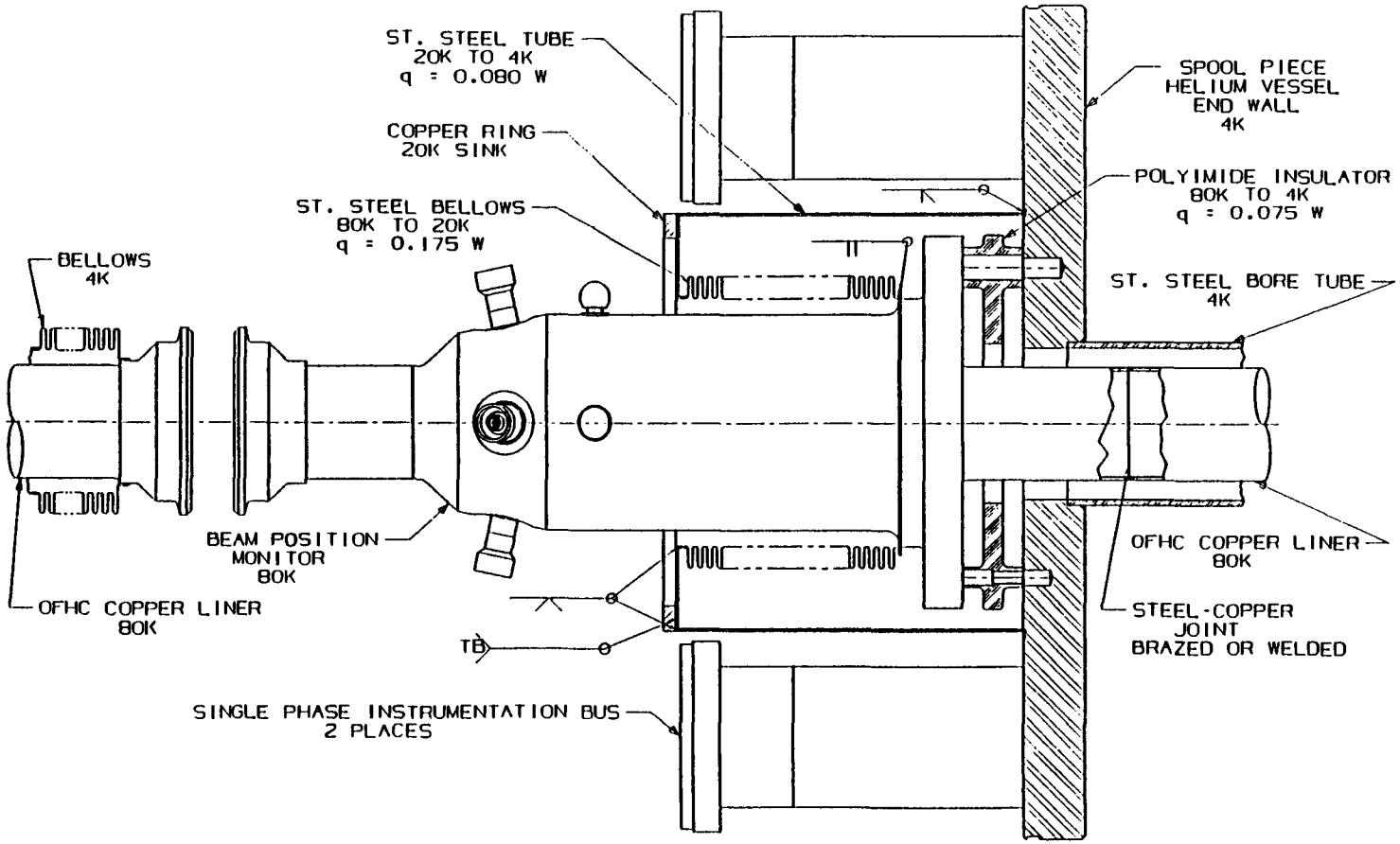

SSC Laboratory 80K SR Liner Program

80K CONCEPT/ ISOMETRIC VIEW

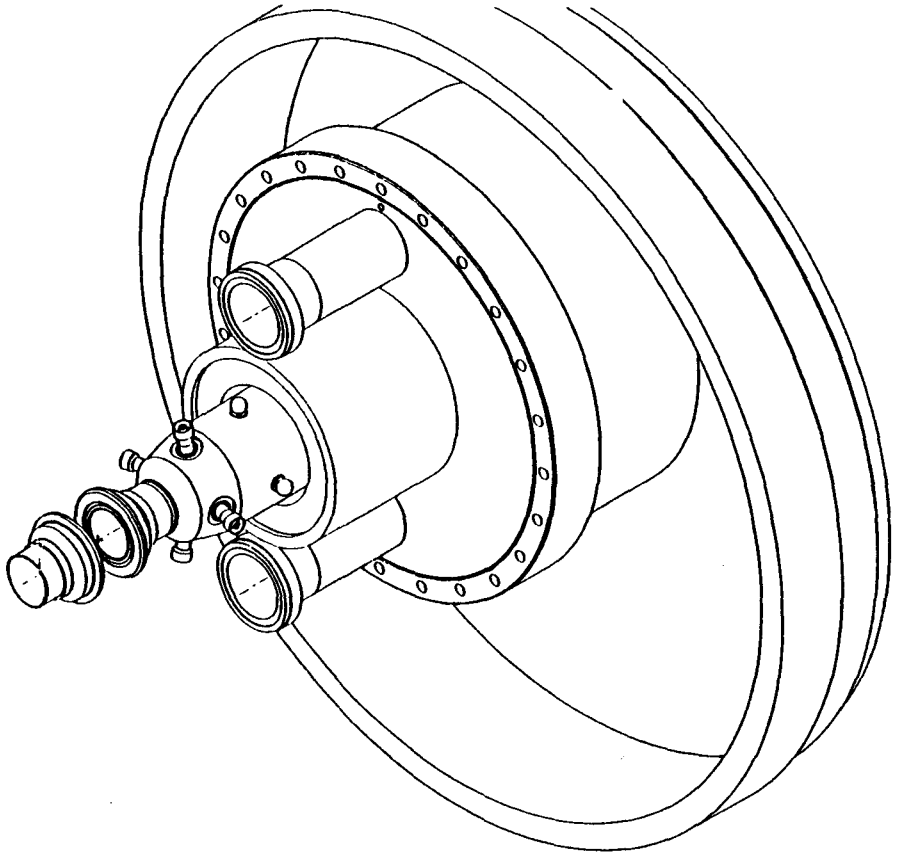

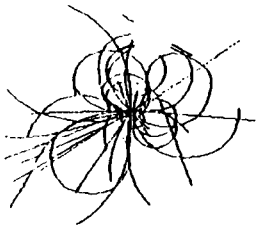

SSC Laboratory 80K SR Liner Program

ASD BEAM INSTRUMENTATION

Potential Design #3

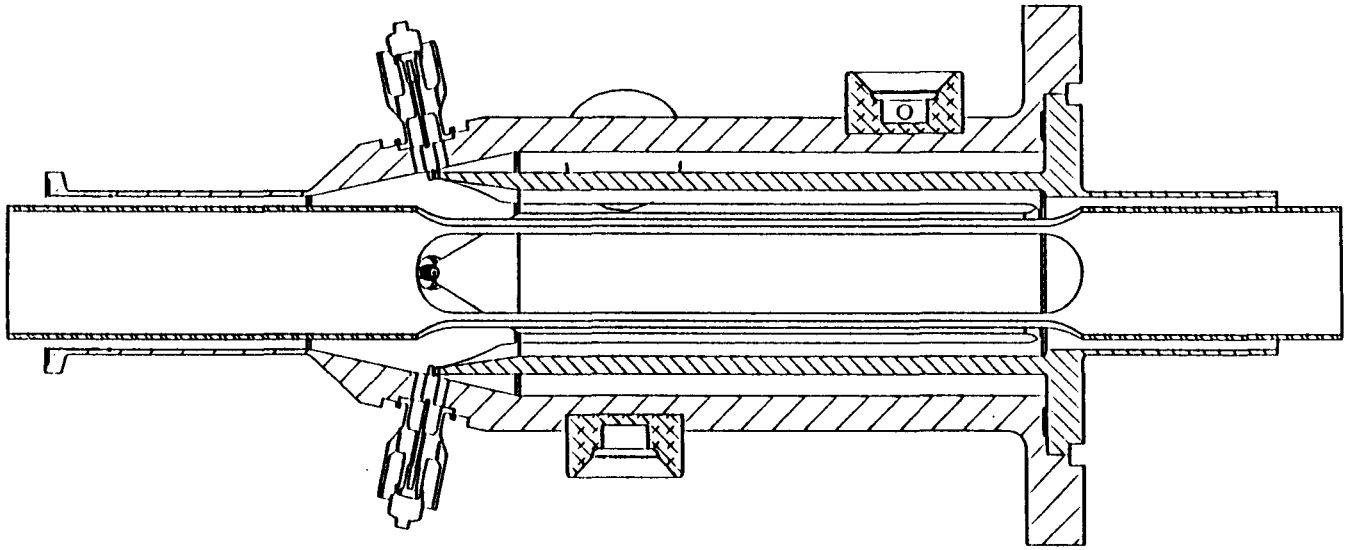

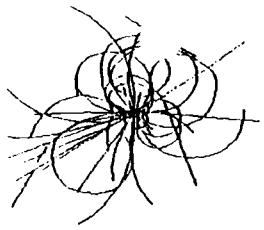

SSC Laboratory 80K SR Liner Program

COMPARISON OF BPM CONCEPTS

Parameter	80K BPM Concept	4K BPM Concept
Temperature	80 Kelvin	4 Kelvin
Accuracy	Increased stack-up. Measure offset.	No Impact.
Radiation	Requires insulator. PI or SS	No Impact.
Reliability	Radiation effect on PI. Complexity.	Many more weld joints.
Heat Leak	~235mW/4K ~3mW/meter	~533mW/4K Absorbs SR heat.
Impedance	No Impact.	+22% to 65% arcs resistive wall.
Vacuum	May require PI in beam vacuum.	No Impact.
Overpressure	Additional bellows required.	No Impact.

This Page Intentionally Left Blank

SECTION 6

Cryosorber Concept and Analysis

R. Kersevan

SECTION 6

Cryosorber Concepts and Analysis

Roberto Kersevan

Superconducting Super Collider Laboratory*
2550 Beckleymeade Avenue
Dallas, TX 75237

1.0 INTRODUCTION

Table 1 reports the main parameters which are relevant to the discussion of vacuum issues in the collider's arc regions.[1]

TABLE 1. RELEVANT PARAMETERS.

Beam energy	20 TeV
Beam current	72 mA
Magnetic field	6.6 T
Superconducting (SC) magnet temperature	4.2 K
Synchrotron radiation (SR) photon flux	1.0×10^{16} ph/s/m
SR critical energy	284 eV
SR power	140 mW/m, 8.9 kW/ring
Hydrogen density corresponding to 150 hr luminosity lifetime	3.0×10^{8} mol/cm^3
Hydrogen density leading to quench/cryo limit	4.0×10^{10} mol/cm^3 (0.6 W/m deposited downstream)
Hydrogen saturation density at 4.2 K	2.0×10^{12} mol/cm^3
Hydrogen density increase due to desorption of 1 monolayer in a 33 mm ID tube	7.3×10^{15} mol/cm^3 (0.2 Torr at 293 K)

As already pointed out by others,[2] these unique machine parameters lead to a vacuum environment which has not been encountered so far in any of the existing particle accelerators. The concomitant presence of a large fraction of the vacuum chamber being cooled down to liquid helium (LHe) temperature combined with the generation of a copious synchrotron radiation (SR) photon flux, which in turn translates into a SR-induced outgassing, need a new approach to the problem to be applied. Few measurements of the SR-induced outgassing yield at LHe temperature can be found in literature,[3] and, therefore, a series of such measurements are in progress.[4] Another key issue to be raised is related to some not well known effects which seem to arise in such a vacuum environment, namely the possibility of having some "recycling" of the already cryosorbed species.[3] Other problems arising from longitudinal and transverse beam impedance

* Operated by the Universities Research Association, Inc., for the U. S. Department of Energy under Contract No. DE-AC35-89ER40486.

requirements lead us to the necessity of "screening" the proton beam from the presence of discontinuities or radio-frequency (RF) absorbing materials. A possible common solution to these problems is obtained by introducing a perforated liner inside the bore tube.[5] Together with the liner, a suitable material capable of removing the molecules presents another means of reducing the molecular density in the proton beam region. Such a material, working at cryogenic temperatures, is called a cryosorber, and is able to 'trap' the molecules due to physisorption and/or chemisorption bonding. There exist a lot of different materials with such characteristics, both organic and inorganic.

The scope of this paper is to review some of the possible choices for a cryosorber and the ongoing activity at the SSCL and other laboratories.

2.0 CRYOSORBER REQUIREMENTS

2.1 Introduction

Synchrotron radiation is well known to cause outgassing from the exposed surfaces: the desorbed molecules subsequently move with a random motion, characteristic of ultra-high vacuum conditions, and finally reach a surface where they are absorbed, either chemically or physically. In the former case, the gas species will be permanently trapped and they will not be of concern to us. In the latter case, represented for instance by the surface of the cold bore tube at 4.2 K, the gas species can undergo several different behaviors. CO, CO_2, CH_4 and H_2O would all be cryopumped, since their saturation vapor pressures at this temperature are incommensurably low, see Figure 1, forming thick condensate layers regardless of the gas load. H_2 and He would behave differently: they would first be cryosorbed on the cold surface, but after absorption of a modest quantity, their saturation vapor pressures would rise to unacceptable levels.[6] The quantity referred to here is on the order of a fraction of a monolayer, and therefore depends primarily on the surface area of the cold bore tube. If a value of $3.0 \cdot 10^{15}$ mol/cm^2 is taken as the monolayer surface concentration, a very modest value of 0.11 Torr liter/m is obtained even assuming a full monolayer coverage (cold bore tube ID = 42 mm, no correction for surface roughness), and this translates into a time period of only 15 days at the nominal SR photon flux of $1.0 \cdot 10^{16}$ ph/s/m and assuming a desorption yield of $3.0 \cdot 10^{-4}$ mol/ph. It should be noted here, that there is experimental evidence[4,6] that the equilibrium pressures of H_2 and He steeply increase, a 'brick wall' behavior, as the surface density is just a fraction of a monolayer, see Figure 2. After reaching this high equilibrium vapor pressure, the cryosorbed layer must be pumped out, since the equilibrium density is much higher than the quench/cryo limit density, see Table 1. After warming the system up to temperatures of several tens of degrees K, the gas species can be removed by roughing pumps. This warm up procedure would require many days to be performed, since it would involve the whole cold mass inside the cryostat.

The introduction of a cryosorber would greatly reduce the problem for He and H_2, since its primary feature is an effective surface which is several times bigger than the geometrical ('projected') surface, up to 4 orders of magnitude.[7] Therefore, the brick wall would be moved to longer time periods, thus reducing the number of warm ups.

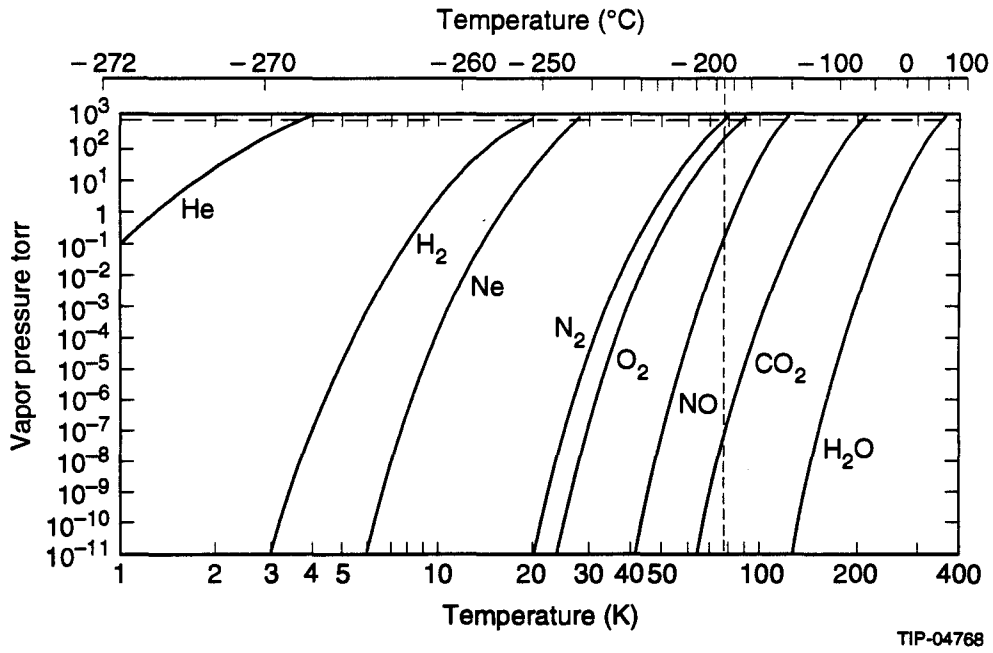

Figure 1. Vapor Pressure Curves of Some Common Gases.[12]

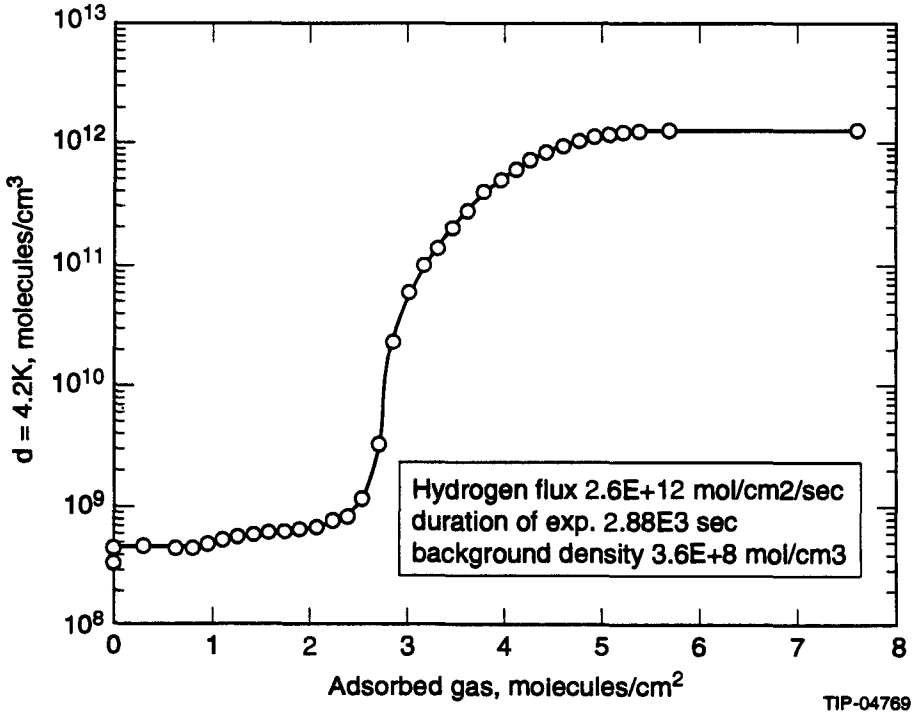

Figure 2. Hydrogen Isotherms Measured on Silves Electrodeposited Copper on Nitronic 40 SS, BINP, Run #3.

2.2 Cryosorber Material Specifications

The cryosorber material is required to have the following characteristics[2]:

- Effective pumping speed of 1200–3000 l/s/m for H_2, at an average temperature of 80 K;
- Pumping capacity of 5–20 Torr l/m, with a gas composition of 45% H_2, 10% CO_2, 20% CO, 20% H_2O and 5% CH_4;
- In situ activation temperature not higher than 300 K;
- In situ regeneration temperature lower than 80 K for H_2 and 300 K for all other gases, and pumping capacity recovery fraction greater than 98% per cycle for up to 25 cycles;
- Recovery of pumping speed and capacity higher than 90% after an accidental vent to atmosphere;
- Survival to 100 quenches over a period of 25 years;
- Radiation dose tolerance of 1400 MRad over 25 years;
- "Good" behavior for RF impedance issues;
- Sufficiently low emissivity so as to reduce the heat leak to the 4 K system;
- The bonding/brazing material, when required, must also comply with the last four mentioned items for the cryosorber.

3.0 CRYOSORBER MATERIAL OPTIONS

3.1 Introduction

The word cryosorber usually refers to any material, either a chemical element or a combination/alloy of chemical elements, which can be used for the purpose of increasing the pumping speed and/or pumping capacity of a cryogenic system.[7] In order to accomplish that, porous materials are usually used in order to have a large effective surface area: these porous materials are generally in the form of small particles bonded, brazed or embedded in a solid matrix which gives them a good mechanical and thermal stability. There exist dozens of different cryosorbers, but only a very limited number of them are suitable for installation in the vacuum environment of the SSC. The radiation dose tolerance of 1400 MRad over 25 years of operation of the SSC seems to pose the strongest constraint on the selection of the cryosorber material, but the total pumping capacity is also important. The selection is also linked to the operational temperature of the liner. At the moment three different temperatures are envisaged, 80, 20 and 4 K. In the first case, which originally motivated the study being presented here, the cryosorber must be placed in good thermal contact with the bore tube at 4 K. The acceptance tests of the SSC magnets, *i.e.* the measurement of their magnetic field quality, require the cryosorber to be installed after the measurement, and this poses a further constraint on the selection of the bonding and brazing techniques and materials. There exist, for instance, the possibilities of plasma/laser welding of a metallic strip inside a long tube comparable to the dipole bore tube, and in this case the cryosorber could be installed by welding a coated strip after the magnetic measurements. For the 20- and 4 K liner options there is the attractive possibility of installing the cryosorber on the outside of the liner, thus removing the need for a welding in situ. In this case other issues should be addressed, such as the compatibility of the concomitant presence of the holes and the cryosorber on the liner. The maximum in situ activation temperature of 300 K poses an additional constraint to the selection of the material. As long as RF impedance issues are concerned, the ideal cryosorber should be a strong RF absorber, in order to reduce the interference between the radiated wake fields and the bunched beam.[8]

3.2 Cryosorber Materials

There exist many different types of cryosorber materials. Here is a partial list of those which have been initially taken into consideration for our application.[9] A brief discussion of each of them follows:

- Zeolites;
- Activated charcoals;
- Porous metals;
- Gas condensates.

See Figures 3, 4, and 5 for the absorption isotherms of different gas species on these cryosorber materials at different temperatures.

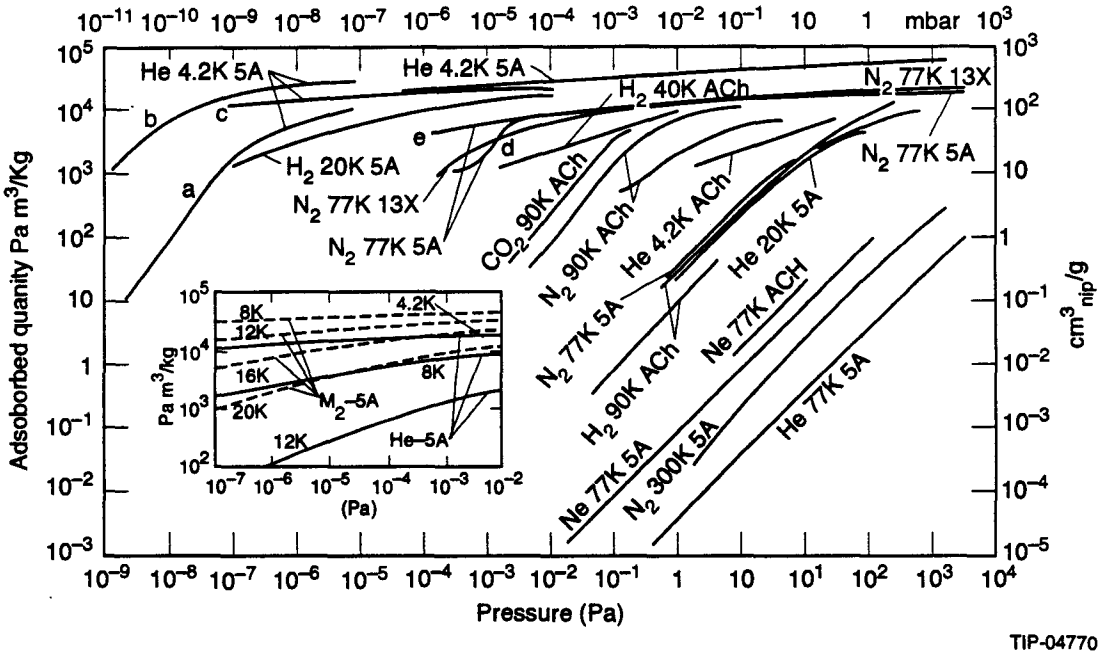

Figure 3. Isotherms for the Absorption of He, Ne, H_2, N_2, CO_2 on Molecular Sieves (5A, 13X) and Charcoal (ACh).[7]

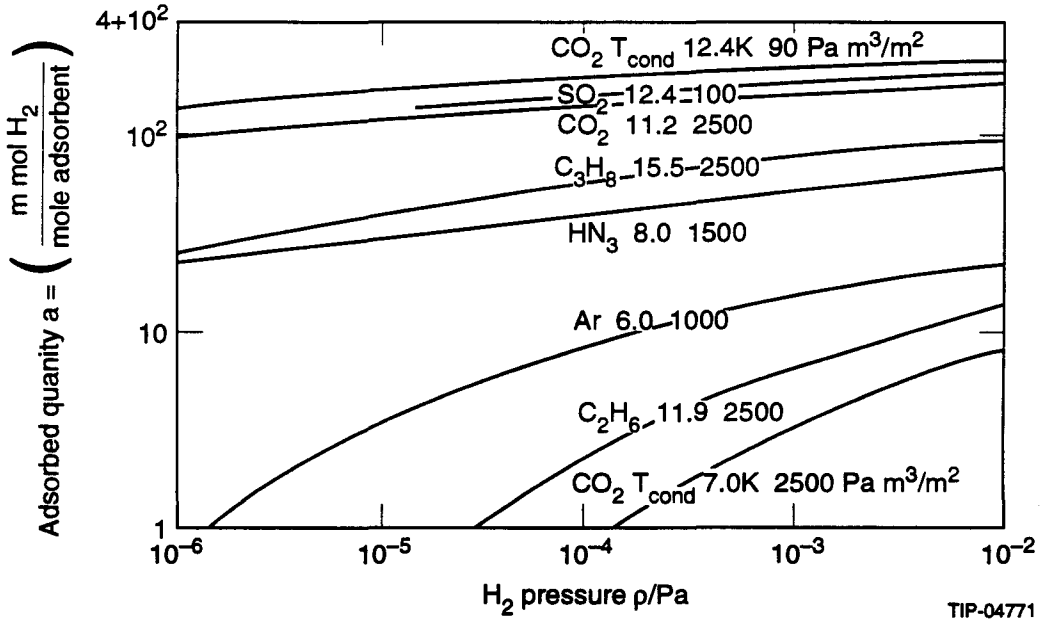

Figure 4. Isotherms of Absorption of He on Various Solids at 4.2 K.[7] Molecular Sieve 5A, 1.8 mm thick.

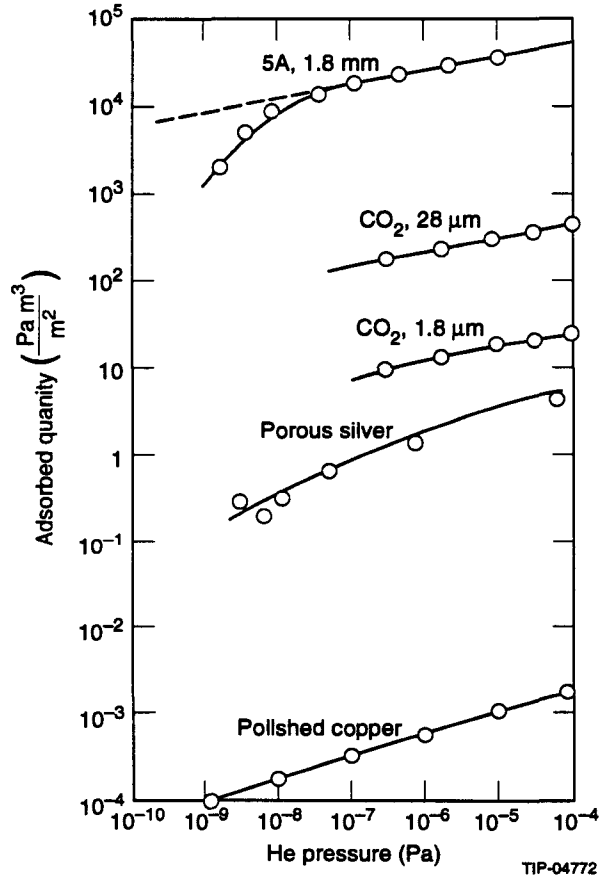

Figure 5. Isotherm of Absorption of H_2 on Various Gas Condensates.[7]

3.3 Zeolites

Zeolites[7] are a class of synthetic materials used as molecular sieves for vacuum applications. They are crystallized alkaline or alkaline earth aluminosilicates containing water of crystallization. Their structure is composed of SiO_4 and AlO_4 tetrahedrons, which form a polyhedron with a cavity at its center. The cavities of the individual polyhedrons are connected with each other by pores ('windows') which have a free diameter on the order of one nanometer.

Absorbed water considerably lowers the absorption capacity for other gases. For instance, the capacity for some molecular sieves is reduced to zero when they absorb 7 percent by weight of water.[10] This is probably due to a blockage of the pore openings by hydrated cations. In practice moisture content of 2 percent should not be exceeded: this value is absorbed from atmospheric air in just a few hours. Molecular sieves require regeneration temperatures in the range of 200–300 C for periods on the order of 24 hours. In addition to that, zeolites are not good RF absorbers.

3.4 Activated Charcoals

Activated charcoals are carbonaceous particles in the form of granules which are bonded/brazed into a matrix.[10] Overall, they exhibit better vacuum performance than zeolites. This behavior can be ascribed to the presence of a higher number of micro-pores whose dimensions are variable as opposed to the fixed size of the zeolites' cavity entrances. This leads to higher specific surfaces and therefore higher capacities. Moreover, charcoals are not so sensitive to the presence of water vapor, and they are able to produce a sufficiently high pumping speed/capacity even without a bake-out. Zeolites are, nevertheless, usually characterized by a lower base pressure as compared to charcoals. Charcoals are generally good RF absorbers.

Charcoal particles by themselves do not fulfill the mechanical requirements for the installation inside the bore tube. In order to prevent the formation of particles and/or microdust, which could prove detrimental to the proton beam lifetime, they need to be made strongly adherent to the surface, either by direct bonding (brazing, epoxy), or by embedding them in a matrix. There are several ways of doing this:

- Carbon films: carbon coatings with good mechanical properties and low gas desorption have already been used as a means of reducing RF breakdown inside stainless steel waveguides.[11] There are both "wet" and gas plasma techniques for obtaining these coatings. The College of William and Mary (W&M) and CEBAF are developing such techniques as part of a statement of work (SOW) with the SSCL;
- Polyurethane and polystirene binders: they can have a stainless steel net as support and give them the required mechanical characteristics. SAES Getters is developing an R&D program on such cryosorbers as part of a SOW with the SSCL;
- Another SOW involves Grumman Aerospace and Lawrence Livermore National Laboratory (LLNL). They should provide the SSCL with a workable solution for the cryosorber based on charcoal, and relying on the extensive experience of both Grumman and LLNL on the subject.

3.5 Porous Metals

Some metals can be etched/sputtered in several different ways so as to produce a highly corrugated surface, characterized by a high effective surface area:

- Ag, Zn, Mg;
- PdO deposited on Al_2O_3;
- Anodized coatings. As part of the SOW with CEBAF and W&M, aluminum anodization is being studied.

Even if their effective surfaces are high when compared to bare metals, the pumping capacities are low as compared to zeolites and charcoals. Porous metals are also very sensitive to H_2O, and require a bake out for full activation.

3.6 Gas Condensates

The bonding of a gas to a solid surface by cryosorption is based on the interaction of the gas particles with the molecules of the solid. Substances used as absorbents are those to which the gas is bonded by van der Waals forces, and which have a higher characteristic temperature (*i.e.* a higher melting point) than the gas to be absorbed.[7]

A condensate layer can be obtained by admitting a constant gas flow of the absorbent and keeping the cold surface at the condensation temperature T_{cond}. The layer thickness should not exceed 100 mm, so as to maintain the maximum temperature difference in the condensate layer below 10^{-2} K. The generation of a constant and uniform gas flow and cooling cycle in the tubular geometry of the SSC vacuum chamber constitutes the primary difficulty for the exploitation of this cryopumping technique.

Cryotrapping of H_2 condensates is not widely studied. The ratio of the condensable to non-condensable depends strongly on the conditions of the condensate formation. The presence of thermal radiation would prevent the system from obtaining low ultimate pressures.[6]

It is not clear what the behavior of gas condensates regarding RF absorption could be, but they should very likely be considered as transparent to RF waves.

4.0 IMPACT OF THE INSTALLATION OF A CRYOSORBER ON ASST-II

The installation of a cryosorber in the Accelerator Systems String Test facility, phase two (ASST-II) will require additional study, in order to verify the compatibility with the existing hardware and the need for new components to be installed. At the moment, this issue cannot be addressed more specifically, since more data on the measurement of the cryosorber's characteristics are required. For the 80 K liner configuration, the cryosorber would presumably be inserted as a retrofit device, prior to the insertion of the liner itself. The requirement of a good mechanical/thermal contact between the 4 K bore tube and the cryosorber support will require the development of in situ installation techniques which are being considered. The cryosorber could be deposited on one or more metallic strips that, in turn, would be welded inside the bore tube. For the 4 K and 20-K liner temperature options, the cryosorber could conceivably be deposited on the outer side of the liner. This is one of the issues being addressed by the SOWs with CEBAF/W&M and Grumman/LLNL.

5.0 TESTS TO BE PERFORMED ON ASST-II

Most of the items which have been outlined before should be tested or measured on the ASST-II facility, thus giving a real insight about the collider configuration. In order to do so, some modifications in the existing hardware, and the development of some diagnostics are required:

- Effective pumping speed and pumping capacity: to measure these quantities, a distributed leak system and a connection to the beam tube (both inside the liner) are necessary. The former allows for a simulation of the SR-induced outgassing, while the latter is used for obtaining the pressure readings in the system. The vacuum gauge could be of the Bayard-Alpert (BA) extractor type, allowing measurements in the 10^{-12} Torr range (at room temperature). Operation of such a gauge immersed in LHe at 4 K has already been reported.[10] The distributed leak system needs a connection to room temperature, where a UHV dome with gauges for calibration of the leaks would be installed: a similar experimental setup has been used at the Budker Institute of Nuclear Physics (BINP), Novosibirsk, Russia;

- Activation and regeneration, recovery of pumping speed: the same hardware and diagnostics mentioned above are used. The identification of a suitable temperature range for regeneration of the cryosorber requires several warm-ups of the cold mass, up to temperatures on the order of several tens of K;
- In order to test the mechanical stability of the cryosorber after several quenches or due to vacuum failures, an inspection of the cryosorber is foreseen. This allows the detection of the detachment of solid particles and mechanical problems of the cryosorber/substrate system.

6.0 PARALLEL TESTS

Some of the items listed above cannot conceivably be tested on the ASST-II. Testing the behavior of the cryosorber under radiation doses of 1400 MRad, its RF absorption characteristics, or the effect of its emissivity on the cryogenic system would probably be difficult. Therefore, these quantities are to be considered part of separate measurements, to be carried out both at the SSCL and other laboratories. An extensive study of the desorption characteristics of several materials under SR photon bombardment is underway.[4] Two different SR light sources have been used so far: VEPP-2M at BINP (two beamlines) and the VUV ring at Brookhaven National Laboratory (BNL), Upton, Long Island NY. The former has been used for photodesorption experiments both at room temperature and cryogenic temperatures, 77 K and 4.2 K. The latter has run one beam line at room temperature, and another beamline is going to be installed in the future. For this purpose, the design of a cryostat is underway. It will allow the installation of a 1m-long beam tube, and its irradiation with SR photons of energy and flux comparable to those expected in the collider, 284 eV critical energy and 10^{16} photons/m. Its design is derived by that developed at BINP, see Figure 6. Running these beamlines with vacuum configurations involving liners and cryosorbers is foreseen.

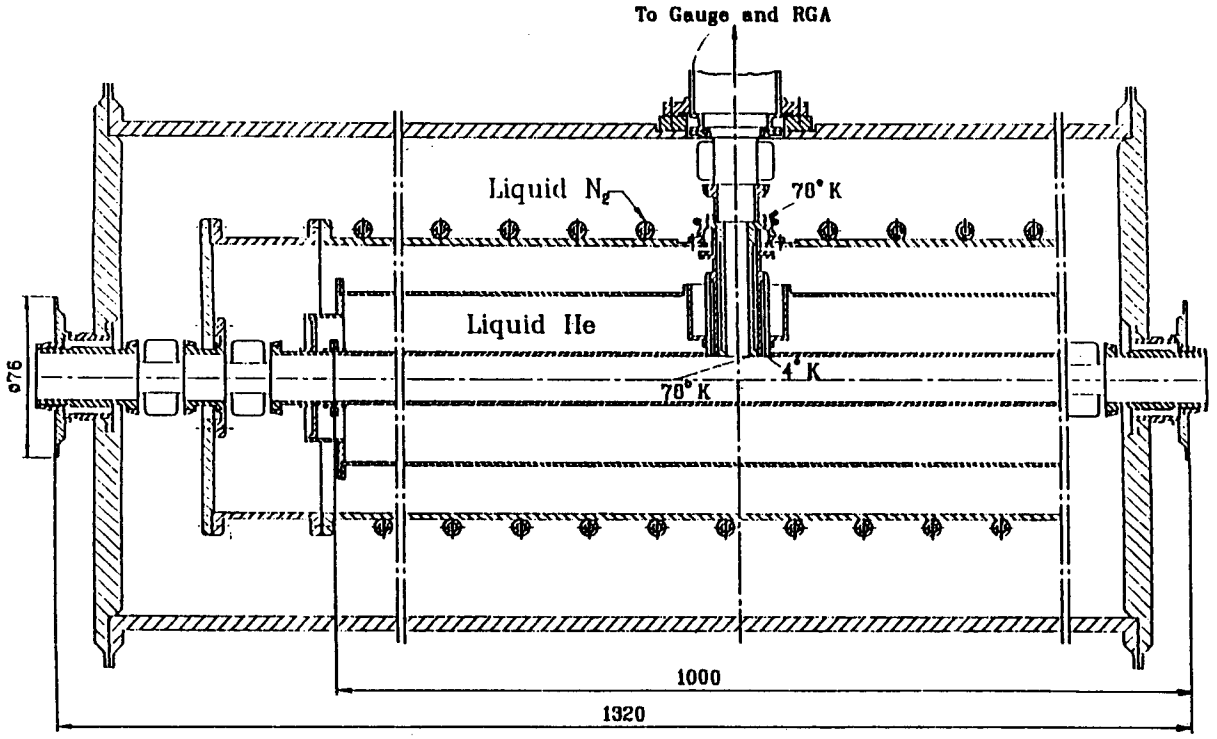

Figure 6. Schematic of the LHe Cryostat Developed at BINP for SR Photodesorption Experiments.

7.0 DRAWINGS, SPECIFICATIONS

A complete set of drawings concerning the cryosorber system is necessary, especially the part referring to the diagnostic equipment described previously. As further data on the cryosorber materials under test become available, specifications and dimensioning of the required hardware will be given. Also, specifications concerning the installation technique for the cryosorber will be derived from the experiences of the SSCL contractors that are developing the cryosorbers.

8.0 SCHEDULE

A definition of the milestones for the development of the cryosorber in ASST-II is strongly linked to that specified in all the mentioned SOWs with CEBAF/W&M, SAES, Grumman/LLNL, BINP and BNL. By, approximately, the end of 1994 all the cited SOWs will be completed, and in the meantime, while additional data become available, a detailed schedule will be done. The main issue here seems to be the operational temperature of the liner.

REFERENCES

1. Q-S. Shu, ed., "Proceedings of the Internal Technical Review of the 80 K Bore Tube Liner for ASST," SSCL Publication, (1993).
2. W. Turner, ibidem.
3. H. Jöstlein, "Vacuum Technology for the SSC," FNAL Report TM-1631 [SSC-N-677] (1989).
4. I. Maslennikov, W. Turner *et al.*, "Photodesorption Experiments on SSC Collider Beam Tube Configurations," *Proceedings Particle Accelerator Conference 93*, Washington (1993), to be published.
5. A. Mathewson, "Vacuum Technology for Superconducting Colliders," ibidem.
6. C. Benvenuti, *et al., J. Vac. Sci. Technol.* **13** (6), (1976).
7. R. H. Haefer, *Cryopumping, Theory and Practice,* Oxford University Press, New York (1989).
8. W. Chou, ref. 1.
9. W. Turner, ed., *Proceedings of the 2nd Proton Collider Vacuum Technical Meeting,* SSCL Publication (1993), to be published.
10. G. Rao, ibidem.
11. D. Manos, ibidem.
12. M. H. Hablanian, *High-Vacuum Technology, a Practical Guide,* (Marcel Dekker, New York, 1990).

This Page Intentionally Left Blank

SECTION 7

80 K Liner Component and Assembly Detail Design

G. Morales, R. Mihelic, C. Murray,
Q. S. Shu, K. Yu, and J. Zbasnik

SECTION 7

80 K Liner Component and Assembly Detail Design

G. Morales, R. Mihelic, C. Murray, Q. S. Shu, K. Yu, and J. Zbasnik

Superconducting Super Collider Laboratory*
2550 Beckleymeade Ave.
Dallas, Texas 75237-3997

1.0 INTRODUCTION

The operating energy of 20 TeV and beam current of 0.072 A of the Superconducting Super Collider (SSC) will produce considerable photodesorbed gases in the beam vacuum.[1] These gases may greatly reduce the beam lifetime, and the scattered beam power may lead to quenching of the superconducting magnets. One method being considered to minimize these gases is to install an 80 K liner inside of the magnets[2] (see Figure 1).

A prototype liner has been developed for installation and testing in a half cell at the Accelerator System String Test (ASST). This 80 K liner design consists of a perforated tube located coaxially inside of the magnet bore tube and sustained at 80 K with GHe pressurized cooling tubes.

This report describes the components that make up the prototype and their assembly in the ASST.

2.0 ASSEMBLIES

The prototype is designed to be a retrofit that can be installed through the magnet interconnect. The method adopted calls for assembling every component around the liner tube and inserting this assembly through the magnet interconnect. The installation is completed with a kit that connects the cooling tubes and the liner tubes.

The prototype is broken up into five assemblies that contain all the necessary components for installation. The first assembly includes all of the components necessary to install the cryosorber in the beam tube. The second assembly includes all of the components needed to install the liner through the lead end of the dipole magnet. The third assembly contains all the components needed to install the liner through the lead end of the quadrupole magnet. The fourth assembly consists of all the components needed to connect the quadrupole liner to the beam position monitor (BPM). The last assembly contains all of the components needed to install the liner in the spool magnet.

Appropriate cryosorbing materials are still being researched; therefore, no details are available for the first assembly.

The second assembly contains the dipole liner with its cryogenic box and a kit consisting of all the connections needed to connect the cooling and liner tubes (see Figure 2). The major component of the assembly consists of a dipole liner tube with brazed cooling tubes, supports, and a turnbuckle sleeve (see Figures 3, 4, 5, 6, and 7). Then the cryogenic box is assembled, around this (see Figure 8). The assembly is completed by connecting the cooling tubes and liner tubes with the tube fittings, the RF flexible sleeves,

* Operated by the Universities Research Association, Inc., for the U.S. Department of Energy under Contract No. DE-AC35-89ER40486.

The third assembly contains the quadrupole liner with its cryogenic box and a kit containing all of the connections for the cooling and liner tubes (see Figure 13). The major component of the assembly consists of a quadrupole liner with a brazed heat exchanger, supports and a turnbuckle sleeve (see Figure 14, 15 and 16). The cryogenic box is then assembled around this (see Figure 17). The assembly is completed by connecting the cooling and liner tubes with the tube fittings, the RF flexible sleeve, the turnbuckle nut, the jam nut, and the 80 K liner extension tubes; these components are contained in the kit (see Figures 18 and 1b).

The fourth section contains a liner tube, a cryogenic box, a bellow, and a kit to connect the cooling tubes (see Figure 19). The major component is made up of a section of quadrupole liner with a brazed heat exchanger (see Figures 19 and 20). An RF joint assembly connects the BPM to the liner tube (see Figures 19 and 21). A bellow connects the RF assembly and the cryogenic box (see Figure 22). The assembly is completed by connecting the cooling and liner tubes with the tube fittings, turnbuckle nut, jam nut, and the 80 K liner extension tubes; these components are contained in the kit (see Figures 18, 1c and 19).

The final assembly contains the spool liner, cryogenic box with a piece of liner tube and a kit to connect the cooling tubes (see Figures 23 and 1c). The major component is the BPM with a liner tube attached to it; a turnbuckle sleeve is brazed to the other end of the liner tube (see Figure 1c). The other major component is made up of a cryogenic box with a liner tube and a compact heat exchanger (see Figures 1c and 20). With the kit the two major components and cooling tubes are connected.

3.0 DRAWING TREE

Figures 3, 18 23, 24, and 25 are a graphical representation of the components that make up the 80 K liner prototype.

4.0 CONCLUSIONS

Most of the components for the prototype have been designed. The assembly of the BPM and its connection to the liner have not been detailed yet. Also, the installation of the cryosorbing material has to be developed.

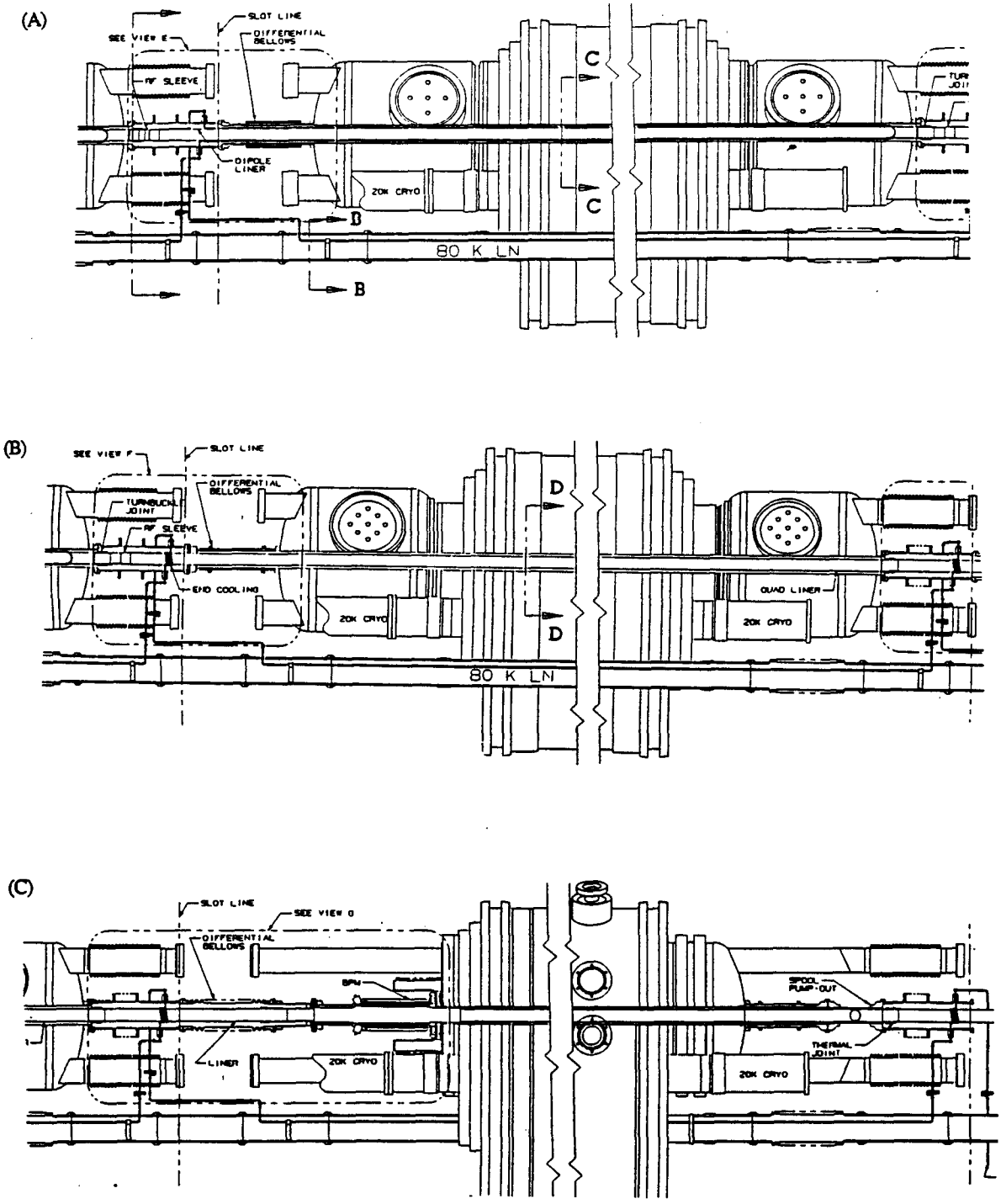

Figure 1. (A) Dipole Liner. (B) Quadrupole Liner. (C) Spool Liner.

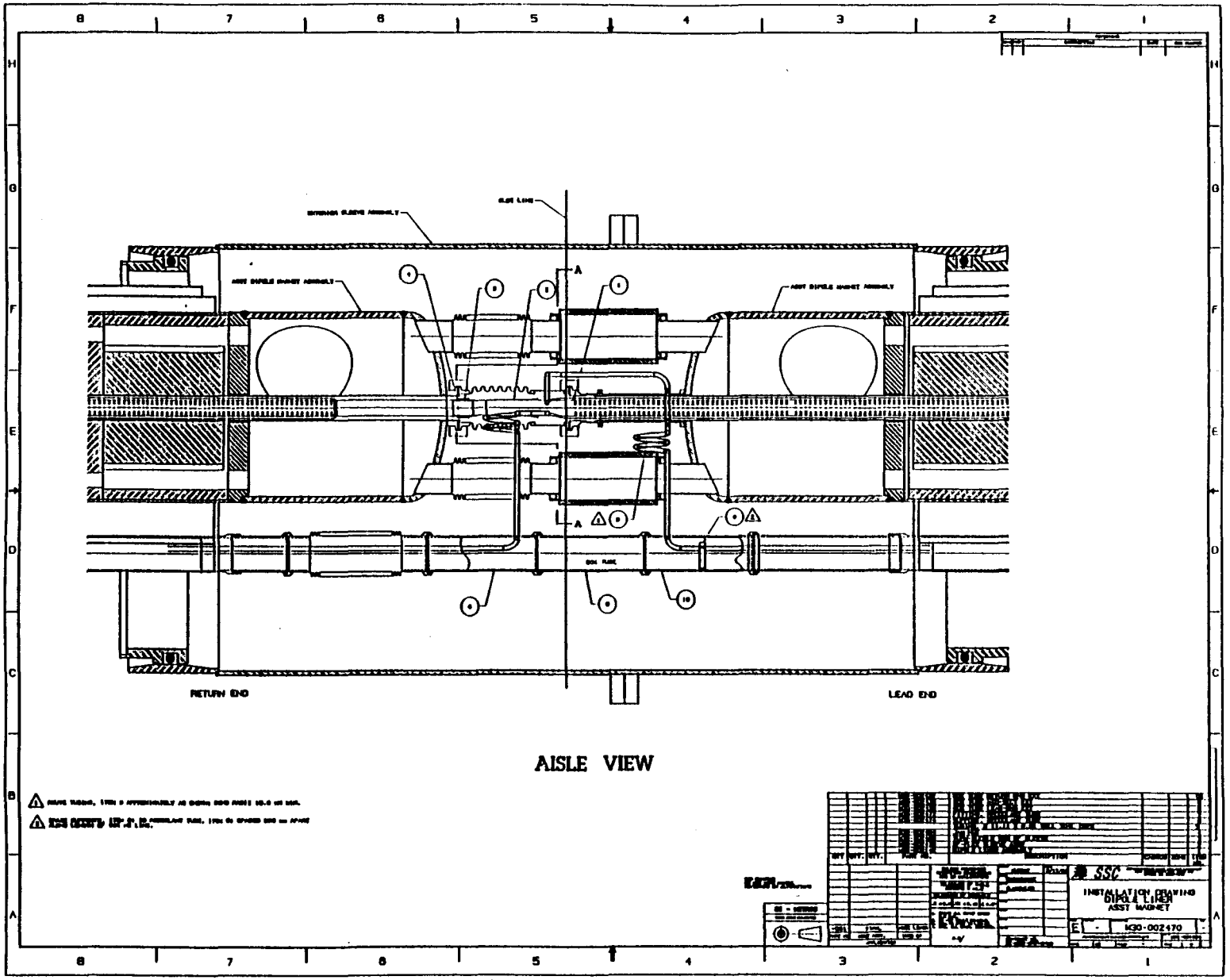

Figure 2.Assembly of Dipole Liner.

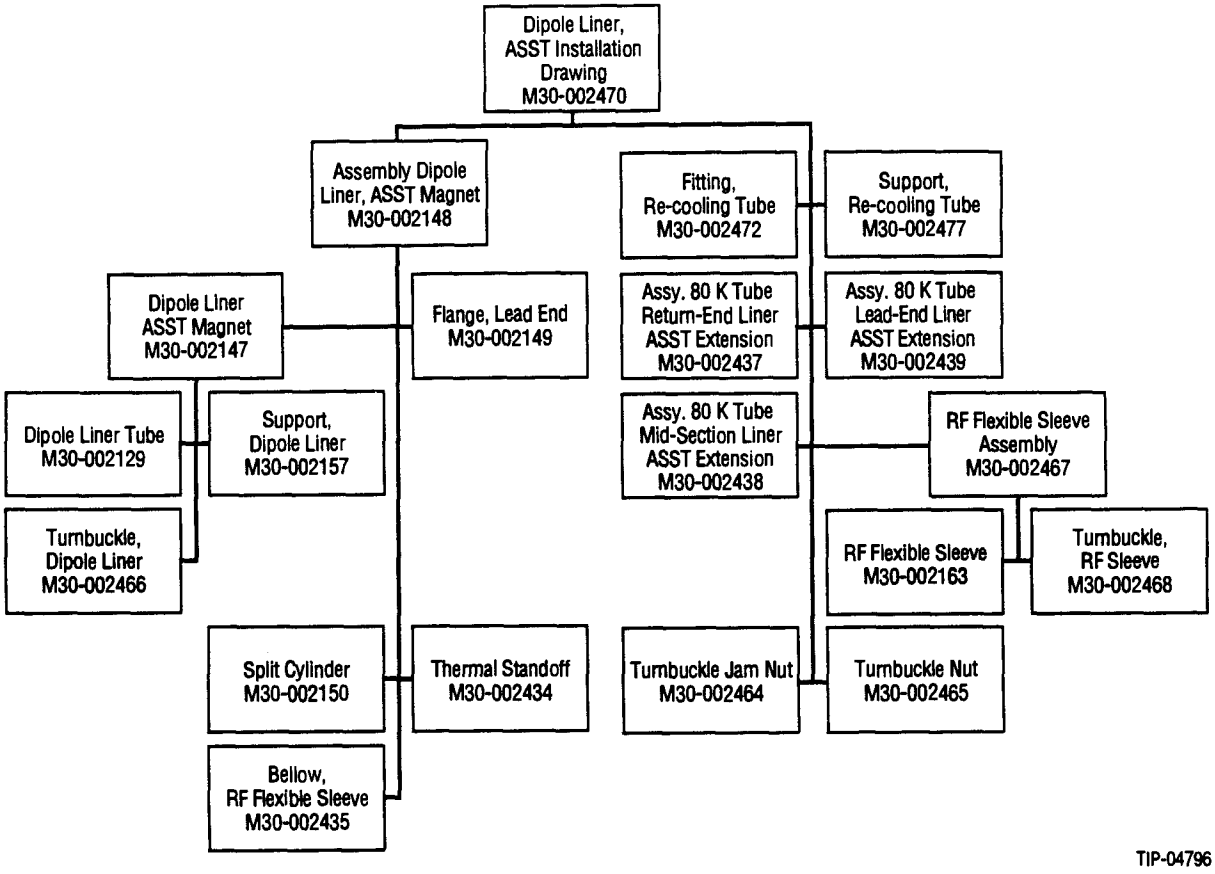

Figure 3. Dipole Liner Drawing Tree.

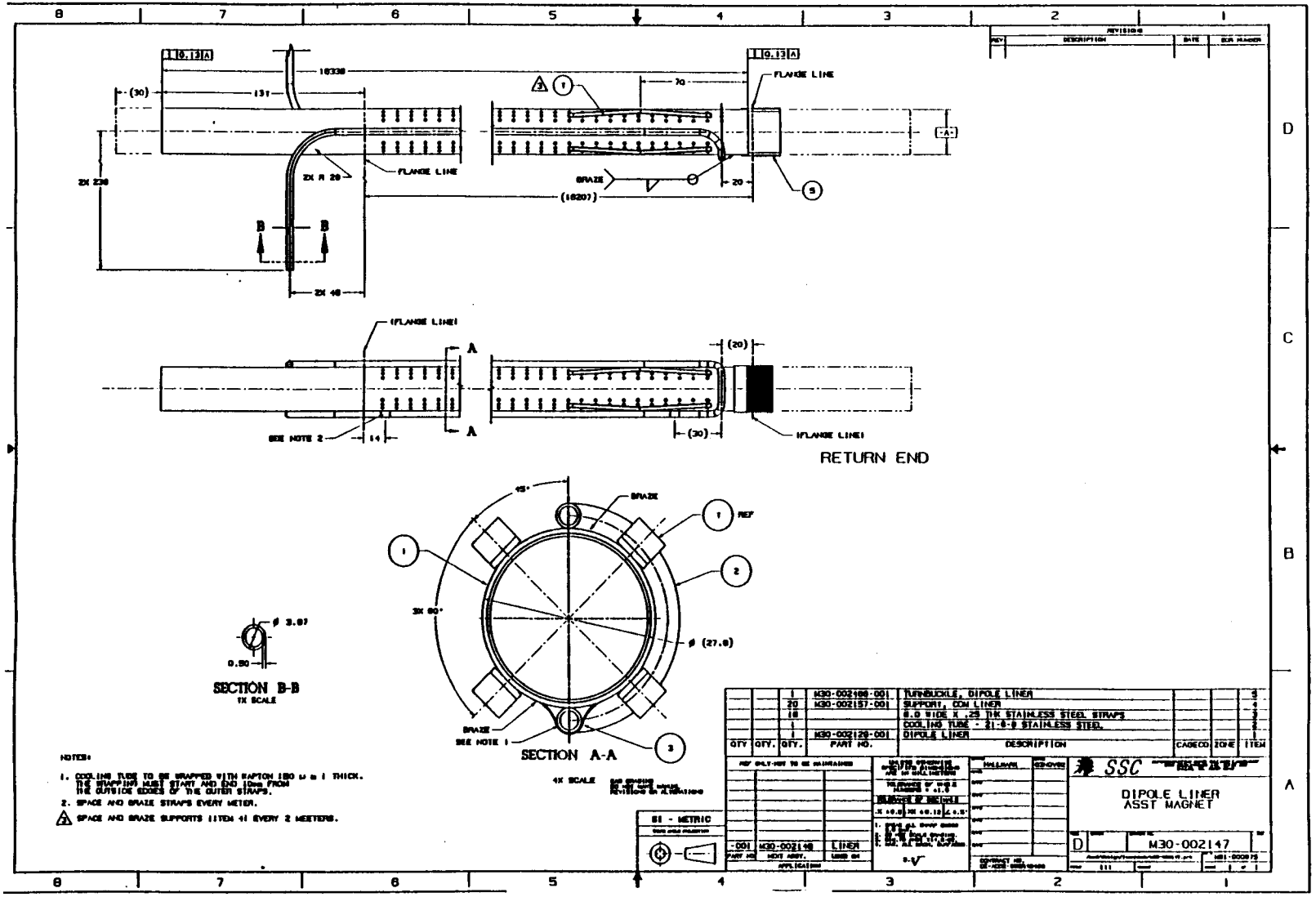

Figure 4. Dipole Liner Tube Assembly.

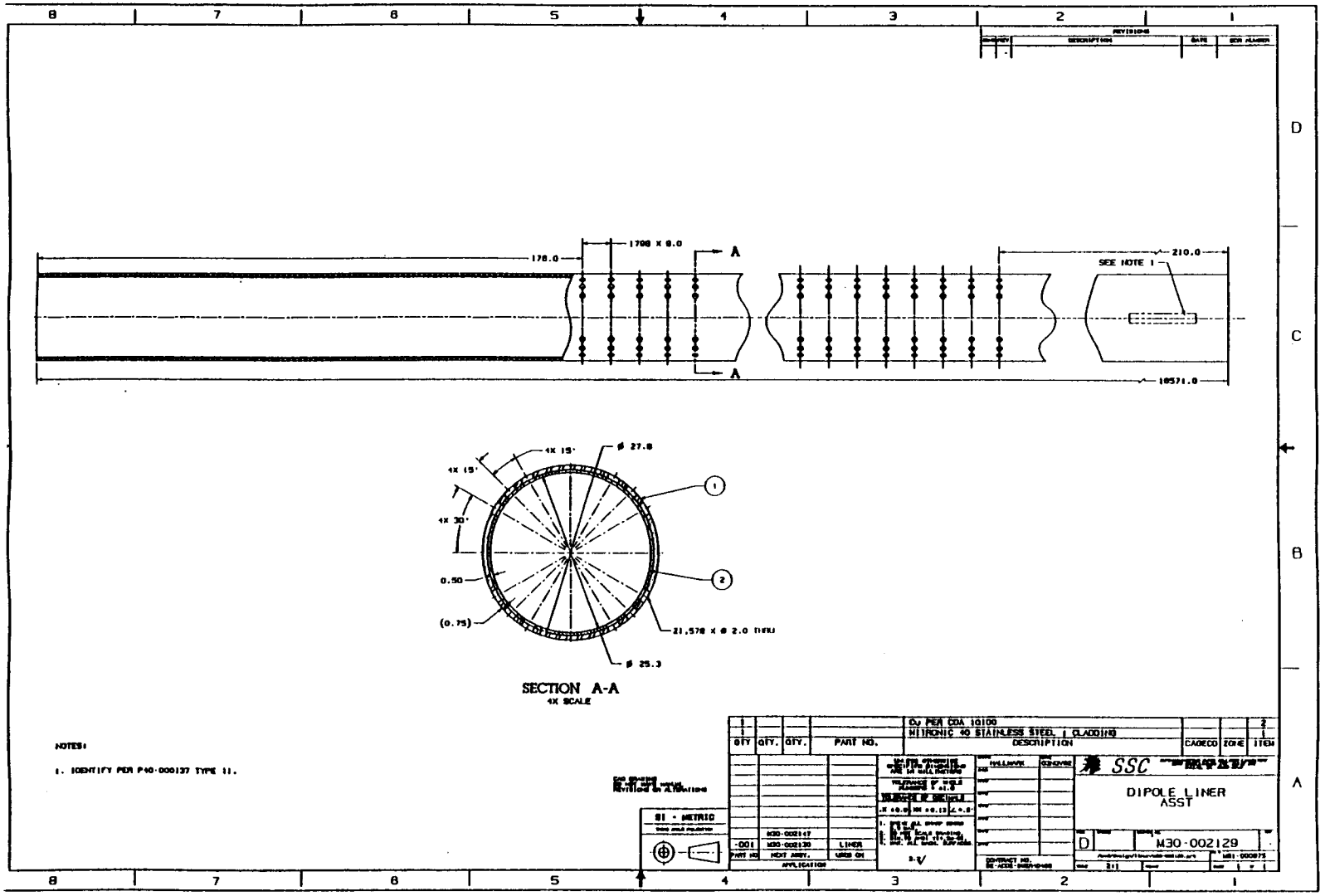

Figure 5. Dipole Liner Tube.

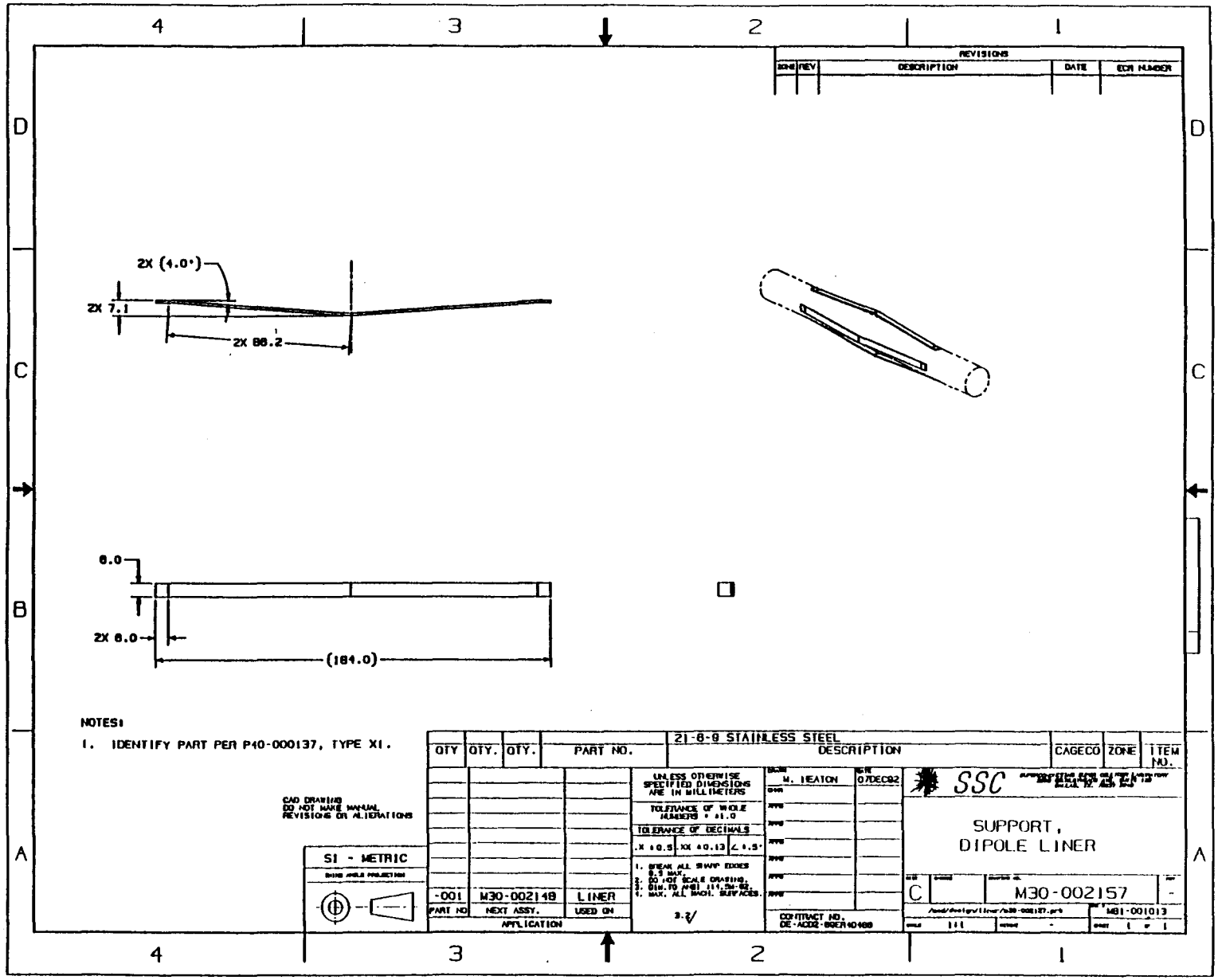

Figure 6. Dipole Liner Supports.

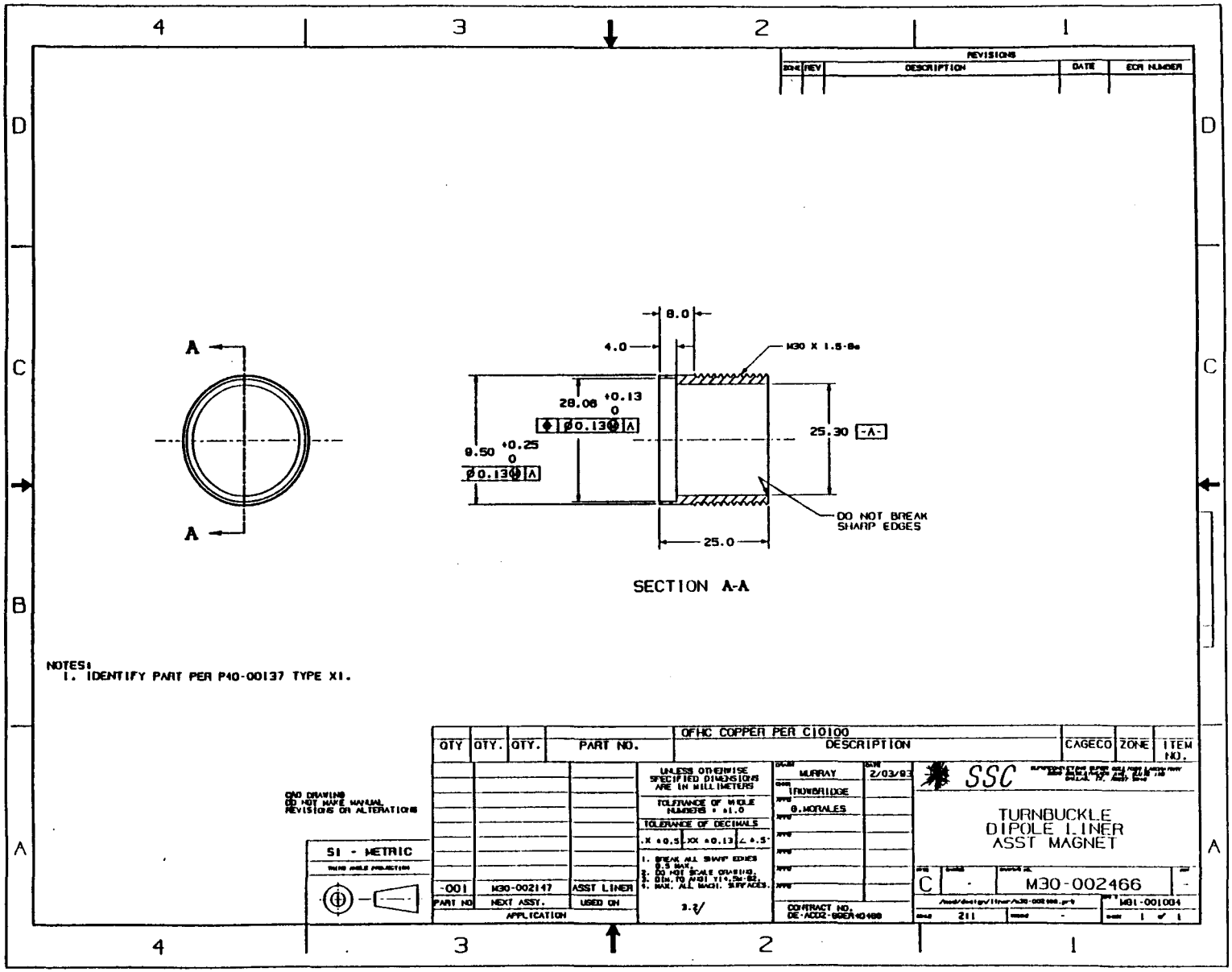

Figure 7. Turnbuckle Sleeve for Dipole Liner.

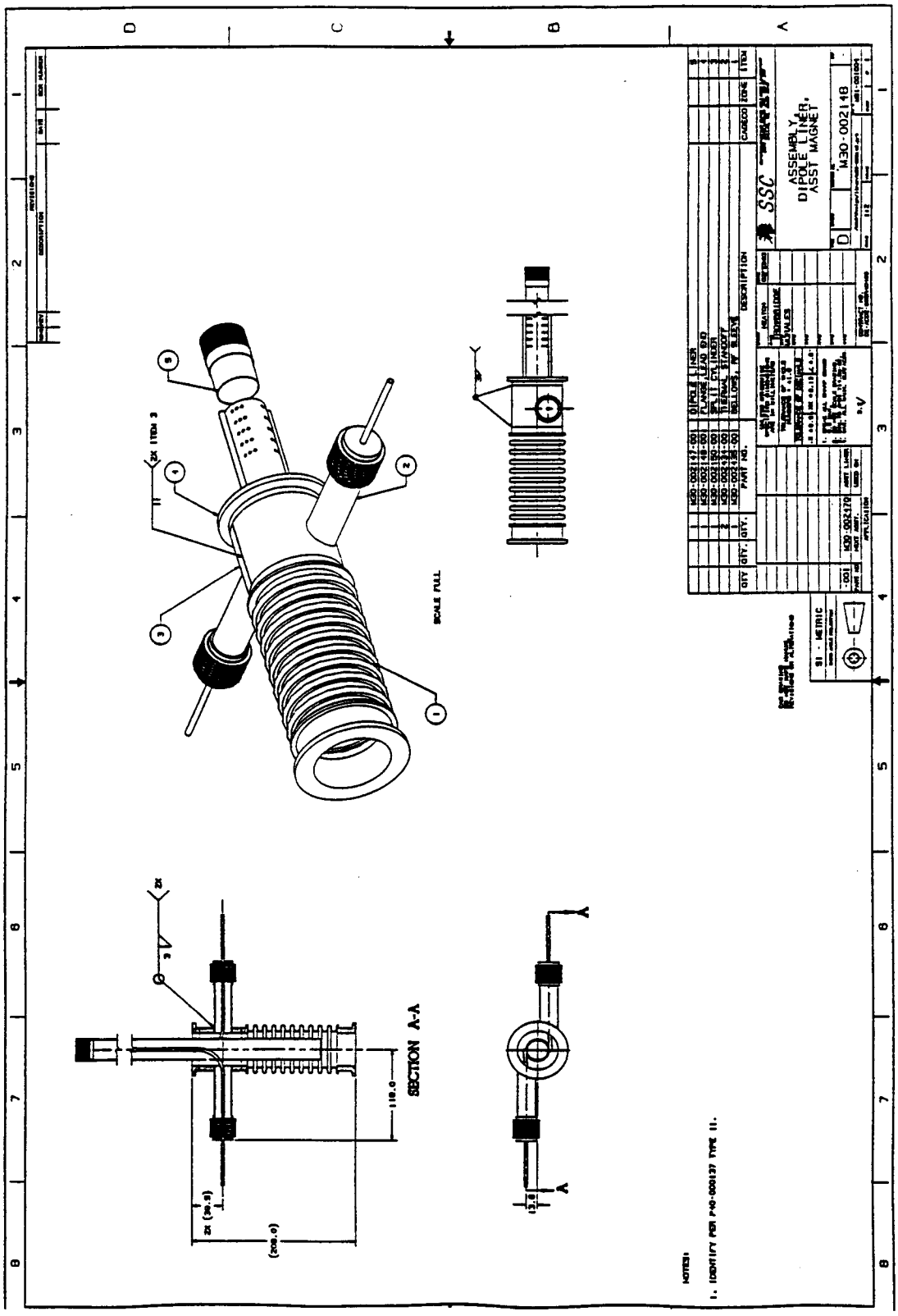

Figure 8. Dipole Liner.

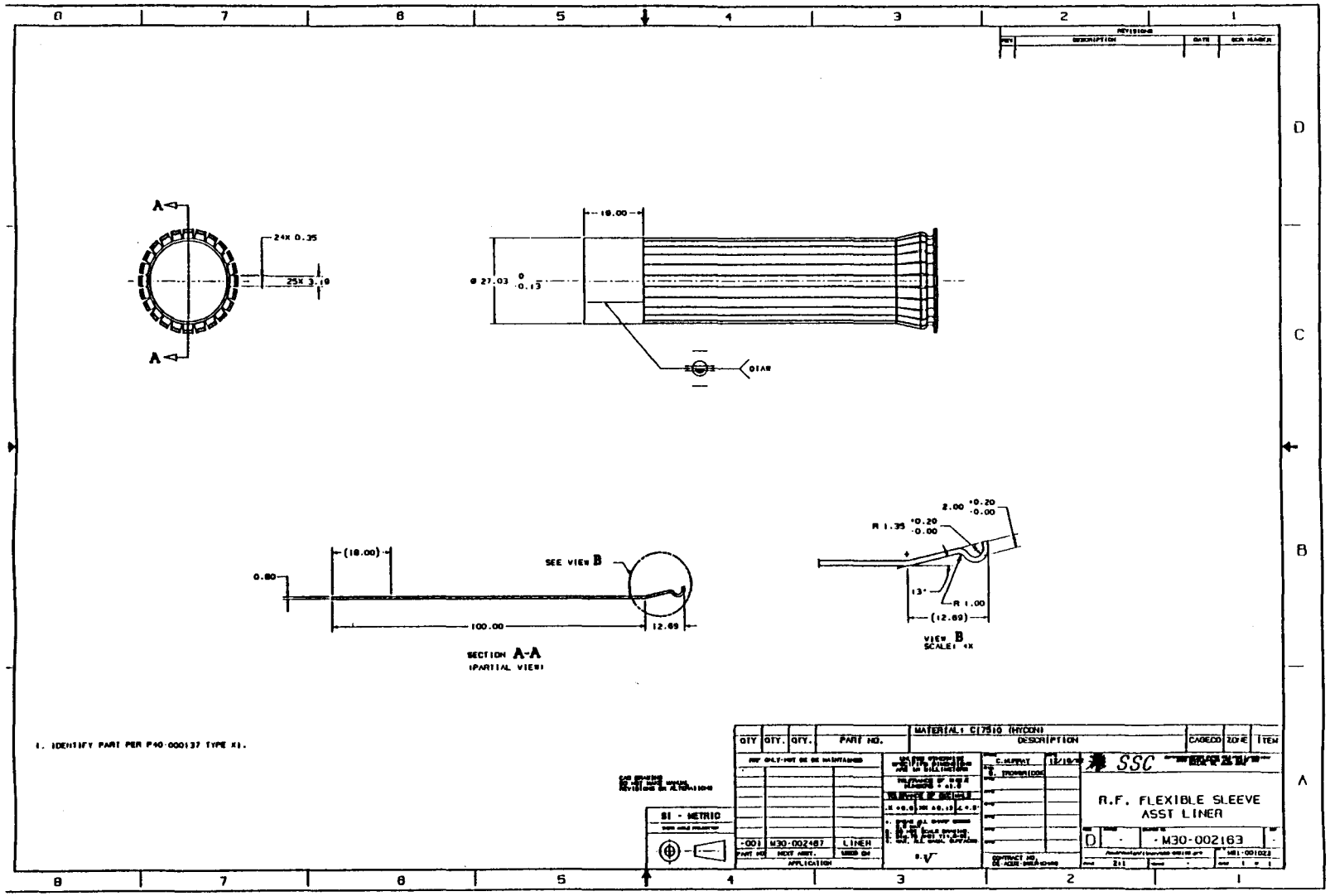

Figure 9. RF Flexible Sleeve.

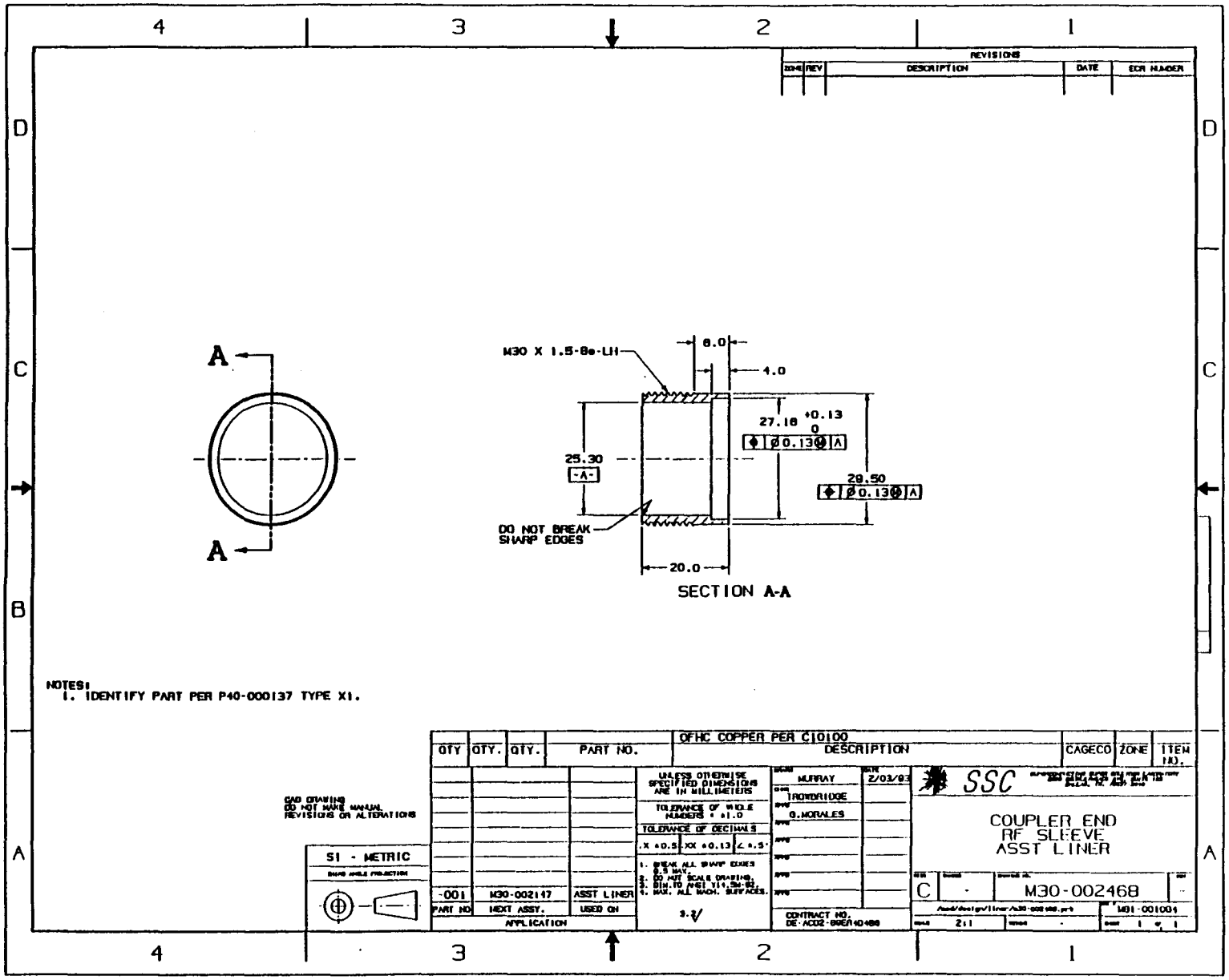

Figure 10.Turnbuckle Sleeve for Quadrupole Liner.

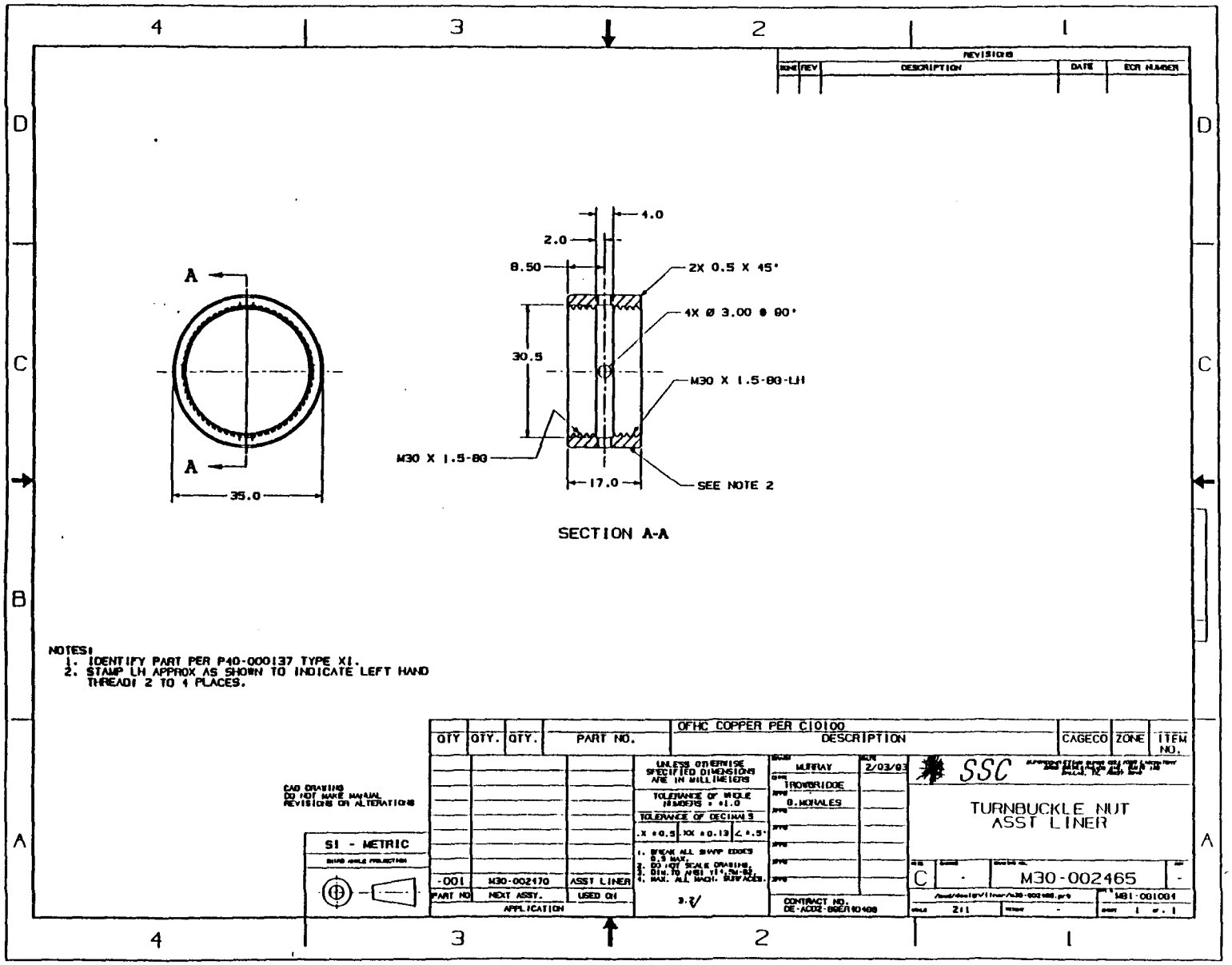

Figure 11. Turnbuckle Nut.

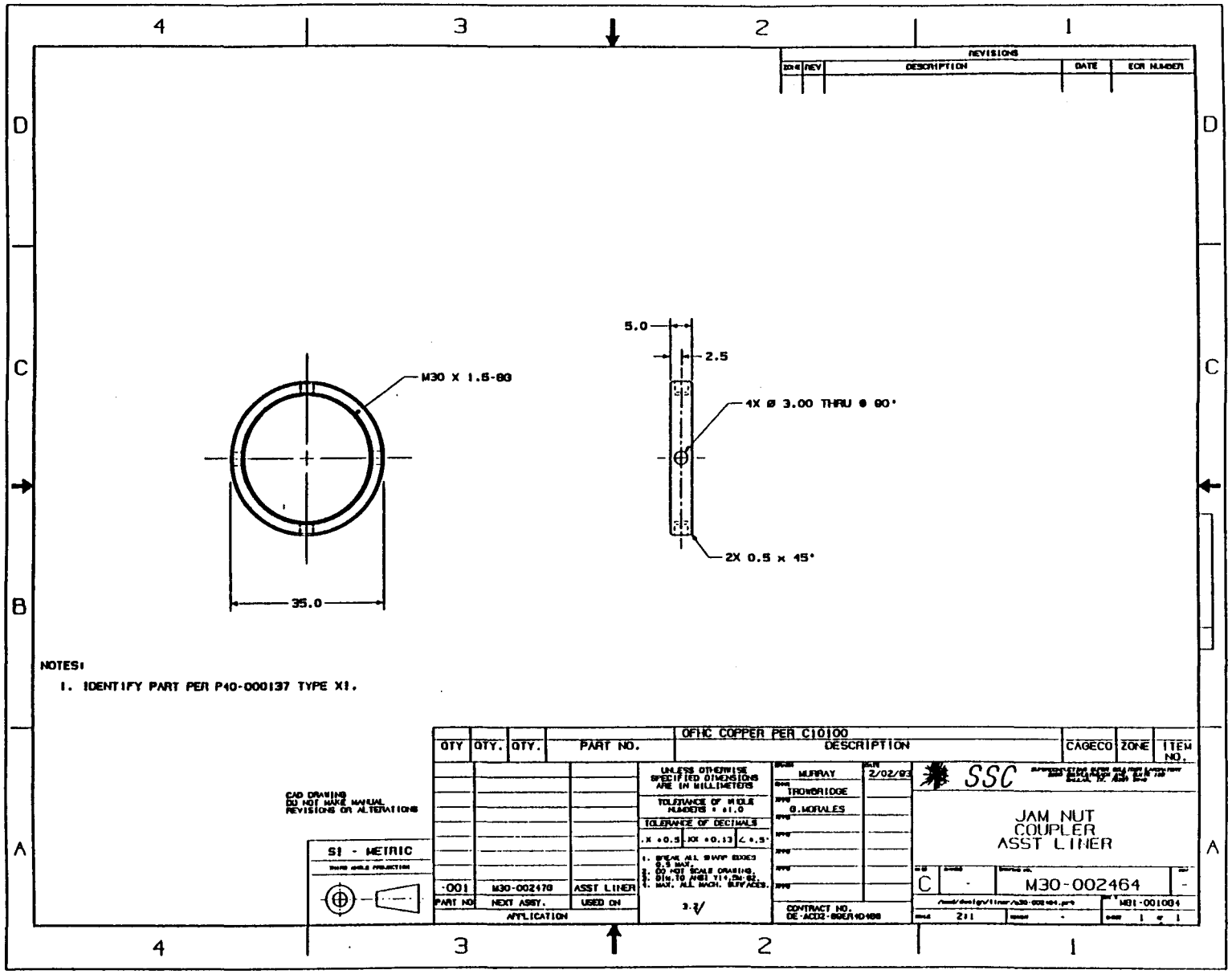

Figure 12. Jam Nut.

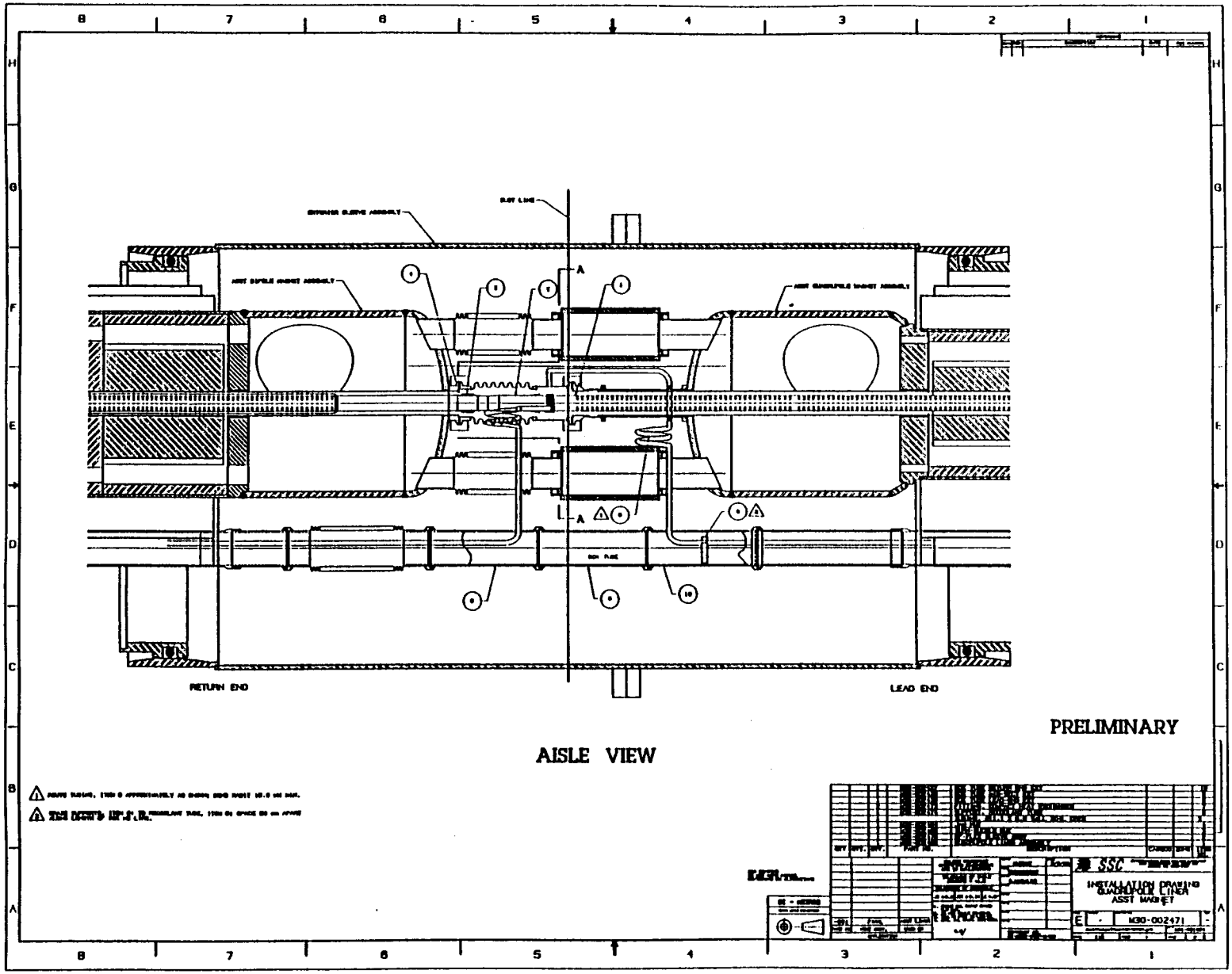

Figure 13. Quadrupole Liner Assembly.

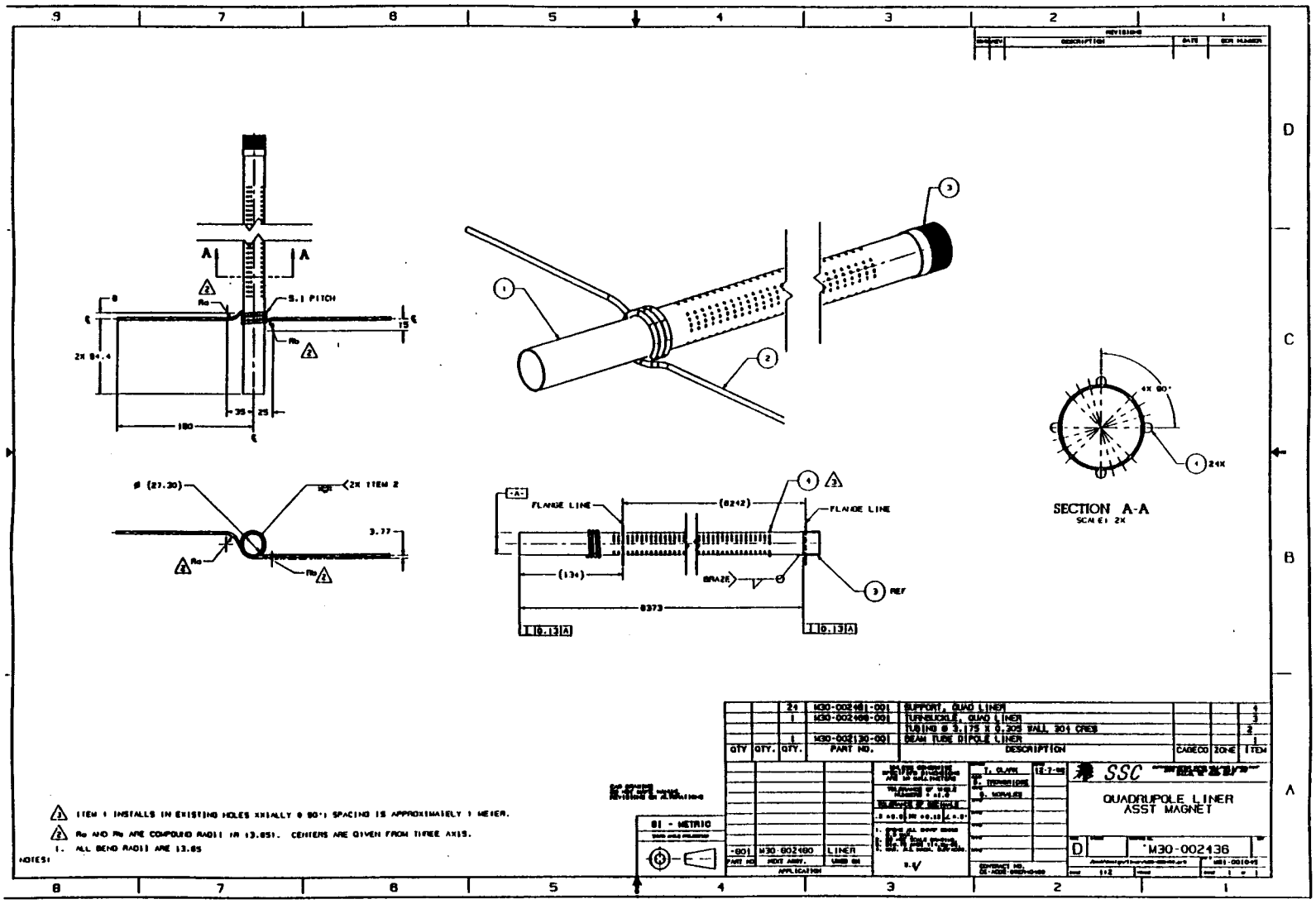

Figure 14. Quadrupole Liner Tube Assembly.

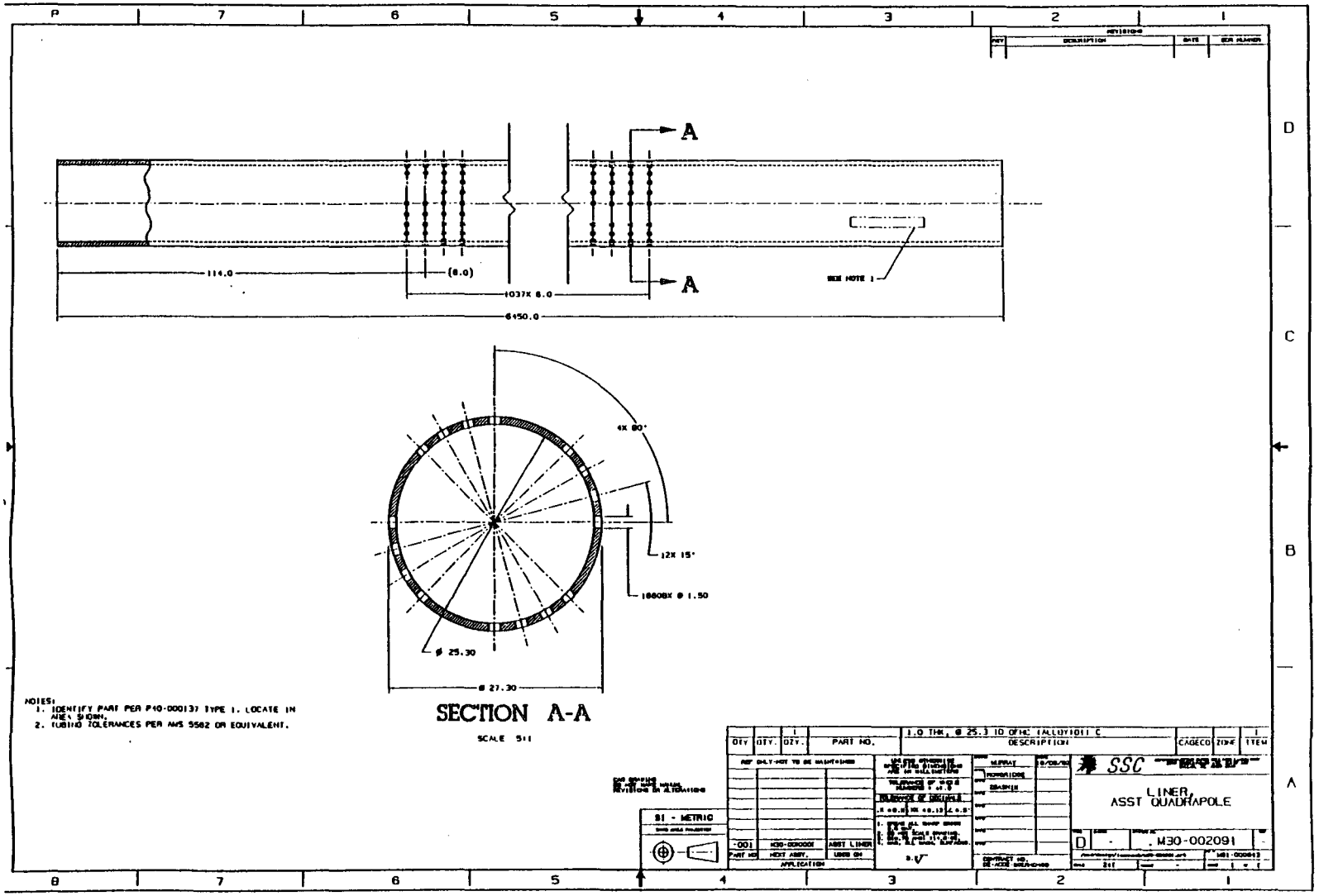

Figure 15. Quadrupole Liner Tube.

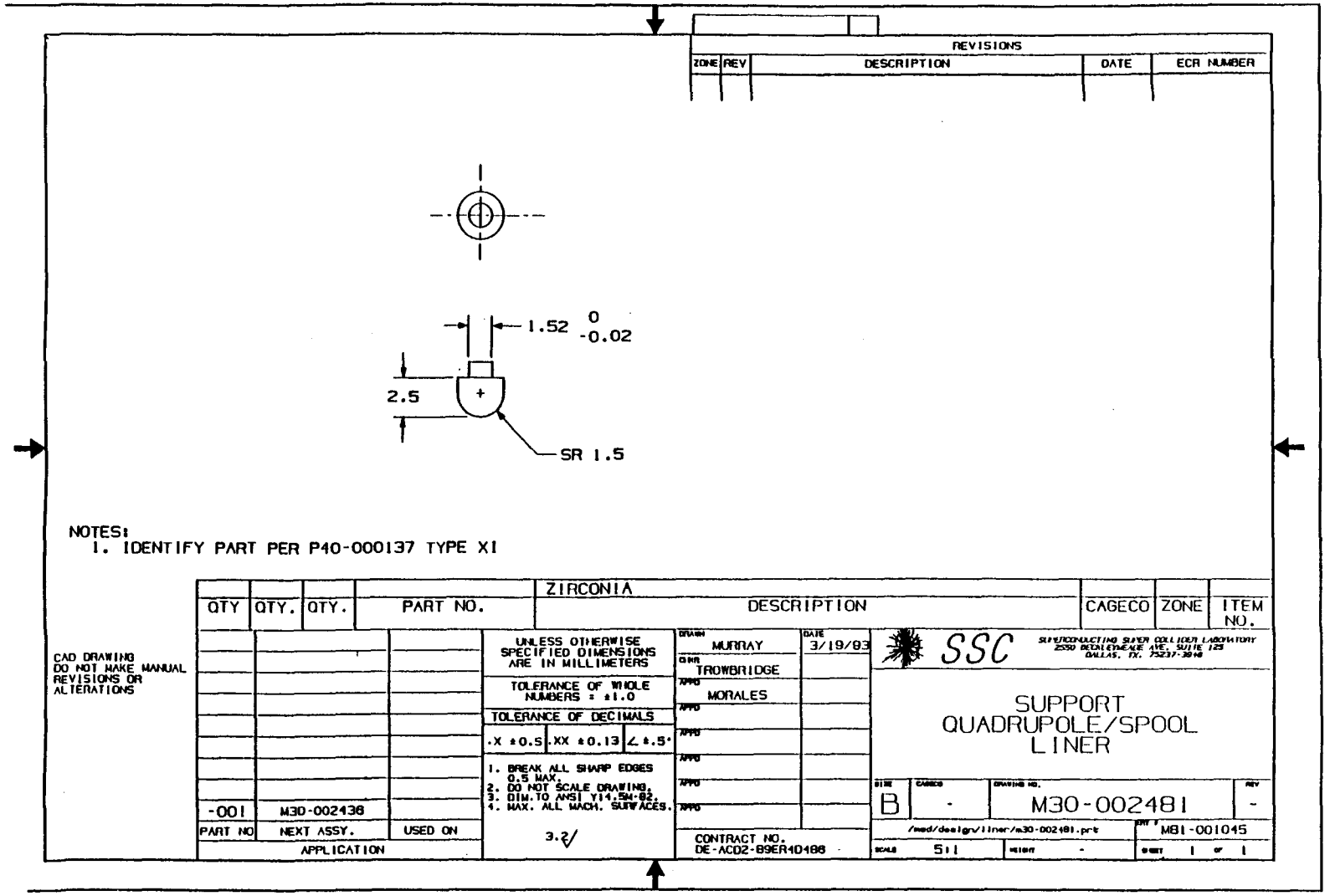

Figure 16. Quadrupole Liner Supports.

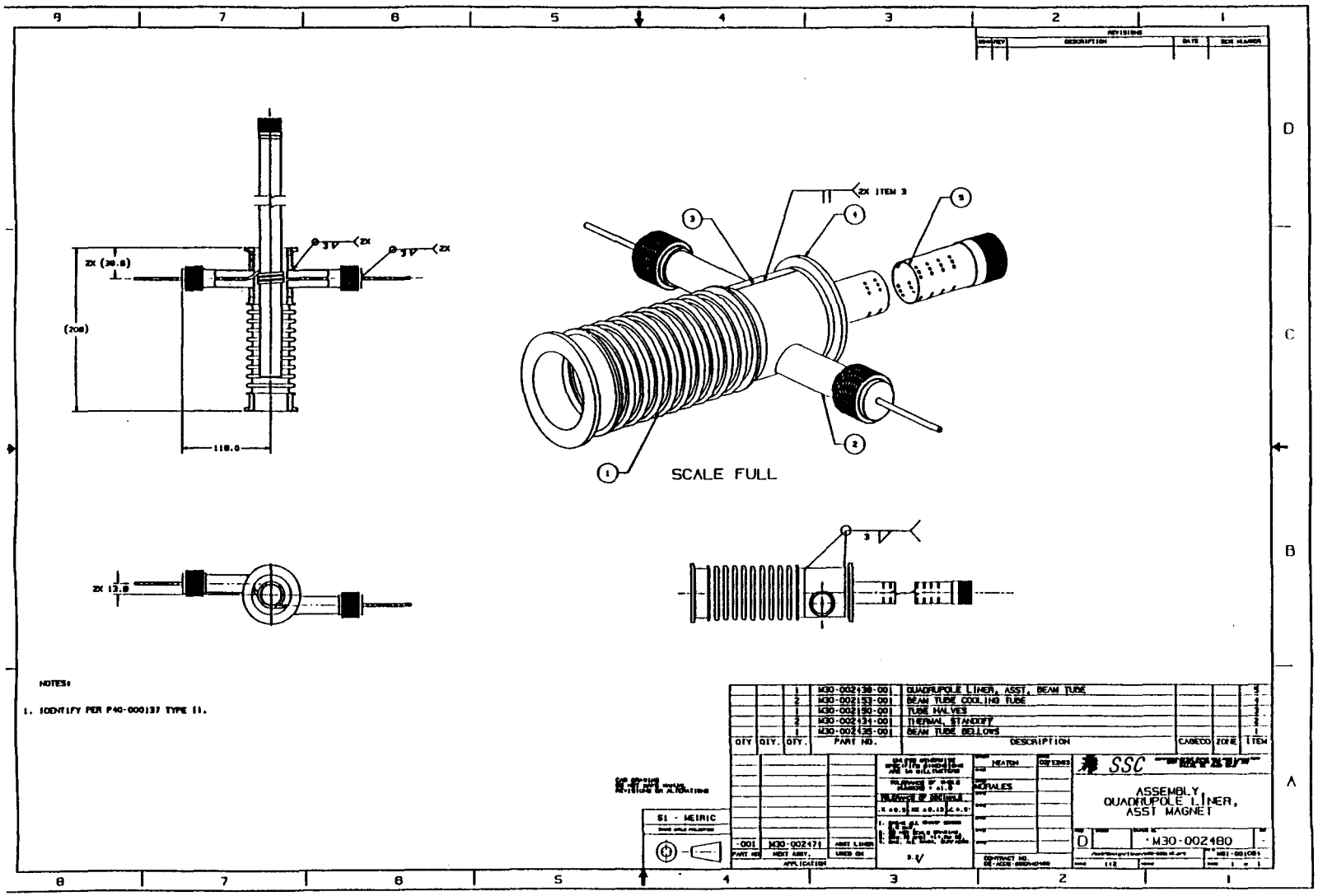

Figure 17. Quadrupole Liner.

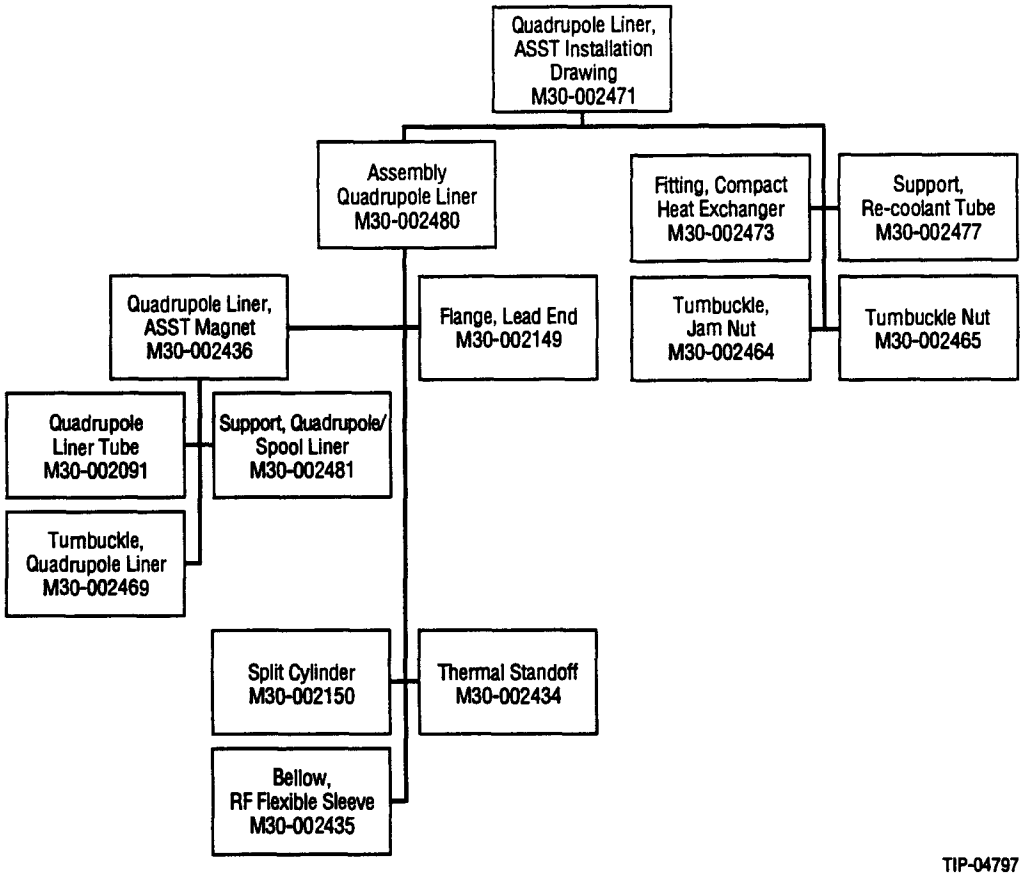

Figure 18. Quadrupole Liner Drawing Tree.

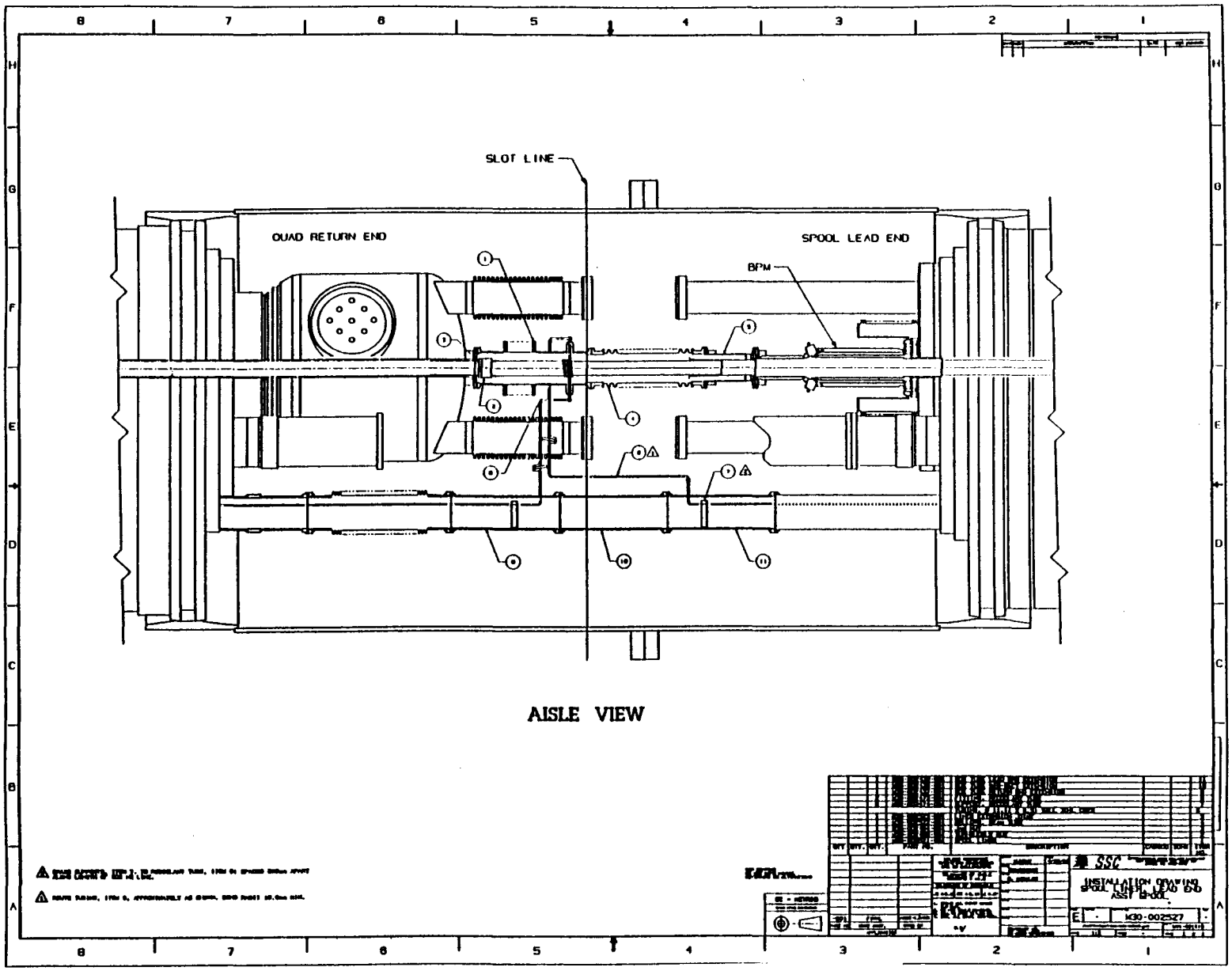

Figure 19. Quadrupole/Spool Liner Interconnect Assembly.

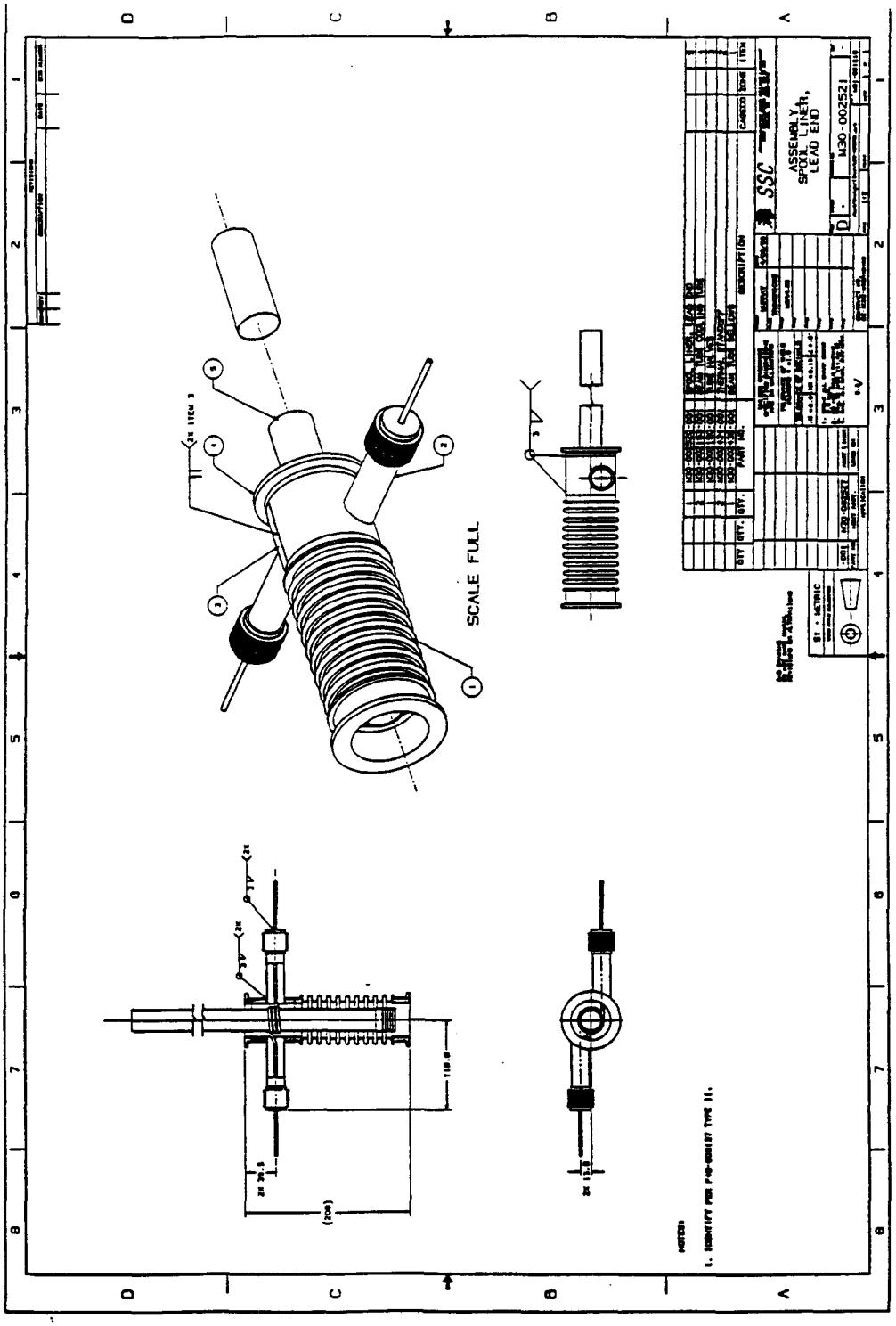

Figure 20. Quadrupole/Spool Liner.

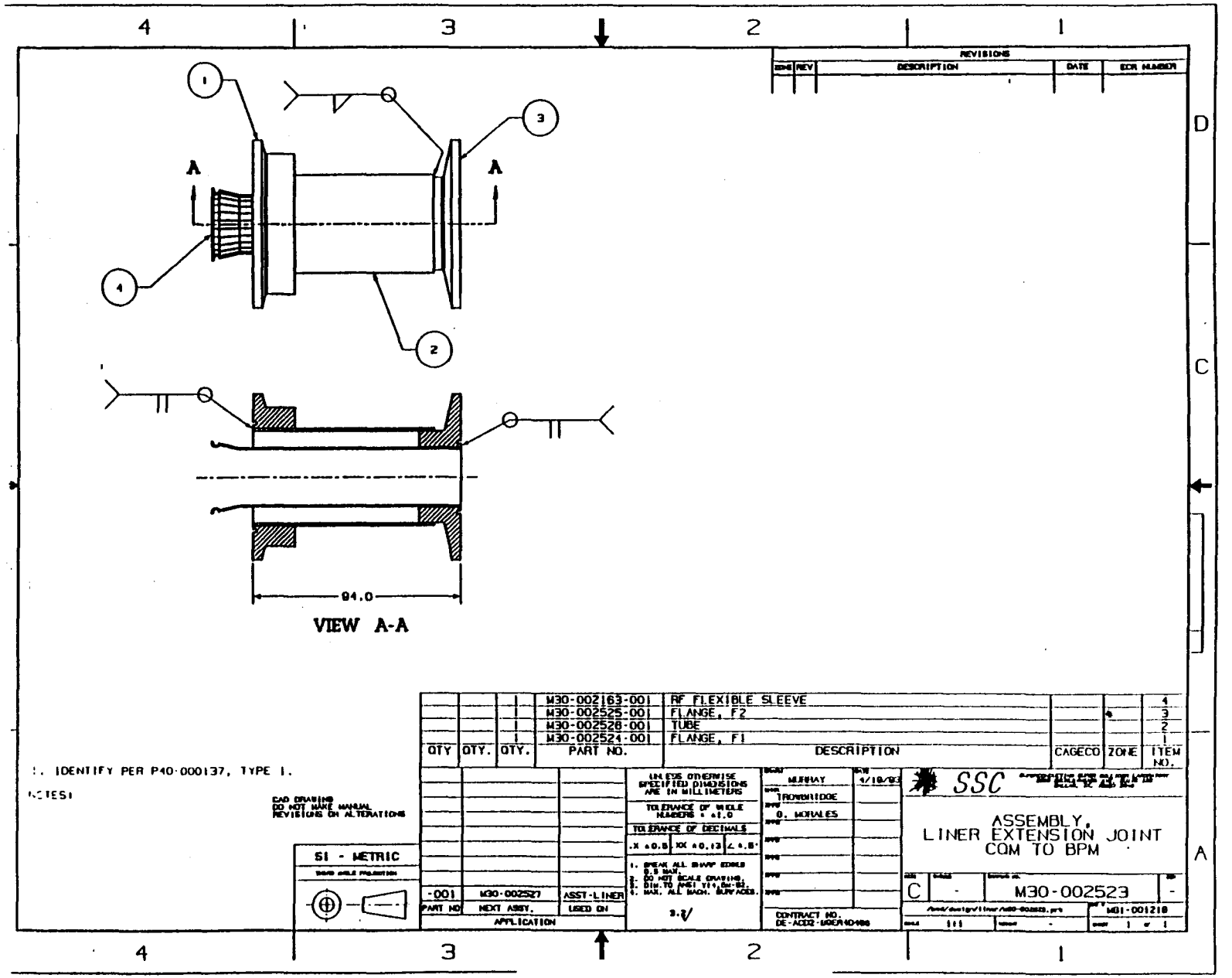

Figure 21. Quadrupole/BPM RF Joint.

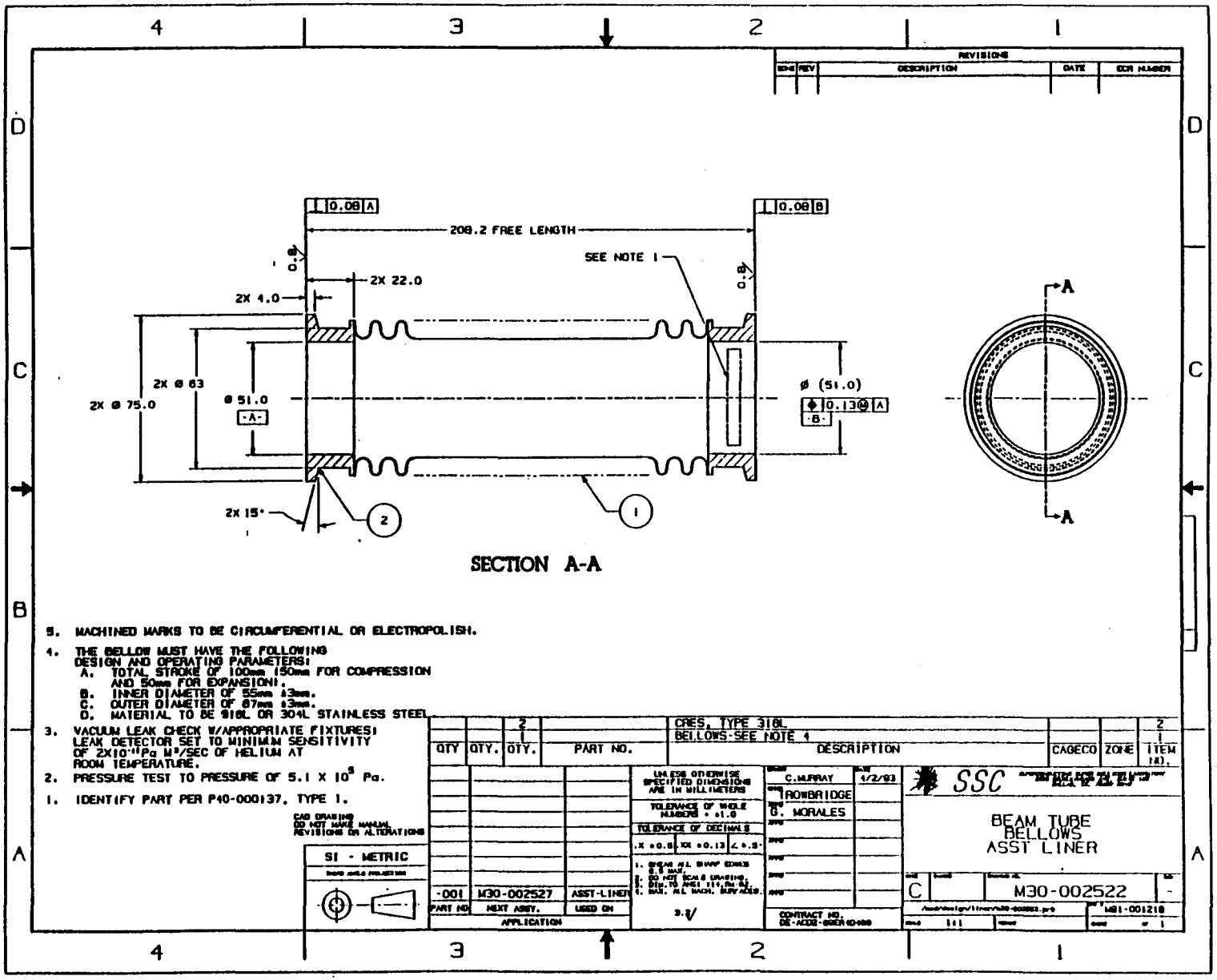

Figure 22. Beam Tube Bellow.

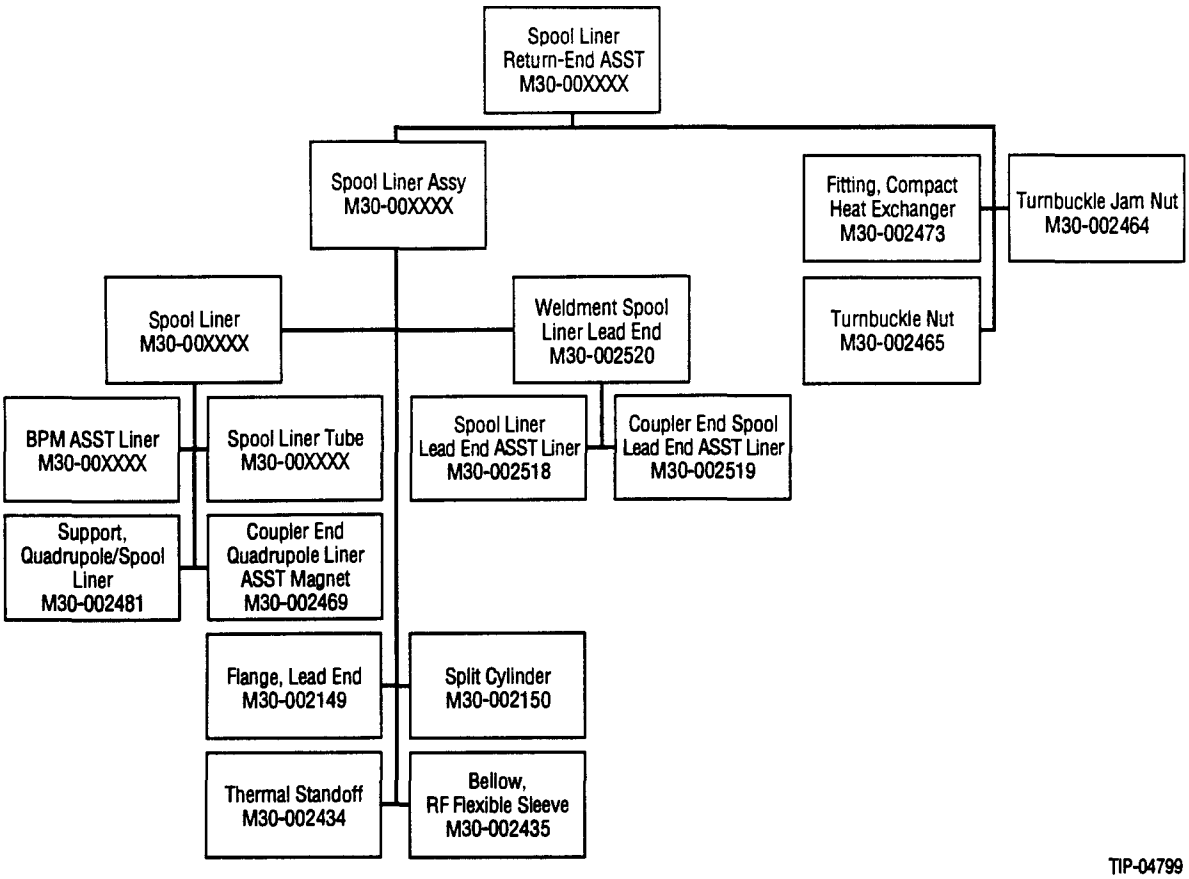

Figure 23. Spool Liner Drawing Tree.

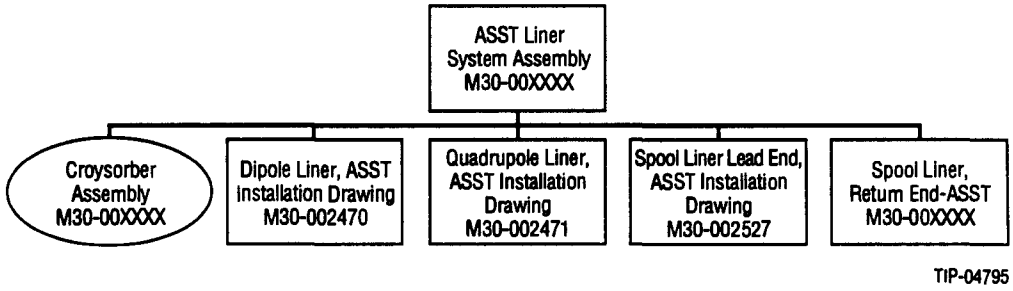

Figure 24. ASST 80 K Liner Drawing Tree.

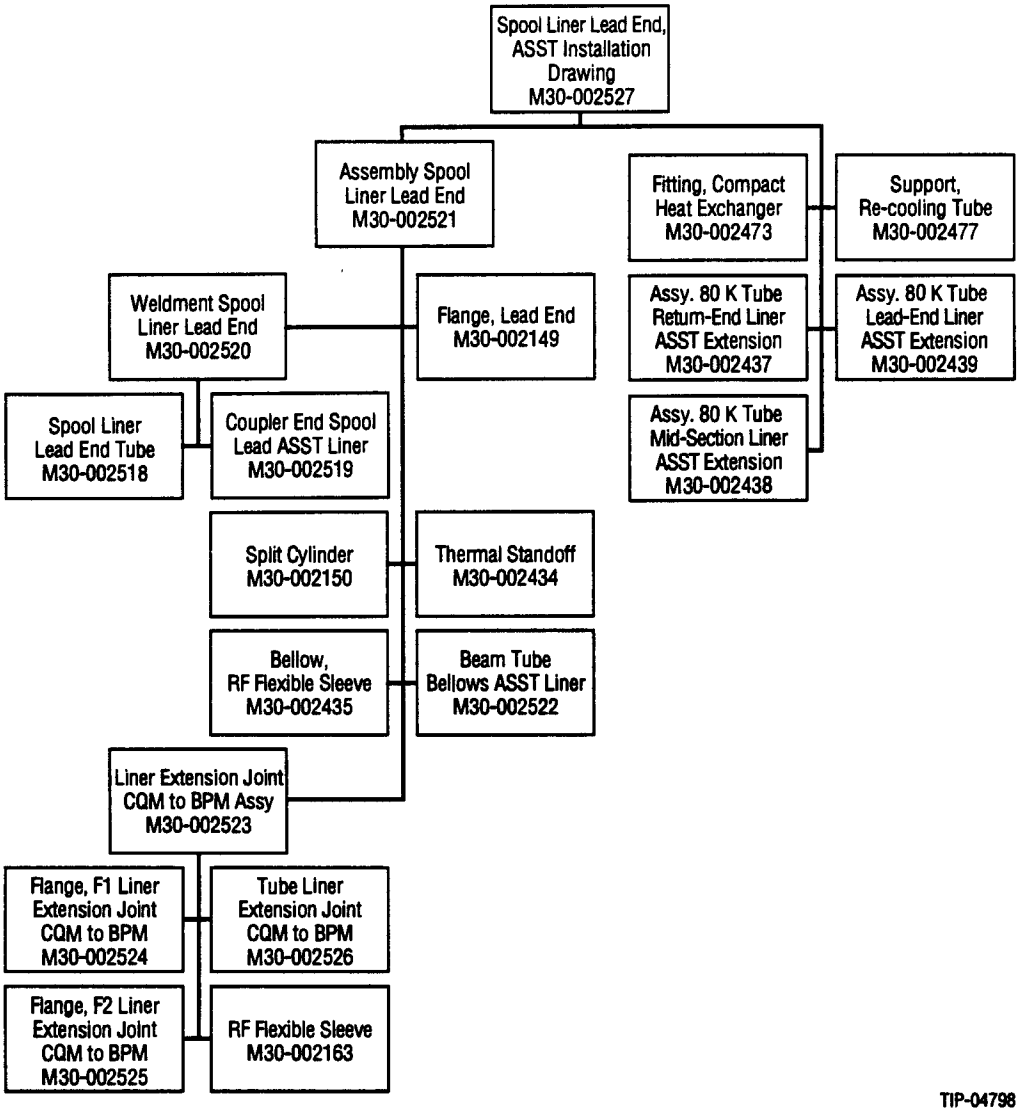

Figure 25. Quadrupole/Spool Section Drawing Tree.

REFERENCES

1. Quan-Sheng Shu, "Design of an 80 K Liner Prototype in SSCL ASST for Synchrotron Light Interception," SSCL-N-818/1 (May, 1993).
2. Quan-Sheng Shu, "Report on the ASST II Liner Status," SSCL-N-805 (November 1992).

This Page Intentionally Left Blank

SECTION 8

Liner Installation into the CDM, CQM, SPXA (SPRA)

D. M. Clark

SECTION 8

Liner Installation into the CDM, CQM, SPXA (SPRA)

Donald M. Clark

Superconducting Super Collider Laboratory*
2550 Beckleymeade Avenue
Dallas, TX 75237

1.0 PURPOSE

The purpose of the liner installation is to identify the components necessary to properly install the 80 K helium liner within the Collider Arc magnets and the specific spool pieces.

2.0 SCOPE

The liner installation is written as if the liner is available during initial magnet installation within the Collider tunnel.

The information presented here identifies how the liner and associated liner components are installed prior to magnet delivery to the Collider tunnel. The details as to identifying specific controlled environments, brazing, welding, cleaning, and vacuum leak checking procedures and processes have purposely been omitted in order to develop direction.

3.0 DEFINITIONS

BPM - Beam Position Monitor located on the lead end of a Spool Piece.

CDM - Collider Dipole Magnet located within the Collider Arc.

CQM - Collider Quadrupole Magnet located within the Collider Arc.

Cryogenic Box - An 80 K heat exchanger incorporating cooling lines, feedthroughs, bellows, RF joint, and flanges that is located on the lead end of the liner.

Liner - A perforated tube placed coaxially inside the bore tube to intercept synchrotron light.

SPRA - Spool Piece with Recooler alternates with the SPXA.

SPXA - Spool Piece without recooler and located adjacent to a CQM.

* Operated by the Universities Research Association, Inc., for the U. S. Department of Energy under Contract No. DE-AC35-89ER40486.

4.0 GENERAL REQUIREMENTS

The following outline presents an overview of the tasks necessary for liner preparation prior to installation within the Collider Arc magnets and Spool Pieces. Also presented is a method by which the liner is installed within the Collider magnets and Spool Pieces.

5.0 LINER INSTALLATION INTO THE CDM, CQM, SPXA (SPRA)

5.1 CDM Liner Installation

1. The liner cryogenic box with 80 K helium cooling tubes shall be installed on the liner prior to installation within the CDM. The cryogenic box installation shall include the demountable joint seals.
2. CDM Liner Installation:

   Insert liner into bore tube from the CDM lead end and slowly slide liner into the bore tube. Liner shall protrude through ends of the CDM.

   Note: Liner shall be supported prior to and during installation to prevent bowing in excess of 25 millimeters in amplitude.
3. The liner shall be installed within the CDM prior to the CDM being positioned within the Collider Arc.

5.2 CQM Liner Installation

1. The liner cryogenic box with 80 K helium cooling tubes shall be installed on the liner prior to installation within the CQM. The cryogenic box installation shall include the demountable joint seals.
2. CQM Liner Installation Procedure:

   Insert liner into bore tube from the CQM lead end and slowly slide liner into the bore tube. Liner shall protrude through ends of the CQM.

   Note: Liner shall be supported prior to and during installation to prevent bowing in excess of 25 millimeters in amplitude.
3. The liner shall be installed within the CQM prior to the CQM being positioned within the Collider Arc.

5.3 Spool Piece Liner Installation

1. The BPM diameters shall be consistent with the 80 K liner. The BPM shall be attached to the liner prior to the installation of the BPM to the lead end plate of the SPXA (SPRA).
2. SPXA (SPRA) Liner Installation:

   Insert liner into bore tube from the SPXA (SPRA) lead end and slowly slide into the bore tube until the BPM is properly fitted against the Spool Piece lead end plate.

   Note: Liner shall be supported prior to and during installation to prevent bowing in excess of 25 millimeters in amplitude.
3. Secure BPM to the Spool Piece lead end plate.

4. The liner cryogenic box with 80 K helium cooling tubes and differential bellows shall be installed on the liner. The cryogenic box installation shall include the demountable joint seals.
5. The SPXA (SPRA) liner shall be installed prior to the Spool Piece being positioned within the Collider Arc.

6.0 DETAILED REQUIREMENTS

The following outline presents a detailed of tasks necessary for the final installation and closing of the liner within the Collider magnets and Spool Piece bore tubes at the Interconnect Regions.

7.0 FINAL INSTALLATION OF CDM, CQM, SPXA (SPRA) LINERS WITHIN THE COLLIDER ARC INTERCONNECT REGIONS

7.1 CDM Liner Final Installation

1. Install and align CDM.
2. Make flange connections of the demountable joint between the cryogenic box lead end and the CDM bore tube return end flange or the SPXA (SPRA) pumpout port tee flange.
3. Ensure liner is positioned within RF Joint and that the liner is free to move in the axial direction as the bellows of the cryogenic box is compressed.
4. Secure RF joint to liner.
5. Make flange connections of the demountable joint between the return end of the cryogenic box and the differential bellows.
6. Make 80 K helium cooling tube connections.
7. Complete all remaining interconnects of the CDM.
8. Repeat steps **5.2.1** through **5.2.7** for the concatenation of the CDM and the SPXA (SPRA).

7.2 CQM Liner Final Installation

1. Install and align CQM.
2. Make flange connections of the demountable joint between the cryogenic box lead end and the CDM bore tube return end flange.
3. Ensure liner is positioned within RF Joint and that the liner is free to move in the axial direction as the bellows of the cryogenic box is compressed.
4. Secure RF Joint to liner.
5. Make flange connections of the demountable joint between the return end of the cryogenic box and the differential bellows.
6. Make 80 K helium cooling tube connections.
7. Complete all remaining interconnects of the CQM.

7.3 (SPXA) Liner Final Installation

1. Install and align SPXA (SPRA).
2. Install Spool Piece cryogenic box/BPM differential bellows.
3. Make flange connections of the demountable joint between the cryogenic box lead end and the CQM bore tube return end flange.
4. Ensure liner is positioned within RF Joint and that the liner is free to move in the axial direction as the bellows of the cryogenic box is compressed.
5. Secure RF Joint to liner.
6. Make flange connections of the demountable joint between the return end of the Spool Piece cryogenic box/BPM differential bellows and BPM lead end flange.
7. Make 80 K helium cooling tube connections.
8. Complete all remaining interconnects of the SPXA (SPRA).

8.0 RESPONSIBILITIES

The structure set forth in the tasks outlined in this liner installation shall be implemented for all documentation regarding liner installation.

It will be the responsibility of the Liner System Design Task Force Committee to provide all detailed information on the liner and specific liner components and the suggested methods for the installation of the liner within the Collider Arc magnets and Spool Pieces.

REFERENCES

E10-000027 ELEMENT SPECIFICATION (Level 3B)
Collider Accelerator Arc Sections

CHAPTER 4

RESULTS AND PLANS FOR ENGINEERING TESTS

SECTION 1

Magnetoresistance of SSC Beam Tube Samples

V. T. Kovachev, M. J. Neal, J. Zbasnik, and M. Tuli

SECTION 1

Magnetoresistance of SSC Beam Tube Samples

V. T. Kovachev, M. J. Neal, , M. Tuli, P. G. Cline,
F. Y. Clark, Q. S. Shu, and J. M. Seuntjens

Superconducting Super Collider Laboratory*
2550 Beckleymeade Ave.
Dallas, TX 75237-3997

J. Zbasnik

Lawrence Livermore Laboratory
P. O. Box 808
Livermore, CA 94550

1.0 INTRODUCTION

The beam tube for the Superconducting Super Collider (SSC) is required to have an inner surface of sufficiently high dc electrical conductivity in order to satisfy beam stability requirements. This high conductivity surface will also help to reduce the parasitic heating of the beam tube due to image currents and may have a positive effect on the beam tube cryogenic budget.[1] The SSC specification on beam tube conductivity is related to the inner diameter; for diameters of technical interest the product of dc electrical conductivity and thickness (σt) should be in the range of $1–2\times10^5\ \Omega^{-1}$ under operating conditions, which include a transverse magnetic field in the range of 7 T.

A competing factor to be considered is that in case of a dipole quench the collapsing field induces eddy currents in the layer, which interact with the collapsing magnetic field, causing large forces and stresses in the beam tube. This requires that the layer be as thin as possible in order to keep the stresses in the beam tube at an acceptable value.

This paper will cover measurements of the dc electrical resistivity with and without transverse magnetic field on samples of stainless steel tubes with inner coatings of copper as well as copper with a thin gold overlay. These samples were produced by different vendors by electroplating with some variations in layer thickness, and post-deposition heat treatment.

These measurements are part of an ongoing experimental program to determine the suitability of these copper-lined stainless steel tubes for use as the proton beam chamber in the SSC. Although in the baseline design the beam tube is cooled to 4.2 K by the supercritical helium used to cool the superconducting magnets, an optional design was considered for reasons unrelated to resistivity, which required the beam tube to be operated at about 80 K. The 77 K measurements reported here were taken to obtain design data for this option.

*Operated by the Universities Research Association, Inc., for the U.S. Department of Energy under Contract No. DE-AC35-89ER40486.

2.0 EXPERIMENTAL DETAILS

The experiment was performed in two phases. Based on discussions with researchers from the National Institute for Science and Technology (NIST)[2] two sample configurations were identified for magnetoresistance measurements. In phase 1, measurements were performed at 4.2 K to determine which configuration would be a more suitable and cost-effective method for an extensive series of follow-on qualification tests. Table 1 lists the samples used in the phase 1 measurements, along with their copper layer thicknesses and post-deposition heat treatments.

TABLE 1. SAMPLES USED IN PHASE 1.

Vendor	Sample ID	Cu Layer Thickness	Heat Treatment
A	Cu-SI-0	50 μm	1 h @190°C
B	Cu-FL-0	38 μm	1 h @230°C

Figure 1 is a tracing taken from a scanning electron micrograph of a typical elecroplated copper layer. In all cases the stainless steel tube is an austenitic ASTM type XM11 with an inner diameter of 32.3 mm and a wall thickness of 1.2 mm. This material is proposed for use in the collider quadrupole magnets, while the current collider dipole design uses type 304LN steel.

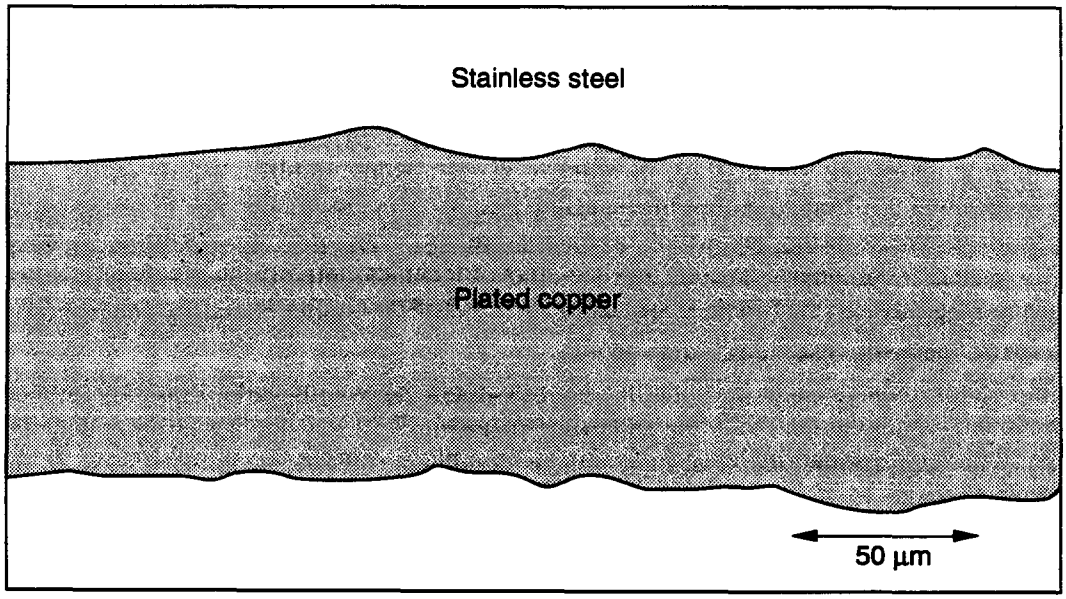

Figure 1. Tracing of a Typical Copper Layer Electrodeposited onto a Stainless Steel Beam Tube.

The first sample configuration is a slit tube, in which 5–10 mm wide rings are sliced from the vendor-supplied beam tube by machining in a lathe. A longitudinal slice is then cut in it to allow the current to flow circumferentially around the ring. A four terminal technique was used in the measurements, in which the sample current was introduced and extracted from the ends of the slit ring specimen (100 mm long), and the voltage is measured over a center 90 mm long section. The 100 mA current was supplied by a LakeShore 120 Current Source, and the voltage was measured using a Hewlett Packard 3458A microvoltmeter.

The second sample configuration was an unslit piece of tube, wherein the current travels axially down the tube. A 35 mm long sample was cut from the vendor-supplied tube by either machining in a lathe or by

diamond sawing. A four-terminal technique was also used in these measurements. A 12 A current was introduced and extracted from the ends of the 35 mm long tubular specimen using a Kepco power supply. The voltage was measured over a center 20 mm-long section using the same Hewlett Packard voltmeter as above. A copper-stabilized NbTi superconductor current lead was soldered around the entire circumference at each end of the tube to provide a uniform current distribution. The voltage taps are 22 gauge copper, soldered circumferentially inboard of the current leads with 60/40 SnPb solder. Polyimide tape was used during the lead attachment to confine the solder.

Phase 2 measurements were carried out at 4.2 and 77 K. For reasons described below only the unslit configuration was used. Again the four-terminal technique was used. To enhance the signal-to-noise ratio measurement, currents of up to 50 A were supplied using a Hewlett Packard 6031A System power supply. The effect of thermal voltages was eliminated by measuring the voltage drop in both current polarities and averaging the result. A Keithley 182 Sensitive Digital Voltmeter was used to measure the voltage drop. The best results were obtained using a 30-A measurement current and the statistical averaging mode of the Keithley voltmeter. In this mode both the digital and analog intrinsic filters are disabled, and a set of 500 voltage readings are stored in a buffer over a period of approximately 30 s. The average voltage and standard deviation were recorded. In order to provide equally uniform current distribution for both 4.2 and 77 K measurements, a large rectangular cross section MRI-type NbTi monofilamentary conductor was used. This conductor has approximately a 3.75 mm^2 cross section and a Cu:SC ratio of 3.7. The measurement current can then be uniformly distributed by the large copper cross section at 77 K and by the superconductor at 4.2 K. Current was introduced to this superconducting current lead at four equidistant points to further ensure a uniform current distribution. Table 2 lists the samples used in phase 2 along with their copper layer thicknesses and post-electrodeposition heat treatments.

TABLE 2. SAMPLES USED IN PHASE 2 MEASUREMENTS.

Vendor	Sample ID	Cu Layer thickness	Heat Treatment
A	Cu-SI-1	109 μm	1 h @ 260°C
A	CuAu-SI-1	108 μm + 2 μm Au	2x1 h @ 190°C
A	Cu-SI-2	97 μm	1 h @ 190°C
B	Cu-FL-0	38 μm	1h @ 230°C
A	Cu-SI-DD	100 μm	Unknown

All magnetoresistance measurements described above were carried out in a solenoid field up to 8 T with the magnetic field perpendicular to the tube axis. The magnetic field was obtained using a 15 T superconducting solenoid magnet with 64 mm aperture, produced commercially by Oxford Instruments, Inc. For the 4.2 K measurements the samples were simply immersed in the magnet helium bath, and for the 77 K measurements the samples were immersed in a liquid nitrogen bath contained in a vacuum-insulated finger inserted into the magnet bore.

3.0 RESULTS AND DISCUSSION

Phase 1 resistance measurements were performed on the tubes listed in Table 1 to assess the differences between the two sample configurations and to check out the procedures. A correction for the parallel resistance of the stainless steel was applied to the measured resistance values in order to obtain the contribution due to the copper. This value is significant at room temperature, much less significant at 77 K, and practically negligible at 4.2 K. The measured resistance, R_T, was taken as the resultant of the resistances of the steel tube and the copper coating in parallel. The resistance of the steel, R_{SS}, was calculated using handbook values for austenitic stainless steel resistivity at 273 K (7.4×10^{-7} Ωm) and 77 K (5.3×10^{-7} Ωm), and the resistance of the copper coating, R_{Cu}, calculated using $R_{Cu} = (R_T * R_{SS}) /$

(R_T - R_{SS}). For the Cu-FL-0 specimen the measured Residual Resistance Ratio (RRR = $R_{273}/R_{4.2}$) for the slit configuration was lower (RRR = 80) than for the unslit tube (RRR = 160). This is evidence that the machining operations needed to prepare the specimen may result in mechanically deforming a significant volume of copper in the measurement path and thereby underestimating the actual RRR value. In the case of the unslit tube, the material between the electrodes is untouched, so no degradation in apparent RRR value is expected. As a result of these measurements the unslit configuration was adopted for phase 2. The unslit configuration also provides a better approximation to the operating conditions for the collider beam tube since the current is along the tube axis and perpendicular to the magnetic field, as is the case with the particle image currents and induced eddy currents in the collider dipoles.

Experimental results for phase 2 magnetoresistance measurements are presented in Table 3. The measurements on several samples were duplicated in order to assess the repeatability of the results. The estimated error in reporting both RRR and $\Delta R/R_0|_{4.2K}$ (ΔR is R_B - R_0) is approximately ± 10%. The error is due in part to variations in Cu coating thickness and to the sample geometry which requires high measurement current and yields low voltage differences. In addition the calculation of R_{Cu} at 273 K described previously may introduce an error, since actual resistivity values may differ from the handbook values, or average thicknesses of copper or steel may differ from the measured thicknesses used in the calculations. In general RRR values are consistent with post deposition heat treatment. Samples Cu-SI-1, however, have a range of RRR values that exceed experimental error. The reason for this could be inhomogeneity in the copper deposition process or in the post deposition heat treatment, since these three samples were cut from different locations of a single 6 m long beam tube. Further study is required to pursue this possibility. The fractional change in resistance, $\Delta R/R_0$, is consistent with RRR data with the exception of sample Cu-SI-1-M3, which shows low $\Delta R/R_0$ and an unrealistically high value of σt.

TABLE 3. RESULTS OF PHASE 2 BEAM TUBE MEASUREMENTS.

Sample ID	RRR	RR (77K)	$\Delta R/R_0$	$\Delta R/R_0$ (7T,77K)	st, Ω^{-1} (7T,4.2K)
Cu-SI-1-M1	170	6.7	5.7	0.11	1.81E+5
Cu-SI-1-M2	88	6.7	3.4	0.21	1.43E+5
Cu-SI-1-M3	126	7.5	2.3	0.06	2.65E+5
Cu-SI-2-M1	65	7.3	2.4	0.20	1.18E+5
Cu-SI-2-M2	60	6.8	1.8	0.07	1.35E+5
CuAu-SI-1-M1	240	6.7	8.1	0.13	1.87E+5
CuAu-SI-1-M2	207	6.4	8.4	0.14	1.53E+5
Cu-SI-DD	269	6.1	12.0	0.12	1.33E+5

Tracings of micrographs of polished copper layers of samples taken from beam tubes Cu-SI-2 and Cu-SI-DD are shown in Figure 2. There is an obvious correlation between the RRR values in Table 3 and the microstructures of these samples. The RRR differences are most likely due to the grain size difference. In the case of small heat treatment differences (*e.g.*, samples Cu-SI-1 and Cu-SI-2) there is a less noticeable grain size difference. It is likely that RRR improvement is due primarily to lattice defect annihilation. According to one manufacturer, the heat treatments described in Table 2 were given primarily to drive off hydrogen and other gases that were trapped in the deposited layer. Trapped hydrogen could affect RRR differences if it was incorporated into the crystal lattice during deposition and then escaped during heat treatment. Exact determination of the major factors driving this is out of the scope of the present work and requires further study.

Figure 3 demonstrates the correlation between $\Delta R/R_0$ at 8 T, 4.2 K and RRR of samples measured in phase 2. Data from samples cut from the same tube are represented by a common symbol shape with individual

samples differentiated from one another by different symbol fill patterns. The property variations discussed in the previous paragraphs can be seen in Figure 3. This data also shows that the 2-μm-thick gold flash of samples CuAu-SI-1 do not degrade the conductivity of the layer. The heat treatment was not sufficient to cause interdiffusion of gold and copper.

The error in RR and $\Delta R/R_0$ at 77 K is of the order of the values calculated. For this reason a cross correlation between RR_{77K} and $\Delta R/R_0|_{77K}$ and 4.2 K data cannot be made. The practical result from the 77 K data is that the $\Delta R/R_0$ is no more than about 20%.

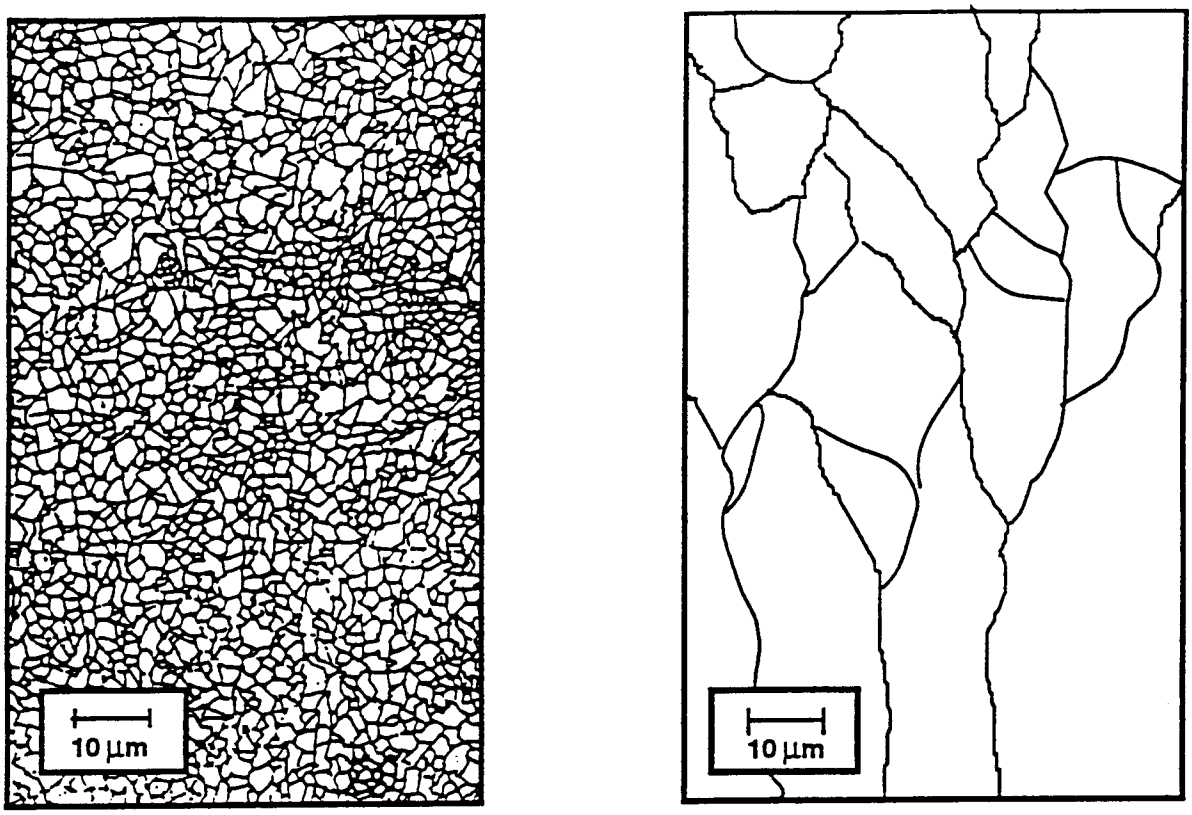

a) Sample Cu-SI-2

b) Sample Cu-SI-DD

Figure 2. Tracings from Micrographs of the Copper Layers of Beam Tubes having Relatively Small (Figure 2a, Sample Cu-SI-2) and Large (Figure 2b, Sample Cu-SI-DD) RRR Values. The Cu-SS Interface is in the direction of the top of the page in both tracings.

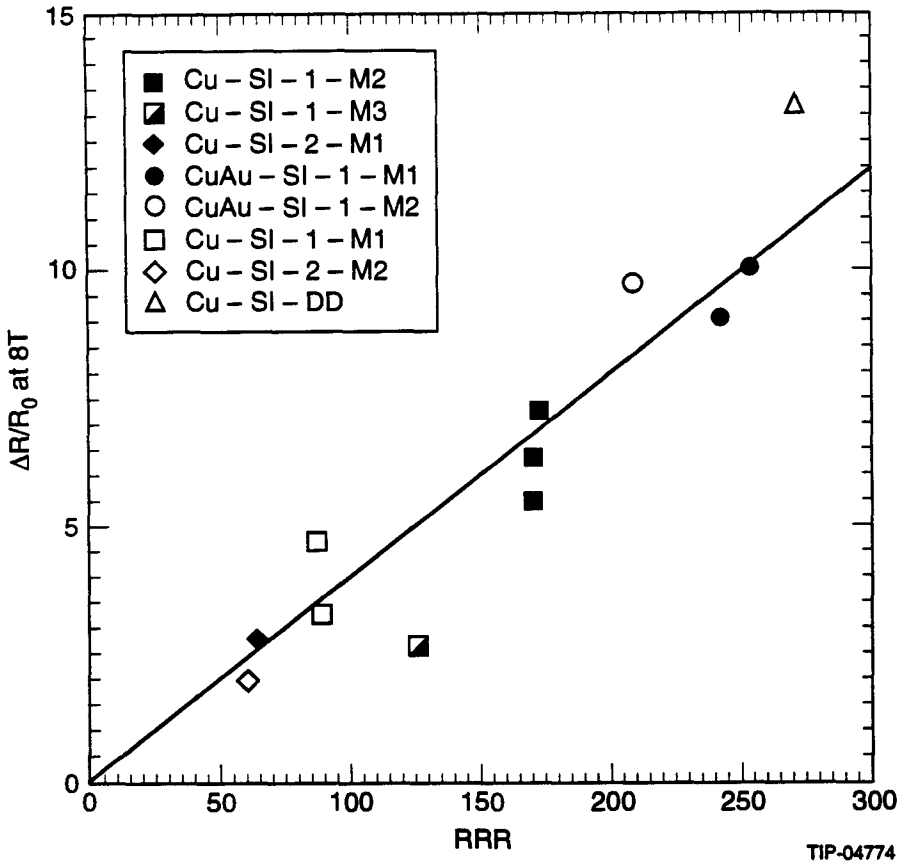

Figure 3. Fractional Change in Resistance at an Applied Field of 8 T as a Function of RRR for all Phase 2 Samples at 4.2 K.

The sample designated as Cu-SI-DD in Table 3 is from a beam tube that was placed in a long (17 m) superconducting dipole, designated as DD0028, that was subjected to a compre-hensive testing program. The magnet was subjected to 12 cooldowns from room temperature to 4.2 K, 81 quench cycles, and 860 power cycles. This represents approximately 10% of the expected lifetime of the magnet. Apparently thermal, quench, and power cycling have little effect on the beam tube RRR. It has been speculated that repeated cooldowns may cause thermal strain buildup due to thermal contraction coefficient mismatch between the conducting layer and the substrate, and that the interaction between the quench current induced in the conducting layer and the dipole field may cause large stresses in the beam tube. There is no evidence of stress buildup in either the resistivity or the microstructure (see Figure 2) due to the imposed operational conditions. The results of the measurements at 4.2 K and 77 K and at fields of 1–8 T are presented in Figure 4, and are compared with the upper and lower limits of magnetoresistance data compiled by NIST[3] (solid lines). The logarithmic plot of fractional resistance change, $\Delta R/R_0$, and the RR × B product (in Tesla) is a standard Kohler plot. Our data are in general within the NIST uncertainty band and are in agreement with Kohler's rule. For RR × B values greater than about 30 there is some data slightly above the NIST upper limit.

In Figure 5 the conductivity-thickness product (σt) criterion is plotted as a function of magnetic induction for two samples with different RRR values. As expected, the σt criterion difference at fields above 6 T is rather small. The large RRR does not provide significant enhancement of σt.

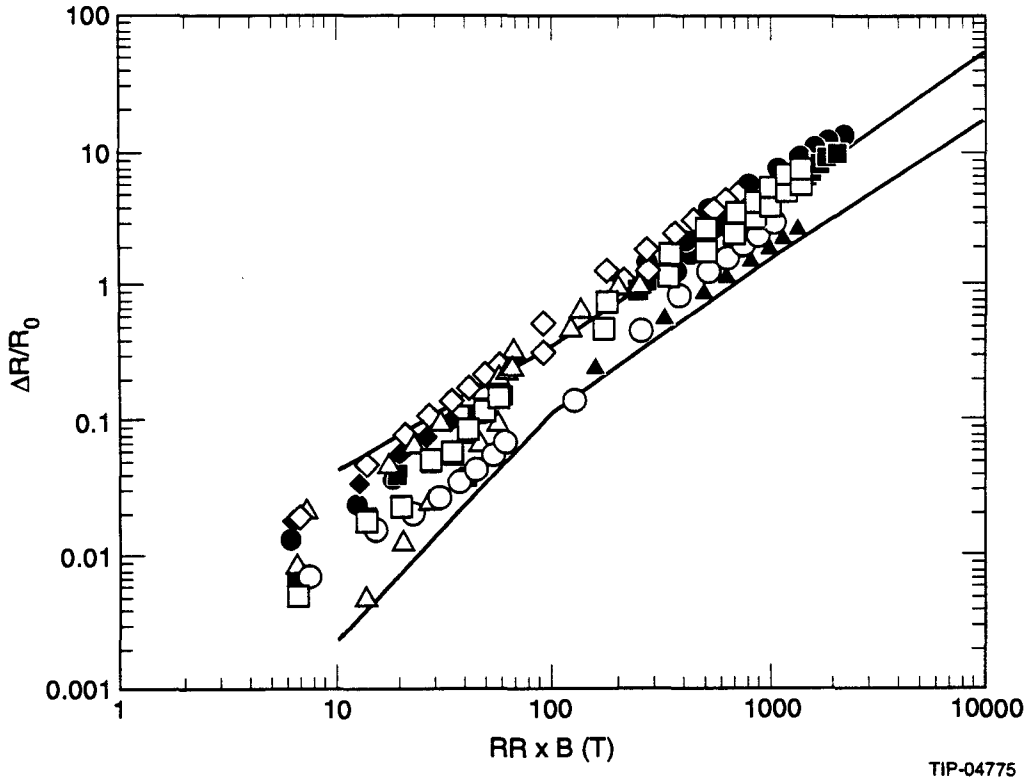

Figure 4. Fractional Change in Resistance as a Function of the Product of the Residual Resistance and Magnetic Induction (Kohler Plot) for all Samples Measured in Phase 2 at 4.2 K and 77 K.

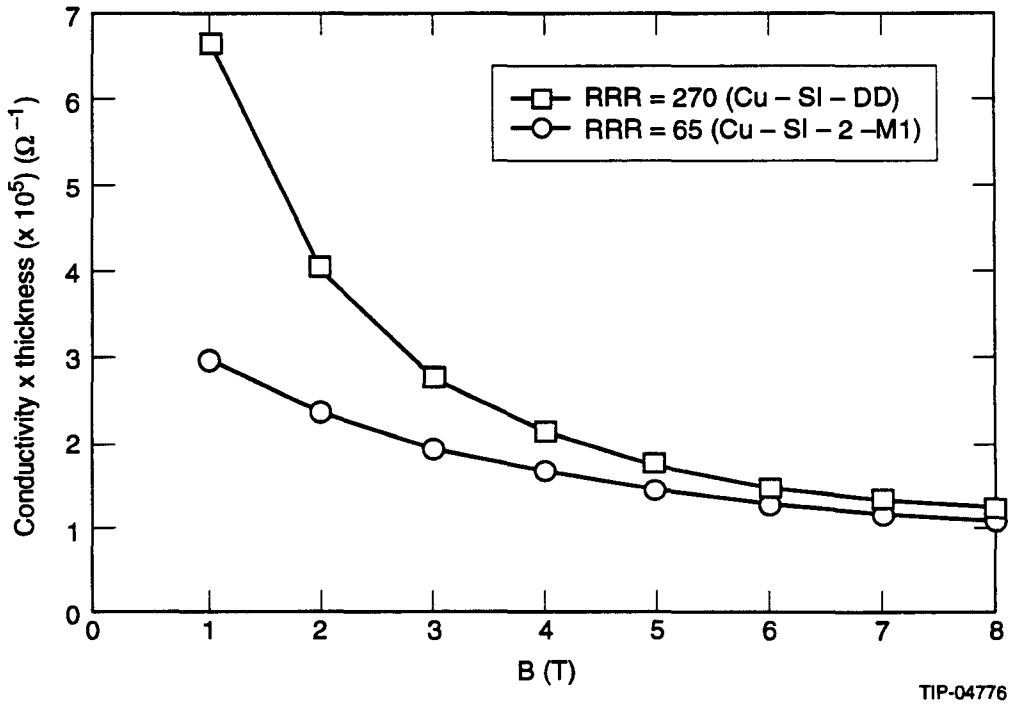

Figure 5. Product of DC Conductivity at 4.2 K and Copper Layer Thickness (σt) as a Function of Magnetic Induction.

4.0 CONCLUSION

It is certain that the deposition technology, the post-deposition heat treatment, and thickness can be optimized further to determine the most suitable and cost-effective method for SSC tube design and production. These measurements show that the enhancement of RRR causes little improvement in σt at the collider operating field of 6.7 T. Therefore this criterion must be met primarily by adjusting the coating thickness. At 4.2 K, copper layer thicknesses of 150–200 μm will be appropriate, depending on tube diameter. If an 80 K option for the beam tube is adopted, the only effective variable for meeting the SSC specification will be the copper layer thickness. In this case high RRR material gives no advantage, and low RRR material will be sufficient.

The proposed beam tube qualification tests will include about 20 samples from different vendors having different deposition techniques, copper layer thicknesses, and post-deposition heat treatments. Only a few additional magnetoresistance tests will have to be performed, and the majority of the planned testing will be simple thickness and RRR-type measurements.

REFERENCES

1. O. Bintinger, "Measurement of residual resistibity ratio in the presence of a magnetic field for various copper platings of stainless steel beam tubes," SSC-N-184, (1986).
2. L. Goodrich, private communication, (1992).
3. N. J. Simon and R. P. Reed, *Cryogenic Properties of Copper and Copper Alloys, Fracture and Deformation Div.,* NBS, Boulder, CO, (1987).

This Page Intentionally Left Blank

SECTION 2

Thermal Conductance of a Prototype Mechanical Support and the "Magic" Joint

J. Maddocks and A. Yücel

SECTION 2

Thermal Conductance of a Prototype Mechanical Support and the "Magic" Joint

J. Maddocks and A. Yücel

Superconducting Super Collider Laboratory*
2550 Beckleymeade Avenue
Dallas, Texas 75237

1.0 INTRODUCTION

As a first step in estimating the heat leak of a dipole support, the thermal contact conductance between support legs and magnet bore tube is assumed to be perfect. The result is an unrealistic estimate of 0.06 W per leg, which translates into 0.12 W per dipole, assuming 4 contact points and one support every 2 meters. Since contact conductance is difficult to calculate accurately, and may be as poor as the conductance of the stainless steel legs themselves, a test was devised to measure the actual heat flow through a prototype support and an average contact conductance.

2.0 TEST APPARATUS

A schematic of the test apparatus is shown in Figure 1. The support used is an early prototype, which has been machined from a piece of Nitronic 40 stainless steel tubing. As indicated in Figure 1, it has two end rings which hold the four legs together in a single unit. The end rings fit tightly over a short piece of liner tubing and are thermally bonded to it with copper-impregnated grease.

The liner tube (no holes) is plated with 50 μm of copper on the inner surface. Four 2.2 kΩ metal film resistors serve as a heater. They are varnished into brass sleeves that are soldered to the Cu surface of the liner tube and wired in series. Thermometers are located on the inside surface of each leg directly behind each contact point. In addition, one thermometer is located on the liner tube and another is located on one end ring near a support leg. Three thermometers are carbon ceramic resistors, and three are standard silicon diodes.

The whole assembly is placed in a stainless steel vacuum container and immersed in a saturated helium bath at 4.2 K. Upon insertion of the support assembly into the vacuum container, the contact points of each leg are deflected by 0.75 mm. Room temperature measurements of the spring constant and calculations of the same give a spring constant for each support leg of about 20 kN/m. Thus, precompression of each leg in the amount of 0.75 mm upon insertion into the vacuum can results in a nominal force per contact equal to that expected in the collider.

* Operated by the Universities Research Association, Inc., for the U.S. Department of Energy under Contract No. DE-AC35-89ER40486.

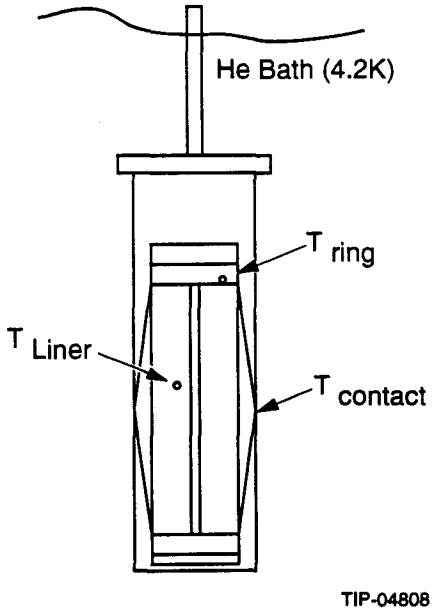

Figure 1. Schematic of Heat Leak Test Apparatus.

3.0 PROCEDURE

The insulating vacuum is pumped to approximately 1×10^{-5} Torr at room temperature using a diffusion pump. During the transfer of liquid, a helium leak detector remains open to the vacuum space. Once the apparatus is immersed in LHe and no leaks have been observed, the detector is valved off.

When the heater is turned on, temperatures slowly rise to steady state values. The time constant for steady state is in the order of a few hours for liner temperatures above 20 K. As a matter of practice, the heater is turned up to full capacity and the liner temperature monitored until it is close to the desired value. The heat is then slowly reduced until a steady temperature is achieved. This process takes approximately one half hour. Accuracy of the method was verified on several occasions by allowing the perceived steady state to remain for a few hours. In all cases, the temperatures changed by less than a few percent.

The heater is powered with a dc voltage supply. A precision resistor in series with the heater provides a means of measuring the current, which together with the applied voltage provides a measure of the heat input. When the steady state is achieved, the heat input as well as the temperatures are recorded. In this way, the heat leak of the support is measured for liner temperatures ranging from 10 K to 100 K.

Heat leak measurements are repeated, over the entire temperature range, for a series of contact surface preparations. The first data were obtained with the support and inner vacuum container wall in "as delivered" condition. This means simply that the contact surfaces were oxidized and the contact area undefined. Later, the inner wall of the vacuum container was polished to remove the oxide layer, and the contact area defined. The definition was accomplished by welding beads of stainless steel rod to the contact points, filing them to a specified 2 mm × 3 mm area with a jeweler's file, and lapping them slightly to seat well against the wall of the vacuum can. Since highly polished surfaces (submicron roughness) present the least resistance to heat flow, our treatment was intended to produce a uniformly rough surface.

4.0 DATA ANALYSIS

The total heat leak as a function of liner temperature for a number of cases is shown in Figure 2. Scatter in the data indicates the contact resistance is reproducible to approximately ± 15%. In addition, oxide on the "as delivered" contact surfaces seems to have little effect on the heat leak, as expected for rough surfaces. For a liner temperature of 80 K, the measured heat leak is 0.04 W per leg, a reduction of 30% from the estimate obtained by neglecting contact resistance.

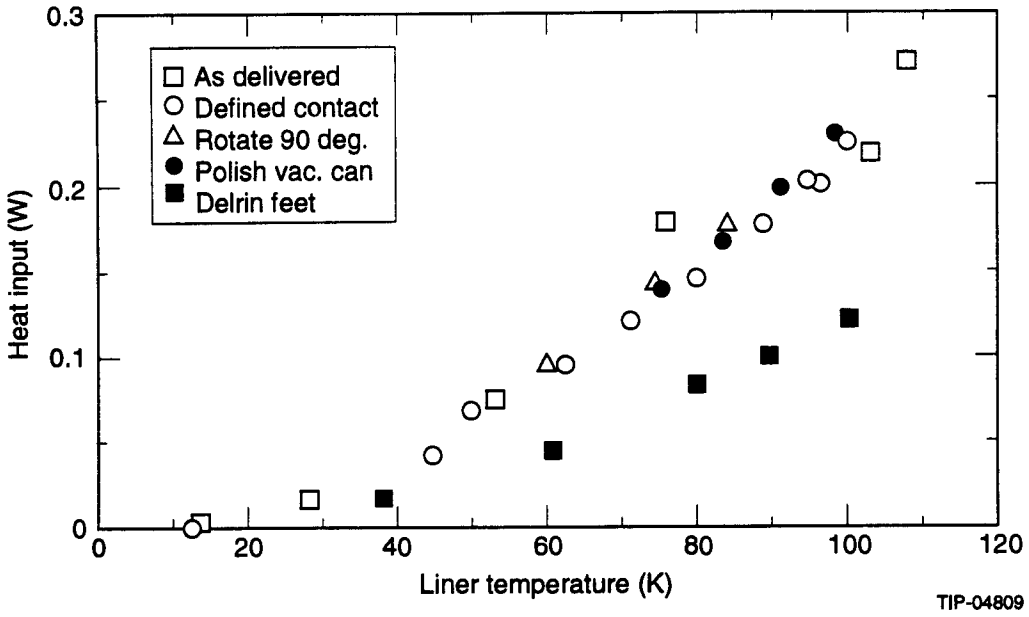

Figure 2. Measured Heat Load of a Mechanical Support Prototype, as a Function of Liner Temperature.

Since none of the various contact surface preparations had a significant effect on the heat leak, one might conclude that surface preparation is inconsequential. It is true that rough surfaces show little dependence on oxide layers in agreement with the results of this test. It is also possible, though, that carefully polishing the support contacts to submicron roughness could increase the heat leak significantly. Evidence for this will be presented shortly.

As a check of the total heat leak measurement, the heat leak through each leg is computed from ΔT across the leg and the thermal conductivity of stainless steel. The sum over all four legs agrees reasonably well with the total heat leak measured at all temperatures. This indicates that there are no significant parallel heat paths, as for instance through gas conduction, radiation, or instrumentation leads.

The same method can be used to determine an average value of contact conductance (h_c), measured in units of W/m^2K. Assume the heat leak through each leg (Q_i) is one fourth of the measured total. Then Q_i is given by,

$$Q_i = A_c \int h_c \, dT, \tag{1}$$

where A_c is the nominal contact area, and h_c is given by,

$$h_c = \alpha T^n. \tag{2}$$

In Eq. (2) α is a function of applied force and surface roughness. Substituting Eq. (2) into Eq. (1) and integrating, results in an expression for $T_{contact}$.

$$T_{contact} = [\,(n+1)Q_i/\alpha A_c + T_{bath}^{n+1}\,]^{1/(n+1)}. \quad (3)$$

Practically speaking, T_{bath}^{n+1} is much less than the leading term and can be neglected. Average values of α and n are extracted from a log-log plot of $T_{contact}$ versus Q_i as shown if Figure 3. The result indicates n = 1.5 and α= 0.75. The value of n compares favorably with stainless to stainless conductances published in the literature.[1] The measured value of 0.75 for α, however, is about two orders of magnitude lower than that of Reference 1, under a similarly applied load.

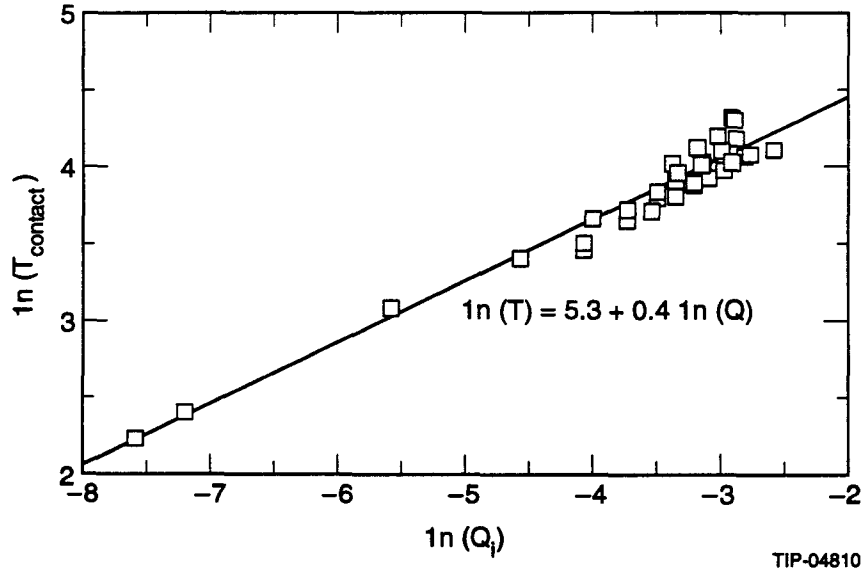

Figure 3. Log-Log Plot of Equation (3) Neglecting the T_{bath} Term, From Which Values of α and n Are Derived.

The published values of Reference 1 are for contact conductance between foils of 302 stainless steel, which presumably are smooth surfaces compared to the nominally rough surfaces of the present test. This probably explains why the values of α vary by a factor of approximately 100. Rough surfaces have less actual contact area per nominal contact area than smooth surfaces do. The clear implication is that care must be taken not to polish the contact surfaces if heat leak reduction is desired.

In order to test the effect of buttons on the heat leak, each contact point of a second support was fitted with a Delrin button. The buttons were attached by press fitting into holes drilled at the points of contact. Only the total heat leak and liner temperature were measured, so that no conductance can be extracted from the data. The data are included in Figure 2. Although Delrin is an unacceptable material for use in the bore tube, the data give an indication of the effect of attaching some sort of plastic buttons to the supports should an acceptable material be identified. In this case the heat leak is reduced by approximately a factor of two.

5.0 THERMAL CONDUCTANCE OF THE "MAGIC" JOINT

A threaded joint, located between the quadrupole liner and its end cooling heat exchanger, must have a large thermal conductance. The turnbuckle type joint, dubbed the magic joint, is made entirely of copper. In order to test the conductance of the joint, a prototype is fitted with a heater and thermometer at one end and enclosed in a vacuum can. The other end is held at a constant temperature of 77 K by immersing the whole apparatus in a liquid nitrogen bath.

The procedure is simply to measure the warm end temperature for several values of heat input. A worst case heat load (Q) is taken to be the dynamic heat load at 10 times the baseline luminosity, approximately 2.1 W. Thus, the temperature is measured for several heat loads up to 2.2 W.

The results are shown in Figure 4, where ΔT is the difference between the warm end temperature and the LN_2 bath temperature of 77 K, and Q is the heater power. Since the temperature rise is small, the conductance ($h = Q/\Delta T$) is constant as would be expected. Note that the contact area is not well defined so that the conductance has not been normalized to an apparent contact area as was done in the support analysis.

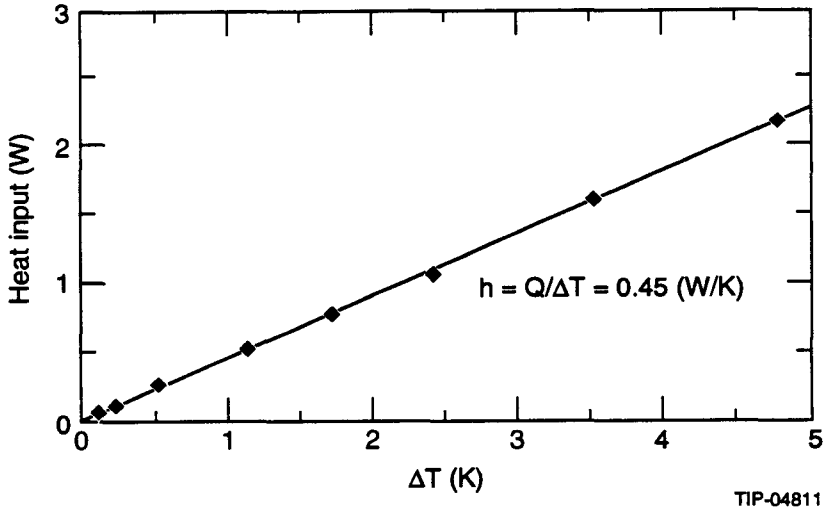

Figure 4. Heater Power as a Function of Temperature Rise Across the Magic Joint.

In addition, it is important to know what the applied contact force is. In this test the joint is only "finger tight". Presumably, the conductance can easily be increased, perhaps as much as an order of magnitude, by using a torque wrench for tightening. Therefore, this test should represent the worst case both from the heat load and conductance viewpoints. In the future, however, tests should be conducted to establish a means of tightening the joint uniformly and to develop a specification for tightening.

Finally, Figure 4 indicates that for a heat load equivalent to the maximum baseline load of 0.7 W, the temperature rise is only 1.5 K. For a heat load equivalent to the maximum upgrade load of 2.2 W, the temperature rise is 4.8 K. In both cases the temperature rise is 5 times smaller than the expected maximum temperature rise of the liner. Given that the joint conductance can certainly be increased by tightening, it is concluded that the magic joint itself presents no insurmountable problems.

This Page Intentionally Left Blank

REFERENCES

1. D. N. Lyon, and W. R. Parrish, "Low Temperature Thermal Conductivities of Two High Compressive Strength Materials," *Cryogenics*, 7:21 (1967).

This Page Intentionally Left Blank

SECTION 3

Preliminary ASST Test Plan for an 80 K Liner

P. Kraushaar

SECTION 3

Preliminary ASST Test Plan for an 80 K Liner

P. Kraushaar

Superconducting Super Collider Laboratory*
2550 Beckleymeade Avenue
Dallas, Texas 75237

1.0 INTRODUCTION

Early in the effort to develop a design for a sychrotron radiation liner for the Collider lattice, the development team acknowledged that testing the proposed design would be necessary. Although individual components of the 80 K liner system could be tested in small scale component tests setups, to test the entire system would require a string of magnets at least a half-cell in length which included spool pieces. Fortunately, the Superconducting Super Collider Laboratory (SSCL) has this testing capability at the Accelerator Systems String Test (ASST) Facility located at the N15 site.

The ASST Testing Facility is managed by the Collider Machine Group within the Project Management Office (PMO). The facility is open to the physicists and engineers in the divisions who wish to propose tests or experiments that require a string of magnets and the systems necessary to support their operation. Although the facility is managed and operated by the ASST Test Group with the Collider Machine Group, the testing program is reviewed and approved by the ASST Program Steering Committee. The membership of this committee is drawn from the technical management in the Magnet Systems Division (MSD), the Accelerator Systems Division (ASD), and the machine groups (Collider and HEB) in PMO.

The ASST Testing Facility provides a unique capability to test components and systems related to the operation of superconducting magnets. Primarily, test data can be acquired in four basic areas. These areas are cryogenic, power, vacuum, and mechanical. Cryogenic related measurements typically involve the thermal heat leak performance of a component such as a magnet or spool piece. The power testing is primarily related to the quench response of the components and magnet systems but has also included ramp rate dependant effects. The two vacuum systems that can be used for testing are the cryostat insulating vacuum and the beam tube vacuum. Finally, in the mechanical area, installation related testing along with vibation response data can be acquired.

2.0 THE LINER TESTING OBJECTIVES

In July, 1992, William Turner submitted test request P-002 to the ASST Test Group, proposing a test of the 80 K synchrotron radiation liner that was under development by a working group that he lead. The details on the motivation for a synchrotron radiation liner for the Collider accelerator and the engineering design information are presented elsewhere in the Liner Internal Technical Review (ITR) review book.[1] The test request called for the testing of the liner system in a half-cell of magnets under operating currents and temperatures expected in the normal collider operations. The program was estimated to take twenty six (26) weeks and was of high priority due to its possible impact on the collider magnet design.

* Operated by the Universities Research Association, Inc., for the U.S. Department of Energy under Contract No. DE-AC35-89ER40486.

The proposed testing program that grew out of the request as the design effort proceeded had a number of goals or objectives. One was the developement and testing of the 80 K liner installation and operating procedures. Another was the determination of the thermal performance of the liner system in both pre- and post-magnet quenching conditions. Related to that was the need to measure the mechanical stability of the liner under quench conditions. Since the liner included a cryosorber, its performance and the ability to regenerate the beam tube vacuum needed to be measured. Related to this was a measurement of the systems ability to recover from a vacuum accident. The main reason for the liner was to intercept the synchrotron radiation heat load from the beam. This heat load was to be simulated in the testing and its effect on the liner temperature measured. Finally, the impedance of the liner system was to be measured at the liner operating temperatures. This list is not all inclusive, but does give the major areas in which operating experience and test data were required by the design team and could be obtained at the ASST.

3.0 THE PROPOSED TESTING SCHEDULE

The definition of a testing schedule within an R&D program is always a difficult task since there are always more requests for test time than time available. The liner test request was given high priority by the laboratory management and with the direction to the test group to accommodate the test at the expense of others. This was done and the liner program scheduled to start in the first quarter of FY 94. The preliminary program was assembled with estimates for the time required to conduct each segment. The estimated test times are shown in Table 1. These estimates are believed to be accurate within 20%.

TABLE 1. ESTIMATE OF LINER TEST PROGRAM DURATION.

Installation of Liner into a Half Cell	90 - 120 days
Commission of the Full Cell String	30 days
Time to Reach Thermal Equilibrium	21 days
Heat Leak Measurements on Liner	28 days
Liner System Quench Response Study (25 Quenches)	15 days
Vacuum Regeneration Tests - 10 Cycles	10 days
Vacuum Recovery Tests - 6 Cycles	12 days
Radiation Heat Load & Temperature	28 days
Total Program Duration	234 - 264 days

4.0 QUESTIONS UNANSWERED AT PROGRAM CANCELLATION

Unfortunately, the 80 K liner program was cancelled prior to the construction of a prototype liner that could be installed in the magnet string at the ASST. This has resulted in the withdrawal of the test request and the cancellation of the testing program planned for the liner system. This represents the loss of an opportunity to validate by test the results of a significant engineering effort.

The test program planning was underway at the time of cancellation. However, there were still may unanswered questions related to how the test would be instrumented and conducted. The selection of the temperature sensors, the mounting technique to be used and the positions of the sensors had not been decided, nor had detailed test plans for each of the areas of testing been written yet.

The present opportunity to test this system has passed since the full cell of ASST magnets are now installed and ready for testing. The scheduled testing time for the liner test has been reallocated to other test requests. The next opportunity to test a liner system of some design would be in the production magnet string test which is tentatively scheduled for FY 95 but is still subject to approval by the Project Management Office.

REFERENCES

1. Internal Technical Review of the 80 K ASST Liner Design, Dallas, TX. April 29-30, 1993.

This Page Intentionally Left Blank

SECTION 4

Quench Survivability Test

R. Richardson, Q. S. Shu,
W. Turner, and J. Zbasnik

Introduction and Background

- By the late 1980's it was well recognized that Lorentz forces acting on the Cu lined collider beam tube during a CDM quench could cause permanent deformation*
  - At 20 K and zero helium external pressure the calculated yield Lorentz equatorial pressure P_{max} was in the 400 psi range
  - Scaling this analysis for the 80 K point design (R=12.9 mm, h=0.75 mm) gives P_{max} = 325 psi
- Lorentz pressures for the 80 K liner point design are 50-60 psi, hence we expect a > 4 safety margin against tube collapse
  - Does not include effect of holes
  - Does not address fatigue cracking, copper debonding, asymmetric forces, etc.
- 100 quench cycle survivability is required. Experimental data are needed

* K. Ng and J. Peterson, "Allowable Stress In the SSC Beam Tube During a Quench", SSC-168, March, 1988

SSC Laboratory

80K
Synchrotron Radiation
Liner Program

Maximum equatorial pressure:

$$Pm = B\dot{B}tb/\rho$$

$B\dot{B} \cong 150\ T^2/s$
$b = 12.7$ mm
$t = 0.5$ mm
$\rho = 2.6 \times 10^{-9}$ ohm-m

=> $Pm = 3.7$ atm $= 54$ psi

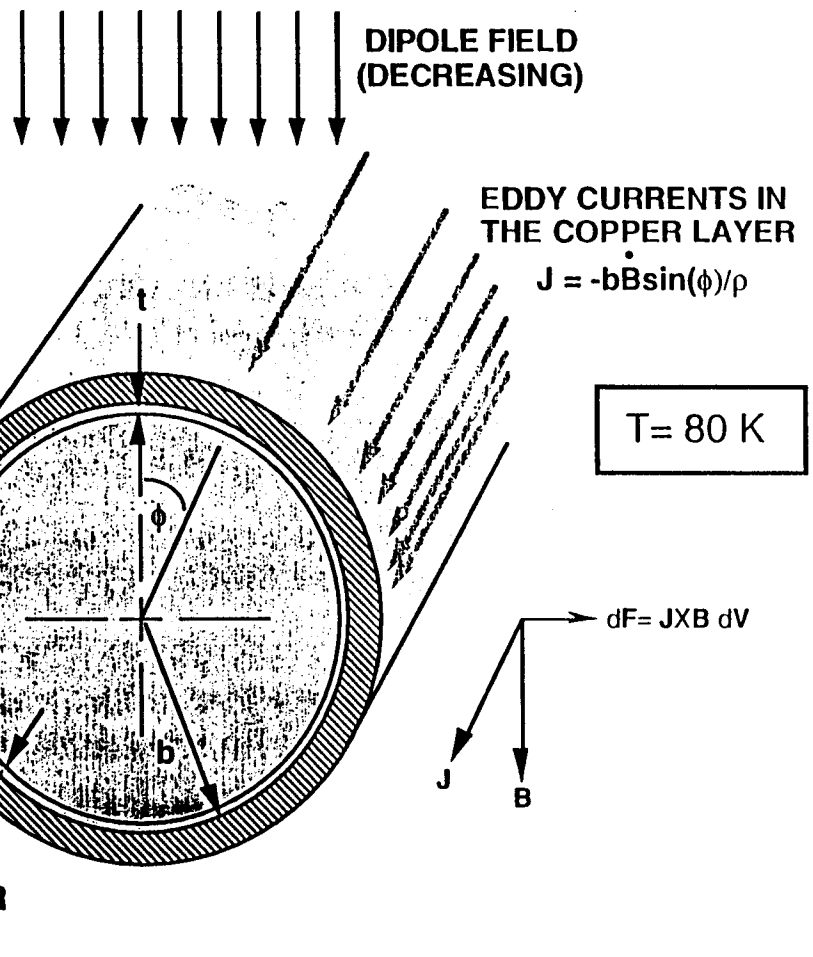

R. Richardson

29-30 April, 1993

Goals of Quench Survivability Experiments

- Assess the mechanical and electrical degradation, if any, of a collider prototypical 80 K liner when subjected to > 100 full-field quench cycles
- Provide sufficient diagnostic instrumentation and inspection to identify and quantify the processes affecting liner performance
- Generate a technical report summarizing test results with recommendations for any further study of problem areas

SSC Laboratory

80K
Synchrotron Radiation
Liner Program

Technical Approach

- Insert a 1m long prototype liner, including supports, into a CDM operating in the vertical cryostat
  - Do not quench magnet for tests; use dump resistor
  - Adjust dump resistance to give correct peak $\dot{B}B$ and approximate B(t)
- Instrument liner with strain gages, temperature probes, current probes, and accelerometers
- Measure wall current and temperature to set boundary conditions
- Measure strain to determine max stress
- Use accelerometer to to detect mechanical movement (other methods such as video photography or position sensors may be required)
- Inspect liner after set number of quench cycles for cracking, flaking, or similar signs of mechanical failure

Apparatus: Schematic Layout of Cryogenic System

Vacuum system, power system, and instrumentation not shown

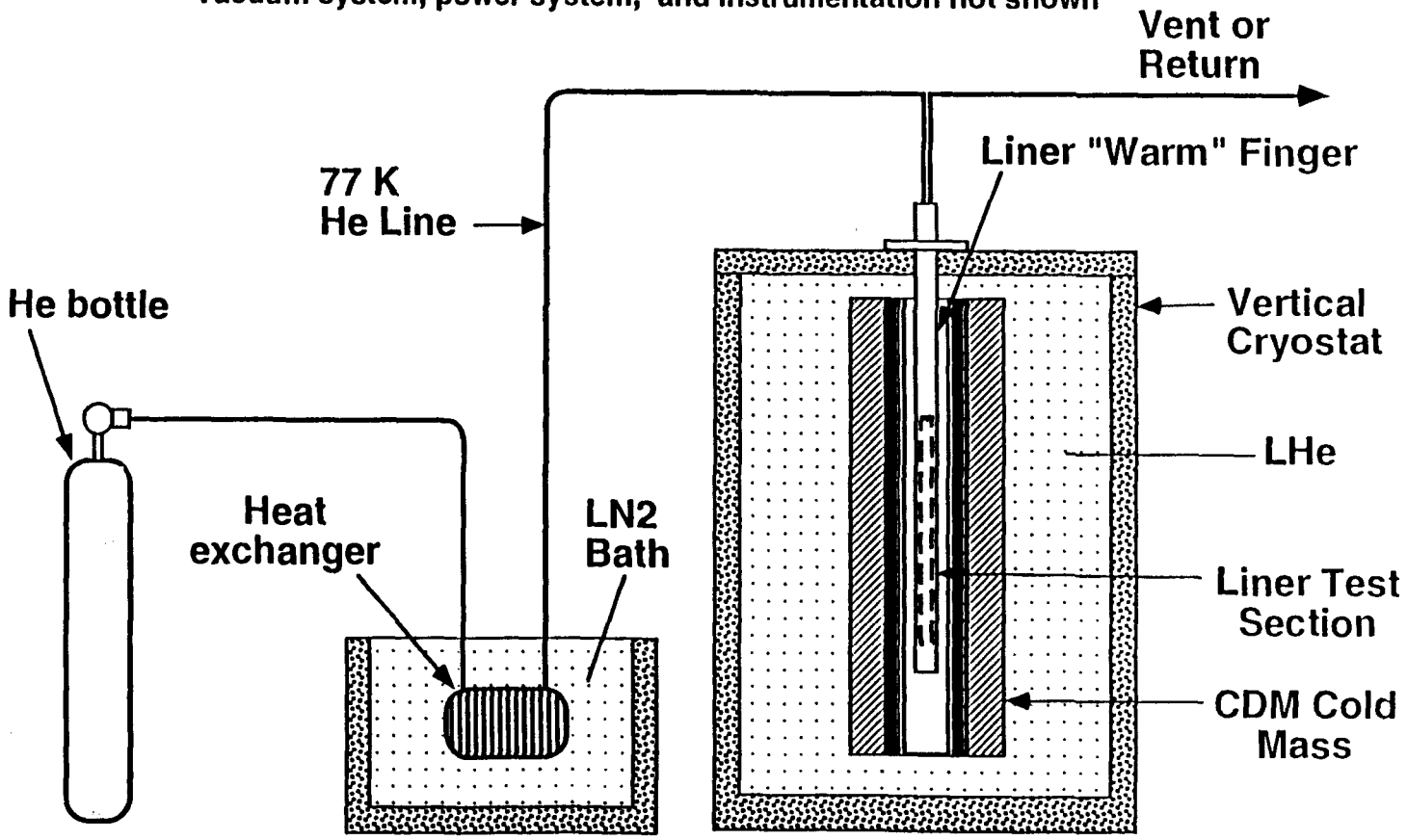

R. Richardson

29-30 April, 1993

SSC Laboratory

80K
Synchrotron Radiation
Liner Program

Liner and 77 K He Line Assembly (Schematic)

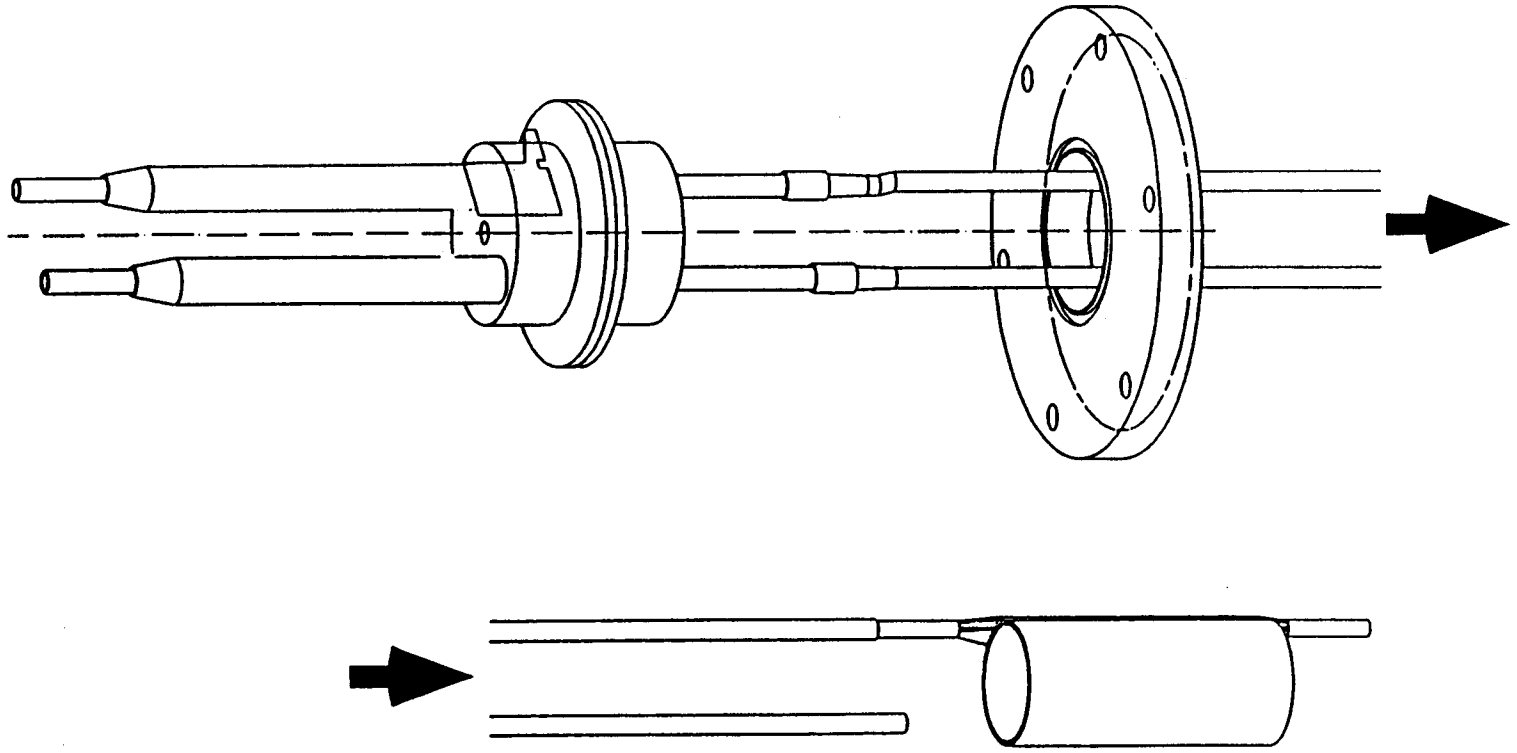

R. Richardson

29-30 April, 1993

Warm Finger: Preliminary Assembly

Shown: flange section with cryo feed-thrus

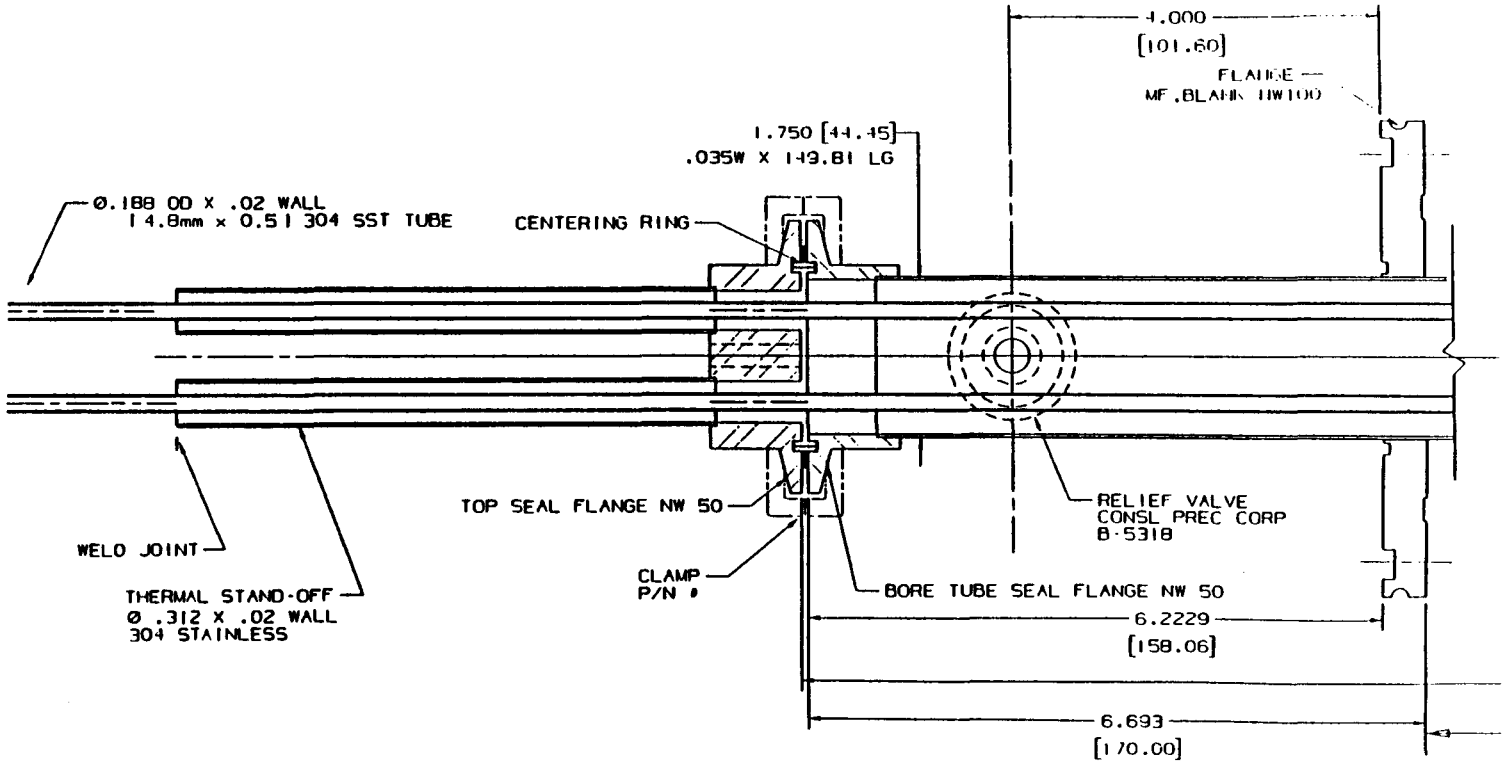

R. Richardson

29-30 April, 1993

SSC Laboratory

80K
Synchrotron Radiation
Liner Program

Warm Finger: Preliminary Assembly

Shown: Liner section with He return lines and strain gages

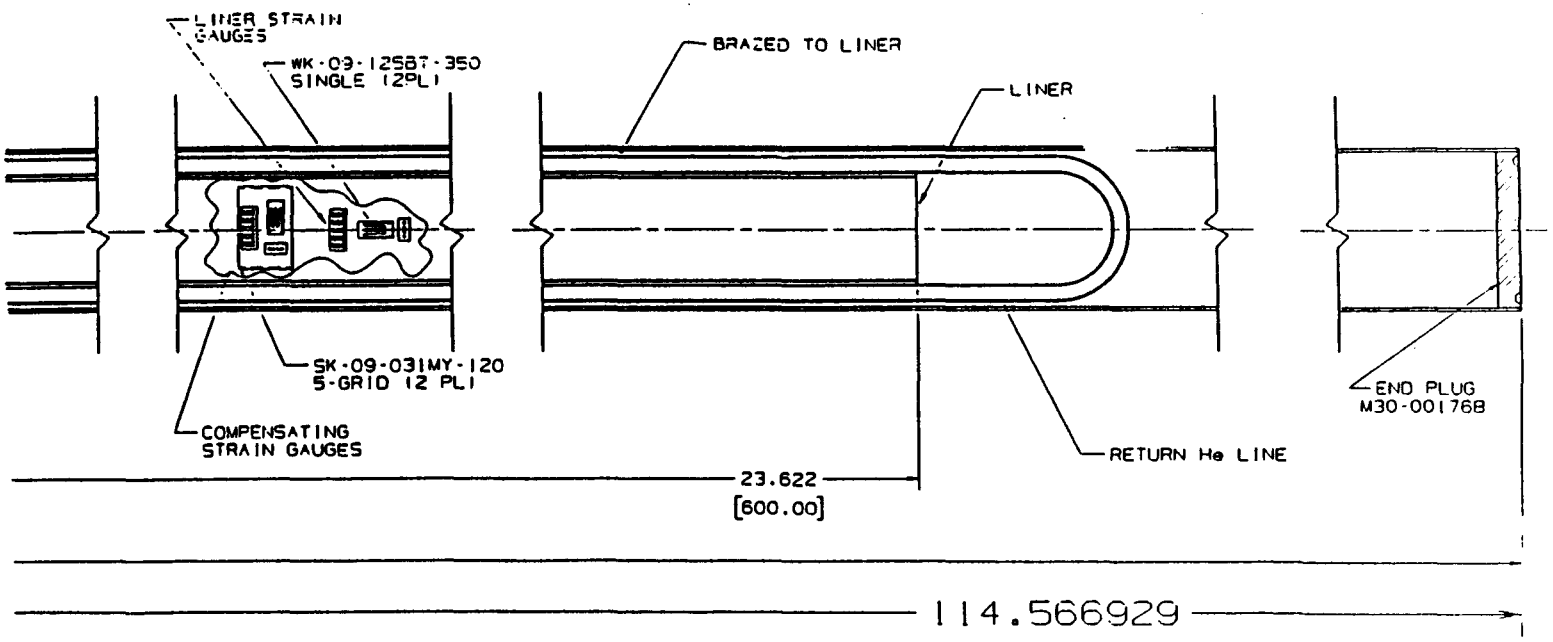

R. Richardson

29-30 April, 1993

"Cartoon" of insrumented Liner

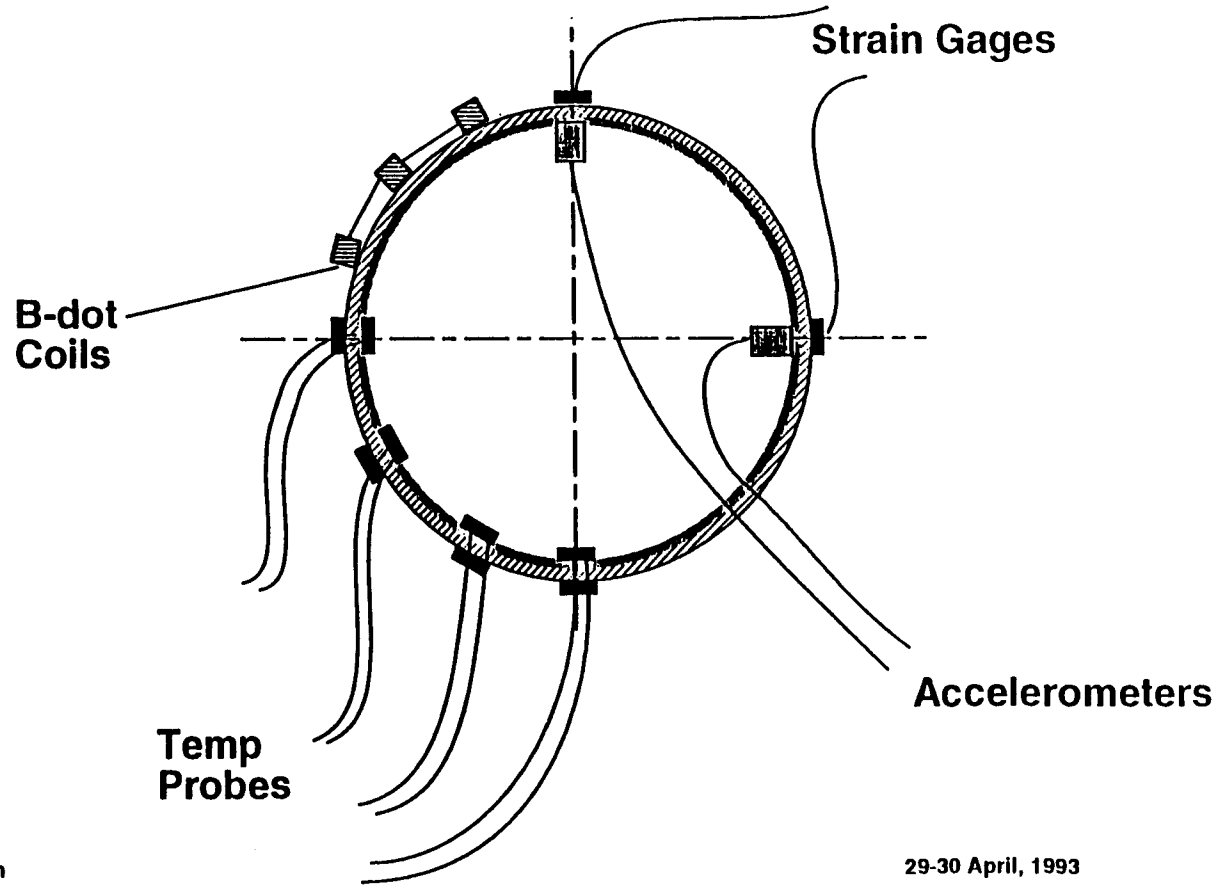

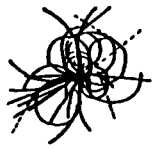

SSC Laboratory

80K
Synchrotron Radiation
Liner Program

Diagnostics: Technical Issues

- Instrumentation requirements are typical for this class of experiment
  - Less than 20 channels of 1kHz analog; 1k record lengths
  - 1mV strain gage signals; >10 mV levels from other sensors

- Principal technical difficulty is the large $\dot{B}$ from the decaying CDM field. Past experimenters have had problems with this environment
  - Voltages couple into transducers and cables; ground loops and EMI add to pickup and noise
  - Strain gages must be carefully located to null the pickup and compensating (or cancellation) geometry must be used
  - $\dot{B}$ probes must be wired to buck main field
  - Measurement techniques may need development before useful data can be taken

SECTION 5

RF Surface Resistivity at Low T and High H Test Plan

W. Chou

Surface Resistance Measurement at Los Alamos National Laboratory

Statement of Work:

To carry out the measurements of the surface resistance of various types of beam tubes supplied by the SSCL. These beam tubes will consist of several electroplated copper tubes that are in procurement as well as new types of tubes that are being developed. The tubes will be about 0.5 to 1 meter long. The number of tubes to be measured will be about 20. The measurements will be under the following conditions:

a. At low temperatures (300K, 80K, 4K and continuous variation) and at dc or low frequencies.
b. At low temperatures (300K, 80K, 4K and continuous variation) and at rf frequencies (from 100 MHz up to above 8 GHz).
c. At low temperatures (300K, 80K, 4K and continuous variation), in high static magnetic fields (up to 6.6 Tesla) and at dc or low frequencies.
d. At low temperatures (300K, 80K, 4K and continuous variation), in high static magnetic fields (up to 6.6 Tesla) and at rf frequencies (from 100 MHz up to above 8 GHz).

Period of Performance:

From effective date of contract to January 31st, 1994.

Deliverables:

1) Results of the measurements and comparisons with the previous measurements and with the theoretical models.
2) Monthly progress reports, to accompany monthly invoices, for all of above activities.

Project Benefits:

The parasitic heating of the beam tube by the proton beam is an important issue in the design of the Collider. The heat power is determined by the surface resistance of the beam tube, of which the environment is a combination of several extreme conditions -- low temperatures, strong static magnetic fields and high frequency ac fields (which are excited by the proton beam). The present heat load budget of the parasitic heating is based on some value of the surface resistance that has not yet been measured for the Collider beam tube under these conditions. (There are some early partial results. But the data exhibited inconsistency and need to be redone.) It is, therefore, essential to perform the measurements as described in the Statement of Work in order to obtain the reliable data of the surface resistance and to assure that the heat load on the cryogenic systems would not exceed the design value.

The AT-1 Group of the LANL has an extensive knowledge on the rf measurements. Mr. George Spalek, who will be responsible for this work, has many years experience in this field and is highly recommended by his colleagues. It is believed that he is capable to perform the work and to obtain the results that are crucially needed by the SSCL in a timely manner.

Attachment:

The proposal from AT-1, LANL.

PROPOSAL FOR MEASUREMENT OF SURFACE RESISTANCE OF COPPER COATING OF COLD BORE TUBE FOR SSC MAGNETS

INTRODUCTION

The superconducting main ring magnets for the SSC will have a cold bore tube made of stainless steel coated on the inside surface by a copper layer 100 to 200 microns thick. For beam stability reasons, the resistivity and rf surface resistance of this Copper coating need to be as low as possible. Measurements of the resistivity and rf surface resistance of the Copper coatings are therefore needed to determine whether they are low enough to meet SSC specifications. These measurements need to be made at various temperatures, frequencies, and in the presence or absence of high magnetic fields.
Samples to be measured would be 0.5m to 1m long with internal diameters of 24mm and 33mm. Wall thickness will be less than 3mm.
This note outlines how the measurements without high magnetic fields could be performed by Los Alamos National Laboratory's (LANL) Accelerator Technology (AT) division personnel and estimates the effort required to perform them (see APPENDIX). The estimates were made under the following assumptions:

a)to save costs, formal fabrication drawings would not be produced
b)no formal design reviews would be held
c)a number of iterations would be needed on some of the designs to achieve accuracy needed
d)the measurements would be done in our 1.1m deep cryostat to save costs and be independent of superconducting work being carried out in the same laboratory (samples longer than 1m would require the additional construction of a larger cryostat insert and the use of a much deeper cryostat with increased He consumption)
e)funding comes from line item construction funds

Estimates of the effort required to perform measurements with high magnetic fields will be provided at a later date.
The measurements without high magnetic fields would be done at LANL. The high magnetic field measurement apparatus would be designed and constructed at LANL and then taken down to the SSC lab where the measurements would be performed in the SSC magnet lab.

OUTLINE OF MEASUREMENTS

The measurements can be divided into three categories:

a)DC and very low frequency resistivity measurements
b)rf surface resistance measurements in the range 100MHz<f<1GHz
c)rf surface resistance measurements in the range f>5GHz

Because of the nature of these measurements some of them cannot be performed at all temperatures or in the presence of magnetic fields. The table below lists the measurements and the conditions under which they can be performed.

		Temperature		
Measurement	300K	80K	4K	continuous
DC	yes (no B)	yes (B?)	yes (B)	yes (B?)
f<1GHz	yes (Cu, no B)	yes(Cu, B?)	yes(no B)	no
>5GHz	yes(no B)	yes(B?)	yes(B)	yes(B?)

The meanings of the entries in the table are:

B	measurement can be made with high magnetic field
B?	possibly with magnetic field if sample can be @80K without quenching magnet
no B	measurement cannot be made in high magnetic field
Cu	measurement not very accurate, can only be made relative to another copper sample
continuous	measurement with continuous variation of temperature from 4K to 300K

The reasons for some of the constraints on the measurements will become obvious when the measurements are described in more detail below.

AT DIVISION CAPABILITIES

AT division has a wide variety of rf test equipment applicable to this measurement task such as:

network analyzers	10MHz->20GHz
frequency synthesizers	1MHz->18GHz,10mW
rf power meters	1MHz->18GHz,1nw->100mW
signal generators	0.1Hz->10MHz
rf amplifiers	10MHz->20GHz, 100mW
TWT amplifiers	1GHz->4GHz, 200W
power amplifier	800MHz, 100W

Cryogenic equipment on hand includes:

liquid Helium Dewars	500 liter
cryostats	depths from 1.1m to 4m
temperature sensors	down to 2K
liquid He level sensors	
vacuum pumps for He pumping to 10Torr at high volume	

In addition the staff of AT division has wide experience in the design and construction of rf structures, both normal and superconducting.

DC MEASUREMENTS

For the DC measurement of the Cu resistivity, the usual four probe method can be used. Two of the probes are used to drive a current through the sample while the other two probes measure the voltage across the sample using a lock-in amplifier.
It is assumed that the cold tube sample dimensions are:

Cu coating thickness	200microns
stainless steel tube thickness	3mm
stainless steel tube length	0.5m
stainless steel tube ID	24mm

At room temperature, using the dimensions above, the measured resistance of the sample should be roughly 0.7 of the Copper liner's. As the temperature is lowered, the stainless steel resistance remains constant while the copper resistance decreases in correspondence to its residual resistivity ratio (RRR). Thus at low temperatures the stainless steel contribution becomes negligible compared to the Copper conductivity.
With exciting currents of 100mA, the voltages that need to be measured with the lock-in amplifier are in the range of 60nV for a Copper RRR of 1,000. Voltages in the range of 15nV can be measured with the lock-in amplifier, but to increase accuracy, it is planned to drive the sample with currents of the order of 1A. Noise suppression will be the most challenging part of these measurements. In order to be able to measure sample resistance as a function of temperature, the measurement will be computerized.
The mechanical arrangement of the measurement in a cryostat without high magnetic field is shown in Figure 1. The sample will be placed inside a metal tube for noise suppression and the assembly mounted inside a stainless steel vessel immersed in liquid Helium. The liquid Helium will not wet the sample. Helium gas and radiation heat exchange will cool the sample to low temperatures. Diode sensors will monitor the sample temperature at two places. A helium displacer made of closed cell styrofoam will be used to save liquid Helium costs. Helium level will be monitored using a commercial level sensor. A similar arrangement will be used for the rf measurements in the same cryostat modified to accommodate rf probes, etc.
The measurement sequence will be:

a)solid Cu cylinders sized to duplicate expected resistances of the room temperature and low temperature beam tube samples will be used to perfect the measurement techniques and determine best way of suppressing system noise
b)a stainless steel tube without the Cu coating will be cooled down in the cryostat and its resistance measured as a function of temperature as the tube is allowed to warm up to room temperature, the results will be used to subtract the stainless steel resistance from the Cu coated sample tests (if needed)
c)a sample of the actual beam tube will then be tested, taking care that air does not contact the Cu coating while the tube is at low temperature so as not to oxidize this coating because of Oxygen condensation on its surface

RF MEASUREMENTS 100MHz<f<1GHz

Frequencies in the range 100MHz to 1GHz are far below the cutoff frequencies for propagation of electromagnetic waves in the SSC beam tube so neither TE nor TM modes

of the tube can be used to measure its surface resistance. Instead, a rod can be suspended in the tube to form an odd or even number of half wavelengths TEM resonator. If the rod is made of Niobium, then at temperatures below 9K the resonator Q will be determined only by the surface resistance of the copper coating of the beam tube. By changing the length of the rod and driving the resonator at its half wavelength, full wavelength, one and a half wavelength, etc. resonances , the rf surface resistance of the Cu coating can be measured over a wide range of discrete frequencies (as long as no appreciable rf power is radiated from the ends of the beam tube) .
A conceptual design of such a coaxial resonator arrangement is shown in Figure 2. The center conductor of the coaxial resonator is supported at its midpoint by a low loss tangent dielectric (sapphire, quartz, or boron nitride) cradle. This cradle does not affect the Q of the resonances that have a magnetic field maximum at the center of the rod.
Two methods of rf coupling to the resonator are shown in Figure 2. One method is to loop couple to the resonator magnetic fields at its center point. Another way of coupling to the resonator is by means of an electric probe in the fringe fields of the resonator.
Superfish code calculations of the resonator Q will be used to extract the rf surface resistance of the Cu coating from the measurements.
At temperatures higher than 9K or in the presence of very high magnetic fields, the Nb center conductor cannot be used for accurate measurements. Under these conditions, the center conductor would be replaced by a well polished Cu rod. For calibration purposes, the rod's surface resistance could be measured directly by making the outer conductor of the resonator superconducting and measuring its Q. This rod would then be used with the beam tube samples to measure the Cu coating's surface resistance relative to that of the rod's. This would be a relatively low accuracy relative measurement.

RF MEASUREMENTS f>5GHz

At these higher frequencies, the beam tube itself can be made into a TE or TM mode resonator by closing off the ends with end caps. The rf seal between the sample and the end caps has to be well made so as not to degrade the cavity Q by a large amount. To check the quality of this seal, it can be placed at the standing wave current node of particular resonances (so that it doesn't affect their Q's). Analytical calculations are then used to extract the surface resistance of the Cu coating at these and adjacent resonances whose Q's would be affected by bad rf joints. If the results are consistent, the rf seal resistance is negligible. If rf seal problems are encountered, choke joints can be adapted to the end caps to ~~reduce~~ make better seals at given frequencies.
For a beam tube with 33mm inside diameter, the approximate cut-off frequencies for the different modes are:

TE11	~5.4GHz
TM01	~6.94GHz
TE21	~8.84GHz
TM11,TE01	~11.09GHz
TE31	~12.16GHz

Since only one mode can be excited between 5.4GHz and 6.94GHz, surface resistance measurements in this range should be relatively easy. In the lower part of the range 5.25GHz to 8.84GHz, the waveguide wavelengths of the TE11 and TM01 are substantially different from each other so not many of their resonant frequencies are expected to overlap and mode mixing should not be a problem unless the modes are coupled strongly because of mechanical deformations of the beam tube (which are expected to be small).

Above 8.84GHz, mode mixing might become a problem since more modes can be excited and TE and TM resonances are more likely to overlap. Whether the surface resistance can reliably be extracted from the measurements at such high frequencies can only be determined experimentally.
Figure 3 shows a sketch of the experimental apparatus for the measurements in this frequency range.

CHAPTER 5

DOCUMENT CONTROL

SECTION 1

ASST Liner Interface Documentation

R. Mihelic

INTERFACE CONTROL DOCUMENTATION

WHAT IS IT?

Documentation that details and controls both physical and functional interfaces between major hardware elements.

It consists of drawings and specifications.

SSC Laboratory

80K
Synchrotron Radiation
Liner Program

INTERFACE CONTROL DOCUMENTATION

WHY IS IT NEEDED?

Interface Control Documentation is a tool used by management to:

- Ensure independently developed hardware elements mate properly.
- System performance requirements are not exceeded (i.e. budgets are allocated to individual hardware elements).
- Individual hardware elements are defined (i.e. work package boundaries are clearly defined and there are no "cracks", all pieces are addressed)

INTERFACE CONTROL DOCUMENTATION

WAS FORMAL DOCUMENTATION NEEDED FOR THE ASST LINER EFFORT?

Not as a precursor to ASST efforts
because:

- Mating hardware elements and designs already existed. Additional definition was redundant.
- The extremely close coordination and openness of diverse Liner design and analysis efforts provided "built-in" timely assessment and resolution of interface issues.
- Clear definition of specific ASST II hardware configurations (i.e. specific magnets and test objectives) was on a different schedule to the liner program.
- Collider ICD issues such as welding and hardware stayout zones or alignment hardware limitations and impacts, for example, were to be part of the "results" of the ASST II Liner R&D effort that would feed a Collider LIner program.
- Remember that ASST magnets, spools, interconnects, cryogenics, etc are similar to but not identical to Collider configurations. The real ICD issues are those of the Collider ICD's.

SSC Laboratory

80K
Synchrotron Radiation
Liner Program

INTERFACE CONTROL DOCUMENTATION

KEY ASST DESIGN OBJECTIVES ESTABLISHED EARLY IN EFFORT:

- The Liner hardware designs would be a minimum impact to existing designs and hardware (and still meet performance objectives).
- The Liner hardware designs would be developed for ASST but concepts should be compatible with Collider hardware efforts.
- Commonality (minimizing number of parts) was stressed.
- Schedule was clearly a major design driver (designs for ASST should minimize risk, use established or achievable near term technologies).

INTERFACE CONTROL DOCUMENTATION

KEY INTERFACE AREAS FOR THE 80K LINER SYSTEM:

- Liner Tube Size, location and size tolerances, magnetic and thermal budgets.
- Welding & Assembly Stayout Zones in the Interconnect Regions
- Liner He Cooling Line Routing:
  - Through 13m & 15m CDM's
  - Through CQM
  - Through, Into & Out of entire family of Arc Spools
  - Through or around Empty Cryostats
  - Through or around all other Arc Beam Line components.
  - From/To Cryoplants and Tunnel
  - etc, etc.
- Replacement of existing interconnect parts with liner system parts (i.e. Liner Cryobox replaces Beam Bellows, Liner He/LN2 Heat Exchangers replace Extension Tubes, etc.)
- Liner/BPM/Spool interfaces
- Liner program interface to all arc hardware programs

SSC Laboratory

80K
Synchrotron Radiation
Liner Program

INTERFACE CONTROL DOCUMENTATION

FUTURE OBJECTIVES:

- Initiate a Collider Liner Program.
- Initiate SSC coordinated requirements for a Collider Liner System.
- Provide SSC program decision milestones for the Collider Liner effort.
- Develop Collider Liner System conceptual design.
- Begin dialogue on updates to existing Collider ICD documentation to address the potential of a Liner System.

Beam Tube Liner Design Reference

Table 1. Geometry

Magnet Parameter	Collider CDM	ASST CDM	Collider CQM	ASST CQM	Collider Spool	ASST Spool
Slot Length (m)	15.815[4]	16.415[6]	5.85[5]		4.575[1]	
Min. Inner Coil Diameter (mm)	50	49.566[8]	40	40	42[2]	
Min. Clear Aperture Diameter (mm)				35.00[16]	40[2]	
Beam Tube O.D. (mm)	37 ±.15[18]	44.6[9] 44.45[14,17] 44.679/ 44.602[19]		34.54[16]	34.54[1] 34.92[10]	44.4[10]
Beam Tube Wall (mm)	2.12 ±.21[18]	1.3±.05[6] 1.24[17] 1.346/ 1.245[19]		1.12[16]	1.12[1] 1.24[11]	1.5[11]
Beam Tube I.D. (mm)	32.3[12]	42±.14[6] 41.96/ 41.81[14] 41.02[15]	32.3[12]	32.3[3]	32.3[3] 32.44[10]	41.4[10]
Sagitta, nom. (mm)	2.3[13]	none[7]	none	none	none	none

[1] Collider 3B Arc Specification E10-000027 (July '92, unreleased), Table 3.2.1.9-II, Dimensions of Spools, page 61.

[2] Collider 3B Arc Specification E10-000027 (July '92, unreleased), Table 3.2.1.8-I thru V, pages 54-58.

[3] Derived from O.D. and Wall Thickness specifications.

[4] Collider Magnet ICD E10-000004 (Rev. -. 6/24/92, unreleased), Section 3.2.2.1, page 5, also Collider 3B Arc Specification E10-000027 (July '92, unreleased), Table 3.2.2-I, page 93.

[5] Collider Magnet ICD E10-000004 (Rev. -. 6/24/92, unreleased), Section 3.2.2.2, page 5, also Collider 3B Arc Specification E10-000027 (July '92, unreleased), Table 3.2.2-I, page 93.

[6] 50mm Collider Dipole Magnet Requirements & Specifications (Yellow Book, 8/16/91) Section 1.2.2.

[7] 50mm Collider Dipole Magnet Requirements & Specifications (Yellow Book, 8/16/91) Section 1.4.

[8] 50mm Collider Dipole Magnet Requirements & Specifications (Yellow Book, 8/16/91) Section 2.2.

[9] Derived from I.D. and Wall Thickness specifications.

[10] Donald Clark Presentation Memo (7/28/92).

[11] Derived from I.D. and O.D. specifications.

[12] Collider 3B Arc Specification E10-000027 (July '92, unreleased), Section 3.2.2.2, pages 93.

[13] Currently not specified in requirements documents, number from Marc Metrolis, MSD Systems.

[14] Per DCA-318 as built QA Travellers (Memo from FNAL Bill Higinbotham, Beam Tube I.D. 8/9/91). (note: ASTM 18 Gage 1-3/4" O.D. 316L Welded Pipe)

[15] See note 14. (Note: welds allow 1.615" ball thru - 41.02mm)

[16] Per M30-000997, Bore Tube, Wrapped, Quadrupole, ASST (note: Nitronic 40).

[17] FNAL Drawing, 0102-MB-292493, SSC 50mm Long Cold Mass Beam Tube (interim) (316L SS, welded, 1-3/4" O.D.)

[18] GD Drawing, M3A-103051-1, Beam Tube.

[19] FNAL Drawing, 0102-MB-292158, SSC 50mm Long Cold Mass Beam Tube (Nitronic 40)

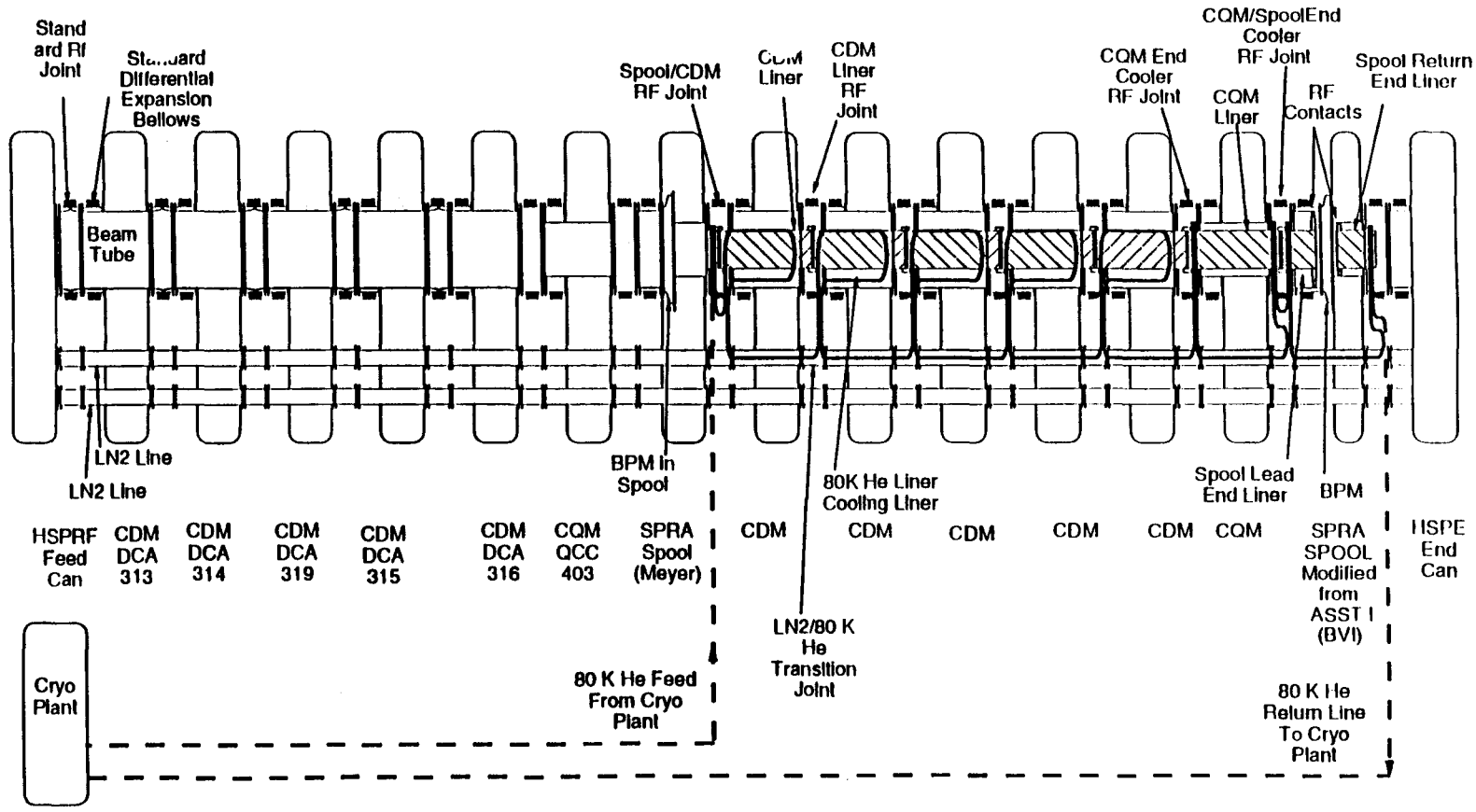

Beam Tube Liner ASST Full Cell System Layout

Control Room

Preliminary

RRM 10/2/92

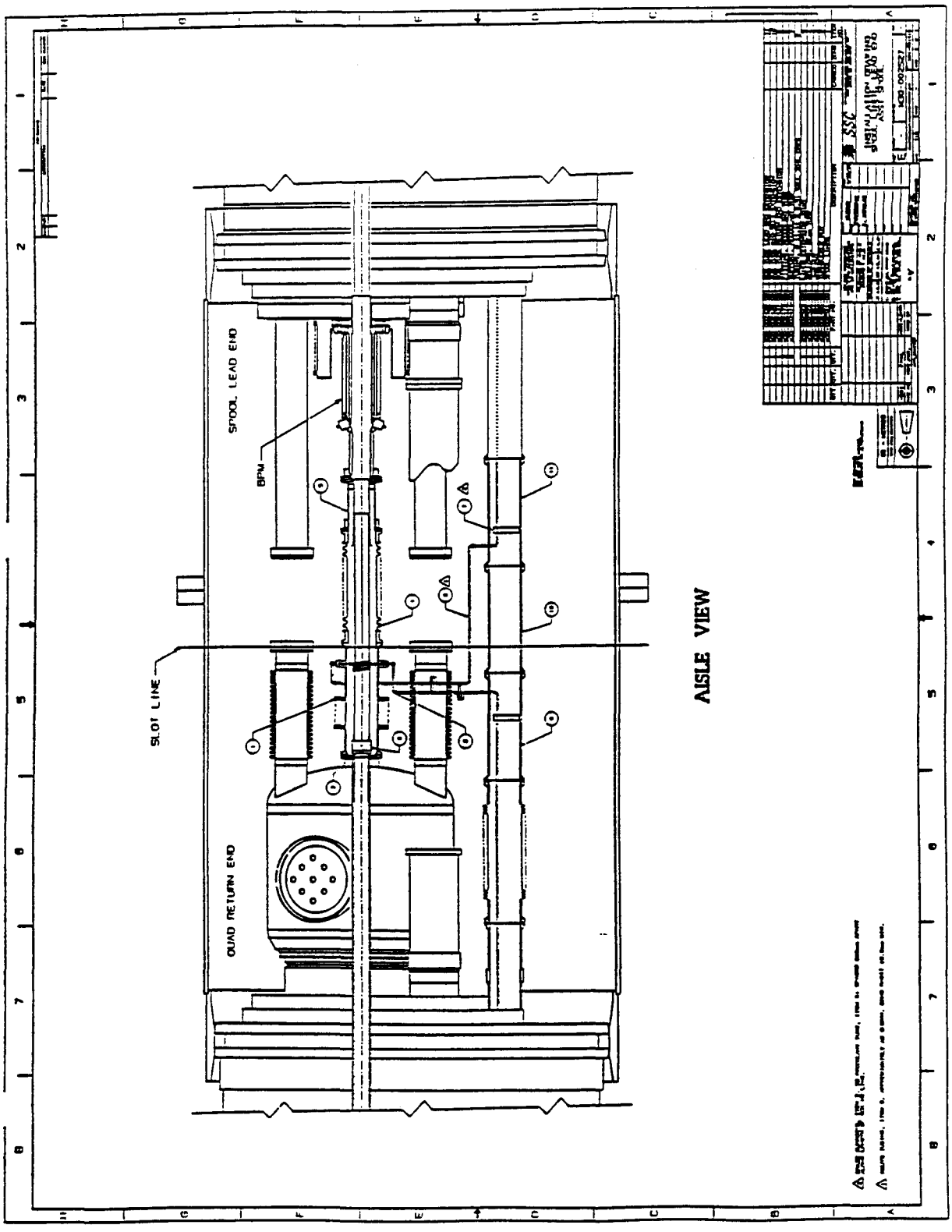
SPOOL LEAD END
BPM
SLOT LINE
QUAD RETURN END
AISLE VIEW

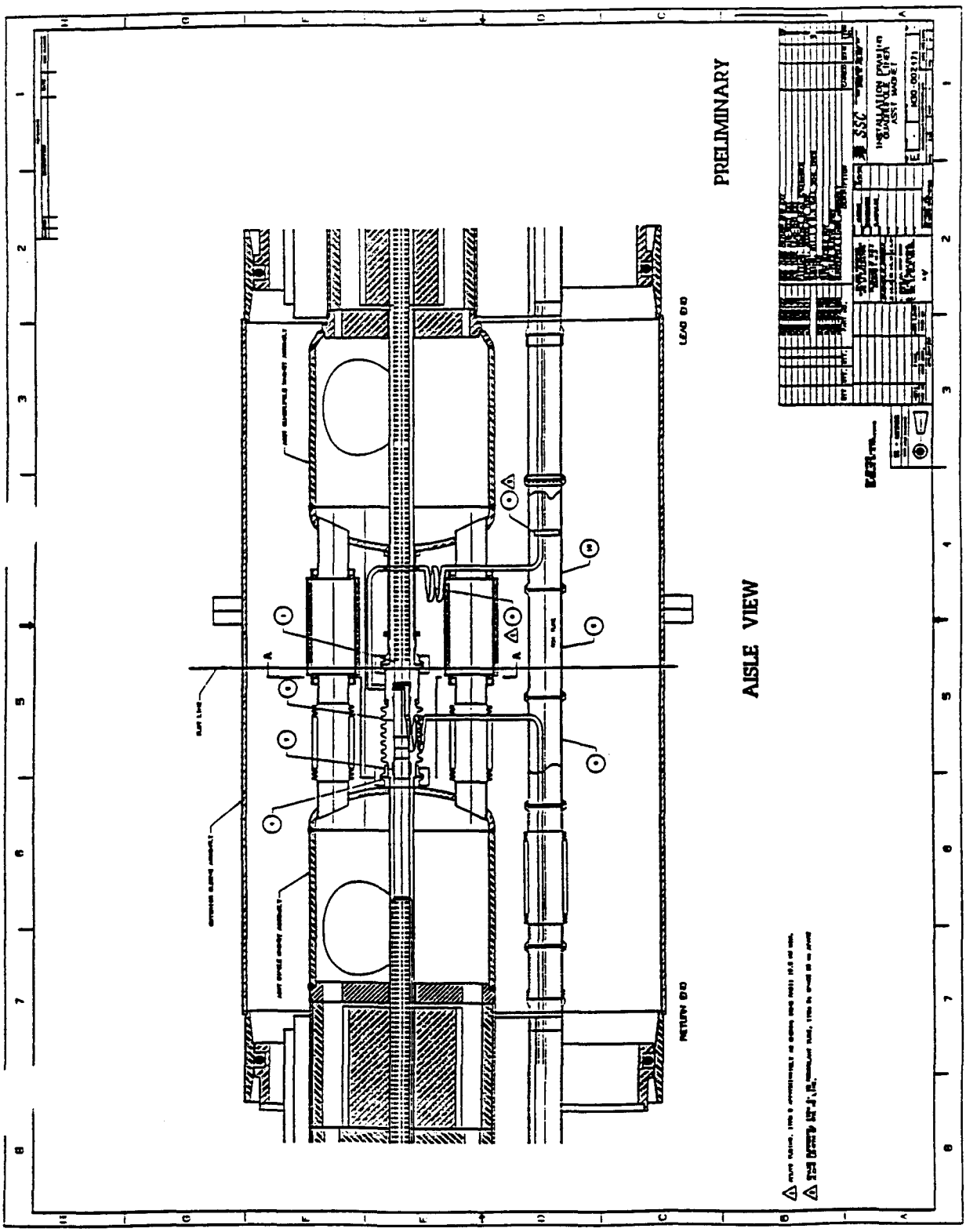
PRELIMINARY
AISLE VIEW

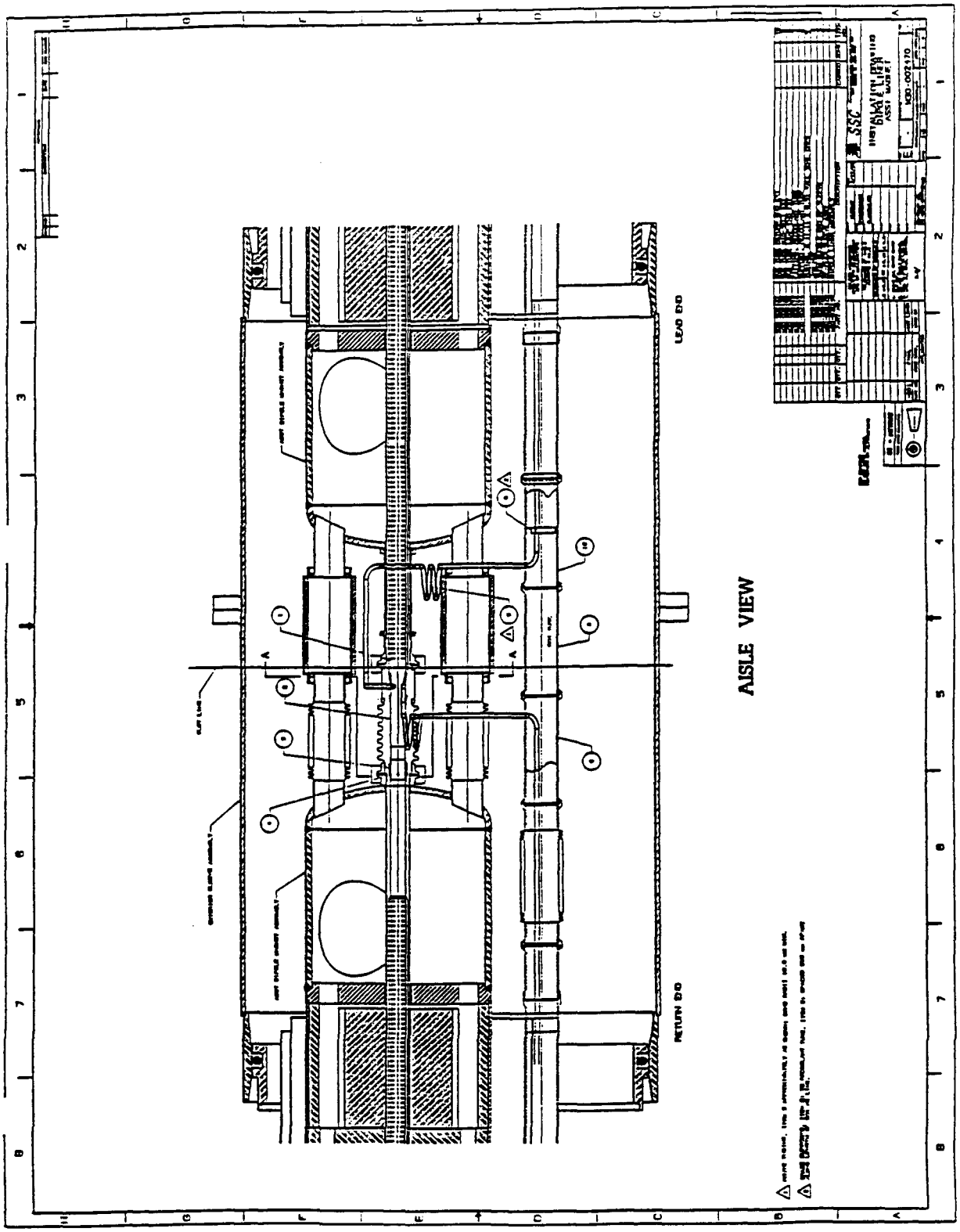
AISLE VIEW
LEAD END
RETURN END

SSC Laboratory 80K SR Liner Program

IMPROVED 80K BPM CONCEPT

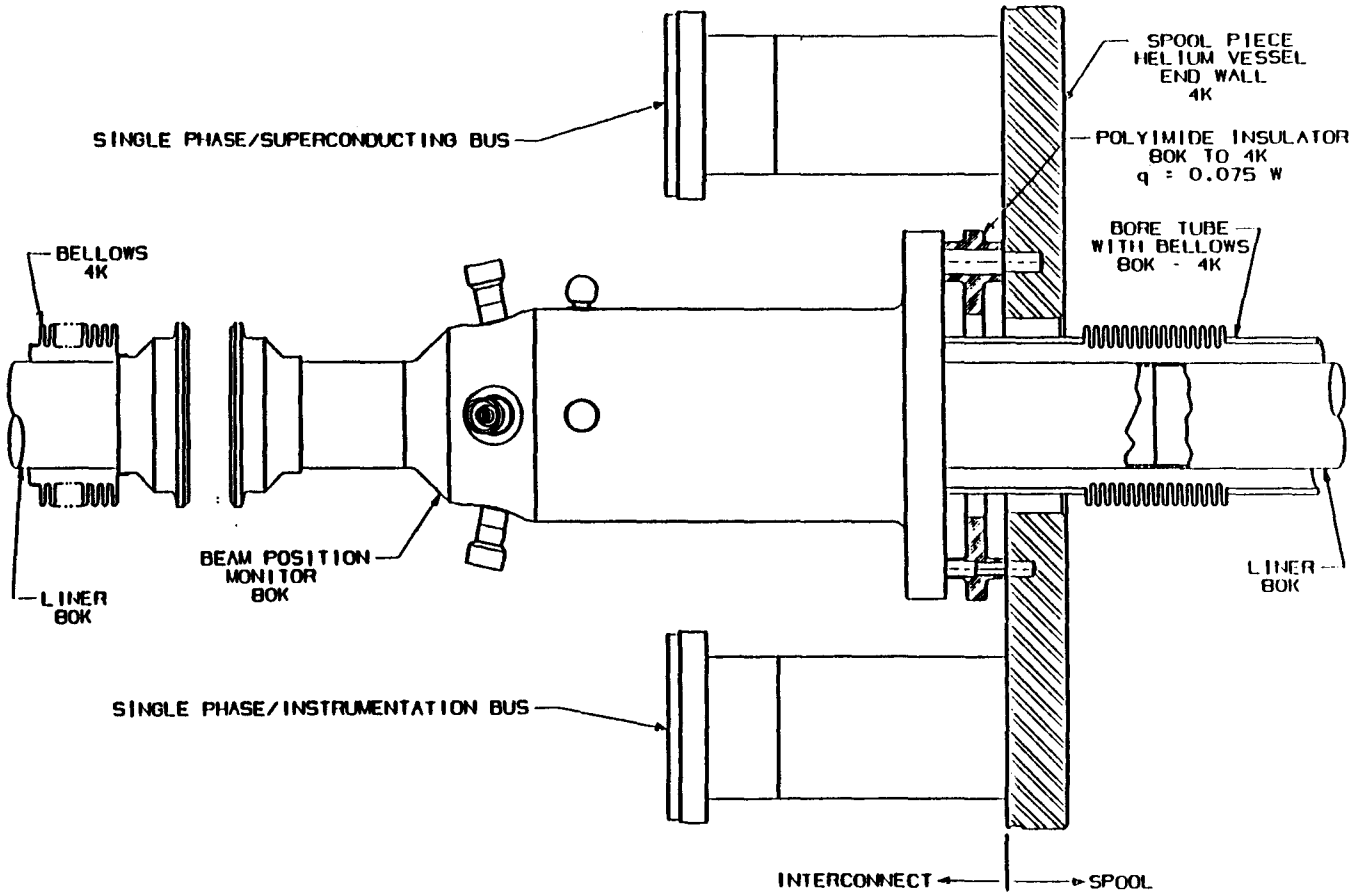

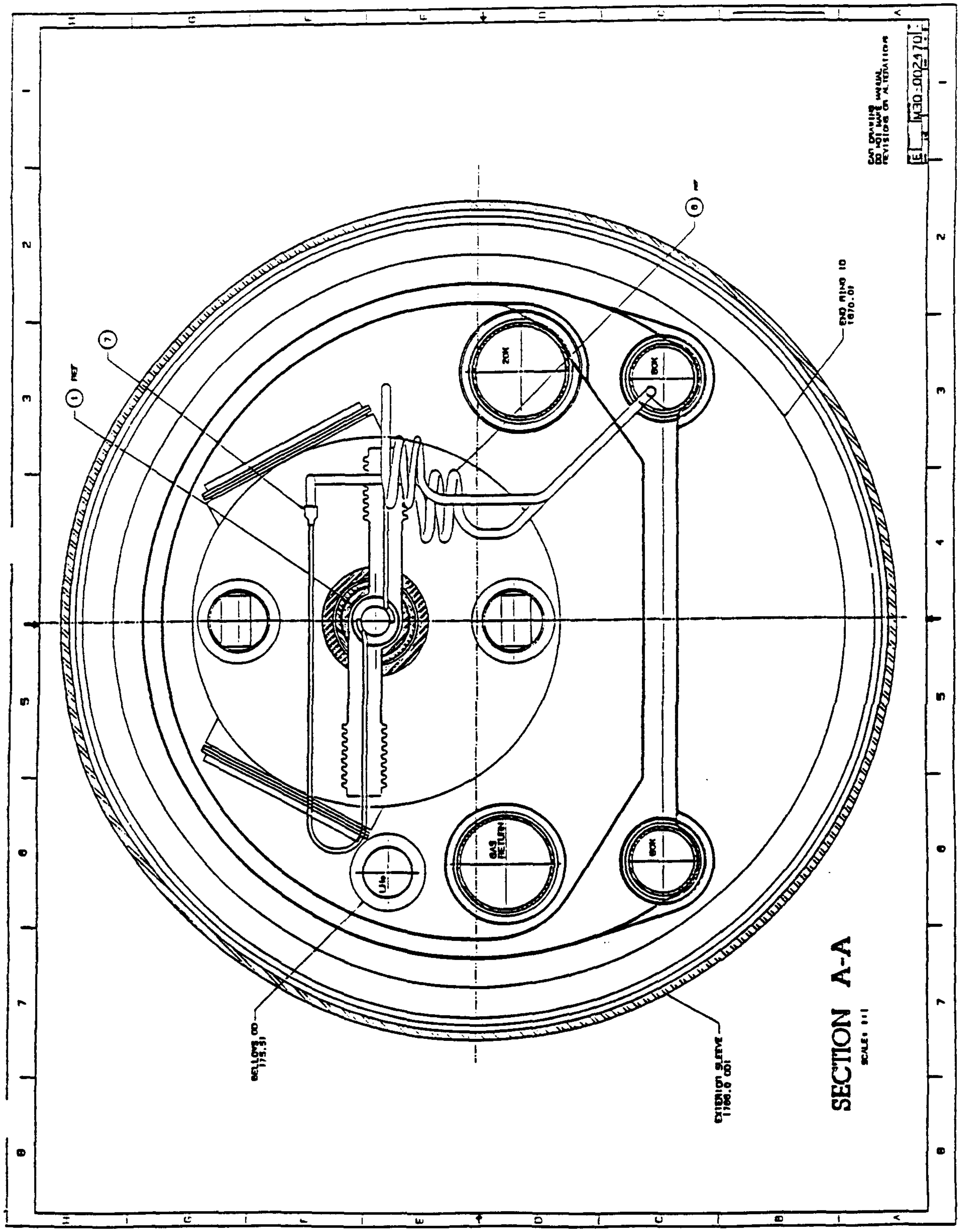
BELLOWS OD
(175.3)
GAS RETURN
20K
80K
80K
EXTERIOR SLEEVE
END RING ID
SECTION A-A
SCALE: 1:1
CAD DRAWING
DO NOT MAKE MANUAL
REVISIONS OR ALTERATIONS
E
M30-002470